

SYNTHETIC METHODS TOWARDS STRAINED AROMATIC NANOHOOPS AND
THEIR APPLICATION IN ELECTRONICS

by

EVAN RASHIED DARZI

A DISSERTATION

Presented to the Department of Chemistry and Biochemistry
and the Graduate School of the University of Oregon
in partial fulfillment of the requirements
for the degree of
Doctor of Philosophy

December 2016

DISSERTATION APPROVAL PAGE

Student: Evan Rashied Darzi

Title: Synthetic Methods Towards Strained Aromatic Nanohoops and their Application in Electronics

This dissertation has been accepted and approved in partial fulfillment of the requirements for the Doctor of Philosophy degree in the Department of Chemistry and Biochemistry by:

David Tyler	Chairperson
Ramesh Jasti	Advisor
Mike Haley	Core Member
John Halliwill	Institutional Representative

and

Scott L. Pratt	Dean of the Graduate School
----------------	-----------------------------

Original approval signatures are on file with the University of Oregon Graduate School.

Degree awarded December 2016

© 2016 Evan Rashied Darzi

DISSERTATION ABSTRACT

Evan Rashied Darzi

Doctor of Philosophy

Department of Chemistry and Biochemistry

December 2016

Title: Synthetic Methods Towards Strained Aromatic Nanohoops and their Application in Electronics

Carbon nanohoops represent an interesting and exciting structural motif with many potential material applications. To this end we have developed design several synthetic strategies to access a wide variety of functionalized hoops. Chapter **I** outlines the current state of the “Nanohoop” field focusing on the size-dependent properties of [5]-[12]cycloparaphenylene. This introduction walks through the interesting properties highlighting several interesting phenomena associated with nanohoops including their photophysical and electronic properties.

To appreciate these properties it is necessary to understand the synthetic advances that lead to their fundamental understanding. Chapter **II** outlines the original size-selective synthesis of [7]-[12]cycloparaphenylene and their fluorescence quantum yields. Chapter **III** describes the seminal synthesis of the smallest nanohoop to date, [5]CPP utilizing a series of mild reactions. In Chapter **IV**, the key step from this synthesis was expanded into a strain building coupling strategy not only for the synthesis of nanohoops but also for natural products.

With scalable strategies available, we designed a series of nitrogen doped nanohoops in the pursuit of true donor-acceptor systems as a means to tune the

electronics of nanohoops. Chapter V details the design principals that were uncovered and highlight the unique properties that can only be achieved in the nanohoop scaffold.

This dissertation includes previously published and co-authored material.

CURRICULUM VITAE

NAME OF AUTHOR: Evan Rashied Darzi

GRADUATE AND UNDERGRADUATE SCHOOLS ATTENDED:

University of Oregon, Eugene
Boston University, Boston
Arizona State University, Tempe

DEGREES AWARDED:

Doctor of Philosophy, Chemistry, 2016, University of Oregon
Master of Art, Chemistry, 2014, Boston University
Master of Science, Chemistry, 2011, Arizona State University
Bachelor of Science, Medicinal Biochemistry, 2008, Arizona State University

AREAS OF SPECIAL INTEREST:

Synthetic Organic Chemistry
Physical Organic Chemistry
Organic Materials

PROFESSIONAL EXPERIENCE:

Teaching Fellow, University of Oregon, 2015-2016
Teaching Fellow, Boston University, 2011-2013
Teaching Assistant, Arizona State University, 2007-2011

GRANTS, AWARDS, AND HONORS:

Poster Award, International Symposium on Novel Aromatic Compounds, 2015
Flash Talk Award, Physical Organic Chemistry Gordon Conference, 2015
Travel Award, Division of Organic Chemistry, National Organic Symposium,
2015

Flash Talk Award, Fusion Conference: From Carbon-Rich Molecules to Carbon Based Materials, 2014

Ignition Award, Boston University, 2013

Feldman Travel Award, Boston University, 2013

Distinguished Teaching Assistant Award, Arizona State University, 2009-2010

University Scholarship, Arizona State University, 2004-2008

PUBLICATIONS:

Taber, B.; Gervasi, C.; Mills, J.; Kislitsyn, D.; Darzi, E. D.; Crowley, W.; Jasti, R.; Nazin, G. Quantum Confinement of Surface Electrons by Molecular Nanohoop Corrals. *J. Phys. Chem. Lett.* **2016**, *7*, 3073-3077.

Jackson, E. P.; Sisto, T. J.; Darzi, E.R.; Jasti, R.; Probing Diels-Alder Reactivity on a Model CNT Sidewall. *Tetrahedron* **2016**, *72*, 3754-3758.

Van Raden, J. M.; Darzi, E. R.; Zakharov, L. N.; Jasti, R. Synthesis and Characterization of a Highly Strained Donor- Acceptor Nanohoop. *Org. Biomol. Chem.* **2016**, *14*, 5721-5727.

Darzi, E. R.; Hirst, E. S.; Webber, C. D.; Zakharov, L. N.; Lonergan, M. C.; Jasti, R. Synthesis, Properties, and Design Principles of Donor-Acceptor Nanohoop. *ACS Cent. Sci.* **2015**, *1*, 335-342.

Hines D. A.; Darzi, E. R.; Hirst, E. S.; Jasti, R.; Kamat, P. V. Carbon Nanohoos: Excited Singlet and Triplet Behavior of Aza[8]CPP and 1,15-Diaza[8]CPP. *J. Phys. Chem. A* **2015**, *119*, 8083-8089.

Darzi, E. R.; Jasti, R. The Dynamic, Size-Dependent Properties of [5]-[12]-Cycloparaphenylenes. *Chem. Soc. Rev.* **2015**, *44*, 6401-6410.

Evans, P. J.; Darzi, E. R.; Jasti, R. Efficient Room-Temperature Synthesis of a Highly Strained Carbon Nanohoop Fragment of Buckminsterfullerene. *Nat. Chem.* **2014**, *6*, 404-408.

Hines, D. A.; Darzi, E. R.; Jasti, R.; Kamat, P. V. Carbon Nanohoos: Excited Singlet and Triplet Behavior of [9]- and [12]-Cycloparaphenylene. *J. Phys. Chem. A* **2014**, *118*, 1595-1600.

Li, P.; Sisto, T. J.; Darzi, E. R.; Jasti, R. The Effects of Cyclic Conjugation and Bending on the Optoelectronic Properties of Paraphenylenes. *Org. Lett.* **2014**, *16*, 182-185.

Darzi, E. R.; Sisto, T. J.; Jasti, R. Selective Syntheses of [7]–[12]Cycloparaphenylenes Using Orthogonal Suzuki–Miyaura Cross-Coupling Reactions. *J. Org. Chem.* **2012**, *77*, 6624-6628.

ACKNOWLEDGMENTS

First, I would like to thank my advisor Professor Ramesh Jasti for bringing me into the lab and teaching me about research and academics. I am forever indebted to those that built the Jasti lab from the early days. Dr. Paul Evans, Dr. Elizabeth Hirst, Dr. Matthew Golder, Dr. Thomas Sisto each taught me an invaluable skill that helped mold the scientist I have become. I would like to extend a special thank you to Professor Jianlong Xia for patiently teaching me everything I know about computational chemistry.

I would like to thank those that inspired and supported me through the highs and lows of grad school including my first year colleagues Penghao Li, Dr. Joel Beatty, Dr. Mitch Keylor, and Gina Kim. Thanks to all the current Jasti lab members including Jeff Van Raden, Curtis Colwell, Erik Leonhardt, and Terri Lovell. A special thanks to Brittany White for being an excellent coworker and friend.

Additionally I would like to thank those professors who have given me guidance during my tenure in graduate school including Professor John Porco, Professor Scott Schaus, and Professor Aaron Beeler. I would like to thank the chair of my doctoral committee including Professor David Tyler who has given numerous key suggestions that helped expand and improve my work. A huge thank you to Professor Michael Haley for warmly welcoming us to the University of Oregon, teaching us how to garden like true Northwesterners, and for introducing me to the wonderful physical organic international community. Thanks to Professor John Halliwill for completing my dissertation committee.

I have drawn constant inspiration and support from my parents. Thank you to my dad Khalil Darzi for teaching me about perseverance and hard work. Thank you to my

mother Cynthia Avazpour for teaching me how to lead by example and no matter what keep a good attitude and treat everyone with respect. Thank you to my sibling, Taylor and Layla Darzi and my step parents Kim Darzi and Reza Avazpour.

Finally I would like to thank my wife Gabrielle Darzi for being my guiding light during this long and arduous process. You have been so understanding and supportive and I cannot thank you enough for all you have contributed to the subsequent work. I am lucky to have such a strong person in my life.

Dedicated to my wife Gabrielle Macias and my parents Khalil Darzi and Cynthia
Avazpour

TABLE OF CONTENTS

Chapter	Page
I. THE DYNAMIC, SIZE-DEPENDANT PROPERTIES OF [5]-[12] CYCLOPARAPHENYLENES.....	1
I.1. Key Learning Points	2
I.2. Introduction	2
I.3. Synthetic Approaches to [n]Cycloparaphenylenes.....	5
I.4. Structural Features of [n]Cycloparaphenylenes	7
I.5. Nuclear Magnetic Resonance Spectroscopy of [n]CPPs.....	11
I.6. Raman Spectroscopy of [n]CPPs.....	13
I.7. Electrochemistry	16
I.8. Carbon Nanohoop Photophysics	17
I.9. Conclusion	21
I.10. Bridge to Chapter II.....	21
II. SELECTIVE SYNTHESIS OF [7]-[12] CYCLOPARAPHENYLENES USING ORTHOGONAL SUZUKI-MIYAJIWA CROSS-COUPLED REACTIONS	23
II.1. Introduction	23
II.2. Synthesis.....	24
II.3. Fluorescence Quantum Yield.....	26
II.4. Conclusion.....	27
II.5. Experimental Section	27
II.5.1. General Experimental Details	27
II.5.2. Synthetic Schemes.....	28

Chapter	Page
II.5.4. Synthetic Details	31
II.5.5. NMR Spectra.....	37
II.5.6. Fluorescence Quantum Yield Data	50
II.5.7. Computational Details.....	51
II.6. Bridge to Chapter III	76
III. EFFICIENT ROOM-TEMPERATURE SYNTHESIS OF A HIGHLY STRAINED CARBON NANOHOOP FRAGMENT OF BUCKMINSTERFULLERENE	77
III.1. Introduction.....	77
III.2. Results and Discussion	79
III.2.1. Synthesis of [5] Cycloparaphenylene	79
III.2.2. NMR Spectroscopy of [5]Cycloparaphenylene	81
III.2.3. Solid State Analysis of [5]Cycloparaphenylene	82
III.2.4. Photophysical Characterization of [5]Cycloparaphenylene.....	83
III.2.5. Electrochemical Properties of [5]Cycloparaphenylene	84
III.3. Conclusion	85
III.4. Experimental Section.....	85
III.4.1. General Experimental Details	85
III.4.2. Synthetic Details	86
III.4.3. NMR Spectra	89
III.4.4. Optical Characterization	91
III.4.5. Electrochemical Characterization	93
III.4.6. Computational Details	95

Chapter	Page
III.4.7. Crystallographic Details.....	129
III.5. Bridge to Chapter IV.....	130
IV. AN OPERATIONALLY SIMPLE AND MILD OXIDATIVE HOMOCOUPLING OF ARYL BORONIC ESTERS TO ACCESS CONFORMATIONALLY CONSTRAINED MACROCYCLES	131
IV.1. Introduction.....	131
IV.2. Results and Discussion.	133
IV.2.1. Reaction Optimization.....	133
IV.2.2. Direct Comparison to Suzuki-Miyaura Cross-Coupling	138
IV.2.3. Direct Comparison to Yamamoto-Coupling.....	140
IV.2.4. Substrate Scope.....	141
IV.2.5. Structural Analysis.....	144
IV.2.6. NMR Studies	146
IV.3. Conclusion.....	148
IV.4. Experimental Details	149
IV.4.1. Synthetic Details.....	149
IV.4.2. NMR Experiments	174
IV.4.3. NMR Spectra.	175
IV.4.4. Crystallographic Details	193
IV.4.5. Computational Details	196
IV.5. Bridge to Chapter V.....	225
V. SYNTHESIS, PROPERTIES, AND DESIGN PRINCIPLES OF DONOR-ACCEPTOR NANOHOOPS	226
V.1. Introduction.....	226

Chapter	Page
V.2. Results and Discussion.....	229
V.2.1. Synthesis of Aza-and Donor–Acceptor Nanohoops.....	229
V.2.2. Solid-State Packing Morphology of Aza-and Donor–Acceptor Nanohoops	231
V.2.3. Electrochemical Properties of Aza-and Donor– Acceptor Nanohoops	232
V.2.4. Optical Properties of Aza-and Donor–Acceptor Nanohoops	235
V.3. Methods.....	237
V.4. Significance and Outlook.....	238
V.5. Conclusion.	240
V.6. Experimental Details.....	241
V.6.1. General Experimental Details.....	241
V.6.2. Synthetic Details	243
V.6.3. NMR Spectra.....	257
V.6.4. Crystallographic Details.....	272
V.6.5. Electrochemical Details.	274
V.6.6. Photophysical Details.....	275
V.6.7. Computational Details.....	280
CONCLUDING REMARKS.....	336
REFERENCES CITED.....	337

LIST OF FIGURES

Figure	Page
I.1. Inspirational bottom up syntheses of curved PAHs.....	3
I.2. [<i>n</i>]CPPs are fragments of (n,n) armchair CNTs.....	4
I.3. Linear paraphenylenes and most conjugated materials have a narrowing HOMO–LUMO gap as conjugation length increases. Cyclic paraphenylenes on the other hand show the opposite trend. Data taken from ref. 19	5
I.4. Point group of (a) even <i>n</i> = 6, 8, 10, and 12 and odd <i>n</i> = 5, 7, 9, 11 [<i>n</i>]CPPs. (b) Torsional angle Θ of cyclic and linear paraphenylenes. Reproduced with permission. Copyright © Elsevier.....	8
I.5. Crystal packing of [5]-[12]CPP in the solid state. (a) Side on view of crystal packing mode. (b) Top down view of [6]CPP and [8]CPP illustrating the long range channel present in [6]-[12]CPP. (c) Close intermolecular interactions found in [6]CPP and [8]CPP crystal structures.....	10
I.6. (a) ¹ H NMR spectra of [5]-[12]CPP, (b) ¹³ C spectra of <i>C_{ortho}</i> for [5]-[12]CPP, and ¹³ C spectra of <i>C_{ipso}</i> for [5]-[12]CPP	12
I.7. (a) Representative [<i>n</i>]CPP bonds and torsional angle highlighted in green. (b) Raman spectra of [6]-[12]CPP (c) Raman frequency vs [<i>n</i>]CPP and (d) percent quinoidization vs [<i>n</i>]CPP. Reproduced with permission. Copyright © Wiley	14
I.8. Cartoon of the pressure induced (a) irreversible deformation of [6]CPP (b) reversible deformation of [12]CPP (c) reversible host guest complexation of [6]CPP@[12]CPP and (d) charge transfer from [10]CPP to C ₆₀	16
I.9. UV/VIS (solid) and fluorescence (dashed) spectra for [5]-[12]CPP. No fluorescence is observed for [6]CPP or [5]CPP.....	19
I.10. Calculated (B3LYP/6-31G*) (d) HOMO, HOMO-1, LUMO, and LUMO+1 energy levels (B3LYP/6-31G*). HOMO-1 and HOMO-2 are nearly degenerate as are LUMO+1 and LUMO+2. For clarity purposes only HOMO-1 and LUMO+1 energies were used. Data taken from reference 19	19
I.11. a) Minimized geometries of the ground state and first excited state. b) Orbital visualization of S1, S2, S3, and S1' transitions. c) Transition dipole for [12]CPP illustrating the self-trapping S1' state. Reproduced with permission. Copyright© ACS.....	20
II.1. [<i>n</i>]Cycloparaphenylene	23

Figure	Page
II.2. The quantum yields of [6]-[12]cycloparaphenylene	27
III.1. Classic Strained Hydrocarbons and Trends in Small Cycloparaphenylenes	78
III.2. Synthesis of [5]Cycloparaphenylene with DFT Structure of III.2 and Refined Crystal Structures of III.3 , and [5]CPP	80
III.3. Crystal Data of [5]CPP Showing Structure (Left, ORTEP Ellipsoids Displayed at 50% Probability), Boat Angle (top right) and Herringbone Packing (Bottom Right).....	83
III.4. UV-Vis Absorbance (1 $\mu\text{g/mL}$, 0.1 mg/mL Inset) of [5]CPP Showing Major and Minor Absorbances	84
III.5. Cyclic Voltammograms Showing Oxidation (Left) and Reduction (Right) Events for [5]CPP in Tetrahydrofuran	84
III.6. UV-Vis of [5]CPP in Dichloromethane, Minor Absorption is Shown in the Top Right Corner	92
III.7. Beer-Lambert Plots for the Determination of Extinction Coefficient of [5]CPP ($\epsilon_{335\text{nm}} = 5.70 \times 10^4 \text{ M}^{-1}\text{cm}^{-1}$, $\epsilon_{501\text{nm}} = 4.50 \times 10^2 \text{ M}^{-1}\text{cm}^{-1}$).....	93
III.8. Cyclic Voltammetry of [5]CPP	94
III.9. Homodesmotic reactions used to calculate strain of macrocyclic compounds III.2 , III.3 , and [5]CPP	95
III.10. Calculated UV-Vis for [5]CPP Determined by TD-DFT Method Using B3LYP/6-31g*	96
III.11. Calculated HOMO and LUMO of Ground State [5]CPP at B3LYP/6-31g* Level of Theory.....	98
III.12. ORTEP Representation of X-ray Crystallographic Structure 3 (CCDC Registry #974188).....	129
III.13. ORTEP Representation of X-ray Crystallographic Structure [5]CPP (CCDC Registry #974187).....	130
IV.1. Common Intramolecular Macrocyclization Strategies	133
IV.2. Seminal Report of the Oxidative Homocoupling of an Aryl Diboronic Ester to Form Strained Macrocycle IV.2	133

Figure	Page
IV.3. Proposed Catalytic Cycle by Adamo.....	133
IV.4. Direct Comparison of an Intramolecular Suzuki-Miyaura Cross-Coupling of IV.10 and Intramolecular Oxidative Homocoupling of Diboronic Ester IV.11 to Give Macrocycle IV.4	139
IV.5. Direct Comparison of Reductive Yamamoto Coupling of Dibromide IV.5 and the Oxidative Homocoupling Diboronic Esters IV.1 to Form Macrocycle IV.2	140
IV.6. ¹ H NMR Profile of Reaction Over 2 h.....	146
IV.7. In Situ Reduction of PdCl ₂ (PPh ₃) ₂ Using TBAF in <i>d</i> ₈ THF.....	147
IV.8. ORTEP Representation of X-ray Crystallographic Structure Macrocycle IV.2	193
IV.9. ORTEP Representation of X-ray Crystallographic Structure Macrocycle IV.12	193
IV.10. ORTEP Representation of X-ray Crystallographic Structure Dichloride IV.19	194
IV.11. ORTEP Representation of X-ray Crystallographic Structure Macrocycle IV.21	195
IV.12. ORTEP Representation of X-ray Crystallographic Structure Macrocycle IV.23	195
V.1. Wrapping a Linear Polymer into a Cyclic Isomer Leads to Dramatic Modulation of the Electronic Structure. Calculated HOMO–LUMO Energy Gaps are Taken from Reference 7	227
V.2. (a) Nitrogen Doped CNT. (b) Azafullerene. (c) Targeted Compounds V.1 Aza[8]CPP, V.2 1,15-Diaza[8]CPP, V.3 1,15,31-Triaza[8]–CPP, V.4 N-methylaza[8]CPP Triflate, and V.5 N,N-dimethyl-1,15-diaza[8]CPP Ditriflate ...	228
V.3. ORTEP, Side-on Packing, and Top-Down Packing of (a) V.1 and (b) V.5 . (c) Head to Tail Interaction Between One Pyridinium Acceptor and a Neighboring Electron-rich Phenylene Donor in Compound V.5	232
V.4. Cyclic Voltammetry of [8]CPP and V.1 – V.5	233

Figure	Page
V.5. DFT Calculated HOMO and LUMO Energy Levels and Orbital Distributions for [8]CPP and Nano hoops V.1– V.6	234
V.6. (a) Scaled (For Clarity) UV–Vis Absorbance (Solid Lines) and Fluorescence (Dashed Lines) of Compounds [8]CPP (Blue), Aza[8]CPP V.1 (Green), 1,15-Diaza[8]CPP V.2 (Yellow), and 1,15,31-Triaza[8]CPP V.3 (Red) in Dichloromethane. (b) Scaled (For Clarity) UV–Vis (Solid Lines) and Fluorescence (Dashed Lines) for Compounds [8]CPP (Blue), N-methylaza[8]CPP Triflate V.4 (Orange), and N,N-dimethyl-1,15-diaza[8]CPP Ditriflate V.5 (Red) in Dichloromethane.....	236
V.7. TD-DFT Orbital Transitions for (a) [8]CPP, (b) 1,15-Diaza[8]CPP V.2 , and (c) N,N-dimethyl-1,15-diaza[8]CPP Ditriflate V.5 . Pictorial Orbital Transitions for V.1 , V.3 , and V.4 are Found in Figure V.26	236
V.8. Theoretical HOMO and LUMO Energies for (a) N,N-dimethyl-1,8-diaza[8]CPP, (b) N,N-dimethyl-1,21-diaza[8]CPP, and (c) N,N-dimethyl-1,26-diaza[8]CPP	239
V.9. The Effect of Acceptor (Red), Donor (Blue), and Donor-Acceptor Moieties on the HOMO and LUMO Energies of [6]CPP and Linear [6]OPP Frameworks.....	240
V.10. ORTEP Representation of X-ray Crystallographic Structure Aza[8]CPP V.1	272
V.11. ORTEP Representation of X-ray Crystallographic Structure N,N-dimethyl-1,15-diaza[8]CPP Ditriflate V.5	273
V.12. ORTEP Representation of X-ray Crystallographic Structure V.8d	273
V.13. Published Crystallographic Information for [8]CPP. (a) ORTEP Representation of X-ray Crystallographic Structure [8]CPP (CCDC Registry 871414) (b) Side-on Packing (c) and Top-Down Packing.....	274
V.14. Beer-Lambert plot of V.1 at 341 nm. ($\epsilon = 2.8 \times 10^4 \text{ M}^{-1} \text{ cm}^{-1}$).....	275
V.15. Beer-Lambert plot of V.1 at 400 nm. ($\epsilon = 0.25 \times 10^4 \text{ M}^{-1} \text{ cm}^{-1}$).....	275
V.16. Beer-Lambert plot of V.2 at 343 nm. ($\epsilon = 9.2 \times 10^4 \text{ M}^{-1} \text{ cm}^{-1}$).....	276
V.17. Beer-Lambert plot of V.2 at 400 nm. ($\epsilon = 0.73 \times 10^4 \text{ M}^{-1} \text{ cm}^{-1}$).....	276
V.18. Beer-Lambert plot of V.3 at 350 nm. ($\epsilon = 1.1 \times 10^4 \text{ M}^{-1} \text{ cm}^{-1}$).....	277
V.19. Beer-Lambert plot of V.3 at 400 nm. ($\epsilon = 0.089 \times 10^4 \text{ M}^{-1} \text{ cm}^{-1}$).....	277

Figure	Page
V.20. Beer-Lambert plot of V.4 at 340 nm. ($\epsilon = 2.9 \times 10^4 \text{ M}^{-1} \text{ cm}^{-1}$).....	278
V.21. Beer-Lambert plot of V.4 at 450 nm. ($\epsilon = 0.019 \times 10^4 \text{ M}^{-1} \text{ cm}^{-1}$).....	278
V.22. Beer-Lambert plot of V.5 at 348 nm. ($\epsilon = 4.9 \times 10^4 \text{ M}^{-1} \text{ cm}^{-1}$).....	279
V.23. Beer-Lambert plot of V.5 at 400 nm. ($\epsilon = 5.5 \times 10^4 \text{ M}^{-1} \text{ cm}^{-1}$).....	279
V.24. Beer-Lambert plot of V.5 at 450 nm. ($\epsilon = 0.98 \times 10^4 \text{ M}^{-1} \text{ cm}^{-1}$).....	280
V.25. TD-DFT (B3LYP/6-31g*) Plot for Compounds V.1- V.5 and [8]CPP	280
V.26. TD-DFT (B3LYP/6-31g*) Major Transitions and Orbital Densities for Compounds V.1- V.5 and [8]CPP	281
V.27. TD-DFT (B3LYP/6-31g*) Plots for Theoretical Structures <i>N,N</i> -Dimethyl- 1,26-diaza[8]CPP, <i>N,N</i> -Dimethyl-1,21-diaza[8]CPP, and <i>N,N</i> -Dimethyl-1,8-diaza[8]CPP	284

LIST OF TABLES

Table	Page
I.1. Calculated B3LYP/6-31G(d) Total Strain, Strain Per Benzene Ring, Displacement Angle, and Diameter of [5]–[12]CPP. ^a Reference 18. ^b Reference 43	7
I.2. Published Oxidation and Reduction Potentials of [n]CPPs (V vs Fc/Fc+). a Reference 18. b Reference 15. c Reference 21. d Reference 39. e Reference 19.....	17
I.3. Summary of Experimental Photophysical Properties for [5]-[12]CPP. ^a Reference 18. ^b Reference 22. ^c Reference 15. ^d Reference 14. ^e Reference 13. ^f Reference 6. ^g Reference 11. ^h Reference 17. ⁱ Reference 35. ^j Reference 54. ^k Reference 53. ^l Reference 39	18
III.1. Summary of Homodesmotic Reactions Used to Calculate Strain of Macrocyclic Compounds III.2 , III.3 , and [5]CPP	96
III.2. Major Electronic Transitions for [5]CPP Determined by TD-DFT Method Using B3LYP/6-31g*	96
III.3. Calculated Total Energies Reduced, Excited, and Oxidized [5]CPP and the Corresponding ΔE from the Neutral Ground State at the Restricted or Unrestricted B3LYP/6-31g* Level of Theory	97
IV.1. Optimization of Oxidative Homocoupling of Diboronic Ester III.1 to Strained Macrocycle III.2	135
IV.2. Solid State Analysis of Macrocycles IV.2 , IV.4 , IV.12 , IV.21 , and IV.23	144
V.1. Experimental Cathodic Peak Potentials, Maximum Absorbance, Extinction Coefficients, and Emission Maxima for [8]CPP and V.1 – V.5	237
V.2. Major Electronic Transitions for Aza[8]CPP V.1 Determined by TD-DFT Method Using B3LYP/6-31g*	281
V.3. Major Electronic Transitions for 1,15-diaza[8]CPP V.2 Determined by TD-DFT Method Using B3LYP/6-31g*.....	282
V.4. Major Electronic Transitions for 1,15,31-triaza[8]CPP V.3 Determined by TD-DFT Method Using B3LYP/6-31g*.....	283
V.5. Major Electronic Transitions for N-methylaza[8]CPP Triflate V.4 Determined by TD-DFT Method Using B3LYP/6-31g*	283

Table	Page
V.6. Major Electronic Transitions for 1,15,31-triaza[8]CPP V.3 Determined by TD-DFT Method Using B3LYP/6-31g*	283
V.7. Major Electronic Transitions for N,N-Dimethyl-1,26-diaza[8]CPP Determined by TD-DFT Method Using B3LYP/6-31g*	284
V.8. Major Electronic Transitions for N,N-Dimethyl-1,21-diaza[8]CPP Determined by TD-DFT Method Using B3LYP/6-31g*	284
V.9. Major Electronic Transitions for N,N-Dimethyl-1,8-diaza[8]CPP Determined by TD-DFT Method Using B3LYP/6-31g*	285

LIST OF SCHEMES

Scheme	Page
I.1. General Synthetic Routes Used to Access [n]CPPs by (a) Jasti, (b) Itami, and (c) Yamago	6
II.1. Orthogonal Suzuki-Miyaura Cross-coupling Reactions to Prepare Terminal Dichlorides II.1 and II.2 . ^a Conditions to Prepare II.1 : Fragment II.3 (1 equiv.), Fragment II.4 (1 equiv.), Pd(PPh ₃) ₄ (10 mol%), NaHCO ₃ (1M aq.), 2-propanol, 85 °C. Conditions to Prepare II.2 : Fragment II.3 (2 equiv.), Fragment II.5 (1 equiv.), Pd(PPh ₃) ₄ (10 mol%), NaHCO ₃ (1M aq.), 2-propanol, 85 °C.....	24
II.2. Divergent Macrocyclizations for the Precursors to [7]-[9]CPP. ^a Conditions: Dichloride II.1 , Diboronate II.6 , II.7 , or II.5 , Pd ₂ (dba) ₃ (10 mol%), S-Phos, K ₃ PO ₄ , DMF, H ₂ O, 125 °C (155 °C for II.8). DFT Optimized Geometries of Macrocycles II.8 , II.9 , and II.10 are Shown	25
II.3. Divergent Macrocyclizations for the Precursors to [10]-[12]CPP. ^a Conditions: Dichloride II.2 , Diboronate II.6 , II.7 , or II.5 , Pd ₂ (dba) ₃ , S-Phos, K ₃ PO ₄ , DMF, H ₂ O, 125 °C. DFT Optimized Geometries of Macrocycles II.11 , II.12 , and II.13 are Shown	25
II.4. General Aromatization Reaction Utilizing Sodium Naphthalide.....	26
IV.1. Synthesis of a Six-Ring DiBpin IV.11 and the Analogues Six-ring Bpin-Cl IV.10 Towards Macrocycle IV.4	138
IV.2. Synthesis of a Strained Tetraphenylene Containing Macrocycle IV.12 Utilizing an Oxidative Homocoupling of Diboronic Ester IV.15	141
IV.3. Synthesis of Strained Alkyne Containing Macrocycle IV.21 Utilizing an Oxidative Homocoupling of Diboronic Acid IV.20	142
IV.4. Formal Synthesis of Acerogenin E Utilizing an Oxidative Homocoupling of Diboronic Ester IV.27	143

CHAPTER I
THE DYNAMIC, SIZE-DEPENDANT PROPERTIES OF [5]-[12]
CYCLOPARAPHENYLENES

This chapter is based on a review published in *Chemical Society Reviews* in 2015. The material covered was written by me and appears as it was published with final edits done by Professor Ramesh Jasti.

Chapter **II** is based on published work in the *Journal of Organic Chemistry* (2012). The manuscripts was written my meself and Dr. Thomas Sisto. The initial synthetic route was devised by Professor Ramesh Jasti and Dr. Thomas Sisto.

Chapter **III** is based on published work in *Nature Chemistry* (2014). The manuscript was prepared by Dr. Paul Evans and myself. The oxidative homocoupling was devised by myself while the remaining synthetic route was equally contributed by Dr. Paul Evans and myself. Editing of the manuscript was provided by Professor Ramesh Jasti.

Chapter **IV** is based on unpublished work. The manuscript was written by myself and edited by Professor Ramesh Jasti. Brittany White is responsible for the formal synthesis of Acerogenin E. Lance Loventhal is responsible for the alkyne containing macrocycle. I devised the mechanistic studies and the synthesis of the remaining compounds.

Chapter **V** is based on published work in *ACS Central Science* (2015). The manuscript was written by myself and was edited by Professor Ramesh Jasti. The synthesis of nitrogen containing nano hoops was contributed by Dr. Elizabeth Hirst and myself. All remaining compounds were synthesized by myself. The electrochemical studies were performed by Dr. Christopher Weber and Professor Mark Lonergan. X-ray crystallography was performed by Dr. Lev Zakharov.

[*n*]Cycloparaphenylenes (or “carbon nano hoops”) are cyclic fragments of carbon nanotubes that consist of *n* para linked benzene rings. These strained, all sp² hybridized macrocycles, have size-dependent optical and electronic properties that are the most dynamic at the smallest size regime where *n* = 5–12. This review highlights the unique physical phenomena surrounding this class of polycyclic aromatic hydrocarbons,

specifically emphasizing the novel structural, optical, and electronic properties of [5]–[12]CPPs.

I.1. Key learning points.

(1) [n]CPPs have a narrowing HOMO–LUMO gap as the number of benzene rings n decreases. This trend is contrary to linear [n]paraphenylenes and most other conjugated macromolecules which have a narrowing HOMO–LUMO gap as n and conjugation length is increased.

(2) Strain induces torsional angle minimization as nano hoops become smaller. This torsional angle minimization leads to an effective increase in conjugation length for smaller sizes.

(3) HOMO–LUMO optical transitions are Laporte forbidden due to a conservation of orbital symmetry for the centrosymmetric CPPs. Absorbance maxima for all [n]CPPs are virtually identical and can be attributed to nearly degenerate HOMO–1 to LUMO or HOMO–2 to LUMO transitions, and HOMO to LUMO+1 or HOMO to LUMO+2 transitions.

(4) Fluorescence is red-shifted and quantum efficiency decreases as nano hoops become smaller. This phenomenon is accounted for by a violation of the Frank–Condon principal resulting in the relaxation from S2 and S3 states to geometrically relaxed S10 state. In larger [n]CPPs (where $n \geq 7$) the S10 state breaks the symmetry of the ground state causing emission to the S0 state with decreasing quantum efficiency and redshifting fluorescence from [12]CPP to [7]CPP. In smaller [n]CPPs (where $n \leq 6$) the S1' state conserves the symmetry of the ground state and so emission to the S0 state is forbidden and no fluorescence is observed.

(5) [n]CPPs organize in the solid state with long range channels and sub van der Waals radius intermolecular carbon–carbon interactions.

I.2. Introduction.

Synthetic chemists often pursue structurally unique molecules in anticipation that these unexplored architectures might impart physical properties that are not present in more common motifs.¹ The field of polycyclic aromatic hydrocarbon (PAH) chemistry is rich with examples, commencing with the historic work in the field by Kekule in 1865 when he first elucidated the cyclic six electron aromatic structure of benzene.² In more recent

years, curved and distorted nonplanar PAHs have attracted significant attention from the scientific community in that these structures push the boundaries of our understanding of aromaticity and electron delocalization. Buckminsterfullerenes and carbon nanotubes (CNTs) have drawn special interest due to their unprecedented material properties and promise in the field of nanotechnology. Pioneers such as Herges with the synthesis of the picotube, Scott with the bottom-up synthesis of C₆₀, and Nakamura with the synthesis of a caged acene belt (Fig. I.1) have paved the way for the rational synthesis of new PAHs that continue to push the frontiers of our understanding of these unique structures.³⁻⁵

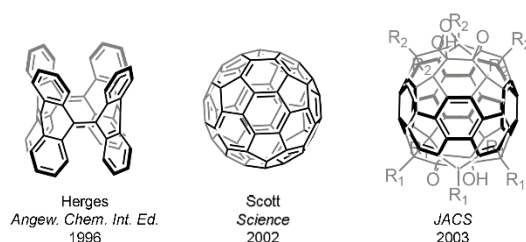


Figure I.1. Inspirational bottom up syntheses of curved PAHs.

The [n]cycloparaphenylenes ([n]CPPs), which can be envisioned as the shortest cross-section of an [n,n] armchair CNT (Fig. I.2.), are towards uniform armchair CNT growth.⁶⁻⁸ The [n]CPPs were first envisioned (although not synthesized) by Parekh and Guha in 1933, many years before the discovery of CNTs.⁹ Another 60 years passed until Vögtle examined synthetic routes to [n]CPPs.¹⁰ Although he too was unsuccessful at preparing [n]CPPs, many of the proposed strategies laid the foundation for the eventual realization of the [n]CPPs in 2008 by Jasti and Bertozzi.¹¹ Since the first synthesis in 2008, [5]–[16]CPP, and [18]CPP have been accessed along with several substituted analogues.¹¹⁻³⁰ Moreover, initial work has suggested that these molecular templates indeed have potential as controlling elements for CNT synthesis.⁸

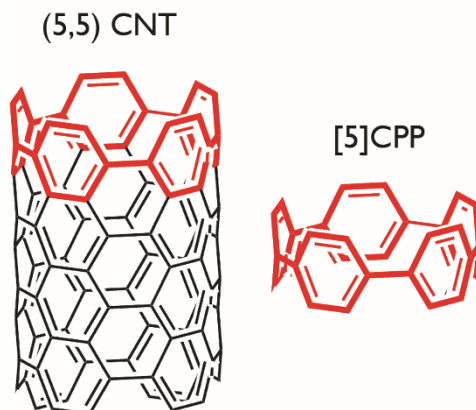


Figure I.2. $[n]$ CPPs are fragments of (n,n) armchair CNTs.

In conjunction with their synthesis, numerous size-dependent properties of these molecules have been elucidated that are unique to this class of structures.^{11,19,31–39} These properties are proving to be fascinating in their own right and promising for future materials science applications—aside from CPPs use as CNT templates. $[n]$ CPPs have a narrowing HOMO–LUMO gap as the number of benzene rings, n , decreases.^{19,35} This is in direct contrast to the open chain linear paraphenylenes and most other conjugated materials which show narrowing HOMO–LUMO gaps with increased number of aromatic rings (Fig. I.3).⁴⁰ In fact, $[n]$ CPPs have more narrow HOMO–LUMO gaps than even the very longest linear paraphenylene highlighting their potential as new organic semiconducting materials. In addition, all $[n]$ CPPs curiously share a common absorbance maximum while the emission is red-shifted as the hoop size decreases.^{11,19,35,41} These novel size-dependent optoelectronic properties are most dynamic in the smaller size regime of the $[n]$ CPPs where $n = 5–12$. In this tutorial review, we highlight the unusual physical properties of CPPs in this smaller size regime, focusing on both experimental and theoretical data, and where applicable providing rationale for these unique physical properties.

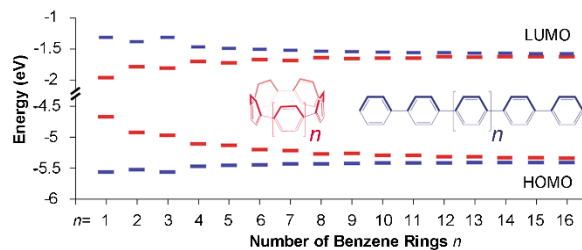
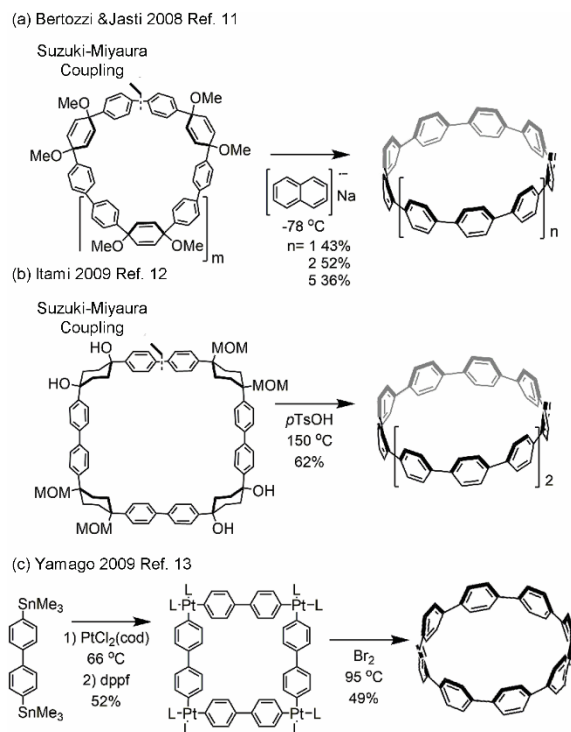


Figure I.3. Linear paraphenylenes and most conjugated materials have a narrowing HOMO–LUMO gap as conjugation length increases. Cyclic paraphenylenes on the other hand show the opposite trend. Data taken from ref. 19.

I.3. Synthetic Approaches to $[n]$ Cycloparaphenylenes.

Synthetic approaches to the CPPs have been thoroughly discussed elsewhere, so we only provide a brief synopsis of strategies that led to the isolation of these structures. Although these molecules are structurally simple, the high strain energy of the non-planar benzene rings renders their synthesis challenging. The first synthesis of $[n]$ CPPs was reported by Jasti and Bertozzi in 2008 yielding $[9]$ –, $[12]$ –, and $[18]$ CPP in milligram quantities (Scheme I.1.a.).¹¹ The key to this synthetic approach was the use of ridged 1,4-syn-dimethoxy-2,5-cyclohexadienes as masked benzene rings.⁴² This appropriately substituted cyclohexadiene unit is able to alleviate strain and allow for Suzuki–Miyaura cross-coupling/macrocyclization to macrocycles of varying size. In the final reductive aromatization step, these cyclohexadiene containing macrocycles are treated with lithium naphthalenide at -78 °C to reveal the fully benzenoid hoops. This synthetic strategy has since been extended and optimized to afford $[5]$ – $[12]$ CPP in a size selective and scalable manner.^{11,14–18}



Scheme I.1. General Synthetic Routes Used to Access $[n]$ CPPs by (a) Jasti, (b) Itami, and (c) Yamago.

In 2009, the Itami group introduced a slightly different approach to selectively synthesize $[12]$ CPP (Scheme I.1.b.).¹² This strategy utilized a substituted 1,4-syn-diarylcyclohexane units as a masked benzene ring to build low strain macrocyclic precursors.¹⁰ It is worth noting that these cyclohexane units are reduced versions of benzene rings, whereas the Jasti/Bertozzi cyclohexadiene approach uses oxidized versions of benzene rings. The low strain cyclohexane containing macrocycle was subsequently aromatized using *p*-toluenesulfonic acid at 150 °C which initiates an acid-catalyzed dehydrogenation/oxidation event to reveal $[12]$ CPP. Recent advances to this strategy include nickel mediated intramolecular reductive homocouplings of aryl bromides, which has led to higher yields and avoids the derivatization of aryl precursors to boronates. This strategy has been used to access $[7]$ – $[16]$ CPP in a size selective manner.^{12,24–26}

Later in 2009, the Yamago laboratory reported the first synthesis of $[8]$ cycloparaphenylene using an entirely different approach (Scheme I.1.c.).¹³ This strategy relies on formation of a cyclic platinum complex followed by bromine-induced reductive elimination. Recent advances include the introduction of XeF_2 to induce

reductive elimination to prepare even smaller [n]CPPs.²¹ This route has been utilized to access [6]CPP and [8]–[13]CPP in relatively short synthetic sequences and high yields.^{13,19–22} In summary, due to the pioneering work of several groups, a new class of PAHs that remained dormant for decades is now synthetically accessible.

I.4. Structural Features of [n]Cycloparaphenylenes.

The subtle interplay of strain, geometry, and symmetry plays a significant role in many of the interesting properties of [n]CPPs. Intuitively, strain energy increases as the nanohoops become smaller. Itami and coworkers nicely quantified this relationship using a series of homodesmotic reactions at the B3LYP/6-31G(d) level of theory to estimate the strain of [5]–[12]CPP.^{18,43} As seen in Table I.1, the strain increases dramatically with smaller sized [n]CPPs. [12]Cycloparaphenylene, the largest in the series presented, has a sizable 48 kcal mol⁻¹ of strain energy which equates to approximately 4 kcal mol⁻¹ per aryl ring. [5]CPP at the other end of this size regime has an estimated 119 kcal mol⁻¹ of strain energy spread out over only five aryl rings. This works out to nearly 24 kcal mol⁻¹ of strain energy per benzene ring! As a frame of reference the highly strained hydrocarbon cubane was shown to have approximately 169 kcal mol⁻¹ of strain estimated by a similar computational method.⁴⁴


[n]CPP	Calculated Strain (kcal/mol)	Average Strain Per Aryl Ring (kcal/mol)	 a° (degrees)	Diameter (nm)
5	119 ^a	24	15.8	0.67 ^a
6	97 ^b	16	12.6	0.79 ^b
7	84 ^b	12	10.9	0.95 ^b
8	72 ^b	9	9.3	1.1 ^b
9	66 ^b	7	8.3	1.2 ^b
10	58 ^b	6	7.7	1.4 ^b
11	54 ^b	5	6.8	1.5 ^b
12	48 ^b	4	6.2	1.6 ^b

Table I.1. Calculated B3LYP/6-31G(d) total strain, strain per benzene ring, displacement angle, and diameter of [5]–[12]CPP. ^a Reference 18. ^b Reference 43.

As studied by DFT calculations, nanohoop size plays a key role in the geometry and conformation of these nanohoops (Fig. I.4.).^{35,39,41,43,45} As cycloparaphenylene size decreases, torsional angle θ become smaller to compensate for the increasing strain

energy.^{35,45} The minimization of these angles gives rise to better pi overlap and an effective increase in the conjugation between neighboring aryl rings for smaller nanohoops. Increased conjugation due to smaller torsional angles offers one possible explanation (or at least contributing factor) for the observed narrowing of the HOMO–LUMO gap as cycloparaphenylenes become smaller.³⁹ In contrast, linear paraphenylenes, regardless of size, display a conformation in which the torsional angle is consistently 36° (Fig. I.4., red line)—presumably the right balance between avoiding C–H/C–H steric interactions and maximizing pi overlap.⁴⁵ Further subtle effects can be observed when comparing conformations of cycloparaphenylenes with an odd number of benzene rings with those with an even number of benzene rings.^{19,39}

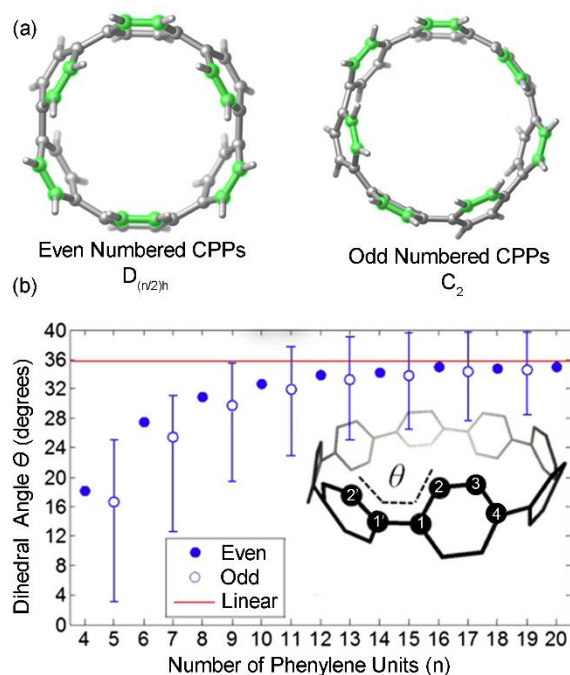


Figure I.4. Point group of (a) even $n = 6, 8, 10,$ and 12 and odd $n = 5, 7, 9, 11$ [n]CPPs. (b) Torsional angle θ of cyclic and linear paraphenylenes. Reproduced with permission. Copyright © Elsevier.

Nanohoops having an even number of benzene rings ($n = 4, 6, 8, 10,$ and 12) have $D_{(n/2)h}$ symmetry with constant torsional angles and an alternating canted aryl–aryl orientation around the hoop (Fig. I.4.a).^{43,45} The increasing strain of smaller hoops leads to a drop in average torsional angle from approximately 34° for [12]CPP down to 28° for

[6]CPP.⁴⁵ Odd sized nanohoops ($n = 5, 7, 9,$ and 11) cannot achieve this alternating structure and instead have C_2 symmetry with a range of torsional angles and always one aryl ring perpendicular to the plane of the hoop creating a helical twist in the minimized geometry (Fig. I.4.a).^{43,45} The increase in strain energy down the odd series leads to a drop in average torsional angle from 32° ([11]CPP) down to 16° ([5]CPP).⁴⁵ The average torsional angles for $[n]$ CPPs where $n \geq 12$ reach a steady state nearly equal to those adopted by linear paraphenylenes, again highlighting the uniqueness of smaller $[n]$ CPPs where $n \leq 12$ (Fig. I.4.b).

Analysis of crystal structures can provide additional insight into the interesting properties and potential solid state application of $[n]$ CPPs. Crystal structures of [5]–[10]CPP, and [12]CPP have all been published in the primary literature.^{13,15,16,18,20,23,24,26} To complete this series we have contributed the structure for [11]CPP for the purpose of this review (CCDC deposition number for [11]CPP 1035794). Fig. I.5. illustrates the solid state structures of [5]–[12]CPP. Solvent molecules are typically present in the cavity of these structures but are often disordered and/or partially missing. For the purpose of clarity, solvent molecules have been removed from these depictions. X-ray crystallography allows us to probe a variety of geometric features of interest. As a benzene ring becomes more increasingly nonplanar, a point should arise when the structure can no longer maintain delocalization and therefore aromaticity. A 2003 computational paper suggested a transition from benzenoid to quinoid electronic structures occurring between [6]CPP and [5]CPP, with [5]CPP being completely quinoidal.⁴⁶ A close analysis of the solid state structure of [5]CPP revealed that the C1–C2 and C2–C3 bond lengths (see Fig. I.4.b. for atom numbering) were nearly equivalent for all rings in the hoop, consistent with a benzenoid structure.¹⁸ Crystal structure of the cycloparaphenylenes also allow for the analysis of the average ring displacement for the different sized nanohoops (Table I.1.). For a frame of reference, the highly distorted aryl ring in the natural product haouamine A, first synthesized by Baran,⁴⁷ has a displacement of 13.61, [2,2]paracyclophane has a displacement of 14.1,⁴⁸ and a [1.1]paracyclophane⁴⁹ adduct crystallized by Kawai and Tsuji has an impressive 25.61 displacement. [5]CPP, the smallest CPP synthesized to date, has an average displacement angle of 15.61 (for all

five rings) and an astounding $119 \text{ kcal mol}^{-1}$ of strain energy! The next CPP in the series yet to be synthetically accessed is [4]CPP and is predicted to have $146.8 \text{ kcal mol}^{-1}$ of strain and an average displacement angle of 19.41° highlighting the increasing synthetic challenge with smaller nanohoops.

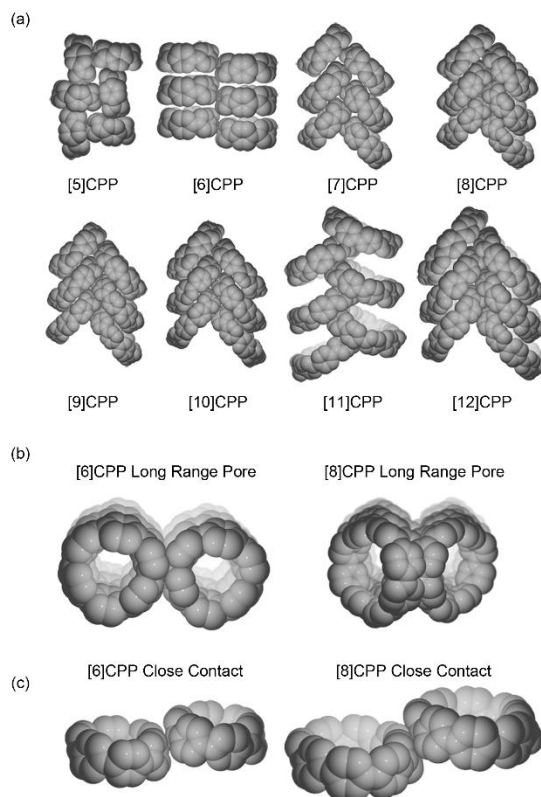


Figure I.5. Crystal packing of [5]-[12]CPP in the solid state. (a) Side on view of crystal packing mode. (b) Top down view of [6]CPP and [8]CPP illustrating the long range channel present in [6]-[12]CPP. (c) Close intermolecular interactions found in [6]CPP and [8]CPP crystal structures.

In addition to the measurements above, X-ray crystallography allows us to examine the solid state packing structures of CPPs. [5]CPP and [7]-[12]CPP all adopt a herringbone packing structure (Fig. I.5.a). [5]CPP shows an especially dense packing with no solvent in the pore of the hoop due to the small cavity size. Each CPP molecule is perfectly nested perpendicular to the plane of all neighboring molecules in the lattice. [11]CPP also shows a unique flavor of herringbone packing. Here each ring is nested inside the pore of its two closest neighbors. [6]CPP provides the most aesthetically

striking and unique packing out of the series. The [6]CPP molecules stack perfectly on top of one another, somewhat reminiscent of an armchair CNT (Fig. I.5.a.). To date no crystalline polymorphs of any [n]CPP have been reported. Attempts in our laboratory to obtain a crystal of [5]-, or [7]-[12]CPP with columnar packing or [6]CPP with herringbone packing has not been achieved. All [n]CPPs except [5]CPP have a long range channel in the solid state which is often occupied by solvent. Two representative examples, [6]CPP and [8]CPP are shown in Fig. I.5.b. by a 90° rotation perpendicular to the page from the side on packing illustrated in Fig. I.5.a. Finally, each [n]CPP has close intermolecular C–C contacts within 3.5 Å. Fig. I.5.c. illustrates a representative example of this interaction for [6]CPP and [8]CPP. The combination of the packing structures, the long range pores, and close intermolecular contacts make [n]CPPs an intriguing candidate for many electronic applications including small molecule sensing, organic field effect transistors (OFETs), or organic photovoltaic devices.

I.5. Nuclear Magnetic Resonance Spectroscopy of [n]CPPs.

Nuclear magnetic resonance (NMR) spectroscopic data for [5]-[12]CPP provides further experimental evidence in regards to the conformation of CPPs and their dynamics. The proton NMR spectra of [5]-[12]CPP (Fig. I.6.a.) each exhibit one singlet peak suggesting all protons in each CPP molecule are in a similar environment on the NMR timescale.¹¹ This equivalency can be explained by rapid wobbling and/or canting motions where individual benzene rings slip past one another. Itami⁴³ and co-workers calculated the activation barrier for this canting motion for [12]CPP as 3.7 kcal mol⁻¹. A second type of fluctuation where benzene rings flip through the centre of the hoop would also lead to an equivalency in the NMR. This process was estimated to have an activation barrier of 7.5 kcal mol⁻¹ for [12]CPP. Although these calculations have not been reported for smaller sized CPPs, as the hoop becomes smaller and the strain energy is increased, a full flip of a benzene ring through the centre of the hoop will become more difficult.^{15,18}

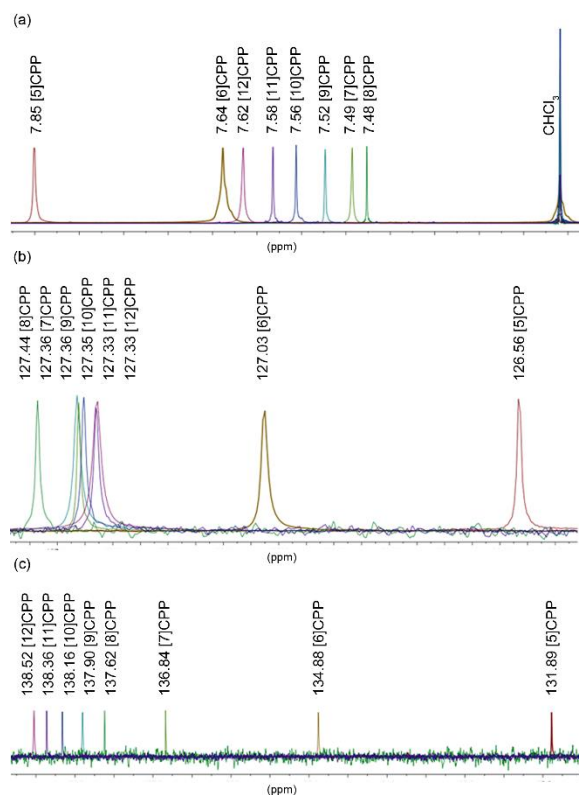


Figure I.6. (a) ^1H NMR spectra of [5]-[12]CPP, (b) ^{13}C spectra of C_{ortho} for [5]-[12]CPP, and ^{13}C spectra of C_{ipso} for [5]-[12]CPP.

The signal in the ^1H NMR spectra of [12]–[8]CPP shows a consistent upfield shift as CPP size gets smaller. [7]–[5]CPP, however, show the opposite trend and their proton signal shifts downfield as CPP size decreases (Fig. I.6.a.). As shown in Fig. I.6.b. and c, each [n]CPP has two distinct carbon signals, where all C_{ortho} carbons (Fig. I.6.b.) are equivalent and all C_{ipso} carbons (Fig. I.6.c.) are equivalent. The signal for the C_{ortho} carbon shifts downfield moving from [12]CPP to [8]CPP and abruptly shifts upfield from [7]CPP to [5]CPP. One possible explanation for these trends is that as the nanohoops become smaller, the torsional angles minimize and thus the ^1H and C_{ortho} ^{13}C signals follow the patterns of the bay regions of extended PAHs. For example, the bay region ^1H signals in phenanthrene shift downfield relative to benzene whereas the ^{13}C NMR shift upfield. These observations have been rationalized by a ring current effect where the proton in the bay region lies perpendicular to the pi system in a deshielding region. The bay region protons are also locked in an eclipsed conformation resulting in a shift of some electron density from the proton onto the attached carbon.⁵⁰ In contrast to the

proton and the C_{ortho} carbon, the C_{ipso} carbons show a gradual shift upfield consistent with an increasing pyramidalization of this carbon.

I.6. Raman Spectroscopy of $[n]$ CPPs.

Raman spectroscopy has proven to be an indispensable tool for characterizing CNTs. Due to CNTs' polymeric nature and high molecular weights, traditional spectroscopies such as NMR, IR, and mass spectrometry provide limited insight into CNT structure. For CNTs, three major Raman modes are used to characterize the diameter and chirality of the nanotube. G^+ bands correlate motions perpendicular to the length of the tube, G^- bands are related to motions parallel to the tube, and radial breathing modes (RBMs) are a result of the expanding and contracting of the tube. Several labs have recently reported the Raman spectra of $[n]$ CPPs offering an experimental glimpse into the structural details of these nanohoops.^{45,51,52}

The Casado⁵¹ group has reported on the Raman spectroscopy of [6]–[12]CPP, offering perhaps the most complete and resolved data to date (Fig. I.7.). A pseudo RBM peak was assigned to minor peaks falling between 200 and 500 cm^{-1} (Fig. I.7.b.). As the hoop becomes smaller and more rigid, the peaks shift to higher wavenumbers. Like CNTs, $[n]$ CPPs show a linear relationship between the frequency and the reciprocal of the nanohoop diameter ($1/d$) establishing this peak as a fingerprint for nanohoop diameter. $[n]$ CPPs, like CNTs, have G^+ bands between 1500 and 1600 cm^{-1} that can be assigned to totally symmetric vibrations parallel to the plane of the hoop (C_{1-1} , $2-3$, and $5-6$) (Fig. I.7.b.). This band was used to experimentally probe the percent quinoidization of each hoop. A flat benzene ring was calculated to have a peak at 1600 cm^{-1} while a quinoidal ring was predicted to be at a lower wavenumbers of 1343 cm^{-1} . As the hoops become smaller, this signal shifts to lower wavenumbers and thus these smaller hoops have more quinoidal character, which is also supported by crystal structure data (vide supra) (Fig. I.7.c.). Fig. I.7.d. shows the empirical percent quinoidization of each nanohoop which closely follows the trends calculated for strain energy. [12]CPP was found to have 3% quinoid character while [6]CPP was found to have nearly 14% quinoid character implying a gradual quinoidization as the hoops become smaller.

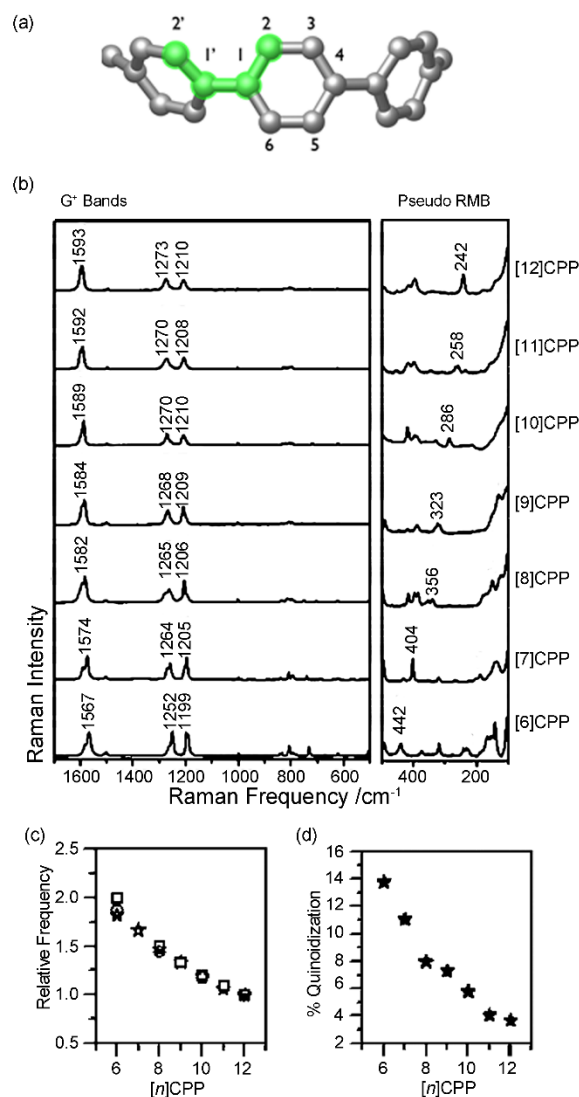


Figure I.7. (a) Representative [n]CPP bonds and torsional angle highlighted in green. (b) Raman spectra of [6]-[12]CPP (c) Raman frequency vs [n]CPP and (d) percent quinoidization vs [n]CPP. Reproduced with permission. Copyright © Wiley.

The Casado⁵¹ group has also shown how Raman spectroscopy can provide a unique tool to describe the effect of pressure on [n]CPPs (Fig. I.8.). Raman spectra were recorded independently for [12]CPP and [6]CPP at ambient pressure and 8 GPa. [12]CPP showed a pressure induced shift of the G⁺ mode indicative of partial planarization of a segment giving it more benzenoid character. Upon release of this pressure the signal rebounded to the ambient state suggesting a reversible flexing of the hoop under pressure (Fig. I.8.b.). [6]CPP also showed significant distortion of the G⁺ mode under 8 GPa, however, the signals did not recover upon release of pressure representative of an

irreversible collapse of the structure (Fig. I.8.a.). When a solid matrix of [12]CPP and [6]CPP were pressurized together, both the [12]CPP and [6]CPP signals were recovered. This was attributed to a pressure induced host guest complex of [6]CPP@[12]CPP where the [12]CPP acts to shield the [6]CPP from irreversible collapse. This complex is the first experimental observations of such ring in ring complexation reminiscent of multi-walled CNTs (Fig. I.8.c.). Next the host guest complex of C_{60} @ [10]CPP was examined under 6 GPa of pressure. First, a Raman spectrum was measured individually for [10]CPP, C_{60} , the radical cation [10]CPP^{•+}, and the radical anion C_{60} . Next a Raman spectrum was measured for the complex C_{60} @ [10]CPP at ambient pressure and 6 GPa. Analysis of these spectra showed that upon application of pressure the [10]CPP signal shifted from 1588 cm^{-1} (neutral compound) to a signal consistent with a radical cation [10]CPP^{•+} at 1569 cm^{-1} . Accompanying these dynamic shifts the neutral C_{60} signal shifted from 1469 cm^{-1} 1463 cm^{-1} indicating the formation of the radical anion C_{60} . These signals recovered to the neutral C_{60} @ [10]CPP when pressure was released suggesting a pressure induced charge transfer event where an electron from the electron rich [10]CPP is given to the electron accepting C_{60} under high pressures (Fig. I.8.d.). The application of pressure to induce a charge transfer event between the electron rich nanohoop to the electron poor fullerene highlights a potential novel materials application of these molecules.

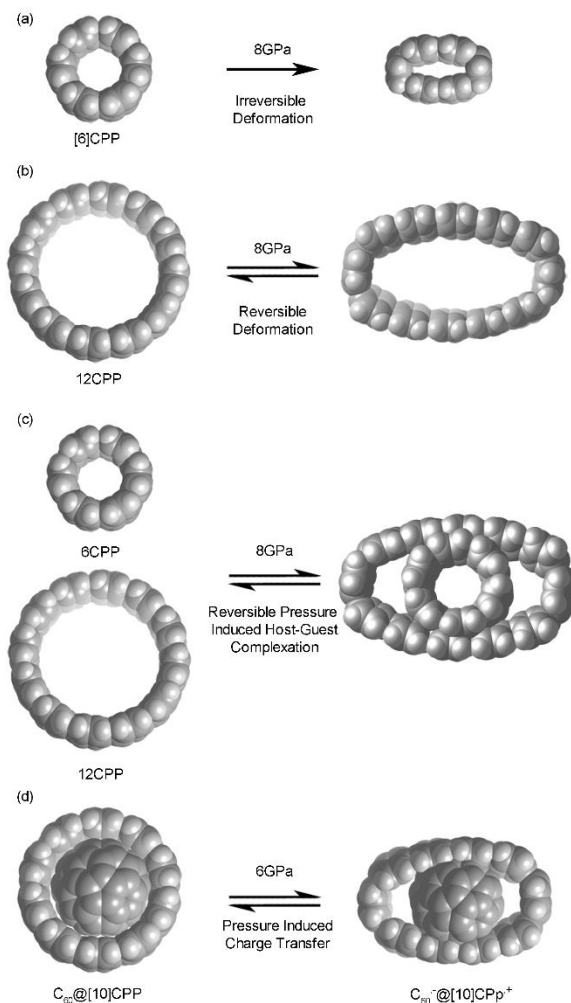


Figure I.8. Cartoon of the pressure induced (a) irreversible deformation of [6]CPP (b) reversible deformation of [12]CPP (c) reversible host guest complexation of [6]CPP@[12]CPP and (d) charge transfer from [10]CPP to C₆₀.

I.7. Electrochemistry.

Cyclic voltammetry has provided the clearest experimental observation of the lowering LUMO and raising HOMO energy as [n]CPP size decreases. Oxidation potentials for [5]–[12]CPP and reduction potentials for [5]CPP and [7]CPP have been reported in the literature (Table I.2.).^{15,18,19,21,39} Although the experimental conditions for the electrochemical experiments are not completely uniform, the nanohoops clearly become easier to reduce and oxidize as the hoop become smaller. Oxidation waves for [5]–[12]CPP demonstrate that as the nanohoops becomes smaller, removal of one electron becomes more facile indicative of a higher energy HOMO. [12]CPP¹⁹ for

example has a half-wave potential of 0.85 V vs. Fc/Fc⁺ while [6]CPP¹⁵ has a half-wave potential of 0.44 V vs. Fc/Fc⁺. Interestingly, [5]CPP¹⁸ uniquely shows two pseudo reversible oxidations at peak potentials of 0.25 and 0.46 V vs. Fc/Fc⁺. Reduction waves are only reported for [5]CPP¹⁸ and [7]CPP, but illustrate that as the hoop becomes smaller the reductions become more facile indicative of a lowering of the LUMO. Again, [5]CPP shows two pseudoreversible reduction peaks with peak potentials at 2.27 and 2.55 V vs. Fc/Fc⁺ while [7]CPP shows only one reversible peak with a half-wave potential of 2.74 V vs. Fc/Fc⁺.

[n]CPP	Oxidation (V)	Reduction (V)
5	0.25 ^{*a} , 0.46 ^{*a}	-2.27 ^{*a} , -2.55 ^{*a}
6	0.44 ^b , 0.30 ^c	NA
7	0.55 ^d	-2.74 ^d
8	0.59 ^e	NA
9	0.70 ^e	NA
10	0.74 ^e	NA
11	0.83 ^e	NA
12	0.85 ^e	NA

Table I.2. Published Oxidation and Reduction Potentials of [n]CPPs (V vs Fc/Fc⁺). ^a Reference 18. ^b Reference 15. ^c Reference 21. ^d Reference 39. ^e Reference 19. *Indicates Pseudo Reversible Wave.

I.8. Carbon Nanohoop Photophysics.

The unique photophysics of the nanohoop structures have been well appreciated since the inception of [n]CPPs. Table I.3. shows a collection of all the absorbance and fluorescence data while Fig. I.9. shows an overlay of [5]–[12]CPP absorbance and fluorescence spectra.^{11,17,19,35,39,52–55} A number of striking features for this homologous series are apparent from this data. First, [5]–[12]CPP have a common absorbance with maxima between 348–350 nm. An explanation for this observation was postulated by the Yamago¹⁹ group using time dependent density function theory (TD-DFT). Due to the centrosymmetric nature of these nanohoops, the HOMO–LUMO transition is Laporte forbidden as the HOMO and LUMO conserve symmetry.³⁵ The HOMO–LUMO transition for even numbered CPPs has an oscillator strength of zero. The HOMO–LUMO transition for odd numbered nanohoops is non-zero due to the inherent lower

symmetry, however the intensity is still very low. [5]–[12]CPP are shown to have degenerate HOMO–1/HOMO–2 and a nearly degenerate LUMO+1/LUMO+2. These orbitals have different symmetries than the HOMO and LUMO and so transitions from HOMO–1 or HOMO–2 to the LUMO are allowed. Likewise a transition from the HOMO to the LUMO+1 or LUMO+2 is also allowed. These distinct transitions have orthogonal transition dipole moments accounting for the relatively high extinction coefficients for all [n]CPPs (Table I.3.). The orbital energy trend for the HOMO–1/HOMO–2 and LUMO+1/ LUMO+2 is opposite that of the HOMO and LUMO. Like linear paraphenylenes and other conjugated materials, these gaps narrow as the hoop becomes larger in stark contrast to the HOMO–LUMO gap which narrows as the hoop becomes smaller.⁴⁰ Fig. I.10. illustrates that the relative magnitude of the transition is conserved across the homo

[n]CPP	Absorbance (nm)	Extinction coefficient ϵ ($M^{-1}cm^{-1}$)	Fluorescence (nm)	Fluorescence Quantum Yield Φ	Singlet Lifetime (ns)	Transient Absorbance (nm)	Phosphorescence (nm)	Triplet Lifetime (ns)
5	335 ^{a,b}	5.7×10^4 ^a	No Fluorescence ^{a,b}	0 ^{a,b}	NA	NA	NA	NA
6	340 ^c	NA	No Fluorescence ^c	0 ^c	NA	NA	NA	NA
7	340 ^d	6.9×10^4 ^l	587 ^d	0.007 ^d	NA	NA	NA	NA
8	340 ^e	1.0×10^5 ^h	533 ^e	0.1 ^h	17.6 ⁱ	708 ^k , 400 ^k	671 ^k	60000 ^k
9	340 ^f	1.2×10^5 ^h	494 ^f	0.38 ^h	10.6 ⁱ , 5.3 ^j	671 ^k , 389 ^k	633 ^k	63000 ^k , 67000 ^j
10	338 ^g	1.3×10^5 ^h	466 ^g	0.65 ^h	6.6 ⁱ	678 ^k , 472 ^k	610 ^k	58000 ^k
11	340 ^g	1.3×10^5 ^h	458 ^g	0.73 ^h	3.8 ⁱ	676 ^k , 487 ^k	600 ^k	64000 ^k
12	339 ^f	1.4×10^5 ^h	450 ^f	0.81 ^d	2.4 ⁱ , 1.9 ^j	668 ^k , 500 ^k	591 ^k	64000 ^k , 110000 ^j

Table I.3. Summary of Experimental Photophysical Properties for [5]–[12]CPP.^a

Reference 18. ^b Reference 22. ^c Reference 15. ^d Reference 14. ^e Reference 13. ^f Reference 6. ^g Reference 11. ^h Reference 17. ⁱ Reference 35. ^j Reference 54. ^k Reference 53. ^l Reference 39.

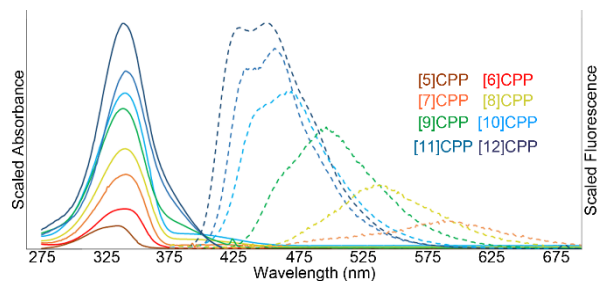


Figure I.9. UV/VIS (solid) and fluorescence (dashed) spectra for [5]-[12]CPP. No fluorescence is observed for [6]CPP or [5]CPP.

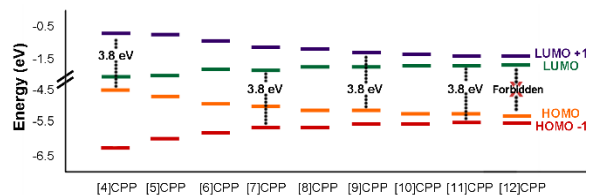


Figure I.10. Calculated (B3LYP/6-31G) (d) HOMO, HOMO-1, LUMO, and LUMO+1 energy levels (B3LYP/6-31G*). HOMO-1 and HOMO-2 are nearly degenerate as are LUMO+1 and LUMO+2. For clarity purposes only HOMO-1 and LUMO+1 energies were used. Data taken from reference 19.

While the absorbance trends can be easily understood computationally, the red-shifting fluorescence and rapid decrease in quantum efficiency with smaller nanohoops are more challenging to model. A number of theoretical papers have attempted to account for these observed properties.^{31,33,34,36–38,41,55} We have chosen to focus on the most recent report by Tretiak³³ since it offers a reasonable and clear explanation of both the observed red-shifting emission and drop in quantum efficiency of smaller nanohoops. According to Kasha's rule,⁵⁶ fluorescence emission typically occurs from the lowest energy excited state S1 to the ground state S0. Due to the Laporte selection rules all $[n]$ CPPs are initially excited to the S2 and S3 states through a combination of HOMO–LUMO+1 or HOMO–LUMO+2 and HOMO–1-LUMO or HOMO–2-LUMO transitions.^{19,35} Nonadiabatic excited state dynamics simulations were used to show that photoexcited S2 and S3 states are able to internally convert to spatial localized S1' states within 50 femtoseconds.³³ This internal conversion to the S1' state (fs timescale) is significantly faster than the experimental fluorescent lifetimes (ns timescale) giving support to this theory.^{32,35,54} Moreover, Tretiak shows that in larger $[n]$ CPPs, where $n \geq 8$, the lowest energy excited state geometry (S1') has partial planarization of five aryl rings leaving the rest of the

hoop in the ground state geometry allowing self-trapping of the excitonic wave function (Fig. I.11.). This localized $S1'$ state has different symmetry from the ground state and thus becomes an allowed $S1'-S0$ transition. In smaller $[n]$ CPPs, where $n \leq 7$, complete delocalization is observed in the lowest energy excited state geometry ($S1'$) conserving the symmetry of the ground state. Therefore, this $S1'-S0$ transition conserves symmetry and is Laporte forbidden accounting for the rapid drop in quantum efficiencies of smaller nanohoops. As stated before, strain induces a decrease in torsional angle which in turn increases the amount of conjugation as nanohoops get smaller therefore enhancing vibrational coupling and reducing the $S1'-S0$ energy resulting in a gradual red-shifting of the fluorescence.³³

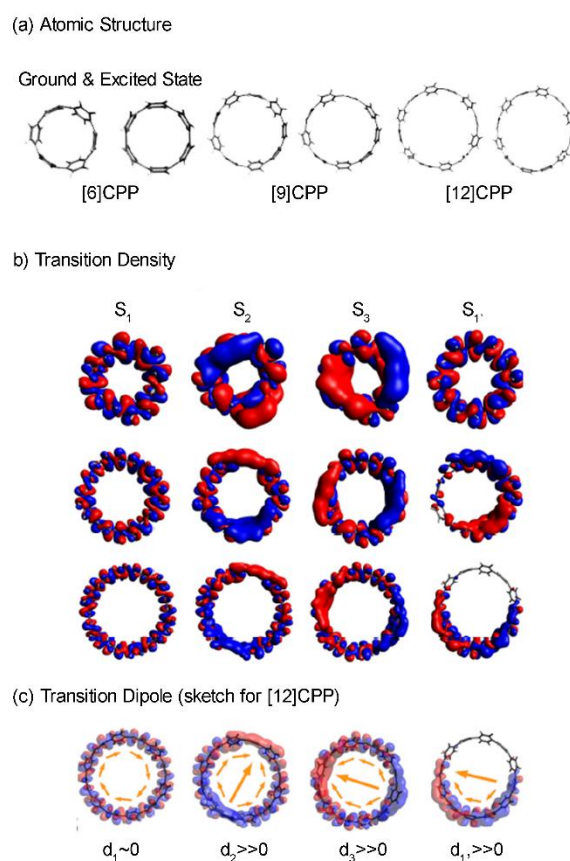


Figure I.11. a) Minimized geometries of the ground state and first excited state. b) Orbital visualization of S_1 , S_2 , S_3 , and $S_{1'}$ transitions. c) Transition dipole for [12]CPP illustrating the self-trapping $S_{1'}$ state. Reproduced with permission. Copyright © ACS.

I.9. Conclusion.

The new molecular family of $[n]$ cycloparaphenylenes or “carbon nano hoops” is a prototypical example of how access to unprecedented architectures can lead to unexpected and unique physical properties. These properties include the narrowing of the HOMO–LUMO gap in $[n]$ CPPs as the hoop size decreases which is in direct contrast with typical conjugated macromolecules. This unique optoelectronic behavior is in accordance with the strain induced decrease in torsional angle and ultimately the increase in conjugation for the smaller nano hoops. The inherent symmetry of these centrosymmetric molecules results in a Laporte forbidden HOMO–LUMO optical transition impacting both the absorbance and emission spectra. The common absorbance observed for $[n]$ CPPs consists of nearly degenerate allowed HOMO to LUMO+1 and LUMO+2 and orthogonal HOMO–1 and HOMO–2 to LUMO optical transitions. A violation of the Frank–Condon principal⁵⁷ allows excited S2 and S3 states to relax to a localized S1’ state. For $[n]$ CPPs where $n \geq 7$, this S1’ state has a different symmetry from the ground state resulting in an allowed S1’ to S0 transition. For $[n]$ CPPs where $n \leq 7$, the S1’ state conserves the ground state symmetry resulting in a forbidden S1’ to S0 transition and thus a decrease in quantum yield in smaller nano hoops. Emission from the S1’ state also accounts for the red-shifting fluorescence observed as nano hoops size decreases. The unique geometric features, solid state packing, and optoelectronic properties make $[n]$ CPPs and their derivatives a fascinating candidate for many electronic applications including small molecule sensing, organic field effect transistors, and organic photovoltaic devices.

I.10. Bridge to Chapter II.

In order to study the interesting size-dependent properties outlined in Chapter I, it was important to develop a rational, size-selective synthesis of $[n]$ cycloparaphenylenes. In Chapter II, we look at the original size-selective synthesis of [7]-[12]cycloparaphenylene and optical characterization of their respective fluorescence quantum yields. This strategy relied on the inherent orthogonality of aryl chlorides and aryl bromides in both lithium halogen exchange as well as Suzuki–Miyaura cross-coupling reactions. Two late stage intermediates, a six-ring dichloride and a nine-ring dichloride, are then Suzuki–Miyaura cross-coupled to a variety of bisboronic acids to give

the corresponding macrocyclic precursors to [7]-[12]CPP. These macrocyclic precursors could then be aromatized to their corresponding nano hoops using sodium naphthalenide.

CHAPTER II

SELECTIVE SYNTHESIS OF [7]-[12] CYCLOPARAPHENYLENES USING ORTHOGONAL SUZUKI-MIYAURA CROSS-COUPLING REACTIONS

Chapter II is based on published work in the *Journal of Organic Chemistry* (2012). The manuscripts was written my meself and Dr. Thomas Sisto. The initial synthetic route was devised by Professor Ramesh Jasti and Dr. Thomas Sisto.

The divergent, selective syntheses of [7]-[12]cycloparaphenylenes have been accomplished utilizing sequential, orthogonal Suzuki-Miyaura cross-coupling reactions from two late stage intermediates. Quantum yields decrease dramatically as cycloparaphenylene size decreases, highlighting the unique photophysical behavior of the smaller cycloparaphenylenes.

II.1. Introduction.

The [n]cycloparaphenylenes ([n]CPPs) are macrocyclic molecules consisting of n benzene rings linked at the *para* position (Fig. II.1.). Recently, these strained molecules have received significant interest due to their potential application in carbon nanotube synthesis,¹⁻⁵ as well as for their unique optical⁶⁻¹¹ and supramolecular properties.¹² Several synthetic routes, both selective and unselective, to various sizes of CPPs have been reported in the last few years.^{6-8,13-22} Many of these selective routes, however, use a large excess (10 equivalents) of complex, multi-step intermediates to impart selectivity, which in turn hampers their potential scalability and synthetic ease.^{13,15,18} Utilizing a more chemoselective approach, we recently reported the selective synthesis of [7]CPP using orthogonal Suzuki-Miyaura cross-coupling reactions.⁸ While investigating this highly strained molecule, we were intrigued by the possibility that this approach might be applied to a general, selective synthesis of multiple [n]CPPs. Herein we report the selective, divergent syntheses of [7]-[12]CPPs using orthogonal Suzuki-Miyaura cross-coupling reactions.⁹

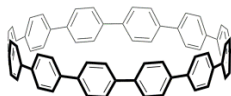
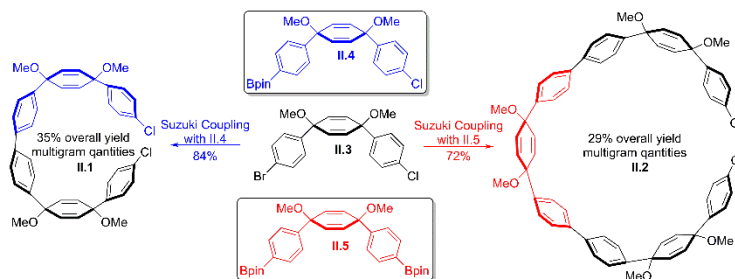


Figure II.1. [n]Cycloparaphenylene.

II.2. Synthesis.

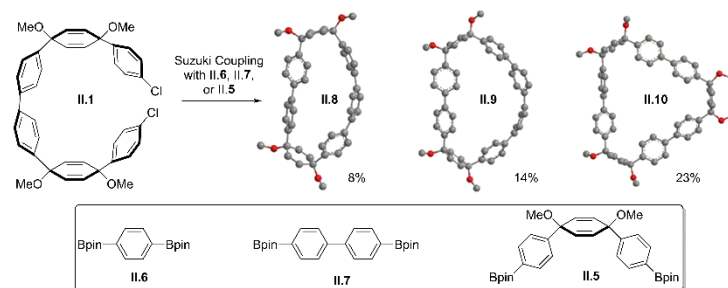
Our synthetic strategy hinges on the gram-scale preparation of two late stage precursors (**II.1** and **II.2**, Scheme II.1.). Dichlorides **II.1** and **II.2** provide a platform to divergently prepare [7]-[12]CPP in only two additional steps (Schemes II.2.-II.4.). To access both dichlorides, we first prepared three different cyclohexadiene fragments (**II.3**, **II.4**, and **II.5**) in a diastereoselective manner by methodology we have recently reported.^{8,24,25} Suzuki-Miyaura cross-coupling of **II.3** and **II.4** using Pd(PPh₃)₄ as the catalyst yields dichloride **II.1** in 84% (Scheme II.1.) as previously reported.⁸ The same reaction conditions also afford the larger terminal dichloride **II.2** in 72% by employing two equivalents of cyclohexadiene **II.3** and one equivalent of bisboronate **II.5**. Both dichlorides can be prepared easily on multigram scale. Advantageously, under these Suzuki-Miyaura cross-coupling conditions we observe no reactivity of the aryl chloride functionality.



Scheme II.1. Orthogonal Suzuki-Miyaura Cross-coupling Reactions to Prepare Terminal Dichlorides **II.1** and **II.2**.^a Conditions to Prepare **II.1**: Fragment **II.3** (1 equiv.), Fragment **II.4** (1 equiv.), Pd(PPh₃)₄ (10 mol%), NaHCO₃ (1M aq.), 2-propanol, 85 °C. Conditions to Prepare **II.2**: Fragment **II.3** (2 equiv.), Fragment **II.5** (1 equiv.), Pd(PPh₃)₄ (10 mol%), NaHCO₃ (1M aq.), 2-propanol, 85 °C.

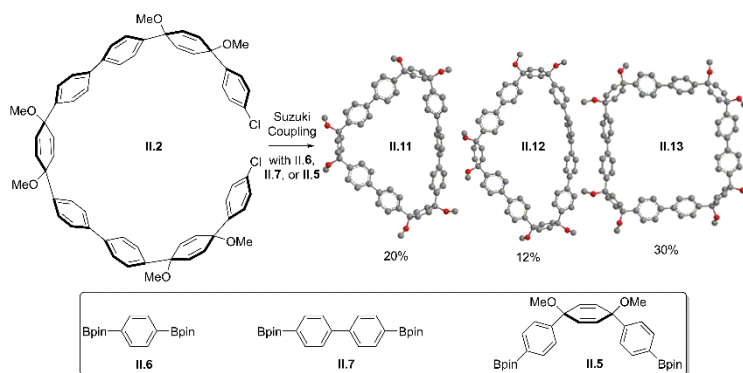
With the dichlorides **II.1** and **II.2** in hand, we next turned our attention towards the synthesis of the macrocyclic precursors to [8]-[12]CPP. Using Buchwald's S-Phos ligand,²⁶ we have previously reported the Suzuki-Miyaura cross-coupling/macrocyclization of dichloride **II.1** with diboronic pinacol ester **II.6** to prepare macrocycle **II.8** (Scheme II.2.).⁸ We were hopeful that these same conditions could be used to prepare the macrocyclic precursors to [8]- and [9]CPP by altering the boronate component. Gratifyingly, dichloride **II.1** underwent cross-coupling and macrocyclization

with either boronate **II.7** or **II.5** to give macrocycles **II.9** and **II.10** respectively (14% and 23% yield).



Scheme II.2. Divergent Macrocyclizations for the Precursors to [7]-[9]CPP.^a Conditions: Dichloride **II.1**, Diboronate **6**, **7**, or **5**, Pd₂(dba)₃ (10 mol%), S-Phos, K₃PO₄, DMF, H₂O, 125 °C (155 °C for **II.8**). DFT Optimized Geometries of Macrocycles **II.8**, **II.9**, and **II.10** are Shown.

We then sought to address whether this same methodology would be applicable for the preparation of the larger macrocyclic precursors to [10]-, [11]-, and [12]CPP (Scheme II.3.). Under identical conditions as before, cross-coupling of diboronic pinacol ester **6** and dichloride **2** generated macrocycle **II.11** in 20% yield. Macrocycles **II.12** and **II.13** were produced in 12% and 30% yield via cross-coupling of dichloride **II.2** with boronates **II.7** and **II.5**.

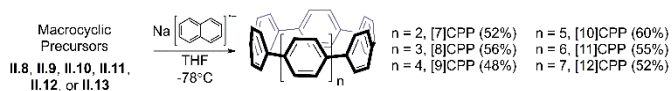


Scheme II.3. Divergent Macrocyclizations for the Precursors to [10]-[12]CPP.^a Conditions: Dichloride **II.2**, Diboronate **II.6**, **II.7**, or **II.5**, Pd₂(dba)₃, S-Phos, K₃PO₄, DMF, H₂O, 125 °C. DFT Optimized Geometries of Macrocycles **II.11**, **II.12**, and **II.13** are Shown.

DFT minimized geometries of each macrocycle are also presented in Schemes II.2. and II.3.²⁷ These minimized geometries were calculated using Gaussian 03 at the B3LYP/6-31(G)²⁷ level of theory. Upon simple visual inspection, macrocycles **II.8**, **II.9**,

and **II.12** suffer from significant strain resulting from the inclusion of several consecutive planar benzene rings. Accordingly, the macrocyclization reactions leading to these structures are the lowest yielding. For example, macrocycles **II.8** and **II.9** contain 3 and 4 consecutive benzene rings, which leads to lower yields. In contrast, macrocycle **II.10** has only 2 consecutive benzene rings, and consequently forms in significantly higher yield. In the larger series (Scheme II.3.), the macrocycle with 4 consecutive benzene rings (**II.12**) forms in the lowest yield. Methodology to prepare less strained macrocyclic precursors by incorporating additional cyclohexadiene units is currently being investigated in our laboratory.

Our synthetic strategy to the cycloparaphenylenes relies on a key reductive aromatization of the oxidized CPP macrocyclic precursors (Scheme II.4.).^{6,8,20,28} We have previously illustrated that single-electron reducing agents (e.g. sodium naphthalenide) can induce efficient aromatization at low temperatures to access even the most highly strained CPPs. Specifically, we have illustrated our reductive aromatization methodology is effective in preparing [6] - and [7]CPP—compounds with 96 and 84 kcal/mol of strain energy.^{8, 20} Each of the new macrocyclic precursors (**II.9- II.13**) were subjected to general reductive aromatization conditions at $-78\text{ }^{\circ}\text{C}$ to afford the resultant cycloparaphenylenes in good yield. [8]-, [9]-, [10]-, [11]-, and [12]CPP were produced in 56%, 48%, 60%, 55%, and 52% respectively.



Scheme II.4. General Aromatization Reaction Utilizing Sodium Naphthalide.

II.3. Fluorescence Quantum Yield.

Recognizing that the cycloparaphenylenes have unique size-dependent optical properties, we were pleased to have each of the [7]-[12]CPPs in hand. All known CPPs have a common absorption maxima around 340 nm regardless of size, while their fluorescence red shifts dramatically with decreasing diameter.^{6,7} Moreover, we have illustrated that [6]CPP has no observable fluorescence²⁰ and [7]CPP has a low quantum yield of 0.007,⁸ while the larger [12]CPP has a quantum efficiency of 0.81.⁸ Recently, Itami and coworkers have reported the absolute quantum yields for [9], [12], [14], [15], and [16] CPP through the use of a fluorescence integrating sphere.¹² In these cases, the

quantum yields are relatively uniform ($\Phi = 0.88$ to 0.90) except for the smaller [9]CPP ($\Phi = 0.73$). Our quantum yield measurements were executed using a relative quantum yield technique reported by Miller and coworkers.²⁹ The data from our studies are illustrated in Figure II.2. We note that there is a large decrease in the quantum efficiencies from [12]-[8]CPP, with [12]CPP having a quantum yield of 0.81 , while [8]CPP displays a quantum efficiency of 0.1 . [9]-, [10]-, and [11]CPP show increasing quantum yields with increasing size— 0.38 ,³⁰ 0.65 , and 0.73 respectively. The photophysical pathways of the smaller CPPs are clearly different from the larger CPPs.

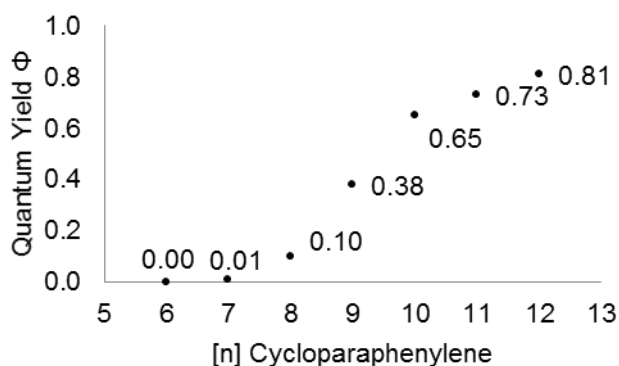


Figure II.2. The quantum yields of [6]-[12]cycloparaphenylene.

II.4. Conclusion.

In conclusion, we have developed a general strategy for the facile synthesis of [7]-[12]CPP from two late stage intermediates that can be prepared on multigram scale. The synthetic route hinges upon chemoselective Suzuki-Miyaura cross-coupling reactions that enable the selective preparation of macrocyclic precursors to the [n]CPPs. With the series of [n]CPPs ($n=7-12$) in hand, we have illustrated the dramatic decrease in quantum yield with decreasing cycloparaphenylene size. The photophysical behavior of CPPs in this smaller size regime warrants further study.

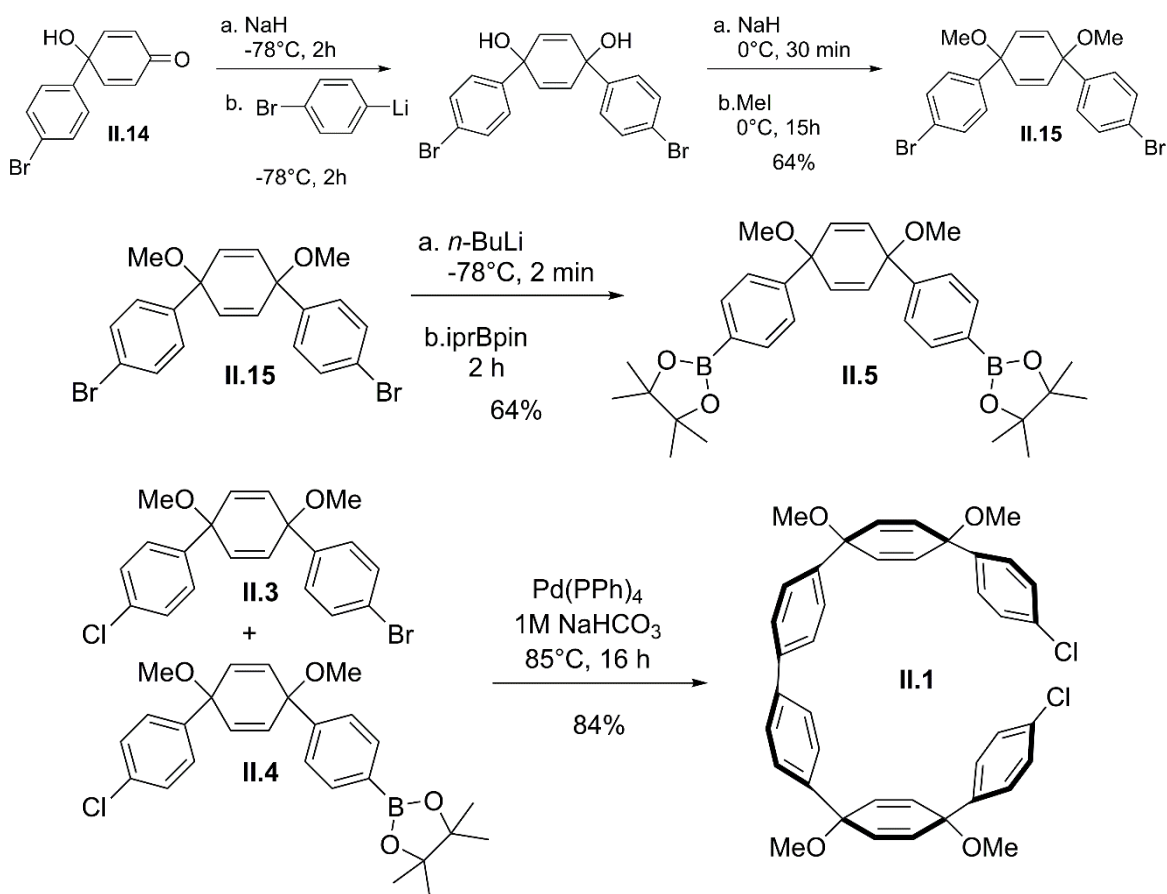
II.5. Experimental Section.

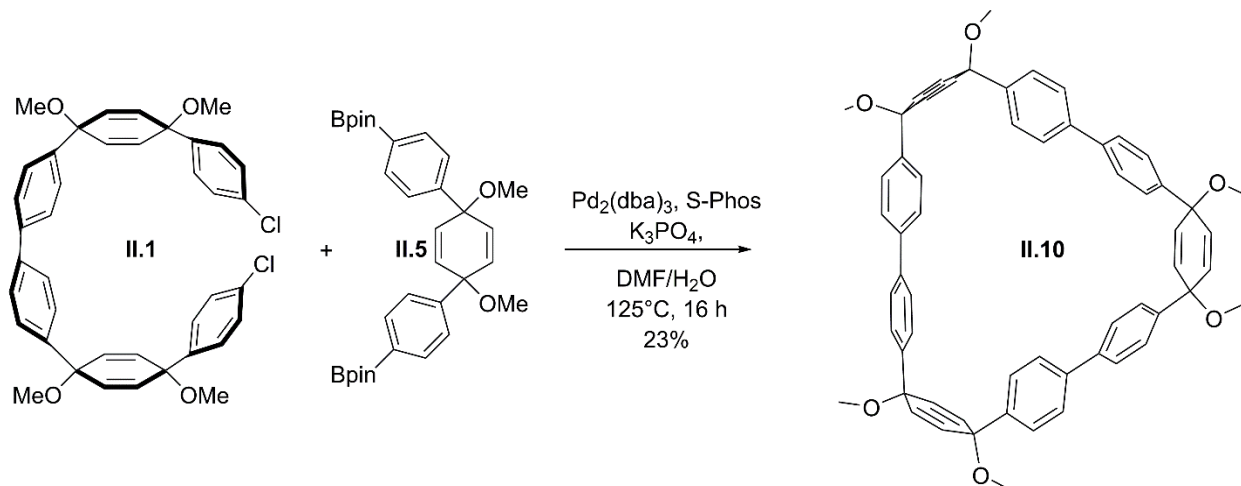
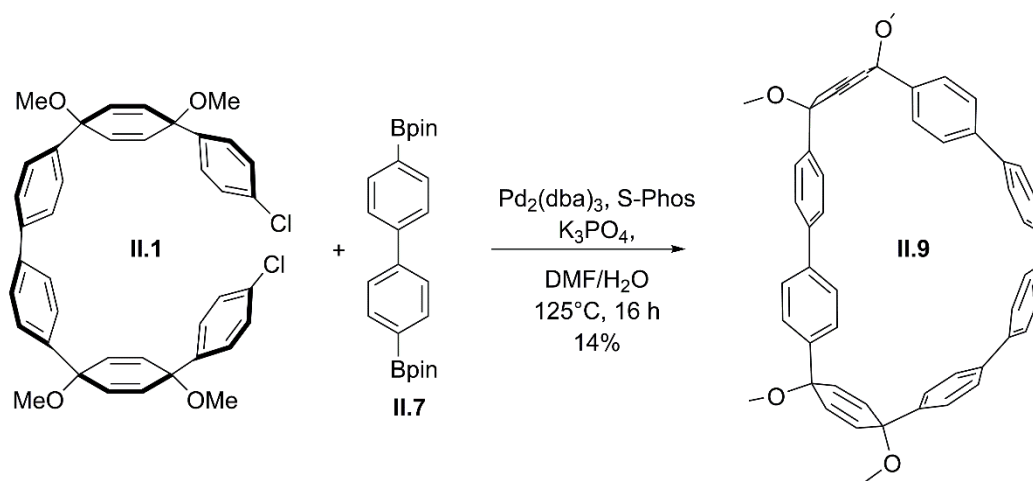
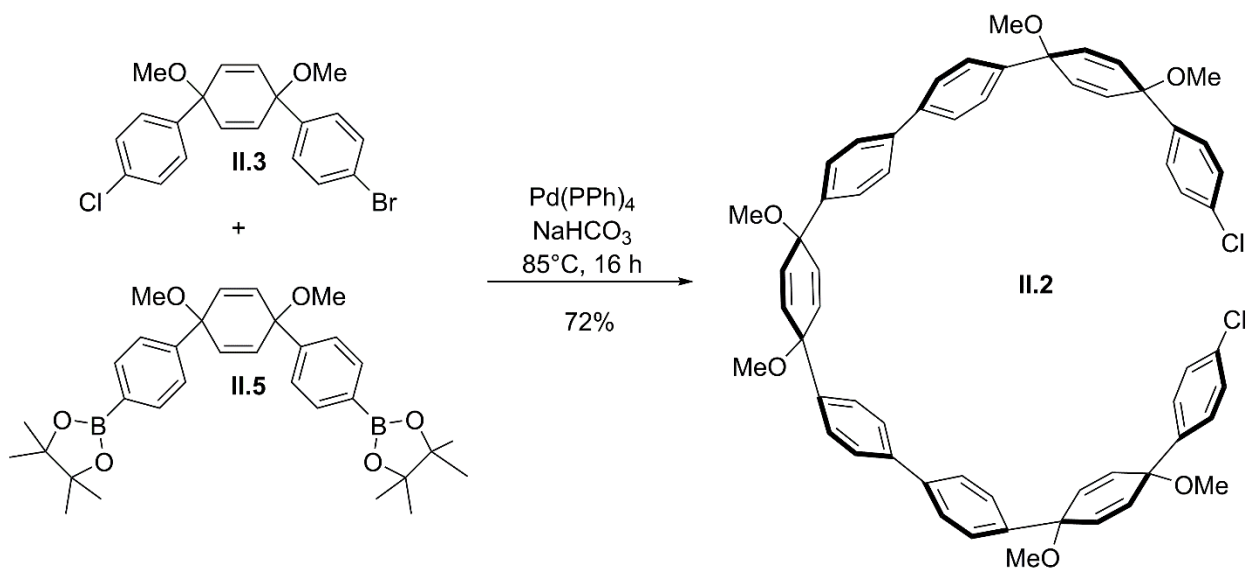
II.5.1. General Experimental Details.

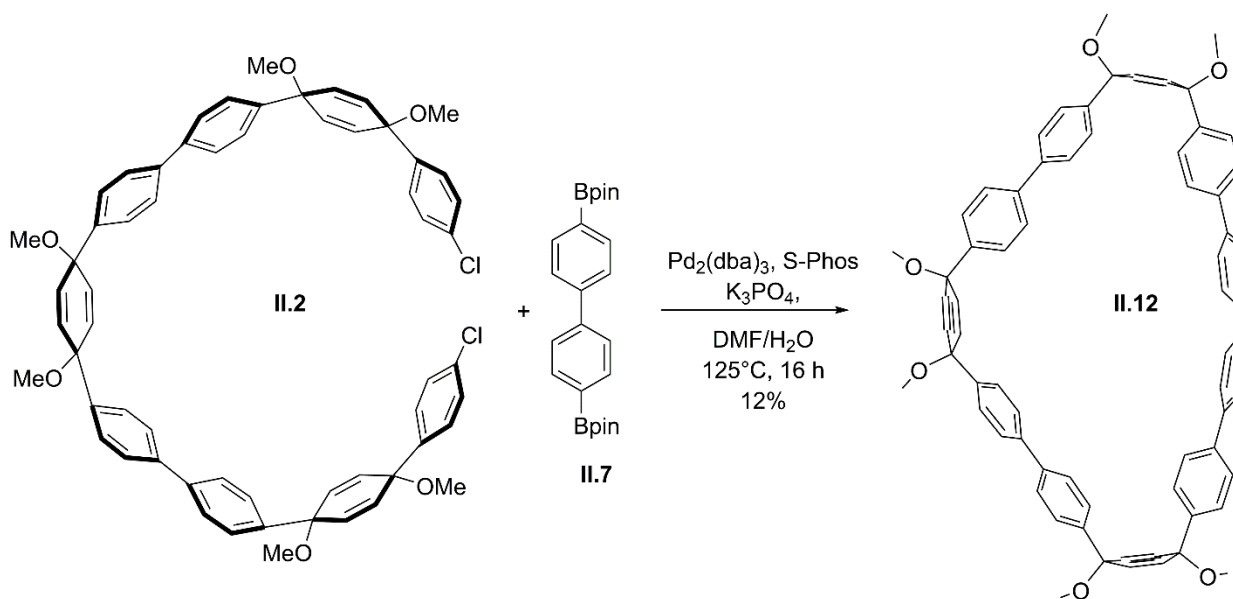
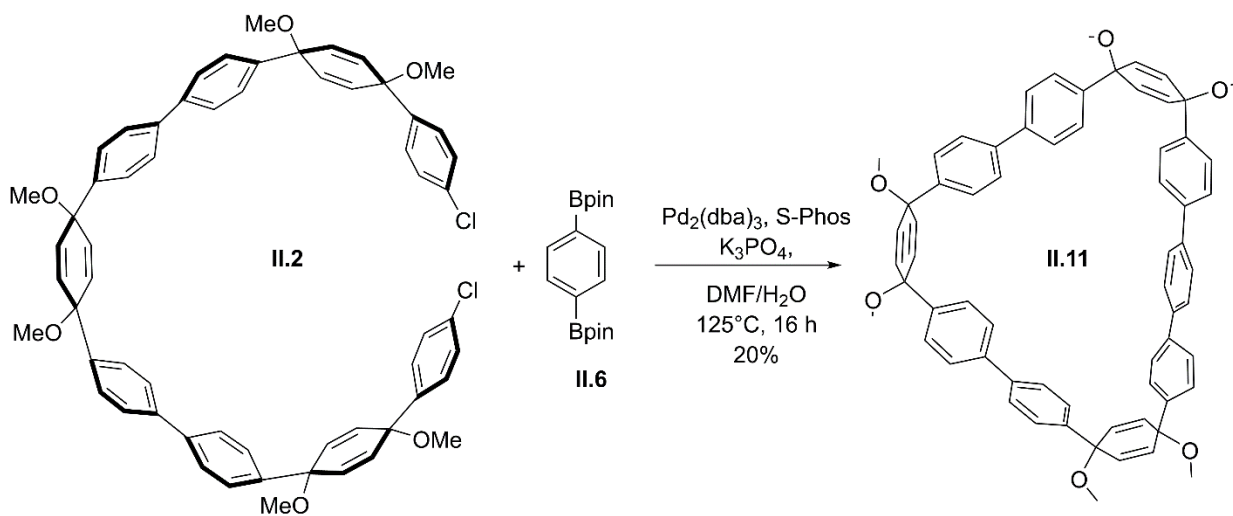
^1H NMR spectra were recorded at 500 MHz while ^{13}C NMR spectra were recorded at 125 MHz. All spectra were referenced to TMS. MALDI-TOF data was obtained using 7,7,8,8-tetracyanoquinodimethane (TCNQ) silver trifluoroacetate matrix. All reagents were obtained commercially. Tetrahydrofuran, dichloromethane, and dimethylformamide were dried by filtration through alumina according to the methods

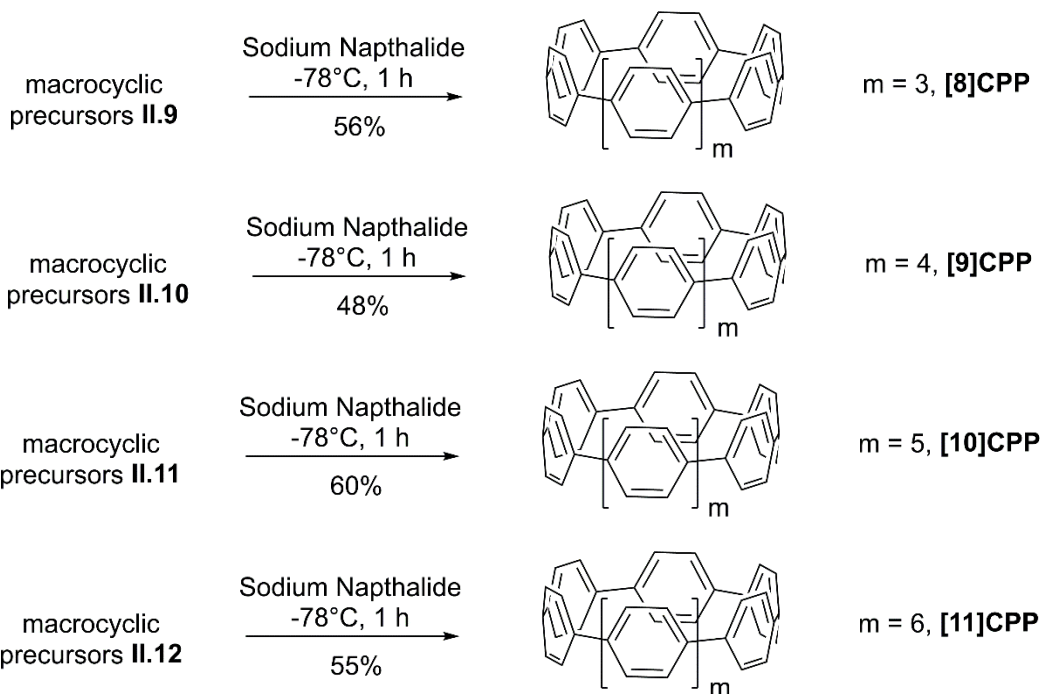
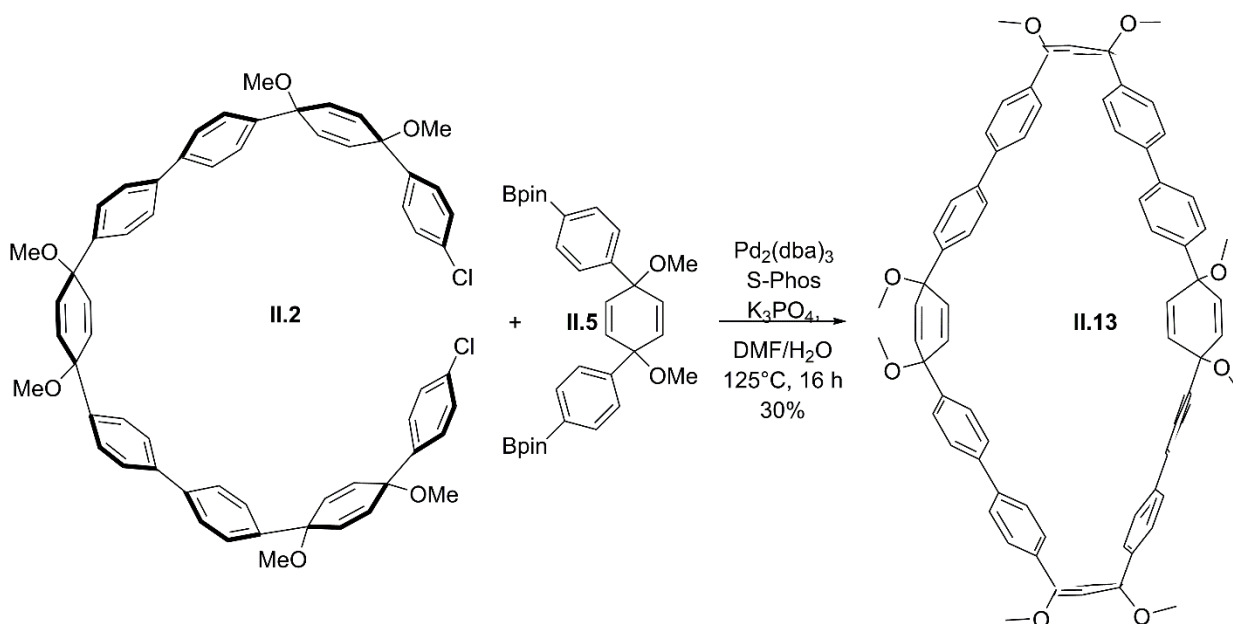
described by Grubbs.³¹ Silica column chromatography was conducted with Zeochem Ceoprep 60 Exo 40-63 μm silica gel while alumina chromatography utilized Sorbent Technologies 50-200 μm Basic Activity II-III Alumina. Thin layer chromatography was performed using Sorbent Technologies Silica Gel XHT TLC plates or Sorbent Technologies Alumina TLC plates respectively. Preparative thin layer chromatography was performed using Watman K6 60 \AA Silica Gel Adsorption Preparative Plates 500 μm thick. Developed plates were visualized using UV light as wavelengths of 254 and 365 nm. All glassware was oven or flame dried and cooled under an inert atmosphere of nitrogen unless otherwise noted. Moisture sensitive reactions were carried out under an inert atmosphere of nitrogen using standard syringe/septa technique.

II.5.2. Synthetic Schemes.









II.5.4. Synthetic Details.

4,4''-dibromo-1',4'-dimethoxy-1',4'-dihydro-1,1':4'1''terphenyl II.15: 4'-bromo-1-hydroxy-[1,1'-biphenyl]-4(1*H*)-one **II.14** was synthesized as previously reported.⁸ To a dry 2 L round bottom flask was added sodium hydride (1.18 g, 29.4 mmol, 1.3 equiv). This solid was washed with dry THF (2x60 mL) to remove excess packing grease. THF (120 mL) was then added and this slurry was cooled to -78°C , at which point **II.14** (6g,

22.6 mmol, 1 equiv) was added drop wise as a solution in THF (60 mL) and stirred for 2 h.

In a separate flame dried flask equipped with a stir bar was added 1,4-dibromobenzene (12.8 g, 54.3 mmol, 2 equiv) and THF (60mL). The reaction was then cooled to $-78\text{ }^{\circ}\text{C}$ at which point *n*-butyllithium in hexanes (22.6 mL, 54.2 mmol, 2.4 equiv) was added drop wise via cannulation to give an off yellow solution. (It is important to note at this point that if the reaction mixture exceeds $-60\text{ }^{\circ}\text{C}$, the reaction mixture will turn brown and must be discarded.) This yellow solution was allowed to stir at $-78\text{ }^{\circ}\text{C}$ for 30 min and was then cannulated to the reaction vessel containing deprotonated **II.14**. This reaction was stirred for 2h at $-78\text{ }^{\circ}\text{C}$ before being carefully quenched with water (15 mL), at which point it was gradually warmed to room temperature.

This solution was then extracted with diethyl ether (3x 20 mL). The pooled organic layer was then washed with saturated brine (50 mL), dried over sodium sulfate, and concentrated under reduced pressure to afford the crude diol as a yellow oil. This crude diol was immediately pushed on to the methylation step to avoid decomposition.

In a separate flame dried 500 mL round bottom flask equipped with a stir bar was added sodium hydride (1.4 g, 58.7 mmol, 2.6 equiv) which was washed with THF (3x60 mL) as before to remove excess grease. Dry THF (60 mL) was then added to the flask and the solution was cooled to $0\text{ }^{\circ}\text{C}$ at which point the crude diol was added drop wise as a solution in THF (60 mL). After the reaction had stirred for 30 min, neat methyl iodide (5.6 mL, 90.4 mmol, 4 equiv) was added drop wise via cannulation. After cannulation, the reaction was allowed to gradually warm to room temperature and stir for 15 h at which point it was carefully quenched with water (50 mL). This solution was extracted with ethyl acetate (3x 30 mL), washed with saturated brine (50 mL), dried over sodium sulfate, and concentrated under reduced pressure. The crude yellow oil was recrystallized in hot hexanes to afford the product **II.15** as a white crystalline solid (6.5 g, 64%, m.p.134-135 $^{\circ}\text{C}$).

^1H NMR (500MHz, CDCl_3) δ (ppm): 3.41 (s, 6H), 6.07 (s, 4H), 7.23 (d, $J=8.5$, 4H), 7.43 (d, $J=9.0$, 4H). ^{13}C (125MHz, CDCl_3) δ (ppm): 52.0, 74.4, 121.7, 127.7, 131.5, 133.3, 142.3. HRMS (Q-TOF ES+) m/z calculated for $\text{C}_{20}\text{H}_{18}\text{Br}_2\text{O}_2$ (M) $^+$: 447.9674, Found

(isotopic pattern): 447.1499, 449.3956. IR (neat): 2982, 2945, 2899, 2825, 1506, 1480, 1451, 1398, 1175, 1025, 1007, 948, 822, 756 cm^{-1} .

Diboronate II.5: To a flame dried flask charged with a stir bar was added **II.15** (5 g, 11.1 mmol, 1 equiv) and THF (50 mL) which was allowed to cool to $-78\text{ }^{\circ}\text{C}$. *n*-butyllithium (10.3 mL, 24.4 mmol, 2.2 equiv) was added drop wise to the stirring THF solution over 2 minutes⁶, immediately neat 2-Isopropoxy-4,4,5,5-tetramethyl-1,3,2-dioxaborolane (9.1 mL, 44.4 mmol, 4 equiv) was added to the solution and allowed to stir for 30 min. Water (20 mL) was used to carefully quench the reaction at which point it was extracted with diethyl ether (3x100 mL), washed with saturated brine (200 mL), dried over sodium sulfate, and concentrated under reduced pressure to afford the crude product as an off white solid. This crude solid was recrystallized in hot hexanes to give the product **II.5** as a white crystalline solid (4.75 g, 79%, m.p. decomposition $> 250\text{ }^{\circ}\text{C}$).

^1H NMR (500 MHz, CDCl_3) δ (ppm): 1.34 (s, 24H), 3.43 (s, 6H), 6.09 (s, 4H), 7.40 (d, $J=8.5$, 4H), 7.75 (d, $J=8.5$, 4H). ^{13}C (125 MHz, CDCl_3) δ (ppm): 24.9, 51.9, 74.9, 83.7, 125.3, 133.2, 134.9, 146.3, C-B not observed. HRMS (Q-TOF ES+) m/z calculated for $\text{C}_{32}\text{H}_{42}\text{B}_2\text{O}_6$ (M-OCH₃)⁺: 514.2978, Found: 514.3044. IR (neat): 2988, 2974, 2938, 2822, 1609, 1398, 1358, 1324, 1272, 1141, 1090, 1080, 1066, 1016, 962, 950, 857, 835, 741 cm^{-1} .

Dichloro II.2: A 250 mL round bottom Schlenk flask was equipped with a stir bar and charged with **II.5** (2 g, 3.7 mmol, 1 equiv), **II.3** (3.0 g, 7.3 mmol, 2 equiv), and tetrakis(triphenylphosphine)palladium(0) (0.43 g, 0.37 mmol, 0.1 equiv). 1 M aqueous sodium bicarbonate (44 mL) and isopropanol (150 mL) were sparged separately with nitrogen for 1 hr. They were then introduced to the Schlenk flask at which point the reaction mixture was heated to $85\text{ }^{\circ}\text{C}$ and vigorously stirred for 16 h.

Once cooled the reaction was extracted with ethyl acetate (3x100 mL), washed with water (10x100 mL), washed with saturated brine (100 mL), dried over sodium sulfate, and concentrated under reduced pressure to give a yellow oil. This oil was purified by flash chromatography (Al_2O_3 , 5:95 ethyl acetate/hexanes) to afford **2** as a white powder (2.5 g, 72%, m.p $148\text{-}150\text{ }^{\circ}\text{C}$).

^1H NMR (500 MHz, CDCl_3) δ (ppm): 3.43 (s, 6H), 3.44 (s, 6H), 3.47 (s, 6H) 6.07 (d, $J=10.5$, 4H), 6.16 (s, 6H), 6.16 (d, $J=10.0$, 4H), 7.27 (d, $J=9$, 4H), 7.34 (d, $J=8.5$, 4H),

7.43 (d, $J=9$, 4H), 7.48 (d, $J=8.5$, 4H), 7.53 (d, $J=8.5$, 4H), 7.53 (d, $J=8.5$, 4H). ^{13}C (125 MHz, CDCl_3) δ (ppm): 52.0, 74.5, 74.6, 74.7, 126.4, 126.4, 127.1, 127.1, 127.5, 128.5, 133.0, 133.4, 139.9, 140.1, 142.0, 142.3, 142.6. MALDI-TOF m/z calculated for $\text{C}_{59}\text{H}_{52}\text{O}_5$ (M-OMe) $^+$: 910.32, Found 910.09. IR (neat): 3028, 2982, 2939, 2897, 2823, 1489, 1399, 1266, 1228, 1176, 1076, 1012, 949, 822, 762, 734 cm^{-1} .

Macrocycle II.9: To a 50 mL reaction tube equipped with a rubber septa and stir bar was added dichloride **II.1** (50 mg, 0.076 mmol, 1 equiv), diboronate **7** (37 mg, 0.092 mmol, 1.2 equiv), tris(dibenzylideneacetone)dipalladium(0) (7 mg, 0.0076 mmol, 0.1 equiv), Buchwald ligand S-Phos (11 mg, 0.024 mmol, 0.32 equiv) and tribasic potassium phosphate (32.5 mg, 0.152 mmol, 2.0 equiv). This tube was then sealed and purged with dry nitrogen for 1.5 h. Water (1.5 ml) and DMF (13.8 ml) were separately freeze-pump-thawed (5x) and introduced into the reaction vessel, which was then dropped into a 125 °C oil bath and stirred vigorously for 16 h.

After cooling, the reaction mixture was washed with water (30 mL), DCM (30 mL), and filtered through a bed of deactivated celite. This solution was extracted with DCM (3x20 mL), washed with water (10 x 20 mL), brine (100 mL) and then dried over sodium sulfate. After concentration the crude mixture was purified by preparative thin layer chromatography (SiO_2 , 5:95 ethyl acetate/dichloromethane) to afford macrocycle **II.9** (7.8 mg, 14% yield, m. p. decomposition >250 °C) as a white solid.

^1H NMR (500 MHz, CDCl_3) δ (ppm): 3.39 (s, 6H), 3.46 (s, 6H), 6.99 (d, $J=10.5$, 4H), 6.26 (d, $J=10.5$, 4H), 7.15 (d, $J=9.0$, 4H), 7.26 (d, $J=8.5$, 4H), 7.37 (d, $J=9.0$, 4H), 7.44 (d, $J=8.5$, 4H), 7.54 (d, $J=8.5$, 4H), 7.77 (d, $J=9.0$, 4H). ^{13}C (125 MHz, CDCl_3) δ (ppm): 51.7, 52.4, 74.5, 74.7, 126.2, 126.6, 126.8, 126.9, 127.8, 128.2, 133.4, 137.9, 139.0, 139.5, 140.5, 141.4, 142.2. MALDI-TOF m/z calculated for $\text{C}_{52}\text{H}_{44}\text{O}_4$ (M) $^+$: 732.32, Found 732.35. IR (neat): 3028, 2937, 2927, 2823, 2610, 1490, 1448, 1396, 1360, 1259, 1174, 1083, 1076, 1014, 1071, 822, 755 cm^{-1} .

Macrocycle II.10: The general procedure above was used with the exception that diboronate **II.5** (50 mg, 0.092 mmol, 1.2 equiv) was used in place of diboronate **II.7** to deliver macrocycle **II.10** (15.74 mg, 23%, m. p. decomposition >250 °C).

^1H NMR (500 MHz, CDCl_3) δ (ppm): 3.48 (s, 18H), 6.15 (s, 12H), 7.48 (d, $J=8.5$, 12H), 7.59 (d, $J=8.5$, 12H). ^{13}C (125 MHz, CDCl_3) δ (ppm): 52.0, 74.9, 126.5, 126.8, 133.5,

139.9, 142.6. MALDI-TOF m/z calculated for $C_{60}H_{54}O_6$ (M)⁺: 870.39, Found 870.50. IR (neat): 2922, 2852, 2824, 1728, 1490, 1464, 1261, 1081, 1022, 951, 820 cm^{-1} .

Macrocycle II.11: The general procedure above was used with the exception that dichloride **II.2** (50 mg, 0.053 mmol, 1 equiv) was used in place of dichloride **II.1** and diboronate **II.6** (21 mg, 0.064 mmol, 1.2 equiv) was used in place of diboronate **II.7** to afford macrocycle **II.11** (10 mg, 20%, m. p. decomposition >250 °C) as a white solid. ¹H NMR (500 MHz, CDCl₃) δ(ppm): 3.43 (s, 6H), 3.47 (s, 6H), 3.49 (s, 6H), 6.12 (d, $J=10.0$, 4H), 6.13 (s, 6H), 6.25 (d, $J=10.5$, 4H), 7.34 (d, $J=8.5$, 4H), 7.47 (d, $J=8.5$, 4H), 7.49 (d, $J=8.5$, 4H), 7.52 (d, $J=8.5$, 4H), 7.56 (d, $J=8.5$, 4H), 7.57 (d, $J=8.5$, 4H), 7.66 (s, 4H). ¹³C (125 MHz, CDCl₃) δ(ppm): 52.0, 52.0, 52.3, 74.0, 75.3, 75.3, 126.4, 126.6, 126.8, 126.8, 127.1, 127.2, 127.7, 133.0, 133.7, 139.8, 139.8, 140.0, 140.2, 142.10, 142.11, 143.0. MALDI-TOF m/z calculated for $C_{66}H_{58}O_6$ (M)⁺: 946.42, Found 946.57. IR (neat): 3028, 2927, 2821, 1654, 1489, 1449, 1174, 1080, 1028, 1005, 949 cm^{-1} .

Macrocycle II.12: The general procedure above was used with the exception that dichloride **II.2** (50 mg, 0.053 mmol, 1 equiv) was used in place of dichloride **II.1** and diboronate **II.7** (26 mg, 0.064 mmol, 1.2 equiv) was used to afford macrocycle **II.12** (6.5 mg, 12%, m. p. decomposition >250 °C) as a white solid. ¹H NMR (500 MHz, CDCl₃) δ(ppm): 3.32 (s, 6H), 3.46 (s, 6H), 3.50 (s, 6H), 6.14 (d, $J=10.5$, 4H), 6.18 (s, 6H), 6.25 (d, $J=10.0$, 4H), 7.32 (d, $J=8.5$, 4H), 7.46 (d, $J=8.5$, 4H), 7.6 (d, $J=8.5$, 4H), 7.49 (d, $J=8.5$, 4H), 7.55 (d, $J=8.5$, 4H), 7.55 (d, $J=8.5$, 4H), 7.66 (d, $J=8.5$, 4H), 7.72 (d, $J=8$, 4H). ¹³C (125 MHz, CDCl₃) δ(ppm): 51.4, 51.9, 52.3, 72.9, 75.2, 75.3, 126.6, 126.6, 126.7, 126.8, 127.0, 127.1, 127.3, 127.6, 132.9, 133.4, 139.3, 139.6, 139.8, 139.9, 140.0, 141.8, 142.0, 142.8. MALDI-TOF m/z calculated for $C_{72}H_{62}O_6$ (M)⁺: 1022.45, Found 1022.42. IR (neat): 3028, 2927, 2821, 1654, 1489, 1449, 1174, 1080, 1028, 1005, 949 cm^{-1} .

Macrocycle II.13: The general procedure above was used with the exception that dichloride **II.2** (50 mg, 0.053 mmol, 1equiv) was used in place of dichloride **II.1** and diboronate **II.5** (35 mg, 0.064 mmol, 1.2 equiv) was used in place of diboronate **7** to afford macrocycle **II.13** (18.5 mg, 30%, m. p. decomposition >250 °C) as a white solid. ¹H NMR (500 MHz, CDCl₃) δ(ppm): 3.45 (s, 24H), 6.15 (s, 16H), 7.44 (d, $J=8.5$, 16H), 7.48 (d, $J=8.5$, 4H). ¹³C (125 MHz, CDCl₃) δ(ppm): 52.0, 74.7, 126.4, 127.1, 133.4,

140.1, 142.5. MALDI-TOF m/z calculated for $C_{72}H_{62}O_6$ (M)⁺: 1160.52, Found 1160.93. IR (neat): 756, 820, 984, 950, 1021, 1082, 1177, 1221, 1359, 1396, 1449, 1492, 1713, 2822, 2855, 2929 cm^{-1} .

[8]CPP: To a dry 25 mL round bottom flask equipped with a glass stir bar was added sodium metal (274 mg, 11.9 mmol) which was subsequently washed with hexanes. Dry THF (12 ml) was added via syringe to the reaction vessel and cooled to 0 °C. Napthalene (1 g, 7.82 mmol) was added to this stirring solution and allowed to gradually warm to room temperature over the course of 18 hrs.

After 18 hrs, a separate flame dried 25 mL flask containing **II.9** (5 mg, 0.007 mmol, 1 equiv), THF (5 mL), and a stir bar was cooled to -78 °C. To this stirring solution was added the deep green 1 M sodium naphthalide solution (0.56 mL, 0.006 mmol, 20.0 equiv per methoxy) drop wise. Upon addition the solution went from clear to a deep purple and was allowed to stir for 1 h. Once the reaction was complete a 1 M solution of iodine in THF (1 mL) was added drop wise.

Aqueous saturated sodium thiosulfate (10 mL) was added and the solution was warmed to room temperature at which point it was diluted with water (20 mL) and extracted with dichloromethane (3x 15 mL). The organic layers were pooled and then washed with saturated brine (20 mL), dried over sodium sulfate, and concentrated under reduced pressure to afford a crude yellow solid. This crude solid was purified by flash chromatography (SiO₂, 50:50 hexane/dichloromethane) to afford **[8]CPP** (2.4 mg, 56%, m. p. decomposition >250 °C) as pale yellow solid.

¹H NMR (500 MHz, CDCl₃) δ(ppm): 7.48 (s, 32H). ¹³C (125 MHz, CDCl₃) δ(ppm): 127.4, 135.6. MALDI-TOF m/z calculated for $C_{48}H_{32}$ (M)⁺: 608.25, Found 608.40. IR (neat): 3958, 2925, 2947, 2934, 2837, 2893, 2852, 1716, 1588, 1484, 1397, 1277, 1254, 1080, 817, 819, 701 cm^{-1} .

[9]CPP: The general procedure above was used, with macrocycle **II.10** (5 mg, 0.006 mmol) in place of **II.11**, to afford **[9]CPP** (1.8 mg, 48%, m. p. decomposition >250 °C) as a pale yellow solid.

¹H NMR (500 MHz, CDCl₃) δ(ppm): 7.52 (s, 36H). ¹³C (125 MHz, CDCl₃) δ(ppm): 127.4, 137.9. MALDI-TOF m/z calculated for $C_{54}H_{36}$ (M)⁺: 688.28, Found 688.24. IR (neat): 2984, 2955, 2928, 2855, 2823, 1481, 1461, 1253, 1089, 816 cm^{-1} .

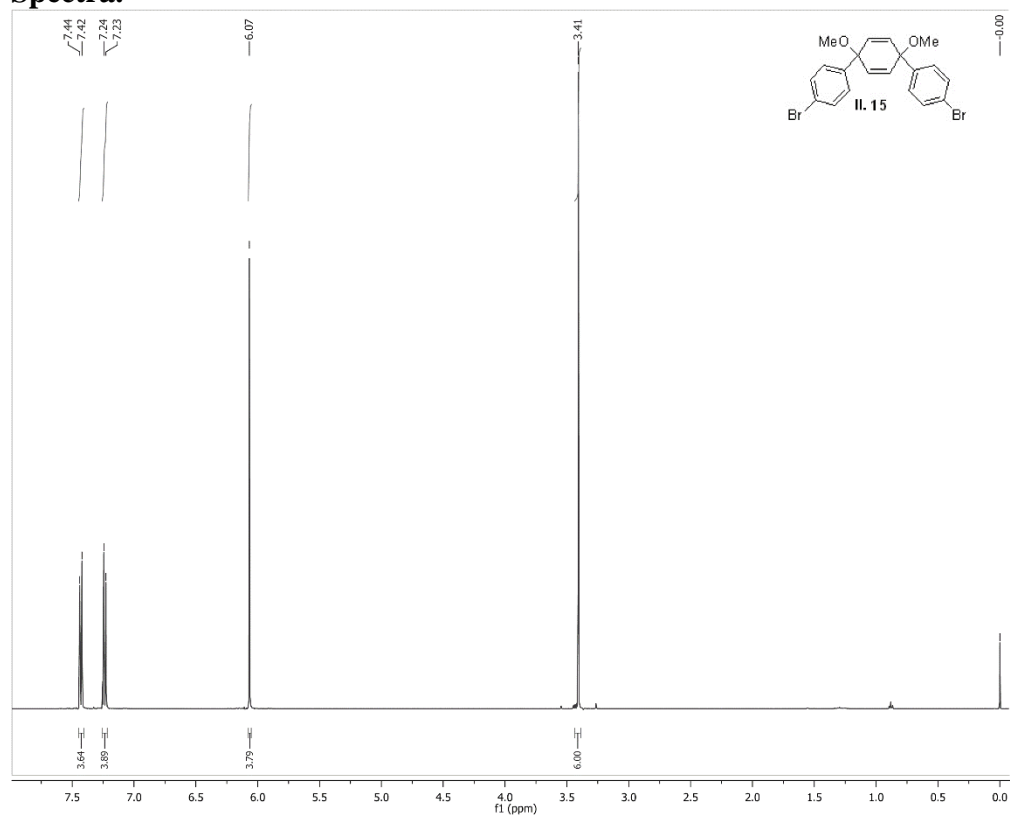
[10]CPP: The general procedure above was used, with macrocycle **II.11** (5 mg, 0.005 mmol) in place of **II.9**, to afford **[10]CPP** (2.5 mg, 60%, m. p. decomposition >250 °C) as a white solid.

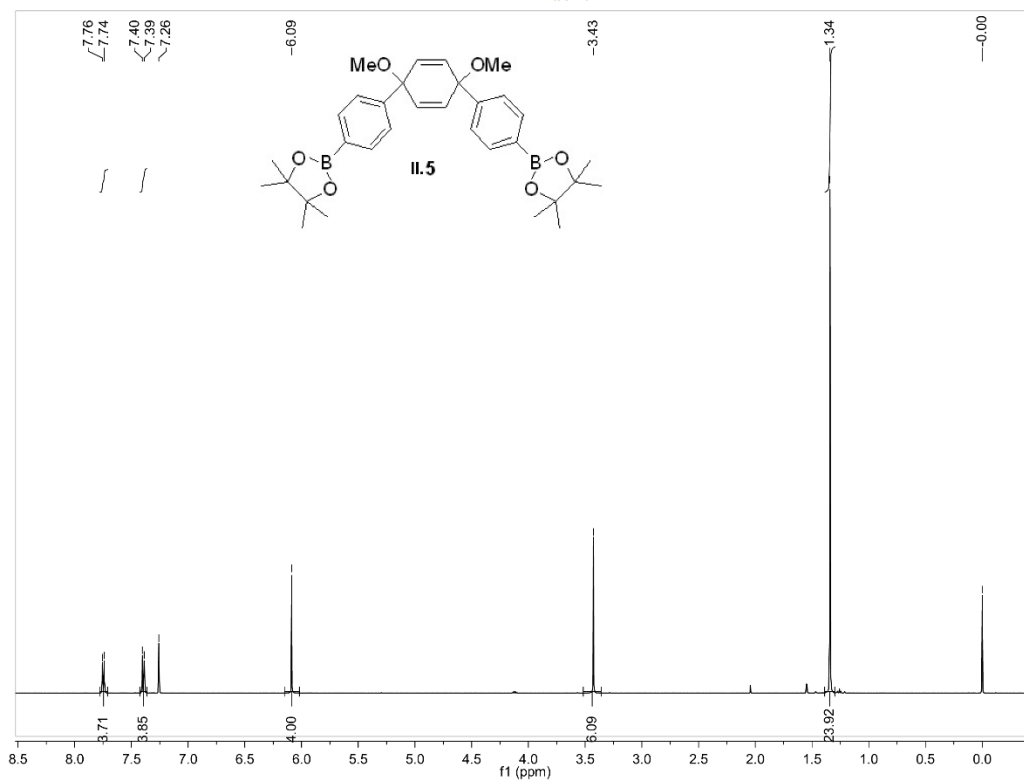
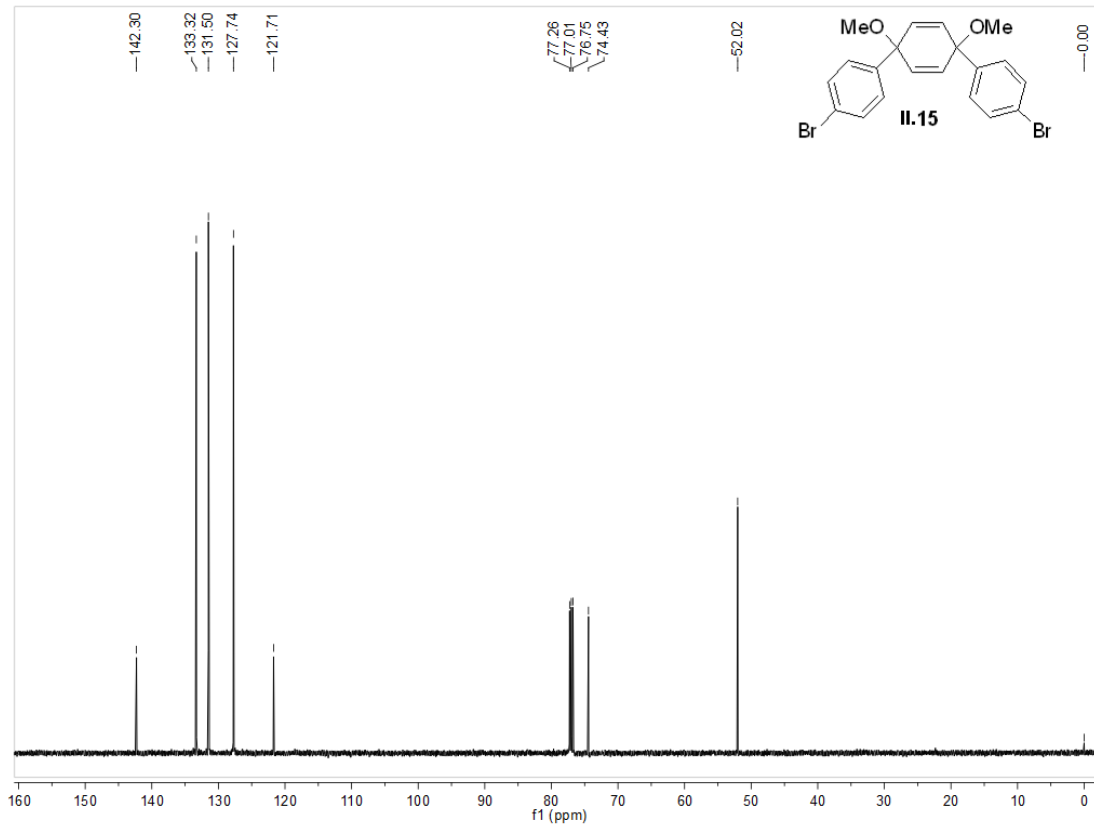
^1H NMR (500 MHz, CDCl_3) δ (ppm): 7.56 (s, 40H). ^{13}C (125 MHz, CDCl_3) δ (ppm): 127.4, 138.2. MALDI-TOF m/z calculated for $\text{C}_{60}\text{H}_{40}$ (M) $^+$: 760.31, Found 760.53. IR (neat): 3029, 2929, 2852, 2820, 1590, 1486, 1395, 1354, 1258, 1082, 949, 816, 758, 734 cm^{-1} .

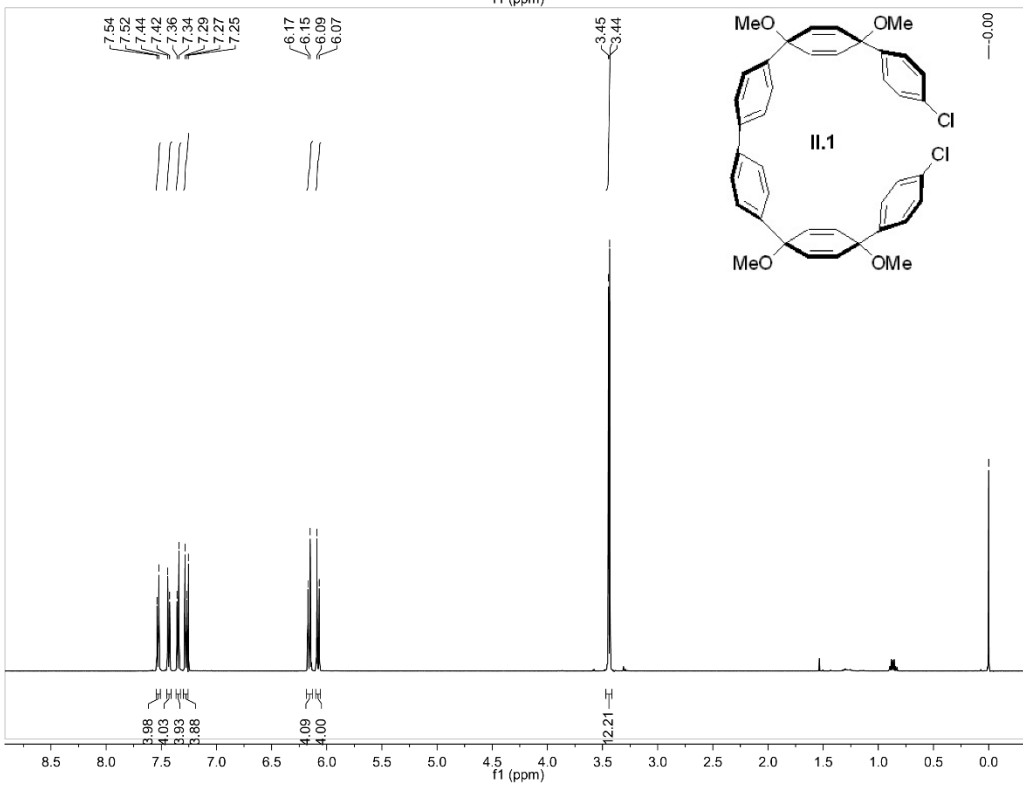
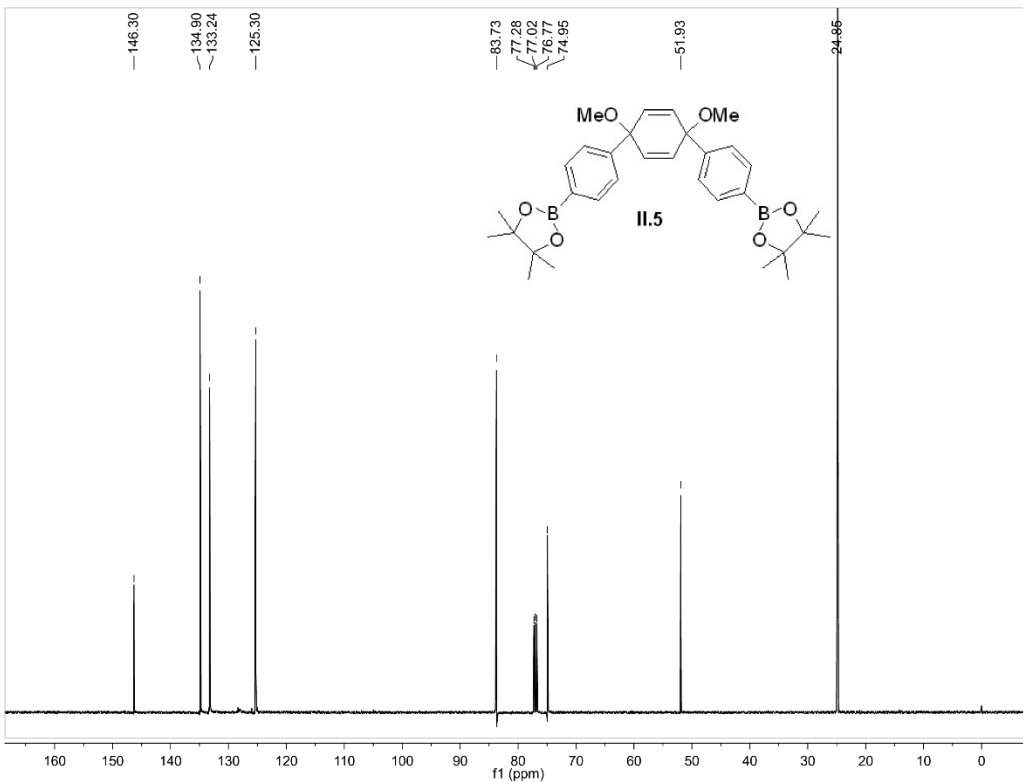
[11]CPP: The general procedure above was used, with macrocycle **II.12** (5 mg, 0.005 mmol) in place of **II.9**, to afford **[11]CPP** (2.3 mg, 55%, m. p. decomposition >250 °C) as a white solid.

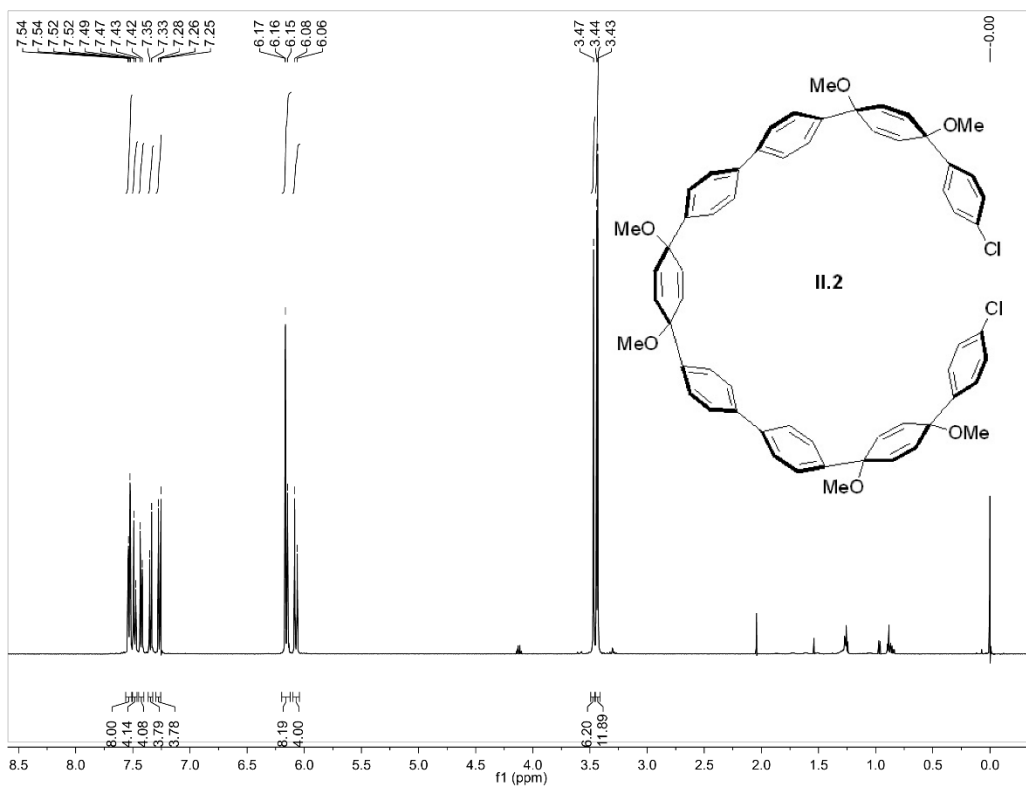
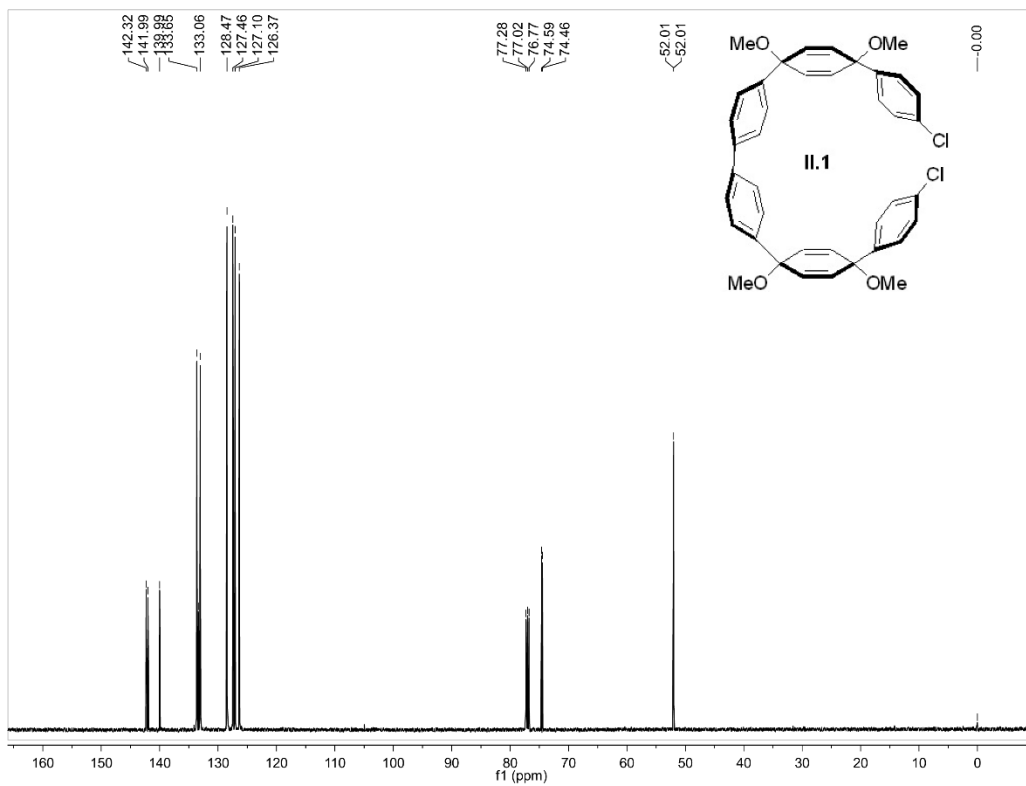
^1H NMR (500 MHz, CDCl_3) δ (ppm): 7.58 (s, 44H). ^{13}C (125 MHz, CDCl_3) δ (ppm): 127.3, 138.4 (Ar). MALDI-TOF m/z calculated for $\text{C}_{72}\text{H}_{62}\text{O}_6$ (M) $^+$: 1022.45, Found 1022.42. IR (neat): 3044, 3030, 3021, 2959, 2950, 2912, 1732, 1593, 1486, 1090, 812, 739, 698 cm^{-1} .

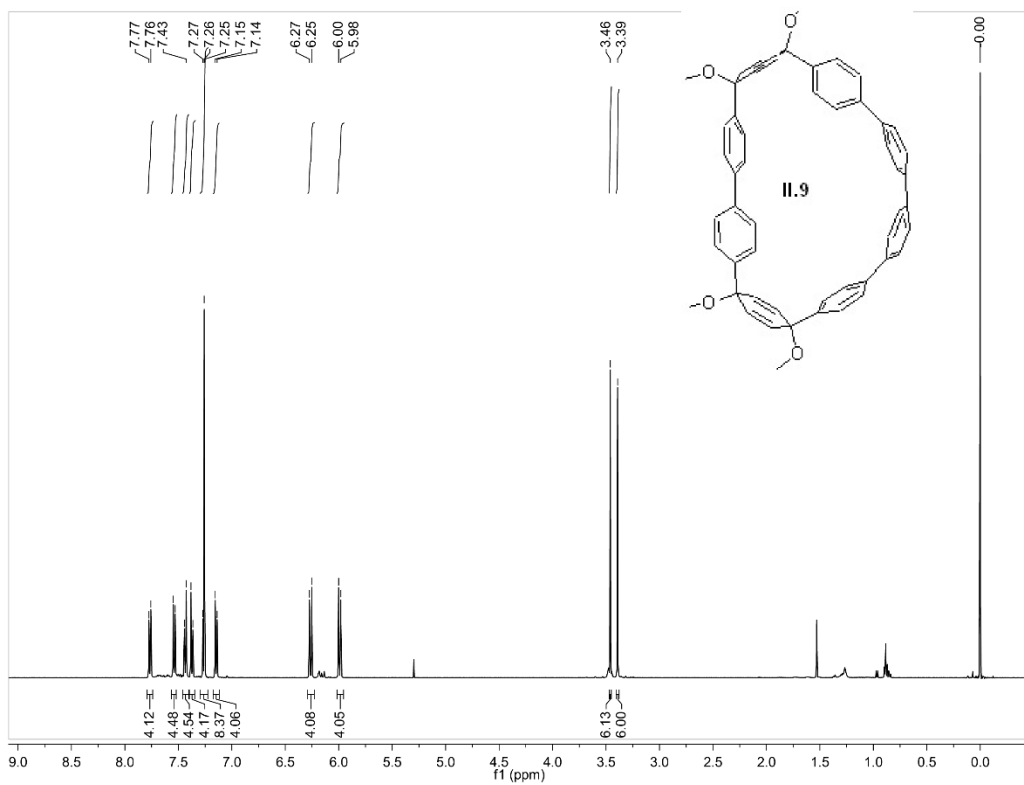
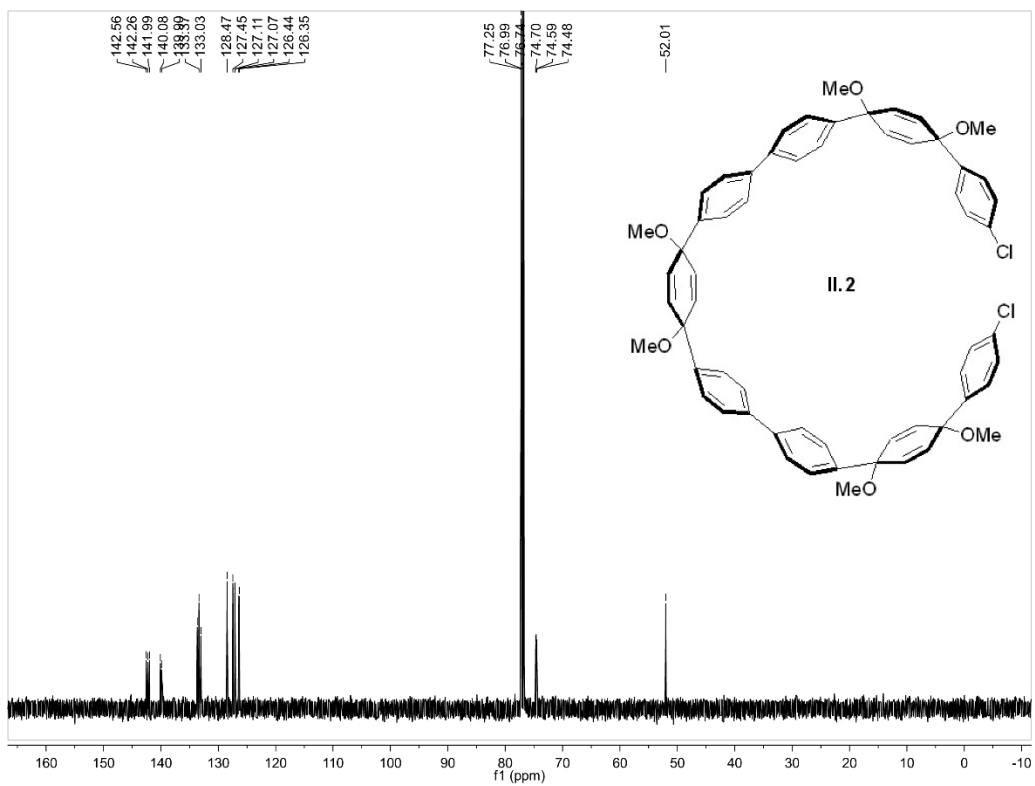
II.5.5. NMR Spectra.

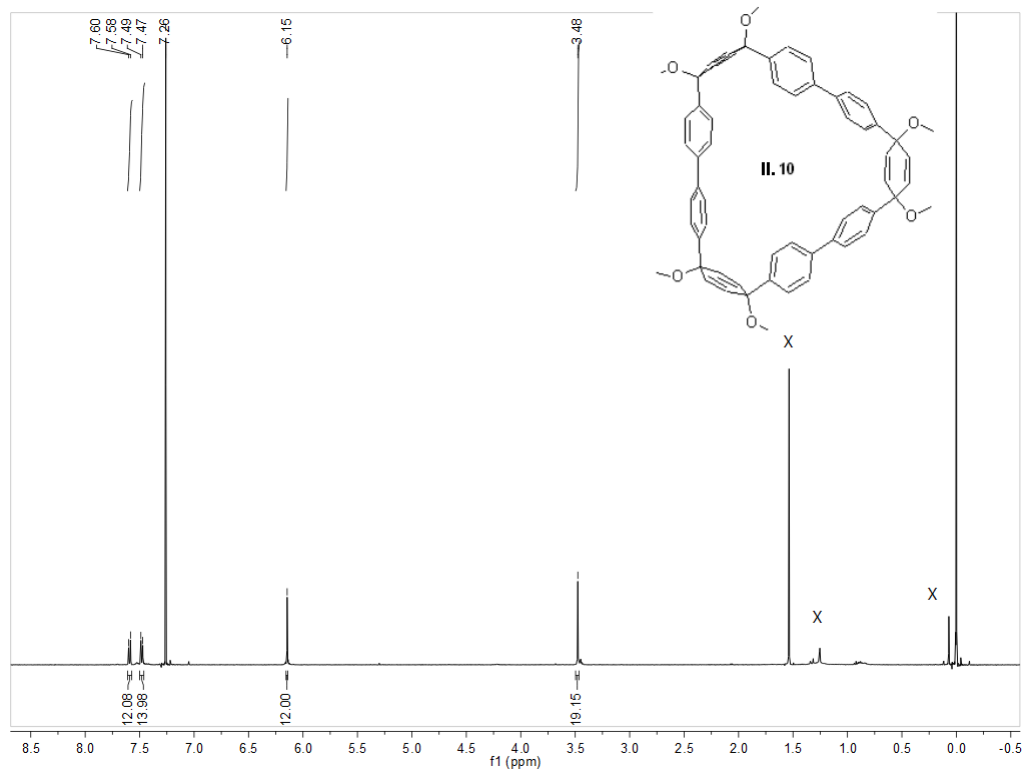
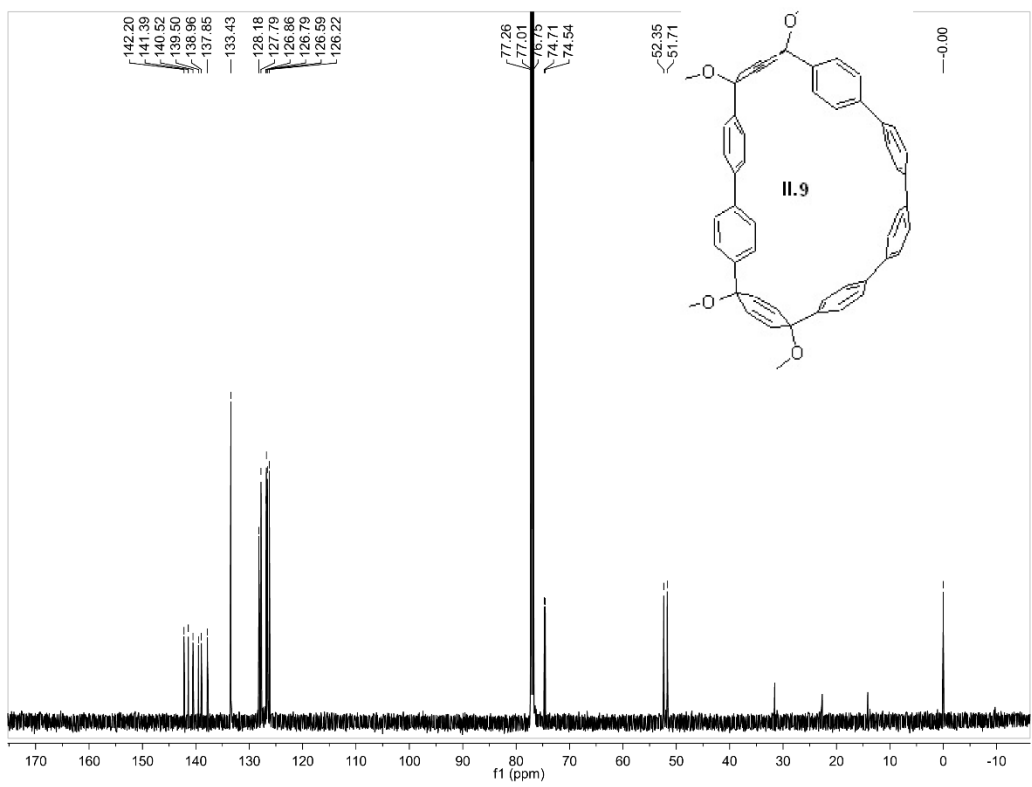


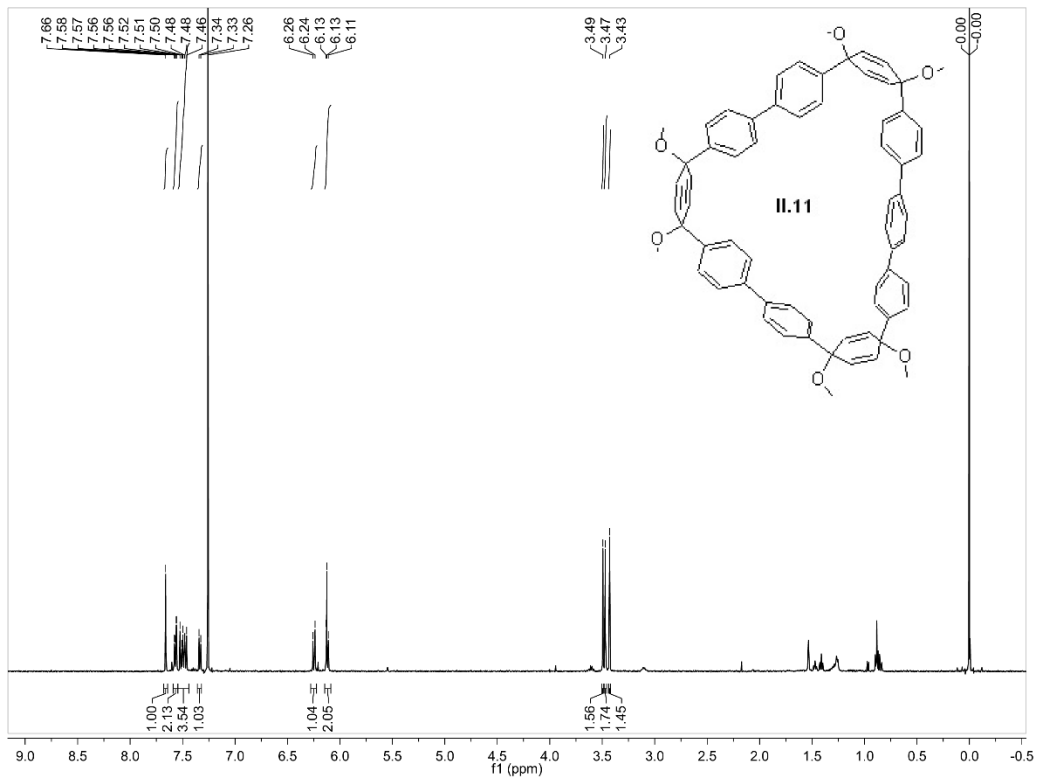
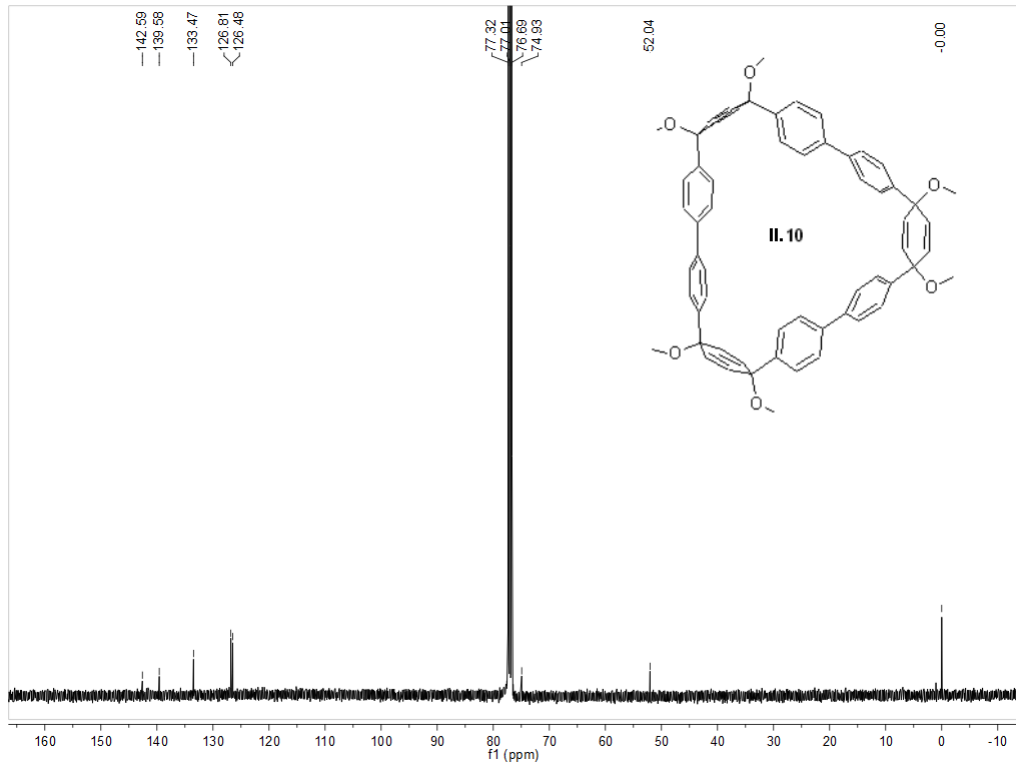


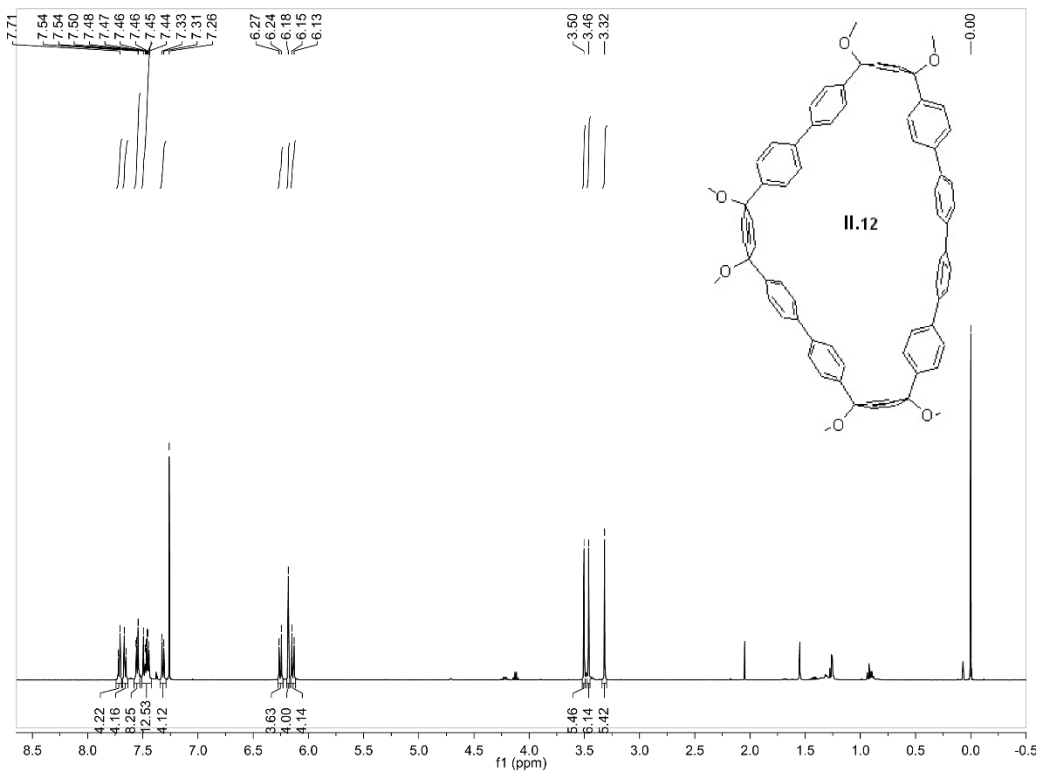
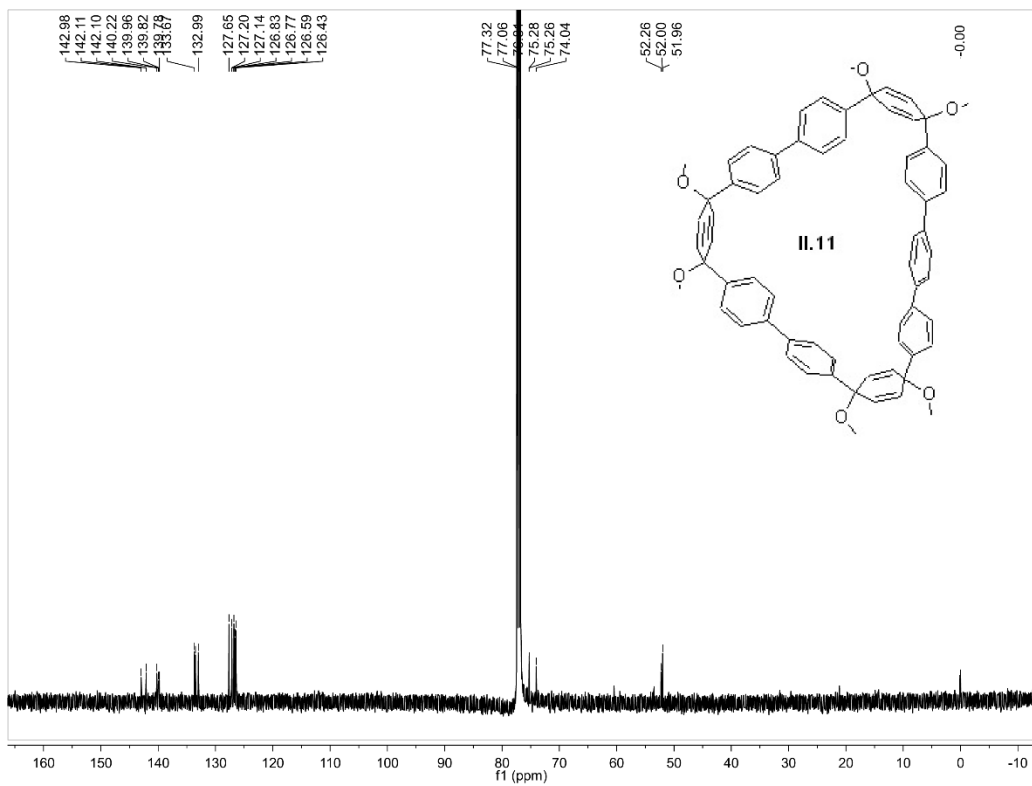


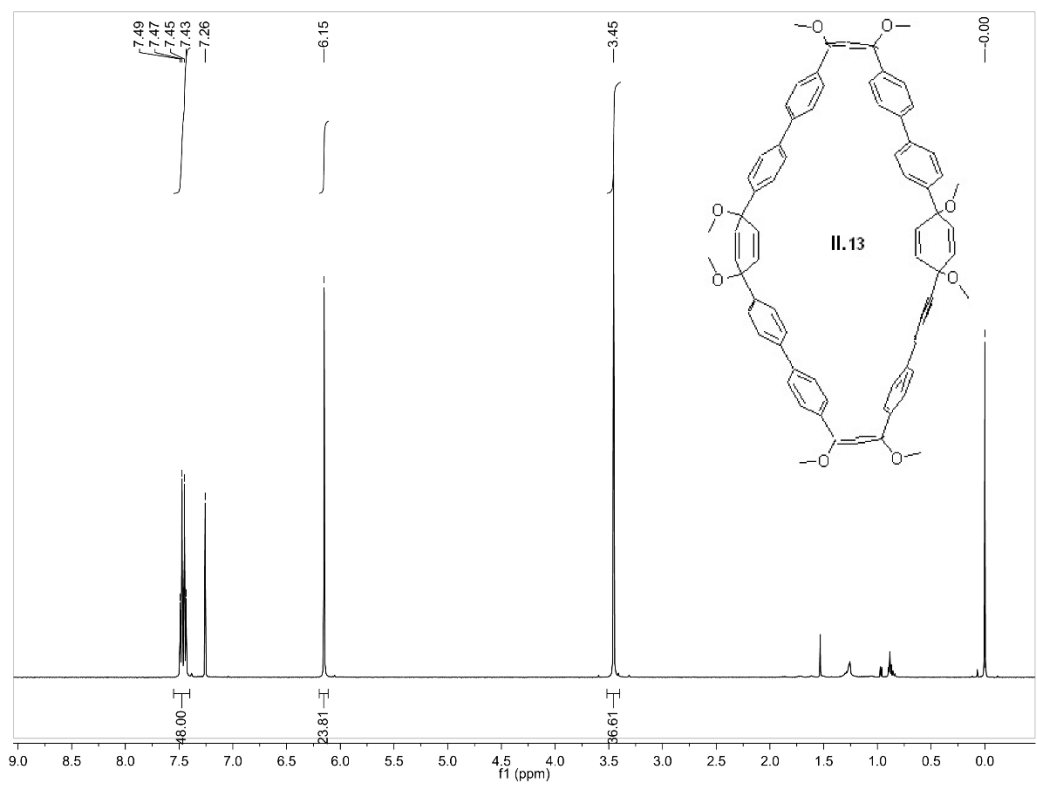
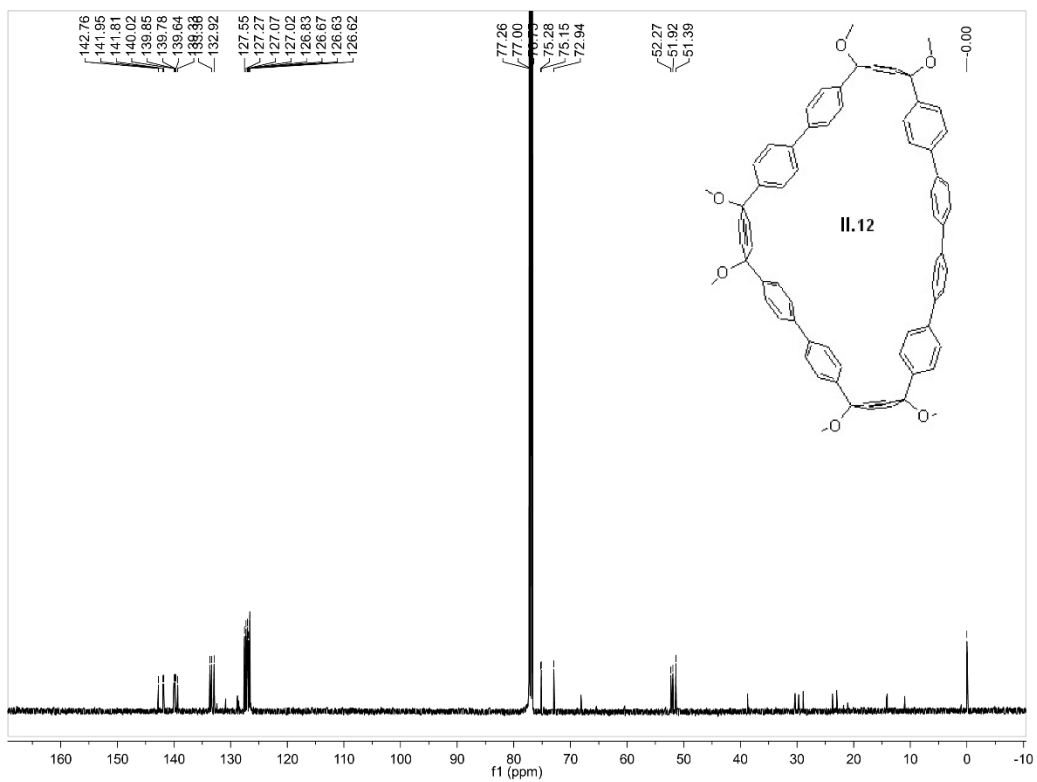


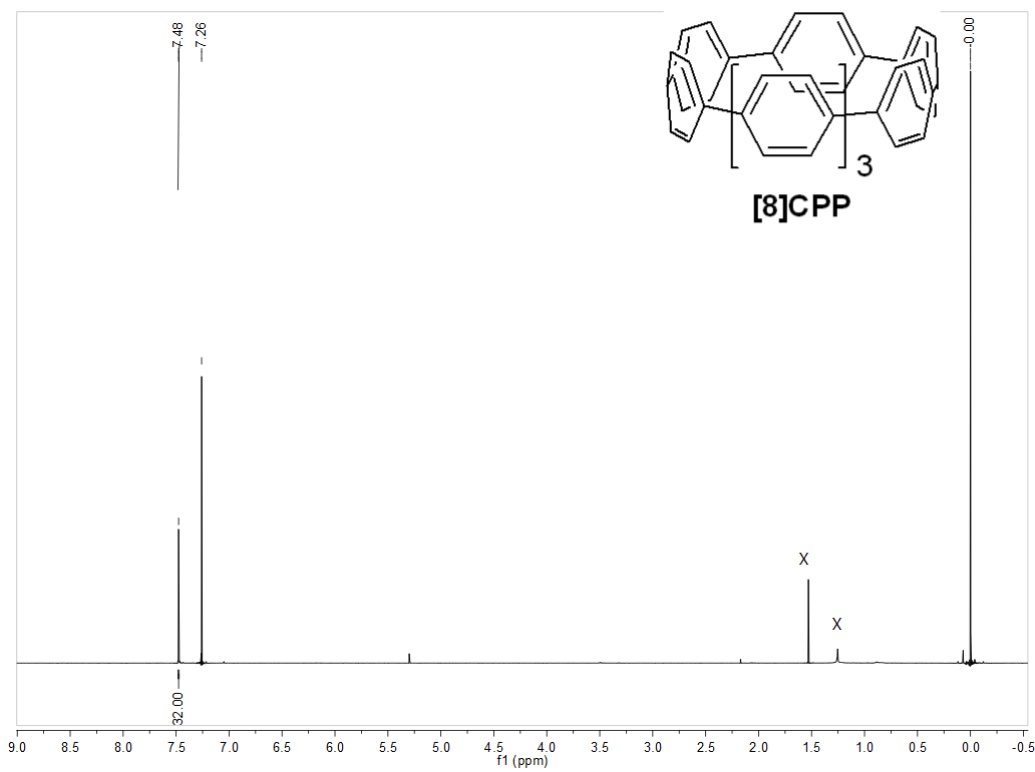
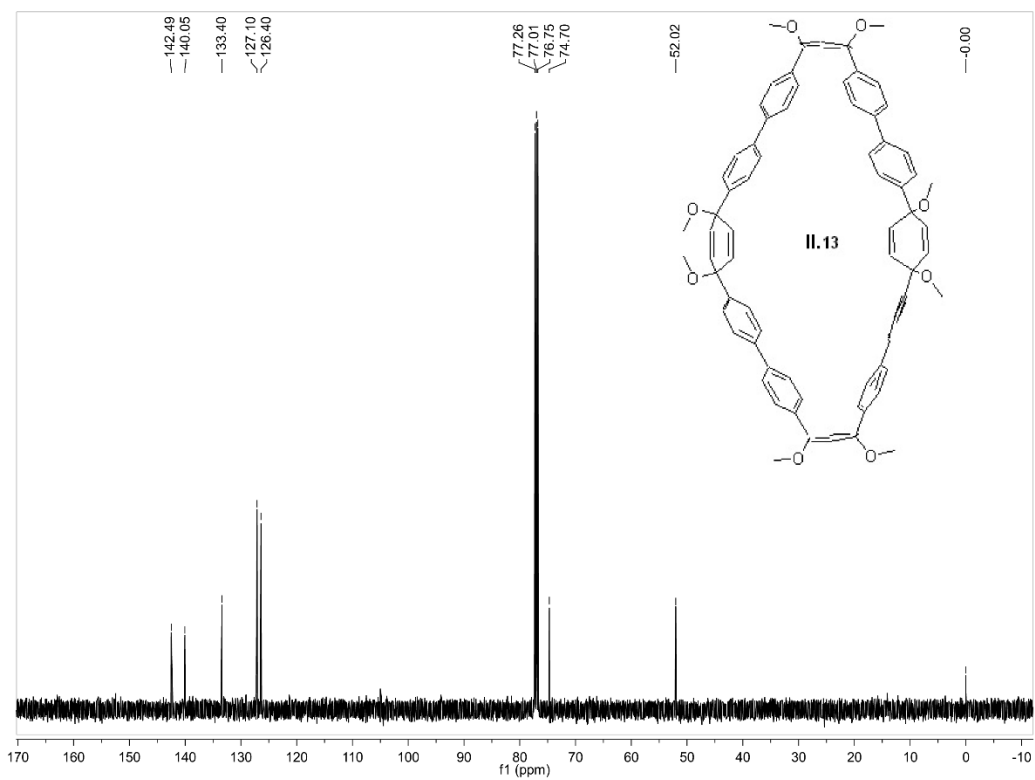


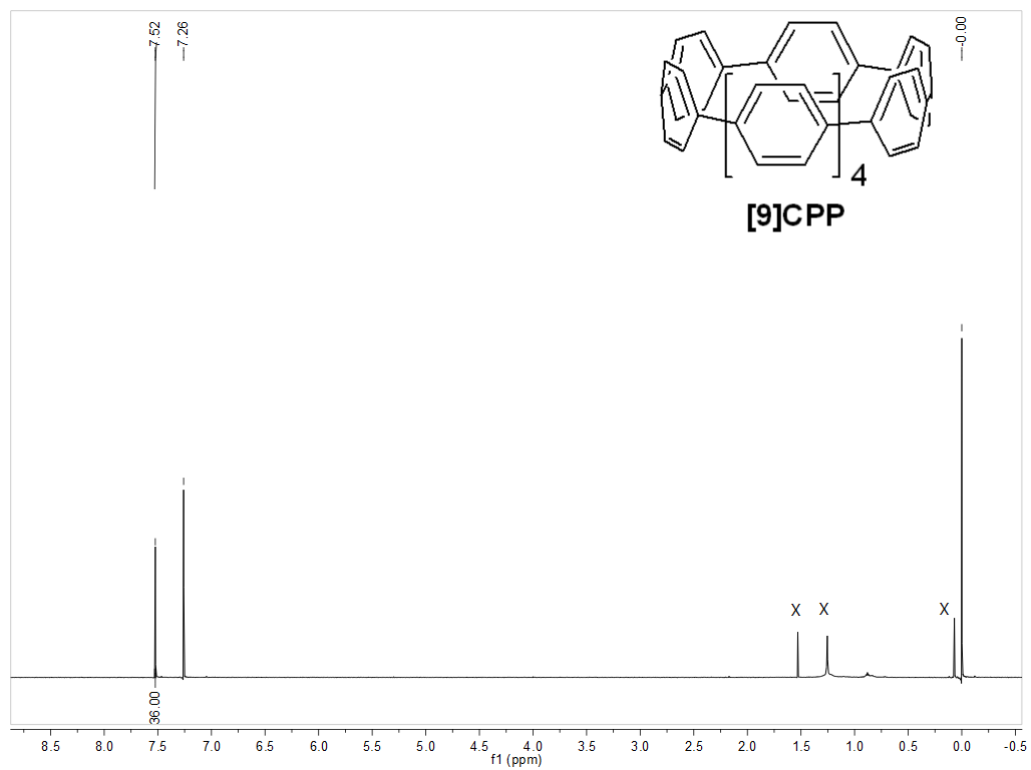
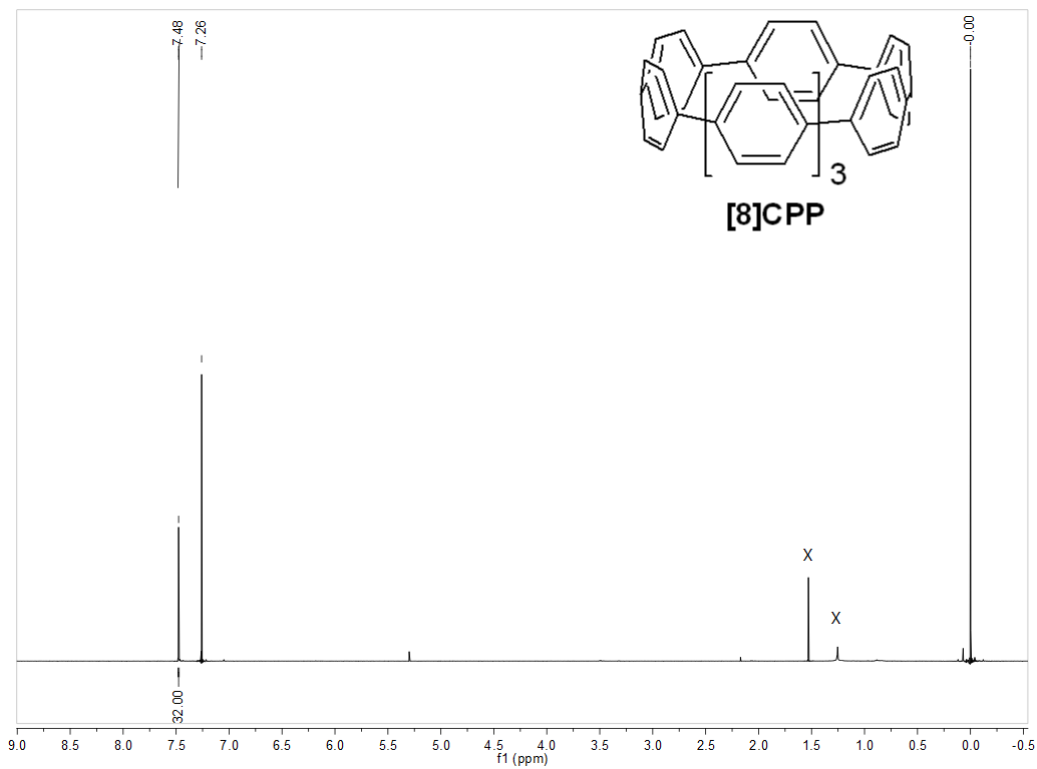


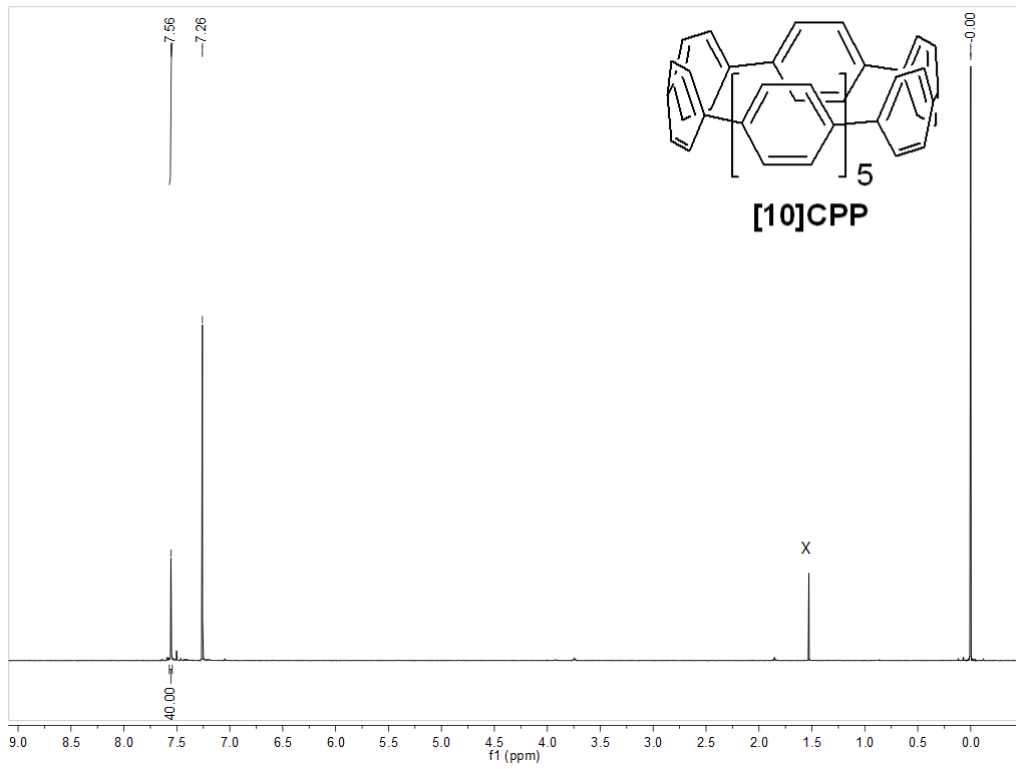
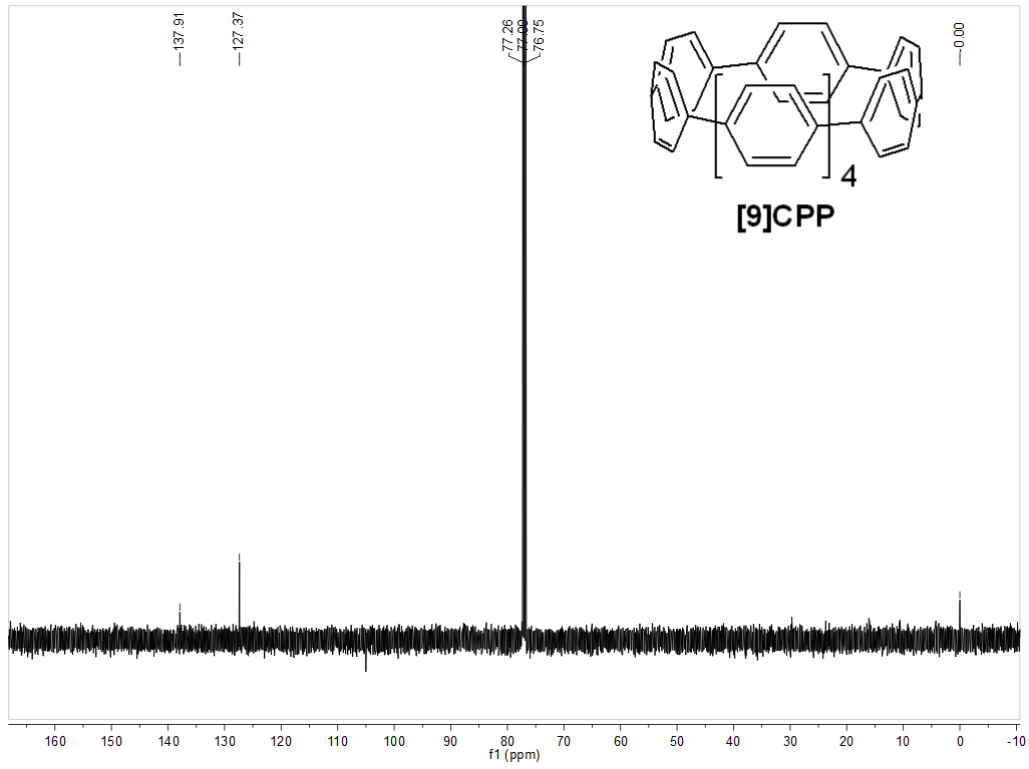


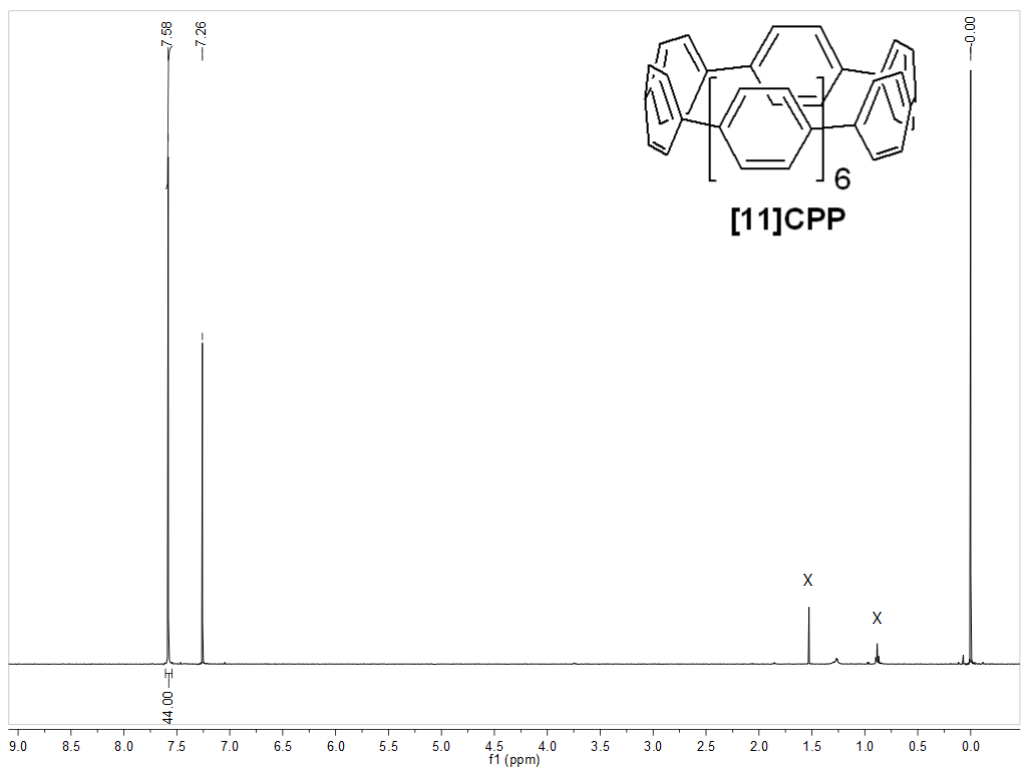
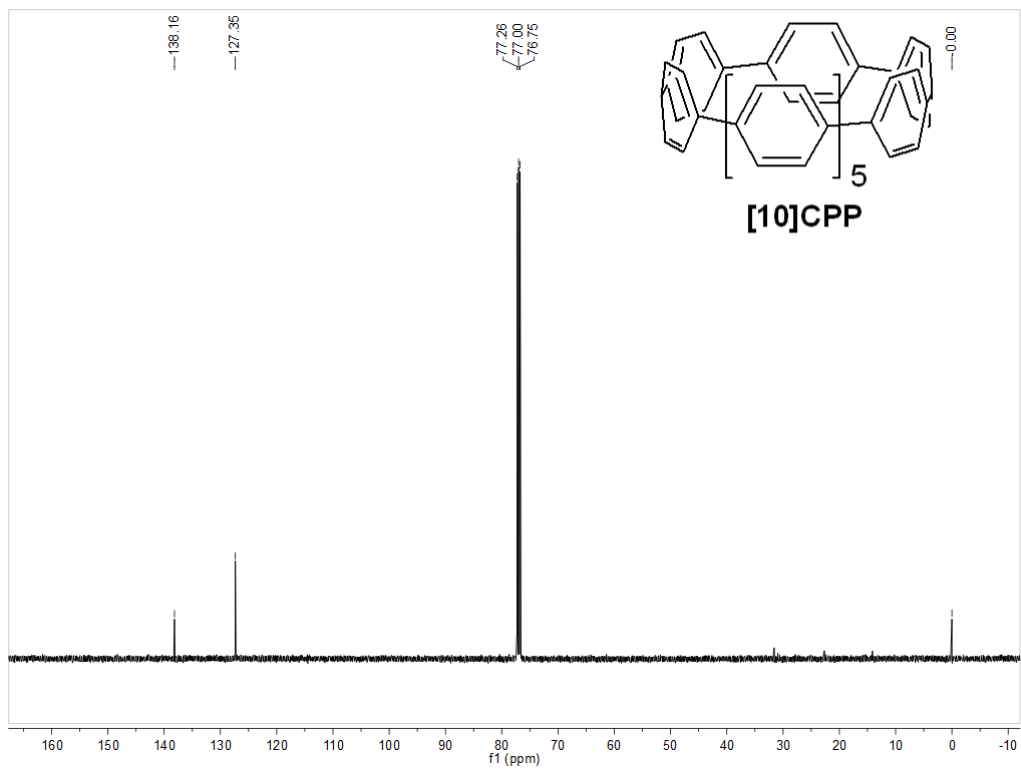


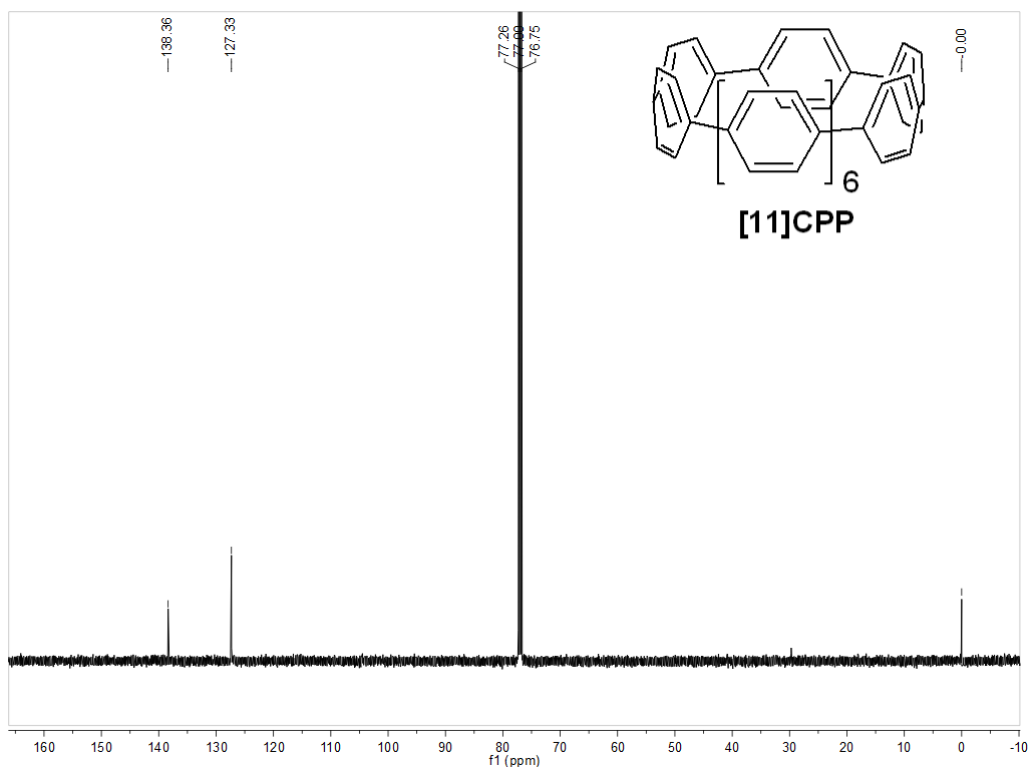






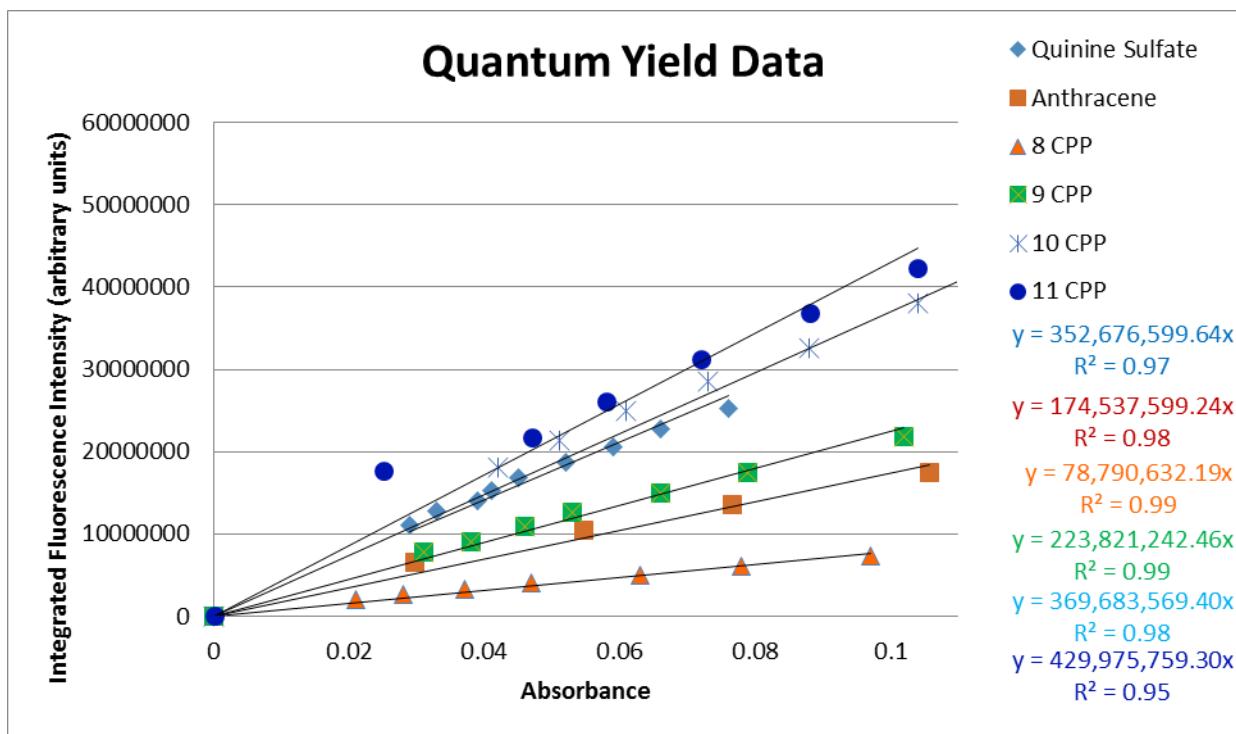






II.5.6. Fluorescence Quantum Yield Data.

Relative quantum yields for [8]cycloparaphenylene, [9]cycloparaphenylene, [10]cycloparaphenylene and [11]cycloparaphenylene (dichloromethane) were determined as described by Williams using anthracene (ethanol) and quinine sulfate (0.1 M H₂SO₄) as standards. All CPP samples were purified by preparative TLC followed by slow crystallization from chloroform with hexanes to give fine crystalline material. The NMR of each crystalline sample was greatly enhanced to make sure there were no traces of impurities. Excitation occurred at 339 nm for all standards and cycloparaphenylene samples. The fluorescence of [8]cycloparaphenylene was integrated from 450 – 650 nm. The fluorescence of [9]cycloparaphenylene was integrated from 400 – 650 nm. The fluorescence of [10]cycloparaphenylene was integrated from 375 – 625 nm. The fluorescence of [11]cycloparaphenylene was integrated from 400 – 600 nm. The fluorescence of [7]cycloparaphenylene and [12]cycloparaphenylene were as previously reported. The fluorescence of anthracene was integrated from 360 – 480 nm. The fluorescence of quinine sulfate was integrated from 400 – 600 nm.



II.5.7. Computational Details.

The Gaussian 03 program² running on an IBM pSeries 655 system was used for optimization of structure 8, 9, 10, 11, 12, and 13 at the (B3LYP/6-31G*) level of theory. Structures were minimized with no symmetry restrictions.

Energy minimized structure of the ground state of [7] macrocycle (**II.8**):

C	-6.11167400	-0.07121700	-1.09765400
C	-3.75193500	-3.53227900	-0.47652400
C	0.63410500	-3.80603600	-1.30293100
C	4.28418400	-1.41238000	-1.29289100
C	5.78908900	1.81919400	-0.88830900
C	1.46815600	1.89665300	-1.00005200
C	-2.82139000	1.15783800	-0.67747300
C	-5.64665300	1.15882400	-1.32023100
C	-4.92585700	-2.78114900	-0.43981100
C	-0.74407600	-3.81107800	-1.10767600
C	3.14858300	-2.21564100	-1.34387200
C	6.33629600	0.60847700	-1.02716300

C	2.86035100	1.88199200	-0.92955600
C	-1.43356100	1.24046800	-0.59843700
C	-5.18287600	2.08560800	-0.21557000
C	-5.06108200	-1.69422500	0.43987600
C	-1.29182000	-3.73179200	0.18453000
C	2.90153400	-3.19226400	-0.36654200
C	6.28177200	-0.47241700	0.03462100
C	3.53373000	2.38073800	0.18962200
C	-0.79671800	2.34583100	-0.01150500
C	-3.63675300	2.17397600	-0.16474900
C	-6.22809900	-0.70213100	0.28142500
C	-2.67614600	-3.23313500	0.37874500
C	1.51887200	-3.71002300	-0.21437000
C	5.21535800	-1.54877800	-0.26085700
C	5.06702000	2.29118600	0.35920600
C	0.68725700	2.41029800	0.04720100
C	-6.19196300	0.37938100	1.34096000
C	-2.87383300	-2.22921000	1.33943000
C	0.96989200	-3.84032400	1.07354500
C	5.05466800	-2.62872200	0.62387100
C	5.37426900	1.35537700	1.50911800
C	1.36872200	2.95428900	1.15103300
C	-3.00906900	3.27516600	0.43711400
C	-5.71333700	1.60491900	1.12283900
C	-4.03900900	-1.47134200	1.36529800
C	-0.40625800	-3.85678100	1.26844100
C	3.92140700	-3.43502300	0.57272400
C	5.91990700	0.14978900	1.36872400
C	2.75977000	2.94228300	1.21847400
C	-1.61868200	3.36056500	0.51008600
O	-5.75149400	3.40578000	-0.34288100

O	-7.42471100	-1.49324000	0.37771500
O	5.58959900	3.56271600	0.80765200
O	7.57499500	-1.06785600	0.25692800
C	-8.64082000	-0.78256800	0.18946200
C	-5.52280800	4.09328700	-1.56321300
C	5.41101400	4.67445700	-0.05508500
C	8.12083100	-1.82318300	-0.81211800
H	-6.39384500	-0.71460200	-1.92868400
H	-3.65759400	-4.33911100	-1.19922300
H	1.02417000	-3.78614200	-2.31702100
H	4.40017300	-0.62001500	-2.02393500
H	5.86291700	2.53129500	-1.70714700
H	0.98023700	1.51183300	-1.89114100
H	-3.27114600	0.28166000	-1.13109800
H	-5.53272000	1.51609100	-2.34056200
H	-5.73455100	-3.01889400	-1.12466200
H	-1.40157600	-3.75896900	-1.97142800
H	2.39129000	-2.00232100	-2.09190200
H	6.84294400	0.35766900	-1.95652000
H	3.42534700	1.46917500	-1.75811900
H	-0.83558000	0.41630300	-0.97625200
H	-6.54314100	0.08713300	2.32868800
H	-2.06312300	-1.96373000	2.01048500
H	1.62284000	-3.80554600	1.94070500
H	5.80362300	-2.80504200	1.39108300
H	5.11573200	1.73623200	2.49331700
H	0.80037000	3.35838200	1.98465200
H	-3.61922600	4.08242900	0.83144400
H	-5.67517700	2.34598600	1.91766400
H	-4.11244700	-0.65025100	2.06893500
H	-0.79839600	-3.87180300	2.28160100

H	3.80197200	-4.22974400	1.30465200
H	6.11195900	-0.47783700	2.23449300
H	3.25688400	3.36486600	2.08695900
H	-1.16495600	4.24270600	0.95449300
H	-9.44073100	-1.51998900	0.29407700
H	-8.77800100	0.00629900	0.94143300
H	-8.70350000	-0.32299800	-0.80670900
H	-4.46389400	4.08558800	-1.85408700
H	-6.12391300	3.68466900	-2.38711300
H	-5.83352800	5.12724700	-1.39014200
H	5.70777900	5.55404200	0.52261700
H	6.04921900	4.61787100	-0.94821500
H	4.36610500	4.79252900	-0.37159400
H	9.01443000	-2.30987200	-0.41234900
H	7.42519400	-2.59299200	-1.17251900
H	8.42251700	-1.19273100	-1.66072600

Total energy: -2077.72961824 a.u.

Energy minimized structure of the ground state of [8] macrocycle (**II.9**):

C	6.55463300	-1.06732100	-1.20184400
C	4.38253300	2.56557300	-1.05158100
C	1.45344700	5.59819600	-0.87881400
C	-2.70351400	4.48626400	-1.36225000
C	-5.10668800	0.88438800	-1.12598400
C	-5.80199200	-2.67994400	-0.91294500
C	-1.46817600	-2.40823200	-0.98576000
C	2.91101200	-1.88678400	-0.68040800
C	5.84960700	-2.19897800	-1.26852400
C	5.17976700	1.42492500	-1.09019700
C	2.75529000	5.10688200	-0.88452400
C	-1.43898400	5.04378500	-1.22575700
C	-4.33512300	2.03851800	-1.20137600

C	-6.58246700	-1.59969700	-0.99600200
C	-2.86169400	-2.42841500	-0.89892700
C	1.51733900	-1.91436900	-0.64032200
C	5.21189900	-2.88082600	-0.07482700
C	6.02110100	1.09961200	-0.02270300
C	3.25525700	4.37060400	0.20355800
C	-0.89033100	5.31043000	0.04298000
C	-4.52622300	3.10889000	-0.31137600
C	-6.78643700	-0.60408400	0.12676300
C	-3.51229300	-3.07642600	0.15645300
C	0.82034500	-3.00322900	-0.08746300
C	3.66943000	-2.94329100	-0.15984200
C	6.75121100	-0.25138900	0.05721600
C	4.38131800	3.41346600	0.06634300
C	0.58684700	5.34607100	0.20245000
C	-3.47196500	4.14951600	-0.23484400
C	-6.10290800	0.74930400	-0.15613400
C	-5.04643200	-3.09979500	0.33020300
C	-0.66505600	-3.02758300	-0.01466600
C	6.23906100	-1.01206000	1.26591800
C	5.30283600	3.14112000	1.09169400
C	1.16328600	4.79833300	1.36321100
C	-3.01997100	4.62413500	1.00903400
C	-6.37118000	1.85487400	0.66763800
C	-5.42623000	-2.21972800	1.50084600
C	-1.32656000	-3.67666300	1.04462900
C	2.98174500	-4.03172400	0.39321200
C	5.57532300	-2.16622500	1.20909800
C	6.11647800	2.01163100	1.04029600
C	2.47155100	4.32812400	1.36717500
C	-1.76187900	5.20451900	1.14276000

C	-5.59877400	3.01196000	0.59297200
C	-6.19956300	-1.14013400	1.41489300
C	-2.71455900	-3.70681200	1.12397500
C	1.58957200	-4.06532400	0.41839600
O	5.75454900	-4.20891000	0.10318900
O	8.14278900	0.09014100	0.23074100
O	-5.46193600	-4.42001200	0.75862200
O	-8.18449800	-0.41428800	0.42723000
C	9.02906700	-1.00866100	0.40110100
C	5.72085900	-5.07773500	-1.01989700
C	-5.26554300	-5.48644300	-0.15695600
C	-8.99580200	0.10439700	-0.61504600
H	7.01850100	-0.65789900	-2.09777100
H	3.68048700	2.75011700	-1.85958300
H	1.08324400	6.11044000	-1.76244300
H	-3.05766500	4.21910200	-2.35398000
H	-4.88430800	0.05782800	-1.79244200
H	-5.70042500	-3.32668500	-1.78189800
H	-1.00077500	-1.92101800	-1.83709000
H	3.41132600	-1.01444900	-1.09062600
H	5.72575400	-2.69404300	-2.22895800
H	5.09884700	0.75911800	-1.94296600
H	3.36952500	5.23401500	-1.77242900
H	-0.82471400	5.15308400	-2.11380500
H	-3.50962600	2.06946700	-1.90533700
H	-7.09359700	-1.38667600	-1.93256700
H	-3.44501400	-1.93623700	-1.67112900
H	0.96357000	-1.05750400	-1.01374200
H	6.44473900	-0.54921700	2.22846800
H	5.35964500	3.80336600	1.95209300
H	0.54323000	4.59754500	2.23064700

H	-3.60513200	4.42883300	1.90344200
H	-7.17483600	1.78979200	1.39576700
H	-5.02978600	-2.53841000	2.46126000
H	-0.74402400	-4.14513100	1.83263200
H	3.54797400	-4.85903200	0.80808500
H	5.23551300	-2.66082700	2.11582300
H	6.81363300	1.81774900	1.84984000
H	2.83555400	3.78628900	2.23573200
H	-1.41813000	5.48068700	2.13549600
H	-5.81172400	3.83759600	1.26738200
H	-6.43954400	-0.55899800	2.30137200
H	-3.19399100	-4.22851000	1.94689200
H	1.09299200	-4.94078500	0.82725300
H	10.02509900	-0.57392000	0.51769700
H	8.78699300	-1.60360300	1.29154200
H	9.02808500	-1.67746500	-0.47042700
H	4.73695100	-5.09258600	-1.50804700
H	6.48613200	-4.81837400	-1.76381400
H	5.93726800	-6.07801800	-0.63465000
H	-5.43954500	-6.40557100	0.40919200
H	-5.97971800	-5.45392500	-0.99140400
H	-4.24425900	-5.50708500	-0.56076900
H	-9.95390000	0.35936000	-0.15420500
H	-8.56530800	1.00943300	-1.06483300
H	-9.17906900	-0.63517500	-1.40704400

Total energy: -2308.77760787 a.u.

Energy minimized structure of the ground state of [9] macrocycle (**II.10**):

C	-5.54463100	-4.32845100	-1.06146300
C	-1.26526600	-3.94414400	-0.85310200
C	3.05243700	-3.46888500	-0.46118100

C	6.44188600	-2.50246900	-1.28095800
C	5.47920700	1.67225700	-0.67077800
C	2.18568500	4.67487900	-0.84063200
C	-0.76146700	7.03924700	-1.16123700
C	-2.59243500	3.07919200	-0.74366700
C	-4.88107300	-0.63632400	-1.12397300
C	-6.26752000	-3.20816900	-1.13827700
C	-2.65666400	-3.96751600	-0.80307100
C	1.66474800	-3.51951900	-0.38107000
C	5.82272600	-3.67290200	-1.42422300
C	6.23013300	0.50154600	-0.70663800
C	2.97340100	3.52322300	-0.85600100
C	0.55642600	7.04453100	-0.95274200
C	-1.91934600	4.29703600	-0.70391600
C	-4.27785800	0.61726700	-1.21928400
C	-6.51218200	-2.26991800	0.02359400
C	-3.33068000	-4.82516300	0.07105600
C	0.99299800	-4.71254000	-0.06171700
C	5.37282800	-4.53907400	-0.26933500
C	5.96572100	-0.55430400	0.17961300
C	3.63856000	3.08788000	0.29717400
C	1.21428900	6.74057500	0.37564600
C	-2.57524200	5.46982400	-0.30872100
C	-4.64634000	1.67084800	-0.36838200
C	-5.88847500	-0.88148900	-0.18638500
C	-4.86226000	-4.81975700	0.19745200
C	-0.48966000	-4.76360400	-0.01726600
C	3.83076000	-4.60584800	-0.20749000
C	6.77728600	-1.86095900	0.04837200
C	4.45461900	1.84527100	0.27499200
C	2.05380600	5.44605000	0.32012600

C	-1.79625000	6.78448700	-0.08707800
C	-3.95316300	2.98326100	-0.40282600
C	-5.23594600	-3.96292000	1.39050600
C	-1.17477800	-5.62486100	0.85734100
C	3.17274000	-5.78941900	0.14617000
C	6.51648900	-2.82419100	1.18499800
C	4.21271600	0.80324600	1.17985500
C	2.74209600	5.02393900	1.46856400
C	-1.14048800	6.69235300	1.27229000
C	-4.61156600	4.17039500	-0.04245600
C	-6.29117000	0.17785600	0.63935800
C	-5.95936400	-2.84470900	1.31388200
C	-2.56564300	-5.66033000	0.89732900
C	1.78078400	-5.84393600	0.20631800
C	5.90322300	-3.99923000	1.04179600
C	4.94694900	-0.38286600	1.12367500
C	3.50378500	3.85879900	1.46385500
C	0.17449200	6.64844200	1.47117700
C	-3.93428800	5.38634800	0.01671800
C	-5.67764200	1.42246600	0.55557100
O	-7.92917700	-2.00823000	0.15235200
O	-5.21137500	-6.20164900	0.43537400
O	-2.70908100	7.89494400	0.03469000
O	2.05328500	7.83780000	0.81479300
O	5.92765900	-5.86922900	-0.33589700
C	-6.58093200	-6.46966200	0.69091800
C	-8.74792100	-3.12599900	0.45911200
C	-3.31521100	8.37043900	-1.15789900
C	3.15619700	8.17995000	-0.00881900
C	5.85328200	-6.54214100	-1.58365300
O	8.18423300	-1.54920900	-0.07601900

C	8.80638400	-0.93989200	1.04445700
H	-5.41694900	-4.96710900	-1.93389100
H	-0.77547900	-3.29168100	-1.57000400
H	3.53646400	-2.53046200	-0.71403700
H	6.73536400	-1.92451000	-2.15364700
H	5.70008300	2.47576000	-1.36876000
H	1.66526000	4.96447700	-1.74798700
H	-1.14195500	7.23216600	-2.16140600
H	-2.03871000	2.18041800	-0.99962000
H	-4.56377300	-1.42696300	-1.79640200
H	-6.74229800	-2.91867700	-2.07437000
H	-3.22051900	-3.31378500	-1.46006100
H	1.09395400	-2.61147100	-0.55224500
H	5.58358700	-4.03140200	-2.42208200
H	7.04079000	0.40423200	-1.42287100
H	3.05405800	2.94037400	-1.76985000
H	1.22046300	7.25649700	-1.78762600
H	-0.85950100	4.32495500	-0.93984100
H	-3.51534500	0.77894700	-1.97587100
H	-4.84282400	-4.30472600	2.34606400
H	-0.61176500	-6.26057600	1.53509300
H	3.75863300	-6.67706000	0.36032500
H	6.84844000	-2.51474800	2.17319700
H	3.41909200	0.90819800	1.91504300
H	2.69171300	5.62297000	2.37293000
H	-1.83342700	6.64248000	2.10829700
H	-5.67130600	4.14636100	0.19530000
H	-7.08845700	0.01842400	1.35780000
H	-6.16644400	-2.25936700	2.20741400
H	-3.06848400	-6.34248700	1.57408900
H	1.29969300	-6.78997600	0.43863400

H	5.74992500	-4.65642600	1.89455200
H	4.70780200	-1.18715500	1.81246300
H	4.02547200	3.55294600	2.36706600
H	0.57176200	6.57466000	2.47961200
H	-4.45901500	6.28100900	0.33433000
H	-5.98050600	2.20568800	1.24427200
H	-6.64680900	-7.54669200	0.86603200
H	-6.94974200	-5.93823100	1.57844700
H	-7.22044100	-6.20772600	-0.16319100
H	-8.70455500	-3.89707000	-0.32223900
H	-8.47906900	-3.58780300	1.41879800
H	-9.76879100	-2.74018300	0.52169300
H	-4.12823100	9.02954300	-0.84108500
H	-2.61468100	8.95262400	-1.77167200
H	-3.73611300	7.55869000	-1.76735100
H	3.73656100	8.91327500	0.55757400
H	3.79652400	7.31544900	-0.23057100
H	2.84352600	8.64361200	-0.95514300
H	6.11869000	-7.58322500	-1.38011500
H	4.84367300	-6.51386500	-2.01639400
H	6.56736000	-6.13577000	-2.31223300
H	9.79149200	-0.61241800	0.70133200
H	8.24803200	-0.06562400	1.40584200
H	8.94526600	-1.64446000	1.87595800

Total energy: -2770.04797540 a.u.

Energy minimized structure of the ground state of [10] macrocycle (**II.11**):

C	4.25549100	-3.29008600	-1.08103400
C	7.66943700	-2.39927300	-0.26188100
C	6.41827700	1.75811500	0.55306600
C	2.20484000	3.99122700	-0.50616400

C	-0.36827200	6.48107900	-1.65433900
C	-2.85037900	3.10623400	-0.66045800
C	-5.86952700	-0.05028600	-0.37529600
C	-7.60677600	-2.50011000	0.13595200
C	-4.43979000	-3.12972200	-0.79424200
C	2.90097200	-3.22794000	-1.39706600
C	7.15139400	-3.51827500	-0.76755100
C	7.17913200	0.60612600	0.73812600
C	2.97463200	2.85778100	-0.25840500
C	0.96266800	6.42938100	-1.57831600
C	-1.98327400	4.17826600	-0.85989200
C	-5.09151100	1.07690800	-0.64052700
C	-7.30085500	-1.46236800	1.26300600
C	-5.57521100	-3.85561300	-0.69736700
C	2.03608300	-4.30110200	-1.12728900
C	6.26609600	-4.46408900	0.01284600
C	6.57052800	-0.61684300	1.05420200
C	4.19718700	2.94390700	0.42752600
C	1.75275700	6.51189600	-0.28930700
C	-2.27196800	5.44586700	-0.34290700
C	-4.93975400	2.10089700	0.30592800
C	-6.53544900	-0.19762300	0.84568700
C	-6.66320300	-3.73764700	0.35870800
C	-3.67962000	-3.52138200	-2.04238500
C	4.79983000	-4.42592500	-0.47086200
C	7.42709900	-1.89921800	1.14739100
C	5.01808600	1.73116100	0.66899100
C	2.62273600	5.25575900	-0.07539200
C	-1.28922000	6.62796400	-0.46266800
C	-4.04627800	3.25961600	0.05913800
C	-6.07750900	-3.45939500	1.73015800

C	-4.52525300	-4.65400500	-2.59067700
C	3.94757000	-5.50961500	-0.21498300
C	6.76708700	-2.97215300	1.98419000
C	4.41655000	0.50700100	1.00150100
C	3.83502500	5.34648100	0.62158800
C	-0.49652100	6.73368500	0.82269700
C	-4.34016100	4.53925600	0.56126800
C	-6.41897600	0.84521700	1.77924600
C	-6.41927700	-2.26522200	2.21176800
C	-5.62148900	-4.80965700	-1.82539600
C	2.59471700	-5.45038300	-0.54172700
C	6.27361000	-4.10476900	1.48433300
C	5.17758700	-0.64430100	1.19311100
C	4.60975700	4.21370900	0.86305100
C	0.83155200	6.68214400	0.89880800
C	-3.46997600	5.60848800	0.36726900
C	-5.63808800	1.96548900	1.51826000
O	-8.48645100	-0.94963600	1.89960500
O	-7.33897200	-5.00542200	0.28877600
O	-2.02131500	7.87418000	-0.51388300
O	2.57981200	7.69666000	-0.25198300
O	6.76663500	-5.81669600	-0.01530400
C	-8.33351800	-5.28474900	1.25461600
C	-9.27300700	-1.84732900	2.66066400
C	-2.78044600	8.12332500	-1.68754500
C	3.42563000	7.92702400	-1.36879900
C	6.96354600	-6.39913000	-1.29474100
O	8.74929500	-1.58060400	1.62996700
C	8.85551600	-1.17284900	2.98555800
H	-8.64730800	-2.81829800	0.23281800
H	-3.75913400	-2.68451600	-2.75858700

H	4.88825800	-2.43224900	-1.28414400
H	8.30064400	-1.75348700	-0.86781800
H	6.91393800	2.68625600	0.28080100
H	1.26788800	3.88859700	-1.04491000
H	-0.84797200	6.39932800	-2.62748600
H	-2.57723200	2.12611500	-1.04110600
H	-5.93167800	-0.82191500	-1.13385200
H	-7.50700300	-2.08373700	-0.86680300
H	-4.09837600	-2.35856600	-0.11484200
H	2.50205200	-2.31367500	-1.82693800
H	7.34412600	-3.77382500	-1.80645800
H	8.25860400	0.64605900	0.62860400
H	2.63636300	1.89330200	-0.62709300
H	1.54258800	6.30490700	-2.49035400
H	-1.06266300	4.01777300	-1.41290400
H	-4.60309600	1.16372700	-1.60726100
H	-5.41365000	-4.17521300	2.20688300
H	-4.26820700	-5.20613600	-3.48754000
H	4.35526500	-6.40637300	0.24165400
H	6.68393700	-2.77815500	3.05059200
H	3.33888000	0.45886000	1.13179200
H	4.16689500	6.31642200	0.97777500
H	-1.09610400	6.87563900	1.71834500
H	-5.27140000	4.70326400	1.09668600
H	-6.94482900	0.76803500	2.72482400
H	-6.07912400	-1.83691200	3.15072300
H	-6.42726100	-5.51619500	-1.97664700
H	1.96418100	-6.31419100	-0.34890000
H	5.81067800	-4.84552000	2.13201800
H	4.67934500	-1.57479300	1.44551300
H	5.53789000	4.31209800	1.41998200

H	1.33590400	6.78210800	1.85670800
H	-3.72027600	6.58906400	0.76024600
H	-5.53704200	2.73035300	2.28325600
H	-8.57149700	-6.34634500	1.14441200
H	-7.98549000	-5.10221400	2.27993300
H	-9.25466600	-4.70710800	1.09072400
H	-9.77788300	-2.59950600	2.03823600
H	-8.69124900	-2.37028100	3.43183900
H	-10.03813500	-1.23615900	3.14699200
H	-3.39864300	8.99759000	-1.46649500
H	-2.14127000	8.35759400	-2.54978400
H	-3.43748300	7.28167200	-1.94678700
H	4.10595700	8.72953400	-1.07095300
H	4.01918000	7.04127900	-1.63463500
H	2.86095600	8.25794000	-2.25094800
H	7.12190300	-7.46686000	-1.12034100
H	6.08960000	-6.27244200	-1.94817300
H	7.85088100	-5.99439900	-1.80002200
H	9.86599200	-0.77187100	3.10249800
H	8.13086000	-0.38808800	3.24206700
H	8.73311400	-2.01466800	3.68040800
C	-1.73780300	-4.59261900	-0.78709100
C	-0.37540200	-4.77969500	-0.57245400
C	0.58423600	-4.18812100	-1.41394600
C	0.11611600	-3.43352100	-2.50105200
C	-1.24781500	-3.23888600	-2.70735000
C	-2.19799800	-3.79900400	-1.84679300
H	-2.45759700	-5.03753700	-0.10493200
H	-0.04879200	-5.35538300	0.28916600
H	0.82676700	-2.99299800	-3.19459900
H	-1.57813800	-2.63234500	-3.54813300

Total energy: -2924.86235588 a.u.

Energy minimized structure of the ground state of [11] macrocycle (**II.12**):

Total energy: -3232.15665363 a.u.

C	-9.23894800	-2.53320200	-1.26378000
C	-5.84436000	-5.32385400	-0.12891800
C	6.83707600	-2.86660800	-0.91360800
C	9.71932400	-0.84325100	-1.29529300
C	6.94979600	2.52286900	-0.95910300
C	2.73404500	4.13140800	-0.91339300
C	-0.71920100	6.21665200	-1.10484300
C	-3.66625900	3.05886100	-0.40904300
C	-7.17881100	0.49733100	-1.02464000
C	-9.45363200	-1.22596800	-1.42428200
C	-7.18580600	-4.94485600	-0.18823500
C	5.51070700	-3.28171700	-0.85371800
C	9.59072000	-2.16573500	-1.39079200
C	8.10567300	1.74579000	-0.95713300
C	3.83436700	3.27055500	-0.95334900
C	0.61221500	6.13655900	-1.06659900
C	-2.60005300	3.95445200	-0.36941400
C	-6.10398800	1.38444800	-0.97920900
C	-9.53439600	-0.23851900	-0.28139700
C	-7.58368600	-3.66127700	0.20688500
C	5.12623800	-4.38794200	-0.08030600
C	9.30205800	-3.06385300	-0.20868200
C	8.31505400	0.76256100	0.02266600
C	4.77524700	3.25402200	0.08355600
C	1.42072200	6.06438100	0.21155700
C	-2.79429400	5.29163400	0.00117700
C	-6.12448300	2.52032000	-0.15473500

C	-8.33213100	0.72199800	-0.26562600
C	-9.04883300	-3.20583100	0.08413100
C	-4.85852700	-4.43624500	0.33055400
C	7.83472000	-3.54558800	-0.20574300
C	9.62071300	-0.06378700	-0.00027300
C	5.97471600	2.37057800	0.04073500
C	2.55541700	5.02526700	0.14807800
C	-1.60469600	6.26157300	0.12494200
C	-4.97836100	3.46577300	-0.10261100
C	-9.41027900	-2.26686300	1.21409100
C	-5.27006000	-3.15438000	0.72999500
C	7.46020900	-4.65790300	0.56282000
C	9.72379100	-1.00440100	1.18024600
C	6.18600100	1.39131100	1.01934000
C	3.49429200	5.00064800	1.19159500
C	-0.80961400	5.91967200	1.36896300
C	-5.16154000	4.81019300	0.26013000
C	-8.36695700	1.85992800	0.55298400
C	-9.61480300	-0.95837300	1.05336800
C	-6.60480000	-2.77268100	0.66669600
C	6.13035100	-5.06989200	0.62746400
C	9.57967300	-2.32566900	1.08477000
C	7.32914400	0.59059500	1.00079800
C	4.57257900	4.12228500	1.16920900
C	0.51689900	5.81121700	1.40178800
C	-4.09150200	5.69911400	0.32876900
C	-7.28373300	2.72981400	0.61638900
O	-10.67912600	0.62803100	-0.44641600
O	-9.83406400	-4.40925900	0.15691300
O	-2.08673200	7.60260500	0.37442200
O	2.00299100	7.36132600	0.52304100

O	10.19791200	-4.19292400	-0.15174800
C	-11.23655400	-4.24142900	0.02170600
C	-11.94660600	-0.01135200	-0.43257700
C	-2.51840300	8.35517200	-0.74965800
C	2.84743800	7.93110500	-0.46504700
C	10.22429000	-5.05086300	-1.28180400
O	10.75651800	0.82982900	-0.07244200
C	10.94780600	1.72267800	1.01297600
H	-9.16249400	-3.19756500	-2.12274700
H	-5.56256200	-6.33140900	-0.42434900
H	7.09294600	-1.99275800	-1.50302000
H	9.91710100	-0.24010600	-2.17768100
H	6.81395500	3.28432700	-1.72292500
H	2.01460200	4.09910800	-1.72584400
H	-1.22468200	6.27793000	-2.06622500
H	-3.46827700	2.02062000	-0.65865700
H	-7.11630300	-0.37348500	-1.66899200
H	-9.56001400	-0.79613400	-2.41868800
H	-7.93448500	-5.65164900	-0.52754600
H	4.75319900	-2.71478400	-1.38721800
H	9.64930300	-2.64034200	-2.36692400
H	8.86802200	1.92109500	-1.71088900
H	3.95758700	2.59619900	-1.79688800
H	1.16811100	6.15224400	-2.00114500
H	-1.59861600	3.60338200	-0.60594400
H	-5.24647000	1.19661700	-1.61833800
H	-9.45267800	-2.72414200	2.20080800
H	-4.52820100	-2.43414900	1.06258700
H	8.22397500	-5.20988700	1.10277800
H	9.90238600	-0.55560300	2.15404100
H	5.44110900	1.24466100	1.79714700

H	3.39377200	5.70537000	2.01175600
H	-1.39710500	5.79227300	2.27469200
H	-6.15939300	5.17866700	0.47802800
H	-9.25549600	2.06820100	1.14049100
H	-9.83601100	-0.32316700	1.90896300
H	-6.88262300	-1.76881000	0.96900500
H	5.86962400	-5.94392000	1.21894200
H	9.65459000	-2.96287800	1.96259100
H	7.44895300	-0.17688200	1.75855500
H	5.29303100	4.13157000	1.98297900
H	1.02194700	5.59547200	2.33946900
H	-4.26133800	6.72305400	0.64152400
H	-7.33535500	3.57818000	1.29200500
H	-11.66838900	-5.24253000	0.09863300
H	-11.65407700	-3.60893900	0.81689700
H	-11.51091400	-3.80566100	-0.94877900
H	-12.05053400	-0.74031500	-1.24806800
H	-12.14325700	-0.52459900	0.51881100
H	-12.68464000	0.78334000	-0.56879700
H	-2.98038100	9.25916300	-0.34336000
H	-1.67865900	8.64796400	-1.39364700
H	-3.26355300	7.82014800	-1.35577500
H	3.29356900	8.81626700	-0.00374600
H	3.65154100	7.24855900	-0.77318600
H	2.28608000	8.24658300	-1.35566900
H	10.77995300	-5.94040100	-0.97280100
H	9.21716400	-5.35414800	-1.59796100
H	10.74609900	-4.59614500	-2.13495000
H	11.74662500	2.40250700	0.70454500
H	10.04647900	2.31029300	1.23317100
H	11.26890500	1.20553200	1.92793100

C	1.71143800	-5.29001400	1.31012200
C	3.08837700	-5.10511000	1.21819300
C	3.69298600	-4.75943300	-0.00135600
C	2.87159400	-4.68463800	-1.13855800
C	1.49760800	-4.87328600	-1.04772600
C	0.88152300	-5.14279900	0.18586200
H	1.26966000	-5.53206100	2.27299800
H	3.69754500	-5.17669500	2.11535500
H	3.31594300	-4.45475700	-2.10296200
H	0.88405700	-4.75297900	-1.93613000
C	-2.80086500	-5.47658900	-0.68903900
C	-1.41990400	-5.65095400	-0.72430300
C	-0.59687800	-5.14210400	0.29450400
C	-1.22244800	-4.51421600	1.38460600
C	-2.60050100	-4.33704800	1.41778300
C	-3.41695200	-4.78122900	0.36424200
H	-3.40580300	-5.83829800	-1.51626300
H	-0.97032500	-6.17244900	-1.56508300
H	-0.61461600	-4.10868000	2.18851000
H	-3.05224100	-3.82770100	2.26443500

Total energy: -3232.15665363 a.u.

Energy minimized structure of the ground state of [12] macrocycle (**II.13**):

C	-1.65680900	8.12608400	2.14298900
C	2.81909000	7.74204000	0.75676200
C	3.85158500	-5.22534700	0.67681400
C	1.65380000	-7.87283900	2.23115400
C	-2.52226800	-7.01334400	1.22901300
C	-5.74254700	-4.15569500	0.32480100
C	-8.92904000	-1.98621500	0.07876400
C	-6.16242000	1.43408100	0.19482600

C	-4.23438800	5.19821400	1.43299400
C	-2.92919600	7.72815500	2.16920400
C	1.62662300	8.43187900	0.96450400
C	4.46312900	-4.03467900	0.29078300
C	2.93642000	-7.51536100	2.25283800
C	-1.37515800	-7.73427500	1.54045000
C	-4.51762200	-4.75800000	0.61248400
C	-8.45365300	-3.22945700	-0.00653800
C	-6.86151300	0.26653000	-0.09936900
C	-4.93732100	4.01360400	1.20382200
C	-3.83872000	7.71458300	0.95989600
C	0.39289200	7.81788400	0.73017100
C	5.80641100	-4.00623800	-0.12037400
C	3.90539400	-7.75568100	1.11715300
C	-0.27656200	-7.75593100	0.66816000
C	-3.88483000	-5.59202400	-0.31952300
C	-7.77681800	-3.80560600	-1.23008100
C	-8.16574800	0.31517300	-0.61080600
C	-5.99758300	3.95673700	0.28474500
C	-4.57986200	6.38020900	0.77025000
C	-0.92854600	8.59165600	0.89855900
C	2.82943500	6.40132200	0.33859700
C	4.55717900	-6.43538700	0.66078500
C	0.97124900	-8.56380900	1.07113700
C	-2.62570000	-6.30226100	0.02109000
C	-6.38756600	-4.38237900	-0.89633800
C	-8.88793500	-0.97555200	-1.04721100
C	-6.74526200	2.70176500	0.01304000
C	-1.79041200	8.41102200	-0.33272500
C	1.58205100	5.77606700	0.15672500
C	5.87975200	-6.42237000	0.20172500

C	1.93019000	-8.76995200	-0.07954400
C	-1.52552800	-6.32136300	-0.84736900
C	-5.74315800	-5.19582400	-1.84080300
C	-8.17604600	-1.54073100	-2.25729400
C	-8.06309500	2.73638500	-0.47147200
C	-5.64462800	6.33220700	-0.14171200
C	-3.06574000	8.02889600	-0.30346100
C	0.39015800	6.47254300	0.33703800
C	6.49348700	-5.23047200	-0.17468200
C	3.21664200	-8.42213700	-0.05437300
C	-0.36534000	-7.02754400	-0.52316700
C	-4.51085800	-5.78005800	-1.56348700
C	-7.67287600	-2.77098400	-2.32951300
C	-8.75219000	1.57029700	-0.79582000
C	-6.32641300	5.14828500	-0.38889400
O	-4.80836300	8.79281100	1.02819600
O	-0.65121000	9.98499500	1.17224900
O	-10.21208400	-0.66104000	-1.53351200
O	-8.58760400	-4.84462400	-1.83731400
O	4.93103700	-8.70858000	1.48204400
C	-0.44006700	10.83937300	0.05805900
C	-5.64741400	8.81732600	2.17339200
C	-11.25980500	-0.56366000	-0.58135700
C	-8.94293400	-5.94314800	-1.01161200
C	5.59342500	-8.49697200	2.72027100
O	0.55719600	-9.83012700	1.64322200
C	-0.06443200	-10.75461700	0.76323300
H	-1.07067500	8.16670300	3.05816600
H	3.75753200	8.27164500	0.89043700
H	2.81423400	-5.21260200	0.99964500
H	1.01732600	-7.68517700	3.09243800

H	-3.36918000	-7.03045300	1.90994100
H	-6.20021200	-3.51096600	1.06903100
H	-9.37961900	-1.65031600	1.00987500
H	-5.13438900	1.35748500	0.53669800
H	-3.41139500	5.19597000	2.14207100
H	-3.37253200	7.42834800	3.11615000
H	1.64996000	9.46388100	1.29561300
H	3.88751400	-3.11330500	0.30599700
H	3.33418900	-7.00737000	3.12816400
H	-1.33474400	-8.31484100	2.45733300
H	-4.04310100	-4.57528700	1.57306100
H	-8.53672900	-3.88680200	0.85618000
H	-6.37253600	-0.69511400	0.03304600
H	-4.66476100	3.12644600	1.76813000
H	-1.31149300	8.60651700	-1.28920400
H	1.54053100	4.72758700	-0.12364600
H	6.43801300	-7.35234000	0.17457700
H	1.52682700	-9.24971500	-0.96844200
H	-1.57095700	-5.76460300	-1.77983700
H	-6.23652800	-5.40317000	-2.78578600
H	-8.10520400	-0.86165700	-3.10321900
H	-8.56718900	3.68989200	-0.59567400
H	-5.93936300	7.24044000	-0.65894600
H	-3.62975900	7.93807800	-1.22826400
H	-0.55630500	5.96451800	0.17056200
H	7.53833100	-5.24441000	-0.47174600
H	3.86334600	-8.63036300	-0.90361900
H	0.47822800	-7.00562600	-1.20700900
H	-4.04715400	-6.43165700	-2.29953200
H	-7.18759200	-3.11196900	-3.24046800
H	-9.75012000	1.63470700	-1.21358600

H	-7.11509600	5.14536000	-1.13470800
H	-0.13547400	11.80248800	0.47681800
H	0.35671900	10.47703300	-0.60754200
H	-1.35728100	10.98232400	-0.52740300
H	-6.14519100	7.85304800	2.34596200
H	-5.09810800	9.10491200	3.08005900
H	-6.40864600	9.57596900	1.97231800
H	-12.12449800	-0.18002400	-1.12990900
H	-11.52034100	-1.54116500	-0.15439900
H	-11.02656800	0.13197500	0.23781200
H	-9.39998800	-6.68209400	-1.67520100
H	-8.07050100	-6.39788500	-0.52276100
H	-9.67757000	-5.66272600	-0.24396500
H	6.43408200	-9.19597500	2.73393000
H	5.98289200	-7.47393600	2.81685800
H	4.94143200	-8.71564900	3.57623100
H	-0.45700900	-11.55490000	1.39634800
H	-0.89678700	-10.30389700	0.20538000
H	0.64945500	-11.19133800	0.05170100
C	8.24056600	-1.49055200	-1.60253700
C	7.51747000	-2.66227600	-1.39681800
C	6.50218300	-2.73154100	-0.42723200
C	6.21100700	-1.55992200	0.29055400
C	6.93058600	-0.38542000	0.08066700
C	7.97569000	-0.33874700	-0.84933400
H	9.03759600	-1.46796600	-2.33918000
H	7.74364500	-3.53788900	-1.99924400
H	5.44340100	-1.57928400	1.05908500
H	6.69227400	0.49757700	0.66672100
C	5.30787700	6.08422900	0.68974800
C	6.52056100	5.48835800	0.36331200

C	6.58981200	4.45707800	-0.58513800
C	5.39570500	4.03431200	-1.17807600
C	4.18265600	4.64981100	-0.86937600
C	4.10837400	5.69705200	0.06319400
H	5.29298300	6.86222900	1.44717300
H	7.43447300	5.83784700	0.83467800
H	5.40969000	3.22810800	-1.90553400
H	3.28718200	4.33215300	-1.39527200
C	8.47881600	3.05356600	0.24688100
C	8.85851000	1.77806200	0.19331100
C	8.82365300	0.93084400	-1.05862800
C	8.29438800	1.72213200	-2.23492300
C	7.91585700	2.99879400	-2.18118800
C	7.96142800	3.84900000	-0.93159600
H	8.54818500	3.60792700	1.17972500
H	9.21131500	1.28866700	1.09813300
H	8.26310200	1.17541400	-3.17459600
H	7.55552200	3.48385700	-3.08542400
O	10.15494400	0.55892200	-1.48958600
O	8.93821300	4.91408500	-1.05414800
C	11.00233000	-0.03080400	-0.51486800
H	10.52144300	-0.87208000	0.00328600
H	11.87288200	-0.40513400	-1.06032200
H	11.34344500	0.70162900	0.22882300
C	8.77725000	5.80581300	-2.14691600
H	9.02367300	5.33110200	-3.10636400
H	7.76082900	6.21919600	-2.20149000
H	9.48154900	6.62395500	-1.97347800

Total energy: -3693.38963079 a.u.

II.6. Bridge to Chapter III.

In Chapter II we were able to establish a size-selective synthesis of [7]-[12]CPP. We were able to use the compounds made to study their fluorescence quantum yield for the first time and showed that as the size became smaller the emission red-shifted and the quantum yield decreased. Although we were able to access these compounds in a size-selective manner, the overall yield were very low and only milligram quantities could be prepared. Chapter III details the serendipitous discovery of a high-yielding mild oxidative homocoupling capable of accessing gram quantities of a five-ring macrocyclic precursor. Treatment of this product with sodium naphthalanide did not produce the anticipated [5]CPP, which had never been reported at the time of this discovery. We found that treating the macrocyclic precursor with sodium naphthalanide at cold temperatures and quenching with a protic source such as methanol gave the dihydro reduced macrocycle lending mechanistic insight into this type of aromatization. Double elimination using lithium diisopropylamide gave [5]CPP for the first time. The details of this compound are discussed in Chapter III.

CHAPTER III

EFFICIENT ROOM-TEMPERATURE SYNTHESIS OF A HIGHLY STRAINED CARBON NANOHOOP FRAGMENT OF BUCKMINSTERFULLERENE

Chapter **III** is based on published work in *Nature Chemistry* (2014). The manuscript was prepared by Dr. Paul Evans and myself. The oxidative homocoupling was devised by myself while the remaining synthetic route was equally contributed by Dr. Paul Evans and myself. Editing of the manuscript was provided by Professor Ramesh Jasti.

[5]Cycloparaphenylene ([5]CPP) which can be envisioned as a carbon nanohoop fragment of C₆₀, the equator of C₇₀ fullerene and the unit-cycle of a [5,5] armchair carbon nanotube was synthesized. Given its calculated 119 kcal/mol of strain energy and severely distorted benzene rings, this synthesis employing a room-temperature macrocyclization of a diboronate precursor, single-electron reduction, and elimination, is remarkably mild and high yielding (27% over 3 steps). Single crystal X-ray diffraction data was obtained to confirm its geometry and previously disputed benzenoid character. First and second pseudoreversible oxidation and reduction events were observed via cyclic voltammetry. The facile synthesis, high solubility, and narrowest optical HOMO/LUMO gap of any *para*-polyphenylene synthesized make [5]CPP a desirable new material for organic electronics and a significant advance in the synthesis of highly distorted aromatic molecules.

III.1. Introduction.

Highly strained hydrocarbons have captivated the imagination of synthetic and physical organic chemists for decades due to their challenging structures and unique properties. The high energy present in these kinetically metastable carbon frameworks requires synthetic ingenuity to overcome, frequently relying on high temperatures (cubane,¹ corannulene²), photochemistry (quadricyclane³), or flash vacuum pyrolysis ([6]paracyclophane,⁴ C₆₀ fullerene⁵). Of particular interest is the extreme bending of aromatic systems and reaching the geometric limit of aromaticity.^{6,7} Cycloparaphenylenes (CPPs), hydrocarbon macrocycles consisting of distorted benzene rings linked at the *para* positions, once only the stuff of theory,⁸ have recently entered the realm of synthetic accessibility. The field of carbon nanohoos, so called because they

are the smallest unit-cycles of armchair carbon nanotubes, has expanded rapidly due to their porous character⁹, electronics,^{10, 11} host-guest capabilities,^{12, 13} synthetic challenge,¹⁴ and usefulness as carbon nanotube precursors.¹⁵ First synthesized in 2008, carbon nano hoops have now been accessed in a variety of sizes ($n = 6-16, 18$)^{9, 13, 16-29} and with several functionalities incorporated.³⁰⁻³³ The strain inherent in these distressed hydrocarbons makes synthesis, especially of the smaller $[n]$ CPPs, very challenging. In addition to synthetic conquest, smaller and smaller CPPs are desired for their solubility and unique electronics. We observe a dramatic increase in strain, reduction of ring-to-ring dihedral angles, and narrowing of the HOMO/LUMO gap (in contrast to the widening gap in oligoparaphenylenes) in CPPs smaller than $[10]$ CPP (Figure III.1).^{17, 34}

Having successfully synthesized $[7]$ CPP, an orange emitting fluorophore, and $[6]$ CPP, which packs into tubes in the solid state, we set our sights on $[5]$ CPP. This new synthetic target has 119 kcal/mol of strain energy, over 20 kcal/mol higher than $[6]$ CPP (97 kcal/mol).^{9, 20, 35, 36}

Classic hydrocarbons



quadricyclane
photolysis
1961

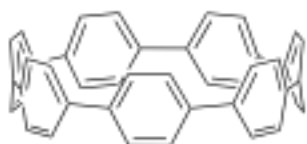


[6]paracyclophane
flash vacuum pyrolysis
1974

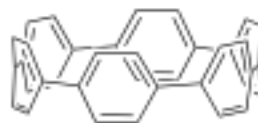


C₆₀ fullerene
flash vacuum pyrolysis
2002

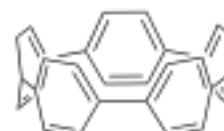
Trends in cycloparaphenylenes



[7]CPP
J. Am. Chem. Soc.
2011



[6]CPP
Angew. Chem., Int. Ed.
2012



[5]CPP
this work



narrowing HOMO/LUMO gap
increasing strain
decreasing dihedral angles

Figure III.1. Classic Strained Hydrocarbons and Trends in Small Cycloparaphenylenes.

III.2. Results and Discussion.

III.2.1. Synthesis of [5] Cycloparaphenylene.

In repeating our synthesis of [10]CPP using bisboronate **III.1** (Figure III.2.), available on the multi-gram scale,¹³ we consistently observed the formation of small amounts of a curious new compound in our macrocyclization reactions. This material appeared to have similar NMR resonances to the 1,4-dimethoxycyclohexa-2,5-diene-containing macrocyclic precursors to cycloparaphenylenes, but with an anomalous singlet in the ¹H NMR spectrum at $\delta = 6.00$ ppm, further upfield than the most shielded phenyl protons in the [6]CPP macrocycle ($\delta = 6.78$ ppm). Mass spectrometric and unrefined single crystal X-ray diffraction data of this mysterious byproduct confirmed, to our surprise and delight, that it was not a larger macrocycle or linear oligomer, but **III.2**, the result of intramolecular boronate homocoupling. This structural data allowed us to assign the singlet at $\delta = 6.00$ ppm as the four phenyl protons on the ring between two cyclohexadiene moieties. As indicated by its multiplicity, this ring spins through the center of the macrocycle bringing the protons within approximately 2.8 Å of the adjacent alkenes and the center of the nearest biphenyl ring, based on our computational investigations. The shielding cones cast by these π -systems account for the dramatic upfield shift of this phenyl signal.³⁷ The formation of **III.2** is encouraged by the rigid, curved geometry of **III.1** in solution. With restricted rotation allowing the boron atoms to swing into proximity, intramolecular macrocyclization at high dilution becomes competitive with intermolecular processes.

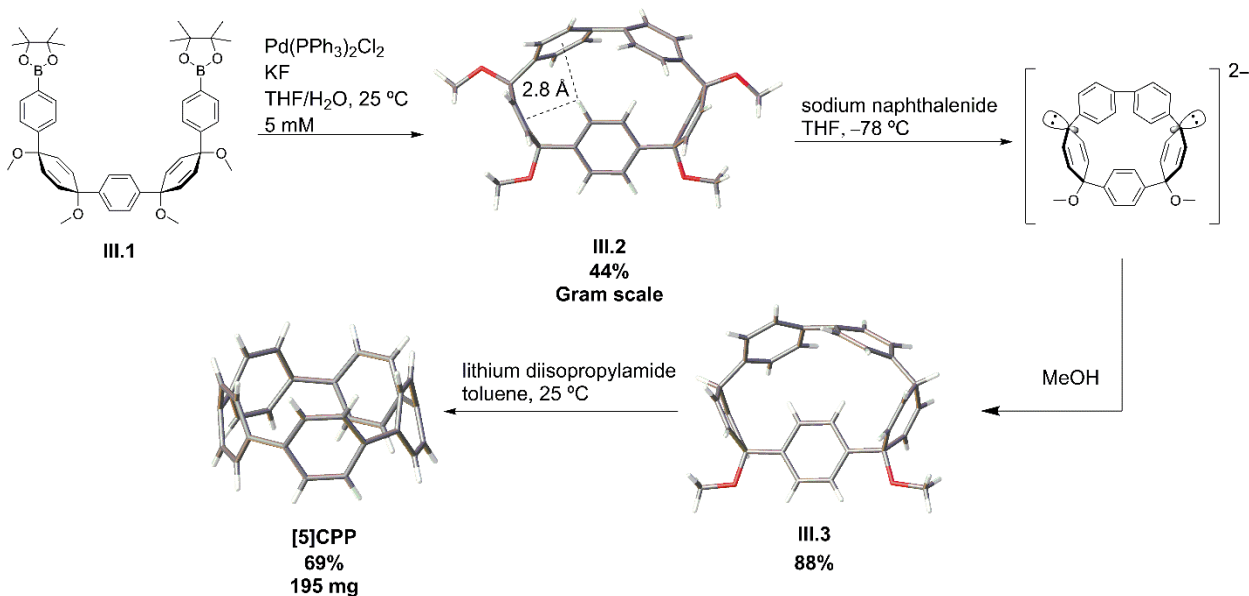


Figure III.2. Synthesis of [5]Cycloparaphenylene with DFT Structure of **III.2** and Refined Crystal Structures of **III.3**, and [5]CPP.

With this observation in mind, optimal conditions for the synthesis of **III.2** were developed. Using a palladium-catalyzed boronate homocoupling performed under air at room temperature,^{38, 39} macrocycle **III.2**, with a strain energy of 32 kcal/mol, was easily prepared. This pivotal discovery allowed for the synthesis of **III.2** on the gram scale at room temperature in one flask and facilitated quick determination of a synthetic route to [5]CPP (*vide infra*).

Reduction of **III.2** with 5 equivalents of sodium naphthalenide at -78 °C in tetrahydrofuran surprisingly did not offer the parent cycloparaphenylene, as is observed with [6]-[12] and [18]CPP.^{13, 16, 19} Instead, the reduction stalls at a stable dianion, which is a deep royal blue in solution. We presume that this is due to unavailable energy at low temperatures to build in the 87 kcal/mol of additional strain necessary for the conversion of **III.2** to [5]CPP via elimination. Previously the most strain overcome by these conditions is 60 kcal/mol for [6]CPP and 67 kcal/mol for [7]CPP.^{9, 20} Allowing this reduction to warm past -70 °C results in a color change to dark brown, and precipitation of insoluble material indicating rapid decomposition.⁴⁰ Sodium naphthalenide reduction at a range of temperatures from -78 °C to room temperature does not yield more than trace (less than 1%) amounts of the desired cycloparaphenylene. However, quenching the dianion with methanol at -78 °C and subsequent removal of naphthalene afforded

reduced macrocycle **III.3** in 88% yield on the half-gram scale. The regioselectivity of this reduction was confirmed by X-ray crystallography and no regioisomers were observed in the reaction mixture.

Since **III.3** has the same oxidation state as **[5]CPP**, we were able to probe the elimination of two equivalents of methanol to generate **[5]CPP** at higher temperatures using a non-nucleophilic, non-reducing base to avoid the decomposition seen with the sodium naphthalenide treatment of **III.2**. Subjecting **III.3** to 30 equivalents of lithium diisopropylamide in toluene at room temperature gratifyingly afforded 195 mg of **[5]CPP**, a 69% isolated yield, as a dark red solid with a deep ruby color in solution.

The structure of **[5]CPP** was confirmed by NMR, MALDI-TOF MS, and IR. Interestingly, **[5]CPP** is soluble in a wide range of common organic solvents including hydrocarbons, aromatic, polar aprotic, halogenated, and ethereal solvents. It should be noted that **[5]CPP**, unless stored under inert atmosphere, decomposes to an insoluble, bright yellow material after about 24 hours. It is possible that this is an oxidation or a nucleophilic decomposition as is seen for [6]paracyclophane.⁴¹

III.2.2. NMR Spectroscopy of [5]Cycloparaphenylene.

With **[5]CPP** in hand, the structure of this new carbon nano hoop was investigated. The ¹H NMR spectrum consists of one singlet, $\delta = 7.86$ ppm and the ¹³C NMR shows two signals at $\delta = 126.74$ and 132.07 ppm. This confirms the lack of rotational isomers, and the free rotation of all phenyl rings through the center of the macrocycle at room temperature. The downfield shift of the proton signal in **[5]CPP** may be explained by the small phenyl-phenyl dihedral angles, calculated to average 16.4°. The tendency of these rings to remain relatively in-plane with each other encourages conjugation throughout the whole molecule and induces a deshielding ring current from the extended π -system in addition to the ring currents around each phenyl ring. Wong's NICS calculations, which suggest that the aromaticity of individual benzene rings decreases with decreasing size in cycloparaphenylenes smaller than **[8]CPP**, may be taken as supporting evidence for the delocalization of the π -system throughout the molecule.³⁴ We first observed this phenomenon in the downfield shift of the ¹H NMR signal for **[6]CPP** ($\delta = 7.64$) relative to other cycloparaphenylenes. Simple bending of a benzene ring alone does not account for such a dramatic downfield shift.⁴²

III.2.3. Solid State Analysis of [5]Cycloparaphenylene.

The refined crystal structure of [5]CPP was obtained from single crystals of [5]CPP that were grown from the slow evaporation of a dichloromethane and hexane solution at 0°C in the dark (Figure III.3.). Though different levels of theory have estimated [5]CPP to be quinoidal or benzenoid^{34, 43}, we now confirm its benzenoid structure by noting the elongated phenyl-phenyl bond lengths (1.49 Å) and the shorter and nearly equivalent phenyl bonds (1.40 Å for the A-B bond and 1.38 Å for the A-A bond). The average phenyl-phenyl dihedral angle for [5]CPP is 12.4°, lower than the calculated 16.4° and much smaller than that of [6]CPP with an average solid state dihedral angle of 26.4°. The most striking feature of this new structure is the nonplanar phenyl rings that adopt a shallow boat conformation in the presence of considerable ring strain. The tertiary carbons in each ring are displaced out of the benzene plane by an average 15.6°. This severe distortion is, to our knowledge, the largest of any distressed benzene isolated, with the exception of [6]- and [7]paracyclophanes.^{42, 44, 45} This includes bent benzenes found in nature and conquered by chemists, such as those in haouamine A (13.6°)⁴⁶ and cavicularin (7.9°)⁴⁷ and the previously most-distorted cycloparaphenylene, [6]CPP (12.7°). The interior of [5]CPP has an average diameter of 6.69 Å, measured by doubling the average distance from the centroid of each ring to the centroid of the molecule. With a size comparable to endohedral fullerenes, it is possible that very small charged guests, such as metal ions or simple organic cations may become encapsulated in [5]CPP's inward-facing π system. Intriguingly, [5]CPP packs in a herringbone fashion, unlike the tubular packing observed for [6]CPP. The unit cells of several visually distinct crystal morphologies have been analyzed to confirm that this result is not anomalous.

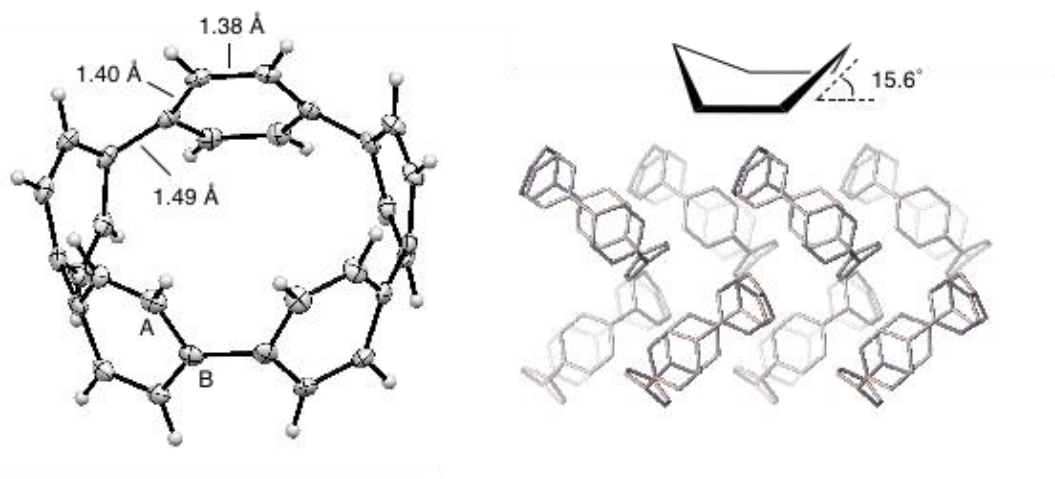


Figure III.3. Crystal Data of [5]CPP Showing Structure (Left, ORTEP Ellipsoids Displayed at 50% Probability), Boat Angle (top right) and Herringbone Packing (Bottom Right).

III.2.4. Photophysical Characterization of [5]Cycloparaphenylene.

[5]CPP absorbs very strongly in the UV with an extinction coefficient of $5.7 \times 10^4 \text{ M}^{-1}\text{cm}^{-1}$ at the maximum, 335 nm (Figure III.4.). This same absorbance is observed in all CPPs and corresponds to a combination of HOMO-2 and HOMO-1 \rightarrow LUMO and HOMO \rightarrow LUMO+1 and LUMO+2 transitions.^{9, 17} Additionally, apparent by its deep red color, [5]CPP displays a very broad second absorbance band centered around 502 nm with a maximum extinction coefficient of $4.5 \times 10^2 \text{ M}^{-1}\text{cm}^{-1}$. This arises from a HOMO-LUMO transition which, forbidden in larger CPPs, starts to manifest in the smaller CPPs. Like [6]CPP, there is no observable fluorescence in [5]CPP due to the weak oscillator strength of the HOMO-LUMO transition.⁴⁸

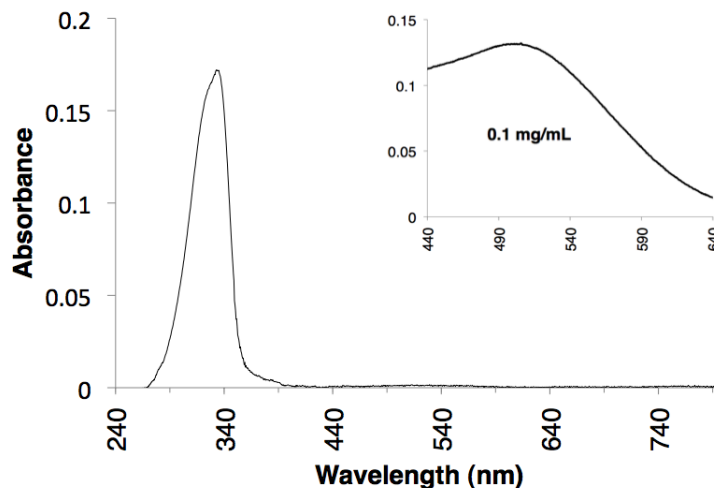


Figure III.4. UV-Vis Absorbance (1 $\mu\text{g/mL}$, 0.1 mg/mL Inset) of [5]CPP Showing Major and Minor Absorbances.

III.2.5. Electrochemical Properties of [5]Cycloparaphenylene.

The oxidation and reduction potentials of [5]CPP, were obtained by cyclic voltammetry, 1 mM in tetrahydrofuran solution with 0.1M nBu₄NPF₆ (Figure III.5). Interestingly, we observed two oxidation events with peak potentials of 0.25 and 0.46 V vs Fc/Fc⁺ and two reductions with peak potentials of -2.27 and -2.55 V vs Fc/Fc⁺. All four events appear to be pseudoreversible one-electron processes. [5]CPP has the lowest oxidation and least-negative reduction potential of any *para*-polyphenylene.¹⁷ The narrow electrochemical gap, combined with crystalline organization in the solid state make [5]CPP an excellent candidate as a new organic semiconductor.

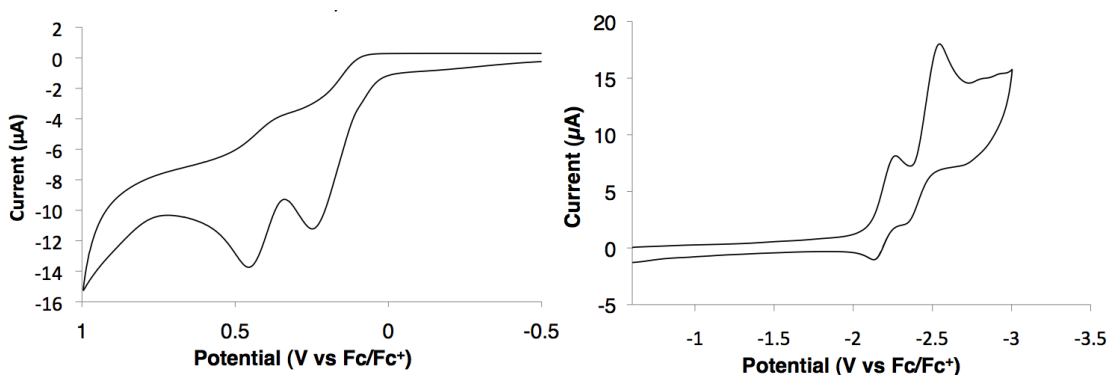


Figure III.5. Cyclic Voltammograms Showing Oxidation (Left) and Reduction (Right) Events for [5]CPP in Tetrahydrofuran.

III.3. Conclusion.

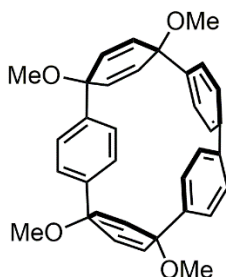
In conclusion we report the synthesis of **[5]CPP**, the smallest carbon nano hoop. Our mild and high-yielding synthesis builds in a remarkable 119 kcal/mol of strain energy in solution without heating. This work illustrates the success of rational chemical design applied to challenging carbon architectures and has offered an easily synthesized nonplanar aromatic hydrocarbon in the same class as corannulene,² C₆₀ fullerene,⁵ or grossly warped nanographene.⁴⁹ Studies of the inclusion of **[5]CPP** in devices and host-guest complexes will be reported in due course.

III.4. Experimental Section.

III.4.1. General Experimental Details.

Moisture and oxygen sensitive reactions were carried out under nitrogen atmosphere using standard syringe/septa technique. All the glassware was thoroughly washed, dried in oven at 140 °C overnight and cooled under nitrogen atmosphere before use. All reagents were obtained commercially. Tetrahydrofuran (THF) and dichloromethane (DCM) were dried by filtration through alumina according to the method described by Grubbs. Silica column chromatography was conducted with Zeochem Zeoprep n60 Eco 40-63 μm silica gel. Thin layer chromatography (TLC) was performed using Sorbent Technologies Silica Gel XHT TLC plates. Developed plates were visualized using UV light at wavelength of 254 and 365 nm. ¹H NMR spectra and ¹³C NMR spectra were recorded respectively at 400 MHz and 125 MHz (or 100 MHz for compound **2**) on a Varian VNMRS. Deuterated chloroform (CDCl₃) was used as NMR solvent for all the compounds and all spectra were referenced to trimethylsilane (TMS). The matrix used for MALDI-TOF was a solution of 7,7,8,8-tetracyanquinodimethane (TCNQ) in THF with 1% silver trifluoroacetate as a promoter.

III.4.2. Synthetic Details.

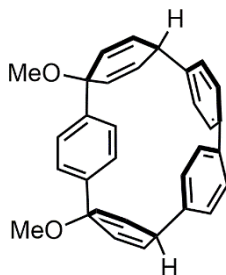


(31S,34s,51S,54s)-31,34,51,54-tetramethoxy-1,2,4(1,4)-tribenzena-3,5(1,4)-dicyclohexanacyclopentaphane-32,35,52,55-tetraene **III.2**

To a 2 L flask equipped with a magnetic stir bar was added diboronic bispinacol ester **III.1** (3.74 g, 4.90 mmol, 1.00 equiv) and tetrahydrofuran (1030 mL). The resulting solution was stirred until all the solid was in solution at which point bis(triphenylphosphine)palladium(II) dichloride (0.346 g, 0.490 mmol, 0.100 equiv) was added followed by H₂O (200 mL). To this yellow solution was added potassium fluoride (0.289 g, 4.90 mmol, 1 equiv). The solution gradually turned bright orange over two hours and was allowed to stir open to air and at room temperature for an additional ten hours at which point palladium black had coated the inside of the flask. The crude reaction mixture was filtered through a pad of Celite to remove palladium. This filter cake was washed with dichloromethane (100 mL). The solution was extracted with dichloromethane (2 x 300 mL) and the resulting organic phase was washed with brine (500 mL). The organic phase was then dried over sodium sulfate and solvent was removed at reduced pressure to give a yellow semisolid. This yellow semisolid was then washed with acetone (100 mL) to dissolve impurities while leaving the product as a white solid which was collected by vacuum filtration. This white solid (1.40 g, 52%) can be further purified on SiO₂ if necessary. The white solid was dissolved in minimal dichloromethane and loaded onto a short pad of silica. The product was eluted in 15% ethyl acetate in dichloromethane to give a pristine crystalline white solid (1.10 g, 44%).

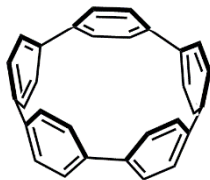
m.p: 311-312°C. ¹H NMR (400 MHz, CDCl₃): δ(ppm) 7.46 (d, J = 9.4 Hz, 4H), 7.43 (d, J = 9.4 Hz, 4H), 6.58 (d, J = 10.2 Hz, 2H), 6.00 (s, 4H), 5.73 (d, J = 10.2 Hz, 2H), 3.46 (s, 6H), 3.26 (s, 6H); ¹³C NMR (100 MHz, CDCl₃): δ(ppm) 141.67, 141.29, 140.02, 133.91, 133.73, 128.90, 127.47, 125.09, 74.96, 73.68, 52.65, 51.27; IR (neat): 3026, 2979, 2936, 2899, 2820, 1594, 1497, 1487, 1464, 1449, 1398, 1306, 1275, 1262, 1221, 1186, 1170,

1075, 1017, 988, 955, 942887, 862, 845, 823, 758, 702, 670, 617, 577, 557, 514, 467 cm^{-1} ; HRMS (Q-TOF, ES+) (m/z): $[\text{M}+\text{Na}]^+$ calcd. for $\text{C}_{34}\text{H}_{32}\text{O}_4$, 527.2198; found, 527.2205.



(31R,34r,51R,54r)-34,54-dimethoxy-1,2,4(1,4)-tribenzena-3,5(1,4)-dicyclohexanacyclopentaphane-32,35,52,55-tetraene **III.3**

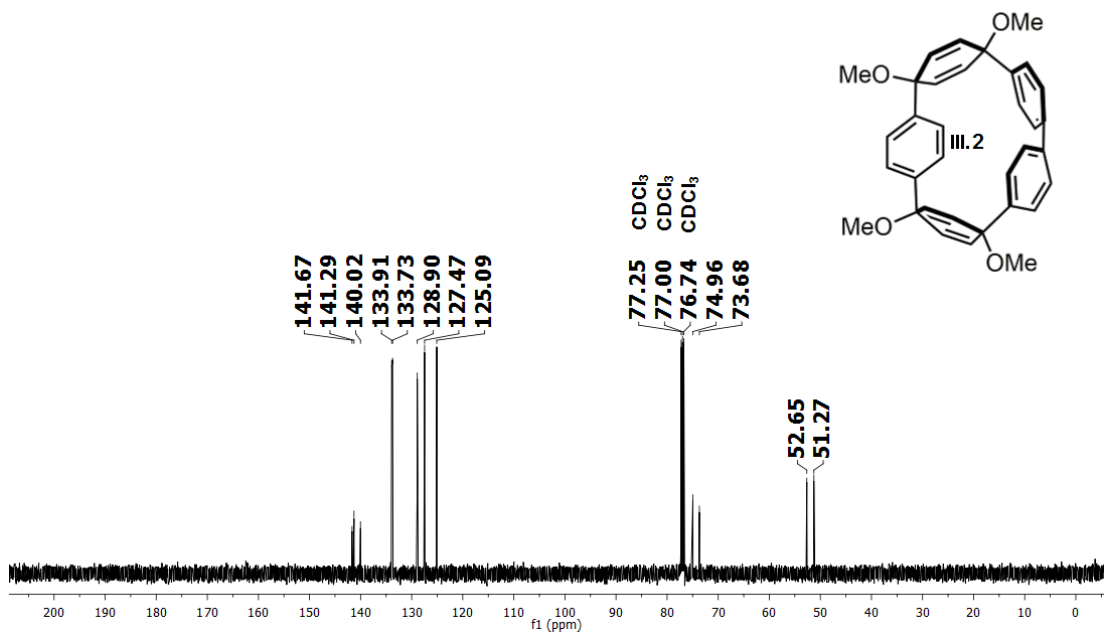
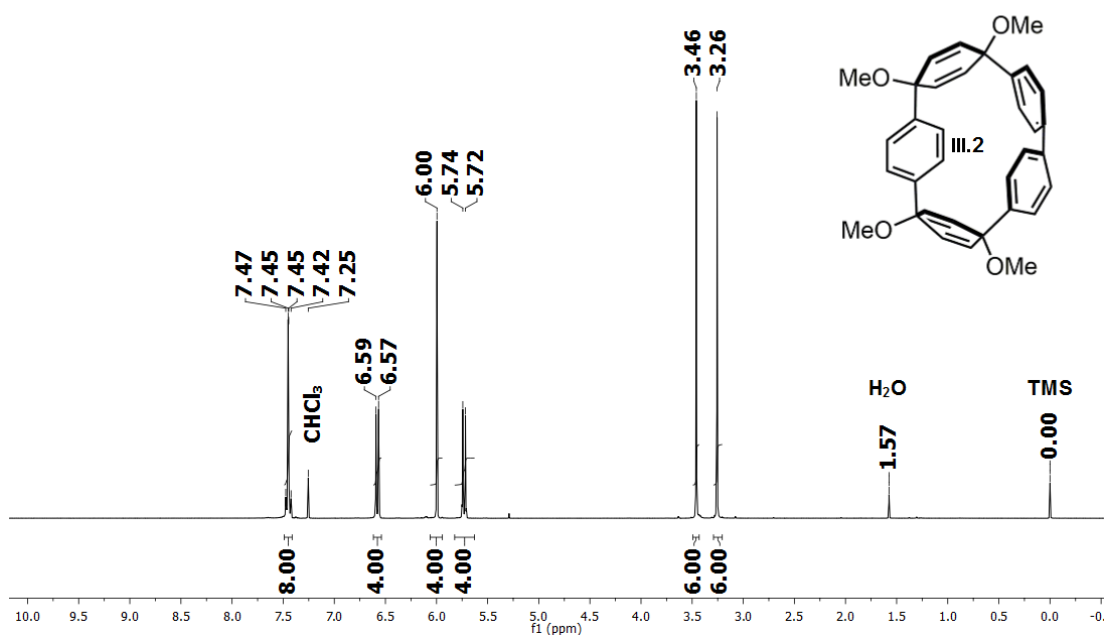
Macrocyclic **III.2** (200 mg, 0.400 mmol, 1.00 equiv) was dissolved in dry THF (150 mL) and cooled to -78°C under N_2 . 1 M sodium naphthalenide (2.00 mL, 2.00 mmol, 50.0 equiv) was added dropwise to the stirring solution to give a deep blue color. This was allowed to stir for 40 minutes at which point 1 mL of methanol was added drop wise to give a clear yellow solution. The reaction was allowed to warm to room temperature at which point water (100 mL) and DCM (100 mL) were added. The aqueous layer was then extracted with DCM (2 x 100 mL). The combined organic layers were washed with water (3 x 100 mL), brine (1 x 100 mL) and dried over sodium sulfate before being filtered and concentrated down to a solid. The crude solid was adsorbed onto silica gel and was washed with hexane (3 x 100 mL) to remove excess naphthalene. The product was eluted with a 1:1 mixture of ethyl acetate and DCM (200 mL). The solvent was then removed under vacuum to give the product as a white solid (160 mg, 91%). m.p: decomp $>350^\circ\text{C}$. ^1H NMR (400 MHz, CDCl_3): δ (ppm) 7.42 (d, $J = 8.6$ Hz, 4H), 7.28 (d, $J = 8.6$ Hz, 4H), (dd, $J = 10.4, 4.9$ Hz, 4H), 6.05 (s, 4H), 5.63 (d, $J = 10.4$ Hz, 4H), 4.27 (t, $J = 4.9$ Hz, 2H), 3.21 (s, 6H); ^{13}C NMR (125 MHz, CDCl_3): δ (ppm) 143.04, 142.01, 138.19, 131.84, 131.60, 128.71, 127.31, 125.18, 74.85, 54.15, 36.39; IR (neat): 3052, 2990, 2930, 2898, 2873, 2820, 1722, 1703, 1665, 1592, 1512, 1487, 1467, 1454, 1397, 1360, 1265, 1220, 1188, 1170, 1068, 1012, 986, 961, 920, 883, 863, 851, 834, 814, 803, 770, 734, 704, 592, 582, 541, 488, 390 cm^{-1} . HRMS (Q-TOF, ES+) (m/z): $[\text{M}+\text{Na}]^+$ calcd. for $\text{C}_{12}\text{H}_{10}\text{ClO}_2$, 467.1987; found, 467.1196.

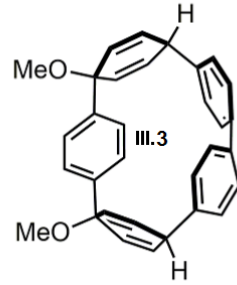
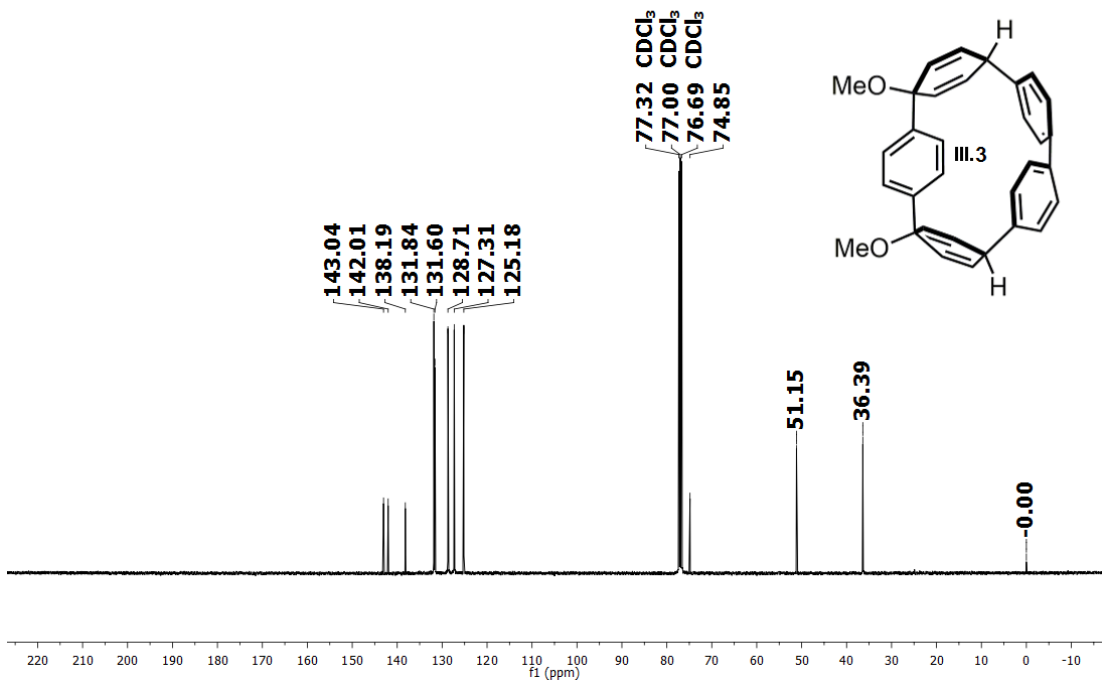
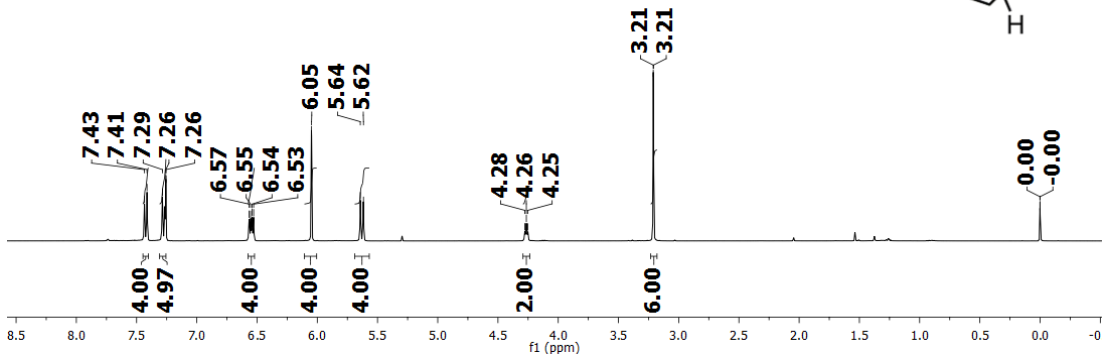
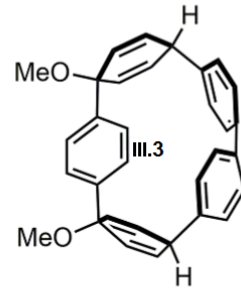
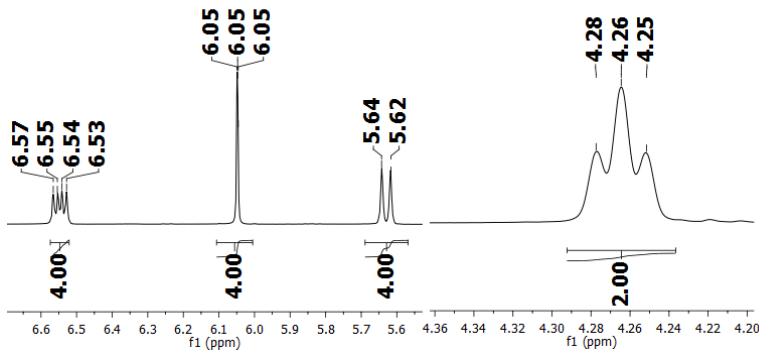


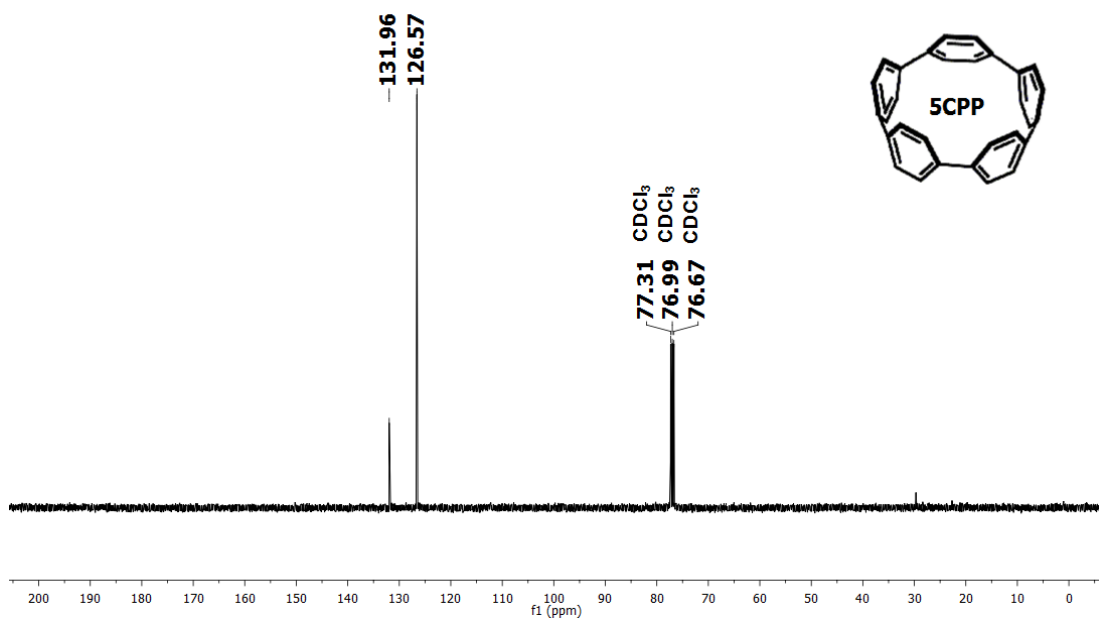
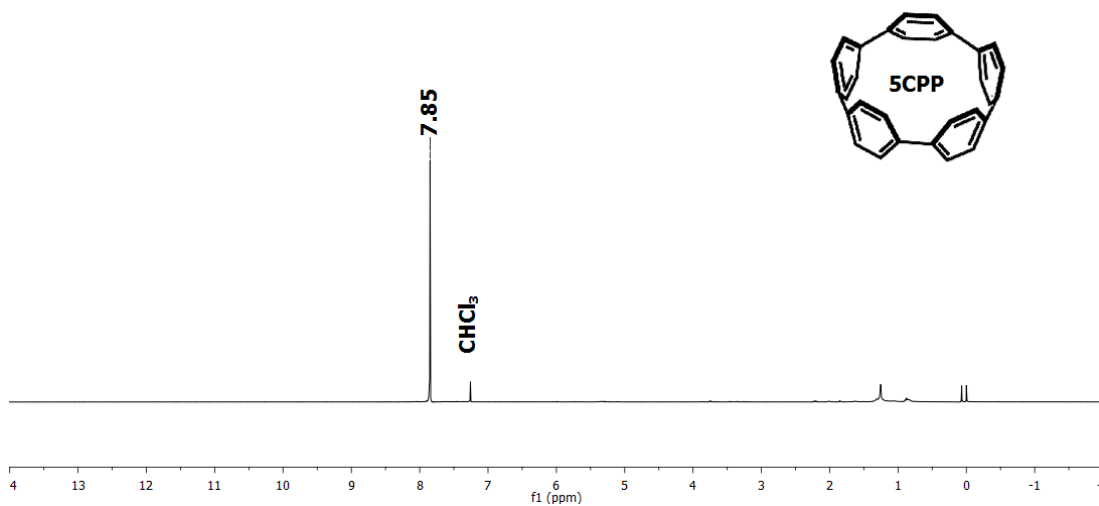
[5]Cycloparaphenylene [5]CPP

Diisopropylamine (5.00 mL, 36.0 mmol, 48.0 equiv) was added to 650 mL of dry toluene in a flame dried round bottom flask under N₂. This solution was cooled to 0 °C at which point 2.3 M n-butyl lithium in hexanes (9.60 mL, 22.0 mmol, 30.0 equiv) was added dropwise and stirred for 20 minutes at 0 °C. Reduced macrocycle **III.3** (330 mg, 0.740 mmol, 1.00 equiv) was dissolved in dry toluene (50.0 mL) and was added dropwise to the stirring solution of lithium diisopropylamide (LDA). The reaction was warmed to room temperature and allowed to stir for 2 hours, resulting in a deep red ruby solution, at which point it was quenched with 200 mL of water. The solution was extracted with toluene (3 × 100 mL). The resulting organic phase was pooled and washed with water (3 × 200 mL), brine (1 × 200 mL) and dried over sodium sulfate before concentration under vacuum. The crude red solid was chromatographed on silica gel in pure DCM to give a solid red band that was collected and concentrated to give [5]CPP as brilliant red needles (195 mg, 69% yield). m.p. decomp >400°C. ¹H NMR (400 MHz, CDCl₃): δ(ppm) 7.85 (s, 20H); ¹³C NMR (125 MHz, CDCl₃): δ(ppm) 131.96, 126.57; IR (neat): 3005, 2956, 2922, 2853, 1666, 1602, 1549, 1508, 1478, 1459, 1415, 1375, 1342, 1299, 1259, 1236, 1180, 1171, 1120, 1079, 1053, 1026, 956, 930, 843, 817, 767, 688, 635, 552, 463, 448, 429 cm⁻¹; MALDI-TOF (*m/z*): [M]⁺ calcd. for C₃₀H₂₀, 380.16; found 380.86.

III.4.3. NMR Spectra.







III.4.4. Optical Characterization.

Absorbance spectra were obtained in a 1 cm quartz cuvette with dichloromethane using a Varian 100 Bio UV-Vis spectrometer. The extinction coefficient was calculated by

measuring the slope of Beer-Lambert plots (absorbance: [5]CPP, 335 nm and 502 nm) and averaging over three independent trials.

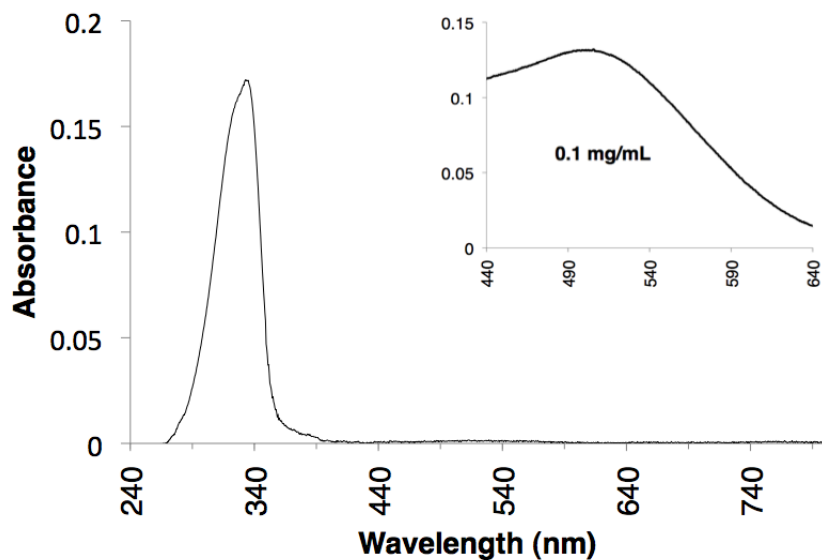


Figure III.6. UV-Vis of [5]CPP in Dichloromethane, Minor Absorption is Shown in the Top Right Corner.

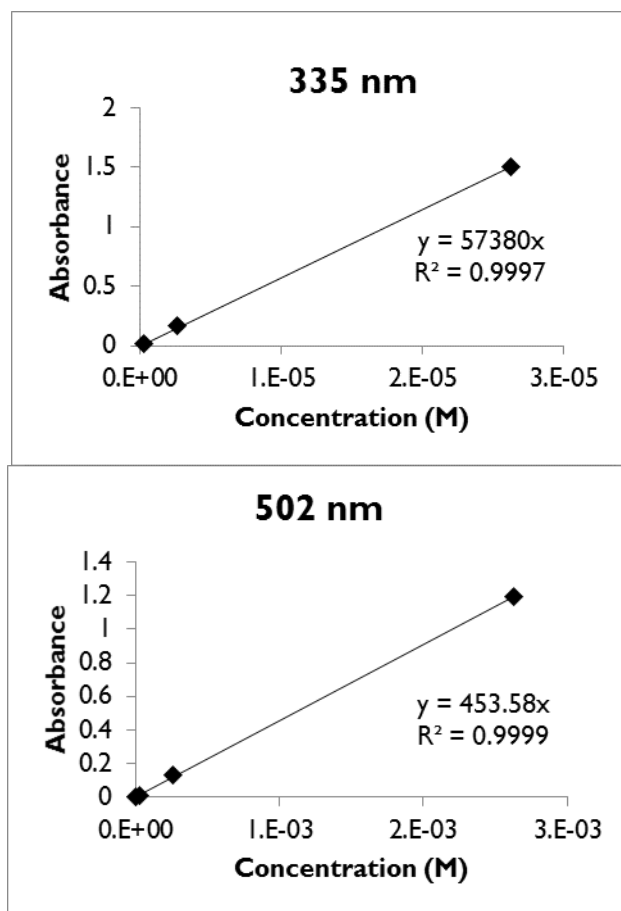
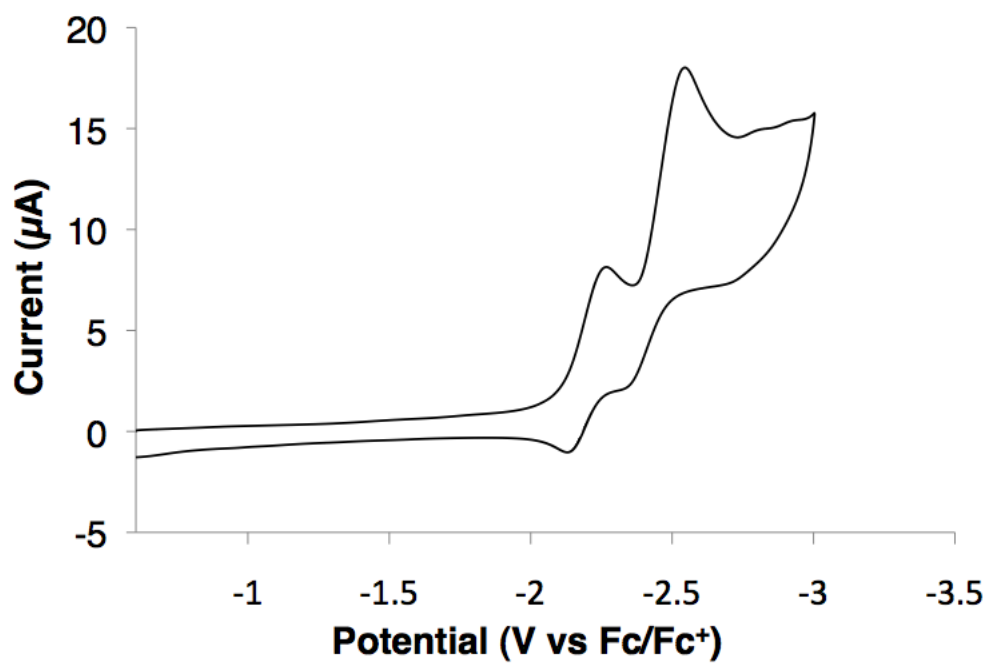
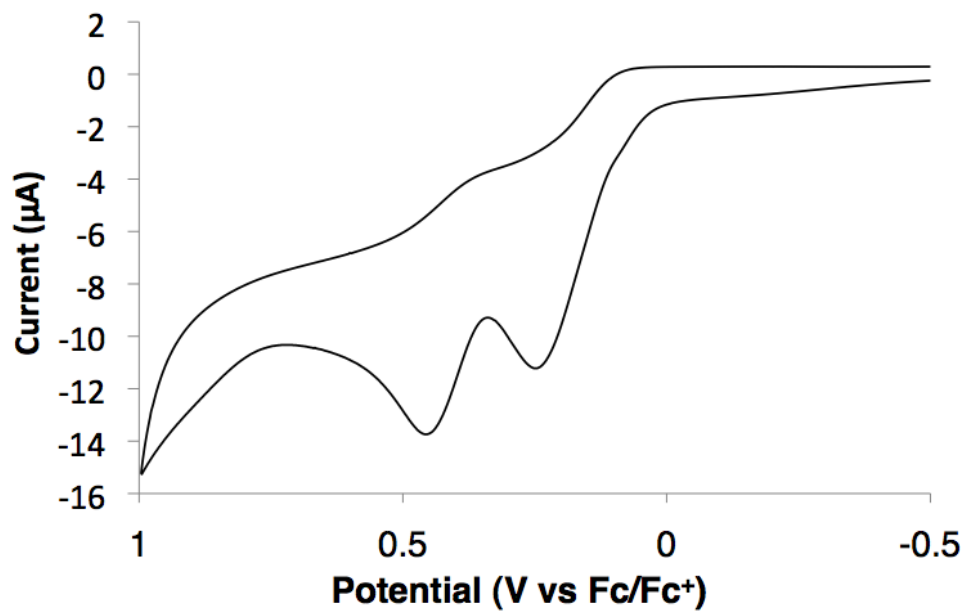


Figure III.7. Beer-Lambert Plots for the Determination of Extinction Coefficient of [5]CPP ($\epsilon_{335\text{nm}} = 5.70 \times 10^4 \text{ M}^{-1}\text{cm}^{-1}$, $\epsilon_{501\text{nm}} = 4.50 \times 10^2 \text{ M}^{-1}\text{cm}^{-1}$).

III.4.5. Electrochemical Characterization.

Cyclic voltammetry experiments were performed using a CH Instruments 1200B potentiostat running CH Instruments software. Measurements were conducted in degassed 0.1 M $n\text{-Bu}_4\text{NPF}_6$ in tetrahydrofuran under an N_2 atmosphere with a glassy carbon working electrode, platinum counter electrode and Ag/AgCl reference electrode. Ferrocene/ferrocenium couple was used as an internal or external reference. Supporting electrolyte tetra-*n*-butylammonium hexafluorophosphate ($n\text{Bu}_4\text{PF}_6$) was purchased from Sigma-Aldrich and was recrystallized from methanol 3 times before use. Solvents were sparged with N_2 prior to data collection.



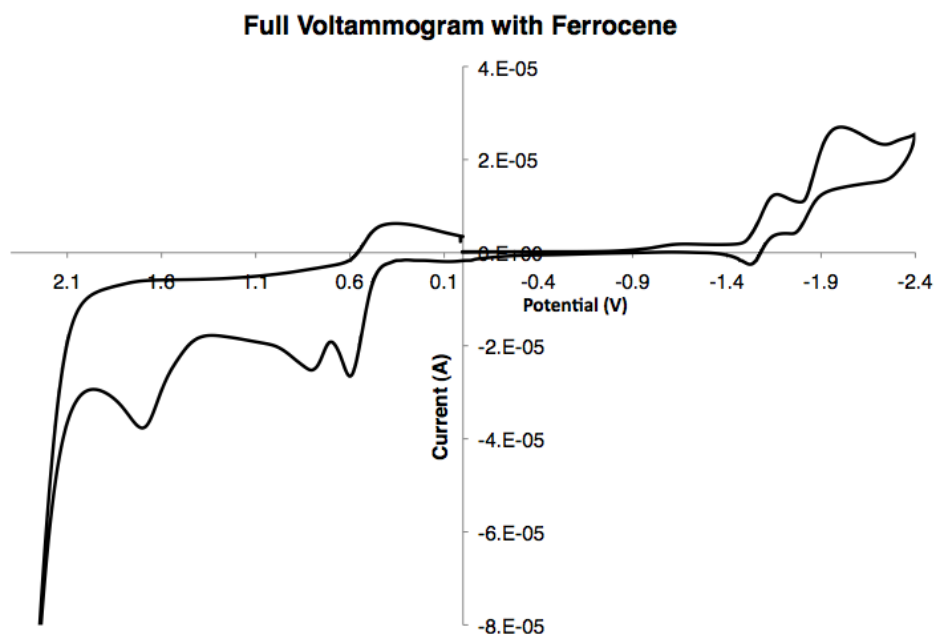


Figure III.8. Cyclic Voltammetry of [5]CPP.

III.4.6. Computational Details.

All calculations were carried out with Gaussian 09 package at B3LYP/6-31g* level of theory.³ All excited state calculations (TD-DFT) were performed on fully optimized structures. The fully optimized structures were confirmed to be true minima by vibrational analysis. Structures were minimized with no symmetry restrictions.

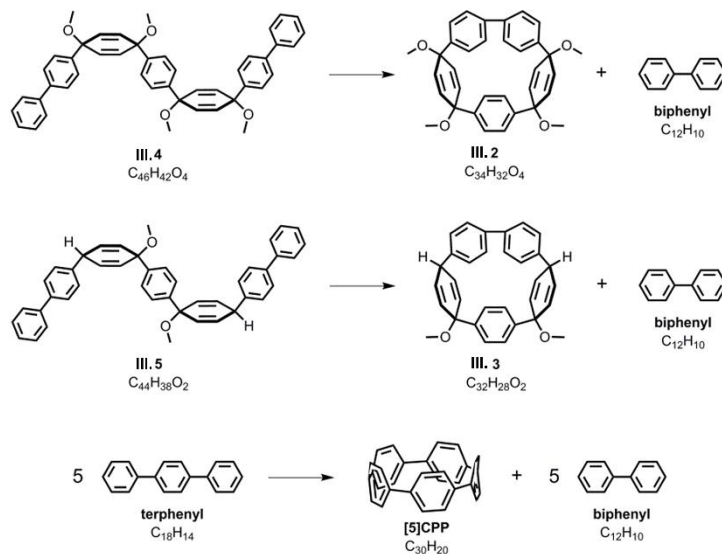


Figure III.9. Homodesmotic reactions used to calculate strain of macrocyclic compounds **III.2**, **III.3**, and **[5]CPP**.

Compound	Total Energy (Hartree)	Strain Energy (Hartree)	Strain Energy (kcal/mol)
biphenyl	-463.30607808		
terphenyl	-694.36374497		
[5]CPP	-1155.09824925	0.19008520	119.3
III.2	-1615.60352147	0.05061031	31.8
III.3	-1386.57340782	0.05555035	34.9
III.4	-2078.96020986		
III.5	-1849.93503625		

Table III.1. Summary of Homodesmotic Reactions Used to Calculate Strain of Macrocyclic Compounds **III.2**, **III.3**, and **[5]CPP**.

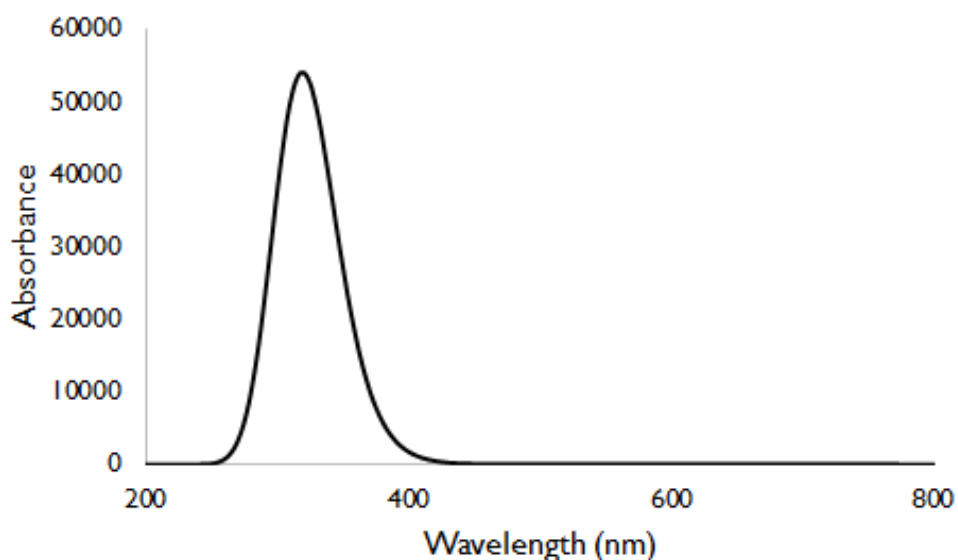


Figure III.10. Calculated UV-Vis for [5]CPP Determined by TD-DFT Method Using B3LYP/6-31g*.

Energy (cm ⁻¹)	Wavelength (nm)	Osc. Strength (f)	Major contribs
16491	606	0.0015	HOMO→LUMO (100%)
27461	364	0.0079	H-1→LUMO (28%) HOMO→L+1 (65%)
27580	363	0.0048	H-2→LUMO (37%) HOMO→L+2 (61%)
28182	355	0.0094	H-1→LUMO (20%) HOMO→L+3 (70%)
28824	347	0.0195	H-2→LUMO (11%) HOMO→L+4 (74%)
31245	320	0.6272	H-1→LUMO (49%) HOMO→L+1 (30%) HOMO→L+3 (16%)

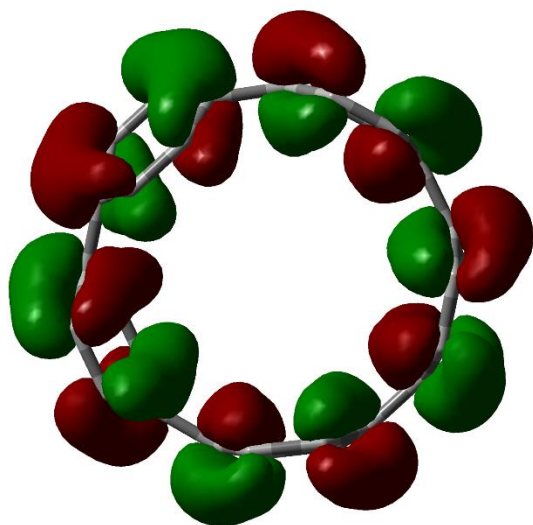
31376	319	0.6398	H-2→LUMO (48%) HOMO→L+2 (33%) HOMO→L+4 (13%)
33154	302	0.001	H-5→LUMO (13%) H-3→LUMO (55%) HOMO→L+5 (18%)
33318	300	0.013	H-6→LUMO (34%) H-4→LUMO (10%) HOMO→L+6 (41%)
33442	299	0.0416	H-5→LUMO (26%) H-3→LUMO (31%) HOMO→L+5 (29%)
33659	297	0.0227	H-4→LUMO (75%)
35402	282	0.008	H-7→LUMO (68%) HOMO→L+8 (21%)

Table III.2. Major Electronic Transitions for [5]CPP Determined by TD-DFT Method Using B3LYP/6-31g*.

Compound	Energy (Hartrees)	ΔE of kcal/mol
[5]CPP ⁻⁴	-1154.443944	363.4330402
[5]CPP ⁻³	-1154.795277	142.9682012
[5]CPP ⁻²	-1155.042566	-12.20813175
[5]CPP ⁻¹	-1155.12962	-66.83564457
[5]CPP Triplet Excited State	-1155.054351	-19.6033371
[5]CPP Singlet Excited State	-1155.096522	-46.06621191
[5]CPP	-1155.023111	0
[5]CPP ⁺¹	-1154.88608	85.98826633
[5]CPP ⁺²	-1154.554144	294.2813002
[5]CPP ⁺³	-1154.050269	610.468052
[5]CPP ⁺⁴	-1153.417265	1007.684317

Table III.3. Calculated Total Energies Reduced, Excited, and Oxidized [5]CPP and the Corresponding ΔE from the Neutral Ground State at the Restricted or Unrestricted B3LYP/6-31g* Level of Theory.

[5]CPP HOMO



[5]CPP LUMO



Figure III.11. Calculated HOMO and LUMO of Ground State [5]CPP at B3LYP/6-31g* Level of Theory.

Cartesian coordinates (in Å) of Macrocycle **III.2**:

C	-0.00287	-2.15455	0.94975
C	1.00735	-2.6536	1.64454
C	2.15923	-2.05156	1.64655
C	2.35105	-0.95233	0.92169
C	1.29157	-0.21789	0.38343
C	0.03908	-0.85687	0.39971
H	0.88004	-3.56362	2.19237
H	2.96855	-2.45974	2.21495
H	1.42822	0.75702	-0.03494
H	-0.83463	-0.38939	-0.00453
C	4.44531	-1.731	1.39713
C	5.68923	-1.99882	1.13241
C	6.35443	-1.26618	0.25379
C	5.84758	-0.04414	-0.23389
C	4.49531	0.2317	0.03526
C	3.81375	-0.74719	0.76234

H	3.91663	-2.32579	2.11248
H	6.1716	-2.82374	1.6137
H	6.45612	0.63075	-0.79898
H	4.01458	1.12168	-0.3141
C	6.6125	-4.73586	-0.10952
C	7.50116	-4.14804	1.0315
C	7.99983	-2.86965	1.00599
C	7.64417	-1.91308	-0.14089
C	7.41089	-2.70387	-1.44145
C	6.94967	-3.9879	-1.42464
H	7.74578	-4.77494	1.86368
H	8.6364	-2.53359	1.79753
H	7.61414	-2.23461	-2.38126
H	6.82439	-4.50131	-2.35511
C	3.10229	-5.99058	1.0281
C	4.50083	-5.79591	0.87241
C	5.0496	-4.68511	0.197
C	4.16251	-3.64444	-0.1799
C	2.61145	-3.85967	-0.00714
C	2.1406	-5.08934	0.52072
H	5.16743	-6.53104	1.27249
H	4.54119	-2.73106	-0.5891
H	1.92254	-3.09455	-0.29662
C	-0.17929	-4.98561	-0.63542
C	0.62123	-5.57023	0.55683
C	-0.1301	-5.20862	1.8775
C	-0.95232	-4.11591	1.99387
C	-1.12256	-3.1378	0.82268
C	-0.96548	-3.87703	-0.51829
H	-0.12047	-5.47574	-1.58467
H	-0.0113	-5.85094	2.72486

H	-1.47282	-3.93961	2.91204
H	-1.48431	-3.51104	-1.37976
O	8.67912	-0.94882	-0.34956
O	6.94391	-6.11944	-0.26277
O	-2.40018	-2.49721	0.86382
C	8.33357	-6.24755	-0.57426
H	8.91723	-5.83147	0.22006
H	8.57907	-7.28256	-0.69255
H	8.54427	-5.72491	-1.48365
C	-2.50529	-1.57838	-0.22737
H	-2.40355	-2.10846	-1.15157
H	-3.45956	-1.09548	-0.19674
H	-1.73116	-0.84408	-0.1506
C	9.89006	-1.61984	-0.70748
H	10.17493	-2.28578	0.08001
H	9.73622	-2.17726	-1.60789
H	10.66504	-0.89859	-0.86268
O	0.65231	-6.99492	0.44206
H	2.76302	-6.86644	1.54046
C	-0.68563	-7.49821	0.43651
H	-1.21935	-7.08029	-0.3914
H	-0.66582	-8.56403	0.34678
H	-1.17328	-7.22638	1.34951

Cartesian coordinates (in Å) of Macrocycle **III.3**:

C	-0.00287	-2.15455	0.94975
C	1.00735	-2.6536	1.64454
C	2.15923	-2.05156	1.64655
C	2.35105	-0.95233	0.92169
C	1.29157	-0.21789	0.38343
C	0.03908	-0.85687	0.39971

H	0.88004	-3.56362	2.19237
H	2.96855	-2.45974	2.21495
H	1.42822	0.75702	-0.03494
H	-0.83463	-0.38939	-0.00453
C	4.44531	-1.731	1.39713
C	5.68923	-1.99882	1.13241
C	6.35443	-1.26618	0.25379
C	5.84758	-0.04414	-0.23389
C	4.49531	0.2317	0.03526
C	3.81375	-0.74719	0.76234
H	3.91663	-2.32579	2.11248
H	6.1716	-2.82374	1.6137
H	6.45612	0.63075	-0.79898
H	4.01458	1.12168	-0.3141
C	6.6125	-4.73586	-0.10952
C	7.50116	-4.14804	1.0315
C	7.99983	-2.86965	1.00599
C	7.64417	-1.91308	-0.14089
C	7.41089	-2.70387	-1.44145
C	6.94967	-3.9879	-1.42464
H	7.74578	-4.77494	1.86368
H	8.6364	-2.53359	1.79753
H	7.61414	-2.23461	-2.38126
H	6.82439	-4.50131	-2.35511
C	3.10229	-5.99058	1.0281
C	4.50083	-5.79591	0.87241
C	5.0496	-4.68511	0.197
C	4.16251	-3.64444	-0.1799
C	2.61145	-3.85967	-0.00714
C	2.1406	-5.08934	0.52072
H	5.16743	-6.53104	1.27249

H	4.54119	-2.73106	-0.5891
H	1.92254	-3.09455	-0.29662
C	-0.17929	-4.98561	-0.63542
C	0.62123	-5.57023	0.55683
C	-0.1301	-5.20862	1.8775
C	-0.95232	-4.11591	1.99387
C	-1.12256	-3.1378	0.82268
C	-0.96548	-3.87703	-0.51829
H	-0.12047	-5.47574	-1.58467
H	-0.0113	-5.85094	2.72486
H	-1.47282	-3.93961	2.91204
H	-1.48431	-3.51104	-1.37976
O	6.94391	-6.11944	-0.26277
C	8.33357	-6.24755	-0.57426
H	8.91723	-5.83147	0.22006
H	8.57907	-7.28256	-0.69255
H	8.54427	-5.72491	-1.48365
O	0.65231	-6.99492	0.44206
H	2.76302	-6.86644	1.54046
C	-0.68563	-7.49821	0.43651
H	-1.21935	-7.08029	-0.3914
H	-0.66582	-8.56403	0.34678
H	-1.17328	-7.22638	1.34951
H	-2.07867	-2.65841	0.85347
H	8.41866	-1.19149	-0.29704

Cartesian coordinates (in Å) of [5]CPP:

C	-1.94207	-0.81005	-1.73001
C	-0.55981	-0.59243	-1.80113
C	-0.1535	0.74847	-1.80697
C	-0.88363	1.70256	-1.08548

C	-2.26658	1.4851	-1.01444
C	-2.73837	0.34164	-1.6736
H	-2.3631	-1.79264	-1.77412
H	0.1356	-1.39927	-1.90244
H	-0.4249	2.57253	-0.66401
H	-2.92489	2.17971	-0.53579
C	-4.44624	-0.69031	-3.25557
C	-4.05251	0.40445	-2.47402
C	-4.77264	1.60484	-2.54062
C	-5.32622	1.91528	-3.79017
C	-5.08776	0.98498	-4.81063
C	-4.99988	-0.37979	-4.50498
H	-4.28287	-1.70104	-2.94451
H	-4.84794	2.27149	-1.70697
H	-5.84827	2.83273	-3.96579
H	-5.28345	-1.13962	-5.20293
C	-4.75833	1.47442	-6.23306
C	-4.37282	0.55279	-7.2156
C	-3.33231	0.9623	-8.06014
C	-2.81328	2.24019	-7.81202
C	-3.65661	3.25803	-7.34665
C	-4.69737	2.84836	-6.50199
H	-4.80458	-0.42402	-7.28183
H	-2.92352	0.31608	-8.80853
H	-3.4846	4.28935	-7.57376
H	-5.36611	3.54882	-6.047
C	0.75902	1.35894	-7.48165
C	0.94308	2.37076	-6.52956
C	0.43675	3.65549	-6.76934
C	-0.75958	3.71329	-7.49754
C	-1.29389	2.47887	-7.89093

C	-0.43703	1.41689	-8.20982
H	1.45911	0.55943	-7.60613
H	0.90135	4.5344	-6.37362
H	-1.26102	4.63887	-7.68966
H	-0.70261	0.66441	-8.92267
C	0.98994	1.19756	-2.73551
C	1.61501	0.26268	-3.57145
C	1.91552	0.70716	-4.86591
C	1.55178	2.02894	-5.15639
C	1.60131	3.00372	-4.15011
C	1.30076	2.55879	-2.85511
H	1.79984	-0.74483	-3.26206
H	2.34308	0.05853	-5.60191
H	1.79927	4.03353	-4.36295
H	1.25616	3.22904	-2.0222

Cartesian coordinates (in Å) of biphenyl:

C	-2.5406	0.29002	0.
C	-1.14544	0.29002	0.
C	-0.44791	1.49777	0.
C	-1.14556	2.70628	-0.0012
C	-2.54038	2.70621	-0.00168
C	-3.23799	1.498	-0.00068
H	-3.09036	-0.66229	0.00045
H	-0.59594	-0.66249	0.00132
H	-0.59536	3.65843	-0.00126
H	-3.09051	3.65849	-0.00263
H	-4.33759	1.49818	-0.00086
C	1.09209	1.49789	0.00089
C	1.78953	2.70621	0.00089
C	1.78969	0.29003	0.0018

C	3.18424	2.70659	0.00112
H	1.23927	3.65829	-0.00061
C	3.18482	0.29024	0.00303
H	1.24016	-0.66241	0.00198
C	3.88216	1.49824	0.00255
H	3.73403	3.65897	0.00049
H	3.73458	-0.66225	0.00417
H	4.98184	1.49879	0.0028

Cartesian coordinates (in Å) of terphenyl:

C	-4.21114	-0.0348	0.
C	-2.81598	-0.0348	0.
C	-2.11844	1.17295	0.
C	-2.81609	2.38146	-0.0012
C	-4.21092	2.38138	-0.00168
C	-4.90852	1.17317	-0.00068
H	-4.7609	-0.98712	0.00045
H	-2.26647	-0.98732	0.00132
H	-2.26589	3.3336	-0.00126
H	-4.76104	3.33366	-0.00263
H	-6.00812	1.17336	-0.00086
C	-0.57844	1.17306	0.00089
C	0.11899	2.38139	0.00089
C	0.11915	-0.03479	0.0018
C	1.51371	2.38177	0.00112
H	-0.43127	3.33347	-0.00061
C	1.51429	-0.03459	0.00303
H	-0.43037	-0.98724	0.00198
C	2.21163	1.17341	0.00255
H	2.0635	3.33415	0.00049
H	2.06404	-0.98708	0.00417
C	3.75162	1.17418	0.00289

C	4.44975	-0.03375	0.00433
C	4.44853	2.38243	0.00166
C	5.84446	-0.03333	0.00521
H	3.90003	-0.98614	0.00608
C	5.84367	2.38302	0.00154
H	3.89846	3.33456	0.00035
C	6.54169	1.17542	0.00345
H	6.3948	-0.98539	0.00697
H	6.39288	3.33583	0.00015
H	7.64137	1.1755	0.00409

Cartesian coordinates (in Å) of open macrocycle **III.4**:

C	1.33985	-6.12655	2.98364
C	2.51154	-6.17337	3.75157
C	2.45903	-6.12711	5.14137
C	1.23352	-6.02422	5.82167
C	0.06358	-5.97323	5.04707
C	0.1156	-6.02626	3.65479
H	3.46874	-6.26514	3.24775
H	3.38199	-6.19856	5.71026
H	-0.90002	-5.8683	5.53794
H	-0.80857	-5.97859	3.08575
C	-5.29765	-1.38575	-5.03747
C	-5.59636	-1.2309	-3.68543
C	-6.3448	-0.13645	-3.23528
C	-6.79276	0.7953	-4.18005
C	-6.49636	0.6359	-5.53162
C	-5.73878	-0.45378	-5.99047
H	-4.73628	-2.2578	-5.36151
H	-5.25136	-1.97669	-2.97593
H	-7.37844	1.64545	-3.85057

H	-6.83666	1.38523	-6.24137
C	-4.80669	-0.96811	0.4719
C	-6.04667	-1.68221	-0.03333
C	-6.83364	-1.2265	-1.01073
C	-6.61448	0.08246	-1.7369
C	-5.44835	0.85231	-1.14487
C	-4.64604	0.3852	-0.18551
H	-6.25717	-2.63361	0.45188
H	-7.69997	-1.79756	-1.33963
H	-5.28114	1.8364	-1.57921
H	-3.81199	0.98039	0.18167
C	-2.03566	-3.58253	0.97934
C	-3.11296	-2.72738	1.219
C	-3.58271	-1.86654	0.22178
C	-2.9465	-1.88594	-1.02658
C	-1.87697	-2.74483	-1.26813
C	-1.40618	-3.6056	-0.26819
H	-3.58713	-2.71859	2.19324
H	-3.2863	-1.22479	-1.81786
H	-1.40745	-2.74831	-2.24804
C	-0.54428	-5.93535	-0.09464
C	-0.21302	-4.53091	-0.55399
C	1.03217	-4.00749	0.12629
C	1.76255	-4.70628	0.99467
C	1.43841	-6.11588	1.44644
C	0.17385	-6.62896	0.7904
H	-1.43521	-6.36811	-0.54575
H	1.32643	-3.00055	-0.16197
H	2.66487	-4.28343	1.43016
H	-0.14878	-7.62734	1.07818
O	-7.81777	0.87843	-1.69082

O	-4.86677	-0.81219	1.90522
O	2.59384	-6.87859	1.02027
C	-5.96081	-0.07004	2.41693
H	-6.92698	-0.53368	2.17586
H	-5.83224	-0.0591	3.50248
H	-5.96807	0.96422	2.04739
C	2.53235	-8.28579	1.20294
H	1.8358	-8.76235	0.49986
H	3.53985	-8.66024	1.00245
H	2.24986	-8.56087	2.22827
C	-8.25989	1.2834	-0.40611
H	-8.49718	0.42622	0.23808
H	-7.52148	1.91304	0.10869
H	-9.16984	1.86574	-0.5733
O	-0.03157	-4.50991	-1.98281
H	-1.68187	-4.24016	1.76387
C	1.00653	-5.33431	-2.49428
H	0.80669	-6.40085	-2.3266
H	1.03749	-5.13939	-3.56931
H	1.98128	-5.09251	-2.05242
C	0.14217	-6.6019	8.01433
C	0.09429	-6.55685	9.40691
C	1.08645	-5.88619	10.124
C	2.12681	-5.25992	9.43437
C	2.17172	-5.30194	8.041
C	1.18059	-5.97466	7.30492
H	-0.62059	-7.15106	7.46942
H	-0.71585	-7.05485	9.93308
H	1.0502	-5.85263	11.20942
H	2.90405	-4.73238	9.98144
H	2.97207	-4.78923	7.51474

C	-3.837	-1.19894	-9.19256
C	-4.14771	-1.06252	-7.8402
C	-5.41387	-0.61088	-7.43079
C	-6.36078	-0.30305	-8.42245
C	-6.05251	-0.44147	-9.77498
C	-4.78902	-0.88897	-10.16569
H	-2.84473	-1.53301	-9.48365
H	-3.39068	-1.28086	-7.09195
H	-7.35428	0.02339	-8.12745
H	-6.80366	-0.20569	-10.5246
H	-4.54787	-0.99387	-11.22026

Cartesian coordinates (in Å) of open macrocycle **III.5**:

C	1.33985	-6.12655	2.98364
C	2.51154	-6.17337	3.75157
C	2.45903	-6.12711	5.14137
C	1.23352	-6.02422	5.82167
C	0.06358	-5.97323	5.04707
C	0.1156	-6.02626	3.65479
H	3.46874	-6.26514	3.24775
H	3.38199	-6.19856	5.71026
H	-0.90002	-5.8683	5.53794
H	-0.80857	-5.97859	3.08575
C	-5.29765	-1.38575	-5.03747
C	-5.59636	-1.2309	-3.68543
C	-6.3448	-0.13645	-3.23528
C	-6.79276	0.7953	-4.18005
C	-6.49636	0.6359	-5.53162
C	-5.73878	-0.45378	-5.99047
H	-4.73628	-2.2578	-5.36151
H	-5.25136	-1.97669	-2.97593

H	-7.37844	1.64545	-3.85057
H	-6.83666	1.38523	-6.24137
C	-4.80669	-0.96811	0.4719
C	-6.04667	-1.68221	-0.03333
C	-6.83364	-1.2265	-1.01073
C	-6.61448	0.08246	-1.7369
C	-5.44835	0.85231	-1.14487
C	-4.64604	0.3852	-0.18551
H	-6.25717	-2.63361	0.45188
H	-7.69997	-1.79756	-1.33963
H	-5.28114	1.8364	-1.57921
H	-3.81199	0.98039	0.18167
C	-2.03566	-3.58253	0.97934
C	-3.11296	-2.72738	1.219
C	-3.58271	-1.86654	0.22178
C	-2.9465	-1.88594	-1.02658
C	-1.87697	-2.74483	-1.26813
C	-1.40618	-3.6056	-0.26819
H	-3.58713	-2.71859	2.19324
H	-3.2863	-1.22479	-1.81786
H	-1.40745	-2.74831	-2.24804
C	-0.54428	-5.93535	-0.09464
C	-0.21302	-4.53091	-0.55399
C	1.03217	-4.00749	0.12629
C	1.76255	-4.70628	0.99467
C	1.43841	-6.11588	1.44644
C	0.17385	-6.62896	0.7904
H	-1.43521	-6.36811	-0.54575
H	1.32643	-3.00055	-0.16197
H	2.66487	-4.28343	1.43016
H	-0.14878	-7.62734	1.07818

O	-4.86677	-0.81219	1.90522
C	-5.96081	-0.07004	2.41693
H	-6.92698	-0.53368	2.17586
H	-5.83224	-0.0591	3.50248
H	-5.96807	0.96422	2.04739
O	-0.03157	-4.50991	-1.98281
H	-1.68187	-4.24016	1.76387
C	1.00653	-5.33431	-2.49428
H	0.80669	-6.40085	-2.3266
H	1.03749	-5.13939	-3.56931
H	1.98128	-5.09251	-2.05242
C	0.14217	-6.6019	8.01433
C	0.09429	-6.55685	9.40691
C	1.08645	-5.88619	10.124
C	2.12681	-5.25992	9.43437
C	2.17172	-5.30194	8.041
C	1.18059	-5.97466	7.30492
H	-0.62059	-7.15106	7.46942
H	-0.71585	-7.05485	9.93308
H	1.0502	-5.85263	11.20942
H	2.90405	-4.73238	9.98144
H	2.97207	-4.78923	7.51474
C	-3.837	-1.19894	-9.19256
C	-4.14771	-1.06252	-7.8402
C	-5.41387	-0.61088	-7.43079
C	-6.36078	-0.30305	-8.42245
C	-6.05251	-0.44147	-9.77498
C	-4.78902	-0.88897	-10.16569
H	-2.84473	-1.53301	-9.48365
H	-3.39068	-1.28086	-7.09195
H	-7.35428	0.02339	-8.12745

H	-6.80366	-0.20569	-10.5246
H	-4.54787	-0.99387	-11.22026
H	-7.50644	0.67249	-1.70274
H	2.29188	-6.67926	1.13164

Cartesian coordinates (in Å) of **[5]CPP⁴⁺**:

C	-2.88209	-1.96002	-1.21329
C	-3.41488	-0.69595	-1.21345
C	-3.46115	0.06808	-0.00008
C	-3.4147	-0.69575	1.21343
C	-2.88198	-1.95986	1.21349
C	-2.36713	-2.5262	0.00014
H	-2.73757	-2.46671	-2.16095
H	-3.67645	-0.23848	-2.16115
H	-3.67614	-0.23804	2.16105
H	-2.73727	-2.46628	2.16127
C	-3.13376	1.47035	-0.00019
C	-2.75482	2.13522	1.21321
C	-2.75448	2.13492	-1.21359
C	-1.71724	3.03263	1.21332
H	-3.19207	1.84102	2.16084
C	-1.71681	3.03226	-1.21354
H	-3.19143	1.84059	-2.16132
C	-1.00481	3.31259	-0.00004
H	-1.36313	3.42286	2.161
H	-1.36239	3.42225	-2.16119
C	1.17961	3.27962	-1.21323
C	2.3537	2.57017	-1.21324
C	2.83982	1.97898	0.00016
C	2.35332	2.56955	1.21364
C	1.17922	3.27909	1.21363

C	0.43003	3.43461	0.00016
H	0.7649	3.60454	-2.16093
H	2.83446	2.3541	-2.16087
H	2.83381	2.35313	2.16132
H	0.76434	3.60366	2.16137
C	-0.39352	-3.46222	-1.2133
C	0.97334	-3.34641	-1.2134
C	1.67107	-3.03155	-0.00003
C	0.97342	-3.34597	1.21349
C	-0.39345	-3.46188	1.21363
C	-1.13434	-3.2704	0.00019
H	-0.90953	-3.56947	-2.16094
H	1.4998	-3.36552	-2.16115
H	1.49999	-3.36484	2.16118
H	-0.90933	-3.56899	2.16137
C	2.75995	-2.08924	-0.00023
C	3.17201	-1.44428	1.21315
C	3.17135	-1.44404	-1.21365
C	3.48439	-0.10855	1.21322
H	3.11493	-1.96832	2.16071
C	3.4837	-0.10827	-1.21353
H	3.11396	-1.96789	-2.1613
C	3.40001	0.65247	-0.00007
H	3.66578	0.38611	2.1609
H	3.66464	0.3866	-2.1612

Cartesian coordinates (in Å) of **[5]CPP⁺³**:

C	-2.78108	-1.71521	-1.20575
C	-3.45161	-0.67932	-1.28584
C	-3.49785	0.08471	-0.07247
C	-3.47438	-0.62465	1.14104
C	-2.89578	-1.99772	1.14111

C	-2.40391	-2.5096	-0.07225
H	-2.52201	-2.03212	-2.2098
H	-3.71315	-0.22184	-2.23354
H	-3.7358	-0.16693	2.08865
H	-2.75109	-2.50415	2.08889
C	-3.17042	1.48697	-0.07258
C	-2.63314	1.99779	1.19825
C	-2.79112	2.15153	-1.28598
C	-1.75385	3.04921	1.14093
H	-3.05996	1.72448	2.15683
C	-1.75342	3.04884	-1.28592
H	-3.22808	1.85721	-2.23371
C	-1.04141	3.32915	-0.07243
H	-1.51003	3.57778	2.05577
H	-1.39899	3.43882	-2.23358
C	1.14301	3.29612	-1.28562
C	2.31708	2.58663	-1.28563
C	2.80317	1.99543	-0.07223
C	2.31669	2.58601	1.14125
C	1.14262	3.29558	1.14124
C	0.39339	3.21897	-0.12582
H	0.7283	3.62105	-2.23332
H	2.79782	2.37055	-2.23326
H	2.87058	2.33652	2.23371
H	0.72774	3.62017	2.08898
C	-0.43032	-3.44568	-1.28569
C	0.93654	-3.3299	-1.28579
C	1.63428	-3.01506	-0.07242
C	0.93662	-3.32946	1.1411
C	-0.29249	-3.21715	1.06123
C	-1.17114	-3.25383	-0.0722

H	-0.94634	-3.55291	-2.23333
H	1.463	-3.34903	-2.23354
H	1.46319	-3.34836	2.08879
H	-0.6938	-3.13447	2.06519
C	2.72319	-2.07278	-0.07262
C	3.13527	-1.42784	1.14076
C	3.1346	-1.4276	-1.28603
C	3.44768	-0.09212	1.14084
H	3.07817	-1.95188	2.08832
C	3.447	-0.09183	-1.28592
H	3.07721	-1.95144	-2.23369
C	3.36333	0.6689	-0.07246
H	3.62909	0.40254	2.08851
H	3.62795	0.40303	-2.23359

Cartesian coordinates (in Å) of **[5]CPP⁺²**:

C	3.30494	-1.12941	1.23592
C	3.49852	0.24571	1.15125
C	3.40515	0.92232	-0.08302
C	3.51865	0.09772	-1.22267
C	3.29495	-1.27313	-1.13835
C	2.9771	-1.88797	0.0916
H	3.23461	-1.56959	2.22583
H	3.53942	0.80698	2.07968
H	3.60536	0.53701	-2.21188
H	3.19427	-1.82521	-2.06777
C	2.70599	2.24136	-0.15409
C	1.99007	2.56702	-1.32411
C	2.30045	2.93345	1.00874
C	0.74703	3.18579	-1.25732
H	2.29168	2.1563	-2.2817

C	1.05851	3.56146	1.0751
H	2.88229	2.85531	1.92297
C	0.1664	3.5202	-0.01803
H	0.14572	3.20976	-2.1606
H	0.72662	3.94851	2.03512
C	-1.70836	2.62599	1.33708
C	-2.68616	1.63763	1.31381
C	-3.29534	1.24827	0.10502
C	-3.15733	2.15483	-0.96803
C	-2.17821	3.14653	-0.94404
C	-1.29652	3.26766	0.1524
H	-1.1182	2.73045	2.2417
H	-2.80578	1.02239	2.20002
H	-3.71243	1.99535	-1.88921
H	-2.00656	3.72629	-1.84746
C	1.13917	-3.06353	1.31873
C	-0.23141	-3.28517	1.24902
C	-0.88699	-3.41075	0.00822
C	-0.0473	-3.69542	-1.09009
C	1.32428	-3.46249	-1.02133
C	1.9188	-2.94229	0.14986
H	1.5502	-2.78231	2.28229
H	-0.81105	-3.14803	2.15636
H	-0.47816	-3.95054	-2.05474
H	1.90079	-3.54277	-1.93848
C	-2.21011	-2.73626	-0.1538
C	-2.4243	-2.00269	-1.33761
C	-3.00808	-2.35815	0.94825
C	-3.06529	-0.76886	-1.31048
H	-1.90065	-2.27853	-2.24712
C	-3.65015	-1.12123	0.97601

H	-3.00884	-2.96124	1.85265
C	-3.52092	-0.21516	-0.09817
H	-3.00536	-0.14683	-2.19804
H	-4.12511	-0.80381	1.90107

Cartesian coordinates (in Å) of **[5]CPP⁺¹**:

C	3.30494	-1.12941	1.23592
C	3.49852	0.24571	1.15125
C	3.40515	0.92232	-0.08302
C	3.51865	0.09772	-1.22267
C	3.29495	-1.27313	-1.13835
C	2.9771	-1.88797	0.0916
H	3.23461	-1.56959	2.22583
H	3.53942	0.80698	2.07968
H	3.60536	0.53701	-2.21188
H	3.19427	-1.82521	-2.06777
C	2.70599	2.24136	-0.15409
C	1.99007	2.56702	-1.32411
C	2.30045	2.93345	1.00874
C	0.74703	3.18579	-1.25732
H	2.29168	2.1563	-2.2817
C	1.05851	3.56146	1.0751
H	2.88229	2.85531	1.92297
C	0.1664	3.5202	-0.01803
H	0.14572	3.20976	-2.1606
H	0.72662	3.94851	2.03512
C	-1.70836	2.62599	1.33708
C	-2.68616	1.63763	1.31381
C	-3.29534	1.24827	0.10502
C	-3.15733	2.15483	-0.96803
C	-2.17821	3.14653	-0.94404

C	-1.29652	3.26766	0.1524
H	-1.1182	2.73045	2.2417
H	-2.80578	1.02239	2.20002
H	-3.71243	1.99535	-1.88921
H	-2.00656	3.72629	-1.84746
C	1.13917	-3.06353	1.31873
C	-0.23141	-3.28517	1.24902
C	-0.88699	-3.41075	0.00822
C	-0.0473	-3.69542	-1.09009
C	1.32428	-3.46249	-1.02133
C	1.9188	-2.94229	0.14986
H	1.5502	-2.78231	2.28229
H	-0.81105	-3.14803	2.15636
H	-0.47816	-3.95054	-2.05474
H	1.90079	-3.54277	-1.93848
C	-2.21011	-2.73626	-0.1538
C	-2.4243	-2.00269	-1.33761
C	-3.00808	-2.35815	0.94825
C	-3.06529	-0.76886	-1.31048
H	-1.90065	-2.27853	-2.24712
C	-3.65015	-1.12123	0.97601
H	-3.00884	-2.96124	1.85265
C	-3.52092	-0.21516	-0.09817
H	-3.00536	-0.14683	-2.19804
H	-4.12511	-0.80381	1.90107

Cartesian coordinates (in Å) of **[5]CPP** Triplet Excited State:

C	2.11264	3.16836	0.95683
C	3.10732	2.19263	0.99128
C	3.27937	1.29632	-0.08577
C	2.68747	1.68736	-1.30241

C	1.69484	2.66044	-1.33614
C	1.24883	3.28495	-0.15474
H	1.91647	3.73735	1.86196
H	3.64743	2.03515	1.92165
H	2.83364	1.08276	-2.19198
H	1.12327	2.76365	-2.25272
C	-0.81587	3.22484	1.23636
C	-0.21948	3.51826	-0.00616
C	-1.097	3.50474	-1.11195
C	-2.32755	2.85643	-1.04014
C	-2.74075	2.20275	0.14207
C	-2.05071	2.59041	1.30927
H	-0.23274	3.29923	2.14889
H	-0.75901	3.85995	-2.08186
H	-2.88939	2.72974	-1.9611
H	-2.36657	2.2243	2.28035
C	-3.41642	0.86936	0.10145
C	-3.46047	0.05282	1.25163
C	-3.21792	-1.31432	1.16882
C	-2.94932	-1.9353	-0.06891
C	-3.34131	-1.19341	-1.20397
C	-3.55614	0.17902	-1.12186
H	-3.50027	0.49802	2.24079
H	-3.05446	-1.85368	2.09669
H	-3.31264	-1.64472	-2.19138
H	-3.66001	0.72946	-2.05197
C	0.10444	-3.73019	1.05993
C	0.93682	-3.39731	-0.03061
C	0.27875	-3.24036	-1.26616
C	-1.09499	-3.03643	-1.32696
C	-1.8745	-2.97065	-0.15436

C	-1.27159	-3.51996	0.9993
H	0.54268	-4.00918	2.01482
H	0.85621	-3.0599	-2.16737
H	-1.51077	-2.71956	-2.27746
H	-1.84835	-3.64373	1.91177
C	3.52142	-0.16494	0.11216
C	3.06287	-0.73114	1.31737
C	2.44057	-1.97475	1.33324
C	2.24973	-2.70588	0.14458
C	3.05118	-2.31095	-0.94915
C	3.67414	-1.06412	-0.96556
H	2.98356	-0.11427	2.20696
H	1.91017	-2.26212	2.23547
H	3.06878	-2.9106	-1.85576
H	4.15383	-0.73557	-1.88427

Cartesian coordinates (in Å) of **[5]CPP** Singlet Excited State:

C	-0.65812	-3.43717	-1.20535
C	0.71495	-3.42566	-1.20527
C	1.44972	-3.16983	-0.00007
C	0.71482	-3.42649	1.20484
C	-0.65827	-3.43803	1.20474
C	-1.39716	-3.19348	-0.00025
H	-1.17514	-3.48828	-2.15866
H	1.23294	-3.46803	-2.15849
H	1.23267	-3.4696	2.15811
H	-1.1754	-3.48991	2.15795
C	-3.04225	-1.73945	-1.20489
C	-2.56955	-2.35808	-0.00007
C	-3.04171	-1.73951	1.20501
C	-3.47757	-0.43734	1.2051

C	-3.4734	0.34127	0.00022
C	-3.47813	-0.43726	-1.2047
H	-2.92318	-2.24514	-2.15821
H	-2.92214	-2.24524	2.15824
H	-3.68699	0.03793	2.1585
H	-3.68803	0.03804	-2.15798
C	-3.03877	1.71389	0.00019
C	-2.5944	2.35273	-1.20479
C	-1.48961	3.16842	-1.20488
C	-0.74814	3.40498	-0.00009
C	-1.4893	3.1684	1.20488
C	-2.5941	2.35272	1.20508
H	-3.03777	2.08257	-2.15828
H	-1.10112	3.51289	-2.15837
H	-1.10054	3.51284	2.15828
H	-3.03726	2.08258	2.15867
C	2.55482	2.39486	-1.20516
C	3.00977	1.76359	-0.00007
C	2.55514	2.39554	1.20476
C	1.43712	3.19291	1.20461
C	0.69185	3.41708	-0.00024
C	1.43681	3.19223	-1.20518
H	3.00249	2.13189	-2.15863
H	3.00309	2.13316	2.15828
H	1.04304	3.53135	2.15799
H	1.04247	3.5301	-2.15864
C	2.60824	-2.31547	0.00019
C	3.07095	-1.68926	-1.2047
C	3.48492	-0.38002	-1.20468
C	3.46704	0.39853	0.00018
C	3.48401	-0.37974	1.20528

C	3.07005	-1.68895	1.2053
H	2.9607	-2.19704	-2.15796
H	3.6872	0.0987	-2.15793
H	3.6855	0.09927	2.15855
H	2.95901	-2.19649	2.1586

Cartesian coordinates (in Å) of **[5]CPP⁻¹**:

C	3.30494	-1.12941	1.23592
C	3.49852	0.24571	1.15125
C	3.40515	0.92232	-0.08302
C	3.51865	0.09772	-1.22267
C	3.29495	-1.27313	-1.13835
C	2.9771	-1.88797	0.0916
H	3.23461	-1.56959	2.22583
H	3.53942	0.80698	2.07968
H	3.60536	0.53701	-2.21188
H	3.19427	-1.82521	-2.06777
C	2.70599	2.24136	-0.15409
C	1.99007	2.56702	-1.32411
C	2.30045	2.93345	1.00874
C	0.74703	3.18579	-1.25732
H	2.29168	2.1563	-2.2817
C	1.05851	3.56146	1.0751
H	2.88229	2.85531	1.92297
C	0.1664	3.5202	-0.01803
H	0.14572	3.20976	-2.1606
H	0.72662	3.94851	2.03512
C	-1.70836	2.62599	1.33708
C	-2.68616	1.63763	1.31381
C	-3.29534	1.24827	0.10502
C	-3.15733	2.15483	-0.96803

C	-2.17821	3.14653	-0.94404
C	-1.29652	3.26766	0.1524
H	-1.1182	2.73045	2.2417
H	-2.80578	1.02239	2.20002
H	-3.71243	1.99535	-1.88921
H	-2.00656	3.72629	-1.84746
C	1.13917	-3.06353	1.31873
C	-0.23141	-3.28517	1.24902
C	-0.88699	-3.41075	0.00822
C	-0.0473	-3.69542	-1.09009
C	1.32428	-3.46249	-1.02133
C	1.9188	-2.94229	0.14986
H	1.5502	-2.78231	2.28229
H	-0.81105	-3.14803	2.15636
H	-0.47816	-3.95054	-2.05474
H	1.90079	-3.54277	-1.93848
C	-2.21011	-2.73626	-0.1538
C	-2.4243	-2.00269	-1.33761
C	-3.00808	-2.35815	0.94825
C	-3.06529	-0.76886	-1.31048
H	-1.90065	-2.27853	-2.24712
C	-3.65015	-1.12123	0.97601
H	-3.00884	-2.96124	1.85265
C	-3.52092	-0.21516	-0.09817
H	-3.00536	-0.14683	-2.19804
H	-4.12511	-0.80381	1.90107

Cartesian coordinates (in Å) of [5]CPP²:

C	3.30494	-1.12941	1.23592
C	3.49852	0.24571	1.15125
C	3.40515	0.92232	-0.08302

C	3.51865	0.09772	-1.22267
C	3.29495	-1.27313	-1.13835
C	2.9771	-1.88797	0.0916
H	3.23461	-1.56959	2.22583
H	3.53942	0.80698	2.07968
H	3.60536	0.53701	-2.21188
H	3.19427	-1.82521	-2.06777
C	2.70599	2.24136	-0.15409
C	1.99007	2.56702	-1.32411
C	2.30045	2.93345	1.00874
C	0.74703	3.18579	-1.25732
H	2.29168	2.1563	-2.2817
C	1.05851	3.56146	1.0751
H	2.88229	2.85531	1.92297
C	0.1664	3.5202	-0.01803
H	0.14572	3.20976	-2.1606
H	0.72662	3.94851	2.03512
C	-1.70836	2.62599	1.33708
C	-2.68616	1.63763	1.31381
C	-3.29534	1.24827	0.10502
C	-3.15733	2.15483	-0.96803
C	-2.17821	3.14653	-0.94404
C	-1.29652	3.26766	0.1524
H	-1.1182	2.73045	2.2417
H	-2.80578	1.02239	2.20002
H	-3.71243	1.99535	-1.88921
H	-2.00656	3.72629	-1.84746
C	1.13917	-3.06353	1.31873
C	-0.23141	-3.28517	1.24902
C	-0.88699	-3.41075	0.00822
C	-0.0473	-3.69542	-1.09009

C	1.32428	-3.46249	-1.02133
C	1.9188	-2.94229	0.14986
H	1.5502	-2.78231	2.28229
H	-0.81105	-3.14803	2.15636
H	-0.47816	-3.95054	-2.05474
H	1.90079	-3.54277	-1.93848
C	-2.21011	-2.73626	-0.1538
C	-2.4243	-2.00269	-1.33761
C	-3.00808	-2.35815	0.94825
C	-3.06529	-0.76886	-1.31048
H	-1.90065	-2.27853	-2.24712
C	-3.65015	-1.12123	0.97601
H	-3.00884	-2.96124	1.85265
C	-3.52092	-0.21516	-0.09817
H	-3.00536	-0.14683	-2.19804
H	-4.12511	-0.80381	1.90107

Cartesian coordinates (in Å) of **[5]CPP³⁻**:

C	-0.07178	3.53887	1.19513
C	-1.41838	3.24401	1.19505
C	-2.10335	2.83251	-0.00005
C	-1.41832	3.244	-1.19512
C	-0.07173	3.53887	-1.19508
C	0.72242	3.4523	0.00004
H	0.41775	3.68242	2.15797
H	-1.92293	3.16967	2.15796
H	-1.92283	3.16969	-2.15804
H	0.41785	3.68236	-2.15791
C	-3.06103	1.75411	-0.00005
C	-3.38889	1.02547	-1.19514
C	-3.38904	1.02552	1.19502

C	-3.52427	-0.34638	-1.19509
H	-3.37471	1.53545	-2.15798
C	-3.52441	-0.34632	1.19504
H	-3.37494	1.53552	2.15785
C	-3.34451	-1.12498	0.00001
H	-3.60977	-0.84907	-2.15802
H	-3.61003	-0.84892	2.15801
C	-2.02275	-2.90556	1.1952
C	-0.75948	-3.45735	1.19518
C	0.03638	-3.5266	0.00002
C	-0.75956	-3.4575	-1.19506
C	-2.02283	-2.90573	-1.19506
C	-2.61461	-2.36888	0.00004
H	-2.50332	-2.73437	2.15805
H	-0.30737	-3.69366	2.15801
H	-0.30756	-3.69389	-2.15792
H	-2.50339	-2.73465	-2.15793
C	2.64735	2.35106	1.19519
C	3.34483	1.16207	1.19518
C	3.50803	0.37997	0.
C	3.34495	1.16219	-1.19511
C	2.64749	2.35117	-1.19506
C	2.04418	2.87504	0.00005
H	2.42052	2.8079	2.15807
H	3.63301	0.74094	2.15799
H	3.63321	0.74116	-2.15794
H	2.42075	2.80807	-2.15794
C	3.36665	-1.05532	-0.00004
C	3.05467	-1.79091	-1.19512
C	3.05484	-1.79105	1.19498
C	2.13886	-2.82124	-1.19512

H	3.41945	-1.43437	-2.15798
C	2.13902	-2.82135	1.195
H	3.4197	-1.43464	2.15785
C	1.44517	-3.21776	-0.00002
H	1.82755	-3.22544	-2.15795
H	1.82785	-3.22558	2.15786

Cartesian coordinates (in Å) of [5]CPP⁴:

C	-0.07178	3.53887	1.19513
C	-1.41838	3.24401	1.19505
C	-2.10335	2.83251	-0.00005
C	-1.41832	3.244	-1.19512
C	-0.07173	3.53887	-1.19508
C	0.72242	3.4523	0.00004
H	0.41775	3.68242	2.15797
H	-1.92293	3.16967	2.15796
H	-1.92283	3.16969	-2.15804
H	0.41785	3.68236	-2.15791
C	-3.06103	1.75411	-0.00005
C	-3.38889	1.02547	-1.19514
C	-3.38904	1.02552	1.19502
C	-3.52427	-0.34638	-1.19509
H	-3.37471	1.53545	-2.15798
C	-3.52441	-0.34632	1.19504
H	-3.37494	1.53552	2.15785
C	-3.34451	-1.12498	0.00001
H	-3.60977	-0.84907	-2.15802
H	-3.61003	-0.84892	2.15801
C	-2.02275	-2.90556	1.1952
C	-0.75948	-3.45735	1.19518
C	0.03638	-3.5266	0.00002

C	-0.75956	-3.4575	-1.19506
C	-2.02283	-2.90573	-1.19506
C	-2.61461	-2.36888	0.00004
H	-2.50332	-2.73437	2.15805
H	-0.30737	-3.69366	2.15801
H	-0.30756	-3.69389	-2.15792
H	-2.50339	-2.73465	-2.15793
C	2.64735	2.35106	1.19519
C	3.34483	1.16207	1.19518
C	3.50803	0.37997	0.
C	3.34495	1.16219	-1.19511
C	2.64749	2.35117	-1.19506
C	2.04418	2.87504	0.00005
H	2.42052	2.8079	2.15807
H	3.63301	0.74094	2.15799
H	3.63321	0.74116	-2.15794
H	2.42075	2.80807	-2.15794
C	3.36665	-1.05532	-0.00004
C	3.05467	-1.79091	-1.19512
C	3.05484	-1.79105	1.19498
C	2.13886	-2.82124	-1.19512
H	3.41945	-1.43437	-2.15798
C	2.13902	-2.82135	1.195
H	3.4197	-1.43464	2.15785
C	1.44517	-3.21776	-0.00002
H	1.82755	-3.22544	-2.15795
H	1.82785	-3.22558	2.15786

III.4.7. Crystallographic Details.

General X-ray data collection: *APEX2* (Bruker, 2006); data reduction: *SAINT* (Bruker, 2006); program(s) used to refine structure: *SHELXL* (Sheldrick, 2008); molecular graphics: *Olex2* (Dolomanov *et al.*, 2009); software used to prepare material for publication: *Olex2* (Dolomanov *et al.*, 2009).

X-ray crystallographic data for compound **III.3**

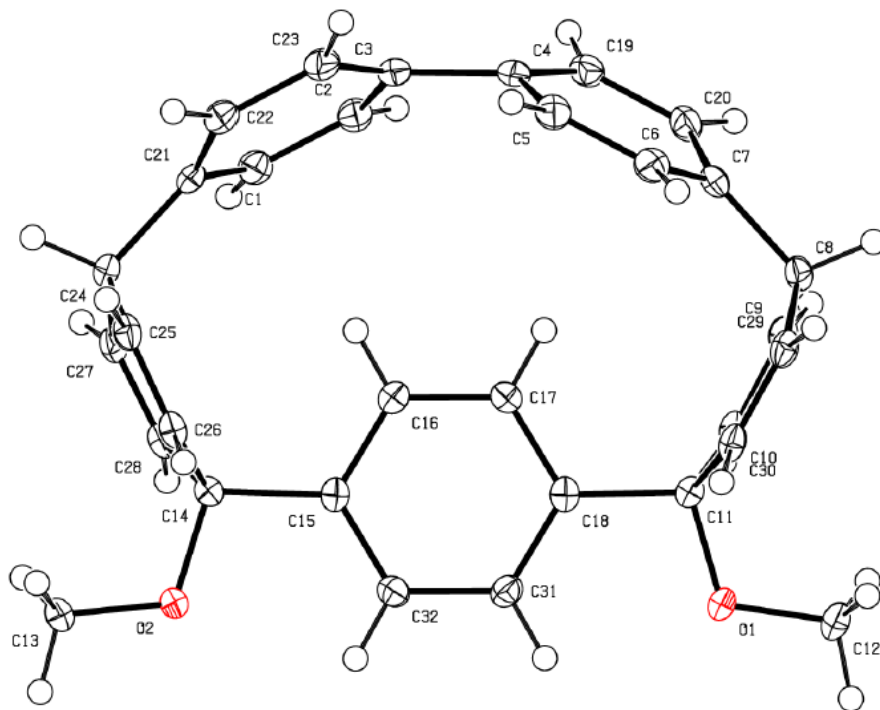


Figure 12. ORTEP Representation of X-ray Crystallographic Structure **III.3** (CCDC Registry #974188).

Crystallographic Data for **III.3**: $C_{32}H_{28}O_2$, $M = 444.54$, $0.11 \times 0.10 \times 0.06$ mm, $T = 100$ K, Monoclinic, space group $P2_1/c$, $a = 17.444$ (3) Å, $b = 10.8686$ (19) Å, $c = 12.1775$ (19), $\beta = 92.014$ (6)°, $V = 2307.3$ (7) Å³, $Z = 4$, $D_c = 1.286$ Mg/m³, $\mu(\text{Cu } K\alpha) = 7.445$ mm⁻¹, $F(000) = 944.0$, $2\theta_{\text{max}} = 133.8^\circ$, 9074 reflections, 3835 independent reflections.

X-ray crystallographic data for compound [5]CPP

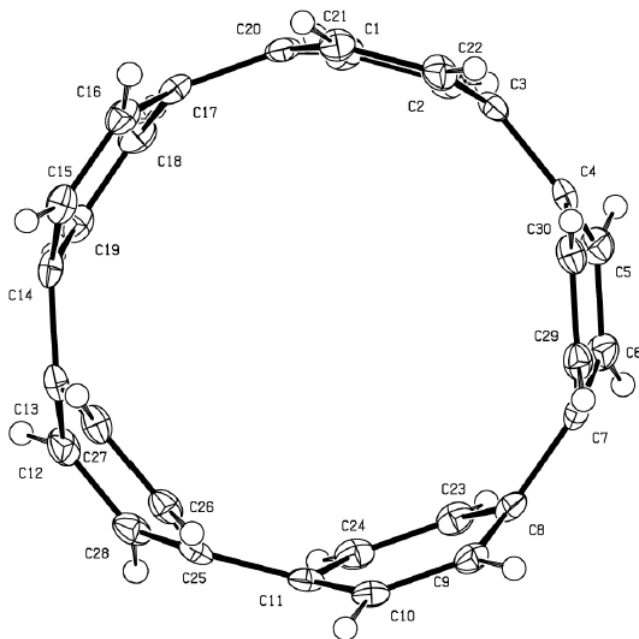


Figure 13. ORTEP Representation of X-ray Crystallographic Structure [5]CPP (CCDC Registry #974187).

Crystallographic Data for [5]CPP: $C_{30}H_{20}$, $M = 380.46$, $0.51 \times 0.44 \times 0.42$ mm, $T = 100$ K, Orthorhombic, space group $Pbca$, $a = 9.8337$ (2) Å, $b = 11.6263$ (3) Å, $c = 35.5613$ (8), $\beta = 66.6^\circ$, $V = 4065.71$ (16) Å³, $Z = 8$, $D_c = 1.243$ Mg/m³, $\mu(\text{Cu } K\alpha) = 7.445$ mm⁻¹, $F(000) = 1600$, $2\theta_{\text{max}} = 133.8^\circ$, 9831 reflections, 3543 independent reflections.

III.5. Bridge to Chapter IV.

Chapter III presented the synthesis of the smallest nanohoop to date, [5]CPP. We recognized the potential power of the key macrocyclization from this study which was carried out at room temperature open to atmosphere and was capable of providing gram quantities of macrocycle. Chapter I highlighted the unique properties of [n]CPPs and showed that the electrochemical properties become more advantageous as the size of the hoop became smaller. Chapter II showed that the smaller more strained nanohoops were more difficult to access often limited by the macrocyclization step. In Chapter IV, we sought to expand on the coupling from Chapter III to optimize standard conditions towards the scalable synthesis of [5]-[7]CPP, a strained alkyne, and a formal synthesis of the natural product Acerogenin E.

CHAPTER IV

AN OPERATIONALLY SIMPLE AND MILD OXIDATIVE HOMOCOUPLING OF ARYL BORONIC ESTERS TO ACCESS CONFORMATIONALLY CONSTRAINED MACROCYCLES

Chapter **IV** is based on unpublished work. The manuscript was written by myself and edited by Professor Ramesh Jasti. Brittany White is responsible for the formal synthesis of Acerogenin E. Lance Loventhal is responsible for the alkyne containing macrocycle. I devised the mechanistic studies and the synthesis of the remaining compounds.

Macrocyclic molecules are widely recognized as useful structural motifs across many disciplines including medicinal and materials chemistry. Although palladium catalyzed oxidative homocoupling of aryl boronic acids and esters to biphenylenes has been recognized as a common byproduct in Suzuki-Miyaura cross-couplings for decades, it has found few applications in the synthesis of challenging molecules. Here we report an oxidative boronic ester homocoupling as a mild method for the synthesis of strained and conformationally restricted macrocycles. Higher yields and better efficiencies are observed for intramolecular diboronic ester homocoupling when directly compared to the analogous intramolecular Suzuki-Miyaura cross-coupling and reductive Yamamoto homocoupling. Substrates include strained polyphenylene macrocycles, strained cycloalkynes, and a formal synthesis of Acerogenin A. The reaction is performed at room temperature, open to atmosphere, and without the need to rigorously exclude water, thus representing an operationally simple alternative to traditional cross-coupling macrocyclizations.

IV.1. Introduction.

Macrocyclic molecules are widely recognized as useful structural motifs across disciplines including material science,¹⁻⁴ medicinal chemistry,^{5,6} and supramolecular chemistry.⁷⁻¹⁴ Synthetic methods towards efficient macrocycle formation, however, remain a challenge and often represent the limiting step in a synthetic sequence. This limitation becomes increasingly apparent when the desired macrocycle is sterically congested, conformationally restricted, or distorted from ideal geometry. Examples of challenging biaryl containing macrocycles range from natural products such as Houamine

A^{15,16} or Vancomycin¹⁷⁻²⁰ to the “bent and battered” benzene rings found in cyclophanes.²¹ These classic examples have served as inspiration to develop reactions capable of accommodating both strained and congested macrocycles under mild transition metal catalyzed conditions. The strain and conformational restriction imparted by the macrocyclic motif is often directly responsible for their desirable properties. Examples include the strain-induced increase in conjugation observed in [n]cycloparaphenylenes ([n]CPPs),^{22,23} strain releasing ring-opening metathesis polymerization of norbornene,^{1,3} and locked conformations that can increase drug binding in medicinal chemistry.⁶

Typical transition metal catalysis for intramolecular biaryl coupling can be broken down into three classes as shown in **Figure IV.1**.²⁴ First, a redox neutral cross-coupling of a nucleophile and electrophile can give strained biaryl macrocycles as in the case of a Suzuki-Miyaura, Negishi, and Stille cross-coupling. Next, a reductive coupling can be used to bring two electrophilic ends together to give the desired macrocyclic structure as in the case of the Yamamoto coupling. Finally, the oxidative homocoupling of nucleophiles such as the widely used Glaser-Hay reaction used to form diynes. The downside of these approaches are the need for an inert oxygen free environment and often harsh conditions in order to accommodate the oxidative insertion step. In 2014 we observed strained macrocycle **IV.2** as a minor byproduct in a Suzuki-Miyaura cross-coupling utilizing diboronic ester **IV.1** (**Figure IV.2**).²⁵ This reaction was found to run efficiently at room temperature and open to air through a palladium catalyzed oxidative homocoupling. This oxidative homocoupling was the key observation in the synthesis and characterization of [5]CPP, a fragment of C₆₀, which contains an estimated 120 kcal/mol of strain. Although this oxidative homocoupling had been established as a side product in Suzuki-Miyaura cross-coupling, there has been little application to complex molecules.²⁶ The major exception to this being the pioneering work by Merlic on the oxidative homocoupling of vinyl boronic esters in the synthesis of complex cyclic dienes.^{27,28} In the ensuing study we sought to optimize a set of standardized conditions for this mild oxidative homocoupling and compare the reactivity to both an analogous intramolecular Suzuki-Miyaura cross-coupling and an intramolecular Yamamoto coupling. We then applied this operationally simple and efficient palladium catalyzed

intramolecular oxidative homocoupling of aryl boronic esters under atmospheric conditions towards the synthesis of strained nanohoop structures, alkynes, and the formal synthesis of Acerogenin E,²⁹ a cyclophane based natural product.

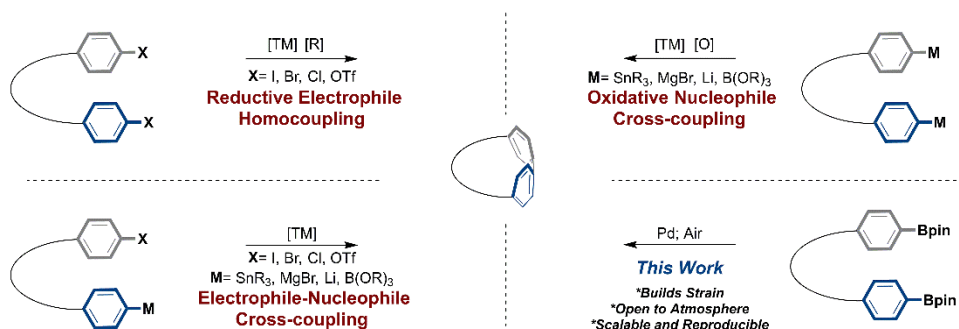


Figure IV.1.: Common Intramolecular Macrocyclization Strategies.

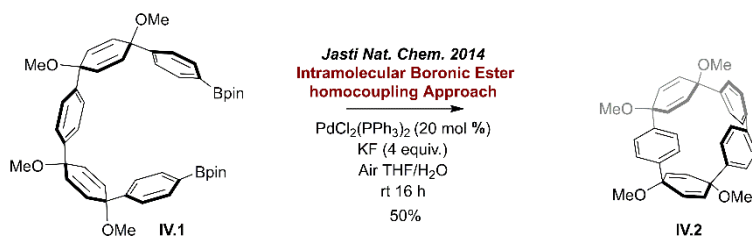


Figure IV.2.: Seminal Report of the Oxidative Homocoupling of Aryl Diboronic Ester IV.1 to Form Strained Macrocycle IV.2.

IV.2. Results and Discussion.

IV.2.1. Reaction Optimization.

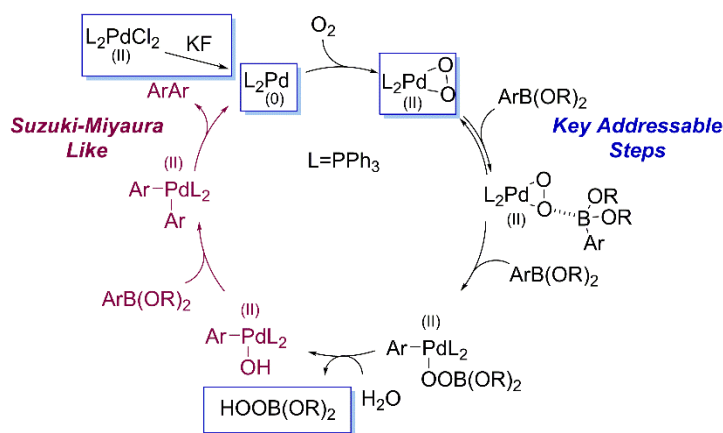


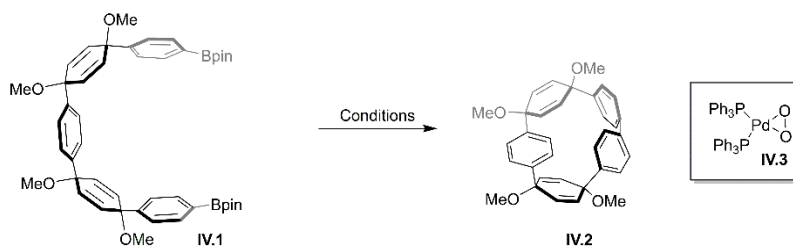
Figure IV.3. Proposed Catalytic Cycle by Adamo.

The palladium catalyzed homocoupling of aryl boronic acids and esters has been identified for decades as the major side product in Suzuki-Miyaura cross-couplings.³⁰ Much of the research associated with this reaction have been dedicated towards better

optimization in Suzuki-Miyaura cross-coupling and limiting this side-reaction.³¹ Although there have been several works demonstrating highly efficient homocoupling of simple boronic acids and esters to make substituted biphenyls, there have been few applications in the synthesis of complex molecules or cyclic motifs.³²⁻³⁷ The reported oxidative homocoupling of nucleophiles (boronic esters) serves as a strategic compliment to electrophile homocoupling and Suzuki-Miyaura cross-coupling. The recent increase in methodologies towards the synthesis and availability of boronic acids and esters without the need for halogenated intermediates increases their synthetic utility as coupling partners. An additional benefit lies in the relative low energy landscape of transmetallation of aryl boronic esters when compared to oxidative insertion of carbon-halogen bonds required in Suzuki-Miyaura cross-coupling and Yamamoto homocoupling reactions.³⁸

The first mechanistic study was performed in 1994 by Pleixitas implicating an initial oxidative insertion into a Ar-B(OH)_2 followed by a transmetallation of a second equivalent of ArB(OH)_2 and finally reductive elimination to give the homocoupled product.³² In 2005 Adamo et. al. proposed an alternative mechanism utilizing the power of DFT calculations to support the experimental observations (**Figure IV.3.**).^{33,34} This cycle begins with the oxidation of a bis-ligated palladium(0) to form palladium(II)di(triphenylphosphine)peroxide **IV.3**. This peroxy intermediate was first suggested by Yoshida³⁶ and had previously been synthesized on large scale by simple oxygenation of $\text{Pd(PPh}_3)_4$.³⁵ Once palladium peroxy activation is complete the oxygen can coordinate an aryl boronic acid or ester. This facilitates the first transmetallation of an aryl group to give a boronic peroxy species. It is important to point out at this point that this first transmetallation step was found both theoretically and experimentally to be second order in boronic acid.³⁴ Water or an alternative base can then nucleophilically attack this peroxide intermediate to give a palladium hydroxo species and one equivalent of hydrogen peroxide. This palladium hydroxo species is closely related to the pre-transmetallation intermediate for Suzuki-Miyaura cross-coupling.^{39,40} In fact, the mechanism is nearly identical from this palladium hydroxo species through the terminal reductive elimination.³⁸ Although the existence of the palladium hydroxo intermediate in Suzuki-Miyaura has been hotly debated, Demark recently showed experimental support

for such a pre-transmetalation intermediate.⁴¹ The key addressable points in the catalytic cycle in figure **IV.3**, are highlighted in blue and will be discussed in more detail in the following optimization.



Entry	Catalyst	Base	Oxidant	Conversion	Yield
1	PdCl ₂ (PPh ₃) ₂ (20 mol%)	KF (4 equiv.)	Air	100	50
2	NiCl ₂ (PPh ₃) ₂ (20 mol%)	KF (4 equiv.)	Air	10	0
3	PtCl ₂ (PPh ₃) ₂ (20 mol%)	KF (4 equiv.)	Air	20	0
4	Pd(dppf)Cl ₂ (20 mol%)	KF (4 equiv.)	Air	100	40
5	Pd(dppp)Cl ₂ (20 mol%)	KF (4 equiv.)	Air	100	30
6	Pd(PEPPSI)(SiP) (20 mol%)	KF (4 equiv.)	Air	60	25
7	Pd(OAc) ₂ (20 mol%)	KF (4 equiv.)	Air	40	20
8	PdCl ₂ (PPh ₃) ₂ (20 mol%)	KF (4 equiv.)	Benzoquinone	100	0
9	PdCl ₂ (PPh ₃) ₂ (20 mol%)	KF (4 equiv.)	Cu(II)Cl	90	0
10	PdCl ₂ (PPh ₃) ₂ (20 mol%)	KF (4 equiv.)	O ₂ (g)	100	0
11	Pd(PPh ₃) ₄ (20 mol%)	NA	Air	100	40
12	Pd(OAc) ₂ (20 mol%)	SPhos (50 mol%)	Air	100	50
13	Pd(dba) ₂ (20 mol%)	NA	Air	100	40
14	(η-O ₂)Pd(PPh ₃) ₂ (20 mol%)	NA	Air	80	42
15	(η-O ₂)Pd(PPh ₃) ₂ (5 mol%)	NA	Air	25	25
16	(η-O ₂)Pd(PPh ₃) ₂ (20 mol%)	NaHCO ₃ (10 equiv.)	Air	100	23
17	PdCl ₂ (PPh ₃) ₂ (5 mol%)	KF (1 equiv.)	Air	100	50
18	PdCl ₂ (PPh ₃) ₂ (100 mol%)	KF (20 equiv.)	Air	100	95

Table IV.1. Optimization of Oxidative Homocoupling of Diboronic Ester **IV.1** to Strained Macrocycle **IV.2**. *Conversion based on recovered starting material.

With the initial observation of an efficient room temperature oxidative homocoupling of **IV.1** to give macrocyclic structure **IV.2** in hand and a greater appreciation for the proposed catalytic cycle, we began to probe various parameters to optimize this reaction. These results are summarized in **table IV.1**. We initially explored the other group 10 transition metals nickel (entry **2**) and platinum (entry **3**) with the same conditions and ligand system reported for palladium (entry **1**). Neither

bis(triphenylphosphine)nickel(II) dichloride, nor bis(triphenylphosphine)platinum dichloride gave any conversion to product. There are two major reasons for the lack of observed reactivity with nickel and platinum. First, Verkade^{42,43} showed that fluoride could be used to efficiently reduce PdCl₂(PPh₃)₂ to the corresponding Pd(PPh₃)₄ in the presence of excess triphenylphosphine however no such reactivity was observed for Ni(II) and only sluggish reduction of Pt(II) to Pt(0). Second, Roth⁴⁴ demonstrated the rate of oxygenation of a variety of M(PPh₃)₄ complexes in solution including Ni, Pd, and Pt. Interestingly Pd binds O₂ with a rate constant over an order of magnitude higher than Ni or Pt. This would significantly hinder the turnover in the proposed catalytic cycle for both Ni and Pt highlighting why Pd is the superior group 10 transition metal for this cycle.

Next a variety of palladium(II) ligand systems were screened (entries **4-7**). These ligands were chosen to cover a wide range of ligand properties including N-heterocyclic carbene, bidentate phosphines, and bulky phosphine ligands. Interesting, there was little variance in conversion and yield when alternate phosphine ligands were used, however NHC's and other nitrogen based ligands were ineffective. This supports the fluoride mediated reduction of the various palladium species through the oxidation of the phosphine ligands to their corresponding phosphine oxides.^{42,43} This insensitivity to phosphine ligand suggests that perhaps the ligands which become oxidized play little role in the observed catalytic cycle.

We then chose to screen the catalyst oxidant based on previously reported boronic acid and ester homocoupling reactions (entries **8-10**). Although less mechanistically understood, the oxidative homocoupling of boronic acids and esters under oxygen free conditions has been explored utilizing a wide variety of chemical oxidants. The most common of which for simple boronic acid homocouplings are benzoquinone (BQ)⁴⁵ and copper (II) salts.⁴⁶ These stoichiometric oxidants prove ineffective in the presented transformation. Although high conversion of starting material was observed, the complex mixture obtained contained no desired product. This could be related to the first transmetallation step from the proposed palladium peroxide species. As was discussed above, this step is second order in boronic acid or ester. The intramolecular nature of this system could allow both boronic esters to structurally preorganized to facilitate the second order transmetallation step. It is not clear how this mechanistic step would be

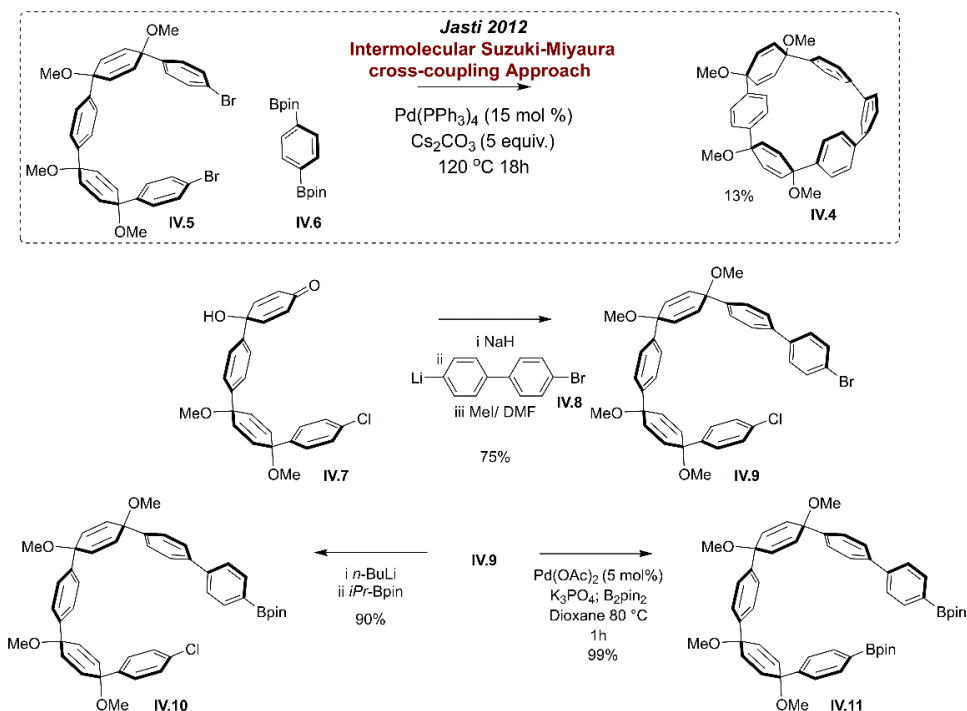
possible in the absence of oxygen. Interestingly we observe that a rigorously pure oxygen environment does not lead to significant increase in yield. This results magnifies the simplicity of reaction set-up since it can be run under normal atmospheric conditions without the need to degas solvents.

It was initially thought that the fluoride would activate the boronic esters to their corresponding fluoroboronates to enhance transmetalation.³⁷ The Lloyd-Jones^{31,47} group showed in 2010 that it was energetically less favorable to transmetallate through such a boronate and likely boronic acids and esters were directly transmetallated from a palladium hydroxo intermediate commonly implicated in the Suzuki-Miyara cross-coupling. As described above, the role of fluoride was more likely used to catalyze the reduction of palladium(II) to palladium(0) through the oxidation of the phosphine ligands to their corresponding phosphine oxides.^{42,43} According to the accepted Adamo catalytic cycle, there is no inherent need for a fluoride source and the catalytic cycle could begin with the O₂ mediated oxidation of palladium(0) source. A bis-ligated palladium(0) was shown to undergo oxidation with molecular oxygen to palladium(II)bis(triphenylphosphine)peroxide **IV.3**.³⁴ This was theoretically and experimentally shown by Adamo to be the active catalyst in this homocoupling cycle. They reported an *in situ* generation of the palladium peroxo species **IV.3** by bubbling O₂ through a solution of substrate and palladium(0). Additionally this circumvented the need for fluoride as discussed above and would require only the addition of water as a base in the hydrogen peroxide forming step. We sought to examine palladium(0) sources (entries **11-13**) could carry out the desired transformation. **Table IV.1.** illustrates that in fact palladium(0) can carry out the desired transformation with reasonably similar conversions and yields. Again the conversion and yield do not vary dramatically between different phosphine ligand similar to what was observed in the case of palladium(II) sources in **table IV.1.** The implicated catalyst, peroxide **IV.3**, was screened under various conditions (entries **14-16**) to determine if in fact this could be a competent catalyst in the desired macrocyclization. This catalyst was freshly prepared according to literature procedures.³⁵ It is worth noting that although this catalyst is bench stable under atmospheric conditions for long periods of time, it was found to explosively decompose on a handful of occasions, especially when exposed to high temperatures or friction.

Under the standard base-free conditions screened above there was moderate conversion and comparable isolated yields of product. However, lower catalyst loading gave poor conversion indicating poor turnover. The addition of an aqueous base allowed for full conversion but gave poor yield in comparison to the base free conditions. These results concluded that the palladium peroxide compound could act as a competent catalyst as reported by Adamo.

Finally, we sought to screen catalyst loading in entries **17** and **18**. Although a full equivalent of palladium (entry **16**) gave full conversion and nearly a quantitative yield, the high catalyst dilution and cost on scale made this impractical. For this reason 5 mol% catalyst (entry **17**) was used in all subsequent reactions. These standard conditions were chosen to reflect a balance between reproducibility, scalability, and ease of set-up. Substrate and catalyst are first dissolved in the appropriate amount of THF and if required, preheated to the desired temperature. This solution is found to be stable for days with no decomposition of starting material and no observed formation of product. The addition of aqueous fluoride initiates the reactions giving a deep orange color initially which fades to a pale yellow. This temporal activation was found to be extremely useful in the subsequent reactions.

IV.2.2. Direct Comparison to Suzuki-Miyaura Cross-Coupling.



Scheme IV.1. Synthesis of a Six-Ring DiBpin **IV.11** and the Analogues Six-ring Bpin-Cl **IV.10** Towards Macrocycle **IV.4**.

With these conditions in hand we initially sought to compare the oxidative homocoupling to a standard Suzuki-Miyaura cross-coupling.³⁰ Strained macrocycle **IV.4** was first reported by our group in the seminal synthesis of [6]CPP in 2012.⁴⁸ The limiting step in this synthetic sequence was the intermolecular Suzuki-Miyaura cross-coupling of dibromide **IV.5** and commercially available diBpin **IV.6**. This gave macrocycle **IV.4** in a paltry 12% yield. The inherent strain associated with this macrocycle was presumed to be the culprit for this low yield. This macrocycle was chosen as a proving ground for our optimized oxidative homocoupling reaction. In order to make a more direct experimental comparison the intramolecular Suzuki-Miyaura precursor **IV.10** was synthesized. To start, addition of 4'-bromo(1,1'-biphenyl)-4-lithium **IV.8** to previously reported ketone **7**⁴⁹ followed by *in situ* methylation of the latent alkoxide gave six-ring bromide **IV.9** in 75% yield. In order to afford the desired Suzuki-Miyaura cross-coupling substrate, bromide **IV.9** was treated with *n*-butyl lithium followed by quenching with isopropoxy Bpin to give boronic ester **IV.10** in 90% yield. Boronic ester homocoupling substrate **IV.11** could be generated by Miyaura borylation^{50,51} of bromide **IV.9** in quantitative yield (an alternative route to diboronic ester **11** can be found in the supporting information).

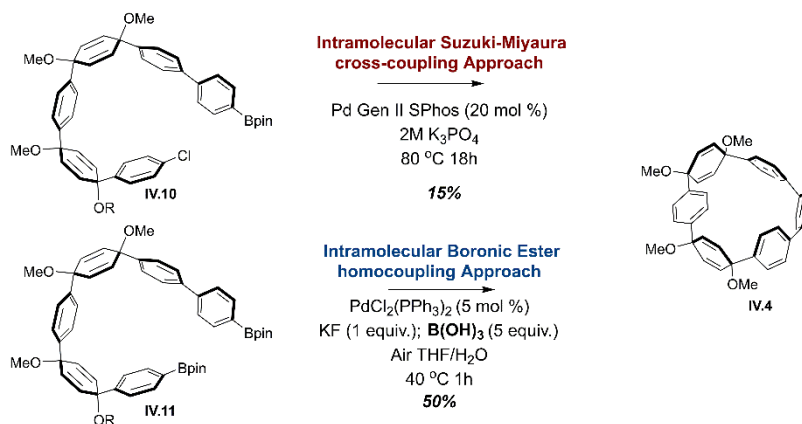


Figure IV.4. Direct Comparison of an Intramolecular Suzuki-Miyaura Cross-Coupling of **IV.10** and Intramolecular Oxidative Homocoupling of Diboronic Ester **IV.11** to Give Macrocycle **IV.4**.

The intramolecular Suzuki-Miyaura macrocyclization of Bpin-chloride **IV.10** was rigorously optimized to give macrocycle **IV.4** in 15% yield, within experimental error for

the originally reported intermolecular Suzuki-Miyaura cross-coupling macrocyclization. The analogous diboronic ester **IV.11** was then subjected to the oxidative homocoupling conditions from entry **IV.16**. To our surprise there was very little conversion after 16h at room temperature with a mere 5% yield of product **IV.4** isolated. The reaction temperature was then increased to 40 °C. After 1h, all starting material was consumed and the isolated yield of macrocycle **IV.4** increased to 25%. It was found that when the temperature was increased, the major byproduct in these reactions was rearrangement of the boronic esters to their corresponding phenols, a common reaction product of boronic acids and esters in the presence of hydrogen peroxide.⁵² Interestingly, the catalytic cycle put forth by Adamo generates one equivalent of hydrogen peroxide per catalyst turn over. The slight increase in temperature appeared to dramatically increase this decomposition pathway so we sought to mitigate this decomposition through the sequestration of the generated hydrogen peroxide species using a sacrificial boron source. Although a modest decrease in phenol was observed with various boronic acid pinacol esters such as B₂pin₂ and HBpin, the more reactive boric acid was found to be superior in peroxide sequestration and led to an increase in yield for macrocycle **IV.4** from 5% to 65%! Of the sacrificial boron sources screened, boric acid is the cheapest due to its wide spread use as an ant pesticide and is also sufficiently water soluble to be removed during an aqueous work up. The observed yield of the diboronic ester homocoupling shows a clear advantage in yield and reaction time over the analogues Suzuki-Miyaura cross-coupling in the synthesis of strained macrocycle **IV.4**.

IV.2.3. Direct Comparison to Yamamoto-Coupling.

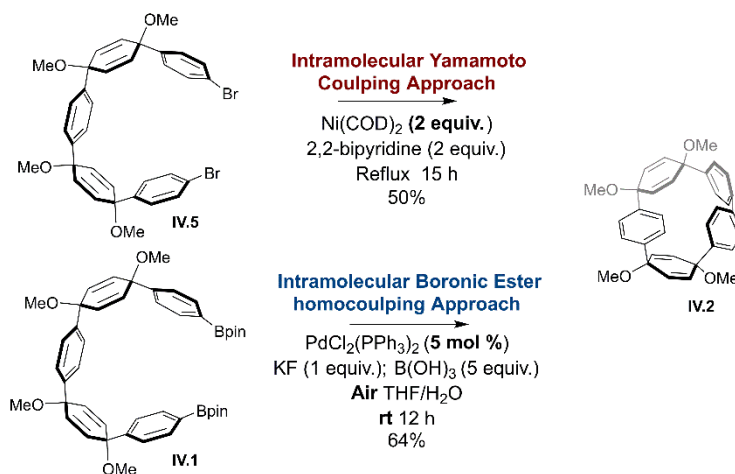
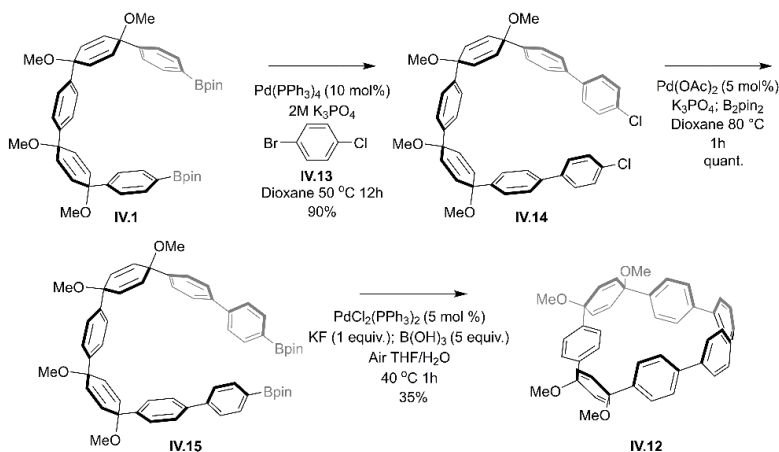


Figure IV.5. Direct Comparison of Reductive Yamamoto Coupling of Dibromide **IV.5** and the Oxidative Homocoupling Diboronic Esters **IV.1** to Form Macrocycle **IV.2**.

With the addition of boric acid to the optimized conditions complete, we sought to compare the oxidative homocoupling of diboronic esters to the analogous electrophile aryl bromide homocoupling, the Yamamoto coupling. Yamago^{53,54} showed that an intramolecular aryl bromide homocoupling could be used to access macrocycle **IV.2** in a comparable 50% yield. Although the yields are comparable, the reaction conditions of the reported Yamamoto reaction require superstoichiometric Ni(COD)₂, *in situ* catalyst generation with **IV.2** equivalents of 2,2'-bipyridine, and harsh refluxing conditions for 15 h. These conditions require a rigorous air and water free environment and are most efficiently carried out in a glove-box. As shown above, comparable yields can be obtained with only 5 mol% of palladium at a lower reaction times. In addition, this reaction can be set up on the bench-top without need to degas solvent or exclude water. At a standard macrocyclization concentration of 1 mM, over 2 L of solvent is required to convert 2 g of starting material **IV.1** to macrocycle **IV.2**. Figure **IV.5**. shows the uncovered 4 L jar that was used for this reaction completely open to atmosphere on the benchtop illustrating how simple the reaction set-up is.

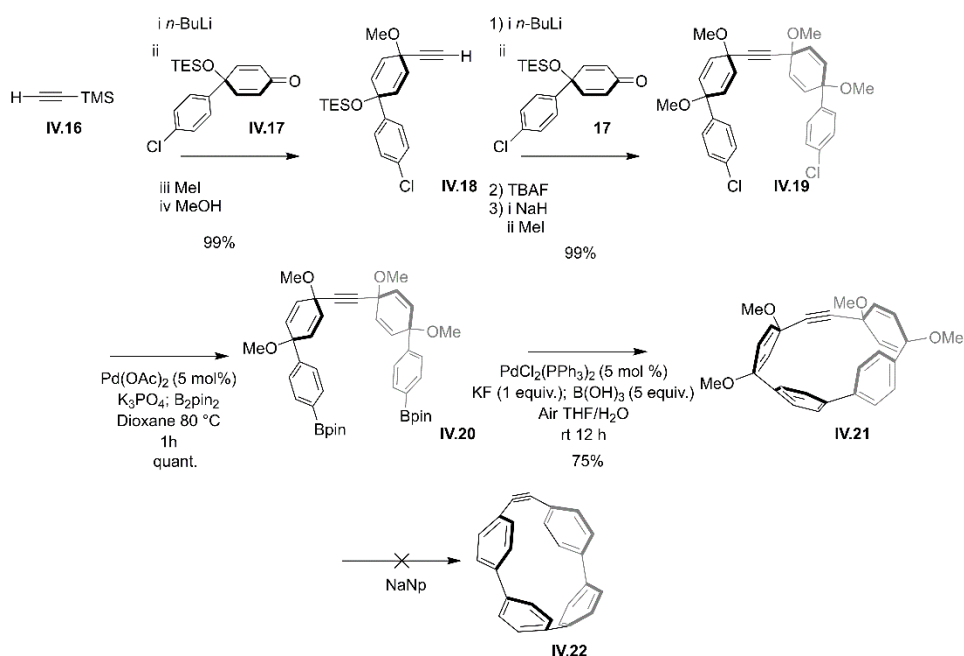
IV.2.4. Substrate Scope.



Scheme IV.4.2. Synthesis of a Strained Tetraphenylene Containing Macrocycle **IV.12** Utilizing an Oxidative Homocoupling of Diboronic Ester **IV.15**.

With standard conditions in hand we sought to screen several additional substrates. In addition to macrocyclic precursors **IV.2** and **IV.4** to [5]- and [6]CPP respectively, we sought to synthesis bent tetraphenylene precursor **IV.12** towards [7]CPP.

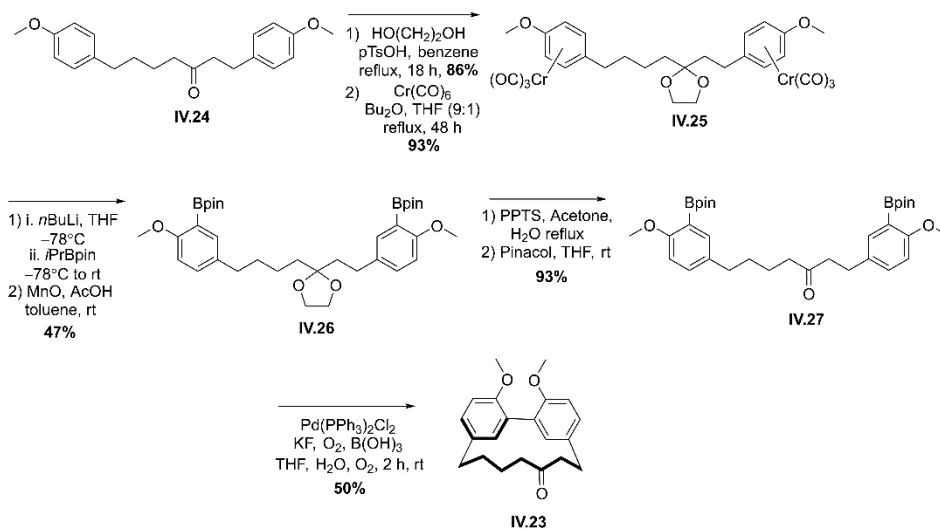
Previous macrocyclic structures with strained tetraphenylene subunits have been reported by our group with notoriously poor yields that rarely eclipse 15%.⁵⁵ Previous synthesis of [7]CPP have been limited by the macrocyclization step by our group in 2011⁵⁶ which relied on an 8% yielding intermolecular Suzuki-Miyaura macrocyclization and the Itami⁵⁷ group in 2014 which relied on a 17% yielding intramolecular Yamamoto coupling. We envisioned a highly strained tetraphenylene containing [7]CPP macrocyclic precursor **IV.12** which could be accessed using the developed oxidative homocoupling of diboronic ester **IV.15**. The required diboronic ester precursor **IV.15** was synthesized by the addition of two aryl rings to five-ring diboronic ester **IV.1** via Suzuki-Miyaura cross-coupling with bromo-chlorobenzene to give seven-ring dichloride **IV.14** in 90% yield. This was then subjected to standard Miyarua borylation conditions to give desired seven-ring diboronic ester **IV.15** in quantitative yield. Seven-ring diboronic ester **IV.15** was then cyclized to give contorted macrocycle **IV.12** in 35% yield, significantly outperforming previous syntheses mentioned above. This macrocycle was then aromatized by treatment with sodium naphthalenide at $-78\text{ }^{\circ}\text{C}$ to give [7]CPP in 45% yield.



Scheme IV.3. Synthesis of Strained Alkyne Containing Macrocycle **IV.21** Utilizing an Oxidative Homocoupling of Diboronic Acid **IV.20**.

Strained alkynes have been a topic of interest for many decades with a recent resurgence due to their application in bioorthogonal metal-free click reactions^{58,59} and

surface functionalization of materials⁶⁰. We sought to introduce an alkyne into a similar scaffold to determine if it was possible to directly bend an alkyne in this reaction. The synthetic design was inspired by Hopf.⁶¹ The desired substrate diboronic ester **IV.20** was synthesized by lithiation of ethynyltrimethylsilane **IV.16** and addition to silyl protected quinol **IV.17** followed by *in situ* methylation. This reaction could be quenched with potassium carbonate to give deprotected alkyne **IV.18** in 90% yield. Alkyne **IV.18** was then treated with *n*-butyl lithium and added to an additional equivalent of protected quinol **IV.17** followed by *in situ* methylation to give alkyne containing dichloride **IV.19** in 85% yield. This was subjected to fluoride mediated silyl ether deprotection followed by alcohol alkylation to give global methyl ether protected dichloride **IV.19** in 95% yield. Miyaura borylation of alkyne containing dichloride **IV.20** gave the desired diboronic ester **IV.20** in quantitative yield. Alkyne containing diboronic ester **IV.20** then subjected to the room temperature oxidative homocoupling conditions to give strained alkyne **IV.21** in an incredible 75% yield! Attempts to aromatize this strained alkyne using sodium naphthalanide were unsuccessful resulting in highly unstable products. Further exploration of **IV.22** and related highly strained alkynes is currently underway.

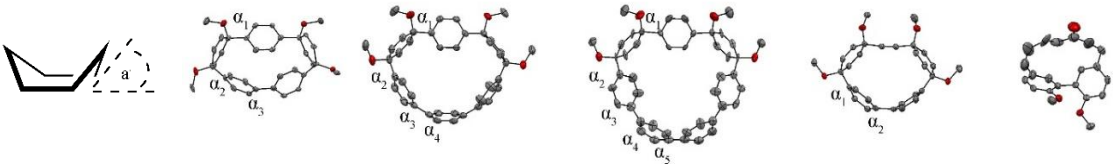


Scheme IV.4. Formal Synthesis of Acerogenin E Utilizing an Oxidative Homocoupling of Diboronic Ester **IV.27**.

The major challenge in the synthetic pursuit of cyclophane containing natural products is often the macrocyclization step.⁵ Biaryl containing cyclophanes are often ridged, contorted, and conformationally restricted adding further challenge in rendering these

molecules accessible. To further prove the versatility of this oxidative homocoupling, we targeted the Acerogenin E macrocyclic precursor **IV.23**. The initial synthesis of this natural product by Usuki²⁹ used an intramolecular Suzuki-Miyaura coupling to construct the cyclic architecture of this molecule. As in our previous syntheses, this late stage coupling proved to be the limiting step of the formal synthesis giving the desired macrocycle in 34% after rigorous optimization. Our synthesis began with the previously reported intermediate **IV.24**. After glycol protection of the ketone, treatment of this compound with Cr(CO)₆ gave metallated **IV.25** in 93% yield. This intermediate was then borylated through deprotonation of the ortho-positions with *n*BuLi at -78 °C followed by quenching with isopropoxybpin to give **IV.28** in 47% yield after demetallation. Deprotection of the ketone using standard conditions gave dibornic ester **IV.27** after protection of the resulting boronic acids with pinacol. Gratifyingly, after subjecting diboronic ester **IV.27** to our optimized oxidative homocoupling conditions, we prepared the desired macrocycle **IV.23** in 2 hours, at room temperature and 50% yield. Further interpretation of the product and overall reaction scheme will be discussed in subsequent sections.

IV.2.5. Structural Analysis.



	IV.2	IV.4	IV.12	IV.21	IV.23
Calculated Total Strain (kcal/mol)	32	38	41	45	4.0
Strain per Backbone Carbon ((kcal/mol)/C)	1.1	1.1	0.98	1.7	0.21
α_1	2.1	2.6	3.5	12	NA
α_2	12	8.0	4.1	14	NA
α_3	12	8.9	4.9	NA	NA
α_4	NA	13	13	NA	NA
α_5	NA	NA	13	NA	NA
Alkyne	NA	NA	NA	6.3	NA

Table IV.2. Solid State Analysis of Macrocycles **IV.2**, **IV.4**, **IV.12**, **IV.21**, and **IV.23**.

Single crystals of macrocycles **IV.2**, **IV.12**, **IV.21** and **IV.23** were grown in order to assess the structural deformation in each compound. Note that crystal structure **IV.4** was previously published and available through the Cambridge Crystallographic Data Centre (CCDC # 852988).⁶² ORTEP models of each are shown in table IV.2. In order to account for disorder or additional impact of packing forces, each structure was also computationally minimized (B3LYP/6-31d*) with comparable values reported in the supporting information. Additionally, homodesmotic reactions for each macrocycle were carried out computationally to afford a relative estimate of macrocyclic strain.^{56,63} These homodesmotic reaction results show a gradual increase in total strain with relatively low strain for **IV.23** at approximately 4.0 kcal/mol. Macrocycles **IV.2**, **IV.4**, **IV.12**, and **IV.21** gradually increase in total strain from 32 kcal/mol for the macrocyclic precursor to [5]CPP up to 45 kcal/mol for alkyne macrocycle **IV.21**. For a frame of reference [12]CPP has a total strain of 48 kcal/mol.²³ However, analysis of the strain per backbone carbon gives a more impressive perspective for the ability of this reaction. These values range from 1.1 (kcal/mol)/carbon up to 1.7 (kcal/mol)/carbon for **IV.21**! [12]CPP registers at a mere 0.3 (kcal/mol)/carbon. In fact the strain built into alkyne macrocycle **IV.21** falls between average strain per carbon in [8]CPP (1.5 (kcal.mol)/carbon) and [7]CPP (2.0 (kcal/mol)/carbon)!²³ Benzene displacement angle α in each crystal structure gives another figure of merit to the difficulty of the parent coupling. As a frame of reference, the inspirational bent benzene in haouamine A has an α of 14°. ⁶⁴ There is a large variation in α for macrocycles **IV.2**, **IV.4**, **IV.12**, and **IV.21** with peak values between 13° and 14°. This falls between [6]CPP (13°) and [5]CPP (16°) which have to be prepared over several high energy steps!²³ Finally, strain can have large implications on the dihedral conformation of polyphenylenes, a feature that give [n]CPPs their previously anomalous narrowing HOMO-LUMO energy gap with decreasing size. A typical free rotating biphenylene has a dihedral angle of 36°, this angle is a result of the balance between minimizing steric interactions between ortho protons and maximizing *pi* overlap of the aromatic systems. Strained paraphenylenes, such as those found in [n]CPPs accommodate this strain by narrowing the biaryl dihedral angles. [12]CPP has an average dihedral angle near that of an unrestricted bipheynelene at approximately 34°. This dips all the way down to 16° for [5]CPP. We see in the paraphenylene containing macrocycles

above that strain is able to force the average dihedral angle down by over 10° for macrocycles **IV.2**, **IV.4**, **IV.12**, and **IV.21**.

IV.2.6. NMR studies.

In order to gain insight into the operating mechanism, we turned to NMR experiments. Adamo showed that in the case of boronic acids, the catalytic cycle could be manipulated to observe various intermediate.³⁴ First, when an excess of boronic acid is used relative to the palladium peroxide, boronate coordination is observed. This can be pushed past the first transmetallation event by the addition of excess boronic acid relative to the palladium. This is supported by kinetic data which that suggested the first transmetallation is second order in respect to the boronate. Next they see an accumulation of the palladium hydroxide intermediate. This is followed by a transmetallation and reductive elimination akin to that of the Suzuki-Miyaura cross-coupling. In our case, the two boronic esters are tethered and are conformationally flexible enough to interact with a single palladium center. This could act to “preorganize” each boronic ester to favor the first transmetallation which had been shown to be second order in the intermolecular case.

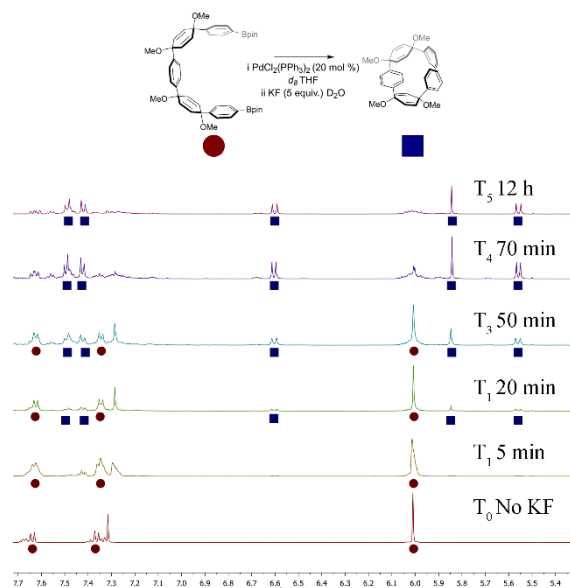


Figure IV.6. ^1H NMR Profile of Reaction Over 2 h.

To test this we carried out a set of NMR experiments in air saturated d_8 THF. First we wanted to qualitatively track the conversion of diboronic ester **IV.1** to macrocycle **IV.2** using the established conditions at room temperature (**Figure IV.6**).

First diboronic ester **IV.1** and $\text{PdCl}_2(\text{PPh}_3)_2$ were dissolved in d_8 THF. This gave a baseline NMR before fluoride activation. KF in D_2O was then injected followed by a collection of the spectra. We see at this first time point no conversion of starting material to product, however we do see signals consistent with phosphine reduction and formation of Pd(0) from $\text{PdCl}_2(\text{PPh}_3)_2$. Within 20 minutes, these signals subside and we begin to see the appearance of product formation. Time points are taken every 20 minutes for 2h and finally an endpoint is taken at 18 h to show full conversion of starting material. At no point during this reaction do we see any signals indicative of the formation of a palladium hydroxide like intermediate nor do we see any signal associated with the pre-reductive elimination step. ^{31}P NMR is able to offer an additional insight into this reaction. In the case of the Adamo experiments, ^{31}P is used to track the phosphorus coordination environment and lend experimental support to the intermediates highlighted above. The ^{31}P spectra evolution of this reaction from the pre-activation state consisting of starting material and catalyst. This data point shows one signal for palladium(II) coordinated triphenylphosphine. At the 20 min time point after fluoride activation this singlet remains along with the emergence of triphenylphosphine oxide formation. Provocatively this signal completely converts to triphenylphosphine oxide by 50 min, however in the ^1H NMR we still see conversion of starting material to product.

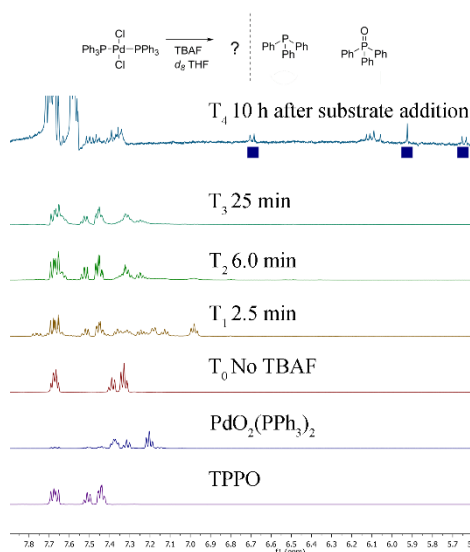


Figure IV.7. *In Situ* Reduction of $\text{PdCl}_2(\text{PPh}_3)_2$ Using TBAF in d_8 THF.

Next, we qualitatively assess the reduction of $\text{PdCl}_2(\text{PPh}_3)_2$ with fluoride. Tetrabutylammonium fluoride was chosen to avoid any miscibility issues (**Figure IV.7.**).

Figure IV.7. shows unbound triphenylphosphine, triphenylphosphine oxide, as well as peroxy palladium species **IV.3** for reference. At T_0 no fluoride is present and only shows the parent Pd(II) species. T_1 , taken 2 min after fluoride addition, shows disappearance of the parent complex entirely and a complicated spectrum with several species. The most prominent species observed are consistent with triphenylphosphine oxide. By T_2 taken at 6 min we observe near quantitative conversion to triphenylphosphine oxide with no apparent formation of peroxy species **IV.3**. This spectra remains relatively unchanged over the remaining time points T_3 and T_4 . At 90 minutes solid substrate **IV.1** was added to the NMR tube along with water. After 12 h the crude NMR (**figure IV.7.**) shows complete consumption of diboronic ester **IV.1** and conversion to macrocycle **IV.2**. These results and those shown in figure **IV.7.** Have led us to speculate that perhaps the discrete peroxy palladium complex **IV.3** is not being generated at each turn of the mechanism, but rather initially full oxidation of phosphine ligands leaves a bare ligandless palladium species. Under these oxidative conditions palladium nanoparticles are known to form. Intriguingly, gold nanoparticles have been shown to effectively carry out the oxidative homocoupling of boronic esters. Further detailed studies are underway to explore this hypothesis.

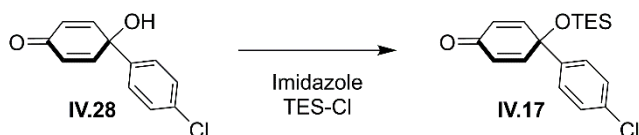
IV.3. Conclusion.

In conclusion we have reported an oxidative homocoupling of aryl boronic esters to form strained and conformationally restricted molecules under atmospheric conditions, short reaction times, and low temperatures. This reaction serves to compliment the both nucleophile-electrophile cross-coupling and electrophile-electrophile homocoupling which have traditionally garner more attention. It was shown to outperform Suzuki-Miyaura cross-coupling on a similar substrate and is more economically viable than Yamamoto coupling to make comparable structures. Although this reaction appears to follow the proposed mechanism put forth by Adamo in 2005, NMR ^1H and ^{31}P suggests the possibility that this reaction proceeds through a heterogenous palladium pathway. Further studies are underway to understand the mechanistic possibility of this supposition. In addition to increased yields, this reaction benefits from the easy of reaction set up. It can be set up and run under ambient atmospheric conditions and is shown to scale nicely. With the ability to build more strained and conformationally

restricted molecules at significantly lower temperature we feel this reaction can find application across many disciplines including medicinal, material, and supramolecular chemistry.

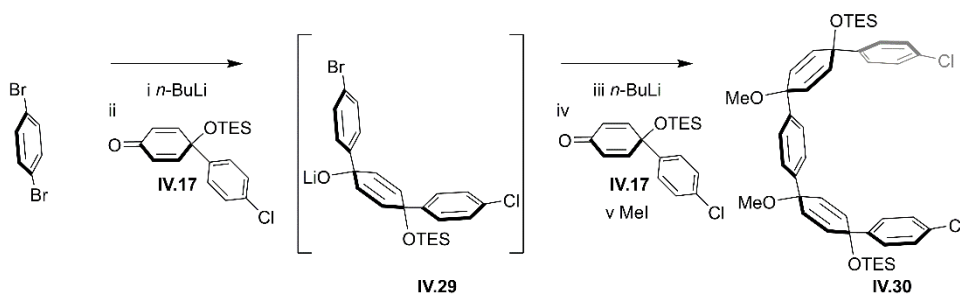
IV.4. Experimental Details.

IV.4.1. Synthetic Details.

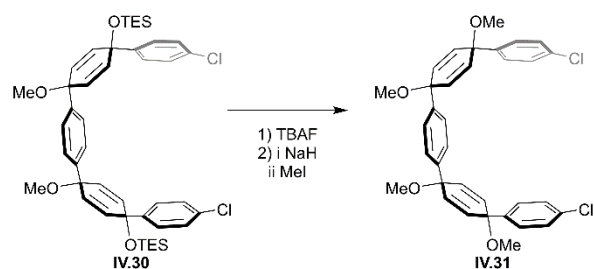


Chloroquinol **IV.28** (16.7 g, 75.6 mmol, 1.00 equiv.) and imidazole (10.3 g, 151 mmol, 2.00 equiv.) were added to a flame dried round bottom flask under N_2 . To this was added dry DMF (378 mL). This was stirred until all solids were in solution. TES-Cl (19.0 mL, 113 mmol, 1.30 equiv.) was then added dropwise to the stirring solution. This solution was heated at 40 °C for 1.5 h at which point the reaction was cooled to room temperature. Water (400 mL) was added to the crude reaction which was then extracted with dichloromethane (3 x 100 mL). Organics were pooled and washed with 5% LiCl (aq) (3 x 100 mL), water (100 mL), and finally brine (300 mL). Organic solution was then dried over sodium sulfate and concentrated to a dark yellow oil. This oil was wet loaded onto silica gel (0 – 5% EtOAc/Hexanes) to afford TES protected chloroquinol **IV.17** as a light yellow oil (23.0 g, 91% yield). This compound should be stored dry at 0 °C to avoid deprotection.

1H NMR (500 MHz, $CDCl_3$): δ 7.37 (d, J = 8.5 Hz, 2H), 7.31 (d, J = 8.5 Hz, 2H), 6.79 (d, J = 10 Hz, 2H), 0.971 (t, J = 7.8 Hz, 9H), 0.658 (q, J = 7.8 Hz, 6 H); ^{13}C NMR (125 MHz, $CDCl_3$): δ 185.75, 151.71, 138.72, 134.08, 128.99, 127.01, 126.87, 72.94, 7.04, 6.37; IR (neat): 2955, 2911, 2876, 1671, 1629, 1604, 1489, 1474, 1387, 1275, 1237, 1164, 1112, 1090, 1060, 1013, 970, 924.43, 879, 834, 746 cm^{-1} .

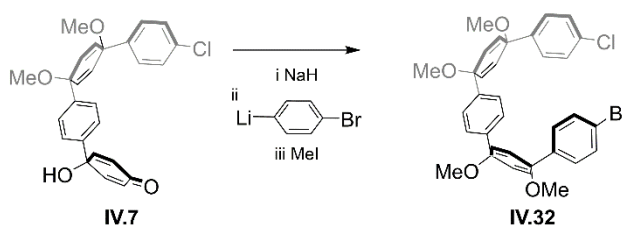


1,4-dibromobenzene (2.00 g, 8.48 mmol, 1.00 equiv.) was added to a flame dried flask under N₂. THF (100 mL) was added and the solution was cooled to -78 °C for 1 h. *n*-BuLi (4.46 mL, 8.48 mmol, 1.00 equiv.) was added dropwise to give a clear solution. **If the reaction turns brown or black it must be discarded.* Upon complete addition of *n*-BuLi TES protected chloroquinol **IV.17** (2.60 mL, 8.48 mmol, 1.00 equiv.) was added dropwise as a neat oil. **If this viscous oil is added too rapidly it will freeze and poor conversion will be observed. This can be added as a cool solution in THF to increase solubility.* This was allowed to stir at -78 °C for 1 h at which point the second equivalent of *n*-BuLi (4.46 mL, 8.48 mmol, 1.00 equiv.) was added rapidly over 4 minutes to the latent alkoxide **IV.29**. Upon complete addition of *n*-BuLi a second equivalent of TES protected chloroquinol **IV.17** (2.60 mL, 8.48 mmol, 1 equiv.) was added as a neat oil. After 1 h MeI (2.64 mL, 42.4 mmol, 5.00 equiv.) was added neat. The cold bath was allowed to expire and the reaction was allowed to stir overnight. MeOH (25 mL) was added to quench the reaction. Reaction was concentrated to a white foam and was dissolved in ethyl acetate (100 mL). Water (100 mL) was added and was extracted with ethyl acetate (3 x 50.0 mL). The organic layer was then washed with water (3 x 100 mL) and brine (100 mL) and was dried over sodium sulfate. This was concentrated to a clear oil which was triturated with cold hexanes (50.0 mL) to give the product **IV.30** as a white crystalline solid (5.26 g, 80% yield) and seemingly only the desired diastereomer. mp 120-121 °C. ¹H NMR (500 MHz, CDCl₃): δ 7.32 (s, 4H), 7.25 (d, *J* = 9.0 Hz, 4H), 7.21 (d, *J* = 9.0 Hz, 4H), 6.12 (d, *J* = 10 Hz, 4H), 5.96 (d, *J* = 10 Hz, 4 H), 3.36 (s, 6H), 0.981 (t, *J* = 8, 18H), 0.663 (q, *J* = 8, 12H); ¹³C NMR (125 MHz, CDCl₃): δ 144.52, 142.81, 135.39, 133.12, 129.40, 128.37, 127.27, 126.46, 74.51, 71.71, 52.22, 7.19, 6.66; IR (neat): 3032.88, 2931.07, 2953.16, 2904.27, 2875.05, 2821.21, 1481.67, 1457.43, 1404.43, 1236.83, 1184.70, 1108.99, 1075.59, 1007.74, 965.10, 869.12, 826.52, 742.60, 723.58 cm⁻¹.



Dichloride **IV.30** (5.00 g, 6.44 mmol, 1.00 equiv.) was dissolved in THF (50.0 mL) under N_2 in a flame dried flask. To this was added TBAF (19.3 mL, 19.3 mmol, 3.00 equiv.). The reaction was allowed to stir for 1 h at which point water (100 mL) was added. This was extracted with DCM (3 x 50.0 mL). The organic layer was washed with water (3 x 50.0 mL) and brine (50.0 mL) and was dried over sodium sulfate. After concentration, the crude oil was dissolved in THF (100 mL) and was cooled to 0 °C for 30 minutes. Solid NaH (773 mg, 19.3 mmol, 3.00 equiv.) was added to this solution and was then stirred for 2 h. At this point MeI (2.01 mL, 32.2 mmol, 5.00 equiv.) was added and the reaction was allowed to stir overnight. Water (100 mL) was added and the reaction was extracted with ethyl acetate (3 x 50.0 mL). The organic layer was washed with water (3 x 50.0 mL) and brine (50.0 mL) and was dried over sodium sulfate. Concentration gave a white solid that was washed with hot hexanes (30.0 mL) to give the product **IV.31** as a white solid (3.52 g, 95% yield).

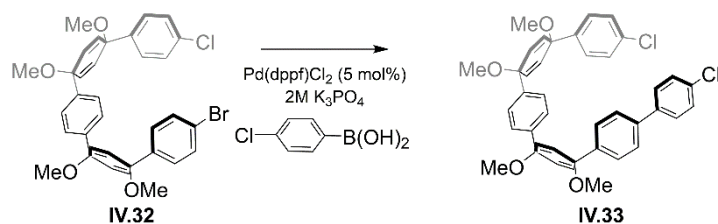
Matched Reported Spectra



Four ring chloroquinol **IV.7** (30.0 g, 69.0 mmol, 1.00 equiv.) was dissolved in dry THF (300 mL) in a flame dried flask under N_2 . This was cooled to -78 °C for 1 h, at this point solid NaH (2.15 g, 89.7 mmol, 1.30 equiv.). This deprotonation was allowed to proceed at -78 °C for 2 h. A separate flame dried flask was charged with 1,4-dibromobenzene (32.5 g, 138 mmol, 2.00 equiv.) which was dissolved in THF (500 mL) and then was cooled to -78 °C for 1 h. *n*-BuLi (55.2 mL, 138 mmol, 2.00 equiv.) was then added dropwise to the cooled 1,4-dibromobenzene. Upon complete *n*-BuLi addition, the

deprotonated choroquinol **7** was rapidly cannulated to the lithiate pot. The addition was allowed to react for 4 h at which point MeI (42.9 mL, 690 mmol, 10.0 equiv.) was added along with DMF (100 mL). This was stirred overnight with the cold bath expiring to room temperature. Water (200 mL) was added to the crude reaction which was then extracted with diethyl ether (3 x 100 mL). Organics were pooled and washed with 5% LiCl (aq) (3 x 200 mL), water (200 mL), and finally brine (200 mL). Organic solution was then dried over sodium sulfate and concentrated to give an off white solid. This was washed with hot hexanes (100 mL) to give the product **IV.32** as a white solid (29.0 g, 68% yield).

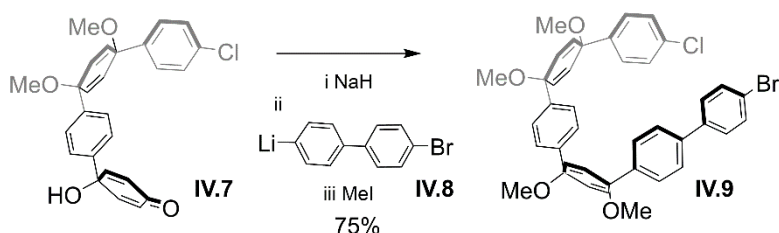
mp 149-150 °C. ¹H NMR (600 MHz, CDCl₃): δ 7.42 (d, *J* = 8.4 Hz, 2H), 7.33 (s, 4H), 7.32 (d, *J* = 9.0 Hz, 2H), 7.26 (d, *J* = 9.0 Hz, 2H), 7.25 (d, *J* = 8.4, 2H), 6.10 (d, *J* = 10.2 Hz, 4H), 6.04 (d, *J* = 10.2, 2H), 6.03 (d, *J* = 10.2 Hz, 2H), 3.41 (s, 12H); ¹³C NMR (150 MHz, CDCl₃): δ 142.78, 142.76, 142.63, 142.09, 133.75, 133.73, 133.47, 133.16, 133.10, 131.50, 128.56, 127.89, 127.54, 126.14, 126.13, 121.68, 74.65, 74.64, 74.57, 74.52, 52.10; HRMS (TOF, ES+) (*m/z*): [M+Na]⁺ calculated for C₃₄H₃₂BrClNaO₄, 641.1070; found: 641.1091. IR (neat): 3023, 2980, 2942, 2893, 2823, 1501, 1482, 1449, 1402, 1360, 1265, 1229, 1172, 1081, 1028, 1010, 985, 951, 825, 801 cm⁻¹.



Five-ring bromo chloride **IV.32** (23.3 g, 37.6 mmol, 1.00 equiv.), 4-chlorophenylboronic acid (7.05 g, 45.1 mmol, 1.20 equiv.), and Pd(dppf)Cl₂ (1.40 g, 1.88 mmol, 5.00 mol%) were added to a flame dried flask. This flask was evacuated and backfilled with N₂ three times. A septum was added and the solids were purged with N₂ for 30 minutes. N₂ sparged dioxane (500 mL) and 2M K₃PO₄ (aq) (50.0 mL) were added to the reaction. The reaction was heated to 80 °C and was allowed to react for 12 h at which point it was cooled to room temperature. The crude mixture was extracted with DCM (3 x 150 mL) and was then washed with water (3 x 200 mL) and brine (200 mL). The organic layer was filtered over activated carbon and was dried on sodium sulfate. The organic layer was

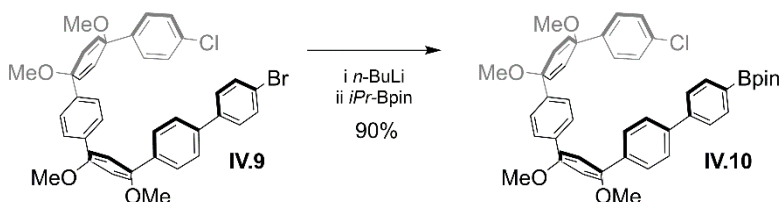
concentrated onto SiO₂ and was dry loaded onto silica gel. The product **IV.33** was eluted (30% EtOAc/Hexanes) to give the product at a white solid (21.8 g, 89% yield).

mp 191-192 °C. ¹H NMR (400 MHz, CDCl₃): δ 7.53 – 7.46 (overlap, 6H), 7.41 – 7.38 (overlap, 4H), 7.36 – 7.36 (overlap, 4H), 7.27 – 7.24 (overlap, 2H), 6.13 (s, 4H), 6.12 (d, *J* = 10, 2H), 6.04 (d, *J* = 10, 2H), 3.46 (s, 3H), 3.45 (s, 3H), 3.42 (s, 3H), 3.42 (s, 3H) ; ¹³C NMR (100 MHz, CDCl₃): δ 143.04, 143.03, 142.72, 142.15, 139.36, 139.31, 133.76, 133.59, 133.55, 133.47, 133.44, 133.20, 129.04, 128.58, 128.49, 127.58, 127.10, 126.66, 126.25, 126.15, 74.77, 74.76, 74.71, 74.60, 52.16; HRMS (TOF, ES+) (*m/z*): [M+Na]⁺ calculated for C₄₀H₃₆Cl₂NaO₄, 673.1888; found: 673.1912. IR (neat): 3029, 2980, 2938, 2896, 2822, 1594, 1501, 1485, 1462, 1449, 1404, 1360, 1264, 1229, 1174, 1157, 1116, 1081, 1029, 985, 951, 876, 818 cm⁻¹.



Four ring chloroquinol **IV.7** (10.0 g, 23.0 mmol, 1.00 equiv.) was dissolved in dry THF (250 mL) in a flame dried flask under N₂. This was cooled to -78 °C for 1 h, at this point solid NaH (1.29 g, 29.9 mmol, 1.30 equiv.). This deprotonation was allowed to proceed at -78 °C for 2 h. A separate flame dried flask was charged with 4,4'-dibromobiphenyl (15.8 g, 50.6 mmol, 2.20 equiv.) which was dissolved in THF (300 mL) and then was cooled to -78 °C for 1 h. *n*-BuLi (20.2 mL, 50.6 mmol, 2.20 equiv.) was then added dropwise to the cooled 4,4'-dibromobiphenyl. Upon complete *n*-BuLi addition, the deprotonated choroquinol **IV.7** was rapidly cannulated to the lithiate pot. The addition was allowed to react for 4 h at which point MeI (14.3 mL, 230 mmol, 10.0 equiv.) was added along with DMF (100 mL). This was stirred overnight with the cold bath expiring to room temperature. Water (100 mL) was added to the crude reaction which was then extracted with DCM (3 x 100 mL). Organics were pooled and washed with 5% LiCl (aq) (3 x 100 mL), water (100 mL), and finally brine (100 mL). Organic solution was then dried over sodium sulfate and concentrated to give an off white solid. This was washed with hot hexanes (500 mL) to give the product **IV.9** as a white solid (12.0 g, 75% yield).

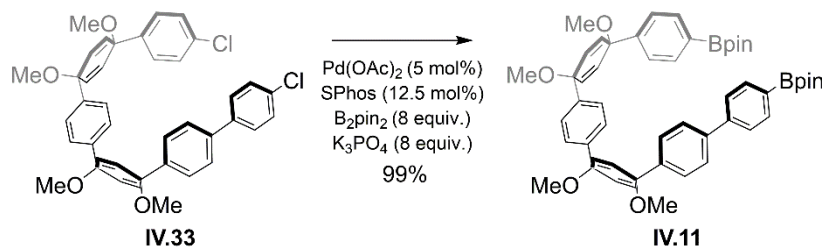
mp 182-184 °C. ^1H NMR (500 MHz, CDCl_3): δ 7.55 (d, $J = 8.5$ Hz, 2H), 7.50 (d, $J = 8.5$ Hz, 2H), 7.47 (d, $J = 9.0$ Hz, 2H), 7.44 (d, $J = 8.5$ Hz, 2H), 7.38 (d, $J = 8.5$ Hz, 2H), 7.33 (d, $J = 9.0$ Hz, 2H), 7.31 (d, $J = 8.5$ Hz, 2H), 7.25 (d, $J = 8.5$ Hz, 2H), 6.12 (s, 4H), 6.11 (d, $J = 10$ Hz, 2H), 6.04 (d, $J = 10$ Hz, 2H), 3.46 (s, 3H), 3.44 (s, 3H), 3.42 (s, 3H), 3.41 (s, 3H); ^{13}C NMR (125 MHz, CDCl_3): δ 143.10, 143.05, 142.73, 142.15, 139.79, 139.38, 133.77, 133.60, 133.48, 133.43, 133.20, 132.00, 128.85, 128.59, 127.59, 127.07, 126.69, 126.26, 126.16, 121.72, 74.78, 74.77, 74.72, 74.60, 52.15; HRMS (TOF, ES^+) (m/z): $[\text{M}+\text{Na}]^+$ calculated for $\text{C}_{40}\text{H}_{36}\text{BrClNaO}_4$, 717.1383; found: 717.1363. IR (neat): 3028, 2980, 2897, 2822, 1608, 1551, 1482, 1449, 1404, 1360, 1264, 1229, 1734, 1144, 1081, 1029, 1013, 1003, 986, 951, 817, 764 cm^{-1} .



A flame dried flask was charged with six ring bromo chloride **IV.9** (1.10 g, 1.58 mmol, 1.00 equiv.) which was dissolved in THF (150 mL) and then was cooled to -78 °C for 1 h. $n\text{-BuLi}$ (0.700 mL, 1.74 mmol, 1.10 equiv.) was then added dropwise over 3 minutes. *Lithiate is not stable for long periods of time (> 30 min.) in solution. Upon complete $n\text{-BuLi}$ addition, isopropoxy pinacolborane (0.650 mL, 3.16 mmol, 2 equiv.) was rapidly added and allowed to react for 2 h. Water (100 mL) was added to quench the crude reaction which was then extracted with DCM (3 x 100 mL). Organics were pooled and washed with water (3 x 100 mL), and finally brine (100 mL). Organic solution was then dried over sodium sulfate and concentrated to give an off white solid. This was washed with cold hexanes (100 mL) to give the product **IV.10** as a white solid (1.06 g, 90% yield).

mp 192-193 °C. ^1H NMR (500 MHz, CDCl_3): δ 7.89 (d, $J = 8.0$ Hz, 2H), 7.61 (d, $J = 8.5$ Hz, 2H), 7.58 (d, $J = 8.5$ Hz, 2H), 7.48 (d, $J = 8.0$ Hz, 2H), 7.40 (d, $J = 8.5$ Hz, 2H), 7.35 (d, $J = 8.5$, 2H), 7.32 (d, $J = 8.5$ Hz, 2H), 7.26 (d, $J = 8.5$ Hz, 2H), 6.16 – 6.11 (overlap, 6H), 6.05 (d, $J = 10$ Hz, 2H), 3.47 (s, 3H), 3.45 (s, 3H), 3.43 (s, 3H), 3.42 (s, 3H); ^{13}C NMR (125 MHz, CDCl_3): δ 143.50, 143.06, 142.93, 142.68, 142.12, 140.36, 135.38, 133.77, 133.50, 133.48, 133.46, 133.16, 128.58, 127.57, 127.34, 126.55, 126.52, 126.25,

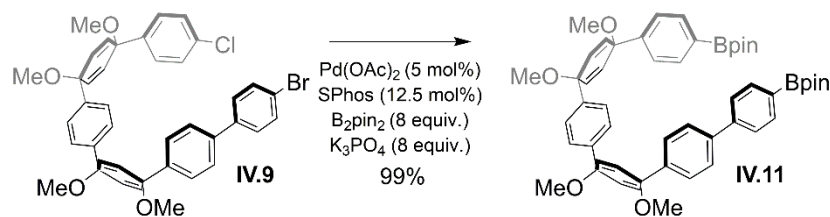
126.15, 83.93, 74.78, 74.70, 74.59, 52.13, 25.01; HRMS (TOF, ES+) (m/z): $[M+Na]^+$ calculated for $C_{46}H_{48}BClNaO_6$, 765.3138; found: 765.3162. IR (neat): 3029, 2978, 2917, 2849, 2823, 1609, 1577, 1540, 1502, 1471, 1449, 1399, 1379, 1361, 1304, 1272, 1229, 1174, 1144, 1082, 1030, 1013, 986, 950, 904, 856, 821, 789 cm^{-1} .



Six ring dichloride **IV.33** (5.00 g, 7.67 mmol, 1.00 equiv.), B_2pin_2 (15.6 g, 61.4 mmol, 8.00 equiv.), K_3PO_4 (13.0 g, 61.4 mmol, 8.00 equiv.), palladium(II) acetate (86.0 mg, 0.383 mmol, 5.00 mol%), and SPhos (787 mg, 1.90 mmol, 25.0 mol%) were added to a flame dried flask. ** K_3PO_4 should be finely ground with a mortar and pestle and oven or flame dried immediately before use for best results.* This flask was evacuated and backfilled with N_2 three times. A septum was added and the solids were purged with N_2 for 30 minutes. N_2 sparged and dried dioxane (150 mL) was added to the reaction. The reaction was heated to 80° C, within 1 minute the reaction turned a deep green which gradually gave way to a pale yellow solution. The reaction was allowed to react for 12 h at which point it was cooled to room temperature and filtered over activated carbon. The crude mixture concentrated and then dissolved in DCM (100 mL) and water (150 mL). This was extracted with dichloromethane (3 x 100 mL) and was then washed with water (3 x 100 mL) and brine (100 mL). The organic layer was dried on sodium sulfate. The organic layer was concentrated to give a white solid. This was washed with cold ethanol (3 x 50.0 mL) to give the product **IV.11** as a white solid (6.34 g, 99% yield).

mp 219-221 °C. 1H NMR (600 MHz, $CDCl_3$): δ 7.87 (d, $J = 8.4$ Hz, 2H), 7.76 (d, $J = 8.4$ Hz, 2H), 7.59 (d, $J = 8.4$ Hz, 2H), 7.57 (d, $J = 8.4$ Hz, 2H), 7.47 (d, $J = 8.4$ Hz, 2H), 7.40 (d, $J = 8.4$ Hz, 2H), 7.38 (d, $J = 9.3$ Hz, 2H), 7.36 (d, $J = 9.3$ Hz, 2H), 6.14 (d, $J = 10.5$ Hz, 2H), 6.12 (d, $J = 10.5$ Hz, 2H), 6.10 (d, $J = 10.8$ Hz, 2H), 6.07 (d, $J = 10.8$ Hz, 2H), 3.46 (s, 3H), 3.44 (s, 3H), 3.43 (s, 3H), 3.42 (s, 3H), 1.36 (s, 12H), 1.31 (s, 12H); ^{13}C NMR (150 MHz, $CDCl_3$): δ 146.56, 143.59, 142.96, 142.91, 142.86, 140.32, 135.37, 135.05, 133.57, 133.45, 133.40, 133.38, 127.38, 126.56, 126.22, 126.20, 125.43, 83.93, 83.90, 75.05,

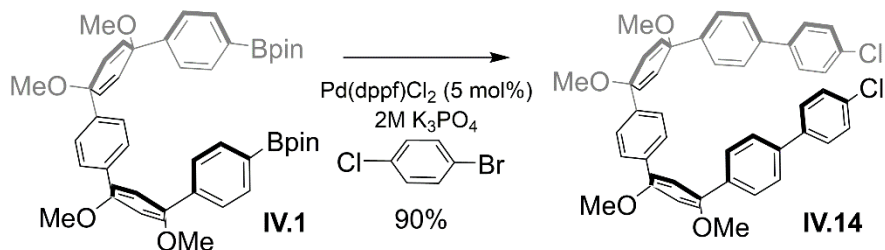
74.82, 74.80, 74.77, 52.15, 52.12, 52.11, 52.10, 25.02, 24.99; HRMS (TOF, ES+) (m/z): $[M+Na]^+$ calculated for $C_{52}H_{60}B_2O_8$, 857.4389; found: 857.4373. IR (neat): 2978, 2938, 2822, 1610, 1397, 1360, 1321, 1272, 1214, 1144, 1086, 1017, 1006, 950, 859, 760 cm^{-1} .



Six ring bromo chloride **IV.9** (2.00 g, 2.87 mmol, 1.00 equiv.), B₂pin₂ (5.80 g, 22.9 mmol, 8.00 equiv.), K₃PO₄ (4.88 g, 22.9 mmol, 8.00 equiv.), palladium(II) acetate (31.0 mg, 0.144 mmol, 5.00 mol%), and SPhos (147 mg, 0.359 mmol, 12.5 mol%) were added to a flame dried flask. *K₃PO₄ should be finely ground with a mortar and pestle and oven or flame dried immediately before use for best results. This flask was evacuated and backfilled with N₂ three times. A septum was added and the solids were purged with N₂ for 30 minutes. N₂ sparged and dried dioxane (50 mL) was added to the reaction. The reaction was heated to 80° C, within 1 minute the reaction turned a deep green which gradually gave way to a pale yellow solution. The reaction was allowed to react for 12 h at which point it was cooled to room temperature and filtered over activated carbon. The crude mixture concentrated and then dissolved in DCM (100 mL) and water (150 mL). This was extracted with dichloromethane (3 x 100 mL) and was then washed with water (3 x 100 mL) and brine (100 mL). The organic layer was dried on sodium sulfate. The organic layer was concentrated to give a white solid. This was washed with cold ethanol (3 x 50.0 mL) to give the product **IV.11** as a white solid (2.40 g, 99% yield).

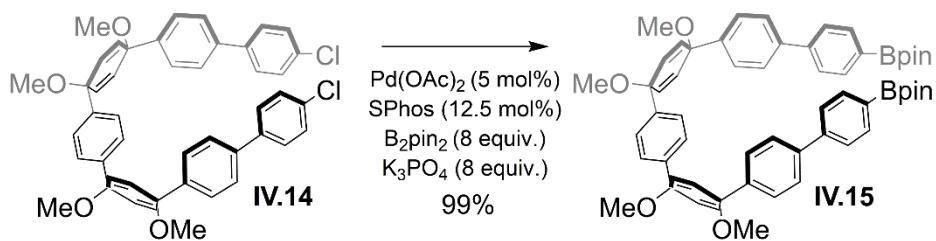
mp 219-221 °C. ¹H NMR (600 MHz, CDCl₃): δ 7.87 (d, $J = 8.4$ Hz, 2H), 7.76 (d, $J = 8.4$ Hz, 2H), 7.59 (d, $J = 8.4$ Hz, 2H), 7.57 (d, $J = 8.4$ Hz, 2H), 7.47 (d, $J = 8.4$ Hz, 2H), 7.40, (d, $J = 8.4$, 2H), 7.38 (d, $J = 9.3$ Hz, 2H), 7.36 (d, $J = 9.3$ Hz, 2H), 6.14 (d, $J = 10.5$ Hz, 2H), 6.12 (d, $J = 10.5$, 2H), 6.10 (d, $J = 10.8$, 2H), 6.07 (d, $J = 10.8$ Hz, 2H), 3.46 (s, 3H), 3.44 (s, 3H), 3.43 (s, 3H), 3.42 (s, 3H), 1.36 (s, 12H), 1.31 (s, 12H); ¹³C NMR (150 MHz, CDCl₃): δ 146.56, 143.59, 142.96, 142.91, 142.86, 140.32, 135.37, 135.05, 133.57, 133.45, 133.40, 133.38, 127.38, 126.56, 126.22, 126.20, 125.43, 83.93, 83.90, 75.05, 74.82, 74.80, 74.77, 52.15, 52.12, 52.11, 52.10, 25.02, 24.99; HRMS (TOF, ES+) (m/z):

$[M+Na]^+$ calculated for $C_{52}H_{60}B_2O_8$, 857.4389; found: 857.4373. IR (neat): 2978, 2938, 2822, 1610, 1397, 1360, 1321, 1272, 1214, 1144, 1086, 1017, 1006, 950, 859, 760 cm^{-1} .



Previously reported five ring diboronate **IV.1** (1.15 g, 1.52 mmol, 1.00 equiv.), 4-bromochlorobenzene (0.639 g, 3.34 mmol, 2.20 equiv.), and $Pd(dppf)Cl_2$ (0.0554 g, 0.0758 mmol, 5.00 mol%) were added to a flame dried flask. This flask was evacuated and backfilled with N_2 three times. A septum was added and the solids were purged with N_2 for 30 minutes. N_2 sparged dioxane (50.0 mL) and 2M K_3PO_4 (aq) (5.00 mL) were added to the reaction. The reaction was heated to 80 °C and was allowed to react for 12 h at which point it was cooled to room temperature. The crude mixture was extracted with DCM (3 x 50.0 mL) and was then washed with water (3 x 50.0 mL) and brine (50.0 mL). The organic layer was filtered over activated carbon and was dried on sodium sulfate. The organic layer was concentrated onto SiO_2 and was dry loaded onto silica gel. The product **IV.14** was washed with hot hexanes (30.0 mL) to give the product at a white solid (0.989 g, 90% yield).

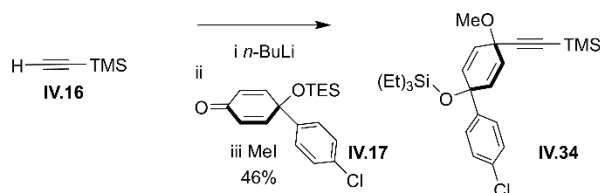
mp 236-237 °C. 1H NMR (600 MHz, $CDCl_3$): δ 7.49 – 7.45 (overlap, 12H), 7.89 (s, 4H), 7.35 (d, $J = 8.4$ Hz, 4H), 6.12 (s, 8H), 3.45 (s, 6H). 3.44 (s, 6H); ^{13}C NMR (150 MHz, $CDCl_3$): δ 143.04, 142.96, 139.31, 139.28, 133.57, 133.55, 133.47, 129.03, 128.43, 127.08, 126.66, 126.24, 74.80, 74.78, 52.19, 52.16; HRMS (TOF, ES+) (m/z): $[M+Na]^+$ calculated for $C_{46}H_{40}Cl_2NaO_4$, 749.2202; found: 749.2196. IR (neat): 2934, 2851, 2819, 1485, 1469, 1388, 1175, 1078, 1051, 1027, 1006, 948, 834, 826, 815, 776 cm^{-1} .



Seven ring dichloride **IV.14** (300 mg, 0.412 mmol, 1.00 equiv.), B_2pin_2 (837 mg, 3.30 mmol, 8.00 equiv.), K_3PO_4 (700 mg, 3.30 mmol, 8.00 equiv.), palladium(II) acetate (9.30

mg, 0.0412 mmol, 10.0 mol%), and SPhos (42.0 mg, 1.03 mmol, 25.0 mol%) were added to a flame dried flask. **K₃PO₄ should be finely ground with a mortar and pestle and oven or flame dried immediately before use for best results.* This flask was evacuated and backfilled with N₂ three times. A septum was added and the solids were purged with N₂ for 30 minutes. N₂ sparged and dried dioxane (20.0 mL) was added to the reaction. The reaction was heated to 80° C, within 1 minute the reaction turned a deep green which gradually gave way to a pale yellow solution. The reaction was allowed to react for 12 h at which point it was cooled to room temperature and filtered over activated carbon. The crude mixture concentrated and then dissolved in DCM (100 mL) and water (150 mL). This was extracted with dichloromethane (3 x 100 mL) and was then washed with water (3 x 100 mL) and brine (100 mL). The organic layer was dried on sodium sulfate. The organic layer was concentrated to give a white solid. This was washed with cold ethanol (20.0 mL) to give the product **IV.15** as a white solid (372 mg, 99% yield).

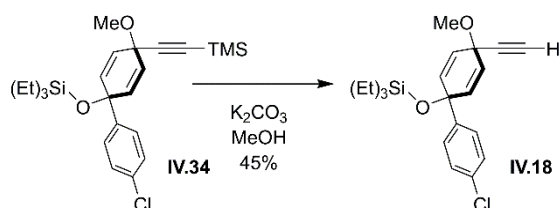
mp 252-253 °C. ¹H NMR (600 MHz, CDCl₃): δ 7.86 (d, *J* = 7.5 Hz, 4H), 7.58 (d, *J* = 8.7 Hz, 4H), 7.55 (d, *J* = 8.7 Hz, 4 H), 7.46 (d, *J* = 7.5 Hz, 4H), 7.39 (s, 4), 6.14 – 6.11 (overlap, 8H), 3.45 (s, 6H), 3.44 (s, 6H), 1.36 (s, 24H); ¹³C NMR (150 MHz, CDCl₃): δ 143.54, 142.94, 142.93, 140.32, 135.38, 133.51, 133.48, 127.36, 126.55, 126.53, 126.24, 83.94, 74.83, 74.81, 52.16, 52.15, 25.03; HRMS (TOF, ES+) (*m/z*): [M+Na]⁺ calculated for C₅₈H₆₄B₂NaO₈, 933.4703; found: 933.4692. IR (neat): 2976, 2939, 2896, 2824, 1610, 1526, 1501, 1450, 1397, 1359, 1323, 1272, 1214, 1167, 1143, 1091, 1077, 1017, 1006, 948, 859, 836, 820, 763, 744 cm⁻¹.



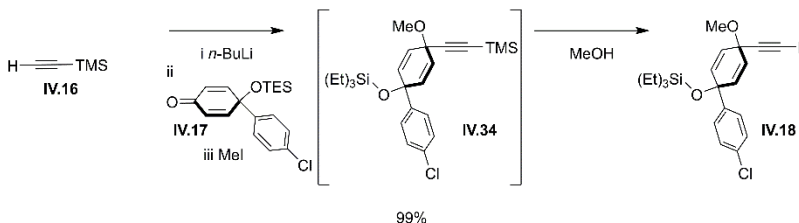
In a flask TMS protected acetylene **IV.16** (4.22 mL, 29.9 mmol, 2.00 equiv.) was dissolved in THF (150 mL) and cooled to -78 °C with stirring for 1 hour. To this flask, *n*-BuLi (2.10 M, 8.50 mL, 18.0 mmol, 1.20 equiv.) at room temperature was added dropwise. The reaction was stirred for 1.5 hours at -78 °C to give the lithiated species as a clear solution. To the lithiated TMS protected acetylene, TES protected chloroketone **IV.17** (5.00 g, 14.9 mmol, 1.00 equiv.) was added neat at -78 °C. The reaction was

stirred for 1.5 hours at $-78\text{ }^{\circ}\text{C}$. After 1.5 hours, the reaction was quenched with methyl iodide (3.72 mL, 60.0 mmol, 4.00 equiv.) at $-78\text{ }^{\circ}\text{C}$. immediately after quenching with methyl iodide, DMF (37.5 mL) was added dropwise and the flask was allowed to warm to room temperature. Upon warming to room temperature, the reaction was stirred at room temperature overnight. After stirring overnight, the mixture was extracted with dichloromethane (3 x 150 mL). The combined organic layers were washed with brine and dried over sodium sulfate before being filtered and concentrated down to the product **IV.34** as an orange-brown oil (2.57 g, 46% yield).

^1H NMR (600 MHz, d-6 acetone): δ 7.51 (d, $J = 8.0$ Hz, 2H), 7.33 (d, $J = 8.0$ Hz, 2H), 6.03 (d, $J = 9.6$ Hz, 2H), 5.96 (d, $J = 9.6$ Hz, 2H), 3.41 (s, 3H), 0.978 (t, $J = 8.1$ Hz, 9H), 0.685 (q, $J = 8.1$ Hz, 6H), 0.209 (s, 9H); ^{13}C NMR (150 MHz, d-6 acetone): δ 145.69, 135.01, 133.40, 129.02, 128.30, 127.12, 72.95, 68.14, 52.16, 7.47, 7.07, 0.05; HRMS (TOF, ES+) (m/z): $[\text{M}+\text{Na}]^+$ calculated for $\text{C}_{24}\text{H}_{35}\text{ClO}_2\text{Si}_2\text{Na}$, 469.1762; found: 469.1751. IR (neat): 2950, 2870, 1490, 1460, 1400, 1250, 1100, 1080, 1060, 1010, 989, 837, 748, 716 cm^{-1} .



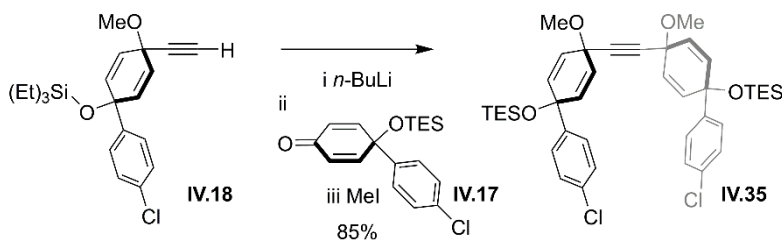
The acetylene addition product **IV.34** was dissolved in MeOH (75.0 mL). To the dissolved oil, K_2CO_3 (4.38 g, 22.3 mmol, 1.50 equiv.) was added. The mixture was stirred at room temperature for 1 hour. After 1 hour, the reaction was poured over ice water and allowed to stir for 10 minutes. After 10 minutes of stirring, the mixture was warmed to room temperature and extracted with ether (3 x 150 mL). The combined organic layers were washed with brine and dried over sodium sulfate before being concentrated down to a orange oil. The oil was then purified via flash chromatography (10% ethyl acetate/hexanes as mobile phase) to afford the product **IV.18** as a yellow oil (2.54 g, 45 % yield).



In a flask TMS protected acetylene **IV.16** (4.05 mL, 28.7 mmol, 1.20 equiv.) was dissolved in THF (150 mL) and cooled to $-78\text{ }^{\circ}\text{C}$ with stirring for 1 hour. To this flask, *n*-BuLi (14.7 mL, 28.7 mmol, 1.2 equiv.) at room temperature was added dropwise. The reaction was stirred for 1.5 hours at $-78\text{ }^{\circ}\text{C}$ to give the lithiated species as a clear solution.

To the lithiated TMS protected acetylene, TES protected chloroquinol **IV.17** (8.00 g, 23.9 mmol, 1 equiv.) was added neat at $-78\text{ }^{\circ}\text{C}$. The reaction was stirred for 1.5 hours at $-78\text{ }^{\circ}\text{C}$. After 1.5 hours, the reaction was quenched with methyl iodide (1.93 mL, 31.1 mmol, 1.3 equiv.) at $-78\text{ }^{\circ}\text{C}$. immediately after quenching with methyl iodide, DMF (0.500 mL) was added dropwise and the flask was allowed to warm to room temperature. Upon warming to room temperature, the reaction was stirred at room temperature overnight. Methanol (100 mL) was then added to reaction and was heated to $40\text{ }^{\circ}\text{C}$ for 2 h. The reaction was then concentrated and extracted with dichloromethane (3 x 50 mL). The combined organic layers were washed with brine and dried over sodium sulfate before being filtered and concentrated down to give product **IV.18** as a clear oil (8.96 g, 99% yield).

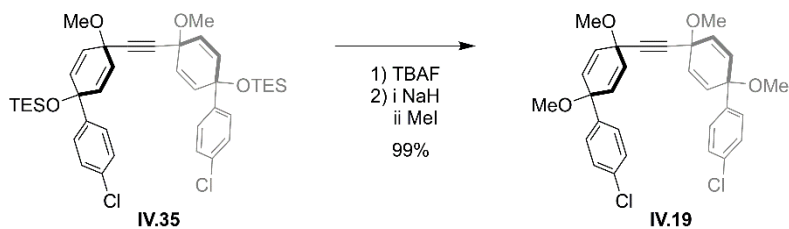
^1H NMR (600 MHz, d-6 acetone): δ 7.48 (d, $J = 8.4\text{ Hz}$, 2H), 7.33 (d, $J = 8.4\text{ Hz}$, 2H), 6.04 (d, $J = 9.8\text{ Hz}$, 2H), 5.95 (d, $J = 9.8\text{ Hz}$, 2H), 3.43 (s, 3H), 3.20 (s, 1H), 0.990 (t, $J = 8.4\text{ Hz}$, 9H), 0.693 (q, $J = 8.4\text{ Hz}$, 6H); ^{13}C NMR (150 MHz, d-6 acetone): δ 145.59, 135.09, 133.61, 129.25, 128.33, 127.11, 83.62, 76.46, 72.85, 67.57, 52.37, 7.74, 7.25; HRMS (TOF, ES+) (m/z): $[\text{M}+\text{Na}]^+$ calculated for $\text{C}_{21}\text{H}_{27}\text{ClO}_2\text{SiNa}$, 397.1367; found: 397.1357. IR (neat): 3290, 3020, 2950, 2940, 2880, 2870, 2820, 1480, 1460, 1400, 1240, 1170, 1100, 1080, 1050, 986, 970, 910, 861, 827, 729, 718, 661, 628, 539 cm^{-1} .



To a flask the acetylene addition product **IV.18** (3 g, 8.00 mmol, 1.2 equiv.) was dissolved in THF (40.0 mL). The flask was then cooled to $-78\text{ }^{\circ}\text{C}$ with stirring for 1 hour. After 1 hour, room temperature *n*-BuLi (2.1 M, 4.1 mL, 8.66 mmol, 1.3 equiv.) was

added drop wise to the flask. The reaction was stirred for 1.5 hours at $-78\text{ }^{\circ}\text{C}$ to give the lithiated acetylene species. After complete formation of the lithiated acetylene species, TES protected chloroketone **IV.17** (2.09 mL, 6.67 mmol, 1.00 equiv.) was added neat to the flask. The reaction was then stirred for 1.5 hours at $-78\text{ }^{\circ}\text{C}$. After the reaction was stirred for 1.5 hours, the reaction was quenched with methyl iodide (1.7 mL, 26.7 mmol, 4 equiv.) at $-78\text{ }^{\circ}\text{C}$. Immediately after quenching with methyl iodide, DMF (4.00 mL) was added drop wise to the flask and the reaction was allowed to warm to room temperature. Upon warming to room temperature, the reaction was stirred at room temperature overnight. After stirring the reaction overnight the mixture was extracted with dichloromethane (3 x 150 mL). The combined organic layers were washed with brine and dried over sodium sulfate before being concentrated down to orange oil. The oil was then purified via flash chromatography (5% ethyl acetate/ hexanes as mobile phase) to afford the product **IV.35** as a clear semi-solid (4.92 g, 85 % yield).

^1H NMR (600 MHz, CDCl_3): δ 7.33 (d, $J = 8.4$ Hz, 4H), 7.09 (d, $J = 8.4$ Hz, 4H), 5.96 (s, 8H), 3.41 (s, 6H), 0.968 (t, $J = 7.8$ Hz, 18H), 0.654 (q, $J = 7.8$ Hz, 12H); ^{13}C NMR (150 MHz, CDCl_3): δ 143.81, 135.07, 132.92, 128.32, 127.00, 125.45, 83.88, 71.91, 67.06, 52.18, 7.16, 6.49; HRMS (TOF, ES+) (m/z): $[\text{M}+\text{Na}]^+$ calculated for $\text{C}_{40}\text{H}_{52}\text{Cl}_2\text{O}_4\text{Si}_2\text{Na}$, 745.2679; found: 745.2694. IR (neat): 2950, 2900, 2870, 2820, 1480, 1450, 1400, 1230, 1180, 1100, 1070, 1010, 990, 959, 905, 861, 826, 768, 715, 645 cm^{-1} .

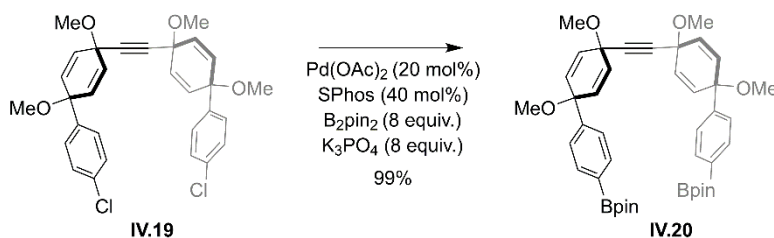


TES protected dichloride **IV.35** (2.50 g, 3.45 mmol, 1.00 equiv.) was dissolved in THF (50.0 mL) under N_2 in a flame dried flask. To this was added TBAF (10.4 mL, 10.4 mmol, 3.00 equiv.). The reaction was allowed to stir for 1 h at which point water (100 mL) was added. This was extracted with DCM (3 x 50.0 mL). The organic layer was washed with water (3 x 50.0 mL) and brine (50.0 mL) and was dried over sodium sulfate. After concentration, the crude oil was dissolved in THF (100 mL) and was cooled to $0\text{ }^{\circ}\text{C}$ for 30 minutes. Solid NaH (414 mg, 10.4 mmol, 3.00 equiv.) was added to this solution and was then stirred for 2 h. At this point MeI (1.07 mL, 17.3 mmol, 5.00 equiv.) was

added and the reaction was allowed to stir overnight. Water (100 mL) was added and the reaction was extracted with ethyl acetate (3 x 50.0 mL). The organic layer was washed with water (3 x 50.0 mL) and brine (50.0 mL) and was dried over sodium sulfate.

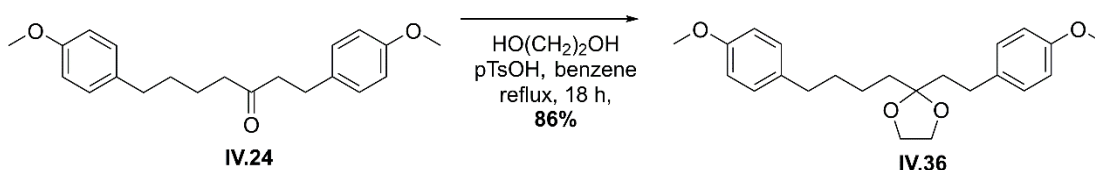
Concentration gave a white solid that was washed with hot hexanes (30.0 mL) to give the product **IV.19** as a white solid (1.79 g, 99% yield). The relative stereochemistry of this product was confirmed by X-ray crystallography.

mp 194-195 °C. ¹H NMR (500 MHz, CDCl₃): δ 7.310 (d, *J* = 8.5 Hz, 4H), 7.11 (d, *J* = 8.5 Hz, 4H), 6.14 (d, *J* = 10, 4H), 5.89 (d, *J* = 10, 4H), 3.39 (s, 6H), 3.34 (s, 6H); ¹³C NMR (125 MHz, CDCl₃): δ 141.46, 133.30, 133.18, 129.57, 128.48, 127.22, 84.66, 74.93, 67.02, 52.26, 51.92; IR (neat): 2982, 2925, 2853, 2826, 1672, 1591, 1484, 1462, 1400, 1266, 1216, 1199, 1184, 1173, 1157, 1133, 1109, 1074, 1023, 1012, 972, 950, 899, 833, 786 cm⁻¹.



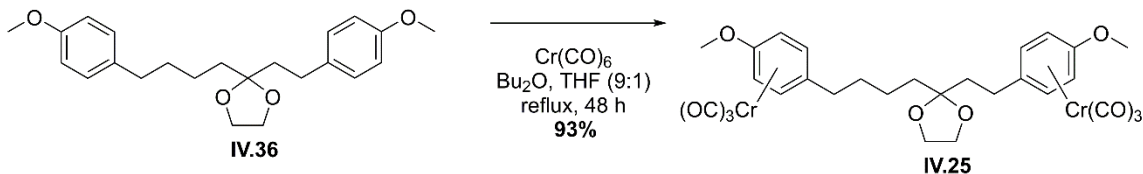
Alkyne dichloride **IV.19** (380 mg, 0.784 mmol, 1.00 equiv.), B₂pin₂ (1.60 g, 6.32 mmol, 8.00 equiv.), K₃PO₄ (1.34 g, 6.32 mmol, 8.00 equiv.), palladium(II) acetate (110 mg, 0.158 mmol, 20.0 mol%), and SPhos (129 mg, 0.316 mmol, 40.0 mol%) were added to a flame dried flask. *K₃PO₄ should be finely ground with a mortar and pestle and oven or flame dried immediately before use for best results. This flask was evacuated and backfilled with N₂ three times. A septum was added and the solids were purged with N₂ for 30 minutes. N₂ sparged and dried dioxane (20.0 mL) was added to the reaction. The reaction was heated to 80° C, within 1 minute the reaction turned a deep green which gradually gave way to a pale yellow solution. The reaction was allowed to react for 12 h at which point it was cooled to room temperature and filtered over activated carbon. The crude mixture concentrated and then dissolved in DCM (100 mL) and water (150 mL). This was extracted with dichloromethane (3 x 100 mL) and was then washed with water (3 x 100 mL) and brine (100 mL). The organic layer was dried on sodium sulfate. The organic layer was concentrated to give a white solid. This was washed with cold ethanol (20.0 mL) to give the product **IV.20** as a white solid (409 mg, 99% yield).

mp 264-265 °C. ¹H NMR (500 MHz, CDCl₃): δ 7.67 (d, *J* = 8.5 Hz, 4H), 7.42 (d, *J* = 8.5 Hz, 4H), 6.15 (d, *J* = 10, 4H), 5.90 (d, *J* = 10, 4H), 3.34 (s, 6H), 3.35 (s, 6H), 1.31 (s, 24H); ¹³C NMR (125 MHz, CDCl₃): δ 145.99, 134.93, 133.07, 129.33, 125.11, 84.55, 83.83, 75.69, 67.05, 52.16, 51.93, 24.99; IR (neat): 3041, 2974, 2928, 2821, 1605, 1506, 1460, 1393, 1358, 1315, 1270, 1214, 1141, 1088, 1013, 946, 964, 855, 780, 729, 659 cm⁻¹.



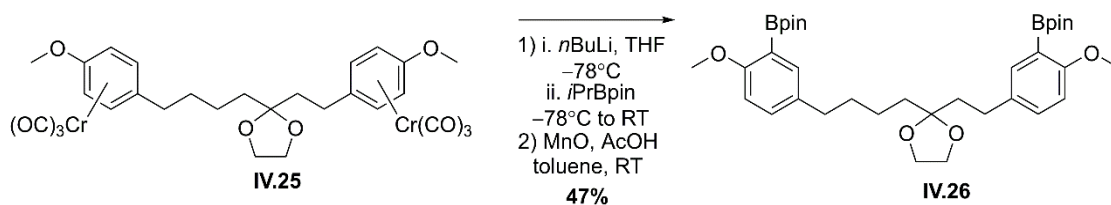
1,7-Bis-(4-methoxyphenyl)-heptane-3-one **IV.24** (6.00 g, 18.4 mmol, 1.00 equiv.) was stirred with *p*-toluene sulfonic acid monohydrate (670 mg 3.68 mmol, 0.200 equiv.) and distilled ethylene glycol (1.50 mL, 27.6 mmol, 1.50 equiv.) in benzene (80.0 mL) in a flask attached to a Dean-Stark apparatus. The reaction mixture was stirred under reflux for 18 hours then cooled to room temperature and quenched with saturated sodium bicarbonate. The resulting organic layer was separated and dried over sodium sulfate to give a light brown oil. The crude reaction mixture was purified via column chromatography (5-30% ethyl acetate/hexanes) to give the product **IV.36** as a white solid after crystallization from hexanes (5.70 g, 86%). mp 44-45 °C.

¹H NMR (600 MHz, CDCl₃): δ 7.09 (d, *J* = 8.7 Hz, 2H), 7.09 (d, *J* = 8.6 Hz, 2H), 6.82 (d, *J* = 8.7 Hz, 2H), 6.82 (d, *J* = 8.6 Hz, 2H), 3.96 (s, 4H), 3.78 (s, 3H), 3.78 (s, 3H), 2.60 (m, 2H), 2.55 (t, *J* = 7.7 Hz, 2H), 1.88 (m, 2H), 1.42 (m, 2H), 1.59 (m, 2H), 1.67 (m, 2H); ¹³C NMR (150 MHz, CDCl₃): δ 157.85, 157.78, 134.83, 134.45, 129.38, 129.31, 113.98, 113.84, 111.51, 65.18, 55.42, 55.40, 39.40, 37.35, 35.12, 32.16, 29.27, 23.72; HRMS (TOF, ES+) (*m/z*): [M+Na]⁺ calculated for C₂₃H₃₀O₄, 393.2042; found: 393.2034. IR (neat): 2940, 2909, 2864, 1611, 1607, 1511, 1464, 1376, 1301, 1255, 1241, 1179, 1172, 1134, 1127, 1062, 1029, 950, 905, 901, 829, 815, 778, 750, 674, 647, 647, 614, 557 cm⁻¹.



1,7-Bis-(4-methoxyphenyl)-heptane-3-[1,3]dioxolane **IV.36** (3.00 g, 8.32 mmol, 1.00 equiv.) and chromium carbonyl (4.76 g, 21.6 mmol, 2.60 equiv.) were charged to a Schlenk flask equipped with a reflux condenser. The mixture was diluted with dibutyl ether (111 mL) and THF (12.0 mL) and subjected to freeze-pump-thaw cycles (3 x 15 min) and then refluxed at 150 °C. At 4 and 24 hours of reaction time, THF (2.00 mL) was added to the top of the reflux condenser to dissolve any chromium carbonyl that sublimed in the condenser. After 48 hours, the reaction mixture was cooled to room temperature and filtered through a pad of silica. The silica pad was rinsed with diethyl ether (3 x 250 mL) and dichloromethane (3 x 250 mL) the resulting filtrate was concentrated to give a yellow solid. The crude reaction mixture was purified via column chromatography (20-70% ethyl acetate/hexane then 70% ethyl acetate/dichloromethane) to give the product **IV.25** as a yellow solid (5.97 g, 93%).

mp 126-127 °C. ¹H NMR (600 MHz, CDCl₃): δ 5.45 (d, *J* = 6.9 Hz, 2H), 5.43 (d, *J* = 6.8 Hz, 2H), 5.11 (d, *J* = 6.6 Hz, 2H), 5.10 (d, *J* = 6.3 Hz, 2H), 1.42 (m, 2H), 3.95 (s, 4H), 3.68 (s, 6H), 2.33 (m, 2H), 2.26 (t, *J* = 7.7 Hz, 2H), 1.84 (m, 2H), 1.62 (m, 2H), 1.55 (m, 2H); ¹³C NMR (150 MHz, CDCl₃): δ 142.28, 142.17, 110.70, 106.36, 106.28, 95.43, 95.37, 78.49, 78.28, 65.23, 55.86, 38.92, 37.14, 34.03, 31.74, 27.98, 23.53; HRMS (TOF, ES+) (*m/z*): [M+Na]⁺ calculated for C₂₉H₃₀Cr₂O₁₀, 665.0548; found: 665.0532. IR (neat): 3091, 3072, 3051, 2977, 2975, 2938, 2908, 2881, 2863, 2834, 1941, 1846, 1841, 1610, 1607, 1542, 1511, 1485, 1462, 1435, 1356, 1278, 1271, 1248, 1245, 1221, 1178, 1134, 1132, 1107, 1075, 1062, 1060, 1028, 1015, 954, 950, 939, 905, 872, 835, 823, 817, 744, 662, 670, 626 cm⁻¹.

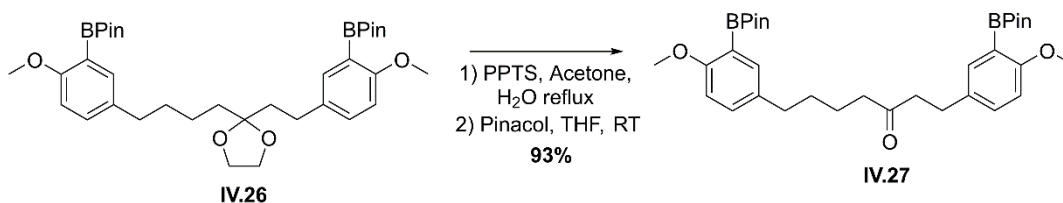


1,7-Bis-[(4-methoxyphenyl)chromium-tricarbonyl]-heptane-3-[1,3]dioxolane **IV.25** (4.55 g, 7.09 mmol, 1.00 equiv) was dissolved in THF (120 mL) and cooled to -78 °C. *n*-BuLi (2.32 M in hexanes, 7.55 mL, 17.5 mmol, 2.50 equiv.) was added to the cooled reaction mixture dropwise and the reaction was stirred at this temperature for 1 hour. 2-Isopropoxy-4,4,5,5-tetramethyl-1,3,2-dioxaborolane (5.00 mL, 24.5 mmol, 3.50 equiv.)

was then added to the mixture dropwise and the reaction was stirred at $-78\text{ }^{\circ}\text{C}$ for 1 hour. The reaction was then quenched with water and warmed to room temperature. The product was extracted with dichloromethane (3 x 100 mL) and the combined organic layers were washed with deionized water (3 x 100 mL), once with brine and dried over sodium sulfate to give the a yellow-orange foam after filtration and concentration. The foam was carried on crude.

To foam from above was added AcOH (10.0 mL) after dilution with toluene (50.0 mL). Activated manganese oxide (4.00 g, 46.0 mmol, 6.50 equiv.) was added in portions to the reaction mixture and this slurry was stirred open to the atmosphere for 16 hours. The reaction was then diluted with EtOAc (20.0 mL) and filtered over a short pad of silica. The pad was rinsed with EtOAc (3 x 125 mL) and filtrate was concentrated to give a yellow oil. The crude reaction mixture was purified via column chromatography (15-50% ethyl acetate/hexane) to give the product **IV.26** as a clear, viscous oil (2.05 g, 47%).

^1H NMR (500 MHz, CDCl_3): δ 7.49 (d, $J = 2.4$ Hz, 1H), 7.47 (d, $J = 2.4$ Hz, 1H), 7.19 (dd, $J = 8.5$ Hz, 2.3 Hz, 1H), 7.19 (dd, $J = 8.4$ Hz, 2.3 Hz, 1H), 6.78 (d, $J = 8.4$ Hz, 1H), 6.77 (d, $J = 8.5$ Hz, 1H), 3.96 (m, 4H), 3.80 (s, 6H), 3.80 (s, 6H), 2.61 (m, 2H), 2.54 (m, 2H), 1.89 (m, 2H), 1.68 (m, 2H), 1.59 (m, 2H), 1.43 (m, 2H), 1.35 (s, 12H), 1.35 (s, 12H); ^{13}C NMR (125 MHz, CDCl_3): δ 162.64, 162.59, 136.67, 136.57, 134.27, 133.80, 132.35, 132.33, 111.56, 110.83, 110.73, 83.54, 83.50, 65.21, 56.18, 39.49, 37.41, 35.09, 32.29, 29.15, 24.97, 23.84; HRMS (TOF, ES+) (m/z): $[\text{M}+\text{Na}]^+$ calculated for $\text{C}_{35}\text{H}_{52}\text{B}_2\text{O}_8$, 645.3759; found: 645.3741. IR (neat): 2974, 2930, 2858, 2830, 1606, 1609, 1492, 1461, 1413, 1369, 1342, 1310, 1276, 1268, 1244, 1204, 1179, 1167, 1140, 1107, 1068, 1026, 965, 947, 912, 856, 824, 813, 763, 745, 731, 691, 673, 578, 553 cm^{-1} .

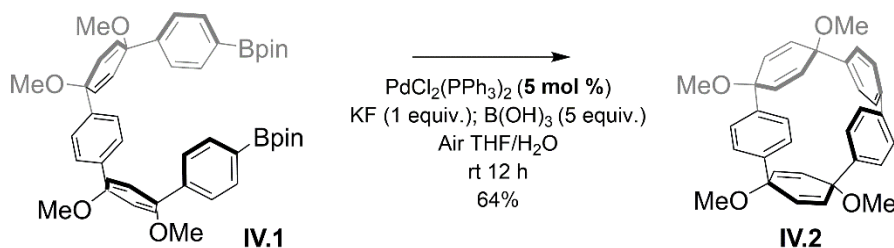


1,7-Bis-[3-(4,4,5,5-tetramethyl-[1,3,2]dioxaborolane-2-yl)4-methoxyphenyl]-heptane-3-[1,3]dioxolane **IV.26** (1.77 g, 2.84 mmol, 1.00 equiv.) was refluxed in acetone (29.0 mL) and water (12.0 mL) with pyridinium paratoluenesulfonate (243 mg, 0.967 mmol, 0.340 equiv.) for 16 hours. The reaction mixture was then cooled to room temperature and

quenched with saturated sodium bicarbonate (15.0 mL). The product was extracted with ethyl acetate (3 x 75.0 mL) and the combined organic layers were washed with deionized water (3 x 100 mL) and brine (1 x 100 mL) then dried over sodium sulfate and concentrated to give a colorless viscous oil. The crude reaction mixture was carried on crude.

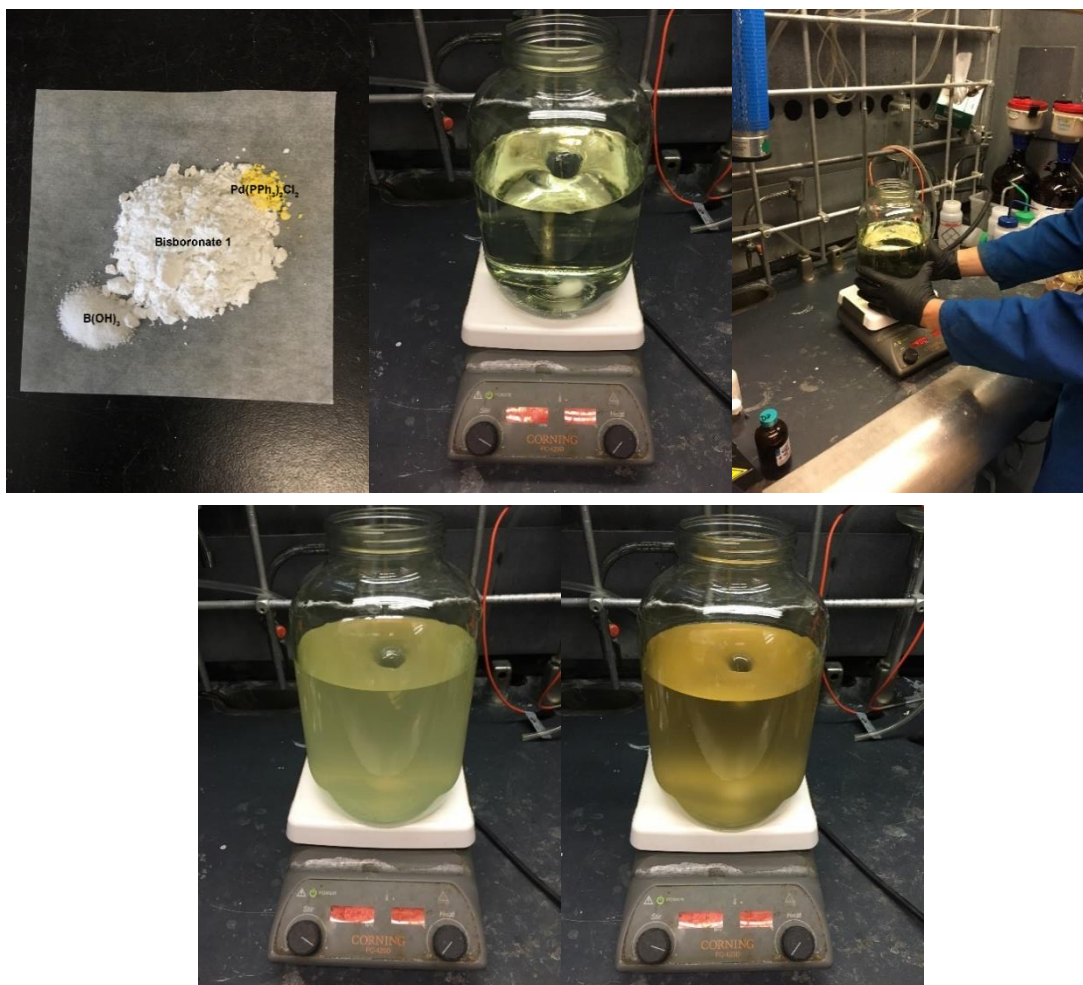
The oil from above was stirred with 2,3-dimethyl-2,3-butanediol (1.01 g, 8.53 mmol, 3 equiv.) in THF (28.0 mL) and molecular sieves for 48 hours. The reaction mixture was then filtered over a pad of celite that was rinsed with dichloromethane (3 x 25.0 mL) and the filtrate was concentrated to give a colorless viscous oil. The crude mixture was purified via column chromatography (15-50% ethyl acetate/hexane) to give the product and 2,3-dimethyl-2,3-butanediol as a mixture. The mixture was then diluted with dichloromethane (50.0 mL) and rinsed with deionized (4 x 10.0 mL) then dried with sodium sulfate and concentrated to give the desired product **IV.27** as a colorless viscous oil (1.54 g, 93%).

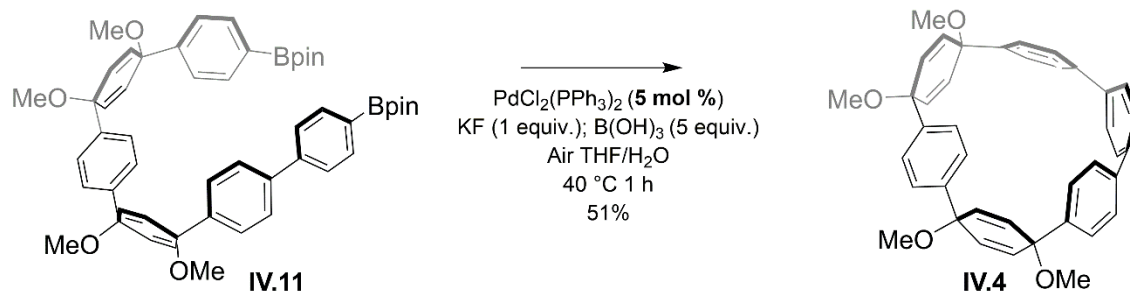
^1H NMR (500 MHz, CDCl_3): δ 7.46 (d, $J = 2.3$ Hz, 1H), 7.45 (d, $J = 2.3$ Hz, 1H), 7.19 (dd, $J = 8.8$ Hz, 2.2 Hz, 1H), 7.17 (dd, $J = 8.9$ Hz, 2.2 Hz, 1H), 6.77 (d, $J = 8.5$ Hz, 1H), 6.77 (d, $J = 8.5$ Hz, 1H), 3.80 (s, 3H), 3.80 (s, 3H), 2.81 (t, $J = 7.7$, 2H), 2.67 (t, $J = 7.7$, 2H), 2.53 (t, $J = 7.2$, 2H), 2.39 (t, $J = 6.9$ 2H), 1.58 (m, 4H), 1.43 (m, 2H), 1.35 (s, 24H); ^{13}C NMR (125 MHz, CDCl_3): δ 210.38, 162.72, 162.54, 136.53, 136.37, 133.71, 132.55, 132.36, 132.26, 110.71, 110.62, 83.47, 83.41, 56.05, 56.01, 44.69, 42.89, 34.77, 31.33, 28.94, 24.88, 23.51; HRMS (TOF, ES+) (m/z): $[\text{M}+\text{Na}]^+$ calculated for $\text{C}_{33}\text{H}_{48}\text{B}_2\text{O}_7$, 601.4395; found: 601.3493. IR (neat): 3535, 2973, 2931, 2856, 2836, 1708, 1606, 1609, 1493, 1460, 1415, 1370, 1343, 1315, 1284, 1267, 1245, 1205, 1176, 1164, 1140, 1107, 1069, 1030, 964, 949, 912, 854, 834, 816, 762, 744, 732, 712, 671, 653, 578, 556 cm^{-1} .



Five-ring diboronate **IV.1** (2.00 g, 2.64 mmol, 1.00 equiv.) was added to a 4 L jar with bis(triphenylphosphine)palladium(II) dichloride (92.5 mg, 0.132 mmol, 5.00 mol%)

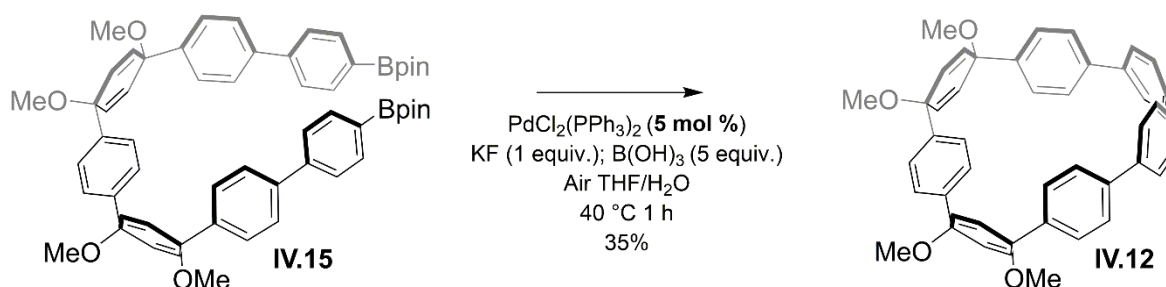
and boric acid (815 mg, 13.2 mmol, 5.00 equiv.). The solid were dissolved in THF (2,600 mL) and the mixture was stirred vigorously for 10 min. Potassium fluoride (153 mg, 2.64 mmol, 1.00 equiv.) was added to the mixture followed by the addition of water (240 mL). The reaction was stirred at room temperature open to the atmosphere for 12 hours. The THF was removed under vacuum and the resulting solution was extracted with dichloromethane (3 x 100 mL). The combined organic layers were washed with deionized water (3 x 100 mL) and brine (100 mL) then dried over sodium sulfate and concentrated to give an off yellow solid. The crude reaction mixture was dissolved in chloroform and purified via GPC to give the desired product **IV.2** as a white crystalline solid (860 mg, 64%). **Alternatively the crude reaction can simply be washed with cold acetone to render the product 90% pure. Single crystals can be grown on large scale by slow diffusion on hexanes into a concentrated solution of the product in dichloromethane.* Characterization consistent with previous reports.





Six-ring diboronic ester **IV.11** (1.00 g, 1.20 mmol, 1.00 equiv.) was added to a 4 L jar with bis(triphenylphosphine)palladium(II) dichloride (42.0 mg, 0.0599 mmol, 5.00 mol%) and boric acid (370 mg, 5.99 mmol, 5.00 equiv.). The solid were dissolved in THF (1,080 mL) and the mixture was stirred vigorously for 10 min while being gently heated to 40 °C. Potassium fluoride (70 mg, 1.20 mmol, 1.00 equiv.) was dissolved in water (120 mL) and was immediately added to the reaction. The reaction was stirred open to the atmosphere for 1 hour. The THF was removed under vacuum and the resulting solution was extracted with dichloromethane (3 x 100 mL). The combined organic layers were washed with deionized water (3 x 100 mL) and brine (1 x 100 mL) then dried over sodium sulfate and concentrated to give a brown oil. The crude reaction mixture was dissolved in chloroform and was purified via GPC to give the desired product **IV.4** as a white crystalline solid (355 mg, 51%).

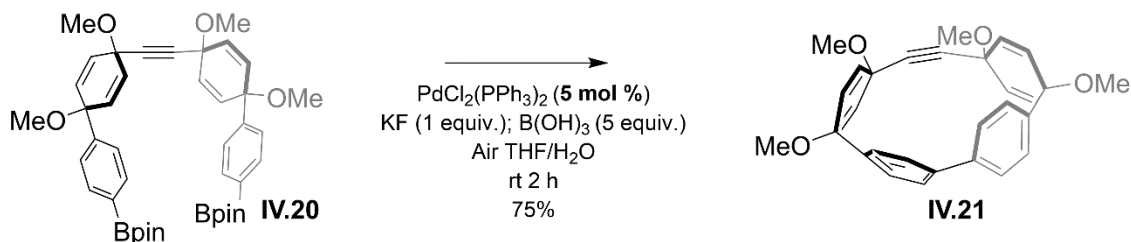
Characterization consistent with previous reports.



Seven-ring diboronic ester **IV.15** (100 mg, 0.110 mmol, 1.00 equiv.) was added to a round bottom flask with bis(triphenylphosphine)palladium(II) dichloride (3.85 mg, 0.00549 mmol, 5.00 mol%) and boric acid (33.9 mg, 0.490 mmol, 5.00 equiv.). The solid were dissolved in THF (100 mL) and the mixture was stirred vigorously for 10 min while being gently heated to 40 °C. Potassium fluoride (6.37 mg, 0.110 mmol, 1.00 equiv.) was dissolved in water (10 mL) and immediately added to the reaction. The reaction was stirred open to the atmosphere for 1 hour. The THF was removed under vacuum and the

resulting solution was extracted with dichloromethane (3 x 100 mL). The combined organic layers were washed with deionized water (3 x 100 mL) and brine (1 x 100 mL) then dried over sodium sulfate and concentrated to give a brown oil. The crude reaction mixture was dissolved in chloroform (3.00 mL) and was purified via GPC to give the desired product **IV.12** as a white crystalline solid (25 mg, 35%).

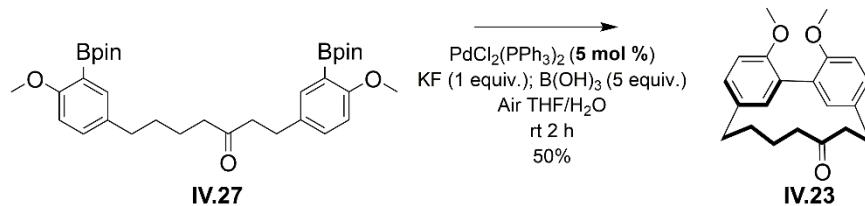
mp 300 °C dec. ^1H NMR (600 MHz, CDCl_3): δ 7.67 (d, J = 9.0 Hz, 4H), 7.41 (d, J = 9.0 Hz, 4H), 7.32 (d, J = 8.4 Hz, 4H), 7.23 (d, J = 8.4 Hz, 4H), 7.18 (s, 4H), 6.17 (d, J = 10.5, 4H), 5.94 (d, J = 10.5, 4H), 3.42 (s, 6H), 3.28 (s, 6H); ^{13}C NMR (150 MHz, CDCl_3): δ 143.24, 141.24, 140.91, 138.20, 138.13, 133.55, 132.33, 128.57, 128.44, 127.54, 126.47, 126.25, 74.02, 73.63, 52.42, 51.48; HRMS (Q-TOF, ES+) (m/z): $[\text{M}+\text{Na}]^+$ calculated for $\text{C}_{46}\text{H}_{40}\text{O}_4$, 679.2824; found: 679.2828. IR (neat): 3020, 2977, 2943, 2897, 2820, 1497, 1477, 1449, 1402, 1264, 1235, 1175, 1113, 1084, 1027, 1014, 983, 971, 944, 909, 895, 816, 787 cm^{-1} .



Four-ring alkyne **IV.20** (420 mg, 0.594 mmol, 1.00 equiv.) was added to a 4 L jar with bis(triphenylphosphine)palladium(II) dichloride (20.9 mg, 0.0297 mmol, 5.00 mol%) and boric acid (184 mg, 2.97 mmol, 5.00 equiv.). The solid were dissolved in THF (535 mL) and the mixture was stirred vigorously for 10 min. Potassium fluoride (34.5 mg, 2.59 mmol, 1.00 equiv.) was dissolved in water (59 mL). The reaction was stirred at room temperature open to the atmosphere for 2 hours. The THF was removed under vacuum and the resulting solution was extracted with dichloromethane (3 x 100 mL). The combined organic layers were washed with deionized water (3 x 100 mL) and brine (1 x 100 mL) then dried over sodium sulfate and concentrated to give a brown oil. The crude reaction mixture was dissolved in chloroform (9.00 mL) and purified via GPC to give the desired product **IV.21** as a white crystalline solid (202 mg, 75%).

mp 300 °C dec. ^1H NMR (500 MHz, CDCl_3): δ 7.26 (d, J = 8 Hz, 4H), 7.12 (d, J = 8 Hz, 4H), 6.34 (d, J = 9.5 Hz, 4H), 5.69 (d, J = 9.5 Hz, 4H), 3.37 (s, 6 H), 3.17 (s, 6H); ^{13}C

NMR (125 MHz, CDCl₃): δ 143.60, 138.95, 134.49, 129.14, 128.66, 128.01, 82.43, 74.19, 67.01, 52.99, 50.97; IR (neat): 3028, 2958, 2923, 2819, 17.28, 1583, 1479, 1460, 1393, 1278, 1262, 1171, 1128, 1069, 1002, 943, 927, 833, 820, 769 cm⁻¹.



1,7-Bis-[3-(4,4,5,5-tetramethyl-[1,3,2]dioxaborolane-2-yl)4-methoxyphenyl]-heptane-3-one **IV.27** (1.50 g, 2.59 mmol, 1.00 equiv.) was added to a 4 L jar with bis(triphenylphosphine)palladium(II) dichloride (91.0 mg, 0.130 mmol, 5.00 mol%) and boric acid (802 mg, 13.0 mmol, 5.00 equiv.). The solid were dissolved in THF (2,590 mL) and the mixture was stirred vigorously for 10 min. Potassium fluoride (151 mg, 2.59 mmol, 1.00 equiv.) was dissolved in water (260 mL) and added immediately to the reaction. The reaction was stirred at room temperature open to the atmosphere for 2 hours. The THF was removed under vacuum and the resulting solution was extracted with dichloromethane (3 x 100 mL). The combined organic layers were washed with deionized water (3 x 100 mL) and brine (1 x 100 mL) then dried over sodium sulfate and concentrated to give a brown oil. The crude reaction mixture was purified via column chromatography (100% dichloromethane) to give the desired product **IV.23** as a white crystalline solid (416 mg, 50%).

mp 145-146 °C. ¹H NMR (600 MHz, CDCl₃): δ 7.08 (dd, J = 8.3 Hz, 2.3 Hz, 1H), 7.07 (dd, J = 8.4 Hz, 2.3 Hz, 1H), 6.84 (d, J = 8.4, 1H), 6.84 (d, J = 8.3 Hz, 1H), 6.74 (d, J = 2.4 Hz, 1H), 6.60 (d, J = 2.5 Hz, 1H), 3.85 (s, 3H), 1.57 (app brs, 1H), 3.82 (s, 3H), 3.22 (app brs, 1H), 2.91 (app brs, 1H), 2.76 (app brs, 2H), 2.67 (t, J = 5.8 2H), 2.60 (app brs, 2H), 1.90 (app brs, 1H), 1.78 (app brs, 2H); ¹³C NMR (150 MHz, CDCl₃): δ 213.94, 155.50, 155.05, 134.97, 134.57, 132.72, 131.68, 129.55, 129.41, 128.54, 128.30, 111.88, 111.55, 56.26, 56.21, 47.27, 42.87, 31.96, 29.93, 25.67, 21.00; HRMS (TOF, ES⁺) (m/z): [M+Na]⁺ calculated for C₂₁H₂₄O₃, 347.1623; found: 347.1616. IR (neat): 3366, 3052, 2998, 2923, 2891, 2837, 2828, 1695, 1606, 1605, 1502, 1463, 1460, 1436, 1404 1366, 1350, 1291, 1287, 1249, 1238, 1177, 1166, 1150, 1134, 1083, 1045, 1025, 993, 903, 905, 890, 818, 809, 803, 757, 732, 728, 702, 680, 644, 648, 502, 585, 584 cm⁻¹.



Entry	Catalyst	Base	Oxidant	Conversion*	Yield
1	PdCl ₂ (PPh ₃) ₂ (20 mol%)	KF (4 equiv.)	Air	100	50
2	NiCl ₂ (PPh ₃) ₂ (20 mol%)	KF (4 equiv.)	Air	10	0
3	PtCl ₂ (PPh ₃) ₂ (20 mol%)	KF (4 equiv.)	Air	20	0
4	Pd(dppf)Cl ₂ (20 mol%)	KF (4 equiv.)	Air	100	40
5	Pd(dppp)Cl ₂ (20 mol%)	KF (4 equiv.)	Air	100	30
6	Pd(PEPPSI)(SiP) (20 mol%)	KF (4 equiv.)	Air	60	25
7	Pd(OAc) ₂ (20 mol%)	KF (4 equiv.)	Air	40	20
8	PdCl ₂ (PPh ₃) ₂ (20 mol%)	KF (4 equiv.)	Benzoquinone	100	0
9	PdCl ₂ (PPh ₃) ₂ (20 mol%)	KF (4 equiv.)	Cu(II)Cl	90	0
10	PdCl ₂ (PPh ₃) ₂ (20 mol%)	KF (4 equiv.)	O ₂ (g)	100	0
11	Pd(PPh ₃) ₄ (20 mol%)	NA	Air	100	40
12	Pd(OAc) ₂ (20 mol%)	SPhos (50 mol%)	Air	100	50
13	Pd(dba) ₂ (20 mol%)	NA	Air	100	40
14	Pd(PPh ₃) ₂ O ₂ (20 mol%)	NA	Air	80	42
15	Pd(PPh ₃) ₂ O ₂ (5 mol%)	NA	Air	25	25
16	Pd(PPh ₃) ₂ O ₂ (20 mol%)	NaHCO ₃ (10 equiv.)	Air	100	23
17	PdCl ₂ (PPh ₃) ₂ (5 mol%)	KF (1 equiv.)	Air	100	50
18	PdCl ₂ (PPh ₃) ₂ (100 mol%)	KF (20 equiv.)	Air	100	95

General Homocoupling Entries 1-10

Diboronate ester **IV.1** (50.0 mg, 0.0659 mmol, 1.00 equiv.) and catalyst (20.0 mol%) were dissolved in THF (60.0 mL). Potassium fluoride (15.3 mg, 0.264 mmol, 4.00 equiv.) was dissolved in water (6.00 mL) and added to the organic solution. This was allowed to stir for 12 h at which point the reaction was concentrated and diluted with water (50.0 mL) and was then extracted with DCM (3 x 20.0 mL). The organics were washed with water (3 x 50.0 mL) and brine (50.0 mL) and was then dried over sodium sulfate. The reaction was concentrated and dissolved in chloroform (3.00 mL) and was purified using gel

permeation chromatography (GPC). Conversion was based on recovered starting material and yields were based on isolated product.

General Homocoupling Entries **11-13**

Diboronic ester **IV.1** (50.0 mg, 0.0659 mmol, 1.00 equiv.) and catalyst (20.0 mol%)* were dissolved in THF (60.0 mL). Water (6.00 mL) and added to the organic solution. This was allowed to stir for 12 h at which point the reaction was concentrated and diluted with water (50.0 mL) and was then extracted with DCM (3 x 20.0 mL). The organics were washed with water (3 x 50.0 mL) and brine (50.0 mL) and was then dried over sodium sulfate. The reaction was concentrated and dissolved in chloroform (3.00 mL) and was purified using gel permeation chromatography (GPC). Conversion was based on recovered starting material and yields were based on isolated product.

**SPhos (50 mol%) was added at this point only for entry 12*

General Homocoupling Entries **14**

Diboronic ester **IV.1** (50.0 mg, 0.0659 mmol, 1.00 equiv.) and palladium peroxide catalyst (20.0 mol%) were dissolved in THF (60.0 mL). Water (6.00 mL) and added to the organic solution, which immediately turned a golden orange. This was allowed to stir for 12 h at which point the reaction was concentrated and diluted with water (50.0 mL) and was then extracted with DCM (3 x 20.0 mL). The organics were washed with water (3 x 50.0 mL) and brine (50.0 mL) and was then dried over sodium sulfate. The reaction was concentrated and dissolved in chloroform (3.00 mL) and was purified using gel permeation chromatography (GPC). Conversion was based on recovered starting material and yields were based on isolated product.

General Homocoupling Entries **15**

Diboronic ester **IV.1** (100 mg, 0.132 mmol, 1.00 equiv.) and palladium catalyst (5.00 mol%) were dissolved in THF (60.0 mL). Water (6.00 mL) and added to the organic solution, which immediately turned a faint golden orange. This was allowed to stir for 12 h at which point the reaction was concentrated and diluted with water (50.0 mL) and was then extracted with DCM (3 x 20.0 mL). The organics were washed with water (3 x 50.0 mL) and brine (50.0 mL) and was then dried over sodium sulfate. The reaction was concentrated and dissolved in chloroform (3.00 mL) and was purified using gel

permeation chromatography (GPC). Conversion was based on recovered starting material and yields were based on isolated product.

General Homocoupling Entries **16**

Diboronic ester **1** (50.0 mg, 0.0659 mmol, 1.00 equiv.) and palladium peroxide catalyst (20.0 mol%) were dissolved in THF (60.0 mL). Sodium bicarbonate (55.4 mg, 0.659 mmol, 10 equiv.) was dissolved in water (6.00 mL) and added to the organic solution. This was allowed to stir for 12 h at which point the reaction was concentrated and diluted with water (50.0 mL) and was then extracted with DCM (3 x 20.0 mL). The organics were washed with water (3 x 50.0 mL) and brine (50.0 mL) and was then dried over sodium sulfate. The reaction was concentrated and dissolved in chloroform (3.00 mL) and was purified using gel permeation chromatography (GPC). Conversion was based on recovered starting material and yields were based on isolated product.

General Homocoupling Entries **17**

Diboronic ester **IV.1** (50.0 mg, 0.0659 mmol, 1.00 equiv.) and catalyst (5.00 mol%) were dissolved in THF (60.0 mL). Potassium fluoride (3.83 mg, 0.0660 mmol, 1.00 equiv.) was dissolved in water (6.00 mL) and added to the organic solution. This was allowed to stir for 12 h at which point the reaction was concentrated and diluted with water (50.0 mL) and was then extracted with DCM (3 x 20.0 mL). The organics were washed with water (3 x 50.0 mL) and brine (50.0 mL) and was then dried over sodium sulfate. The reaction was concentrated and dissolved in chloroform (3.00 mL) and was purified using gel permeation chromatography (GPC). Conversion was based on recovered starting material and yields were based on isolated product.

General Homocoupling Entries **18**

Diboronic ester **IV.1** (50.0 mg, 0.0659 mmol, 1.00 equiv.) and bis(triphenylphosphinepalladium(II) dichloride (92.5 mg, 0.0659 mmol, 1 equiv.) were dissolved in THF (900 mL). Potassium fluoride (153 mg, 2.64 mmol, 20.00 equiv.) was dissolved in water (100 mL) and added to the organic solution. This was allowed to stir for 12 h at which point the reaction was concentrated and diluted with water (50.0 mL) and was then extracted with DCM (3 x 50.0 mL). The organics were washed with water (3 x 50.0 mL) and brine (50.0 mL) and was then dried over sodium sulfate. The reaction was concentrated and dissolved in chloroform (3.00 mL) and was purified using gel

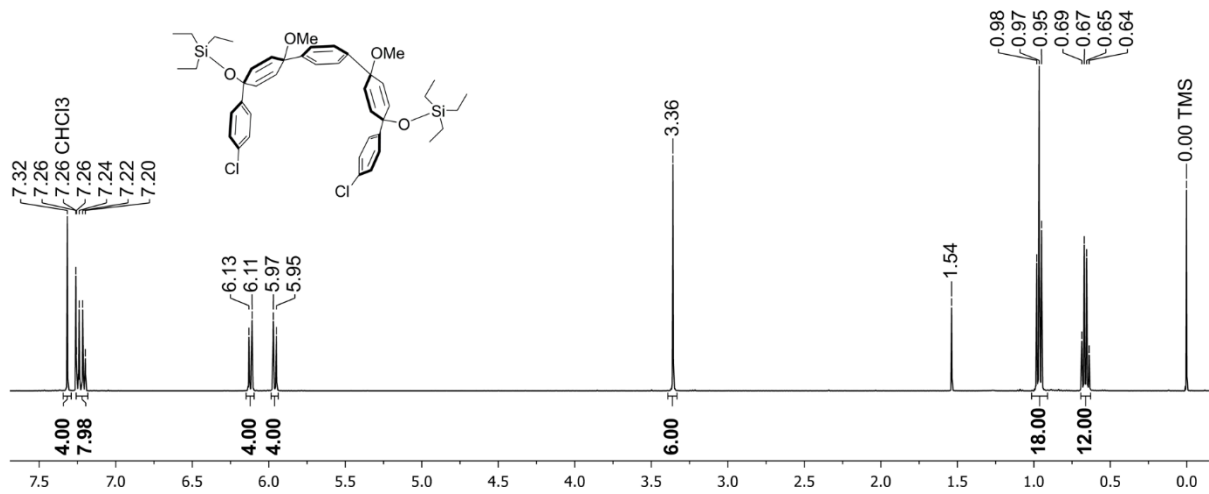
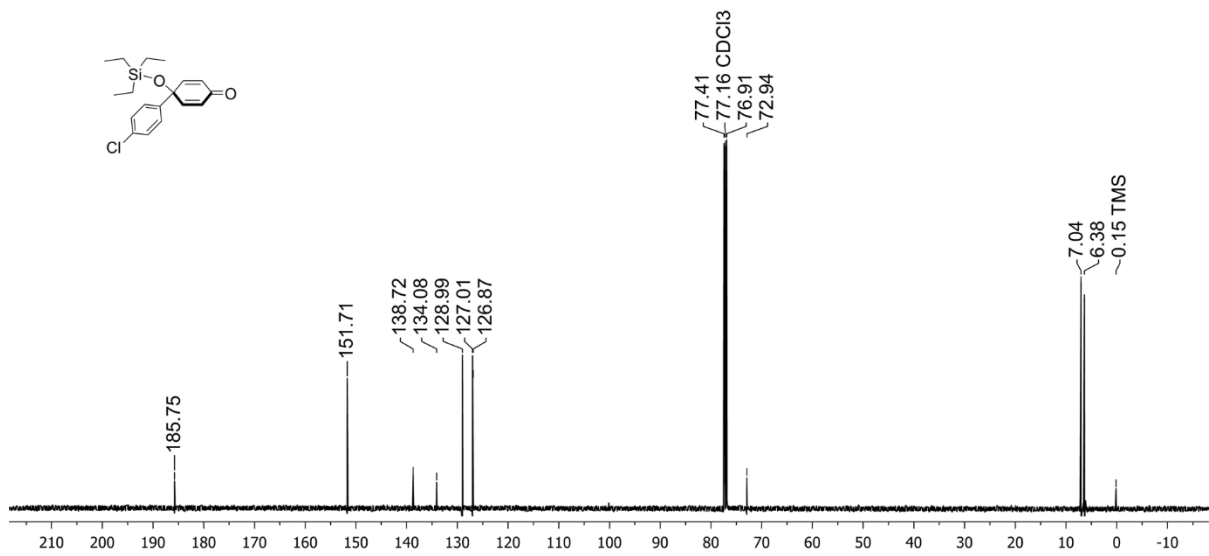
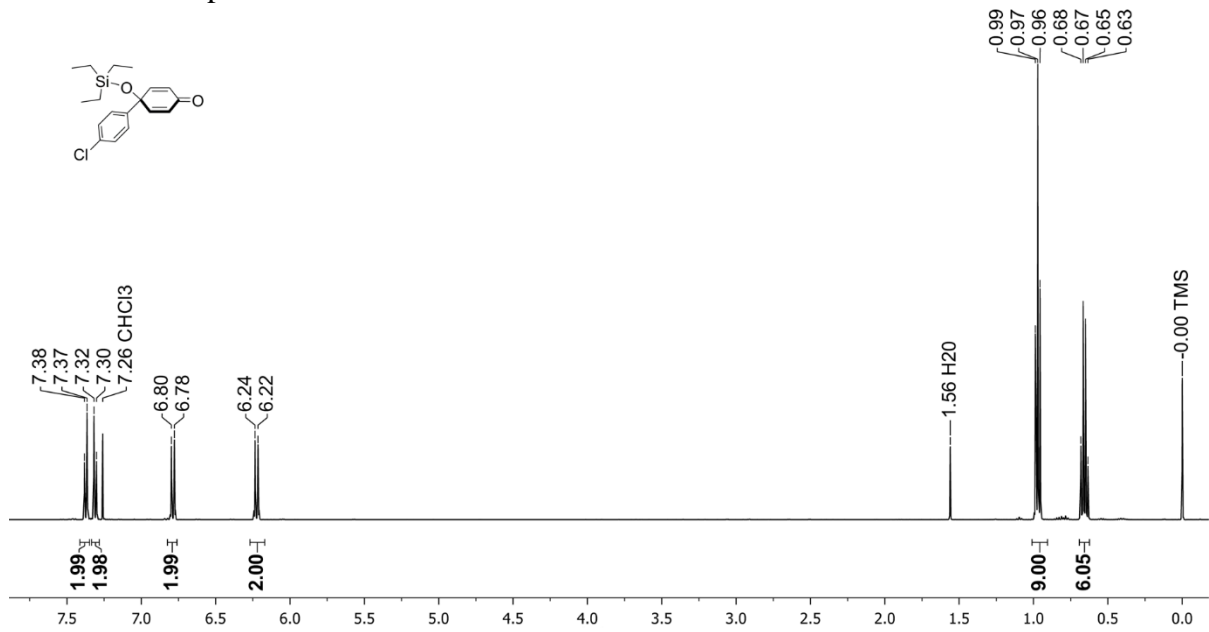
permeation chromatography (GPC). Conversion was based on recovered starting material and yields were based on isolated product. **Reaction concentration and fluoride equivalency are held constant relative to the catalyst and substrate ratio.*

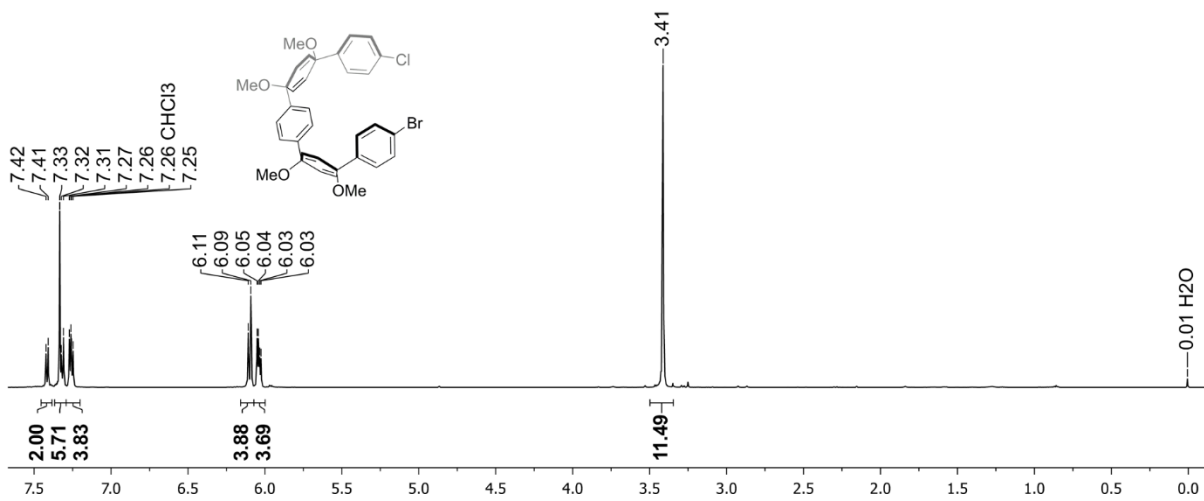
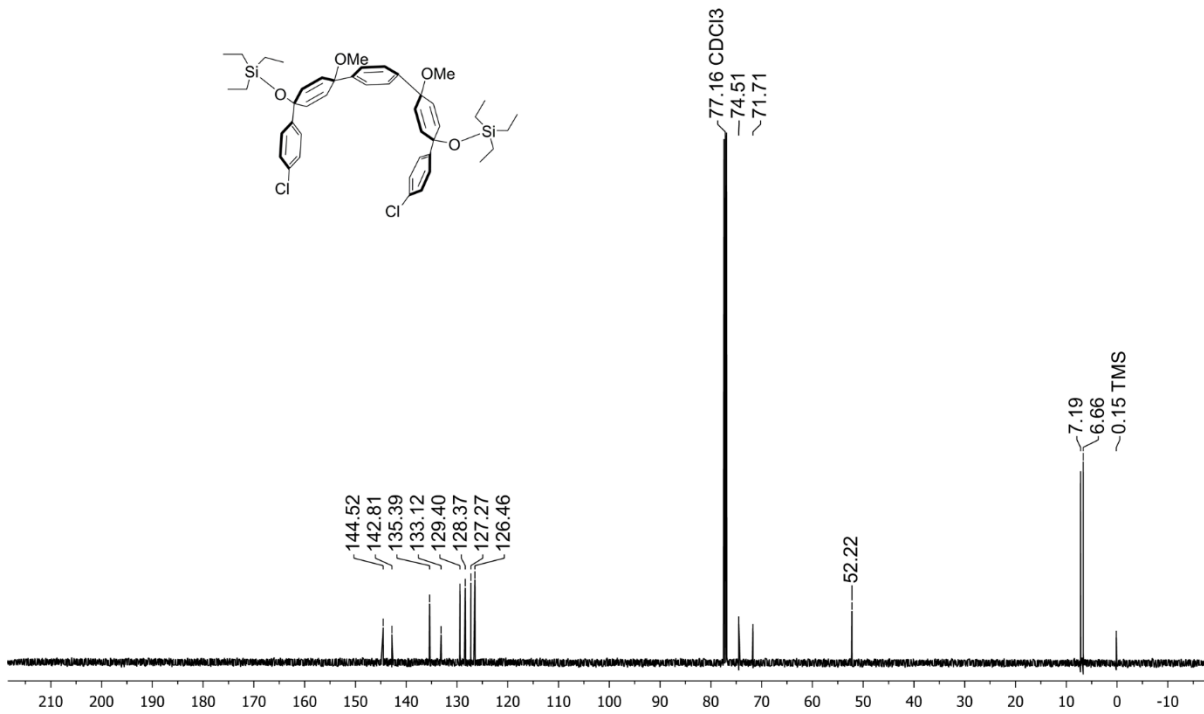
IV.4.2. NMR Experiments.

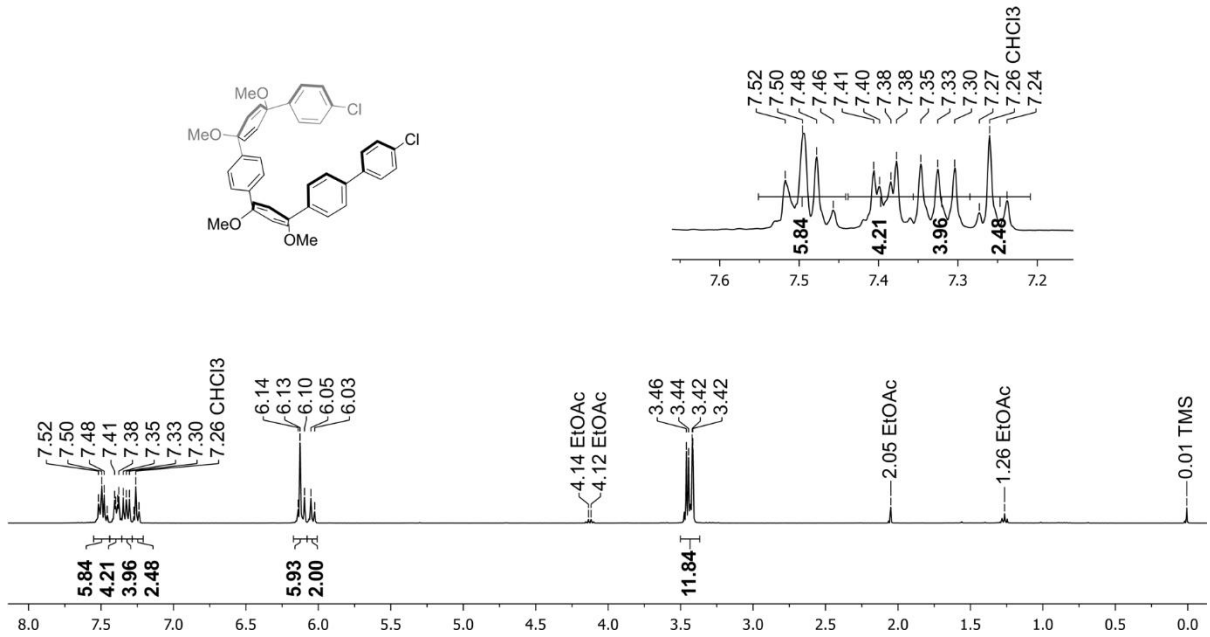
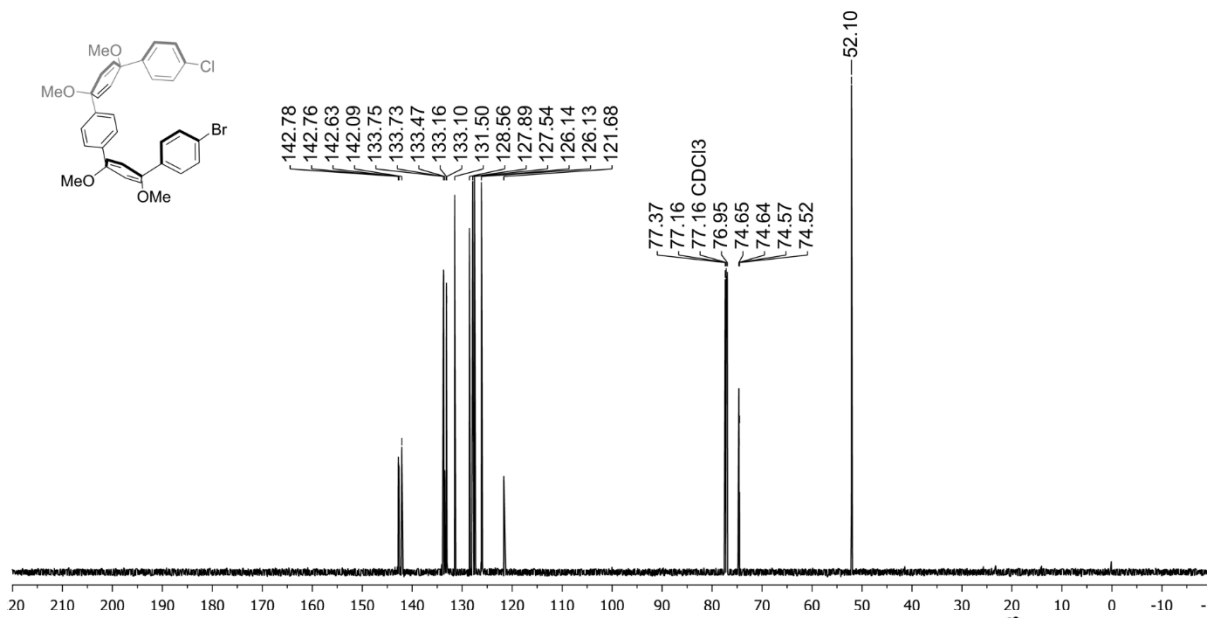
Diboronic ester **IV.1** (5.00 mg, 0.00659 mmol, 1 equiv.) and bis(triphenylphosphine)palladium(II) dichloride (0.925 mg, 0.00132 mmol, 20 mol%) were dissolved in d_8 THF (1.00 mL). 0.100 mL of this stock solution was dissolved in an additional 0.5 mL of d_8 THF. A baseline spectra of this solution was taken as T_0 prior to fluoride activation. Potassium fluoride (153 mg, 2.64 mmol, 40 equiv.) was dissolved in D_2O (1.00 mL). 0.100 mL of this solution was added to the reaction tube and spectra were collected over 12 h.

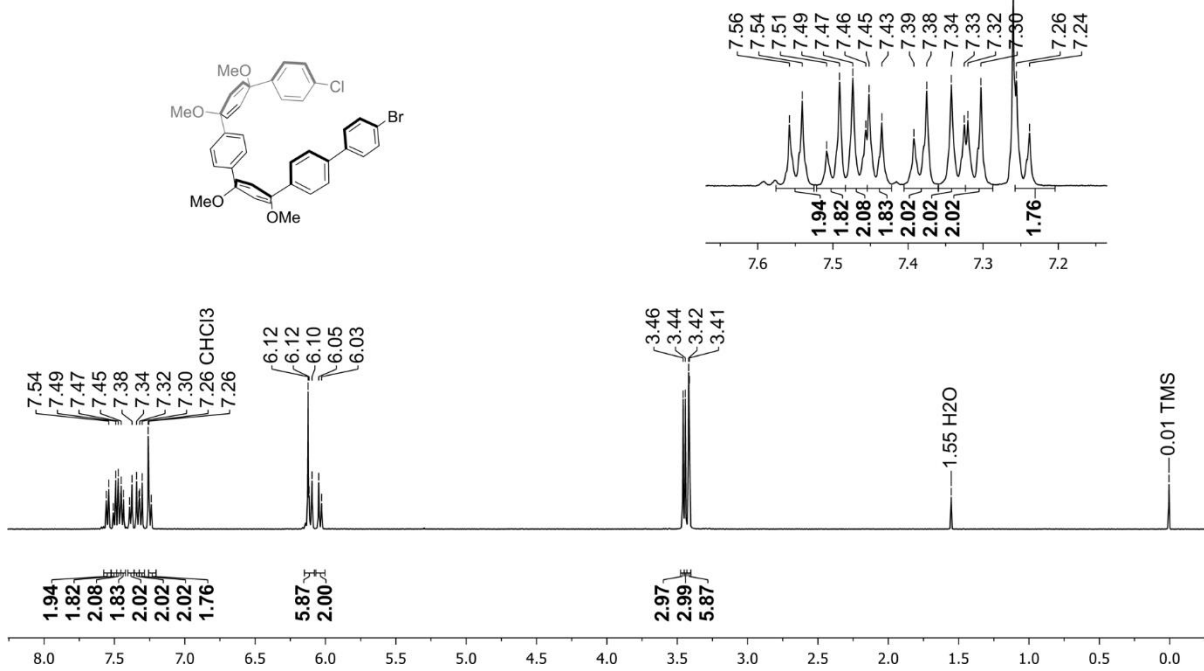
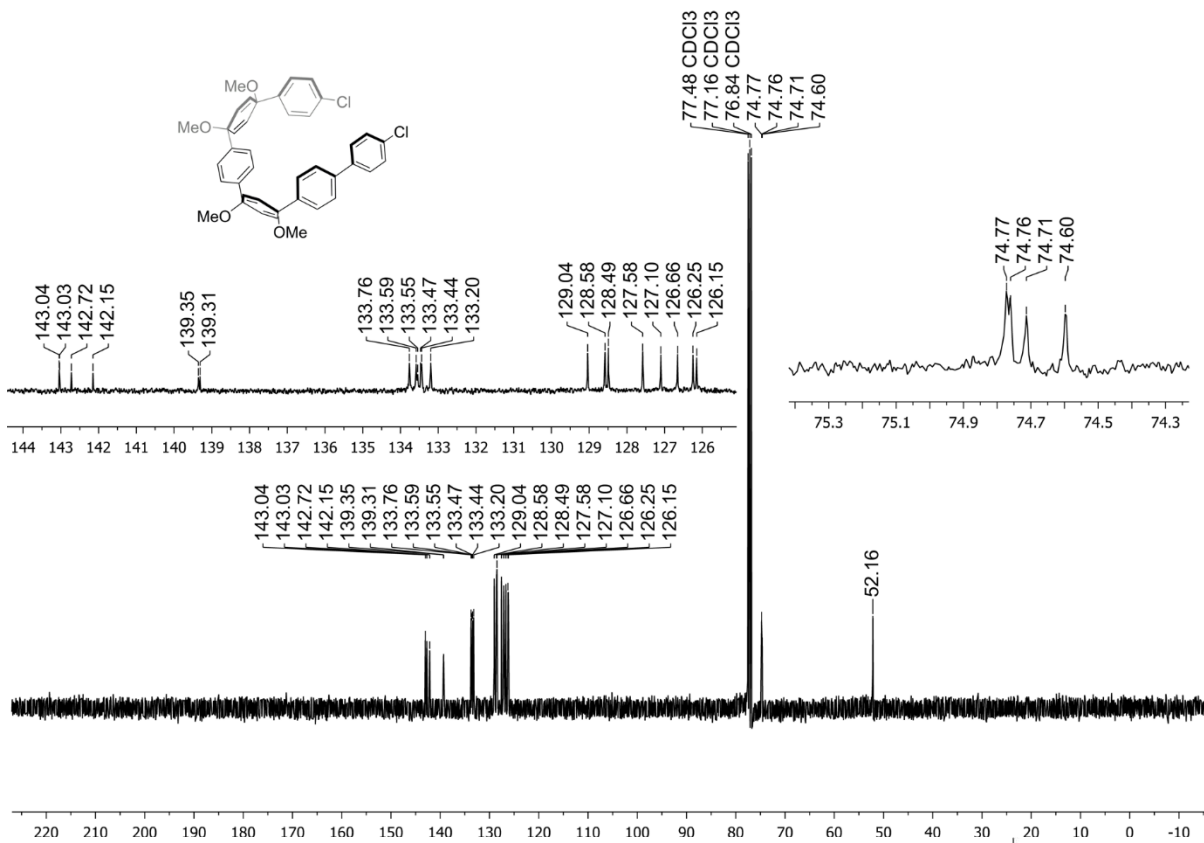
Bis(triphenylphosphine)palladium(II) dichloride (4.50 mg, 0.00640 mmol, 1.00 equiv.) was dissolved in d_8 THF (1.00 mL). A baseline spectra was taken as T_0 prior to fluoride addition. 1.00 M TBAF (0.103 mL, 0.103 mmol, 16.0 equiv.) was injected into the NMR tube and spectra were immediately recorded over 1 h. After all ligated triphenylphosphine appeared to be oxidized, diboronic ester **IV.1** (1.00 mg, 0.00132 mmol, 20 mol%) was added to the tube as a solid. This was allowed to sit at room temperature for 12 h. After 12 h the starting material was qualitatively consumed and product formation was observed.

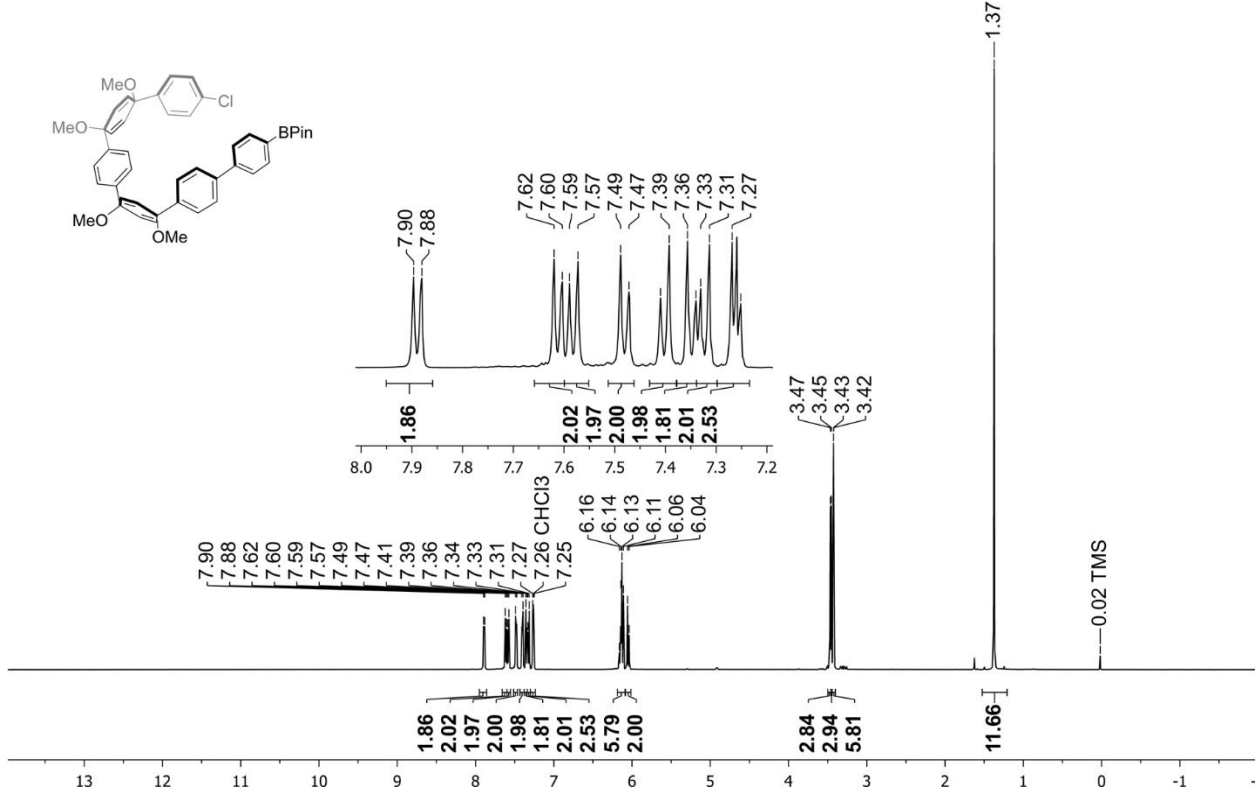
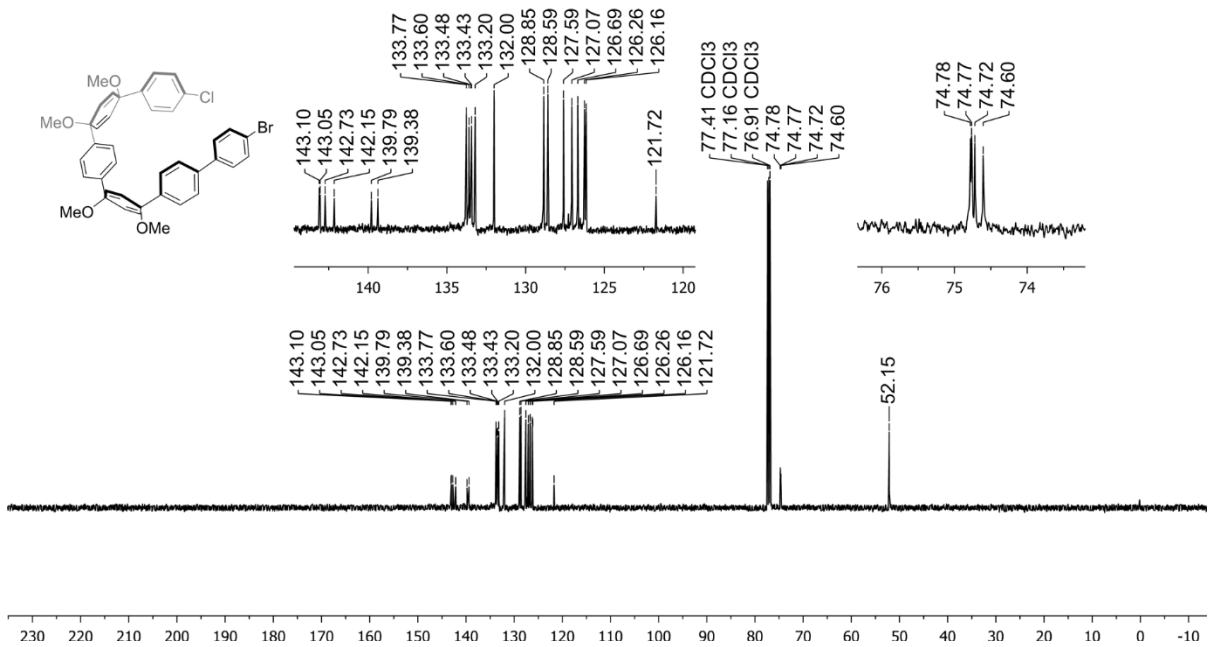
IV.4.3. NMR Spectra.

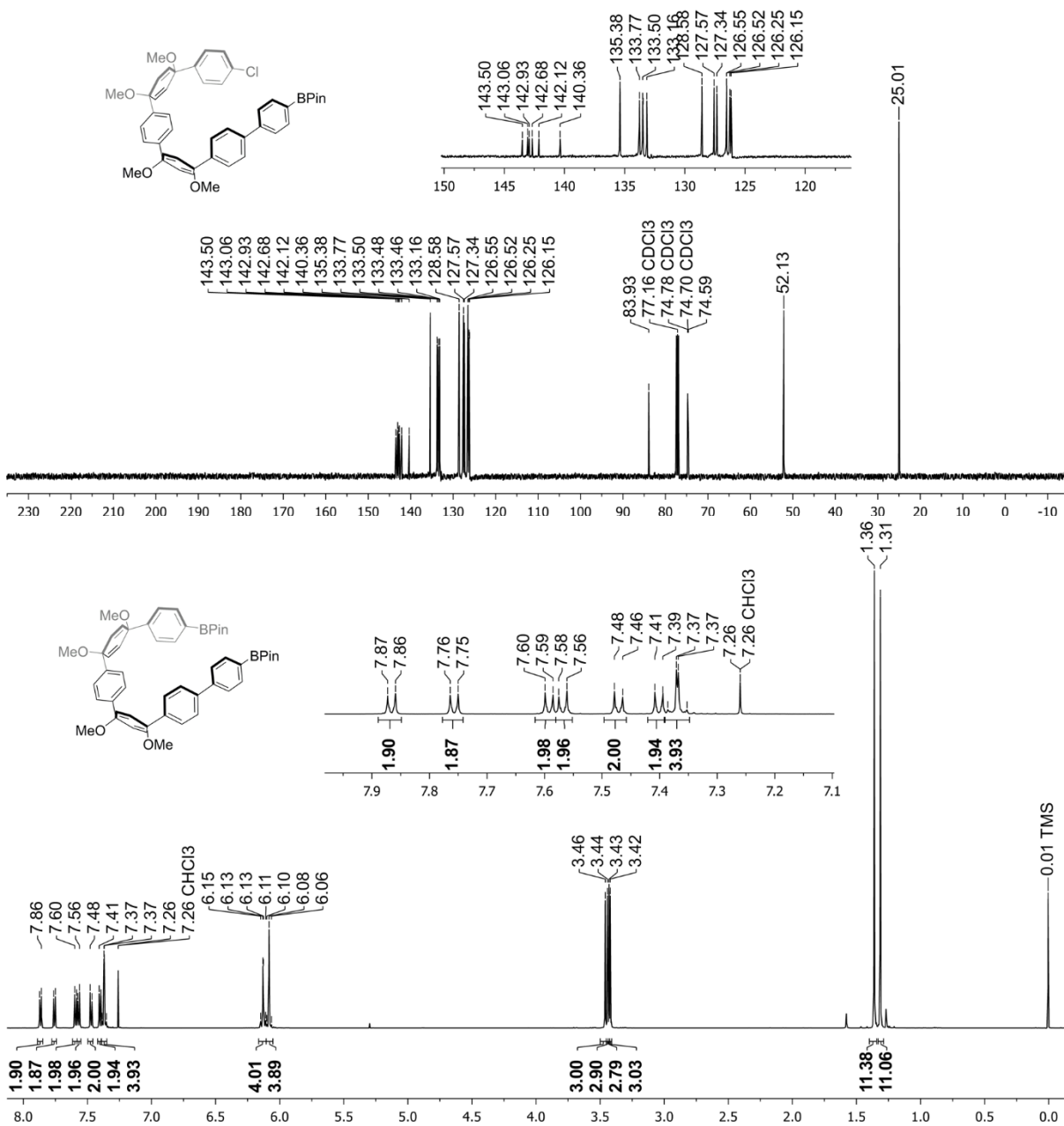


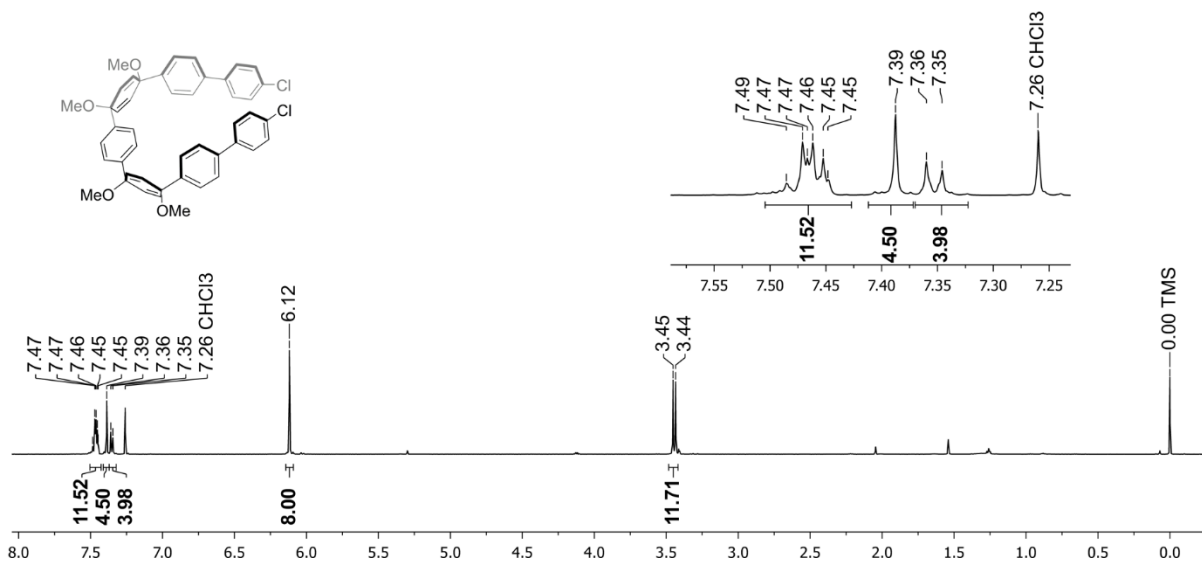
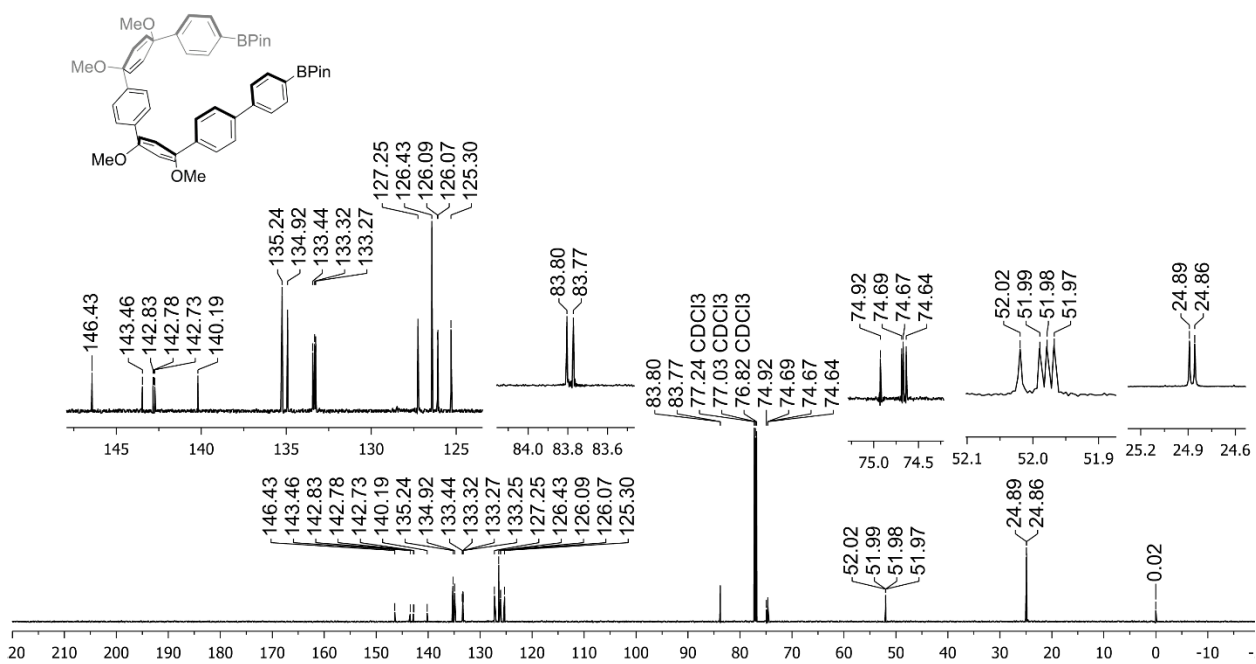


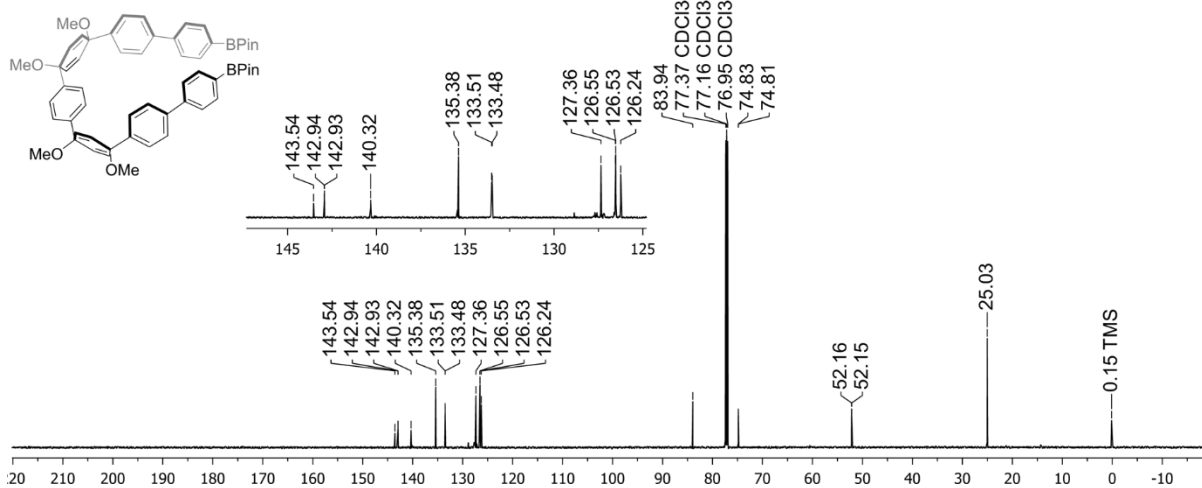
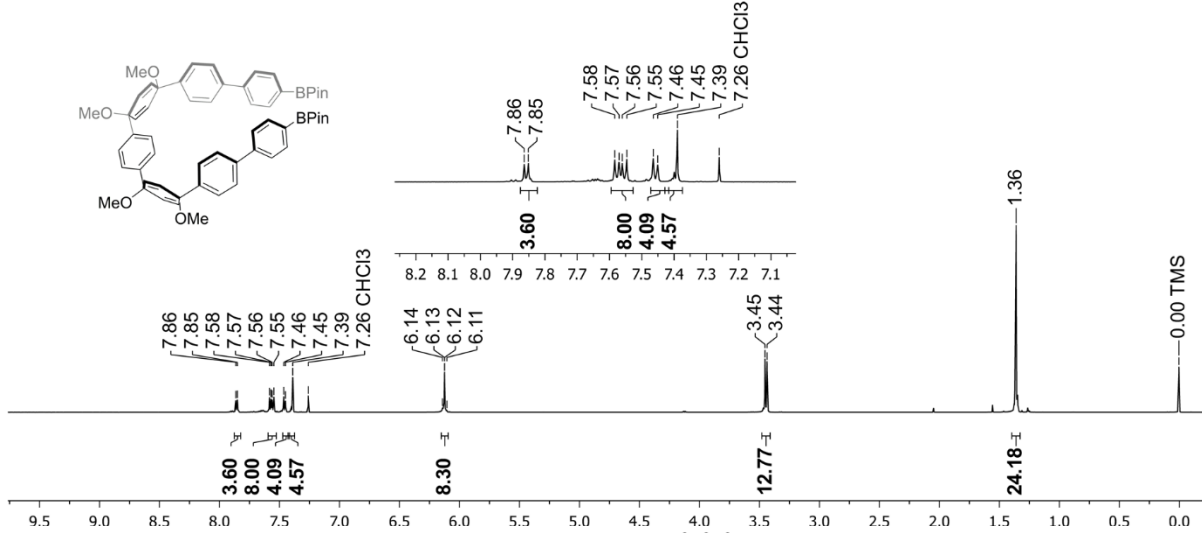
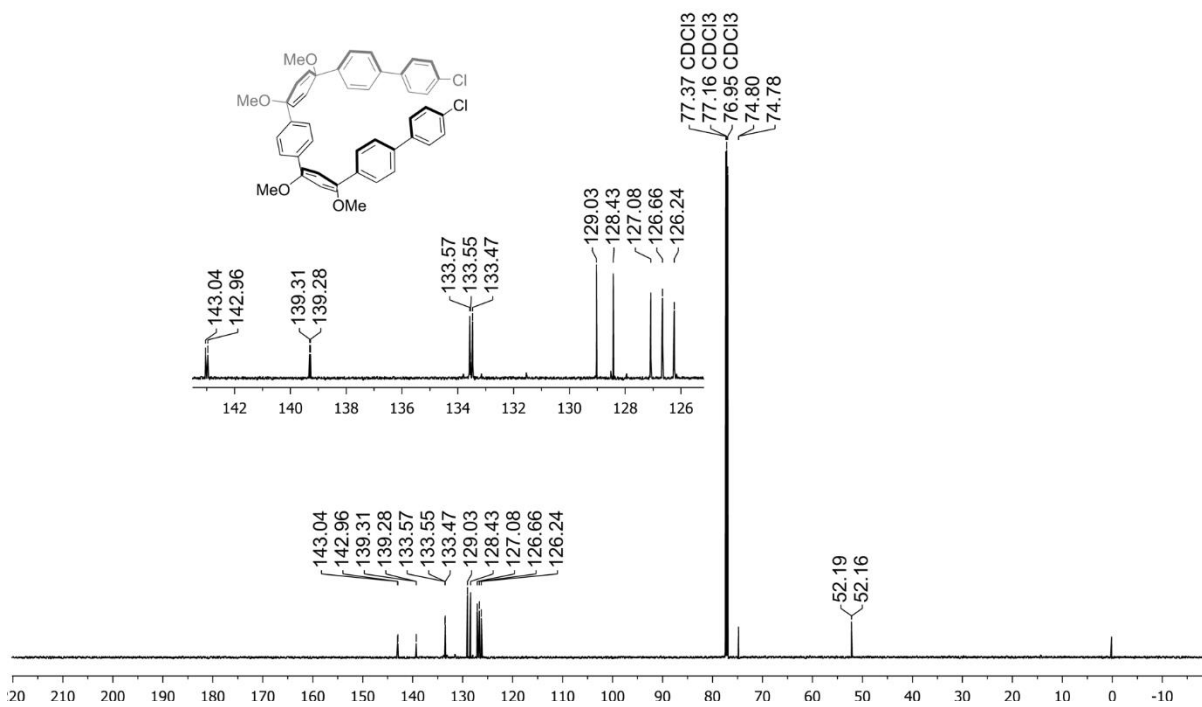


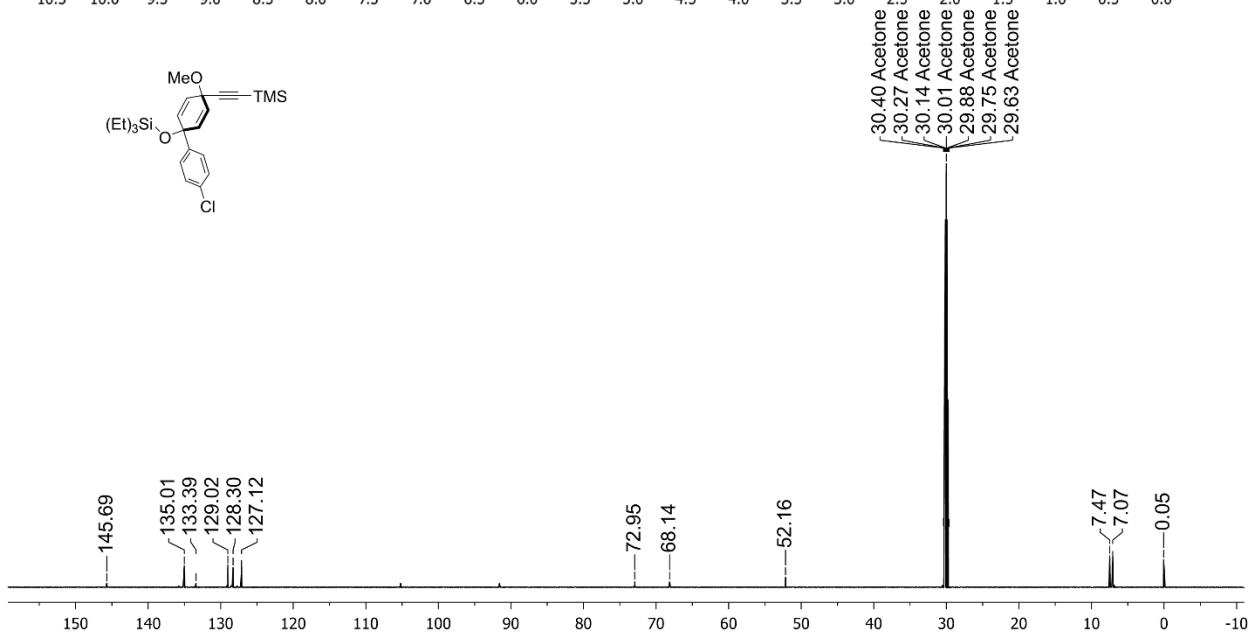
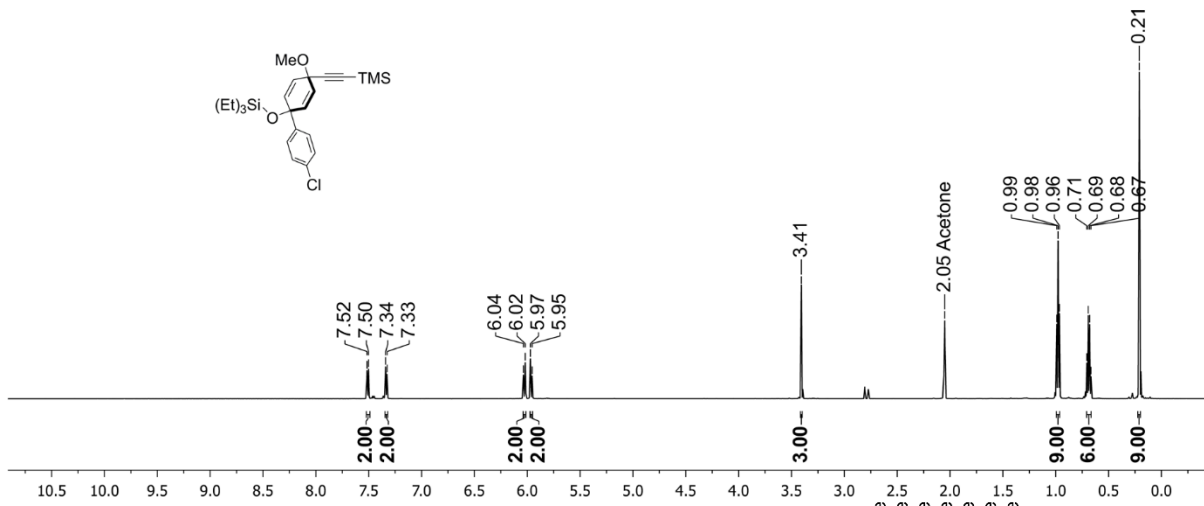


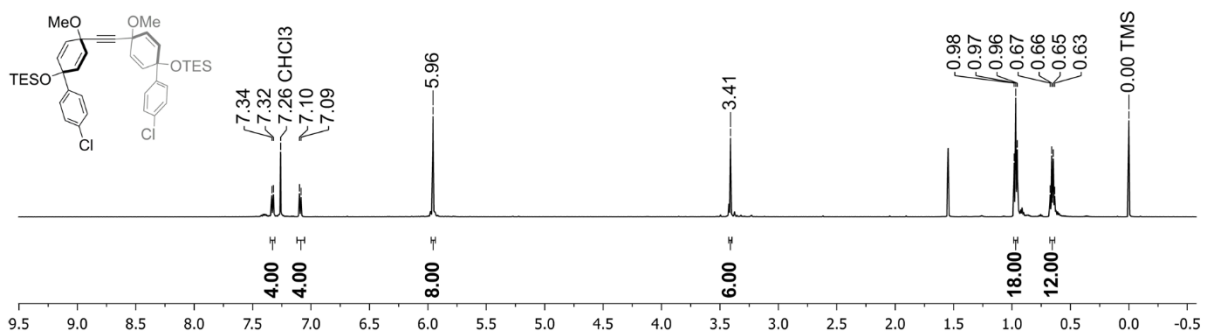
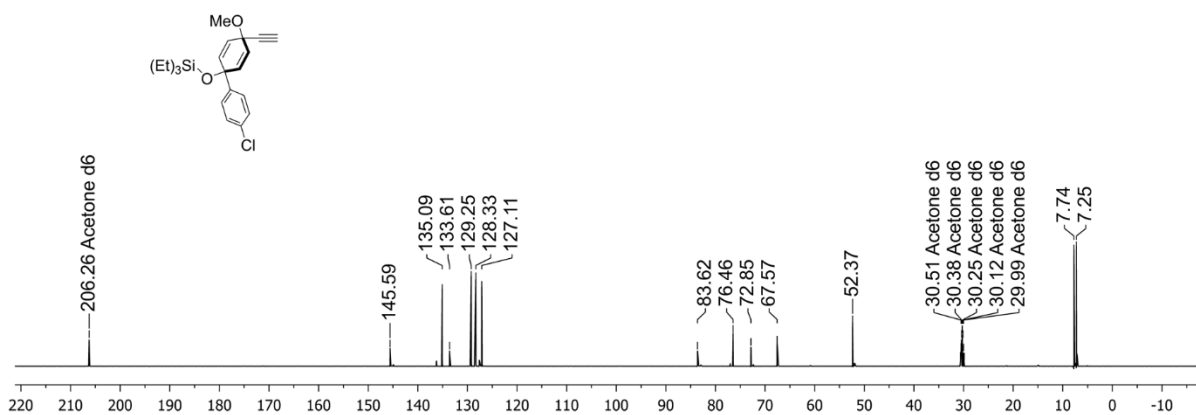
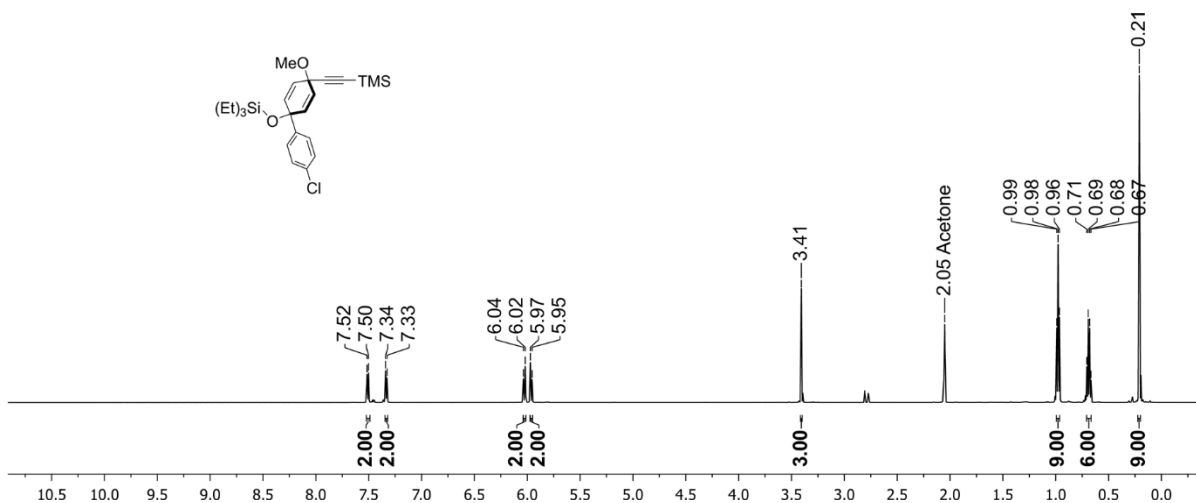


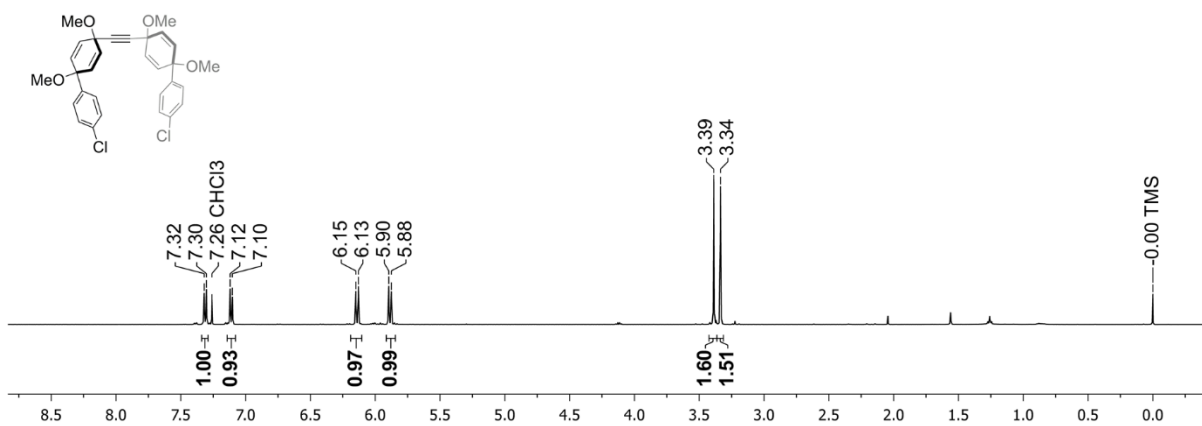
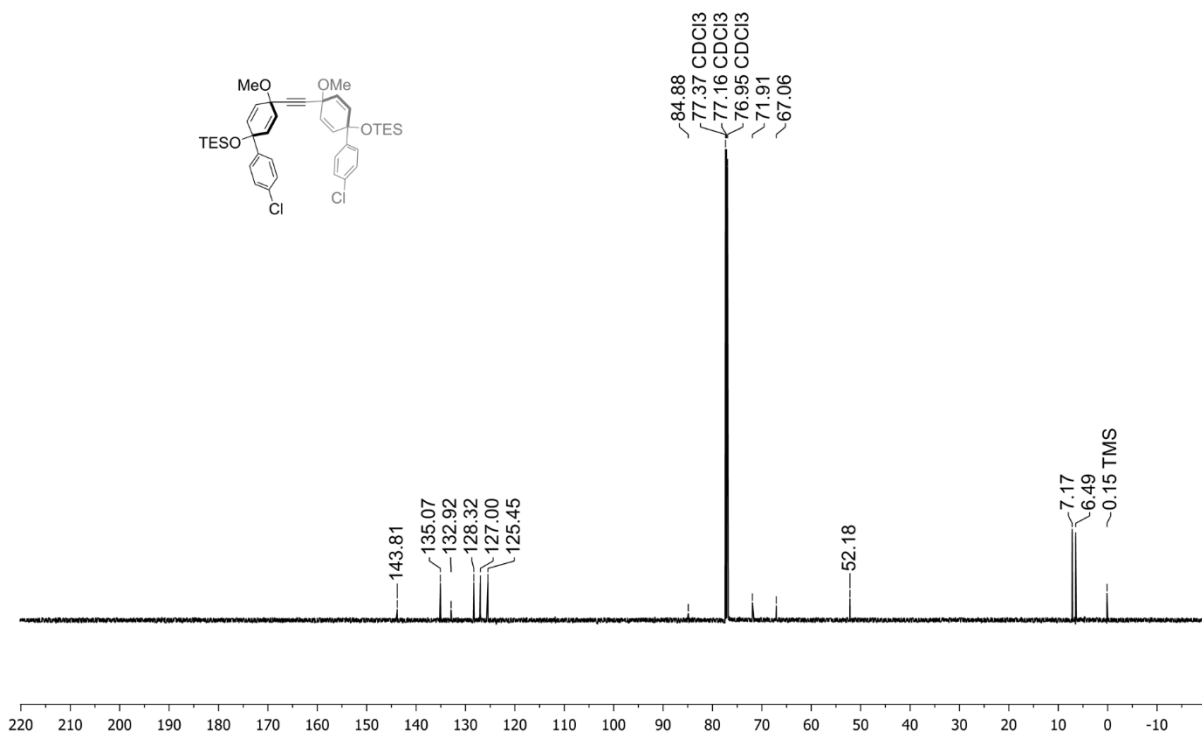


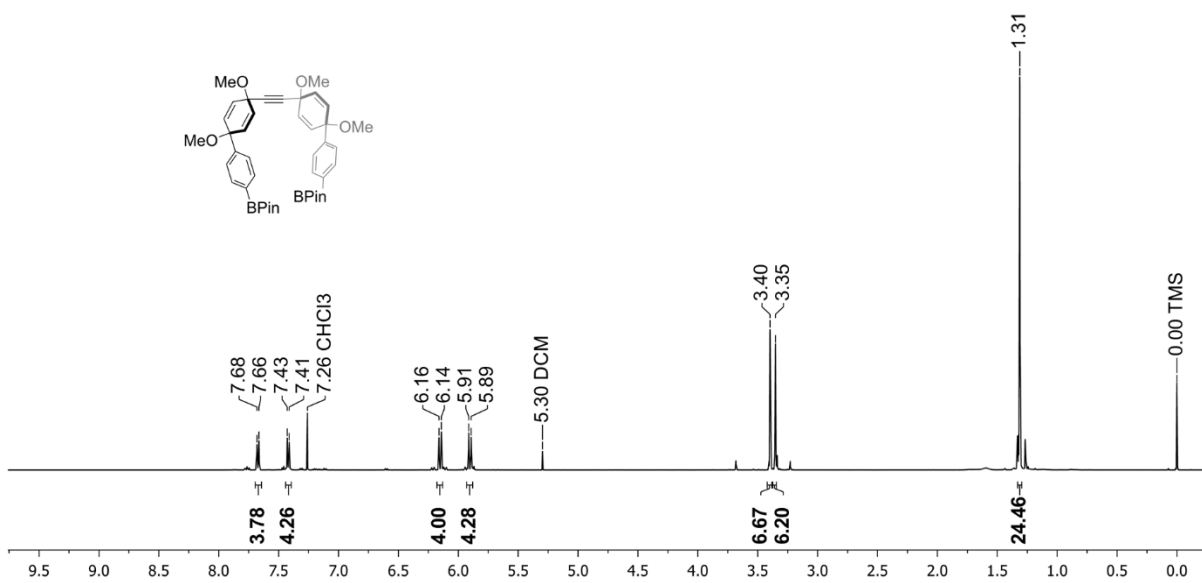
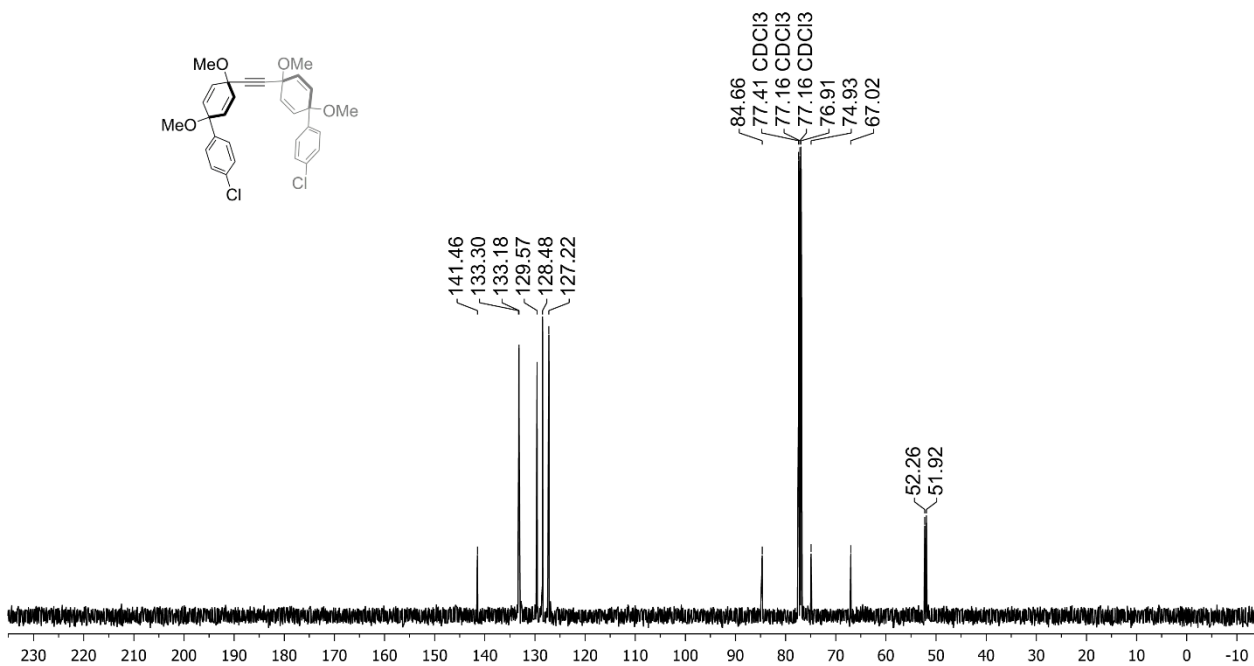


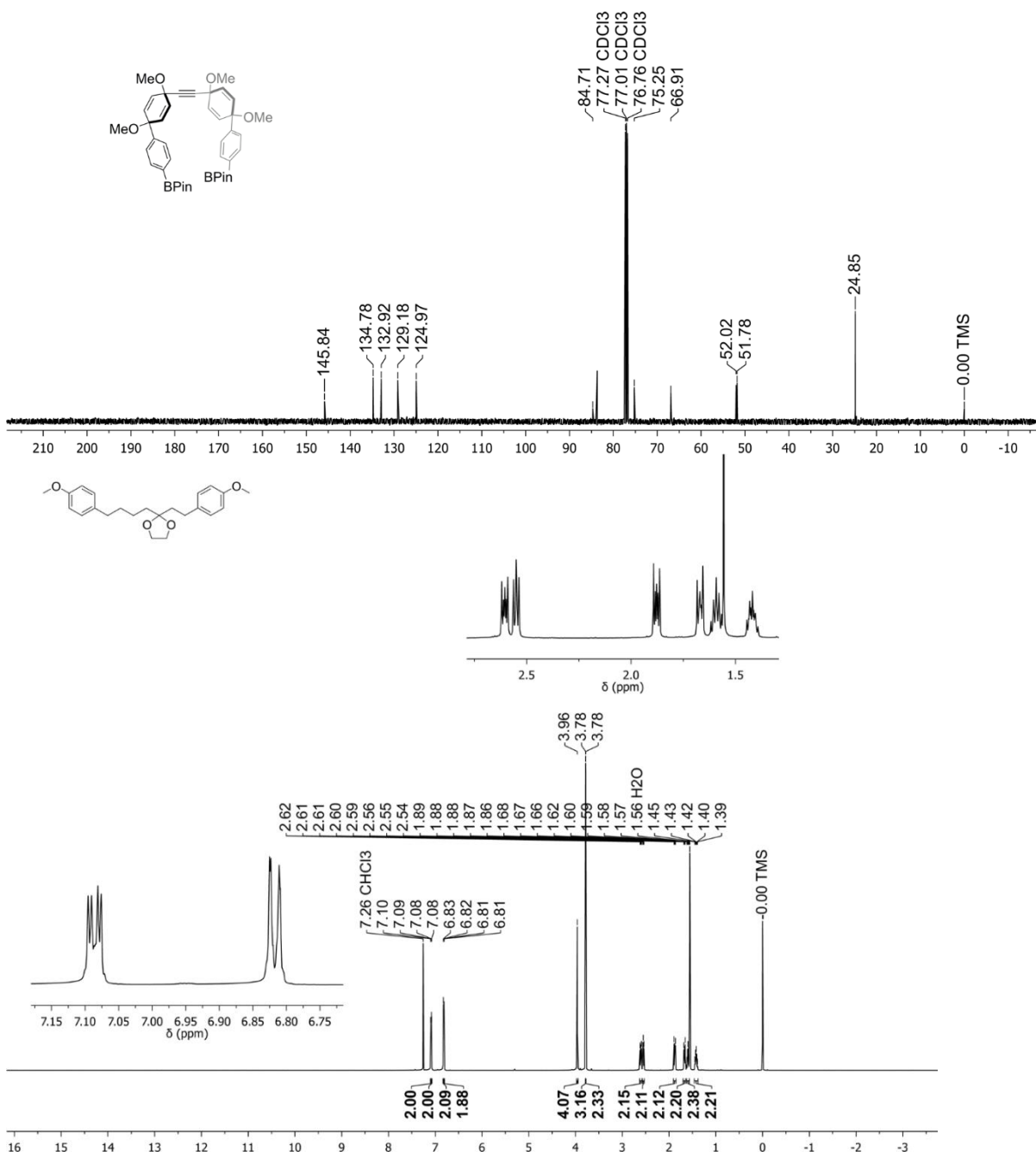


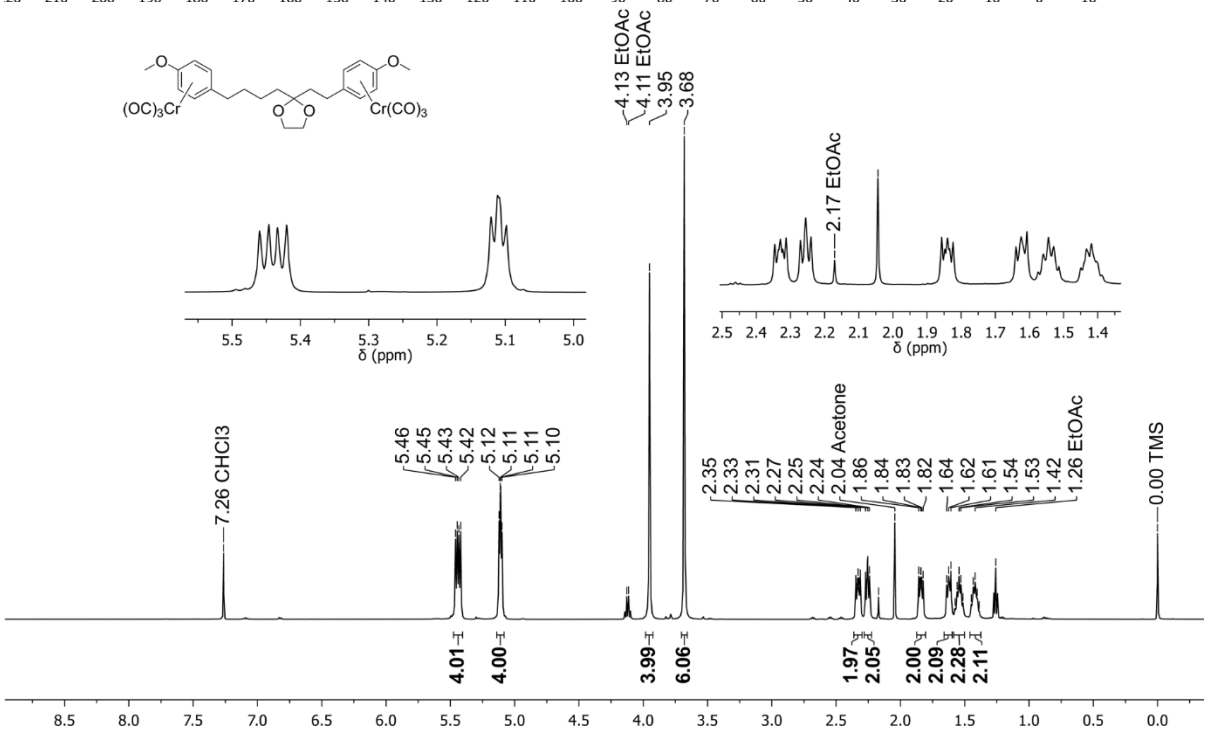
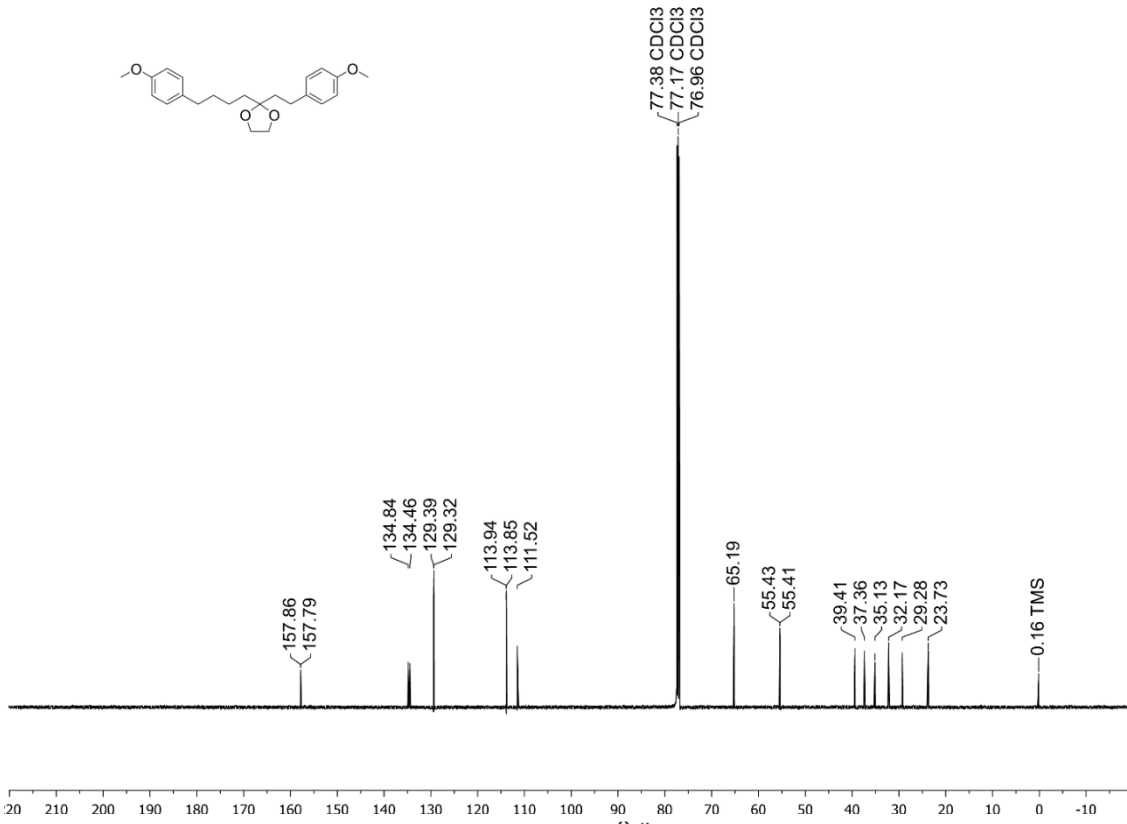


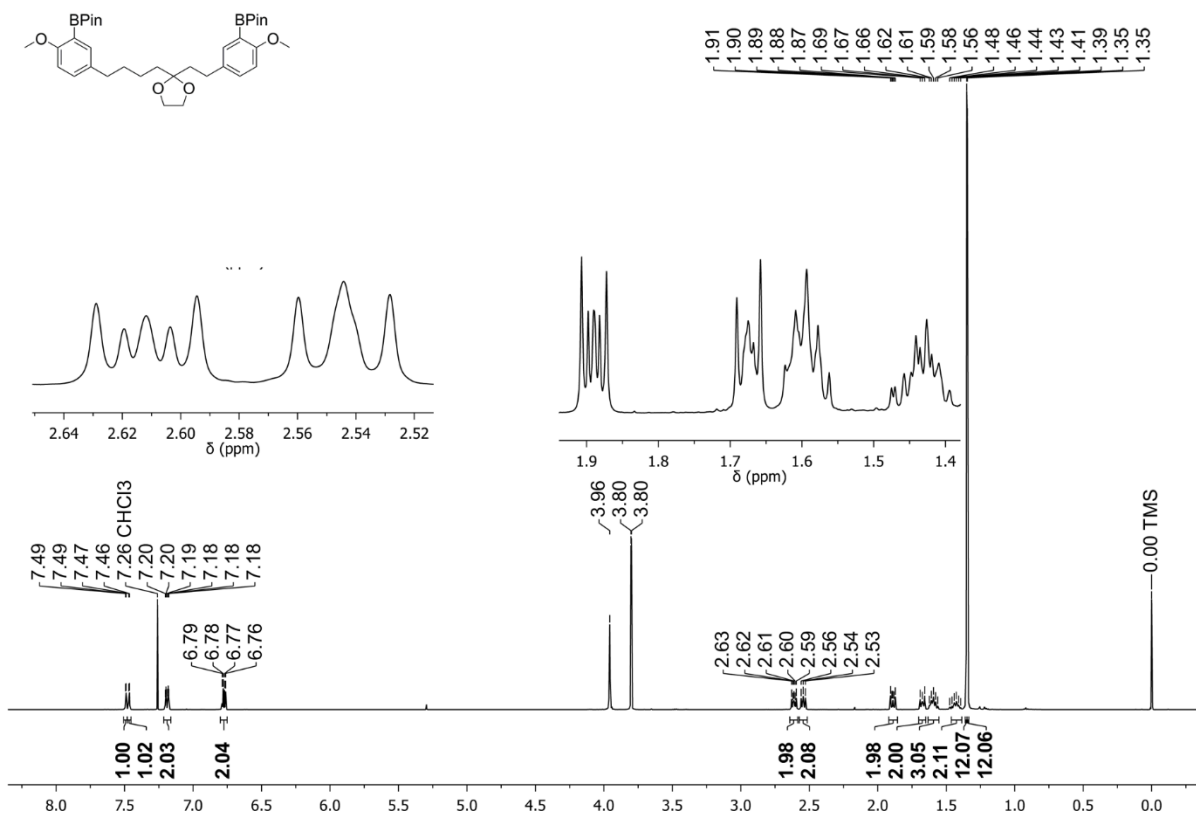
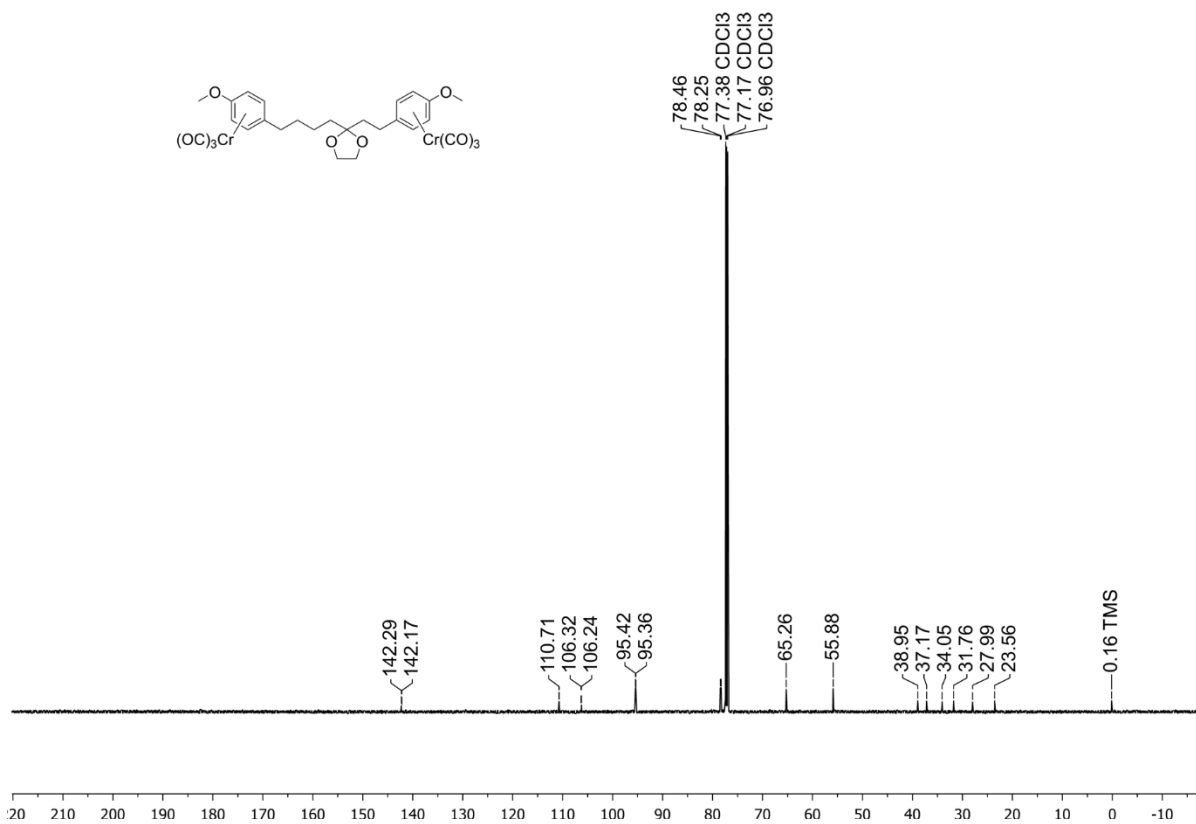


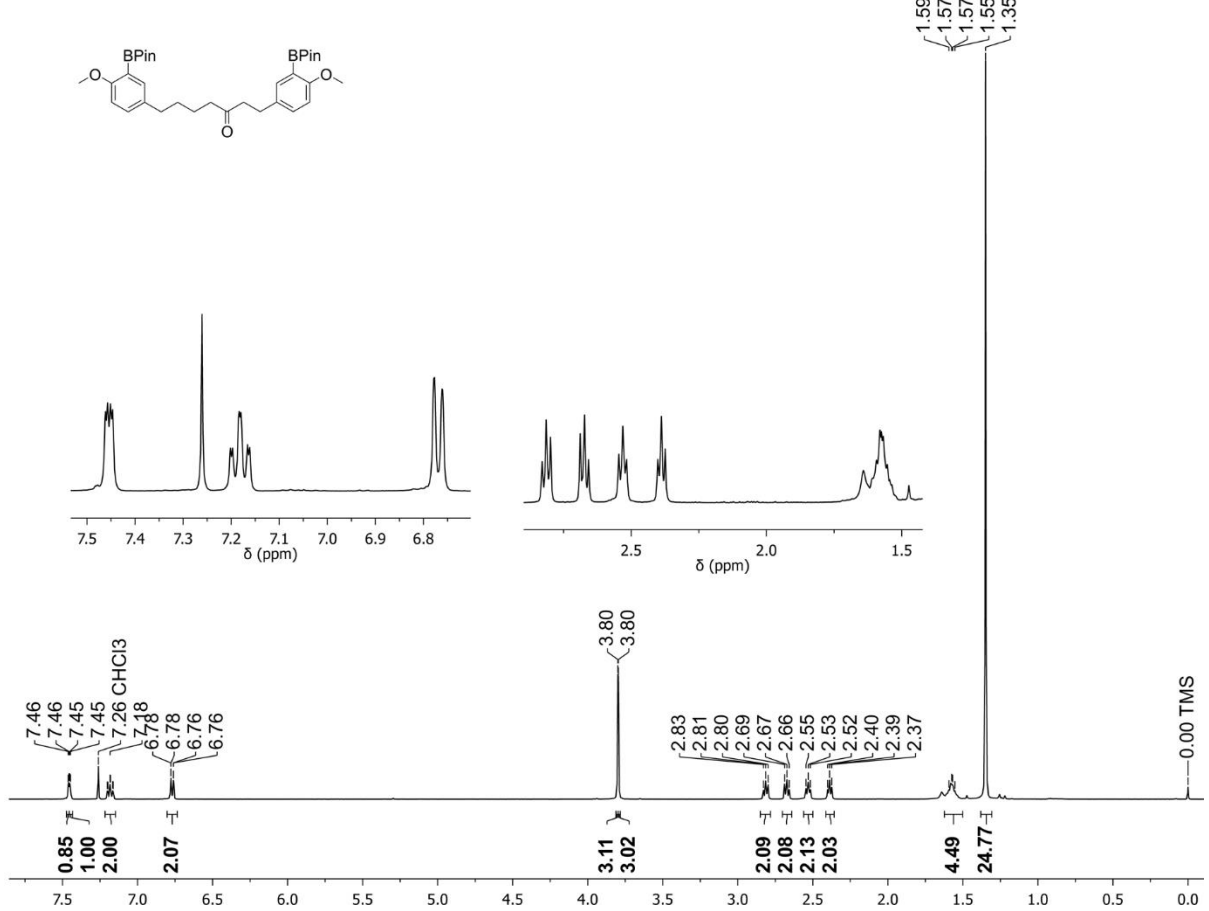
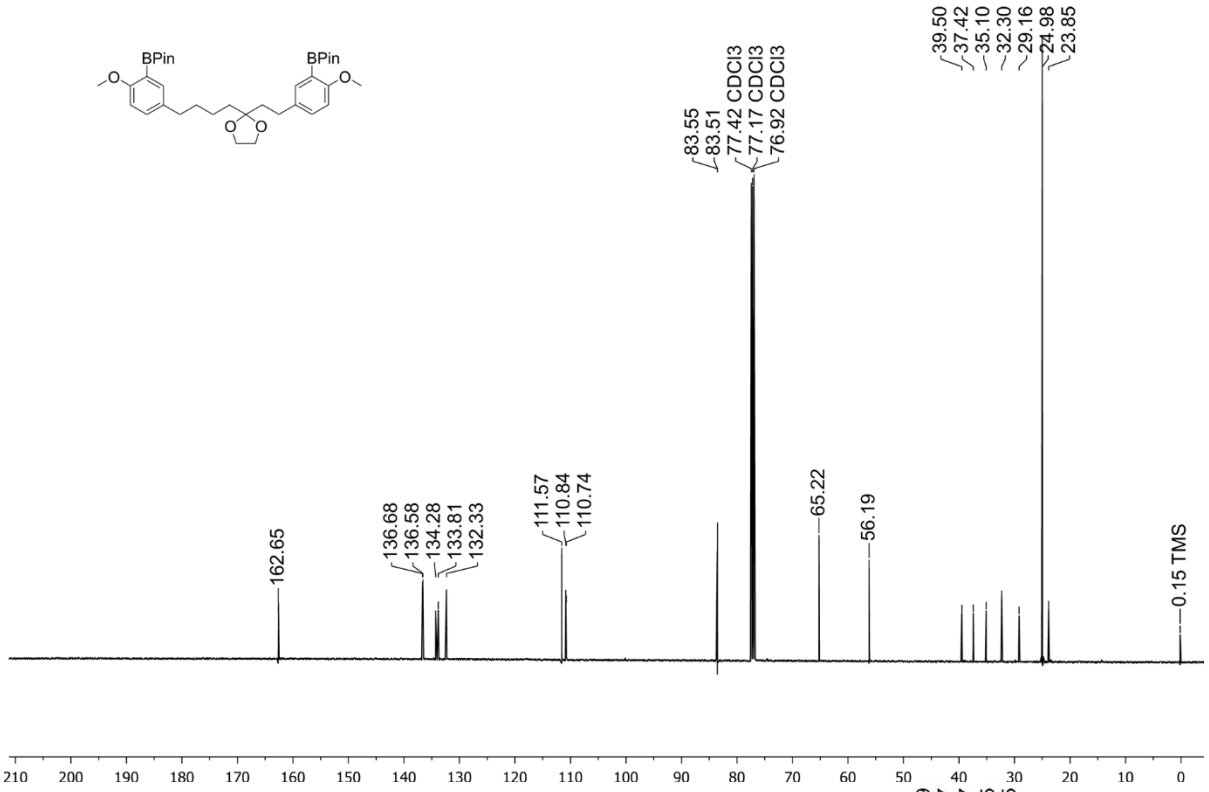


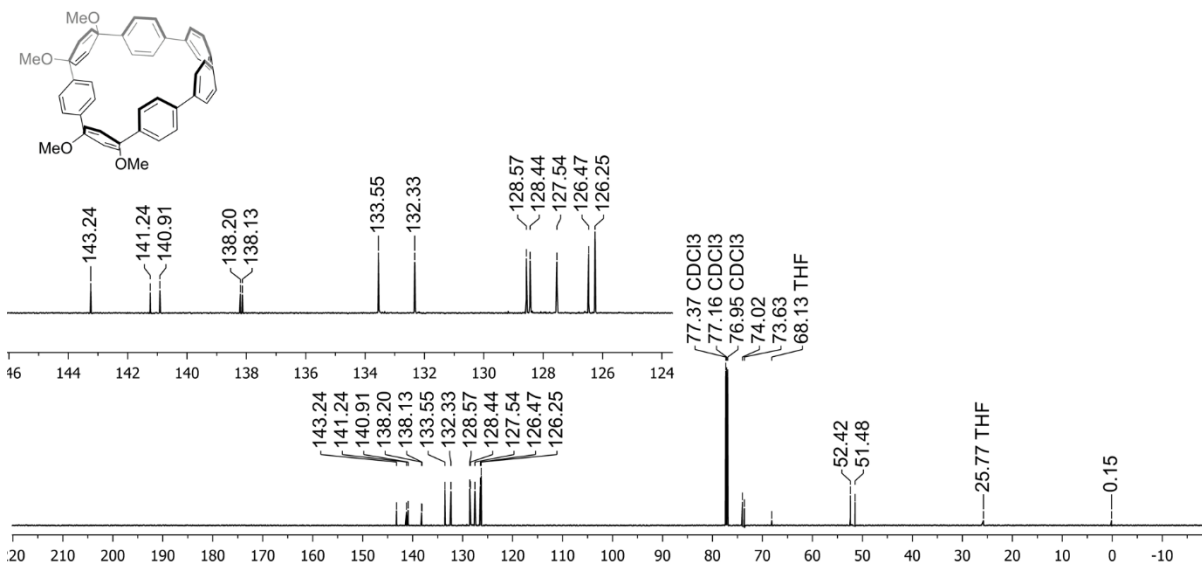
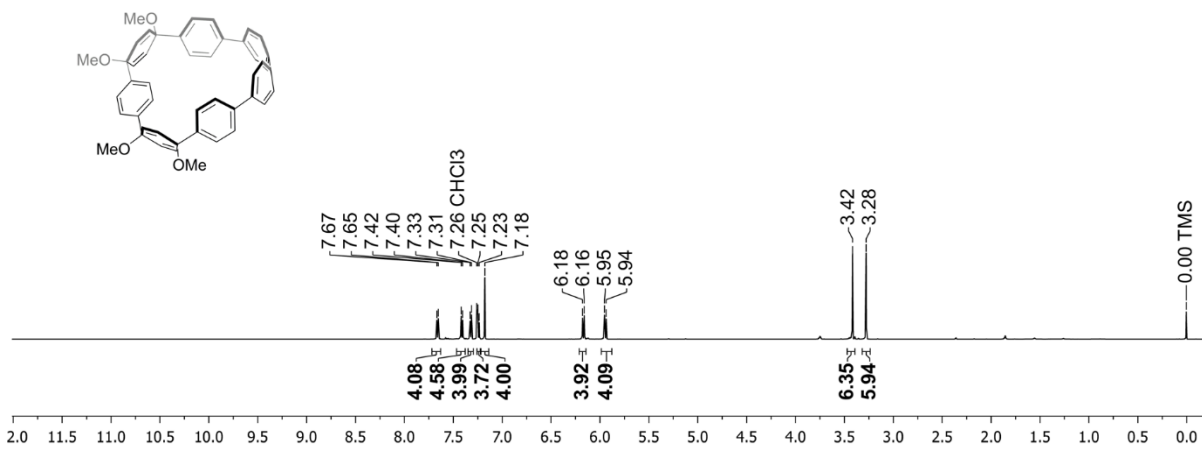
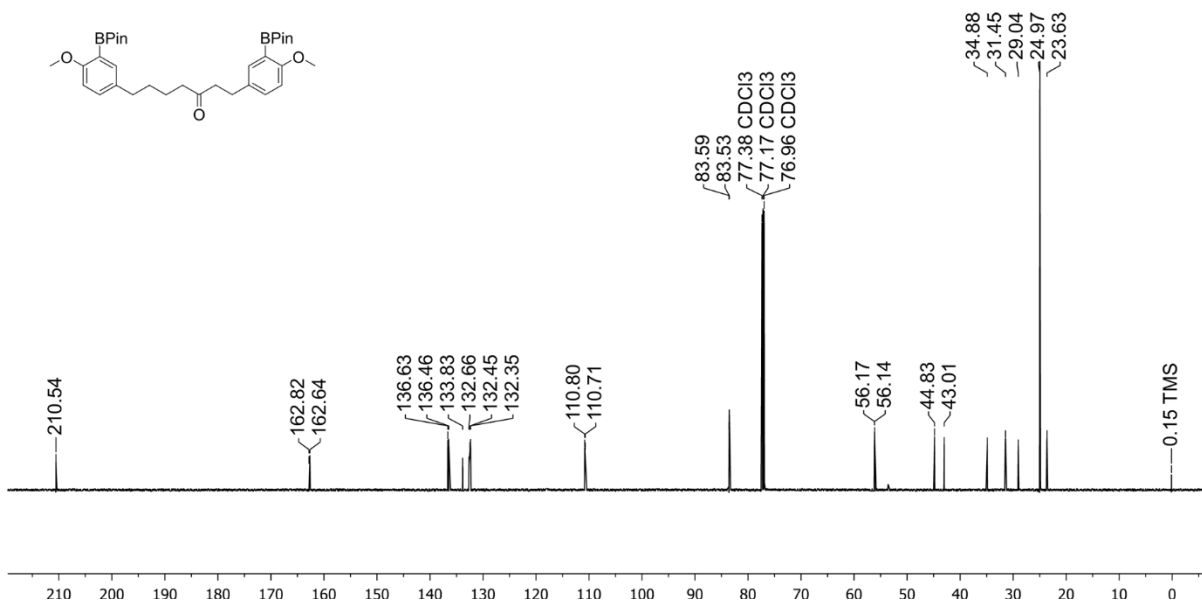


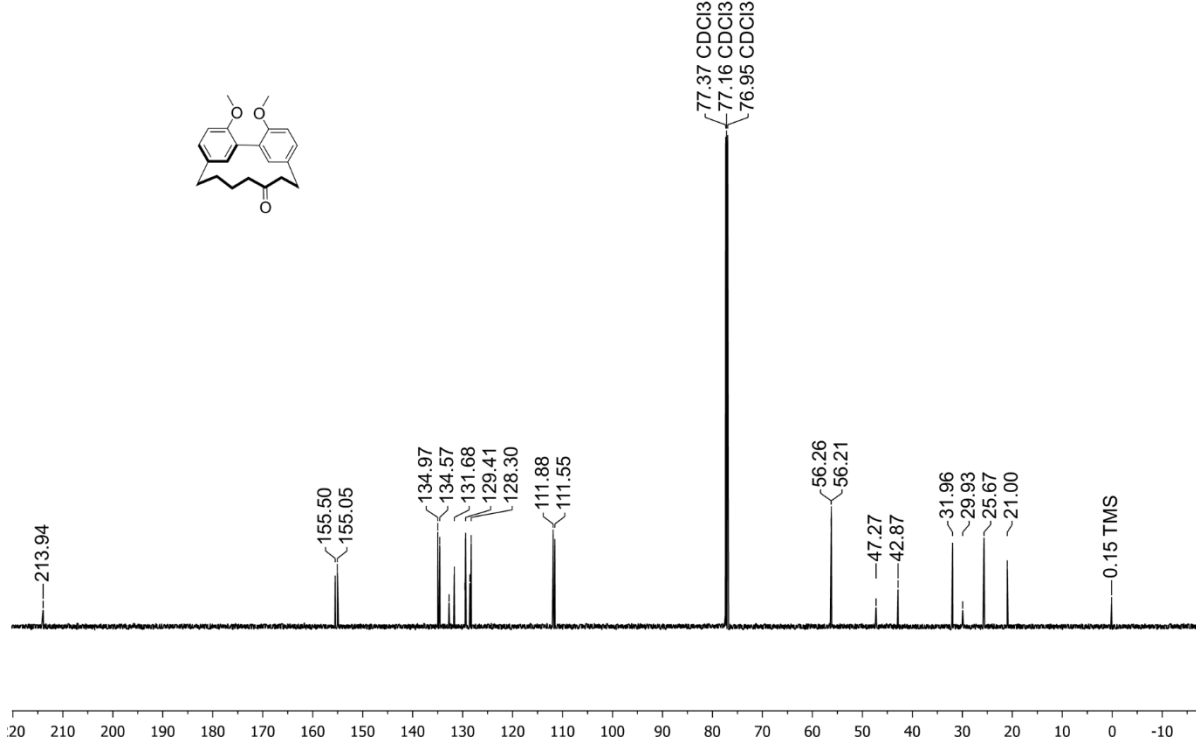
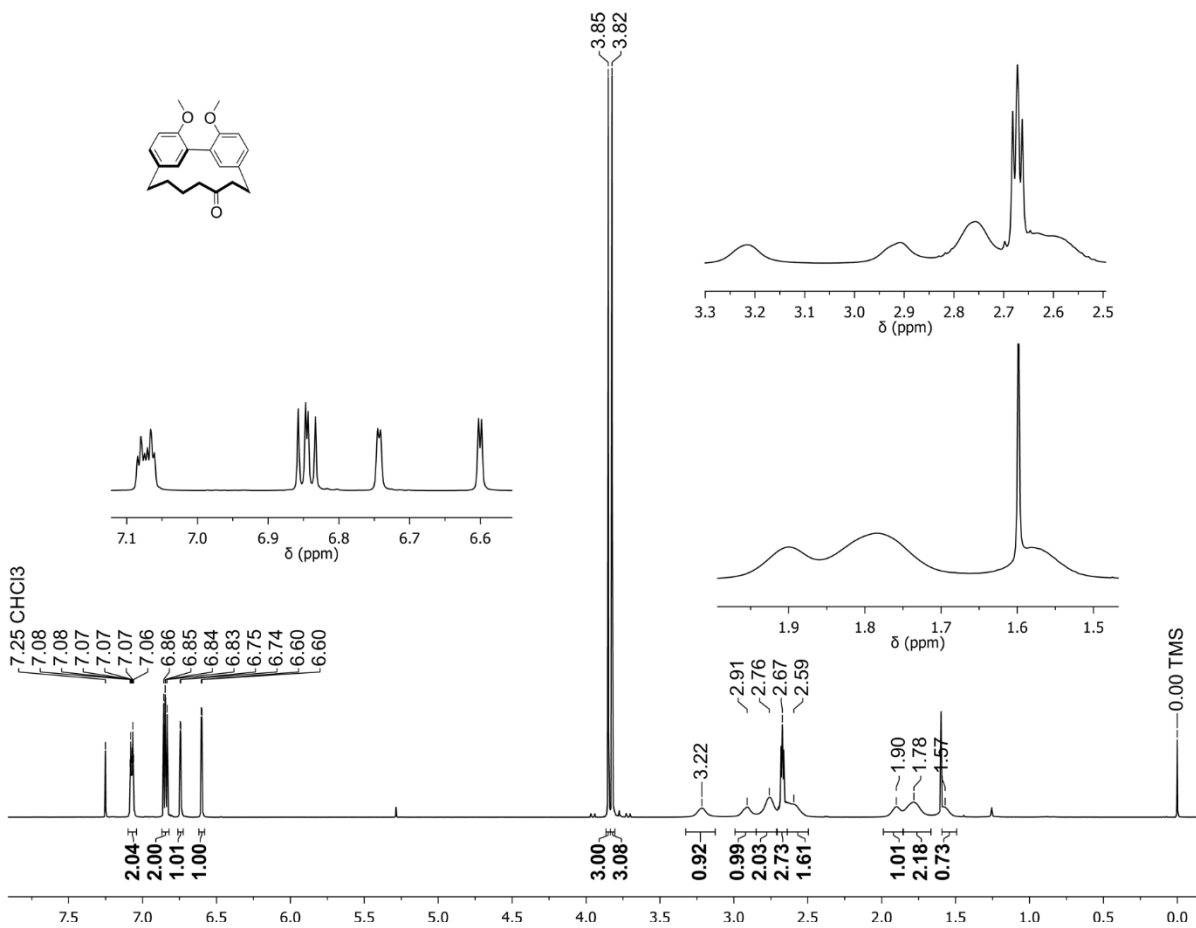












IV.4.5. Crystallographic Details.

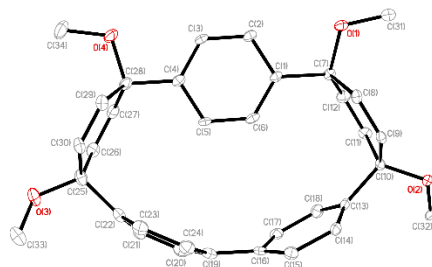


Figure IV.8. ORTEP Representation of X-ray Crystallographic Structure Macrocycle **IV.2.**

Crystallographic Data for **IV.2**: C₃₄H₃₂O₄, M = 504.59, 0.019 x 0.017 x 0.100 mm, T = 173(2) K, Monoclinic, space group Cc, a = 36.9470(18) Å, b = 9.7771(5) Å, c = 38.2483(18) Å, β = 111.093(2)°, V = 12890.90(11) Å³, Z = 20, D_c = 1.300 Mg/m³, μ(Cu) = 0.666 mm⁻¹, F(000) = 5360, 2θ_{max} = 133.8°, 51624 reflections, 19979 independent reflections [R_{int} = 0.0605], R₁ = 0.0557, wR₂ = 0.1448 and GOF = 1.064 for 19979 reflections (14414 parameters) with I > 2σ(I), R₁ = 0.0753, wR₂ = 0.1607 and GOF = 1.034 for all reflections, max/min residual electron density +0.308/-0.368 eÅ⁻³.

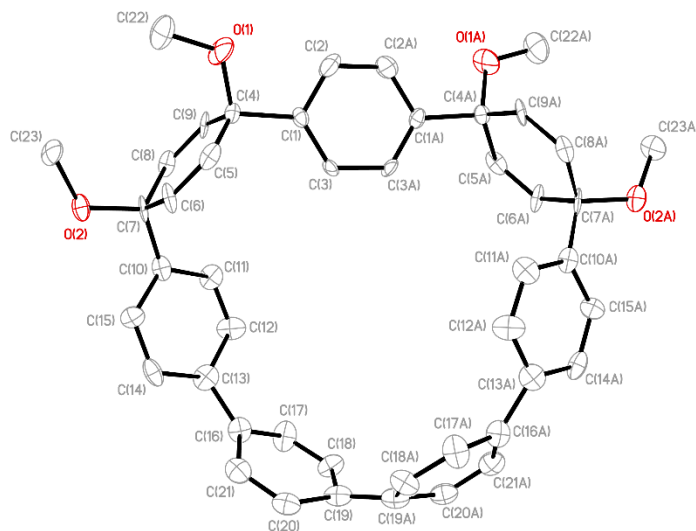


Figure IV.9. ORTEP Representation of X-ray Crystallographic Structure Macrocycle **IV.12.**

Crystallographic Data for **IV.12**: C₅₅H₆₀O₅, M = 801.03, 0.140 x 0.060 x 0.040 mm, T = 173(2) K, Trigonal, space group P₃₂21, a = 25.4957(12) Å, b = 25.4957(12) Å, c = 6.2727(3) Å, β = 90°, V = 3531.2(4) Å³, Z = 3, D_c = 1.130 Mg/m³, μ(Cu) = 0.553 mm⁻¹,

$F(000) = 1290$, $2\theta_{\max} = 135.4^\circ$, 13892 reflections, 2348 independent reflections [$R_{\text{int}} = 0.0718$], $R_1 = 0.0633$, $wR_2 = 0.1558$ and $\text{GOF} = 1.003$ for 2348 reflections (2263 parameters) with $I > 2\sigma(I)$, $R_1 = 0.0728$, $wR_2 = 0.1605$ and $\text{GOF} = 1.003$ for all reflections, max/min residual electron density $+0.243/-0.178 \text{ e}\text{\AA}^3$.

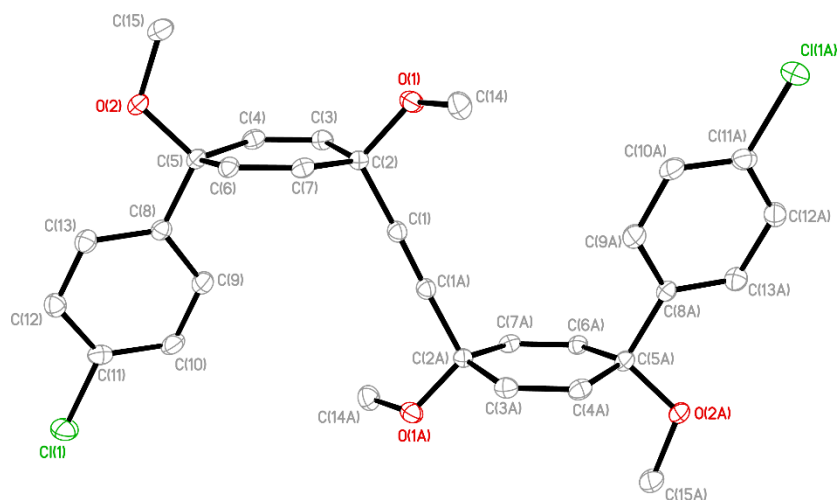


Figure IV.10. ORTEP Representation of X-ray Crystallographic Structure Dichloride **IV.19**.

Crystallographic Data for **IV.19**: $\text{C}_{30}\text{H}_{28}\text{Cl}_2\text{O}_4$, $M = 523.42$, $0.160 \times 0.050 \times 0.030 \text{ mm}$, $T = 173(2) \text{ K}$, Triclinic, space group $P-1$, $a = 6.7057(7) \text{ \AA}$, $b = 10.4349(10) \text{ \AA}$, $c = 10.4710(11) \text{ \AA}$, $\beta = 101.865(8)^\circ$, $V = 639.10(12) \text{ \AA}^3$, $Z = 1$, $D_c = 1.360 \text{ Mg/m}^3$, $\mu(\text{Cu}) = 2.568 \text{ mm}^{-1}$, $F(000) = 274$, $2\theta_{\max} = 135.4^\circ$, 6284 reflections, 2221 independent reflections [$R_{\text{int}} = 0.0450$], $R_1 = 0.0428$, $wR_2 = 0.1104$ and $\text{GOF} = 1.049$ for 2221 reflections (219 parameters) with $I > 2\sigma(I)$, $R_1 = 0.0556$, $wR_2 = 0.1178$ and $\text{GOF} = 1.049$ for all reflections, max/min residual electron density $+0.243/-0.185 \text{ e}\text{\AA}^3$.

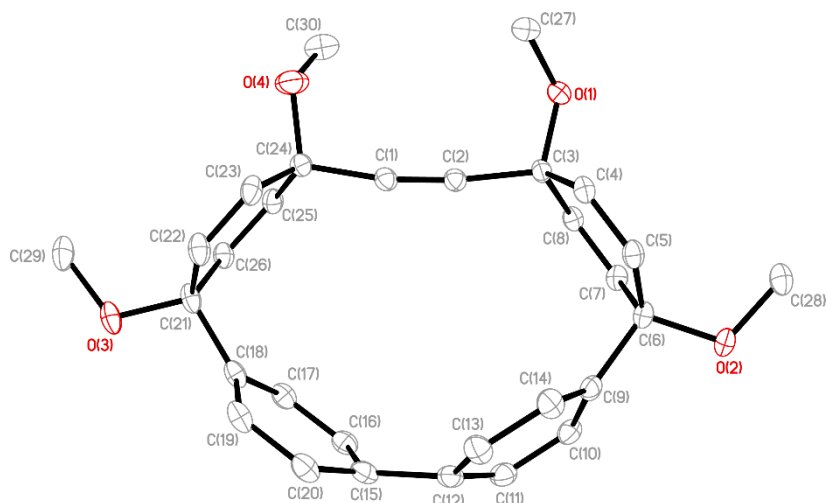


Figure IV.11. ORTEP Representation of X-ray Crystallographic Structure Macrocycle IV.21.

Crystallographic Data for **IV.19**: C₃₀H₂₈O₄, M = 452.52, 0.130 x 0.120 x 0.030 mm, T = 173(2) K, Triclinic, space group P-1, a = 11.7566(13) Å, b = 11.9481(13) Å, c = 18.9210(2) Å, β = 84.064(7)°, V = 2351.2(5) Å³, Z = 4, D_c = 1.278 Mg/m³, μ(Cu) = 0.669 mm⁻¹, F(000) = 960, 2θ_{max} = 135.4°, 29998 reflections, 8217 independent reflections [R_{int} = 0.0303], R₁ = 0.0576, wR₂ = 0.1500 and GOF = 1.055 for 8217 reflections (623 parameters) with I > 2σ(I), R₁ = 0.0676, wR₂ = 0.1576 and GOF = 1.058 for all reflections, max/min residual electron density +1.230/-0.515 eÅ⁻³.

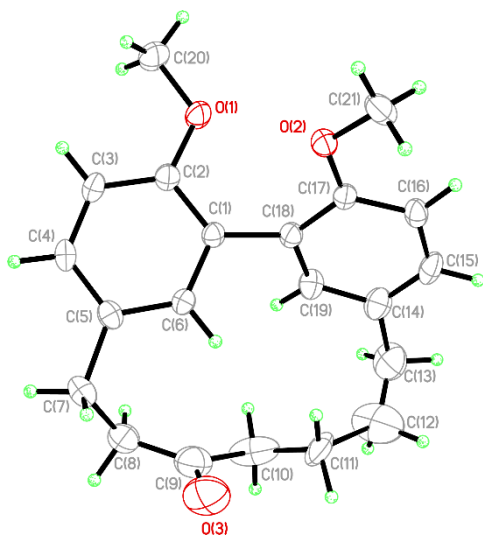


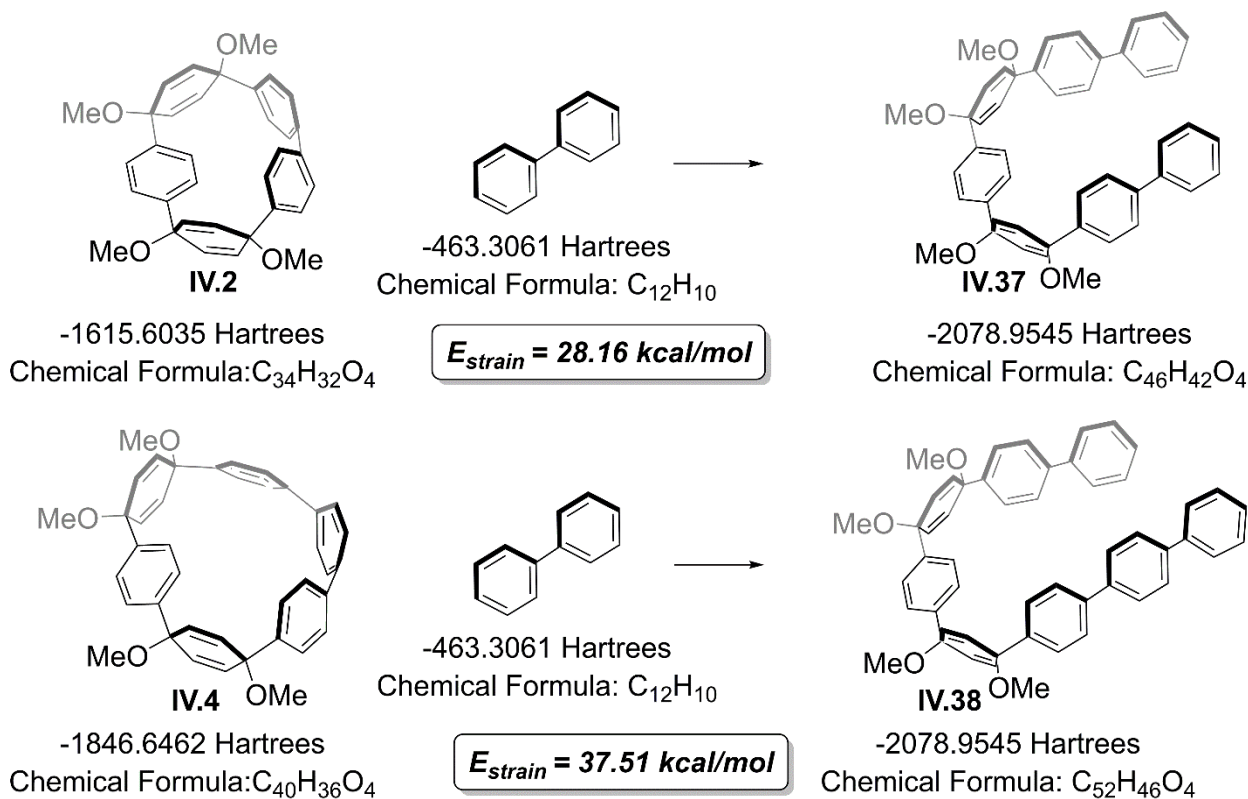
Figure IV.12. ORTEP Representation of X-ray Crystallographic Structure Macrocycle IV.23.

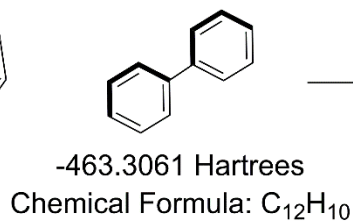
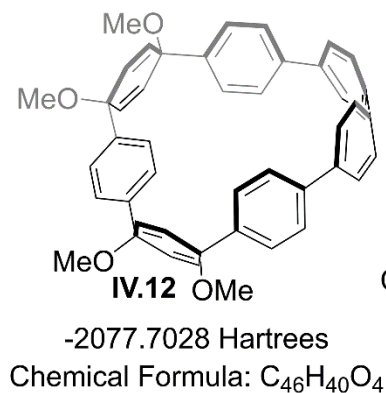
Crystallographic Data for **IV.23**: C₂₁H₂₄O₃, M = 324.40, 0.100 x 0.060 x 0.040 mm, T = 173(2) K, Monoclinic, space group P21/c, a = 10.4271(4) Å, b = 14.8854(5) Å, c = 12.0952(4) Å, β = 113.424(2)°, V = 1722.60(11) Å³, Z = 4, D_c = 1.251 Mg/m³, μ(Cu) = 0.654 mm⁻¹, F(000) = 696, 2θ_{max} = 135.4°, 9981 reflections, 2291 independent reflections [R_{int} = 0.0357], R₁ = 0.1075, wR₂ = 0.2954 and GOF = 1.015 for 2291 reflections (218 parameters) with I > 2σ(I), R₁ = 0.1240, wR₂ = 0.3146 and GOF = 1.015 for all reflections, max/min residual electron density +0.898/-0.521 eÅ³.

IV.4.5. Computational Details.

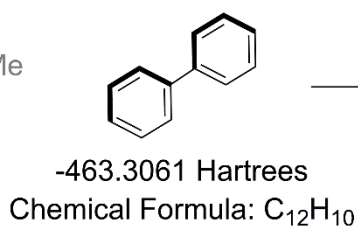
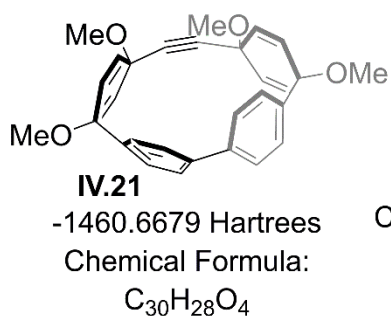
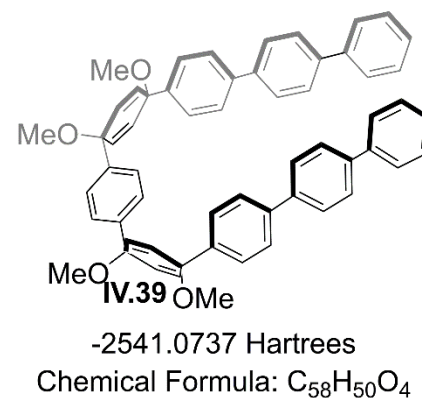
All calculations were carried out with Gaussian 09 package at B3LYP/6-31g* level of theory. Geometries were first optimized in the gas phase. The fully optimized structures were confirmed to be true minima by vibrational analysis. Structures were minimized with no symmetry restrictions.

Homodesmotic reactions for compound IV.2, IV.4, IV.12, IV.21, and IV.23.

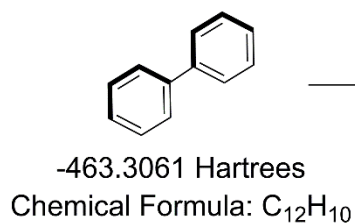
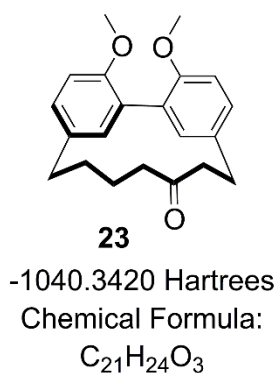
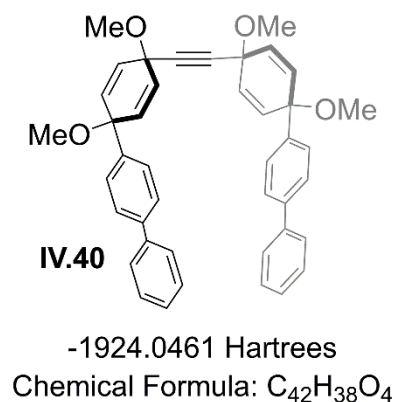




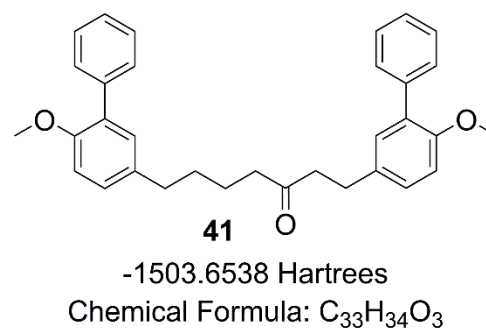
$$E_{\text{strain}} = 40.67 \text{ kcal/mol}$$



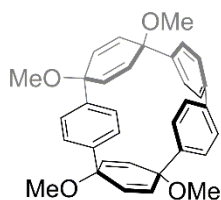
$$E_{\text{strain}} = 45.23 \text{ kcal/mol}$$



$$E_{\text{strain}} = 3.602 \text{ kcal/mol}$$



Minimized Geometries



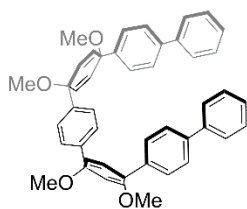
Macrocycle IV.2

C	4.20026	-1.04432	0.08593
C	4.17518	-0.0635	1.24578

C	3.6217	1.14896	1.16703
C	3.04922	1.74283	-0.10969
C	3.52014	0.94539	-1.30724
C	4.04548	-0.27797	-1.22192
H	3.56082	1.79124	2.04377
H	4.57274	-0.43256	2.18945
H	3.38321	1.42967	-2.27225
H	4.35074	-0.81182	-2.11936
C	3.01995	-2.03218	0.20171
C	2.6013	-2.79426	-0.90195
C	2.21715	-2.062	1.34482
C	1.32646	-3.35566	-0.9411
H	3.24232	-2.88211	-1.77432
C	0.94746	-2.62709	1.31172
H	2.52145	-1.53504	2.24141
C	0.42911	-3.17475	0.12791
H	0.99561	-3.85579	-1.84793
H	0.29728	-2.48819	2.16922
C	1.49282	1.81091	-0.23494
C	0.86653	3.05975	-0.17124
C	0.68025	0.66915	-0.15988
C	-0.51678	3.16705	-0.01284
H	1.45876	3.96644	-0.23706
H	1.13893	-0.31415	-0.18431
C	-1.32936	2.03293	0.0645
H	-0.96323	4.15268	0.03967
O	3.47207	3.11876	-0.23464
O	5.39629	-1.83882	0.08058
C	6.60796	-1.11089	-0.05537
H	6.75497	-0.39641	0.76676
H	6.65735	-0.55881	-1.00457

H	7.41151	-1.85141	-0.03205
C	4.8743	3.33469	-0.2883
H	5.38475	2.9945	0.62316
H	5.00744	4.41488	-0.38974
H	5.33702	2.83431	-1.15006
C	-2.87197	2.13271	0.17684
C	-3.60826	1.60672	-1.04221
C	-3.33686	1.38422	1.40802
C	-4.33286	0.48439	-1.06357
H	-3.54546	2.21366	-1.9421
C	-4.0426	0.25525	1.37819
H	-3.06259	1.84593	2.35301
C	-4.44216	-0.47475	0.10837
H	-4.85343	0.20695	-1.97761
H	-4.36041	-0.22065	2.30151
C	-3.47316	-1.67077	-0.06576
C	-3.12265	-2.46325	1.0409
C	-2.74365	-1.86385	-1.2435
C	-1.93018	-3.17934	1.05416
H	-3.73184	-2.43607	1.93977
C	-1.54901	-2.58103	-1.23495
H	-3.02301	-1.33675	-2.15006
C	-1.04678	-3.12114	-0.04118
H	-1.6273	-3.68707	1.96618
H	-0.92332	-2.56277	-2.12247
O	-3.25483	3.49914	0.45242
O	-5.79925	-0.89263	0.34285
C	-3.06061	4.4494	-0.58403
H	-3.81894	4.36009	-1.3741
H	-2.0621	4.37782	-1.03543
H	-3.16554	5.4324	-0.11642

C	-6.36957	-1.76164	-0.61995
H	-6.50886	-1.27733	-1.59774
H	-5.76982	-2.6712	-0.76154
H	-7.35313	-2.03887	-0.23166
C	-0.70419	0.77862	-0.02311
H	-1.31051	-0.12026	0.03458



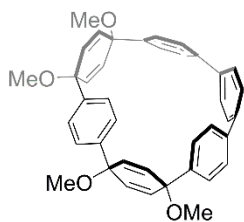
Homodesmotic Product IV.37

C	5.1097	1.65692	0.08801
C	4.363	1.7491	1.40056
C	3.05626	2.00262	1.50097
C	2.13275	2.22262	0.31737
C	2.90411	2.25461	-0.98352
C	4.21309	2.01359	-1.08336
H	2.57307	2.052	2.47515
H	4.9693	1.5862	2.28972
H	2.3121	2.48941	-1.86605
H	4.71266	2.04666	-2.04996
C	5.67937	0.24468	-0.13547
C	6.89666	0.07269	-0.80642
C	4.97632	-0.89277	0.27971
C	7.40353	-1.20205	-1.05712
H	7.4576	0.94473	-1.12052
C	5.47055	-2.17406	0.03546
H	4.03283	-0.78429	0.80523
C	6.68399	-2.31761	-0.6337
H	8.3495	-1.32823	-1.57327
H	4.92168	-3.05015	0.36439

C	1.06285	1.11703	0.30868
C	-0.14711	1.29707	0.98768
C	1.28879	-0.10726	-0.33363
C	-1.10359	0.28185	1.01818
H	-0.34434	2.24237	1.47955
H	2.21744	-0.27099	-0.87206
C	-0.88199	-0.94159	0.37738
H	-2.0361	0.45235	1.54834
O	1.39346	3.45014	0.48363
O	6.26675	2.5171	0.11372
C	6.0193	3.90726	0.25252
H	5.51796	4.14433	1.20042
H	5.41483	4.30561	-0.57335
H	7.00115	4.38727	0.23986
C	2.15928	4.63973	0.58812
H	2.83321	4.62444	1.45527
H	1.43625	5.44996	0.71219
H	2.75515	4.82762	-0.31504
C	-1.94042	-2.06201	0.33968
C	-2.93118	-1.94561	1.47718
C	-2.6462	-2.0291	-0.99846
C	-4.24929	-1.8133	1.32055
H	-2.51571	-1.96347	2.48252
C	-3.96153	-1.90045	-1.15573
H	-1.99535	-2.14114	-1.86182
C	-4.95106	-1.76324	-0.01937
H	-4.88316	-1.72385	2.20022
H	-4.40372	-1.90491	-2.14888
C	-5.74163	-0.4513	-0.20431
C	-6.86036	-0.43045	-1.04798
C	-5.33783	0.74735	0.39455

C	-7.56583	0.74885	-1.28214
H	-7.18259	-1.3528	-1.52013
C	-6.03097	1.93709	0.17045
H	-4.46625	0.7608	1.04155
C	-7.14406	1.92649	-0.66708
H	-8.43347	0.75519	-1.93363
H	-5.71063	2.86124	0.63986
O	-1.28764	-3.35319	0.34439
O	-5.83362	-2.89397	-0.19648
C	-0.62234	-3.73009	1.54054
H	-1.32879	-3.98838	2.34125
H	0.05942	-2.94827	1.90279
H	-0.03837	-4.62057	1.29294
C	-6.77795	-3.14098	0.83518
H	-6.3026	-3.54427	1.73932
H	-7.35132	-2.24216	1.10184
H	-7.46608	-3.89264	0.43941
C	0.33216	-1.11971	-0.29964
H	0.52592	-2.06405	-0.79911
C	7.23941	-3.72812	-0.905
C	8.45371	-3.88278	-1.57434
C	6.52859	-4.85102	-0.48147
C	8.95667	-5.16011	-1.82067
H	9.01349	-2.99732	-1.90879
C	7.03205	-6.12879	-0.72692
H	5.57161	-4.7293	0.04625
C	8.24582	-6.2835	-1.39653
H	9.91348	-5.28211	-2.3488
H	6.47158	-7.01396	-0.39252
H	8.64261	-7.29053	-1.5908
C	-7.91932	3.23356	-0.91638

C	-7.50523	4.41752	-0.30545
C	-9.0354	3.23382	-1.75299
C	-8.20751	5.6013	-0.53062
H	-6.62575	4.41683	0.35467
C	-9.73742	4.41807	-1.9791
H	-9.36181	2.3008	-2.23471
C	-9.32376	5.60169	-1.36799
H	-7.88154	6.53442	-0.04862
H	-10.61712	4.41806	-2.63911
H	-9.87729	6.53519	-1.54541



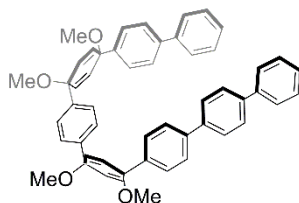
Macrocycle IV.2

C	6.1637	5.52218	-0.2028
C	4.73811	6.11393	-0.29108
C	3.95427	6.29799	0.81712
C	4.46285	5.99533	2.24919
C	5.9892	5.96892	2.29532
C	6.74381	5.70865	1.21189
H	2.96619	6.6889	0.69145
H	4.35899	6.40985	-1.2469
H	6.47855	6.1738	3.22454
H	7.80588	5.66393	1.33408
C	7.10851	6.38771	-1.02598
C	8.41363	6.42913	-0.55443
C	6.71231	7.19128	-2.11133
C	9.06137	7.628	-0.65706
H	8.87141	5.58298	-0.08603
C	7.3878	8.42355	-2.22455

H	5.91969	6.9119	-2.77362
C	8.33826	8.66366	-1.22166
H	10.04949	7.76959	-0.27176
H	7.15129	9.14134	-2.982
C	3.95192	7.13951	3.17883
C	2.92709	6.93176	4.10373
C	4.53425	8.42693	3.0759
C	2.4819	7.99752	4.9081
H	2.48479	5.96272	4.20492
H	5.3682	8.57827	2.42281
C	2.97585	9.30721	4.7264
H	1.74328	7.81459	5.66035
O	3.99483	4.71661	2.68598
O	6.11774	4.14686	-0.59171
C	7.43151	3.58687	-0.51911
H	7.79625	3.66187	0.484
H	8.08416	4.12195	-1.17687
H	7.39716	2.55778	-0.81013
C	4.48857	3.70247	1.807
H	4.13834	3.89013	0.81351
H	4.13833	2.74572	2.13389
H	5.55849	3.71273	1.8159
C	2.29267	10.43168	5.56245
C	3.2111	10.92717	6.71959
C	1.89512	11.63363	4.6868
C	3.94937	12.09848	6.63756
H	3.26075	10.35052	7.61955
C	2.59963	12.78279	4.6192
H	0.99499	11.56169	4.11277
C	3.90601	13.02334	5.38707
H	4.55645	12.38505	7.47077

H	2.2198	13.57359	4.0066
C	5.09724	12.77477	4.44631
C	5.3638	13.73702	3.44993
C	5.89979	11.64167	4.55286
C	6.30431	13.47063	2.44414
H	4.83304	14.6661	3.45056
C	6.902	11.42345	3.60275
H	5.75133	10.94641	5.35253
C	7.01132	12.27122	2.4882
H	6.46831	14.17123	1.6522
H	7.56789	10.59278	3.70992
O	1.09367	9.86619	6.09867
O	3.95481	14.39258	5.79657
C	1.42311	8.74936	6.92875
H	2.05364	9.07412	7.7299
H	1.93623	8.012	6.34745
H	0.52595	8.32628	7.33
C	2.84339	14.67439	6.65111
H	1.93141	14.4927	6.12178
H	2.88726	14.04242	7.51343
H	2.87987	15.69892	6.95755
C	4.01457	9.52149	3.81118
H	4.41558	10.50361	3.67144
C	8.5341	10.01511	-0.57
C	7.98713	11.22728	-1.00755
C	9.21699	9.92894	0.63215
C	7.66088	12.15921	0.00056
H	7.78848	11.42022	-2.04108
C	8.8382	10.79444	1.62888
H	9.96739	9.18429	0.79733
C	7.87409	11.75163	1.3348

H	7.22913	13.10958	-0.23452
H	9.25051	10.71246	2.61284



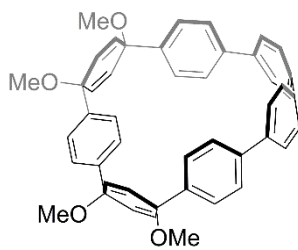
Homodesmotic Product IV.38

C	3.35494	3.45767	0.11392
C	2.53906	3.46924	1.38784
C	1.20692	3.39359	1.42336
C	0.32279	3.26611	0.19654
C	1.13075	3.38123	-1.07723
C	2.46198	3.47222	-1.11318
H	0.67458	3.40272	2.37287
H	3.11808	3.54205	2.30658
H	0.54738	3.38049	-1.9961
H	2.98864	3.54769	-2.06284
C	4.27118	2.22398	0.04449
C	5.5273	2.30636	-0.56952
C	3.8568	0.98354	0.54497
C	6.34218	1.18197	-0.67562
H	5.86622	3.25922	-0.95871
C	4.67369	-0.13961	0.43807
H	2.89298	0.89404	1.03663
C	5.93483	-0.06521	-0.17486
H	7.30199	1.26955	-1.17757
H	4.33911	-1.08103	0.86512
C	-0.42914	1.92573	0.26697
C	-1.67729	1.8448	0.89406
C	0.13576	0.74986	-0.24323
C	-2.33875	0.62143	1.00754

H	-2.13622	2.74691	1.28146
H	1.10054	0.78692	-0.73984
C	-1.77568	-0.5554	0.50307
H	-3.30942	0.58973	1.4941
O	-0.71121	4.27194	0.21868
O	4.25316	4.58617	0.09348
C	3.65238	5.87128	0.08333
H	3.03626	6.04595	0.97543
H	3.03053	6.03217	-0.80757
H	4.47866	6.58674	0.07541
C	-0.27743	5.62253	0.23138
H	0.31969	5.85828	1.12265
H	-1.18732	6.22809	0.24094
H	0.31129	5.87534	-0.66051
C	-2.50162	-1.91381	0.55957
C	-3.53791	-1.96093	1.66115
C	-3.13099	-2.19186	-0.78808
C	-4.83472	-2.20754	1.46831
H	-3.17882	-1.7702	2.67033
C	-4.42447	-2.43843	-0.98138
H	-2.43696	-2.1991	-1.62465
C	-5.46304	-2.47732	0.11819
H	-5.50805	-2.21128	2.32288
H	-4.80487	-2.65033	-1.97752
C	-6.5756	-1.4604	-0.21039
C	-7.61438	-1.82766	-1.07638
C	-6.55047	-0.14981	0.27971
C	-8.6081	-0.91943	-1.43792
H	-7.64457	-2.84065	-1.46419
C	-7.53588	0.77281	-0.07252
H	-5.74956	0.16405	0.94198

C	-8.56078	0.37753	-0.92915
H	-9.41108	-1.21364	-2.10572
H	-7.50846	1.78643	0.31332
O	-1.53613	-2.98156	0.70662
O	-5.99131	-3.82055	0.0406
C	-0.8394	-3.05018	1.94163
H	-1.48326	-3.40025	2.76
H	-0.39381	-2.0862	2.22302
H	-0.03843	-3.77988	1.79529
C	-6.88084	-4.22239	1.07251
H	-6.35757	-4.39198	2.02304
H	-7.69057	-3.49705	1.23317
H	-7.31687	-5.16889	0.74209
C	-0.52679	-0.47012	-0.12713
H	-0.07133	-1.37251	-0.52342
C	6.80711	-1.26057	-0.28594
C	8.20135	-1.15689	-0.14579
C	6.26604	-2.53325	-0.5345
C	9.02762	-2.27379	-0.24978
H	8.6476	-0.19129	0.0735
C	7.07763	-3.66079	-0.63961
H	5.19438	-2.64191	-0.67381
C	8.45713	-3.52147	-0.49628
H	10.10196	-2.18018	-0.13082
H	6.64666	-4.6359	-0.84093
C	9.36257	-4.76179	-0.61198
C	8.8009	-6.01486	-0.85855
C	10.74416	-4.63246	-0.47039
C	9.62065	-7.13841	-0.96283
H	7.71159	-6.1166	-0.96937
C	11.56438	-5.7561	-0.57564

H	11.18702	-3.64489	-0.27622
C	11.00287	-7.00898	-0.82168
H	9.17795	-8.12623	-1.15655
H	12.6537	-5.65377	-0.46437
H	11.64902	-7.895	-0.904
C	-9.65665	1.38693	-1.31874
C	-9.61818	2.68735	-0.81485
C	-10.68759	1.00118	-2.17542
C	-10.61085	3.60155	-1.16707
H	-8.8057	2.99093	-0.13887
C	-11.6801	1.91583	-2.52863
H	-10.71796	-0.02366	-2.5728
C	-11.64197	3.21581	-2.02452
H	-10.58095	4.62638	-0.76944
H	-12.4926	1.61152	-3.20444
H	-12.42451	3.93682	-2.30215



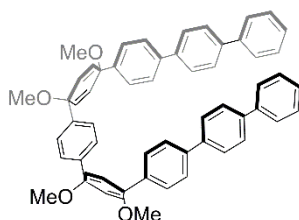
Macrocycle IV.12

C	5.3101	-2.87658	0.3607
C	4.65176	-3.37077	-0.94513
C	3.92676	-4.52517	-0.99641
C	3.25007	-5.15457	0.24633
C	3.85685	-4.58938	1.55371
C	4.57767	-3.43399	1.6004
H	3.815	-5.0165	-1.94001
H	4.78908	-2.80138	-1.84103
H	3.69529	-5.12564	2.4645

H	4.65948	-2.91001	2.52917
C	5.3016	-1.33621	0.40002
C	5.26971	-0.66089	1.63136
C	5.31572	-0.60554	-0.79684
C	5.02967	0.72013	1.65687
H	5.41382	-1.19975	2.54454
C	5.07621	0.77135	-0.7694
H	5.49458	-1.10031	-1.7271
C	4.79112	1.38806	0.45068
H	5.00504	1.25004	2.58626
H	5.08524	1.34059	-1.67482
C	1.7111	-4.86041	0.21338
C	0.90244	-5.80669	-0.42897
C	1.09911	-3.72736	0.79865
C	-0.49218	-5.68354	-0.43222
H	1.3575	-6.6418	-0.92088
H	1.70287	-2.96852	1.2529
C	-1.12507	-4.60617	0.20108
H	-1.08486	-6.42773	-0.92165
O	3.41355	-6.58263	0.21261
O	6.66014	-3.34805	0.39147
C	7.27773	-2.91485	1.60532
H	6.74443	-3.32025	2.4397
H	7.25842	-1.84605	1.65556
H	8.29184	-3.25446	1.63124
C	4.80128	-6.94717	0.22356
H	5.29182	-6.51391	-0.62332
H	4.88906	-8.01511	0.17822
H	5.25903	-6.59079	1.12247
C	-2.69168	-4.6221	0.21332
C	-3.22163	-3.91373	1.48203

C	-3.20997	-3.9357	-1.06997
C	-3.72479	-2.6499	1.46709
H	-3.18729	-4.43934	2.41431
C	-3.70015	-2.66731	-1.08149
H	-3.17205	-4.4792	-1.99045
C	-4.289	-2.00726	0.18243
H	-3.74776	-2.0889	2.37754
H	-3.69839	-2.11816	-1.99953
C	-3.96524	-0.5069	0.18224
C	-3.76667	0.17159	-1.02817
C	-3.85305	0.17542	1.39939
C	-3.23455	1.46354	-1.00904
H	-4.00646	-0.30089	-1.95822
C	-3.32425	1.46716	1.418
H	-4.15778	-0.29476	2.3092
C	-2.88787	2.03569	0.2198
H	-3.07127	1.99725	-1.92389
H	-3.23176	2.00337	2.3386
O	-3.11944	-5.98694	0.2321
O	-5.70744	-2.19923	0.16665
C	-2.63637	-6.62013	1.41875
H	-3.00399	-6.09779	2.27776
H	-1.5671	-6.60233	1.42097
H	-2.977	-7.63397	1.44598
C	-6.00599	-3.59793	0.18313
H	-5.5764	-4.06476	-0.67843
H	-5.59755	-4.03973	1.06891
H	-7.06781	-3.73545	0.17222
C	-0.32489	-3.59808	0.78993
H	-0.78594	-2.74072	1.23476
C	0.45103	4.39052	0.34257

C	-0.18588	4.35797	-0.89819
C	-0.28046	4.38103	1.52686
C	-1.43607	3.74789	-0.9447
H	0.28159	4.74081	-1.78156
C	-1.53047	3.76774	1.4828
H	0.11702	4.78287	2.43496
C	-1.94527	3.23702	0.25396
H	-1.96664	3.63563	-1.86871
H	-2.13173	3.66925	2.36092
C	2.61437	4.1813	1.62516
C	3.74666	3.36886	1.65509
C	4.1177	2.7608	0.44976
C	3.79124	3.35632	-0.77333
C	2.66494	4.16516	-0.79874
C	1.9624	4.28655	0.3957
H	2.23643	4.65591	2.50586
H	4.27932	3.1844	2.56416
H	4.35794	3.16293	-1.66036
H	2.32627	4.62819	-1.70172



Homodesmotic Product IV.39

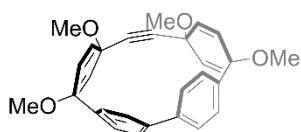
C	4.31714	-6.97658	-1.25434
C	3.55223	-7.84543	-0.24211
C	3.16844	-7.36993	0.96421
C	2.96686	-5.86636	1.22646
C	3.72872	-4.99272	0.21116
C	4.10383	-5.47007	-1.00362
H	2.98224	-8.06239	1.75842

H	3.33454	-8.86229	-0.49327
H	3.95146	-3.97696	0.46336
H	4.2756	-4.78079	-1.80418
C	3.87184	-7.34688	-2.68078
C	3.92009	-6.39665	-3.71018
C	3.41811	-8.64511	-2.94664
C	3.52142	-6.75012	-5.00837
H	4.26087	-5.40307	-3.50595
C	3.02265	-8.99841	-4.2419
H	3.37408	-9.36832	-2.15891
C	3.07611	-8.05319	-5.27413
H	3.55776	-6.0262	-5.7951
H	2.67968	-9.99173	-4.44367
C	1.46707	-5.5506	1.07279
C	0.97451	-5.08152	-0.15202
C	0.59603	-5.72839	2.15682
C	-0.38291	-4.76042	-0.28463
H	1.6356	-4.96461	-0.98548
H	0.97082	-6.09106	3.0913
C	-1.25331	-4.93369	0.79925
H	-0.75529	-4.38412	-1.21441
O	3.39396	-5.55449	2.55458
O	5.71249	-7.24744	-1.09826
C	6.45689	-6.47957	-2.04764
H	6.27265	-5.43761	-1.8882
H	6.15419	-6.74753	-3.03807
H	7.50103	-6.67931	-1.92719
C	4.78884	-5.83999	2.6827
H	4.95846	-6.87883	2.49211
H	5.11238	-5.60142	3.6743
H	5.3396	-5.25291	1.97734

C	-2.74257	-4.57206	0.65269
C	-3.56031	-5.57578	1.48255
C	-2.91469	-3.1251	1.15545
C	-3.96988	-5.30281	2.74067
H	-3.79657	-6.52784	1.05549
C	-3.3128	-2.85323	2.42625
H	-2.69535	-2.31458	0.49247
C	-4.13673	-3.86148	3.2522
H	-4.20297	-6.11519	3.39691
H	-3.06492	-1.9066	2.85846
C	-3.72427	-3.81009	4.73439
C	-3.22177	-2.63119	5.30568
C	-3.85764	-4.96437	5.51406
C	-2.85444	-2.61327	6.66224
H	-3.11867	-1.74822	4.71009
C	-3.49041	-4.9472	6.86238
H	-4.2414	-5.86239	5.07676
C	-2.98754	-3.77559	7.43847
H	-2.4734	-1.71541	7.10205
H	-3.59389	-5.83165	7.45497
O	-3.13347	-4.66526	-0.71922
O	-5.51302	-3.49944	3.11836
C	-2.92629	-6.00148	-1.18374
H	-3.50917	-6.67777	-0.5945
H	-1.88988	-6.25382	-1.09582
H	-3.22505	-6.07262	-2.20861
C	-5.88681	-3.55128	1.73983
H	-5.2774	-2.87321	1.17941
H	-5.74759	-4.54532	1.36927
H	-6.91495	-3.27357	1.63898
C	-0.76708	-5.4322	2.01562

H	-1.43577	-5.58278	2.83733
C	-1.87256	-3.85897	11.63622
C	-1.73154	-2.66943	10.90481
C	-2.3688	-5.00916	11.01137
C	-2.0882	-2.63372	9.54689
H	-1.35211	-1.79011	11.38195
C	-2.72629	-4.97286	9.65903
H	-2.475	-5.9166	11.56795
C	-2.58712	-3.78769	8.9256
H	-1.97993	-1.72773	8.98785
H	-3.10688	-5.85262	9.18367
C	2.28606	-7.89633	-9.03365
C	2.68355	-7.52005	-7.74183
C	2.64371	-8.45501	-6.69724
C	2.20906	-9.76369	-6.94533
C	1.81328	-10.13855	-8.23475
C	1.84991	-9.20593	-9.2781
H	2.31586	-7.18429	-9.83183
H	3.01654	-6.52045	-7.55431
H	2.17992	-10.47744	-6.14868
H	1.48231	-11.13848	-8.42358
C	-1.48492	-3.91088	13.12685
C	-0.99846	-2.76536	13.77104
C	-0.64576	-2.82111	15.127
C	-0.77901	-4.02152	15.83791
C	-1.26676	-5.16628	15.19414
C	-1.6205	-5.11064	13.8394
H	-0.89627	-1.84878	13.22848
H	-0.2748	-1.94673	15.61969
H	-0.50841	-4.06388	16.87222
H	-1.36917	-6.0829	15.73676

H	-1.99407	-5.98497	13.34821
C	1.40894	-9.62729	-10.69072
C	1.43494	-8.7034	-11.74366
C	1.0284	-9.09434	-13.02682
C	0.59811	-10.40841	-13.25645
C	0.57458	-11.33234	-12.20312
C	0.97961	-10.94099	-10.92054
H	1.76461	-7.70065	-11.56845
H	1.04599	-8.38974	-13.83186
H	0.28755	-10.70601	-14.23619
H	0.24753	-12.33636	-12.37789
H	0.96148	-11.64564	-10.11531

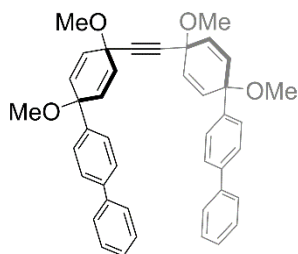


Macrocycle IV.21

C	2.43921	2.81125	-0.498
C	1.91678	3.34286	0.8519
C	2.34788	2.43482	2.04198
C	2.99441	1.24213	1.88086
C	3.59485	0.77538	0.53834
C	3.06922	1.61401	-0.63714
H	2.26588	3.40132	-1.37335
H	2.09779	2.74553	3.03947
H	3.0729	0.59062	2.72707
H	3.18688	1.21901	-1.62342
C	0.49243	3.30235	0.77772
C	-0.7311	3.2142	0.7751
C	-2.14607	3.03199	0.85778
C	-2.39511	2.00966	1.99482
C	-2.6003	2.50107	-0.5193

C	-2.86322	0.75186	1.77496
H	-2.16382	2.29721	2.99985
C	-3.05215	1.23104	-0.71746
H	-2.53156	3.15353	-1.36687
C	-3.42279	0.26496	0.42408
H	-2.81863	0.0546	2.58278
H	-3.13423	0.87592	-1.71932
C	1.76379	-1.89735	-1.23533
C	1.05527	-2.2533	-0.08943
C	1.68538	-2.35176	1.15221
C	2.74687	-1.47698	1.36026
C	3.07477	-0.63689	0.28803
C	2.83281	-1.03586	-1.03107
H	1.47424	-2.21876	-2.21257
H	1.34027	-3.01497	1.91687
H	3.2514	-1.4138	2.30626
H	3.41254	-0.65496	-1.84645
C	-0.45232	-2.36688	-0.14112
C	-1.14469	-2.61106	1.04078
C	-1.12872	-2.07429	-1.32824
C	-2.32368	-1.89217	1.19841
H	-0.76899	-3.26406	1.79811
C	-2.31742	-1.35978	-1.17656
H	-0.73649	-2.32777	-2.29135
C	-2.69808	-1.05014	0.13549
H	-2.89337	-1.94532	2.10374
H	-2.88153	-1.02213	-2.02316
O	-4.85059	0.13383	0.49714
O	-2.85216	4.24936	1.14845
O	2.39425	4.68402	1.0531
O	5.01497	0.8643	0.58428

C	3.82238	4.74057	1.01181
H	4.2232	4.12346	1.78318
H	4.16741	4.39348	0.05755
H	4.14579	5.75171	1.15901
C	5.52383	0.37678	-0.66
H	6.58639	0.49085	-0.67646
H	5.27189	-0.66143	-0.77506
H	5.0849	0.93873	-1.4613
C	-2.61062	5.21624	0.11939
H	-3.16613	6.10891	0.32707
H	-1.56824	5.44593	0.09162
H	-2.91471	4.81713	-0.82869
C	-5.4619	1.37185	0.86599
H	-5.09847	1.667	1.82512
H	-5.22308	2.12317	0.14571
H	-6.52256	1.24256	0.90881



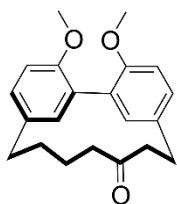
Homodesmotic Product IV.40

C	2.37725	1.30864	-1.34419
C	1.98219	2.26088	-0.21297
C	2.83729	1.95904	1.02219
C	3.39245	0.72758	1.27486
C	3.36159	-0.49777	0.28409
C	2.89096	0.04531	-1.11182
H	2.24571	1.64042	-2.35505
H	3.01115	2.76645	1.71653
H	3.88682	0.60761	2.20722

H	3.00715	-0.59825	-1.9453
C	0.49683	2.12957	0.13876
C	-0.67479	2.0346	0.3632
C	-2.18051	1.91255	0.65165
C	-3.0132	3.13725	0.14774
C	-2.3315	1.83822	2.16396
C	-3.37496	4.21979	0.9479
H	-3.33244	3.16136	-0.86133
C	-2.61814	2.95028	2.97426
H	-2.21123	0.88153	2.62683
C	-3.02236	4.407	2.43238
H	-3.9339	5.00935	0.4919
H	-2.62106	2.77592	4.02447
C	2.16742	-4.12974	0.47859
C	2.61336	-4.26889	1.80149
C	2.83097	-3.27894	2.65693
C	2.93809	-2.02287	2.20401
C	2.79195	-1.80765	0.81972
C	2.2672	-2.82776	-0.04786
H	1.7971	-4.96442	-0.09916
H	2.94978	-3.53539	3.69422
H	3.18933	-1.24867	2.88996
H	2.01092	-2.63234	-1.07227
C	-1.18054	8.05583	2.0266
C	-2.14246	7.73988	1.18971
C	-0.95456	7.54287	3.29319
C	-2.65373	6.52642	1.31599
H	-2.45867	8.46154	0.44096
C	-1.4266	6.23681	3.46395
H	-0.4486	8.10332	4.06813
C	-2.28657	5.72879	2.44819

H	-3.33299	6.1847	0.55823
H	-1.16746	5.67141	4.33318
O	-4.01504	4.93776	3.25726
O	-2.66054	0.73074	-0.00576
O	2.20075	3.63549	-0.59253
O	4.59031	-1.13645	0.17586
C	3.59759	3.8789	-0.75393
H	4.09119	3.68158	0.17226
H	3.97595	3.23415	-1.51404
H	3.77391	4.90231	-1.03731
C	4.26379	-2.38426	-0.54158
H	5.07079	-3.07512	-0.431
H	3.35438	-2.85785	-0.15745
H	4.11548	-2.14786	-1.56705
C	-1.81137	-0.35438	0.33182
H	-2.1418	-1.23374	-0.17876
H	-0.80695	-0.12596	0.03273
H	-1.84583	-0.51172	1.3843
C	-5.14011	4.21173	3.32043
H	-5.55353	4.14549	2.34721
H	-4.92449	3.23947	3.6941
H	-5.80858	4.71554	3.97684
C	3.01164	-5.43686	2.53973
C	3.28466	-5.17349	3.88691
C	3.14752	-6.63823	1.95638
C	3.7759	-6.1806	4.67476
H	3.13261	-4.18121	4.29008
C	3.64826	-7.66377	2.72905
H	2.90244	-6.76018	0.92079
C	3.95672	-7.44049	4.09148
H	4.00489	-5.99933	5.70693

H	3.7911	-8.6166	2.2904
H	4.33459	-8.23304	4.68055
C	-0.32485	8.88494	1.28125
C	0.77138	9.41433	1.81637
C	-0.73278	8.99378	-0.04516
C	1.63467	10.02788	0.94881
H	0.95283	9.32516	2.87127
C	0.10895	9.59515	-0.92811
H	-1.68435	8.5806	-0.36596
C	1.31037	10.11417	-0.42773
H	2.53832	10.42496	1.32184
H	-0.14752	9.65622	-1.96521
H	1.98288	10.58217	-1.09266

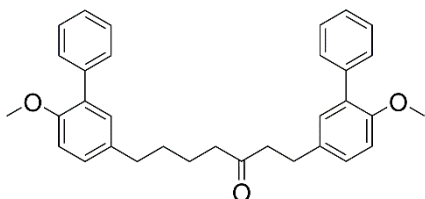


Macrocycle IV.23

C	-2.43541	-0.87566	0.34829
C	-1.05881	-0.6374	0.3189
C	-0.49686	0.35772	1.15865
C	-1.33141	1.32828	1.72085
C	-2.72398	1.15435	1.66329
C	-3.27101	0.02165	1.0314
H	-2.8497	-1.72179	-0.159
H	-3.3709	1.88131	2.10811
H	-4.32668	-0.15017	1.06322
C	1.02783	0.38426	1.40377
C	1.73344	1.49885	0.94242
C	1.76232	-0.65826	2.05791
C	3.12211	1.40491	0.76799

C	3.10737	-0.83301	1.7209
C	3.78915	0.20315	1.06619
H	3.67208	2.24357	0.39503
H	3.61929	-1.73477	1.9848
H	4.82065	0.08507	0.8074
O	1.04401	2.70842	0.61602
O	-0.77282	2.47437	2.36846
C	-1.67312	3.57831	2.24375
H	-2.60764	3.32986	2.7018
H	-1.25523	4.43588	2.72833
H	-1.83013	3.79522	1.20781
C	1.9116	3.82455	0.8313
H	1.39571	4.72961	0.58709
H	2.21109	3.85066	1.85821
H	2.77721	3.72856	0.20967
C	-0.13384	-1.39515	-0.69933
H	-0.10263	-0.8322	-1.60872
H	0.85023	-1.4735	-0.28661
C	1.19512	-1.56278	3.23364
H	0.12576	-1.59962	3.22938
H	1.54021	-1.10486	4.13702
C	-0.65305	-2.80799	-1.01406
H	-1.65166	-2.77824	-1.39723
H	-0.02407	-3.28986	-1.73316
C	1.73298	-3.01306	3.1642
H	2.75697	-2.98111	2.85546
H	1.66623	-3.51157	4.10864
C	0.8351	-3.76297	2.20191
C	-0.59302	-3.51918	0.29077
H	-1.2289	-3.0051	0.9809
H	-0.90894	-4.53902	0.21979

C	0.8598	-3.42583	0.75575
H	1.4976	-4.07087	0.1883
H	1.20487	-2.41831	0.65217
O	0.02333	-4.62205	2.63388



Homodesmotic Product IV.41

C	-1.70304	1.14848	-1.32814
C	-0.8525	0.12486	-1.76691
C	-0.67541	-0.09946	-3.13879
C	-1.34664	0.70189	-4.07192
C	-2.19705	1.72586	-3.6332
C	-2.37559	1.94882	-2.26132
H	-1.83887	1.31925	-0.28063
H	-2.71007	2.33737	-4.3457
H	-3.0254	2.7302	-1.9263
C	3.21179	-0.74554	2.48311
C	2.77854	0.51593	2.05386
C	3.43739	-1.76474	1.5483
C	2.56883	0.75775	0.68945
C	3.22725	-1.52347	0.18392
C	2.79279	-0.26202	-0.24545
H	2.23765	1.72086	0.3615
H	3.39864	-2.30187	-0.52992
H	2.63203	-0.07756	-1.28719
O	2.55052	1.55604	3.00819
O	-1.16435	0.47495	-5.47187
C	-2.35264	0.84928	-6.17365
H	-2.55575	1.88591	-6.00321

H	-2.21638	0.68001	-7.22127
H	-3.17492	0.26216	-5.8214
C	2.80908	2.82485	2.40154
H	2.63891	3.60304	3.11593
H	3.82587	2.86109	2.07019
H	2.15623	2.95984	1.56473
C	-0.11204	-0.75362	-0.74172
H	0.81959	-1.07711	-1.1566
H	0.07097	-0.18712	0.14738
C	3.91653	-3.14909	2.02295
H	3.54447	-3.3357	3.00861
H	4.98629	-3.17089	2.03508
C	-0.97476	-1.98225	-0.39989
H	-1.90658	-1.66021	0.01542
H	-1.15741	-2.54805	-1.28975
C	3.39215	-4.23391	1.06351
H	3.76368	-4.04863	0.07728
H	3.72621	-5.19446	1.39596
C	1.85239	-4.2039	1.04603
C	-0.23241	-2.86114	0.6237
H	-0.05146	-2.29663	1.51445
H	-0.83024	-3.71675	0.85903
C	1.11029	-3.32086	0.02574
H	0.92946	-3.88293	-0.86651
H	1.70853	-2.46472	-0.20693
O	1.20034	-4.90165	1.86546
C	0.25609	-1.22698	-3.62073
C	1.19231	-0.97763	-4.63324
C	0.1671	-2.50247	-3.04703
C	2.03971	-2.00399	-5.07221
H	1.26016	-0.00372	-5.07128

C	1.01393	-3.52902	-3.48649
H	-0.54749	-2.69271	-2.27361
C	1.95035	-3.27983	-4.49909
H	2.75486	-1.81348	-5.84504
H	0.94544	-4.50322	-3.04904
H	2.59701	-4.06355	-4.83448
C	3.44015	-1.01332	3.98242
C	4.73446	-1.25963	4.45967
C	2.35488	-1.0112	4.86925
C	4.94389	-1.50435	5.82348
H	5.56308	-1.26089	3.78268
C	2.56429	-1.25584	6.23339
H	1.36654	-0.82283	4.50517
C	3.85885	-1.50251	6.71053
H	5.93246	-1.69256	6.18765
H	1.73571	-1.25425	6.91069
H	4.01878	-1.68948	7.75198

IV.5. Bridge to Chapter V.

With the completion of Chapter **IV** we had scalable size-selective syntheses capable of providing large quantities even the most strained nanohoops. As discussed in chapter **I**, the smaller more strained nanohoops had properties more advantageous for electronic applications. However, the energetics of these smaller carbon based nanohoops were not tunable over a wide range of optical and electronic properties. Chapter **V** discusses the application of classic donor-acceptor systems in the nanohoop architecture in order to further tune the properties of [8]CPP. These experimental results were then leveraged to elucidate design principles for future donor-acceptor nanohoops.

CHAPTER V

SYNTHESIS, PROPERTIES, AND DESIGN PRINCIPLES OF DONOR–ACCEPTOR NANOHOOPS

Chapter V is based on published work in *ACS Central Science* (2015). The manuscript was written by myself and was edited by Professor Ramesh Jasti. The synthesis of nitrogen containing nanohoops was contributed by Dr. Elizabeth Hirst and myself. All remaining compounds were synthesized by myself. The electrochemical studies were performed by Dr. Christopher Weber and Professor Mark Lonergan. X-ray crystallography was performed by Dr. Lev Zakharov.

We have synthesized a series of aza[8]cycloparaphenylenes containing one, two, and three nitrogens to probe the impact of nitrogen doping on optoelectronic properties and solid state packing. Alkylation of these azananohoops afforded the first donor–acceptor nanohoops where the phenylene backbone acts as the donor and the pyridinium units act as the acceptor. The impact on the optoelectronic properties was then studied experimentally and computationally to provide new insight into the effect of functionalization on nanohoops properties.

V.1. Introduction.

Alternative energy technologies are needed to address increasing worldwide energy demands.¹ Organic materials are poised to play a significant role in these technologies with research focusing on their ability to harvest (organic photovoltaics, OPVs), transport (organic field-effect transistors, OFETs, and molecular wires), and store energy (batteries and capacitors).² Research in polymeric and small molecule based organic electronics has received a dramatic upsurge in recent years for their potential use as lightweight and flexible electronic materials.³ Organic small molecules are relatively cheap, structurally defined, and can be functionalized to systematically study structure–property relationships. Although many strides have been made in the small molecules used to this end, the scaffold diversity is still low with the majority of research focusing on fullerene, oligothiophene, or acene-like motifs. With an understanding of the fundamental phenomena governing charge transport emerging, a more diverse toolbox of organic scaffolds is needed to guide future materials research.⁴

[n]Cycloparaphenylenes ([n]CPPs) possess a unique architecture of fully conjugated bent benzenes linked in the para position to form a nanohoop.⁵ This nanohoop architecture imparts several advantageous properties in relation to their linear counterparts. First, they have a narrowing highest occupied molecular orbital (HOMO)–lowest unoccupied molecular orbital (LUMO) energy gap as the number of benzene units is decreased. This trend is in stark contrast to linear conjugated materials, including poly(*para*-phenylenes) (PPPs), which have a narrowing HOMO–LUMO energy as the molecule becomes larger.⁶ **Figure V.1.** illustrates this dramatic effect where the HOMO–LUMO energy gap for PPPs are comparable to [18]CPP but over an electronvolt (eV) larger than that of [5]CPP.⁷ The calculated energy level deviation can be explained by a strain-induced minimization of the biaryl dihedral angles as the nanohoops become smaller,⁸ which effectively increases conjugation around the hoop. In addition, the smaller nanohoops have increased quinoidal character,⁹ which is also advantageous for charge transport in conjugated systems. Another advantage is the unique solid-state architecture of these compounds which pack into long-range channels with multiple close π – π contacts. The curved nature of these nanohoops also affords a significant increase in solubility without the need for additional solubilizing chains.¹⁰ Finally, the cyclic “infinite” conjugation afforded by the nanohoops framework renders them electronic hybrids between polymers and small molecules.

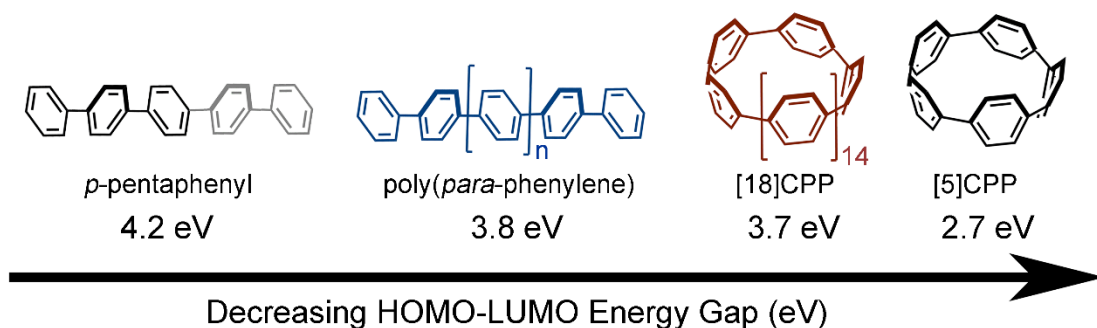


Figure V.1. Wrapping a Linear Polymer into a Cyclic Isomer Leads to Dramatic Modulation of the Electronic Structure. Calculated HOMO–LUMO Energy Gaps are Taken from Reference 7.

Significant effort has been devoted to altering the electronic properties of carbon materials, better tailoring them to specific applications. Doping of materials with a noncarbon element such as nitrogen, boron, phosphorus, or silicon has been one approach

to modify properties.¹¹ Nitrogen doping in particular has been shown to not only enable tuning of electronics but also introduce novel reactivity into these materials. The top-down synthesis of nitrogen-doped carbon nanotubes (CNTs) has led to significant modulation of various properties. Top-down nitrogen doping techniques, however, lead to a number of possible structures as illustrated in **Figure V.2.a.** making direct structure–property relationships difficult to study. Bottom-up organic chemistry approaches, on the other hand, such as those used to access azafullerene (**Figure V.2.b.**), have allowed in-depth studies of these “doped” systems and have facilitated the design of new materials.¹² Although heteroatom incorporation in carbon nanostructures has previously been achieved,¹³ donor–acceptor systems have not been investigated.¹⁴ Herein, we report the bottom-up synthesis of a family of aza[8]CPPs and their donor–acceptor alkylated counterparts—structures in which the pyridinium unit serves as an electron-poor acceptor, and the bent phenylene unit is the electron-rich donor (**Figure V.2.c.**). The effects of structural modifications on optical and electronic properties are presented in the context of experimental and computational studies. In addition, we provide a platform for the design of future donor–acceptor nanostructures with tailored electronic and optical properties.

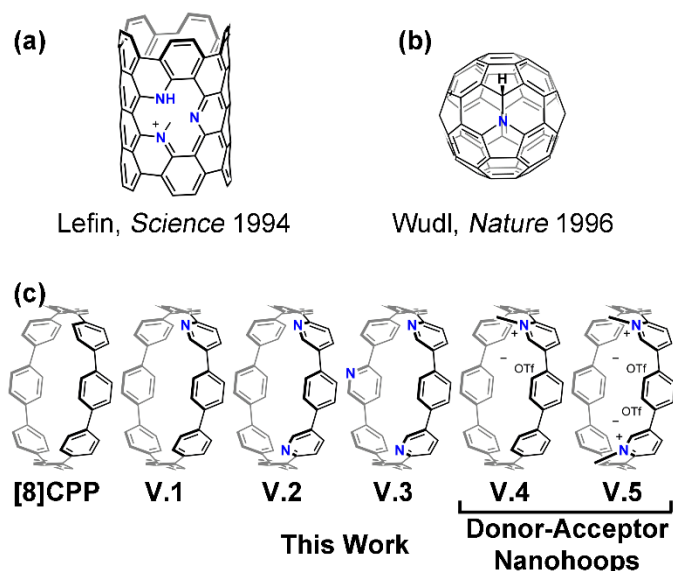
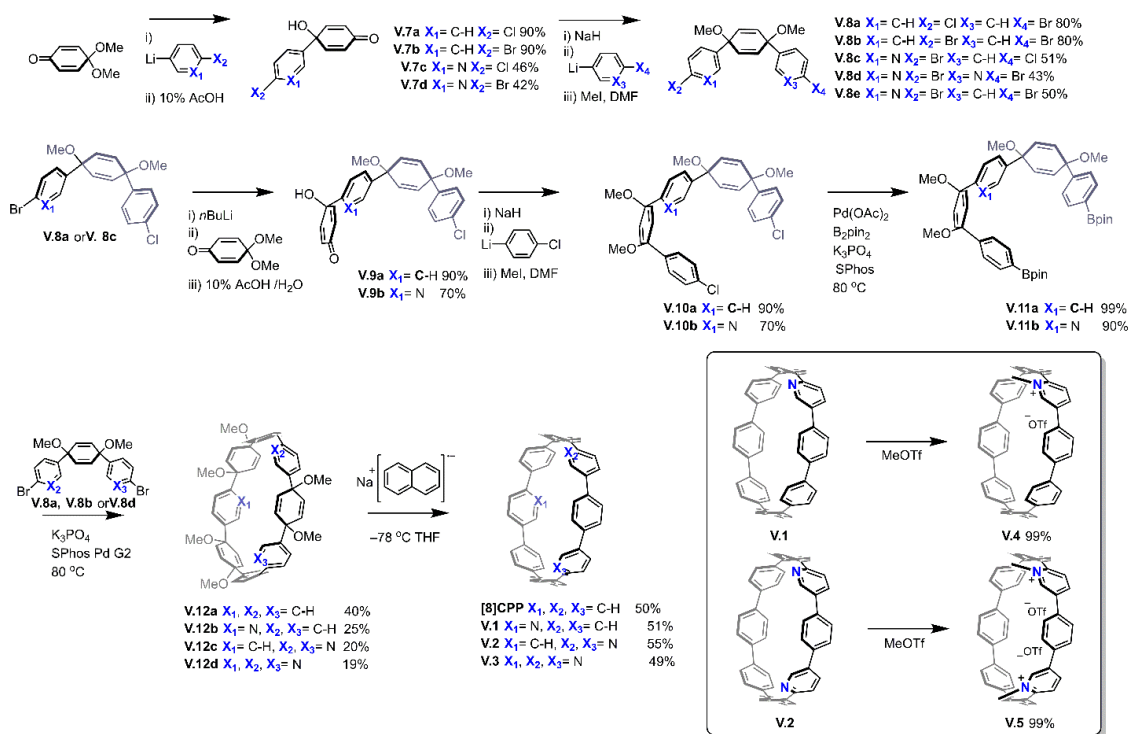


Figure V.2. (a) Nitrogen Doped CNT. (b) Azafullerene. (c) Targeted Compounds **V.1** Aza[8]CPP, **V.2** 1,15-Diaza[8]CPP, **V.3** 1,15,31-Triaza[8]CPP, **V.4** N-methylaza[8]CPP Triflate, and **V.5** N,N-dimethyl-1,15-diaza[8]CPP Ditriflate.

V.2. Results and Discussion.

V.2.1. Synthesis of Aza-and Donor–Acceptor Nano hoops.

Synthesis of nitrogen-doped CPPs was achieved by a scalable and modular route that leverages the inherent orthogonal reactivity of aryl chlorides and bromides to lithium halogen exchange. The synthesis relies on the construction of a dihalo or diboronate macrocyclic precursors containing oxidatively dearomatized cyclohexadiene moieties as masked arenes.¹⁷ Macrocyclization is then achieved by Suzuki-Miyaura crosscoupling reactions followed by a reductive aromatization step to achieve the final nitrogen doped nano hoop structures. The synthesis of key three-ring intermediates **V.8a–e** is summarized in **Scheme V.1** and began with the addition of either 4-chlorophenyllithium, 4-bromophenyllithium, 6-chloro-3-pyridinyl lithium, or 6-bromo-3-pyridinyl lithium to benzoquinone monoketal followed by acid-catalyzed ketal deprotection to give aryl quinols **V.7a–d** in moderate to excellent yields. Quinols **V.7a–d** were then deprotonated with sodium hydride and subjected to nucleophilic addition by the appropriate lithio haloarene to give the syn three-ring fragments **V.8a–e** after in situ alkylation with methyl iodide. Note that regioselective lithiation of 2,5-dibromopyridine was selectively achieved in the 5-position under kinetic control in coordinating solvents such as THF as detailed by Wang et al.¹⁸ X-ray crystallographic analysis of **8e** confirmed the position of the nitrogen atoms and the syn configuration of the arenes ([Supplementary Figure V.10.](#)). Compounds **V.8a** and **V.8c** were then treated with *n*-butyllithium and quenched with quinone monoketal followed by acid catalyzed ketal deprotection to give four-ring quinols **V.9a** and **V.9b** respectively. Quinols **V.9a** and **V.9b** were then treated with sodium hydride and subjected to nucleophilic addition of 4-bromophenyllithium followed by alkylation with methyl iodide to afford five-ring dichlorides **V.10a** and **V.10b**. Five-ring dichlorides **V.10a** and **V.10b** were then transformed to the corresponding bisboronates **V.11a** and **V.11b** through a Miyaura borylation with Pd(OAc)₂, SPhos, and B₂Pin₂. The iterative construction of the macrocyclic precursors allows for the possibility of the introduction of a wide variety of heteroaromatics at varying positions.



Scheme 1. Synthesis of [8]CPP and Targets aza[8]CPPs **V.1–3** and Donor–Acceptor aza[8]CPPs **V.4** and **V.5**.

Suzuki-Miyaura cross-coupling of five-ring bisboronates (**V.11a** or **V.11b**) and three-ring dibromides (**V.8a**, **V.8b**, or **V.8d**) was achieved using Buchwald's second generation SPhos precatalyst to give macrocycles **V.12a–d** in moderate yield (**Scheme V.1**). These macrocycles were then subjected to sodium naphthalenide at $-78\text{ }^\circ\text{C}$ to give [8]CPP, aza[8]CPP (**V.1**), 1,15-diaza[8]CPP (**V.2**), and 1,15,31-triaza[8]CPP (**V.3**). Aza-CPPs **V.1** and **V.2** were then treated with methyl triflate in dry dichloromethane to afford the donor–acceptor monoalkylated N-methylaza[8]CPP triflate **V.4** and N,N-dimethyl-1,15-diaza[8]CPP ditriflate **V.5** quantitatively. Peralkylation of triaza[8]CPP **V.3** did not cleanly afford N,N,N-trimethyl-1,15,31-triaza[8]CPP tritriplate, but rather a complex mixture of inseparable and unidentifiable compounds. Compounds **V.1–5** were thoroughly characterized using ^1H and ^{13}C NMR spectroscopy and mass spectrometry (see [Supporting Information](#)).

V.2.2. Solid-State Packing Morphology of Aza-and Donor– Acceptor Nanohoops.

Single-crystal X-ray structure determination was performed on compounds **V.1** and **V.5**. **Figure V.3.** shows the ORTEP, packing structure, and unique interactions for each compound. Packing motifs of organic materials are critical for understanding intermolecular charge transport.⁴ We were curious to how nitrogen incorporation would affect the nanohoop solid-state packing that is typically observed. The nitrogen in **V.1** is found to be disordered over all 32 possible locations in the solid state. The impact of simple nitrogen incorporation into the [8]CPP backbone is minimal and results in a nearly identical herringbone crystal packing observed for [8]CPP in previous reports (**Supplementary Figure V.13.**)^{17b} Attempts were made to order the nitrogen distribution in the solid state using cocrystallants; however these efforts resulted in similar disorder. In contrast, compound **5** had a dramatically different packing structure compared to **V.1–V.3** and any previously reported [n]CPP. Donor–acceptor nanohoop **V.5** was found to be ordered adopting a trans relationship for the Nmethylpyridinium triflate rings. Each nanohoop in the crystal structure has one face centered donor–acceptor interaction between its own pyridinium ring and a neighbor’s electron-rich phenylene ring. The shortest contacts between these neighboring subunits is 3.35 Å and is highlighted in **Figure V.3.c**. This head to tail packing results in a 2D plane as shown in **Figure V.3.b**. The layers that make up the third dimension of the crystal structure form tubular channels similar to those seen in the solid state packing of [6]CPP.¹⁹ Although the charge transport in nanohoops has not been explored yet, access to multiple packing motifs will help guide future design. The dipole moments of these alkylated nanohoops (SI Computational Coordinates) far exceed any previously reported nanohoops and serve as a new supramolecular design motif for their solid-state structures.

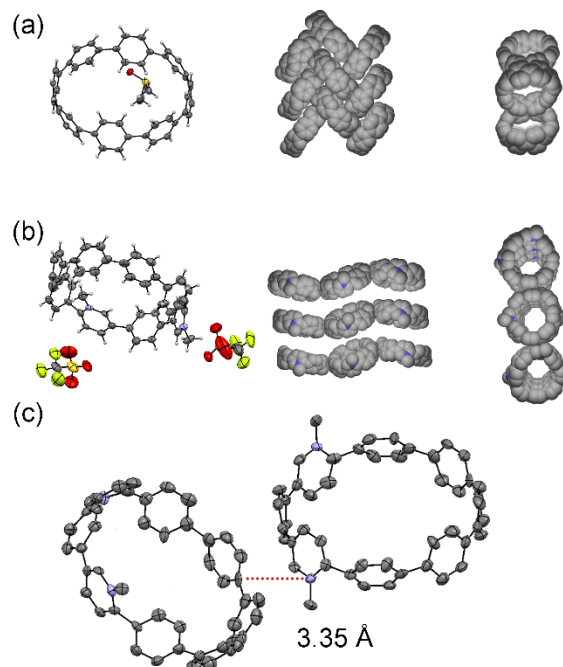


Figure V.3. ORTEP, Side-on Packing, and Top-Down Packing of (a) **V.1** and (b) **V.5**. (c) Head to Tail Interaction Between One Pyridinium Acceptor and a Neighboring Electron-rich Phenylene Donor in Compound **V.5**.

V.2.3. Electrochemical Properties of Aza- and Donor– Acceptor Nano hoops.

A primary goal of this study was to effectively lower the LUMO energy to levels more appropriate for functional electronic materials such as the n-type semiconductor C_{60} . Cyclic voltammetry (CV) was used to probe the reduction properties of [8]CPP and compounds **V.1– V.5**. Oxidations fell outside of the solvent window and thus were not reported. The cathodic peak potentials for the reduction of [8]CPP and **V.1– V.3** were recorded as -2.44 V, -2.39 V, -2.32 V, and -2.39 V respectively versus the ferrocene/ferrocenium couple. Compound **V.4** has a cathodic peak potential at -1.49 V, while **V.5** had two reduction events with peak potentials recorded at -1.36 V and -1.49 V versus the ferrocene/ferrocenium couple. The voltammograms for these compounds are illustrated in **Figure V.4**.

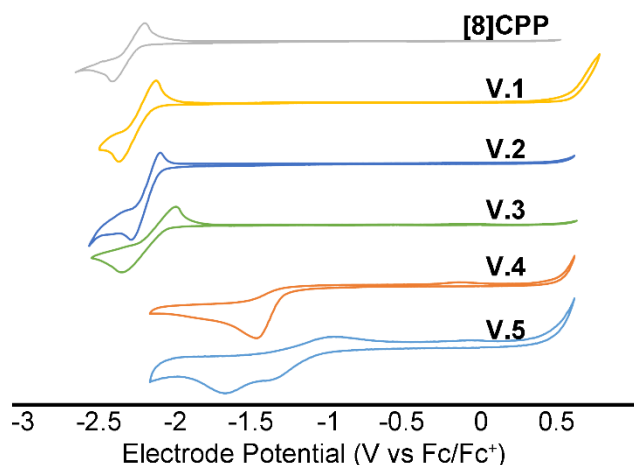


Figure V.4. Cyclic Voltammetry of [8]CPP and **V.1– V.5**.

In order to better understand these effects, we turned to density function theory (DFT) computational analysis (**Figure V.5**). As nitrogen content increases, calculations show a steady decrease in both HOMO and LUMO energies of approximately 0.07 eV from [8]CPP to **V.1**, **V.2**, and **V.3**. Visualization of the HOMO and LUMO orbitals showed nearly complete delocalization around the entire hoop showing a slight increase in the orbital coefficient around the nitrogen containing rings. The similar lowering of both the HOMO and LUMO orbital energies can be rationalized by the similar coefficients localized on the nitrogen for either frontier orbital. Although this nitrogen doping can fine-tune the orbitals energies, it is not sufficient to dramatically alter either the HOMO or LUMO.

Alkylation of these compounds, however, results in a dramatic shifting to less negative cathodic peak potentials in accordance with DFT predictions (**Figure V.5**). Alkylated compounds **V.4** and **V.5** as well as computationally investigated compound N,N,N-trimethyl-1,15,31-triaza[8]CPP (**V.6**) show a dramatic lowering of the LUMO energy level by 1.00, 1.15, and 1.36 eV respectively relative to [8]CPP. This trend again follows the experimental reduction values for **V.4** and **V.5**, which show a dramatic lowering of the cathodic peak potential. Advantageously, this lowering effect was less impactful on the HOMO energy levels of nanohoop **V.4** and **V.5**, resulting in a decreased HOMO energy by only 0.200 and 0.470 eV, respectively, and a net narrowing of the HOMO–LUMO energy gap. In contrast, the theoretical triply alkylated **V.6** HOMO energy is lowered substantially by 1.15 eV. Visualization of the HOMO and LUMO

orbitals helps explain these trends. In both the mono- and bis-alkylated structures, **V.4** and **V.5**, there is a significant dipole moment and localization of the LUMO on the N-methylpyridinium core. The HOMO meanwhile is localized on the bent, electron-rich phenylene backbone with orbital coefficients reaching the highest values directly opposite the N-methylpyridinium rings. Because of minimal contribution from the N-methylpyridinium core, the HOMO energies of **V.4** and **V.5** are very similar to neutral analogues **V.1**– **V.3**, as well as [8]CPP. The separation of the HOMO and LUMO orbital densities is consistent with a donor–acceptor nanostructure motif (vide infra). The calculated triply alkylated **V.6** on the other hand has a much lower dipole moment, and the HOMO and LUMO orbitals are localized evenly over both the phenylene and pyridinium sections. This results in a simultaneous lowering of the HOMO and LUMO orbital energies by over 1 eV therefore maintaining a similar HOMO–LUMO energy gap as the parent compound 1,15,31-triaza[8]CPP (**V.3**). These results suggest that the position of the N-methylpyridinium rings in relation to one another plays a dramatic role in modulation of the frontier molecular orbital energies (vide infra).

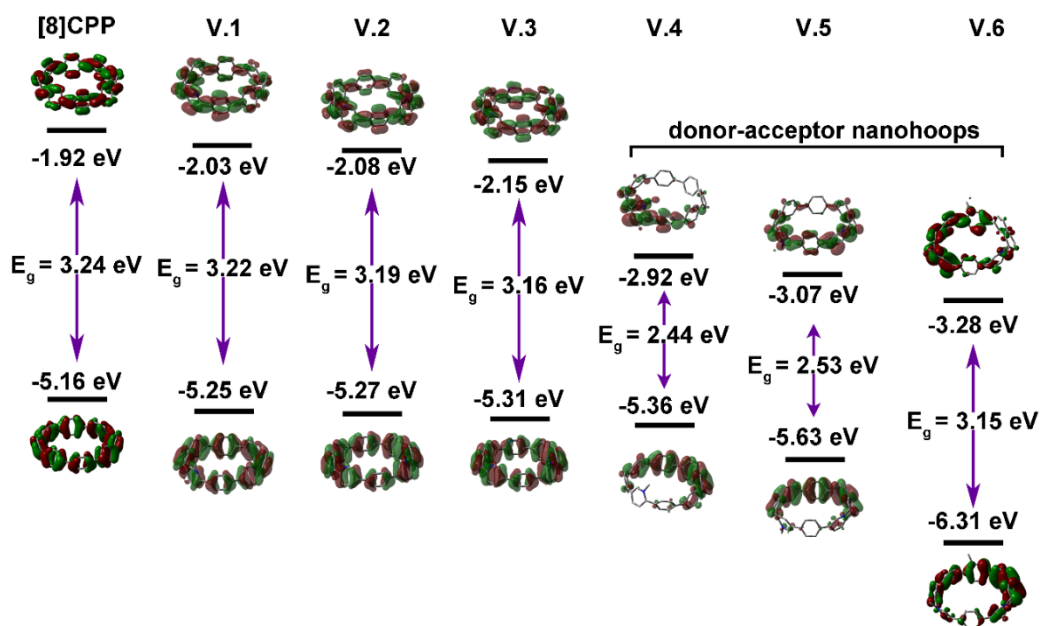


Figure V.5. DFT Calculated HOMO and LUMO Energy Levels and Orbital Distributions for [8]CPP and Nanostructures **V.1**– **V.6**.

V.2.4. Optical Properties of Aza-and Donor–Acceptor Nano hoops.

All [n]CPPs share a common absorbance maximum at 340 nm and show little if any absorbance in the visible spectrum.^{5b} We sought to explore the impact of nitrogen and donor–acceptor incorporation on the optical properties of nano hoops. The UV–vis absorption and fluorescence spectra of [8]CPP and compounds **V.1– V.3** in dichloromethane (DCM) are depicted in **Figure V.6**. Time-dependent density functional theory (TD-DFT) was used to gain a more in depth understanding of the photophysical trends with major transitions depicted in **Figure V.7**. Orbital contributions to major and minor absorbances are outlined in the [Tables V.2.–V.4](#). The major absorption for [8]CPP is 340 nm ($\epsilon = 1.0 \times 10^5 \text{ M}^{-1} \text{ cm}^{-1}$). This absorbance is comprised of four degenerate transitions, HOMO \rightarrow LUMO +1, HOMO \rightarrow LUMO+2, HOMO–1 \rightarrow LUMO, and HOMO–2 \rightarrow LUMO (red transitions in **Figure V.7.a**). Although the HOMO \rightarrow LUMO transition is formally Laporte forbidden with conservation of HOMO and LUMO orbital symmetry, it is still observed as a slight shoulder centered at 400 nm ($\epsilon = 8.5 \times 10^2 \text{ M}^{-1} \text{ cm}^{-1}$) (purple transition in **Figure V.7.a**). The addition of nitrogen breaks the symmetry of the molecule and thus the degeneracy between the HOMO-1 and HOMO-2 as well as the LUMO-1 and LUMO-2 orbital energies. Increasing nitrogen content in **V.1**, **V.2**, and **V.3** leads to a slight red-shifting of major absorbance to 345 nm ($\epsilon = 2.5 \times 10^5 \text{ M}^{-1} \text{ cm}^{-1}$), 349 nm ($\epsilon = 7.30 \times 10^5 \text{ M}^{-1} \text{ cm}^{-1}$), and 353 nm ($\epsilon = 8.94 \times 10^5 \text{ M}^{-1} \text{ cm}^{-1}$) respectively. These absorbances are attributed to the same combination of the HOMO-1 \rightarrow LUMO, HOMO-2 \rightarrow LUMO, HOMO \rightarrow LUMO+1, and HOMO \rightarrow LUMO+2 transitions (red transitions in **Figure V.7.b**) as observed for [8]CPP. The slight red-shifting of these transitions relative to [8]CPP can be accounted for by the increasing electronegative nitrogen content having a slightly greater effect on the LUMO than the HOMO. The shoulder peaks for [8]CPP and aza CPPs **V.1– V.3** around 400 nm have a measured extinction coefficient (ϵ) of $2.5 \times 10^3 \text{ cm}^{-1} \text{ M}^{-1}$, $7.3 \times 10^3 \text{ cm}^{-1} \text{ M}^{-1}$, and $8.9 \times 10^3 \text{ cm}^{-1} \text{ M}^{-1}$, respectively. These lower energy transitions are assigned to the HOMO–LUMO absorbances (purple transitions in **Figure V.7.b**) which have larger oscillator strengths and extinction coefficients over an order of magnitude larger than observed for [8]CPP. The emission for [8]CPP was reported at 533 nm.²⁰ In accordance with the red-shifted absorbance, the fluorescence for compounds **V.1**, **V.2**, and **V.3** are slightly shifted to 541,

544, and 542 nm, respectively. Similar to the solid-state packing and cathodic peak potentials, simple nitrogen incorporation has a marginal effect on the photo-physical properties of these compounds. This minimal modulation of optical and electronic properties is consistent with other reported modified nano hoops that have high symmetry.

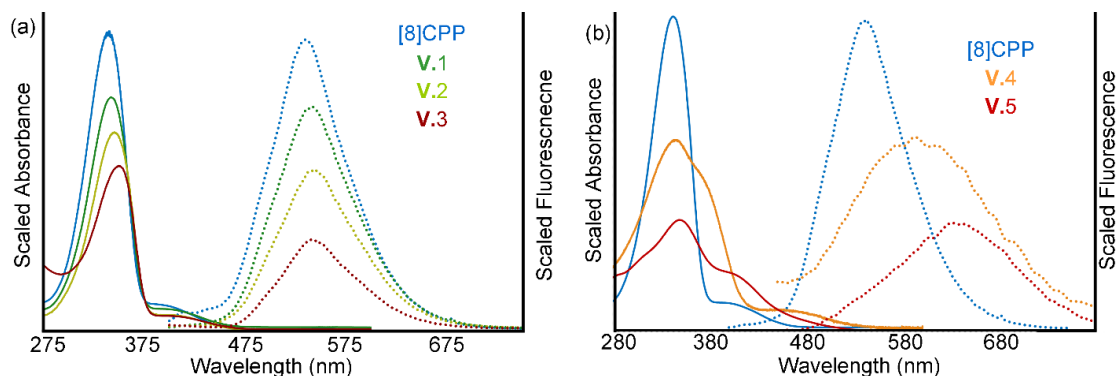


Figure V.6. (a) Scaled (For Clarity) UV–Vis Absorbance (Solid Lines) and Fluorescence (Dashed Lines) of Compounds [8]CPP (Blue), Aza[8]CPP **V.1** (Green), 1,15-Diaza[8]CPP **V.2** (Yellow), and 1,15,31-Triaza[8]CPP **V.3** (Red) in Dichloromethane. (b) Scaled (For Clarity) UV–Vis (Solid Lines) and Fluorescence (Dashed Lines) for Compounds [8]CPP (Blue), N-methylaza[8]CPP Triflate **V.4** (Orange), and N,N-dimethyl-1,15-diaza[8]CPP Ditriflate **V.5** (Red) in Dichloromethane.

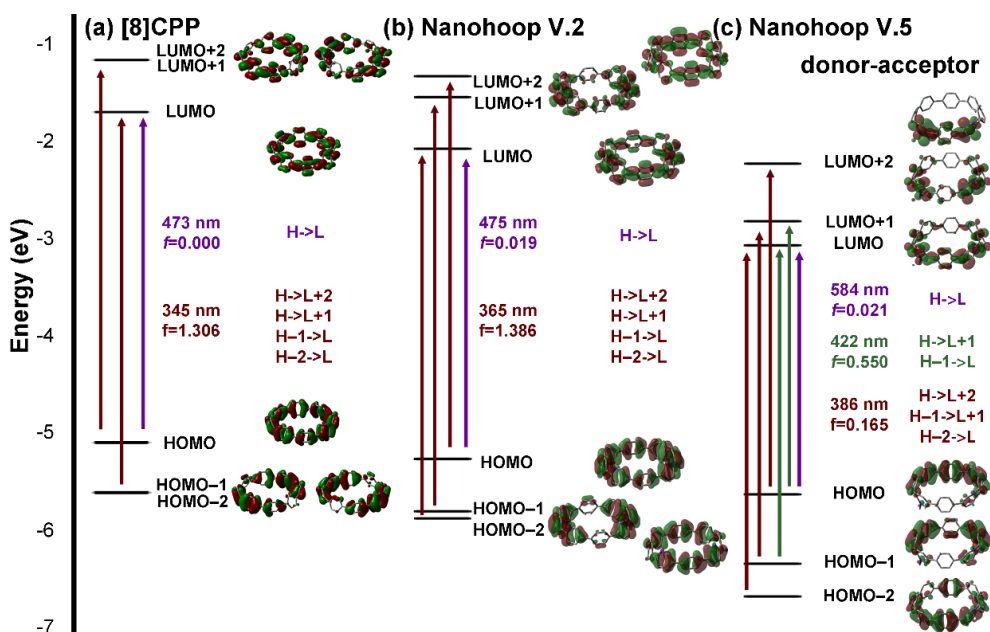


Figure V.7. TD-DFT Orbital Transitions for (a) [8]CPP, (b) 1,15-Diaza[8]CPP **2**, and (c) N,N-dimethyl-1,15-diaza[8]CPP Ditriflate **V.5**. Pictorial Orbital Transitions for **V.1**, **V.3**, and **V.4** are Found in [Figure V.26](#).

Table V.1. Experimental Cathodic Peak Potentials, Maximum Absorbance, Extinction Coefficients, and Emission Maxima for [8]CPP and **V.1– V.5**.

Compound	Cathodic Peak Potential Fc/Fc+ (V)	Max Absorbance (nm)	Extinction Coefficient (M-1 cm-1)	Emission Maximum (nm)
[8]CPP	-2.44	341	1.00E+05	533
V.1	-2.39	345	2.81E+04	541
V.2	-2.32	349	9.21E+04	544
V.3	-2.39	353	1.13E+04	542
V.4	-1.49	345	2.90E+04	598
V.5	-1.36	350	4.91E+04	630

V.3. Methods.

The synthesis and characterization of all new compounds were executed by standard methods and are fully described in the experimental details. The effects of nitrogen incorporation on the electronic structure and properties of [8]CPP were explored in detail for the target molecules **V.1- V.5** using density function theory (DFT) calculations at the B3LYP/6-31g* level of theory using *Gaussian 09*.¹⁵ Ground state geometry optimizations were first performed in the gas phase. Although geometries and orbital densities from these calculations have been shown to correlate well with experimental values, the addition of charged species are known to give inaccurate values for orbital energies. In the gas phase, charged species have high electrostatic interactions, which cause the calculated orbital energies to be inaccurate. Mujica et al. recently showed that this discrepancy can be corrected by minimizing each geometry in the gas phase while omitting the counter ion for charged species.¹⁶ A solvated (acetonitrile) single point energy calculation is then performed using the conductor-like polarization continuum model (CPCM). This method gives stronger correlation between computed frontier orbitals and experimental reduction and oxidation values for both charged and neutral aromatic species. In accordance with this report, all compounds in this work were treated with the outlined workflow described above. Time-dependent density functional theory (TD-DFT) was used to predict and assign optical absorbances again using CPCM with acetonitrile as the solvent. The computed values are redshifted in relation to the experimental spectra. This trend is commonly observed, however, the peak shape and relative intensity matched the experimental results allowing assignment of optical transitions.

V.4. Significance and Outlook.

At the outset of this project, we aimed to use nitrogen incorporation to theoretically and experimentally explore the impact on the HOMO and LUMO energy levels of nanohoops. Gratifyingly we were able to elucidate a strategy that can lower the LUMO energy independent of the HOMO energy in the case of the higher dipole structures **V.4** and **V.5** resulting in a net lower HOMO-LUMO energy gap. The LUMO orbital energy levels achieved through alkylation of the aza[8]CPP are on the cusp of the desirable range of -3.0 eV to -4.0 eV for use as organic electronic materials.²² Also we find that by incorporating multiple *N*-methylpyridinium units in a highly symmetric structure (**V.6**) we are able to drop both the LUMO and HOMO energies equally, a feature that is important when designing organic devices with high open circuit voltages (V_{oc}). With these results and basic understanding in hand, we attempted to further probe the concept of the donor-acceptor nanohoop in order to guide future design.

With the difficulties associated with the synthesis of triply alkylated structure **V.6**, we sought to explore the possibility of attaining similar HOMO-LUMO energy levels by changing the relative positioning in the doubly alkylated diaza[8]CPP scaffold. This effect was computationally studied by changing the relative pyridinium position in the *N,N*-dimethyl-*x,y*-diaza[8]CPP scaffold where *x* and *y* represent the relative position of each nitrogen in the hoop (**Figure V.8.**). The three regioisomers shown, in addition to compound **V.5**, highlight the importance of the relative positioning of the acceptor groups. The (1,8) isomer (**Figure V.8.a.**) has the lowest lying LUMO with orbital localization primarily on the electron-poor pyridinium rings. The HOMO remains localized on the bent, electron-rich phenylene backbone maintaining an energy closer to neutral compound **V.5**. This gives a HOMO-LUMO energy gap of 1.7 eV, a value that coincides with a significant increase in the calculated absorption in the visible spectrum (**Figure V.27.**). When the pyridinium rings are opposite one another in the (1,27) position (**Figure V.8.c.**), a significant increase in orbital coefficients is observed for the HOMO and LUMO on both the pyridinium and phenylene sections resulting in a lowering of both energies, while maintaining a HOMO-LUMO energy gap around 3.0 eV. These results emphasize the need to construct nanohoops with high dipole moments rather than high symmetry, as has been primarily investigated, in order to attain low HOMO-LUMO

energy gap materials.^{13b, 23} This aspect offers yet another control element when designing future donor-acceptor nanohoops.

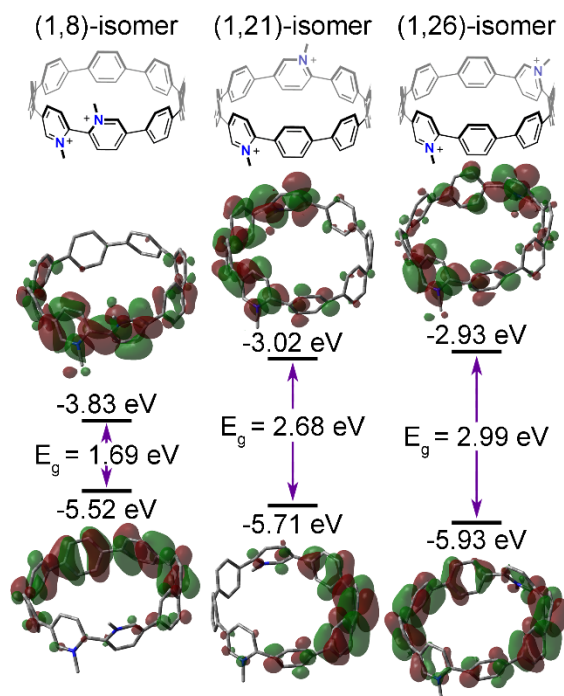


Figure V.8. Theoretical HOMO and LUMO Energies for (a) N,N-dimethyl-1,8-diaza[8]CPP, (b) N,N-dimethyl-1,21-diaza[8]CPP, and (c) N,N-dimethyl-1,26-diaza[8]CPP.

The use of alternating donor and acceptor moieties in organic materials is ubiquitous in both polymeric and small molecule organic electronics and is often used to construct chromophores and narrow HOMO-LUMO energy gaps.²⁴ In the current study, the *N*-methylpyridinium ring acts as the acceptor and the strained paraphenylene backbone serves as the donor. To assess the generality of this finding, we computationally explored a common donor benzodithiophene (BTD) and acceptor benzothiadiazole (BT) in the context of [6]cycloparaphenylene ([6]CPP) and linear [6]oligophenylene ([6]OPP) (**Figure V.9**). As shown, [6]CPP has 1.01 eV narrower HOMO-LUMO energy gap compared to [6]OPP. As expected, the LUMO energy drops for both [6]OPP and [6]CPP when the acceptor BT is incorporated. Interestingly, the addition of the donor BTD leads to a raising of the HOMO energy for the linear [6]OPP, but has little to no effect on the cyclic [6]CPP. Finally, incorporation of both the donor BTD and the acceptor BT leads to a raising of the HOMO energy and lowering in the LUMO energy for the linear [6]OPP,

but only a lowering of the LUMO energy in the case of the cyclic [6]CPP. The HOMO-LUMO energy gap for the donor-acceptor [6]OPP drops to 2.70 eV while the HOMO-LUMO energy gap for the donor-acceptor cyclic [6]CPP remains nearly identical to the BT substituted [6]CPP. This result suggest that the bent CPP backbone itself is a good donor and that addition of complex donor heterocycles is unnecessary therefore simplifying synthetic efforts towards donor-acceptor nanohoops. Advantageously, the bent phenylene backbone acts as a good donor on its own where donor strength can be tuned by changing the size of the hoop. These findings highlight the importance of exploring acceptor-containing nanohoops in future materials.

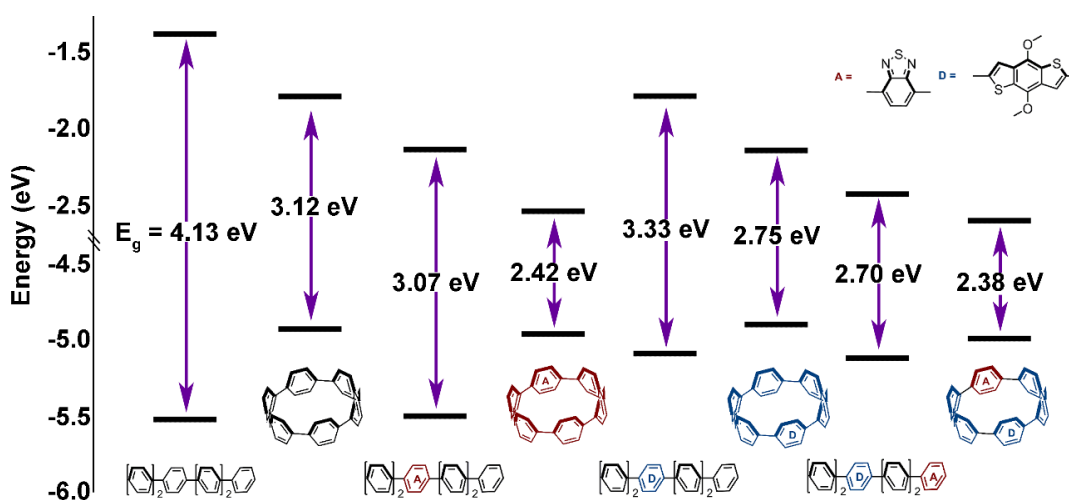


Figure V.9. The Effect of Acceptor (Red), Donor (Blue), and Donor-Acceptor Moieties on the HOMO and LUMO Energies of [6]CPP and Linear [6]OPP Frameworks.

V.5. Conclusion.

In conclusion, the modular syntheses of aza[8]CPPs were developed in order to probe the impact of nitrogen doping on nanohoop optical, electronic, and solid state properties. Increasing nitrogen content led to a slight red shifting in both the absorbance and fluorescence and dropped the cathodic peak potential for reduction on average by 0.07 V. Similar to its modulation of the optical and electronic properties, nitrogen content had little influence on the solid state structure of the nanohoops. Further alkylation of these aza-nanohoops, however, afforded donor-acceptor nanohoops resulting in increased absorbance in the visible spectrum and over a 0.5 V decrease in cathodic peak potential. The high dipole moment (through-bond and through-space) of the alkylated aza-

nanohoops afforded topologically unique solid-state nanohoop packings. The synthesis and characterization of these aza-nanohoops has led to a deeper understanding of the impact of structural modification on the optical and electronic properties of these nanohoops. We find that incorporation of electron-poor acceptors has a more dramatic effect on the electronic structure of nanohoops than incorporation of electron-rich moieties. This feature implies that the bent phenylene architecture intrinsically acts as a good donor, and donor strength can be tuned by nanohoop size. In addition, relative positioning of multiple acceptor groups leads to nanohoops with dramatically different properties. With the ability to modularly construct novel nanohoops and with emerging strategies to introduce functional groups in a mild manner, we have begun to target and examine the donor-acceptor structures with the most promising electronic features.^{5, 25} We anticipate that the donor-acceptor nanohoop architecture will be an important additional tool in the organic materials chemistry tool box.

V.6. Experimental Details.

V.6.1. General Experimental Details.

Moisture sensitive reactions were carried out under an inert atmosphere of nitrogen using standard Schlenk technique. 2,5-dibromopyridine was purchased from Oakwood Scientific. All other starting materials were purchased from TCI America, Alfa Aesar, and Sigma Aldrich.

¹H NMR spectra were recorded at 400 MHz or 500 MHz on a Varian VNMR spectrometer or at 600 MHz on a Bruker Avance-III-HD NMR spectrometer. ¹³C NMR spectra were recorded at 100 MHz or 125 MHz on a Varian VNMR Spectrometer or at 150 MHz on a Bruker Avance-III-HD NMR spectrometer. Deuterated chloroform (CDCl₃) was used as the NMR solvent for compounds **V.1- V.4** and **V.6- V.12d** while deuterated dimethyl sulfoxide (DMSO *d*₆) was used for compound **V.5** due to poor solubility. All the compounds and all spectra were referenced to tetramethylsilane (TMS). Absorbance spectra for **V.1- V.5** were obtained using dichloromethane as the solvent in a 1 cm quartz cuvette on an Agilent Cary 60 UV-Vis spectrophotometer. Emission spectra for **V.1- V.5** were collected using dichloromethane as the solvent in a 1 cm quartz cuvette using a Horiba Jobin Yvon FluoroMax-4 spectrophotometer.

THF, dichloromethane and DMF were dried by filtration through alumina according to the methods described by Grubbs. Silica column chromatography was conducted with Zeochem Zeoprep 60 Eco 40-63 μm silica gel. Thin Layer Chromatography (TLC) was performed using Sorbent Technologies Silica Gel XHT TLC plates. Developed plates were visualized using UV light at wavelengths of 254 and 265 nm. All glassware was oven or flame dried and cooled under an inert atmosphere of nitrogen unless otherwise noted.

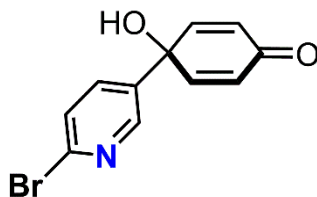
Cyclic voltammetry was conducted utilizing a platinum working electrode, platinum counter electrode, and a silver wire pseudoreference that was separated from the solution via a glass frit. Experiments were performed using a custom designed potentiostat at a scan rate of 50 mV/s. Analyte solutions were freeze-pump-thaw degassed three times and all experiments were conducted under airfree conditions. Analyte solutions were prepared using 0.1M tetrabutylammonium tetrafluoroborate in THF, with analyte concentrations 1-5mM. The Ag pseudoreference was calibrated versus the ferrocene/ferrocinium redox couple following the CV of each compound.

Diffraction intensities were collected at 173 (**V.1**) and 200(2) (**V.5**) on a Bruker Apex2 CCD diffractometer using an Incoatec $I\mu S$ micro-focus source with $\text{CuK}\alpha$ radiation, $\lambda = 1.54178 \text{ \AA}$. Space groups were determined based on systematic absences. Absorption corrections were applied by SADABS. Structures were solved by direct methods and Fourier techniques and refined on F^2 using full matrix least-squares procedures. All non-H atoms were refined with anisotropic thermal parameters. H atoms in both structures were refined in calculated positions in a rigid group model. Crystals of **V.1** were very small and even with using a strong Incoatec Cu $I\mu S$ micro-focus source provided non-zero reflections only up to $2\theta_{\text{max}} = 106.6^\circ$. Only such reflections were involved in the final refinement. The molecule of **1** has C_2 symmetry. The structure of **V.1** has additionally solvent molecule Me_2SO located inside the main molecule. It was found that the crystal structure of **V.5** has six solvent CHCl_3 molecules. One of them is located inside the cation and others fill out empty spaces in the crystal packing. Four of these molecules are highly disordered and were treated by SQUEEZE. The correction of the X-ray data by SQUEEZE is 938 electron/cell; the required value is 928 electron/cell for 16

solvent molecules CHCl_3 in the full unit cell. All calculations were performed by the SHELXL-2013 packages.

Compounds **V.7a**, **V.7b**, **V.8a**, **V.8b**, **V.9a**, **V.10a**, **V.11a**, **V.12a**, and [8]CPP were prepared in accordance with Jasti *et. al.* All spectra matched previously reported.

V.7.2. Synthetic Details.



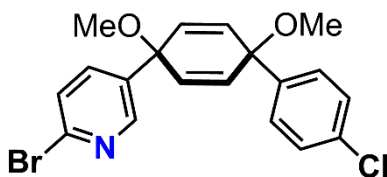
V.7c

nButyllithium (2.50 M in hexanes , 45.0 mL, 112 mmol, 1.15 eq) was diluted into a flask of THF (550 mL) and cooled to $-78\text{ }^\circ\text{C}$. This solution was allowed to cool for another 30 minutes with stirring.³ To this solution was added dropwise a solution of 2,5-dibromopyridine (25.0 g, 107 mmol, 1.10 eq) in THF (100 mL). The reaction was stirred for 30 minutes at $-78\text{ }^\circ\text{C}$ to give the lithiated species as a deep red solution.

In a separate flask, 4,4-dimethoxycyclohexa-2,5-dienone **6** (15.0 g, 97.4 mmol, 1.00 eq) was dissolved in THF (200 mL) and cooled to $-78\text{ }^\circ\text{C}$. To this was added the solution of lithiated 2-bromo-pyridine dropwise by cannula. The reaction was stirred for 3 hours at $-78\text{ }^\circ\text{C}$ after completion of the transfer. After 3 hours, the reaction was quenched with MeOH and allowed to warm to room temperature. The mixture was extracted with ether. After separation of the phases, the aqueous layer was washed with ether (3 x 200 mL). The combined organic layers were washed with brine and dried over sodium sulfate before being filtered and concentrated down to a yellowish-brown semi-solid. The solid was carried on crude.

The solid from above was dissolved in acetone (250 mL). An equal volume of 10% AcOH (250 mL) was added. The solution was stirred at room temperature for 4 hours. The acetone was removed by rotary evaporation. The remaining aqueous layer was extracted with dichloromethane (3 x 100 mL). The combined organic layers were washed with brine and dried over sodium sulfate before being concentrated down to a brown solid. The solid was then purified by recrystallization with absolute ethanol to yield a

pale tan solid (10.7 g, 42% yield). mp 145-147 °C. ¹H NMR (400 MHz, CDCl₃): δ 6.30 (d, *J* = 10 Hz, 2H), 6.85 (d, *J* = 10 Hz, 2H), 7.50 (d, *J* = 8.4 Hz, 1H), 7.61 (dd, *J* = 8.4 Hz, 2.8 Hz, 1H), 8.50 (d, *J* = 2.8 Hz, 1H); ¹³C NMR (125 MHz, CDCl₃): δ 185.14, 149.62, 148.10, 142.38, 136.35, 134.58, 128.44, 127.98, 69.82; HRMS (Q-TOF, ES⁺) (*m/z*): [M+H]⁺ calculated for C₁₁H₈BrNO₂, 265.9817; found: 265.9722. IR (neat): 3396, 3097, 3067, 3045, 2964, 1662, 1616, 1441, 1388, 1237, 1175, 1093, 1016, 921, 861 cm⁻¹.



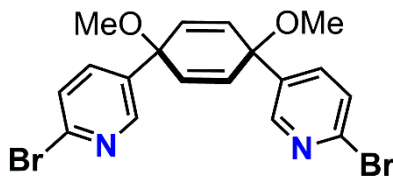
V.8c

To a solution of 4-bromo-1-chlorobenzene (14.9 g, 77.8 mmol, 2.40 eq) in THF (225 mL) at -78 °C. Was added nBuLi (2.5 M in hexanes, 31.0 mL, 77.5 mmol, 2.00 eq). The solution was stirred for 30 minutes at -78 °C and generated a cloudy white suspension. In a separate flask, NaH (1.60 g, 60% suspension in mineral oil, 40.0 mmol, 1.20 eq) was suspended in THF (150 mL) and cooled to -78 °C. Pyridyl quinol **V.7c** (9.10 g, 34.3 mmol, 1.00 eq) was dissolved in THF (50 mL) and added drop wise via cannula to the NaH suspension. The mixture was stirred for 2 hours at -78 °C. At this time, lithiated chlorobenzene was transferred dropwise via cannula into the NaH/Quinol mixture. The reaction was stirred for 3 hours at -78 °C, during which the reaction turned a yellow-brown color. Next, MeI (10.6 mL, 170 mmol, 5.00 eq) and DMF (75 mL) were added and the reaction was allowed to warm to room temperature and stir for 18 hours. Water (100 mL) and ether (250 mL) were added and the phases allowed to separate. The aqueous layer was washed with ether (3 X 250 mL). The combined organic phases were washed with brine before being dried over sodium sulfate. Solvent was removed under reduced pressure to give a brown solid. The crude material was purified by washing with hexanes and recrystallization from hot ethanol (7.00 g, 51%) mp 107-109 °C.

¹H NMR (500 MHz, CDCl₃): δ 3.41 (s, 3H), 3.42 (s, 3H), 6.03 (d, *J* = 8 Hz, 2H), 6.17 (d, *J* = 8 Hz, 2H), 7.30 (bs, 4H), 7.41 (d, *J* = 8.4 Hz, 1H), 7.53 (dd, *J* = 8.4, 2.6 Hz, 1H), 8.31 (d, *J* = 2.6 Hz, 1H); ¹³C NMR (125 MHz, CDCl₃): δ 148.63, 141.64, 141.54, 138.77, 136.67, 134.53, 134.08, 132.80, 129.08, 127.95, 127.50, 74.38, 73.52, 52.40, 52.28.

HRMS (Q-TOF, ES⁺) (*m/z*): [M+H]⁺ calculated for C₁₉H₁₇BrClNO₂, 406.0208; found

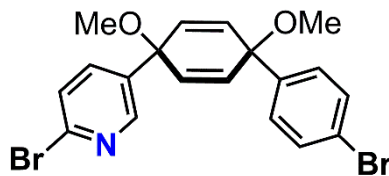
406.0208. IR (neat): 2992, 2924, 2854, 2820, 1572, 1486, 1449, 1398, 1361, 1171, 1070, 1015, 947, 832, 732 cm^{-1} .



V.8d

nButyllithium (2.5 M in hexanes, 1.79 mL, 4.48 mmol, 2.40 eq) was diluted in THF (25 mL) at $-78\text{ }^{\circ}\text{C}$. This solution was allowed to cool for another 30 minutes with stirring.³ To this was added via cannula a solution of 2,5-dibromopyridine (1.10 g, 4.48 mmol, 2.40 eq) in THF (5 mL). The deep red solution was stirred for 30 minutes at $-78\text{ }^{\circ}\text{C}$. In a separate flask, NaH (100 g, 2.26 mmol, 1.20 eq) was suspended in THF (7 mL) and cooled to $-78\text{ }^{\circ}\text{C}$. Quinol **7c** (0.500 g, 1.87 mmol, 1.00 eq) was dissolved in THF (5 mL), and transferred into the NaH solution by cannula. After stirring at $-78\text{ }^{\circ}\text{C}$ for 2 hours, the lithiated 2-bromopyridine was transferred by cannula to this solution. The reaction was stirred for 3 hours at $-78\text{ }^{\circ}\text{C}$. After this time, methyl iodide (0.700 mL, 11.2 mmol, 6.00 eq) and DMF (15 mL) were added. The flask was raised out of the bath and allowed to warm to room temperature over 20 hours. Water (50 mL) and ether (50 mL) were added and the phases allowed to separate. The aqueous layer was washed with ether (3 X 100 mL). The combined organic phases were washed with brine before being dried over sodium sulfate. Solvent was removed under reduced pressure to give a brown solid. The crude material was re-crystallized with hot ethanol yielding a light tan solid (0.350 g, 43%) mp $197\text{-}198\text{ }^{\circ}\text{C}$.

^1H NMR (400 MHz, CDCl_3): δ 3.42 (s, 6H), 6.13 (s, 4H), 7.44 (d, $J = 8.2\text{ Hz}$, 2H), 7.51 (dd, $J = 8.2\text{ Hz}$, 2.2 Hz, 2H), 8.35 (d, $J = 2.2\text{ Hz}$, 2H); ^{13}C NMR (125 MHz, CDCl_3): δ 148.47, 141.84, 138.35, 136.45, 133.73, 128.17, 73.29, 52.41. HRMS (Q-TOF, ES+) (m/z): $[\text{M}+\text{H}]^+$ calculated for $\text{C}_{18}\text{H}_{16}\text{Br}_2\text{N}_2\text{O}_2$, 450.9657; found, 450.9650. IR (neat): 3063, 3008, 2994, 2938, 2896, 2822, 1574, 1556, 1446, 1403, 1359, 1289, 1276, 1233, 1180, 1080, 1054, 1025, 1008, 952, 901, 833 cm^{-1} .

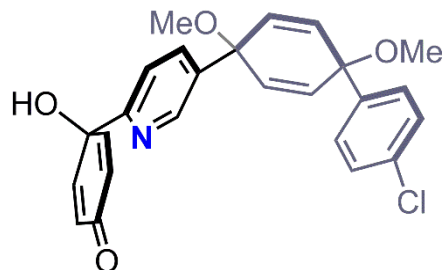


V.8e

To a solution of 1,4-dibromobenzene (10.5 g, 44.5 mmol, 2.40 eq) in THF (225 mL) at $-78\text{ }^{\circ}\text{C}$ was added nBuLi (2.5 M in hexanes, 19 mL, 46.3 mmol, 2.50 eq). The solution was stirred for 30 minutes at $-78\text{ }^{\circ}\text{C}$ and generated a cloudy white suspension.

In a separate flask, NaH (0.890 g, 60% suspension in mineral oil, 22.3 mmol, 1.20 eq) was suspended in THF (80 mL) and cooled to $-78\text{ }^{\circ}\text{C}$. Pyridyl quinol **V.7c** (5.00 g, 18.5 mmol, 1.00 eq) was dissolved in THF (15 mL) and added drop wise via cannula to the NaH suspension. The mixture was stirred for 2 hours at $-78\text{ }^{\circ}\text{C}$. At this time, lithiated bromobenzene was transferred dropwise via cannula into the NaH/Ketone mixture. The reaction was stirred for 3 hours at $-78\text{ }^{\circ}\text{C}$, during which the reaction turned a yellowy-brown color. Next, MeI (5.76 mL, 92.5 mmol, 5.00 eq) and DMF (45 mL) were added and the reaction was allowed to warm to room temperature and stir for 18 hours. Water (100 mL) and ether (250 mL) were added and the phases allowed to separate. The aqueous layer was washed with ether (3 X 100 mL). The combined organic phases were washed with brine before being dried over sodium sulfate. Solvent was removed under reduced pressure to give a brown solid. The crude material was purified by column chromatography (silica gel, 30% Ethyl Acetate in Hexanes eluent) to recover a pale yellow solid which was then recrystallized from hot ethanol to give a light tan solid (4.20 g, 50%) mp $124\text{-}125\text{ }^{\circ}\text{C}$.

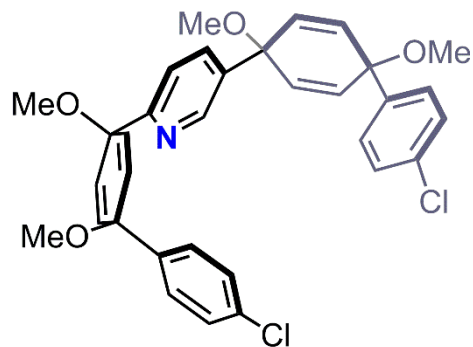
^1H NMR (500 MHz, CDCl_3): δ 3.40 (s, 3H), 3.42 (s, 3H), 6.03 (d, $J = 10\text{ Hz}$, 2H), 6.16 (d, $J = 10\text{ Hz}$, 2H), 7.24 (d, $J = 8.8\text{ Hz}$, 2H), 7.41 (d, $J = 9.3\text{ Hz}$, 1H), 7.46 (d, $J = 8.8\text{ Hz}$, 2H) 7.54 (dd, $J = 9.3, 3\text{ Hz}$, 1H), 8.31 (d, $J = 3\text{ Hz}$, 1H). ^{13}C NMR (125 MHz, CDCl_3): δ 148.75, 141.75, 141.67, 138.89, 136.79, 134.65, 134.22, 132.92, 129.21, 128.08, 127.62, 74.51, 73.65, 52.52, 52.40. HRMS (Q-TOF, ES+) (m/z): $[\text{M}+\text{H}]^+$ calculated for $\text{C}_{19}\text{H}_{17}\text{Br}_2\text{NO}_2$, 449.9704 found 449.9720. IR: 2973, 2939, 2894, 2818, 1570, 1554, 1482, 1447, 1393, 1360, 1288, 1175, 1065, 1029, 1018, 1004, 992, 946, 836 cm^{-1}



V.9b

V.8e (5.80 g, 14.3 mmol, 1.00 eq) was added to a dry flask and dissolved in dry THF (200 mL). The solution was cooled to $-78\text{ }^{\circ}\text{C}$. nBuLi (2.5 M in hexanes, 6.30 mL, 15.7 mmol, 1.10 eq) was added dropwise over 5 minutes resulting in a deep reddish-purple solution. After stirring at $-78\text{ }^{\circ}\text{C}$ for 10 minutes, 4,4-dimethoxycyclohexa-2,5-dienone **V.6** (2.80 g, 18.5 mmol, 1.30 eq) was added neat. The solution then turned yellow-orange. The reaction was stirred for 1 hour before being quenched with H_2O . The aqueous layer was then washed with diethyl ether (3 X 100 mL). The combined organic layers were washed with brine and dried over Na_2SO_4 , and concentrated down to a yellow oil. The oil was dissolved in acetone (50 mL) and 5% AcOH/ H_2O was added (50 mL). The solution was stirred at room temperature for 2 hours. The solution was neutralized with sodium bicarbonate and extracted with diethyl ether (3 X 100 mL). The combined organic layers were washed with brine and dried over Na_2SO_4 . The solution was concentrated under reduced pressure to yield a yellow solid. The solid was purified by column chromatography to give a light tan solid (silica gel, 30% EtOAc/DCM eluent), (4.00 g, 65%). mp $156\text{-}159\text{ }^{\circ}\text{C}$.

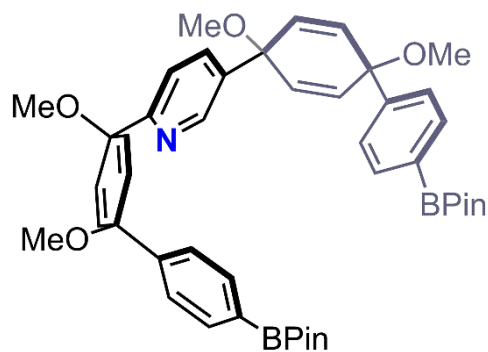
^1H NMR (400 MHz, CDCl_3): δ 3.42 (s, 3H), 3.45 (s, 3H), 6.05 (d, $J = 11\text{ Hz}$, 2H), 6.20 (d, $J = 11\text{ Hz}$, 2H), 6.28 (d, $J = 10.2\text{ Hz}$, 2H), 6.75 (d, $J = 10.2\text{ Hz}$, 2H), 7.20 (d, $J = 8.4\text{ Hz}$, 1H), 7.32 (s, 4H), 7.69 (dd, $J = 8.4, 1.6\text{ Hz}$, 1H), 8.56 (d, $J = 1.6\text{ Hz}$, 1H). ^{13}C NMR (100 MHz, CDCl_3): δ 185.86, 154.71, 150.75, 146.40, 141.62, 139.70, 135.93, 134.53, 134.05, 132.81, 129.00, 128.20, 127.40, 120.40, 74.27, 73.58, 70.97, 52.36, 52.27. HRMS (Q-TOF, ES+) (m/z) calculated for $\text{C}_{25}\text{H}_{22}\text{ClNO}_4$: 436.1316; found, 436.1303. IR: 2938, 2902, 2820, 2106, 1667, 1627, 1481, 1401, 1075, 954, 857, 726 cm^{-1} .



V.10b

Ketone **V.9b** (1.00 g, 2.29 mmol, 1.00 eq) and 5-bromo-2-chloropyridine (0.960 g, 5.00 mmol, 2.20 eq) were added to a dry round bottom flask and dissolved in dry THF (75 mL). The solution was cooled to $-78\text{ }^{\circ}\text{C}$ for 1 hour. To this solution was added NaH (0.100 g, 2.80 mmol, 1.20 eq) as a solid. The reaction was stirred for 2 hours. After 2 hours, nBuLi (2.20 mL, 5.60 mmol, 2.40 eq) was added drop-wise. The reaction was stirred for 2 hours at which time MeI (1.43 mL, 23.0 mmol, 10.0 eq) and dry DMF (10 mL) were added. The reaction was allowed to warm to room temperature overnight while stirring for 18 hours. The reaction was quenched with H_2O and extracted with diethyl ether (3 X 75 mL). The combined organic layers were washed with brine, dried with Na_2SO_4 and concentrated under reduced pressure to give a solid. The solid was washed with cold hexanes to give the product as a white powder (0.900 g, 70%). mp $196.5\text{--}203\text{ }^{\circ}\text{C}$.

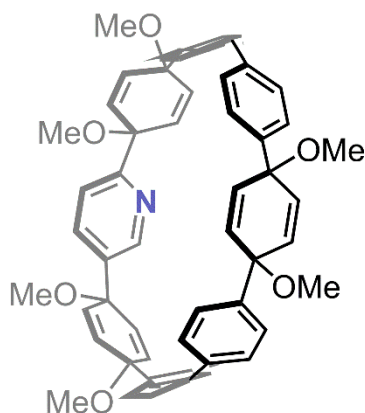
^1H NMR (400 MHz, CDCl_3): δ 3.42 (s, 3H), 3.43 (s, 3H), 3.45 (s, 3H), 3.46 (s, 3H), 6.05 (d, $J = 10.4$ Hz, 2H), 6.07 (d, $J = 10.4$ Hz, 2H), 6.13 (d, $J = 10.4$ Hz, 2H), 6.14 (d, $J = 10.4$ Hz, 2H), 7.24 (d, $J = 8.4$ Hz, 2H), 7.31 (d, $J = 8.8$ Hz, 2H), 7.32 (d, $J = 8.8$ Hz, 2H), 7.51 (d, $J = 8.4$ Hz, 1H) 7.56 (d, $J = 8.4$ Hz, 2H), 7.65 (dd, $J = 8.4, 2.4$ Hz, 1H), 8.59, (d, $J = 2.4$ Hz, 1H); ^{13}C NMR(125 MHz, CDCl_3): δ 161.50, 147.51, 142.26, 141.97, 138.24, 134.72, 133.23, 132.58, 129.05, 128.55, 128.11, 127.64, 120.71, 76.28, 75.07, 74.49, 73.77, 52.44, 52.39, 52.35. HRMS (Q-TOF, ES+) (m/z): $[\text{M}+\text{Z}]^+$ calculated for $\text{C}_{33}\text{H}_{31}\text{Cl}_2\text{NO}_2$, 576.1708; found, 575.1733. IR (neat): 3021, 2939, 2896, 2823, 1590, 1469, 1400, 1368, 1086, 1020, 950, 829, 760, 730 cm^{-1} .



V.11b

Dichloride **V.10b** (0.870 g, 1.51 mmol, 1.00 eq), B_2Pin_2 (2.30 g, 9.06 mmol, 6.00 eq), $Pd(OAc)_2$ (0.0300 g, 0.109 mmol, 0.100 eq), S-Phos (0.250 g, 0.604 mmol, 0.400 eq), and finely ground and oven dried K_3PO_4 (1.92 g, 9.06 mmol, 6.00 eq) were added to a dry flask. The flask was evacuated and backfilled with nitrogen 3 times. The solid was purged with N_2 for 30 minutes. Dry 1,4-dioxane (40 mL) was added to the flask via syringe. The mixture was stirred at $70^\circ C$ overnight. The mixture was cooled to room temperature and filtered through a pad of Celite with a top layer of activated carbon. The filtrate was extracted between DCM and H_2O . The combined organic layers were washed with H_2O followed by brine, before finally being dried over Na_2SO_4 . The solvent was concentrated under reduced pressure to yield a white solid. The solid was washed with hexanes to give the pure product (0.487 g, 45%) mp $232-234^\circ C$.

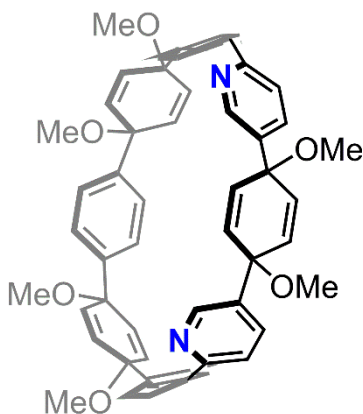
1H NMR (400 MHz, $CDCl_3$): δ 1.33 (m, 24H), 3.45 (multiplet, 12H), 6.12 (m, 8H), 7.39 (m, 3H), 7.55 (m, 3H), 7.75 (m, 4H), 8.73 (bs, 1H). ^{13}C NMR (100 MHz, $CDCl_3$): δ HRMS (Q-TOF, ES+) (m/z): $[M+H]^+$ calculated for $C_{45}H_{55}B_2NO_8$, 760.4207; found, 760.4200. IR (neat): 2979, 2948, 2932, 2826, 1608, 1474, 1393, 1358, 1321, 1274, 1143, 1081, 1016, 950, 854, 758 cm^{-1} .



V.12b

Dibromide **V.8a** (0.585 g, 1.30 mmol, 1.00 eq), diboronate **V.11b** (1.00 g, 1.30 mmol, 1.00 eq), ⁿBu₄Br (0.084 g, 0.260 mmol, 0.200 eq) and Pd(PPh₃)₄ (0.150 g, 0.130 mmol, 0.100 eq), NaHCO₃ (1.10 g, 13.0 mmol, 10.0 eq) were charged to a dried flask, which was then purged with argon. Degassed toluene (225 mL), methanol (25 mL), and water 13 mL (to make base 1 M) were added. The mixture was heated to 90 °C and stirred for 24 hours. The reaction was cooled to room temperature and washed with water. The organic layer was washed with brine and dried over sodium sulfate. The organic layer was concentrated down under reduced pressure to a yellow solid. The solid was purified by column chromatography (silica gel, 30% ethyl acetate in DCM eluent) to recover a white solid. Material was further purified by washes with cold ethyl acetate (0.257 mg, 25%) mp 285 °C dec.

¹H NMR (500 MHz, CDCl₃): δ 3.40-3.48 (m, 18H), 6.02-6.17 (m, 8H), 6.22 (d, *J* = 10 Hz, 2H), 6.32 (d, *J* = 10.0 Hz, 2H), 7.13 (d, *J* = 8.6 Hz, 2H), 7.39 (d, *J* = 8.6 Hz, 2H), 7.50 (m, 12H), 7.93 (m, 2H), 8.26 (m, 1H). ¹³C NMR (125 MHz, CDCl₃): δ 52.11, 52.39, 52.41, 52.43, 52.50, 74.29, 74.41, 74.92, 75.01, 76.13, 119.73, 126.49, 126.52, 126.53, 127.04, 127.13, 132.91, 133.06, 133.10, 133.61, 133.87, 134.65, 135.18, 135.83, 143.10, 143.58, 148.57, 156.25. MALDI-TOF (*m/z*): [M+H]⁺ calculated for C₅₃H₅₀NO₆, 796.36; found, 796.45 and 767.27 (loss of methoxy). IR (neat): 2982, 2926, 2896, 2823, 1589, 1490, 1081, 1069, 1014, 978, 852 cm⁻¹.

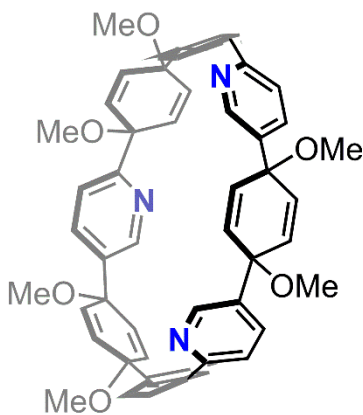


V.12c

Dibromide **V.8d** (0.415 g, 0.920 mmol, 1.00 eq), diboronate **V.11a** (0.700 g, 0.920 mmol, 1.00 eq), ⁿBu₄NBr (0.323 g, 0.184 mmol, 0.200 eq) and Pd(PPh₃)₄ (0.106 g, 0.0920

mmol, 0.100 eq), and NaHCO₃ (0.865 g, 10.0 mmol, 10.0 eq) were charged to a dried flask, which was then evacuated and backfilled with N₂ three times. Degassed toluene (118 mL), methanol (13 mL) and H₂O (10 mL to make base 1M) were added. The mixture was heated to 90 °C and stirred for 24 hours. The reaction was cooled to room temperature and extracted between washed with H₂O. The organic layer was washed with brine and dried over sodium sulfate. The organic layer was concentrated down under reduced pressure to a yellow solid. The solid was purified by column chromatography (silica gel, 30% ethyl acetate in DCM eluent) to give a white solid (140 mg, 20%) mp 290 °C dec.

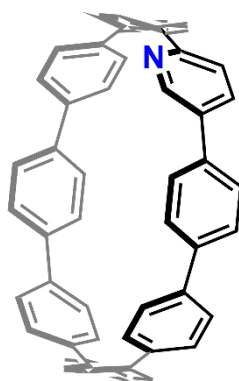
¹H NMR (500 MHz, CDCl₃): δ 3.40 (s, 6H), 3.46 (s, 6H), 3.48 (s, 6H), 6.05 (d, *J* = 10 Hz, 4H), 6.13 (d, *J* = 10 Hz, 4H), 6.28 (s, 4H), 7.51-7.57 (m, 12H), 7.92 (d, *J* = 8.5 Hz, 4H), 8.29 (dd, *J* = 2 Hz, 1 Hz, 2H). ¹³C NMR (125 MHz, CDCl₃): δ 52.11, 52.41, 52.49, 74.33, 74.85, 74.93, 119.99, 126.45, 126.52, 127.20, 133.09, 133.66, 133.79, 134.93, 135.42, 138.28, 143.57, 144.79, 148.12, 156.64. MALDI-TOF (*m/z*): [M+H]⁺ calculated for C₅₂H₄₉N₂O₆, 797.36; found 797.52. IR (neat): 3022, 2983, 2920, 2850, 2821, 1589, 1471, 1390, 1229, 1081, 1068, 101, 102, 978, 829, 662, 610, 543 cm⁻¹.



V.12d

Dibromide **V.8d** (0.178 g, 0.395 mmol, 1.00 eq), diboronate **V.11b** (0.300 g, 0.395 mmol, 1.00 eq), ⁿBu₄Br (0.0250 g, 0.0790 mmol, 0.200 eq) and Pd(PPh₃)₄ (0.0500 g, 0.0400 mmol, 0.100 eq), and NaHCO₃ (0.336 g, 4.00 mmol, 10.0 eq) were charged to a dried flask, which was then evacuated and backfilled with N₂ three time. Degassed toluene (180 mL), methanol (20 mL), and H₂O (4 mL to make base 1M) were added. The mixture was heated to 90 °C and stirred for 24 hours. The reaction was cooled to room

temperature and washed with H₂O. The organic layer was washed with brine and dried over sodium sulfate. The organic layer was concentrated down under reduced pressure to a yellow solid. The solid was purified by column chromatography (silica gel, 40% ethyl acetate in DCM eluent) to recover a white solid (16.0 mg, 16%) mp 290 °C dec. ¹H NMR (500 MHz, CDCl₃): δ 3.42-3.51 (m, 18H), 6.09-6.29 (m, 12H), 7.40 (dd, *J* = 8.3, 2.3 Hz, 1H), 7.49-7.61 (m, 8H), 7.84 (dd, *J* = 8.3, 2.3 Hz, 1H), 7.88-7.95 (m, 4H), 8.30 (s, 1H), 8.32 (s, 1H), 8.80 (d, *J* = 2.3 Hz, 1H). ¹³C NMR (125 MHz, CDCl₃) δ 161.47, 156.55, 156.28, 148.04, 147.92, 144.44, 144.18, 134.85, 134.73, 134.70, 134.67, 134.48, 133.68, 133.57, 131.99, 131.70, 127.06, 126.41, 126.22, 120.83, 119.78, 119.72, 75.39, 74.90, 74.80, 74.72, 74.52, 72.96, 52.36, 52.34, 52.32, 52.7, 51.95. MALDI-TOF (*m/z*): [M+H]⁺ calculated for C₅₁H₄₈N₃O₆, 798.35; found, 799.56. IR: 3023, 2935, 2896, 2822, 1590, 1556, 1470, 1393, 1227, 1175, 1114, 1074, 1014, 948, 825, 771, 753, 730, 662, 645, 610, 573, 543 cm⁻¹.

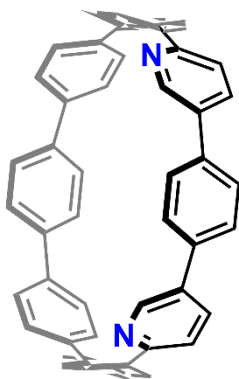


V.1 Aza[8]CPP

To a dry flask charged with 15 mL of THF was added sodium metal (0.200 g, 8.30 mmol) and naphthalene (1.20 g, 9.36 mmol). The solution was stirred for 15 hours at room temperature during which time a dark green solution of sodium naphthalide formed. Macrocyclic **V.12b** (0.200 g, 0.250 mmol, 1.00 eq) was dissolved in dry THF (20 mL) and cooled to -78 °C. To this solution, sodium naphthalide was added dropwise until the solution sustained a dark purple color (approximately 3 eq. per OMe, 3 mL naphthalide). The reaction was stirred for an additional 30 mins at -78 °C. The reaction was quenched with a solution of I₂ in THF (1 mL of 1 M solution). The solution was warmed to room temperature. The mixture was extracted with DCM and was washed with saturated

sodium thiosulfate to quench excess iodine. The aqueous layer was extracted with DCM (3 X 10 mL). The combined organic layers were washed with brine and dried over sodium sulfate. The solvent was removed under reduced pressure to yield an orange solid. The solid was purified by column (5% ether/DCM eluent) followed by preparative TLC with the same solvent system (silica, 5% ether/DCM eluent). The pure product was received as an yellow solid (0.0860 g, 56%) mp 250 °C dec.

^1H NMR (400 MHz, CDCl_3): δ 7.43-7.61 (m, 28H), 7.81-7.84 (m, 2H), 8.76 (s, 1H). ^{13}C NMR (125 MHz, CDCl_3): δ 153.99, 140.85, 137.62, 17.60, 137.47, 137.45, 137.43, 137.42, 134.67, 132.45, 130.16, 128.25, 127.6, 127.51, 127.47, 119.04. MALDI-TOF (m/z): $[\text{M}+\text{H}]^+$ calculated for $\text{C}_{47}\text{H}_{32}\text{N}$, 610.25; found, 609.92. IR (neat): 3023, 2923, 2853, 1567, 1479, 1467, 1390, 1364, 1261, 1224, 1055, 996, 816, 760, 741 cm^{-1} .

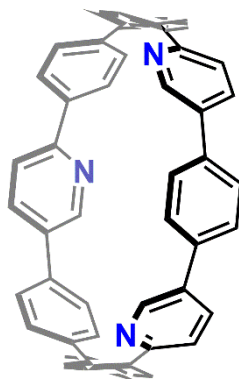


V.2 1,15-Diaza[8]CPP

To a dry flask charged with 15 mL of THF was added sodium metal (0.200 g, 8.30 mmol) and naphthalene (1.20 g, 9.36 mmol). The solution was stirred for 15 hours at room temperature during which time a dark green solution of sodium naphthalide formed. Macrocyclic **12c** (0.174 g, 219 μmol , 1.00 eq) was dissolved in dry THF (20 mL) and cooled to -78 °C. To this solution, sodium naphthalide was added dropwise until the solution sustained a dark purple color (approximately 2 mL of 1 M sodium naphthalide). The reaction was stirred for an additional 3 hours at -78 °C. The reaction was quenched with a solution of I_2 in THF (1 mL of 1 M solution). The solution was warmed to room temperature. The reaction was extracted with DCM and was washed with saturated sodium thiosulfate to quench excess iodine. The aqueous layer was extracted with DCM (3 X 10 mL). The combined organic layers were washed with brine and dried over sodium sulfate. The solvent was removed under reduced pressure to yield an orange

solid. The solid was washed with hexanes to remove excess naphthalene. The solid was then purified by preparatory TLC (silica, 5% MeOH/DCM eluent). The pure product was received as a yellow solid (0.0720 g, 55%) mp 236 °C dec.

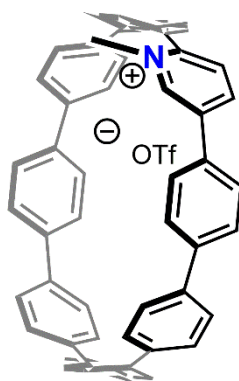
^1H NMR (500 MHz, CDCl_3): δ 7.26-7.86 (m, 28H), 8.75 (s, 2H). ^{13}C NMR (125 MHz, CDCl_3): δ 154.24, 146.86, 138.86, 137.91, 137.64, 137.04, 136.94, 135.31, 132.72, 130.13, 128.28, 127.66, 127.52, 127.47, 127.41, 127.02, 119.07. MALDI-TOF (m/z): $[\text{M}+\text{H}]^+$ calculated for $\text{C}_{46}\text{H}_{31}\text{N}_2$, 611.25; found, 611.26. IR (neat): 2967, 2879, 1472, 880, 830, 739, 556 cm^{-1} .



V.3 1,15,31-Triaza[8]CPP

To a dry flask charged with 15 mL of THF was added sodium metal (0.200 g, 8.30 mmol) and naphthalene (1.20 g, 9.36 mmol). The solution was stirred for 15 hours at room temperature during which time a dark green solution of sodium naphthalide formed. Macrocyclic **V.12d** (0.0500 g, 0.0630 mmol, 1.00 eq) was dissolved in dry THF (15 mL) and cooled to -78 °C. To this solution, sodium naphthalide was added dropwise until the solution sustained a dark purple color (approximately 3 eq per OMe). The reaction was stirred for an additional 30 mins at -78 °C. The reaction was quenched with a solution of I_2 in THF (1 mL of 1 M solution). The solution was warmed to room temperature. The mixture was extracted with DCM and washed with saturated sodium thiosulfate to quench excess iodine. The aqueous layer was extracted with DCM (3 X 10 mL). The combined organic layers were washed with brine and dried over sodium sulfate. The solvent was removed under reduced pressure to yield an orange solid. The solid was washed with a small amount of hexanes to remove most of the excess naphthalene. The residue was then purified by preparatory TLC (silica, 20% ether/DCM eluent). The pure product was received as a yellow solid (0.0190 g, 50%) mp 230 °C dec.

^1H NMR (500 MHz, CDCl_3): δ 7.51-7.61 (m, 17H), 7.79-7.86 (m, 9H), 8.75-8.77 (m, 3H). ^{13}C NMR (125 MHz, CDCl_3): δ 154.13, 154.11, 153.94, 146.89, 138.83, 138.48, 138.40, 137.79, 137.30, 137.23, 135.26, 135.23, 135.02, 132.67, 132.65, 132.59, 130.22, 130.09, 128.29, 128.23, 127.77, 127.76, 127.47, 127.17, 127.02, 119.20, 119.15, 119.06. MALDI-TOF (m/z): $[\text{M}+\text{H}]^+$ calculated for $\text{C}_{45}\text{H}_{30}\text{N}_3$, 612.24; found, 612.32. IR (neat): 3026, 2924, 2853, 1733, 1567, 1463, 1363, 1263, 1228, 1174, 1153, 1114, 1077, 1015, 948, 911, 819, 740, 699, 664, 650 cm^{-1} .

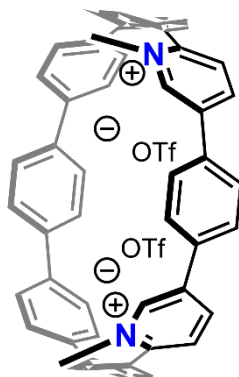


V.4 *N*-methylaza[8]CPP Triflate

Aza[8]CPP **V.1** (0.0230 g, 0.0377 mmol, 1 equiv) was added to a flame dry flask charged under nitrogen. 20 mL of dry dichloromethane was added. Once all solids had dissolved methyl triflate (0.0200 mL, 0.189 mmol, 5 equiv) was added dropwise. This was allowed to stir for 18 hours during which the color turned from a bright fluorescent yellow to a dull orange. The reaction was quenched by addition of saturated ammonium chloride (20 mL). The aqueous layer was extracted with DCM (3 X 10 mL). The combined organic layers were washed with brine and dried over sodium sulfate. The solvent was removed under reduced pressure to yield a red/ orange solid (0.0290 g, 99%). Single crystal was grown by slow liquid diffusion by layering toluene onto a concentrated dichloromethane solution of **V.4**. mp 230 °C dec.

^1H NMR (600 MHz, CDCl_3): δ 9.29 (s, 1H), 7.91 (d, $J = 9$ Hz, 1H), 7.70 (d, $J = 9$ Hz, 1H), 7.64-7.26 (m, 19H), 4.76 (s, 3H). ^{13}C NMR (150 MHz, CDCl_3): δ 151.90, 145.48, 142.88, 141.61, 141.40, 139.48, 138.87, 138.23, 137.95, 137.82, 137.60, 137.50, 137.22, 136.81, 136.64, 136.30, 131.06, 130.24, 129.54, 129.37, 128.46, 127.92, 127.70, 127.57, 121.58 (q, $J_{\text{C-F}}$ 318 Hz), 47.96. ESI-MS (m/z): $[\text{M}+\text{Na}]^+$ calculated for

$C_{49}H_{34}NF_3NNaO_3S^+$, 796.2109; found, 796.2096. IR (neat): 3025, 2923, 1585, 1486, 1260, 1165, 1029, 822, 730, 638 cm^{-1} .

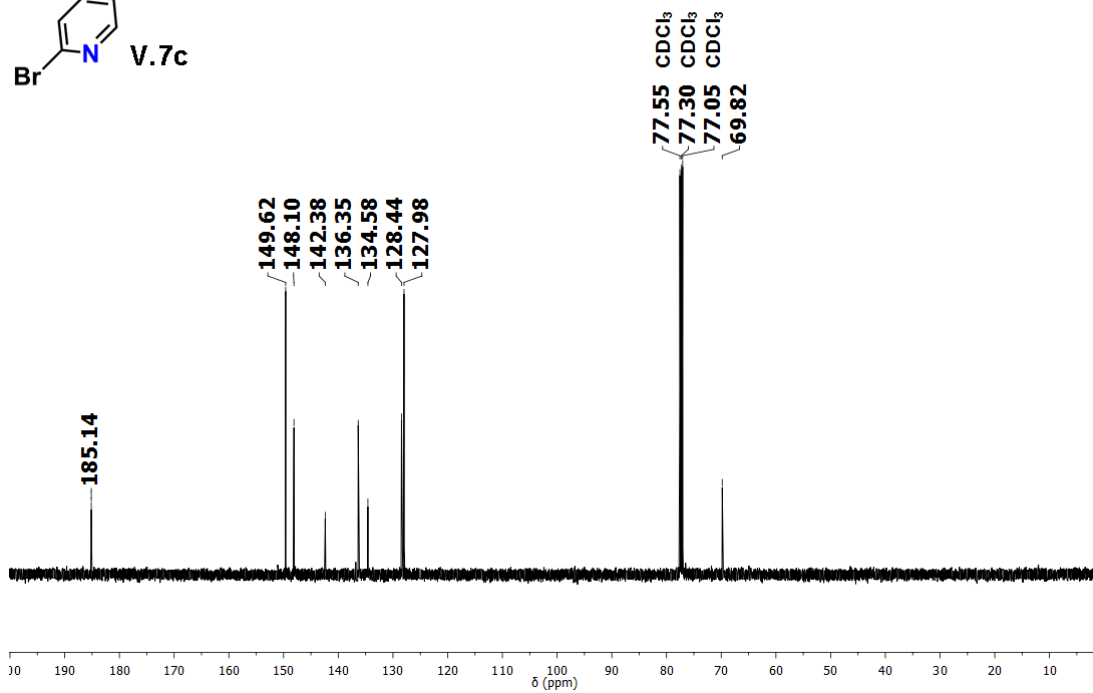
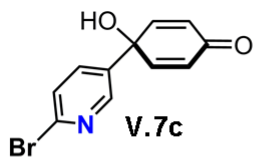
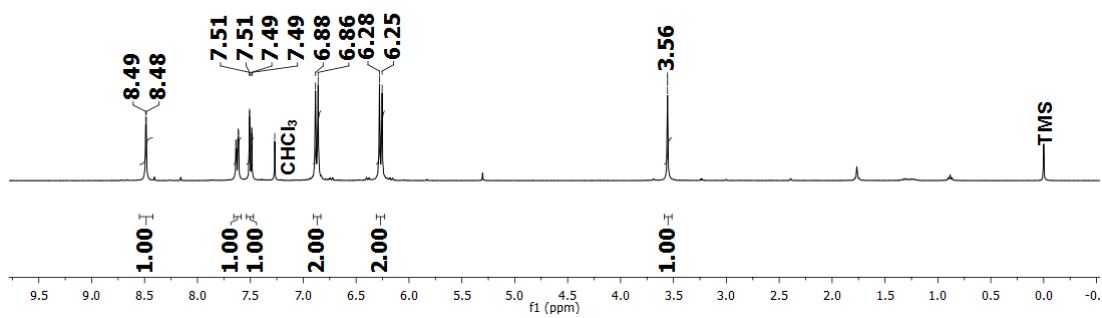
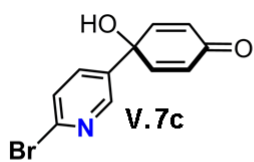


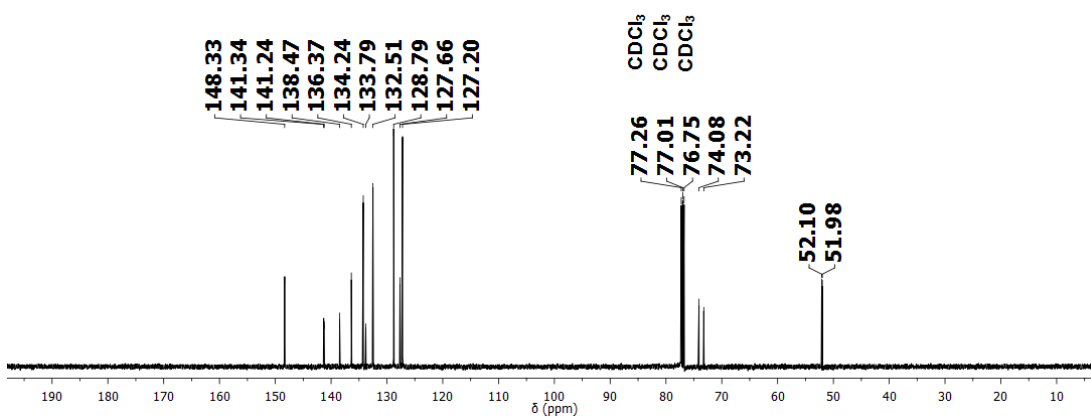
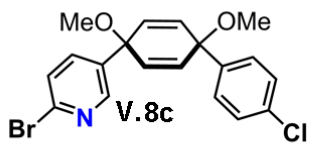
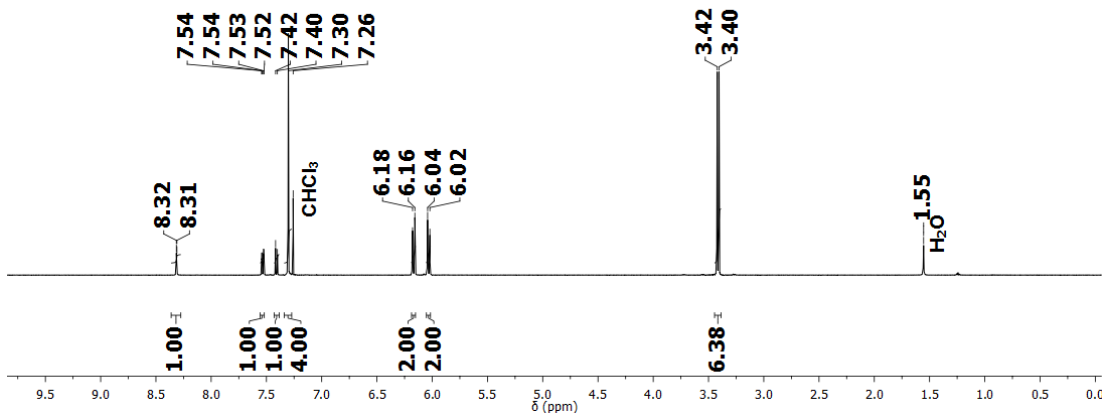
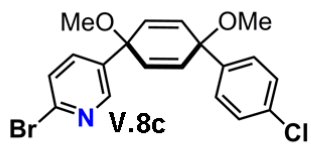
V.5 *N,N*-dimethyl-1,15-diaza[8]CPP Ditriflate

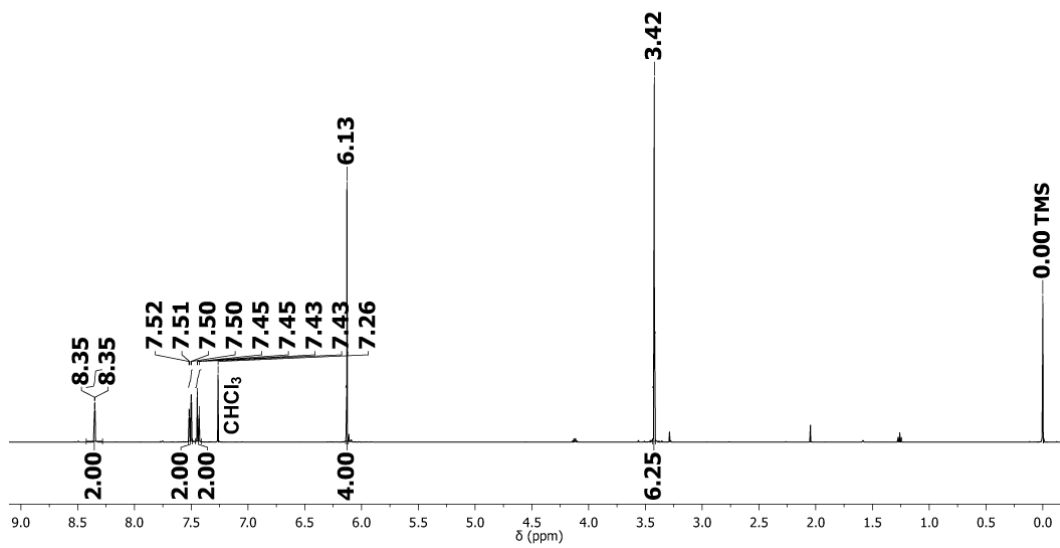
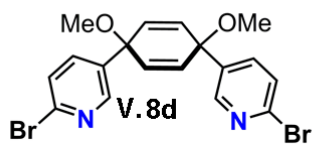
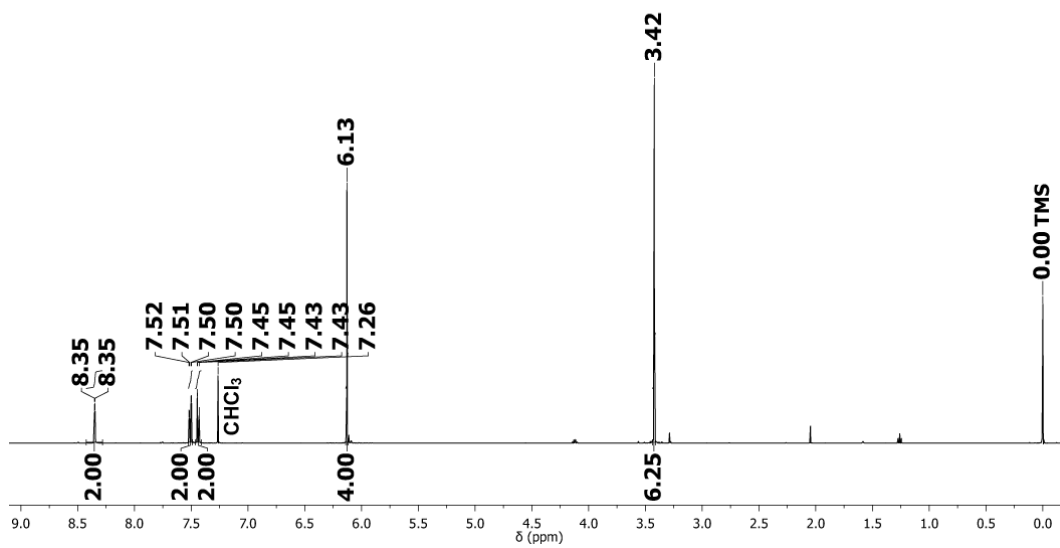
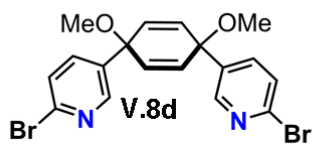
1,15-diaza[8]CPP2N V.2 (0.0170 g, 0.0383 mmol, 1 equiv) was added to a flame dry flask charged under nitrogen. 20 mL of dry dichloromethane was added. Once all solids had dissolved methyl triflate (0.0280 mL, 0.283 mmol, 10 equiv) was added dropwise. This was allowed to stir for 18 hours during which the color turned from a bright fluorescent yellow to a dull orange. The reaction was quenched by addition of saturated ammonium chloride (20 mL). The aqueous layer was extracted with DCM (3 X 10 mL). The combined organic layers were washed with brine and dried over sodium sulfate. The solvent was removed under reduced pressure to yield a red/ orange solid (0.0263 g, 99%). Single crystals were grown by slow evaporation of $CDCl_3$. mp 230 °C dec.

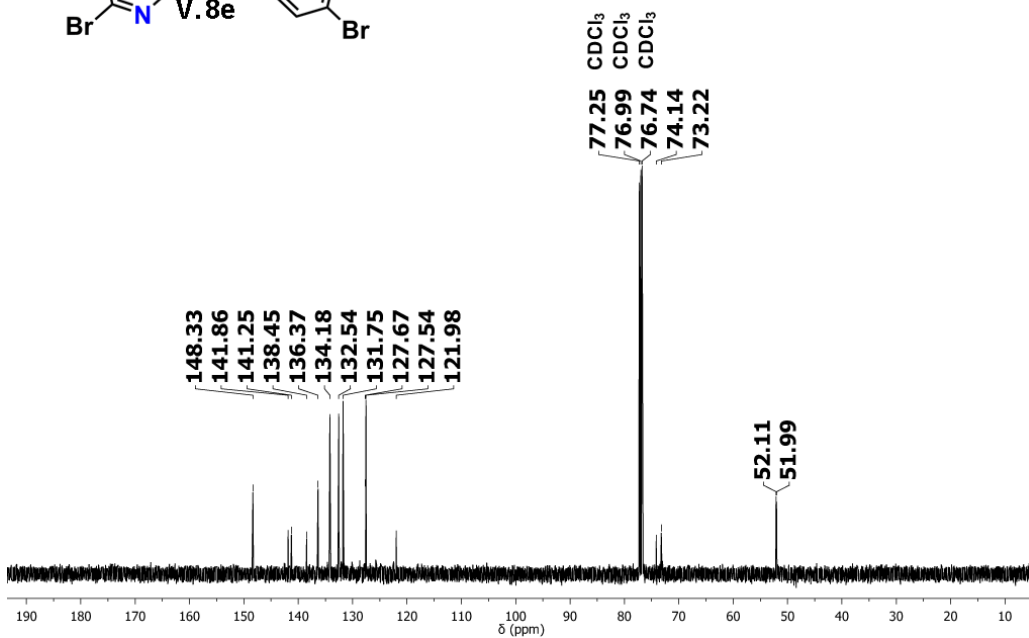
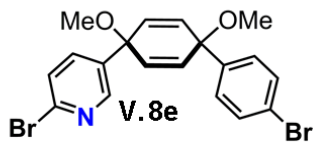
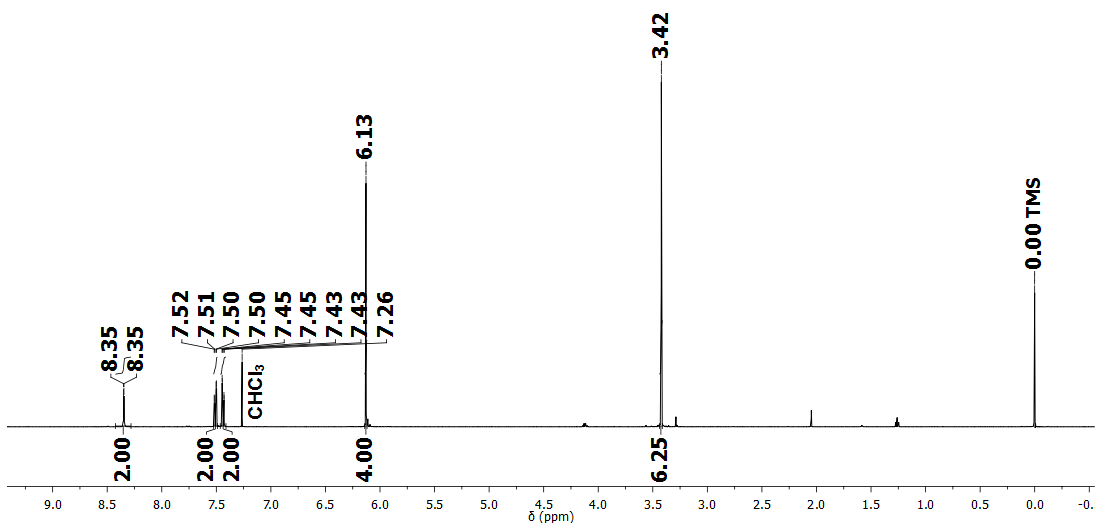
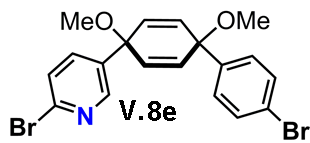
1H NMR (600 MHz, DMSO d_6): δ 9.63 (s, 2H), 8.40 (d, $J = 9$ Hz, 2H), 8.05 (s, 4H), 7.82-7.62 (m, 24H), 4.58 (s, 6H). ^{13}C NMR (150 MHz, DMSO): δ 151.89, 144.09, 143.03, 141.14, 137.80, 136.32, 136.09, 133.76, 133.54, 131.27, 129.93, 129.61, 129.39, 128.46, 128.08, 127.26, 127.16, 120.68 (q, $J_{C-F} = 320$ Hz), 47.57. ESI-MS (m/z): $[M+Na]^+$ calculated for $C_{50}H_{36}F_6N_2NaO_6S_2$, 961.1816; found, 961.1819. IR (neat): 3058, 2925, 2854, 1590. 1523, 1435, 1258, 1166, 1030, 825. 734, 638, 574 cm^{-1} .

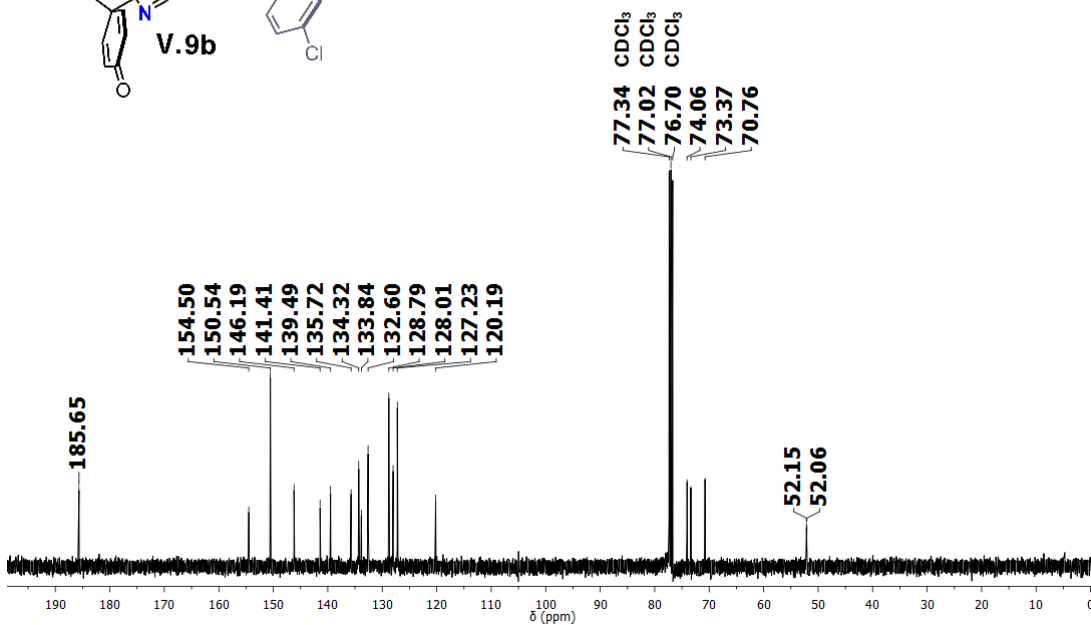
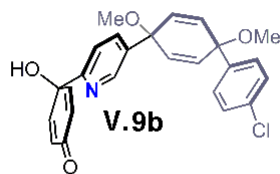
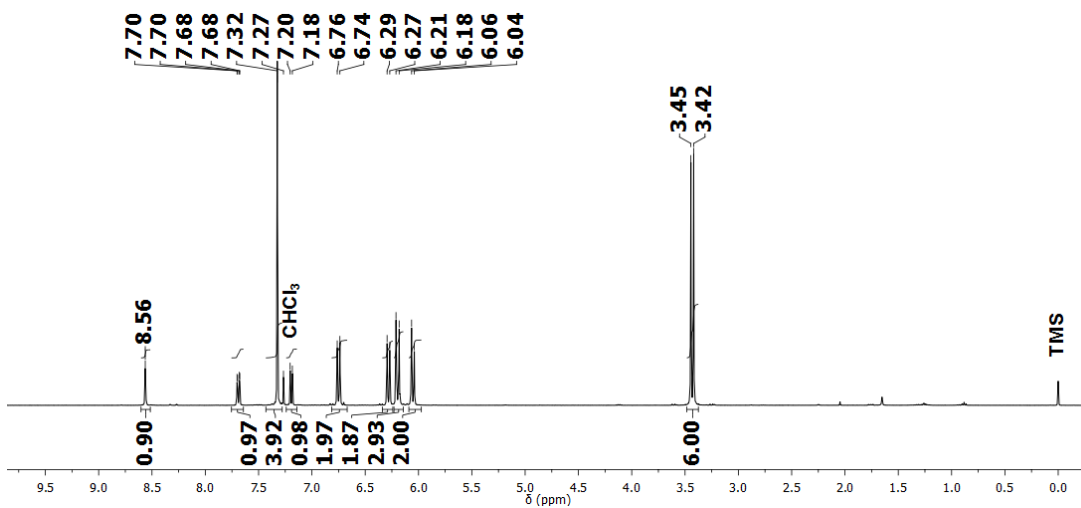
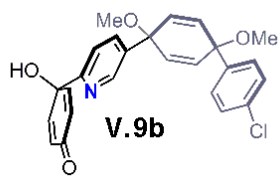
V.6.3. NMR Spectra.

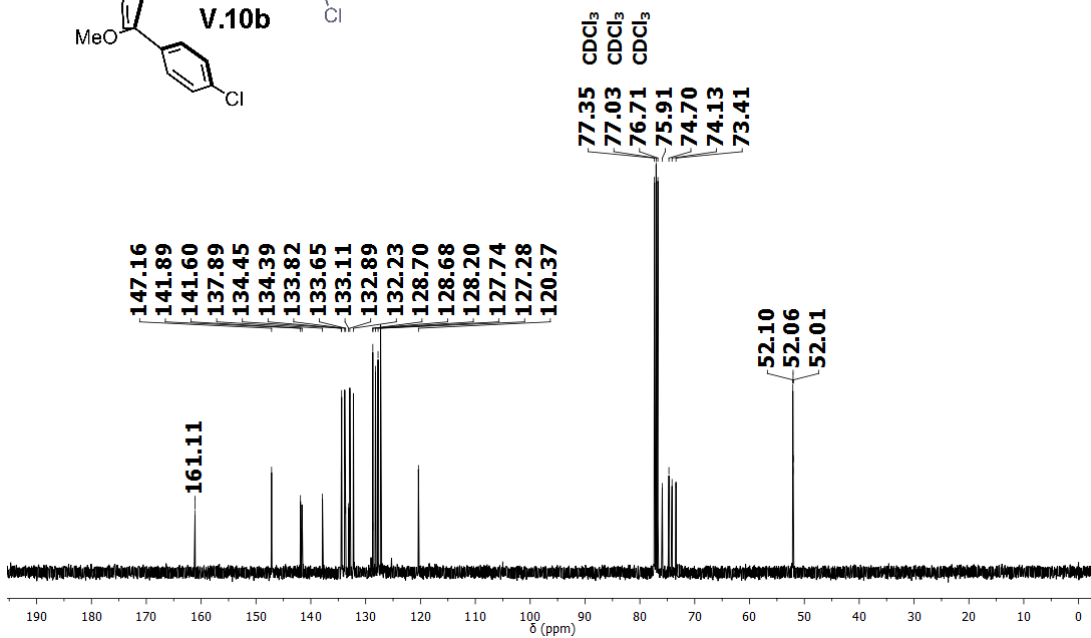
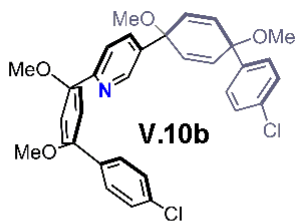
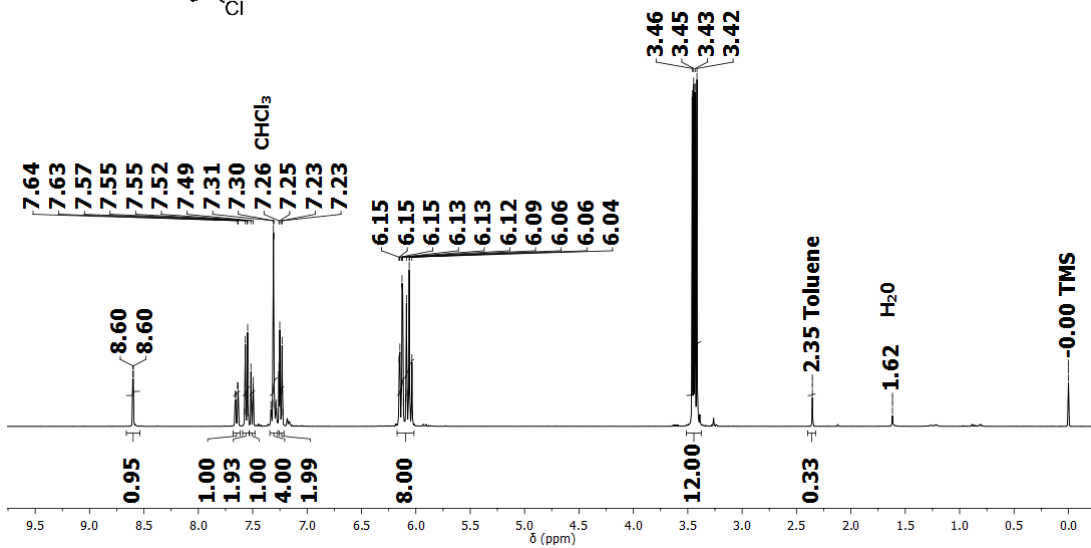
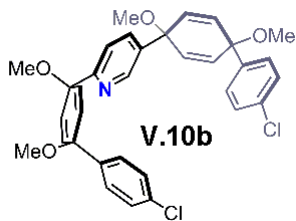


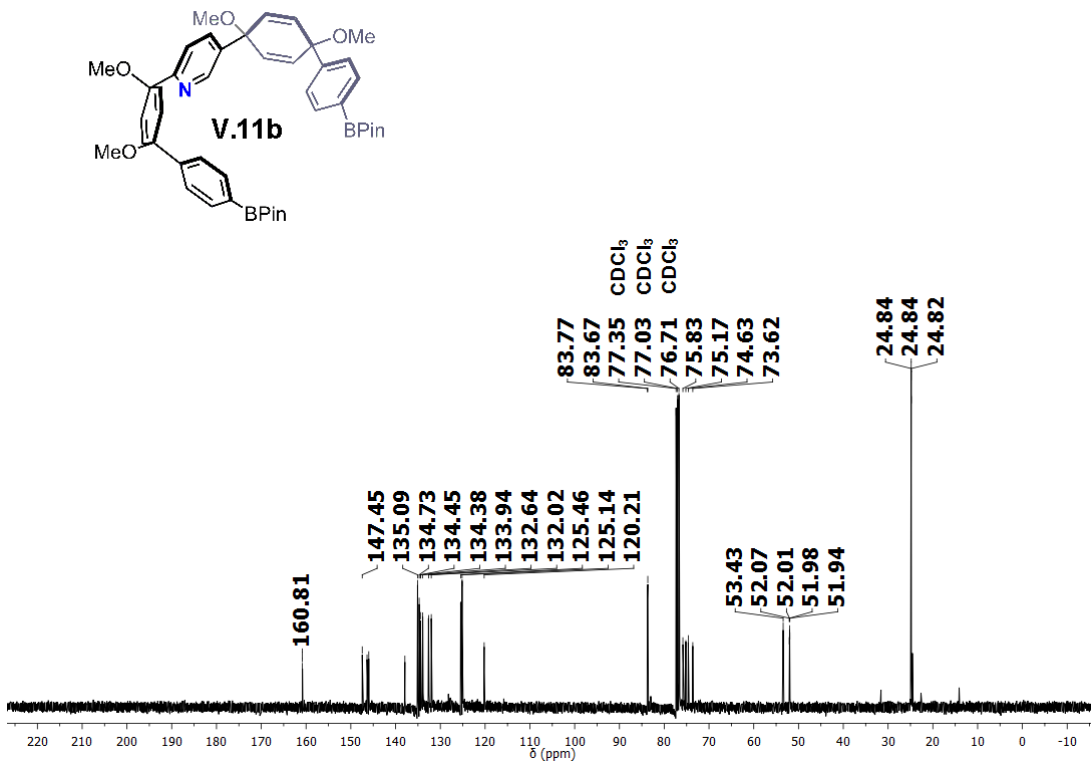
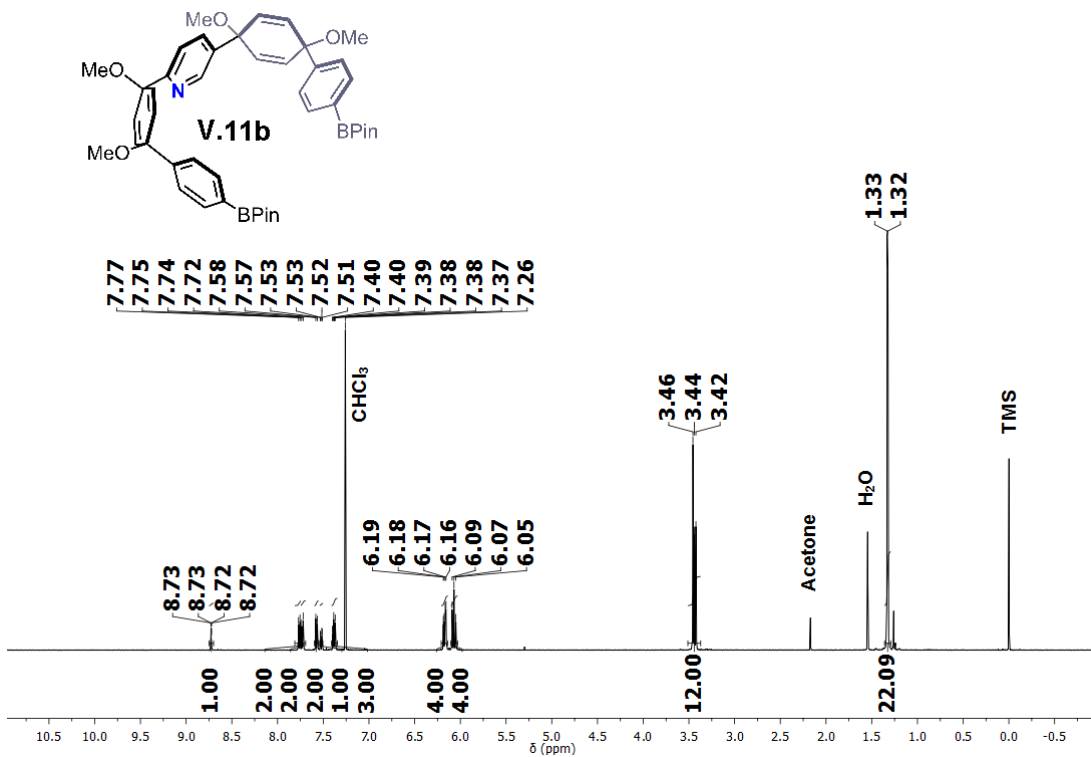


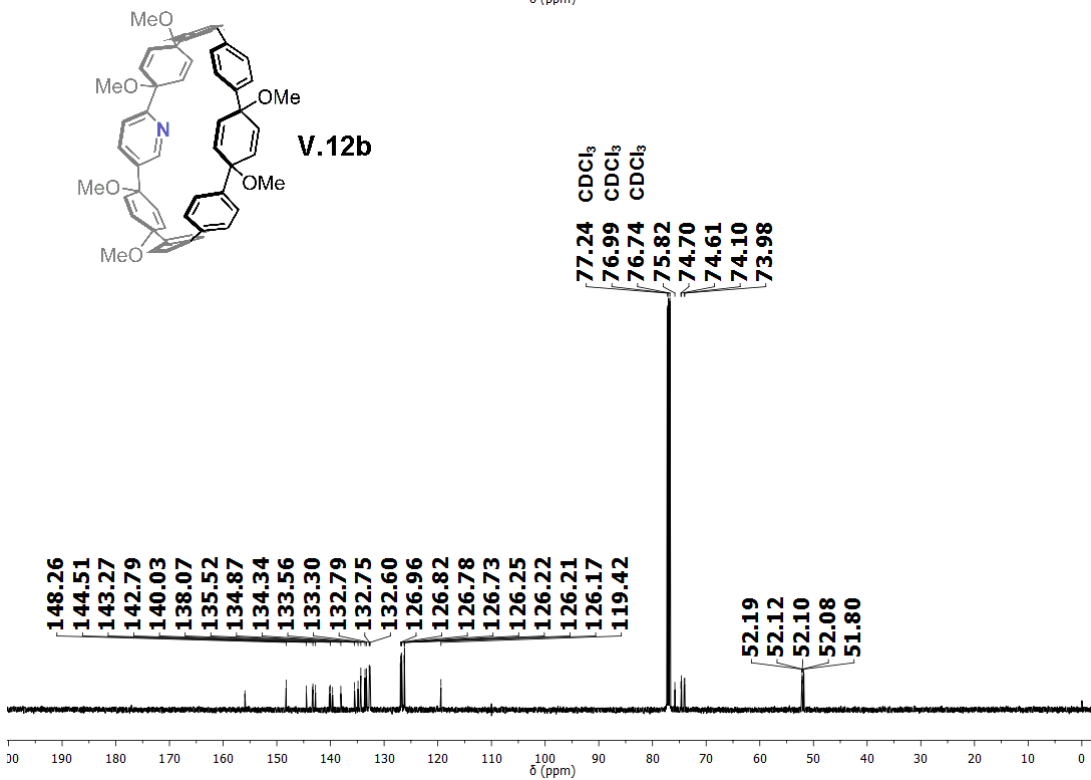
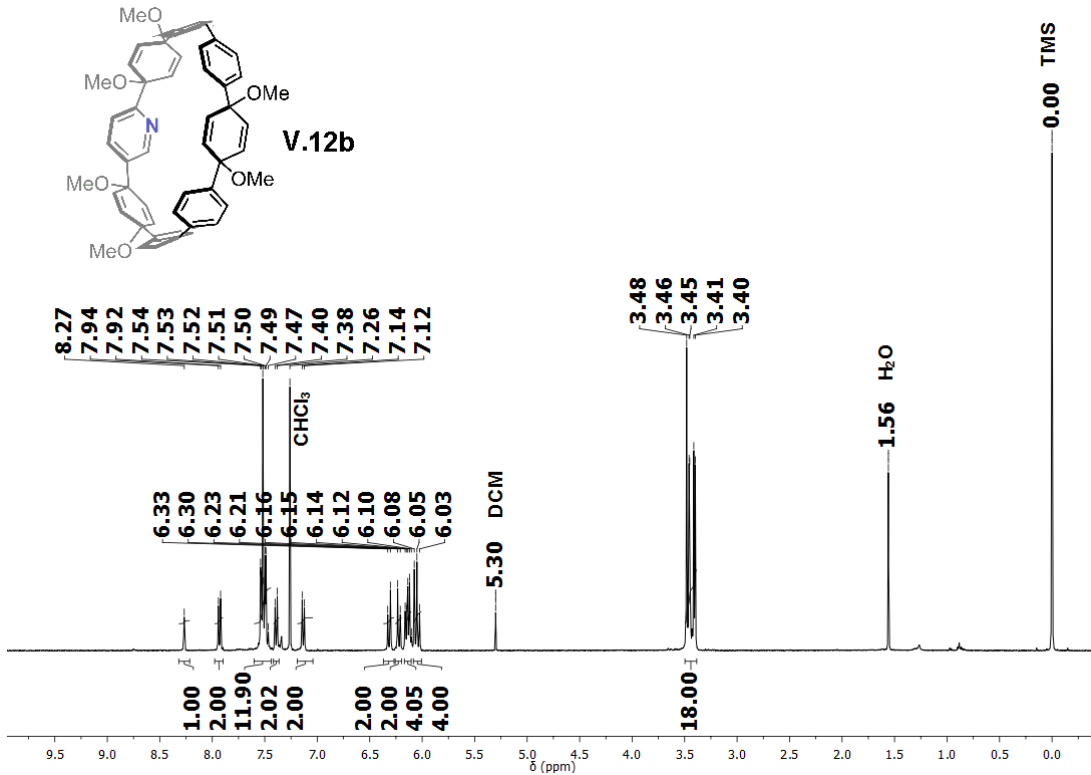


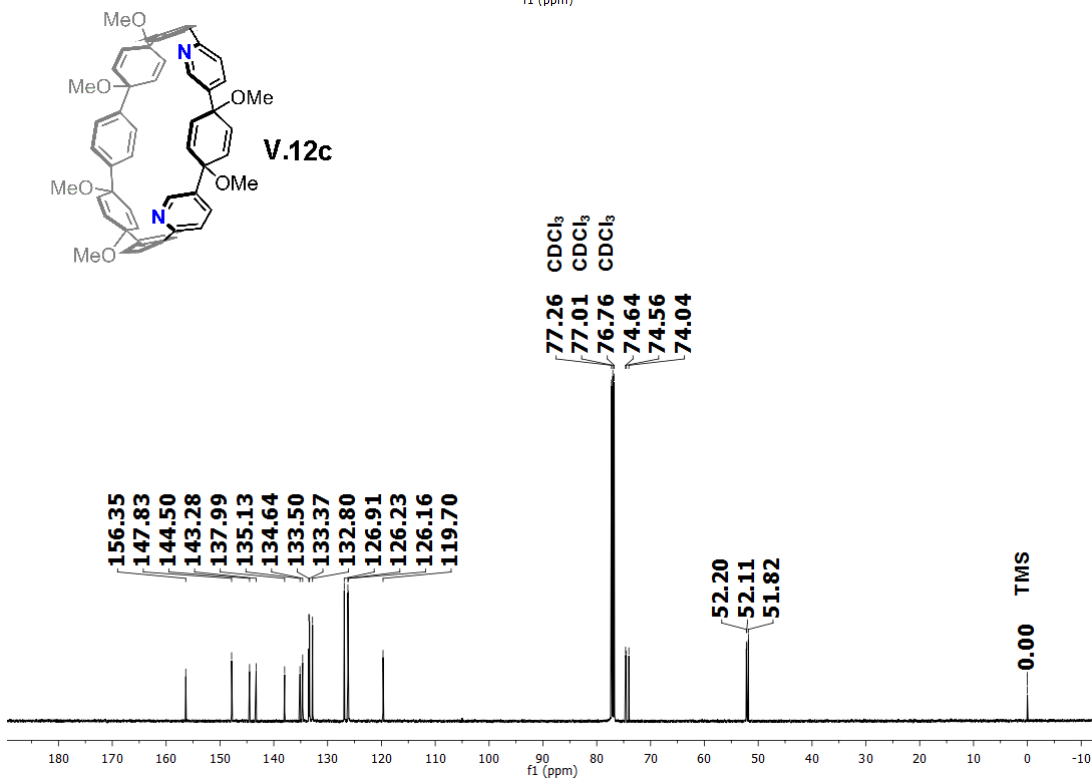
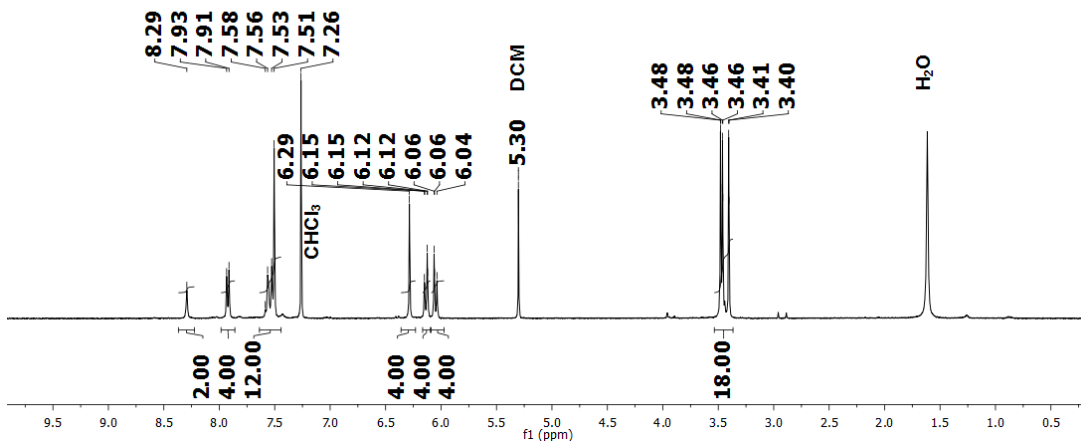
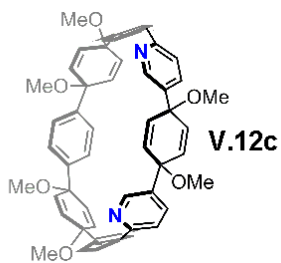


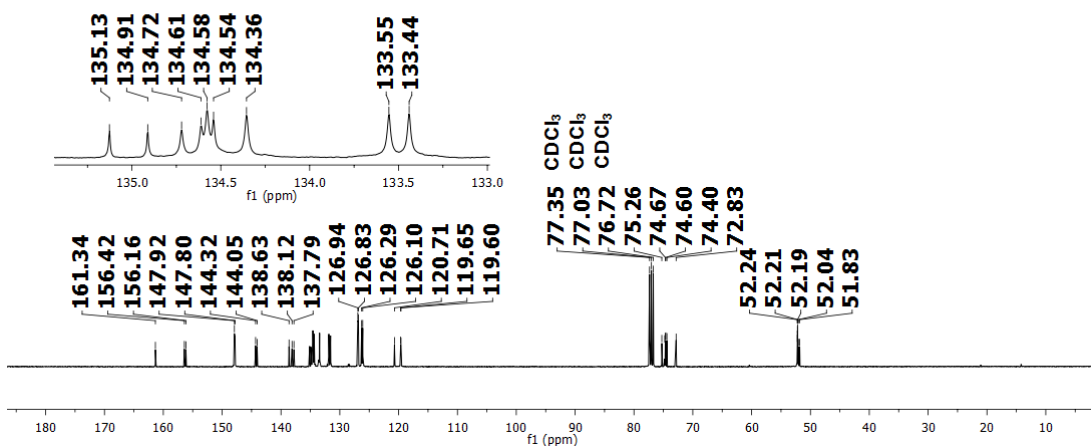
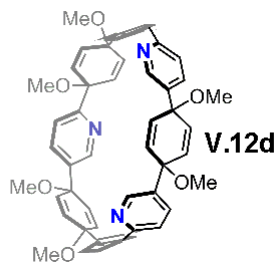
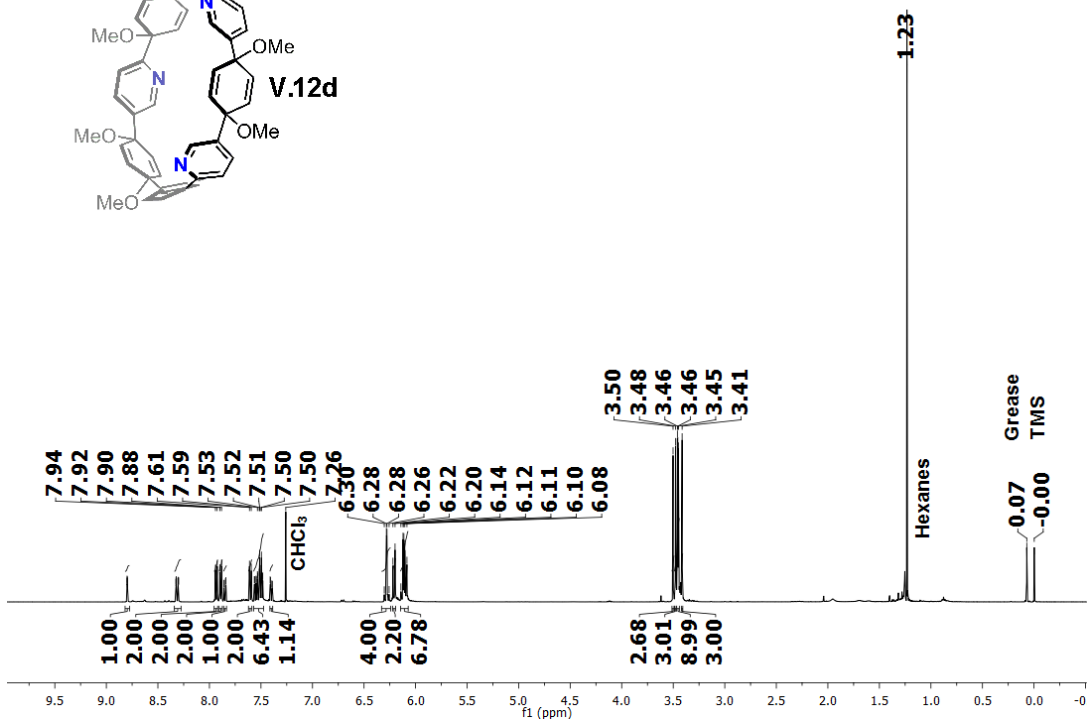
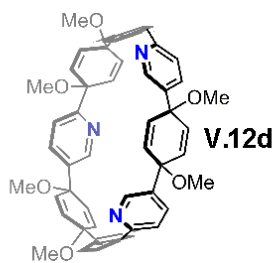


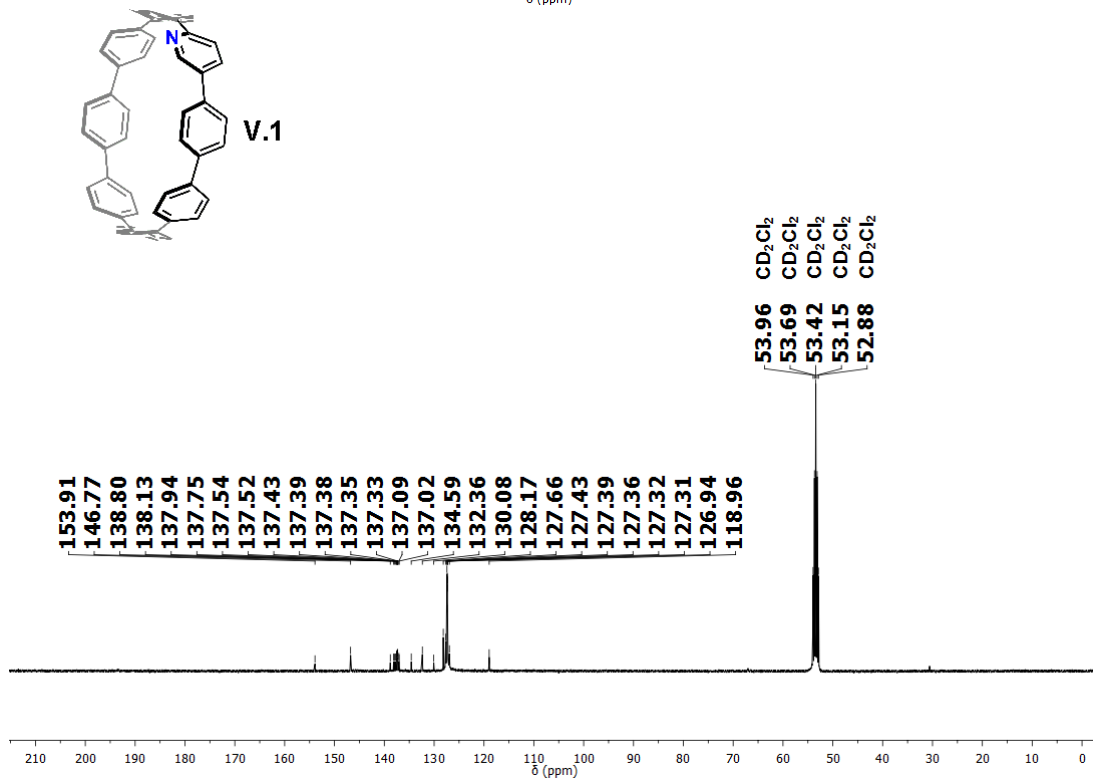
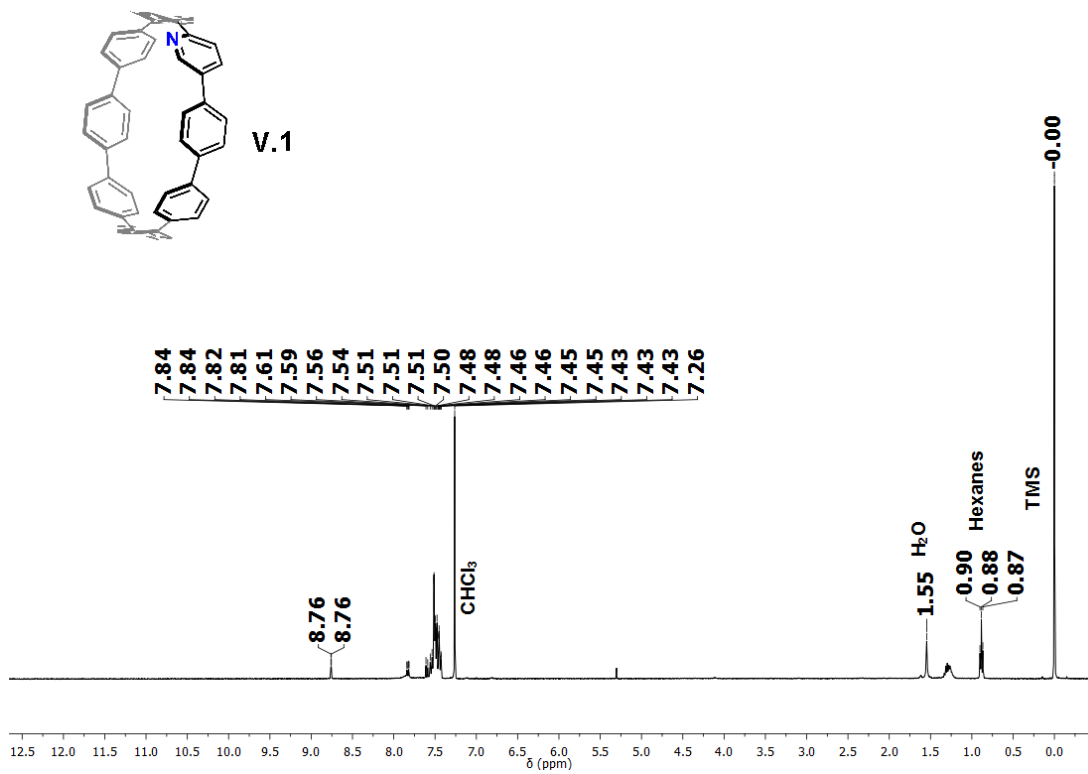


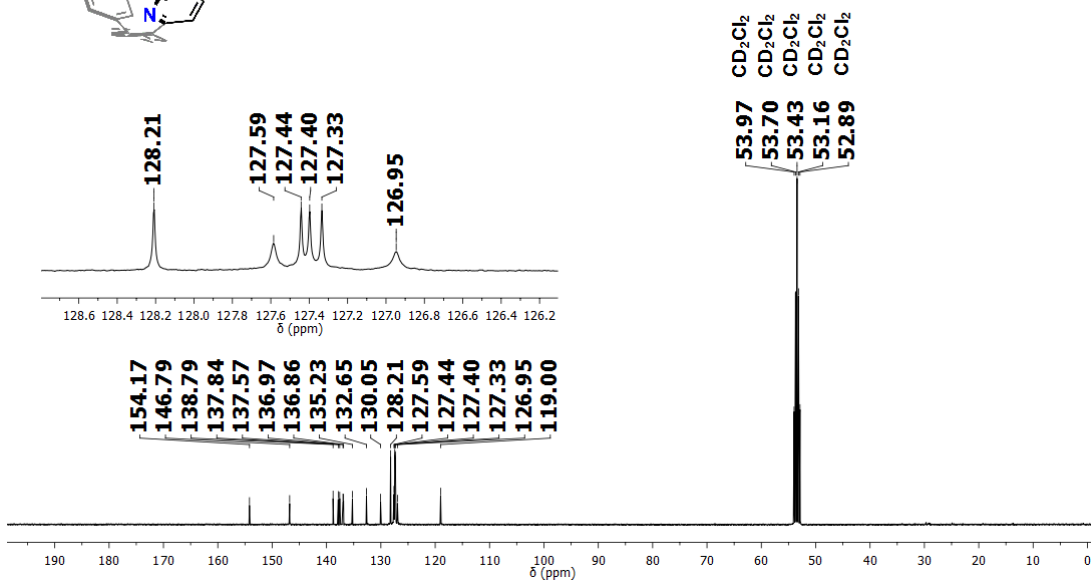
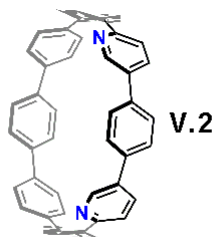
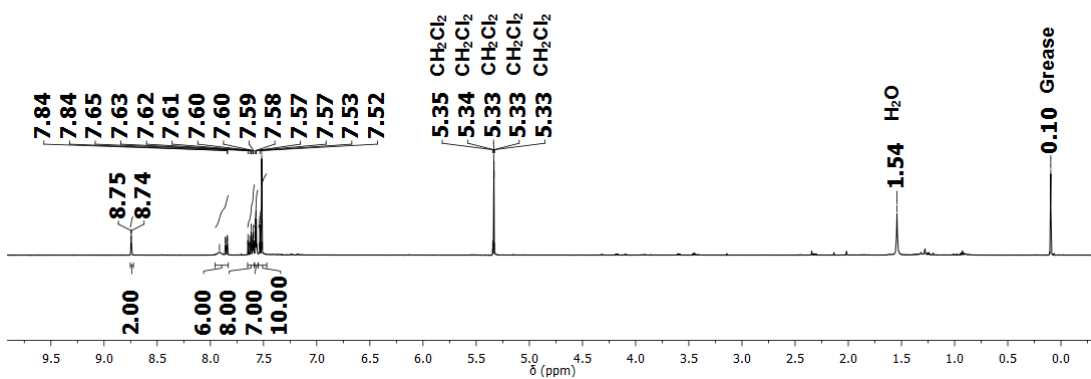
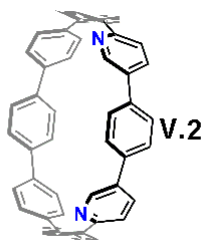


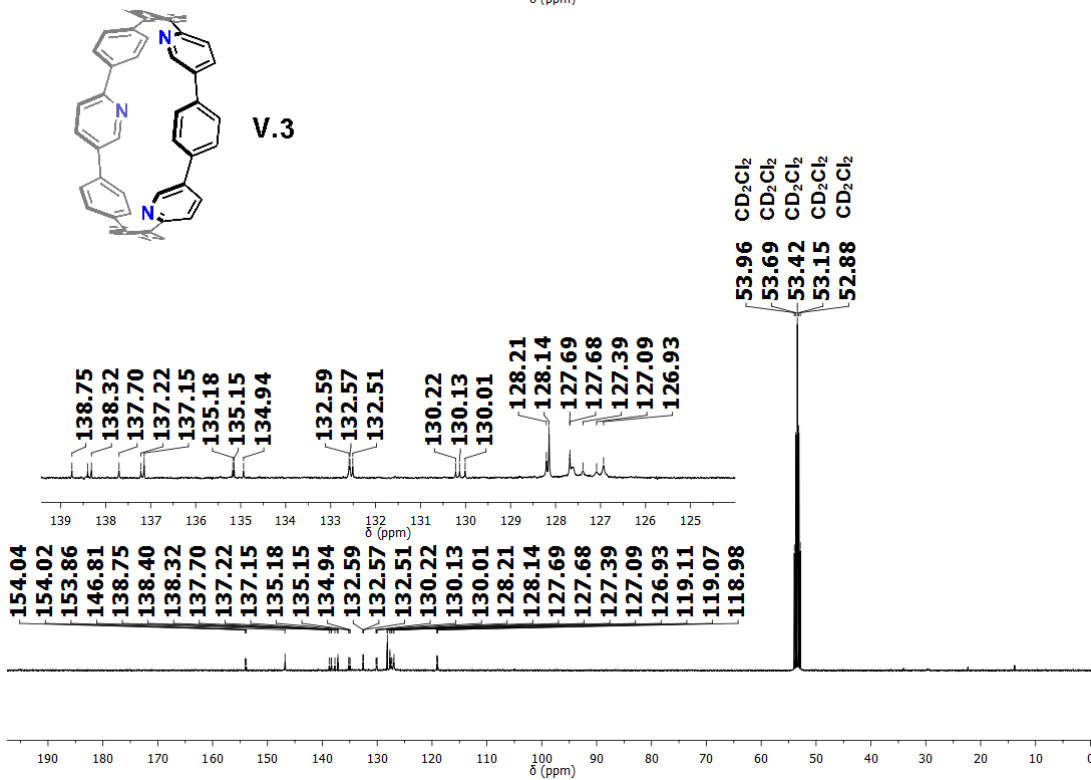
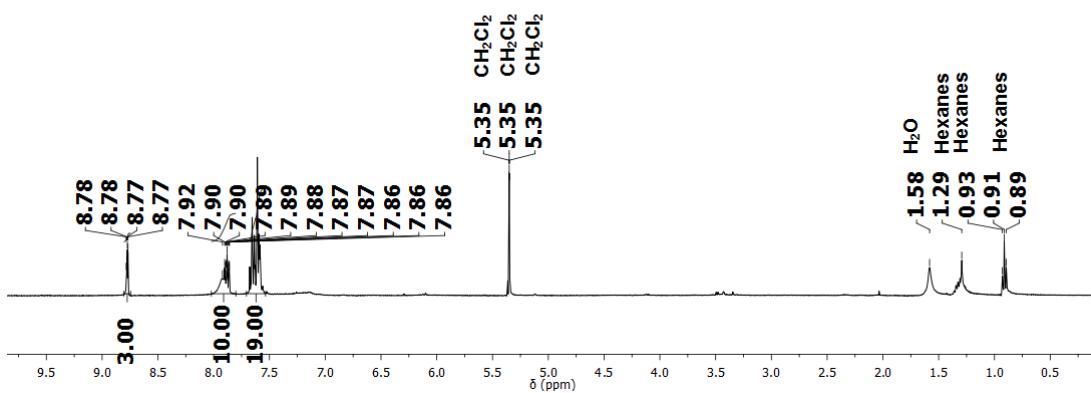
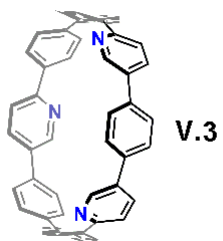


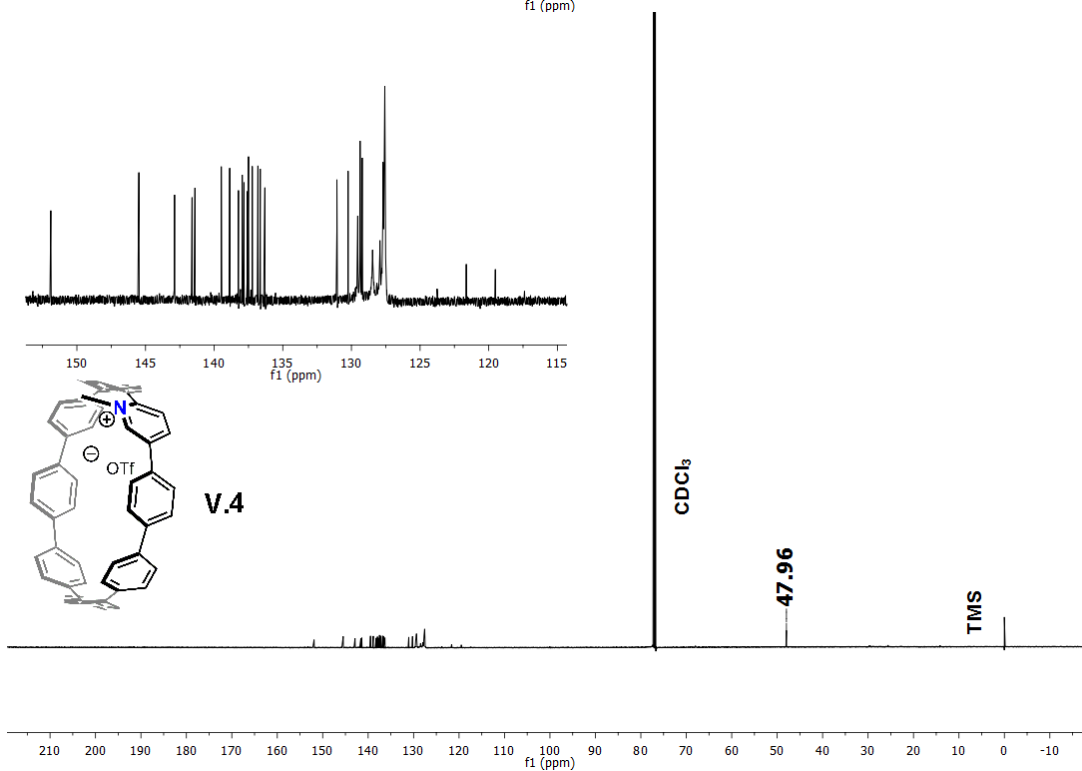
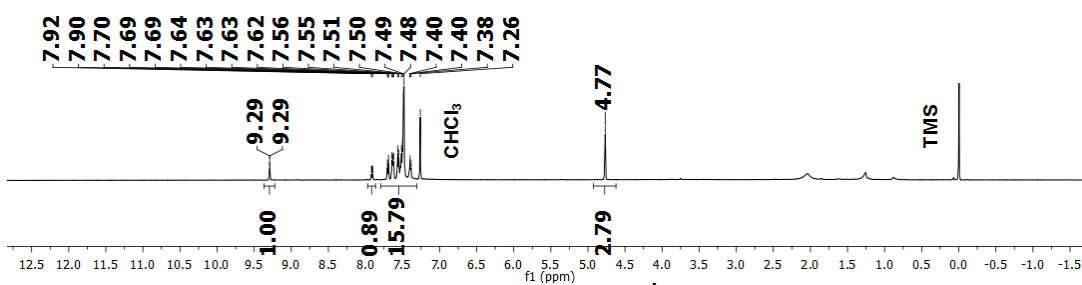
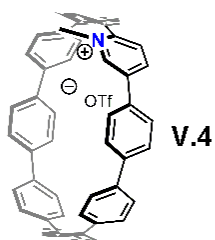


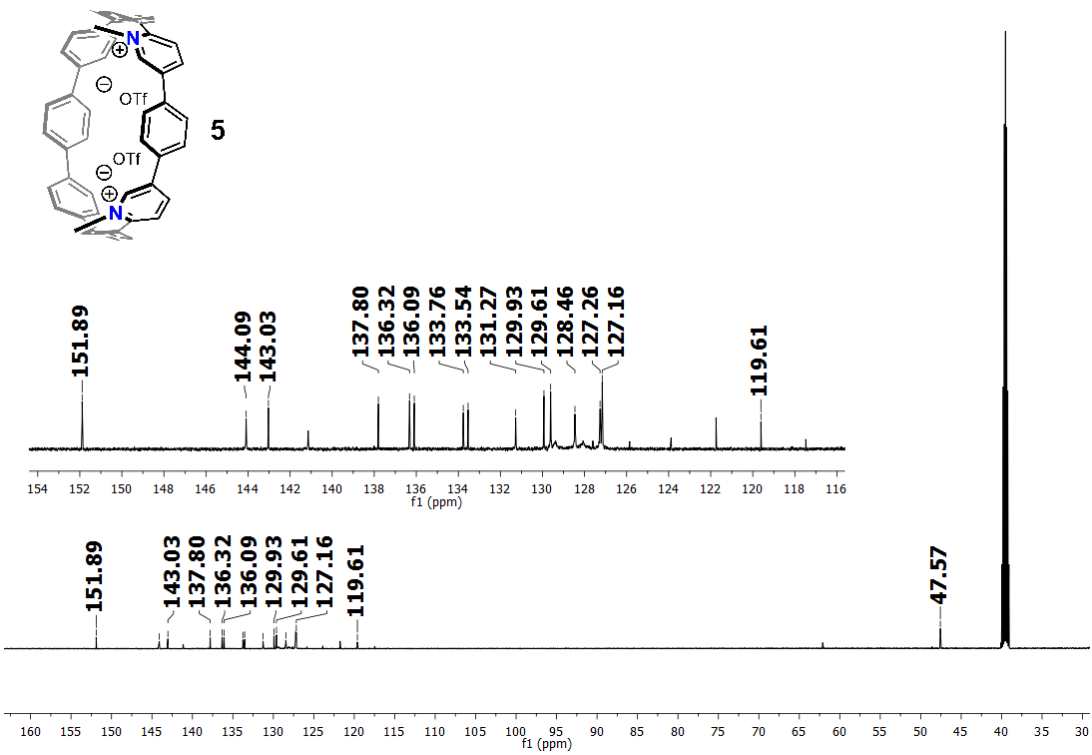
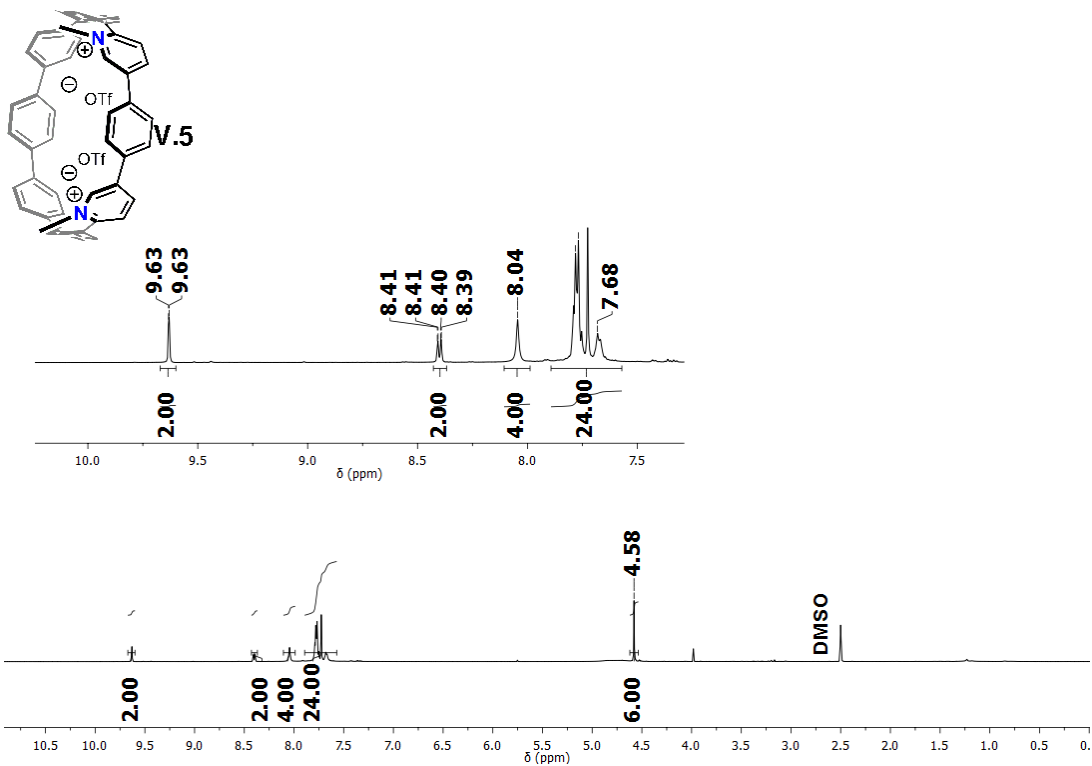












V.6.4. Crystallographic Details.

V.1

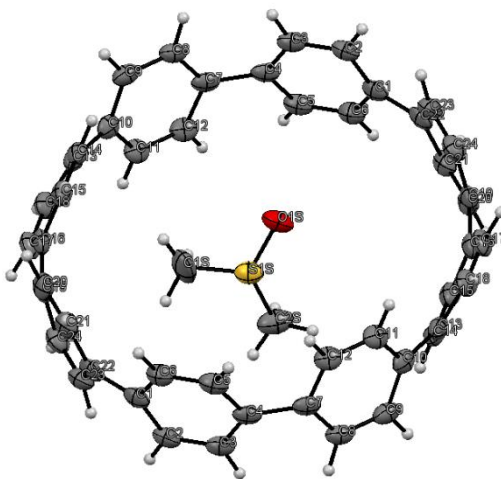


Figure V.10. ORTEP Representation of X-ray Crystallographic Structure Aza[8]CPP

V.1.

Crystallographic Data for **V.1**: $C_{52}H_{44}O_2S_2$, $M = 6764.99$, $0.05 \times 0.04 \times 0.02$ mm, $T = 173(2)$ K, Monoclinic, space group $P2_1/c$, $a = 13.3179(5)$ Å, $b = 9.3373(4)$ Å, $c = 16.7050(8)$ Å, $\beta = 105.759(2)^\circ$, $V = 1999.24(15)$ Å³, $Z = 2$, $D_c = 1.271$ Mg/m³, $\mu(\text{Mo}) = 1.526$ mm⁻¹, $F(000) = 808$, $2\theta_{\text{max}} = 106.6^\circ$, 17195 reflections, 2315 independent reflections [$R_{\text{int}} = 0.0592$], $R_1 = 0.0468$, $wR_2 = 0.1139$ and $\text{GOF} = 1.078$ for 2317 reflections (253 parameters) with $I > 2\sigma(I)$, $R_1 = 0.0625$, $wR_2 = 0.1228$ and $\text{GOF} = 1.078$ for all reflections, max/min residual electron density $+0.332/-0.402$ eÅ⁻³.

V.5

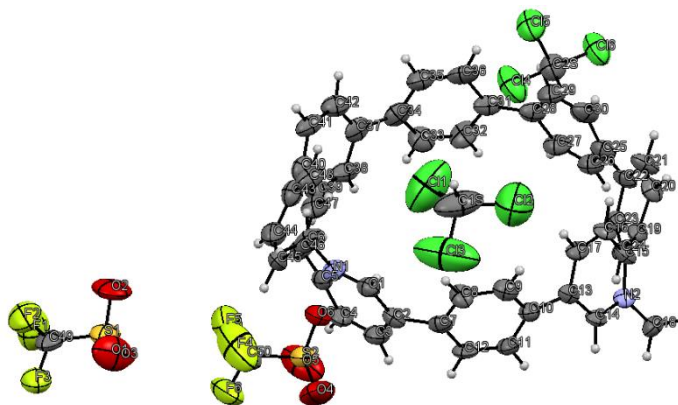


Figure V.11. ORTEP Representation of X-ray Crystallographic Structure *N,N*-dimethyl-1,15-diaza[8]CPP Ditriflate **V.5**.

Crystallographic Data for **V.5**: $C_{56}H_{42}Cl_{18}F_6N_2O_6S_2$, $M = 1655.13$, $0.13 \times 0.08 \times 0.03$ mm, $T = 200(2)$ K, Monoclinic, space group $P2_1/c$, $a = 24.745(12)$ Å, $b = 10.384(5)$ Å, $c = 27.866(13)$ Å, $\beta = 96.257(11)^\circ$, $V = 7117(6)$ Å³, $Z = 4$, $D_c = 1.545$ Mg/m³, $\mu(\text{Mo}) = 7.445$ mm⁻¹, $F(000) = 3328$, $2\theta_{\text{max}} = 135.3^\circ$, 29341 reflections, 7210 independent reflections [$R_{\text{int}} = 0.0828$], $R1 = 0.1035$, $wR2 = 0.3177$ and $\text{GOF} = 1.036$ for 7210 reflections (667 parameters) with $I > 2\sigma(I)$, $R1 = 0.1285$, $wR2 = 0.3387$ and $\text{GOF} = 1.036$ for all reflections, max/min residual electron density $+0.649/-0.497$ eÅ³.

V.8d

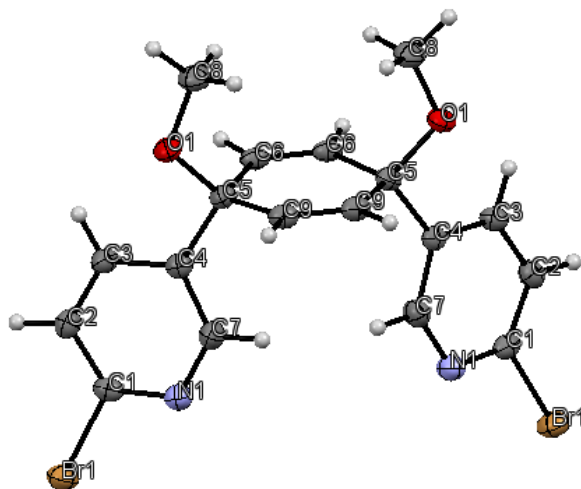


Figure V.12. ORTEP Representation of X-ray Crystallographic Structure **V.8d**.

Crystallographic Data for **V.8d**: $C_{18}H_{16}Br_2N_2O_2$, $M = 452.15$, $0.22 \times 0.08 \times 0.03$ mm, $T = 100$ K, Orthorhombic, space group $Pnma$, $a = 12.562(10)$ Å, $b = 20.755(17)$ Å, $c =$

6.453 (5) Å, $V = 1682.4 (2) \text{ \AA}^3$, $Z = 4$, $D_c = 1.785 \text{ Mg/m}^3$, $\mu(\text{Cu}) = 6.23 \text{ mm}^{-1}$, $F(000) = 896$, $2\theta_{\text{max}} = 131.68^\circ$, 16796 reflections, 1497 independent reflections [$R_{\text{int}} = 0.0468$], $R1 = 0.0308$, $wR2 = 0.0806$ and $\text{GOF} = 0.930$ for 1497 reflections (110 parameters) with $I > 2\sigma(I)$, $R1 = 0.0333$, $wR2 = 0.0806$ and $\text{GOF} = 0.930$ for all reflections, max/min residual electron density $+0.89/-0.39 \text{ e\AA}^3$.

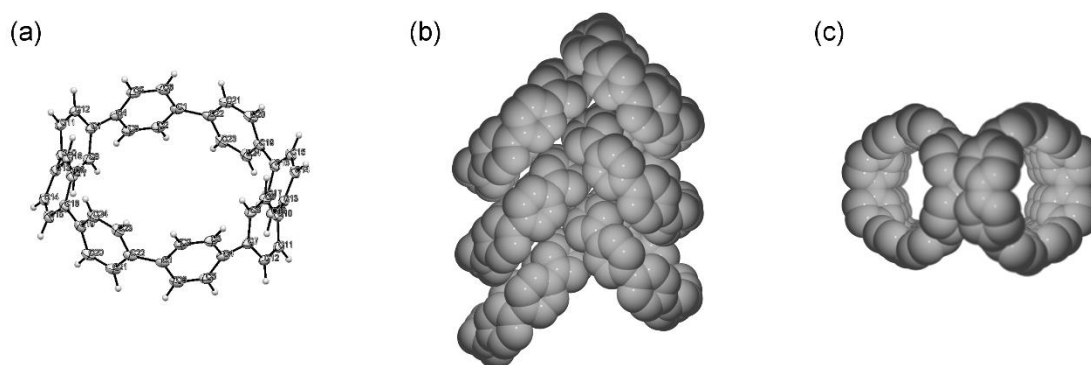


Figure V.13. Published Crystallographic Information for [8]CPP. (a) ORTEP Representation of X-ray Crystallographic Structure [8]CPP (CCDC Registry 871414) (b) Side-on Packing (c) and Top-Down Packing.

V.6.5. Electrochemical Details.

Cyclic voltammetry was conducted utilizing a platinum working electrode, platinum counter electrode, and a silver wire pseudoreference that was separated from the solution via a glass frit. Experiments were performed using a custom designed potentiostat at a scan rate of 50 mV/s. Analyte solutions were freeze-pump-thaw degassed three times and all experiments were conducted under airfree conditions. Analyte solutions were prepared using 0.1M tetrabutylammonium tetrafluoroborate in THF, with analyte concentrations 1-5mM. The Ag pseudoreference was calibrated versus the ferrocene/ferrocinium redox couple following the CV of each compound.

V.6.6. Photophysical Details.

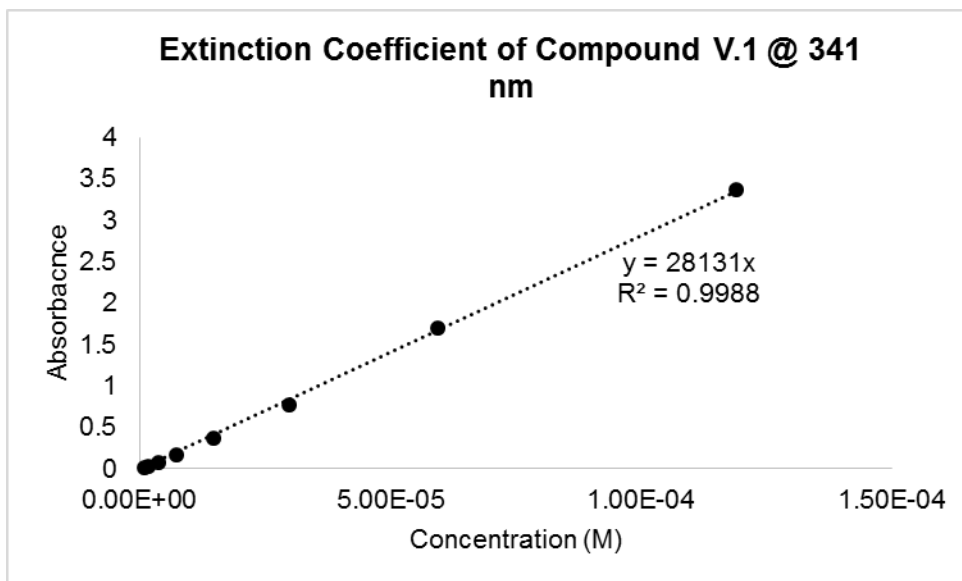


Figure V.14. Beer-Lambert plot of V.1 at 341 nm. ($\epsilon = 2.8 \times 10^4 \text{ M}^{-1} \text{ cm}^{-1}$)

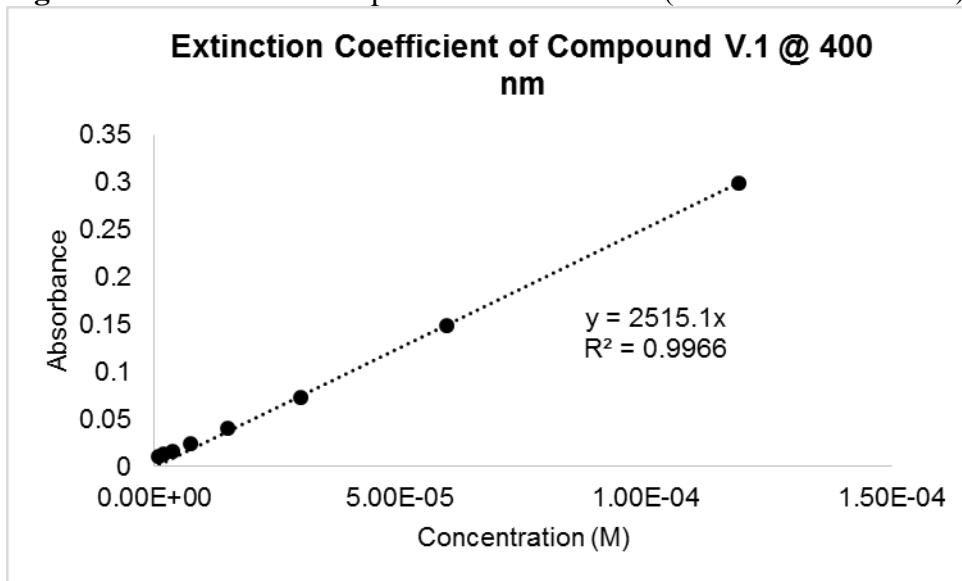


Figure V.15. Beer-Lambert plot of V.1 at 400 nm. ($\epsilon = 0.25 \times 10^4 \text{ M}^{-1} \text{ cm}^{-1}$)

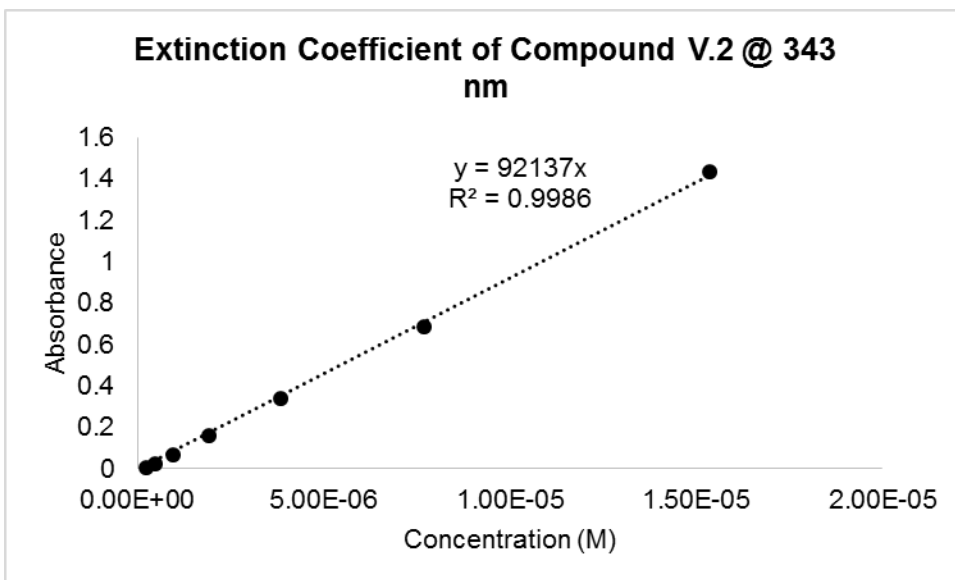


Figure V.16. Beer-Lambert plot of V.2 at 343 nm. ($\epsilon = 9.2 \times 10^4 \text{ M}^{-1} \text{ cm}^{-1}$)

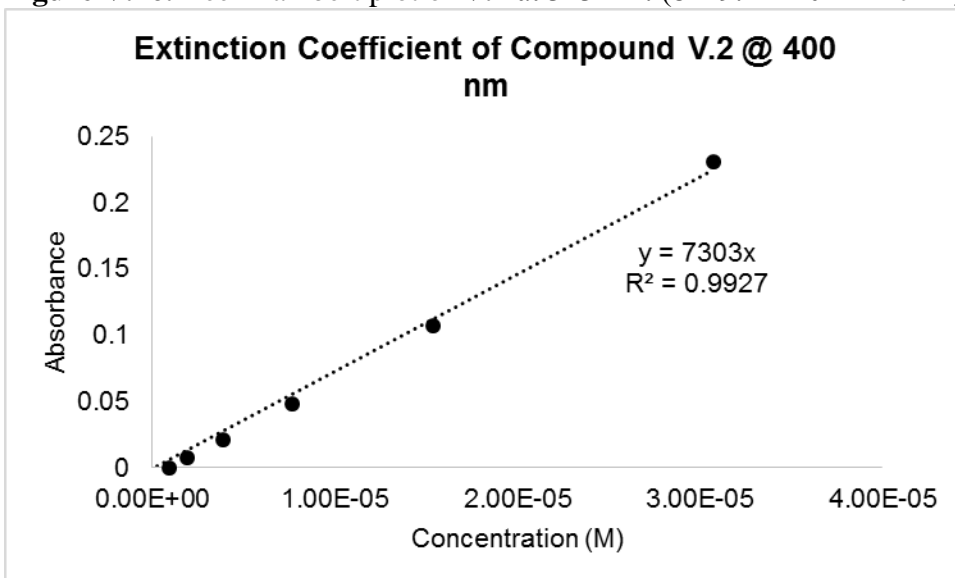


Figure V.17. Beer-Lambert plot of V.2 at 400 nm. ($\epsilon = 0.73 \times 10^4 \text{ M}^{-1} \text{ cm}^{-1}$)

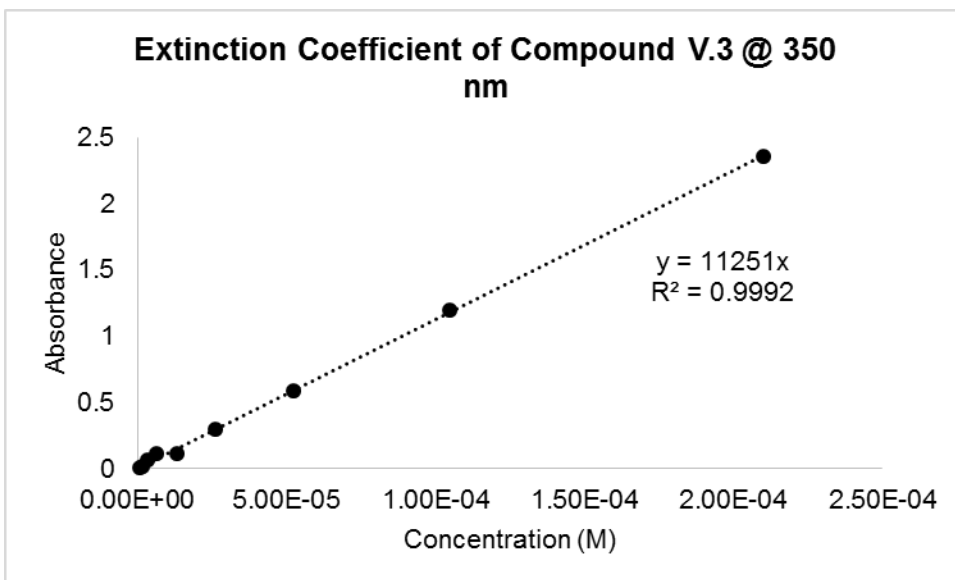


Figure V.18. Beer-Lambert plot of V.3 at 350 nm. ($\epsilon = 1.1 \times 10^4 \text{ M}^{-1} \text{ cm}^{-1}$)

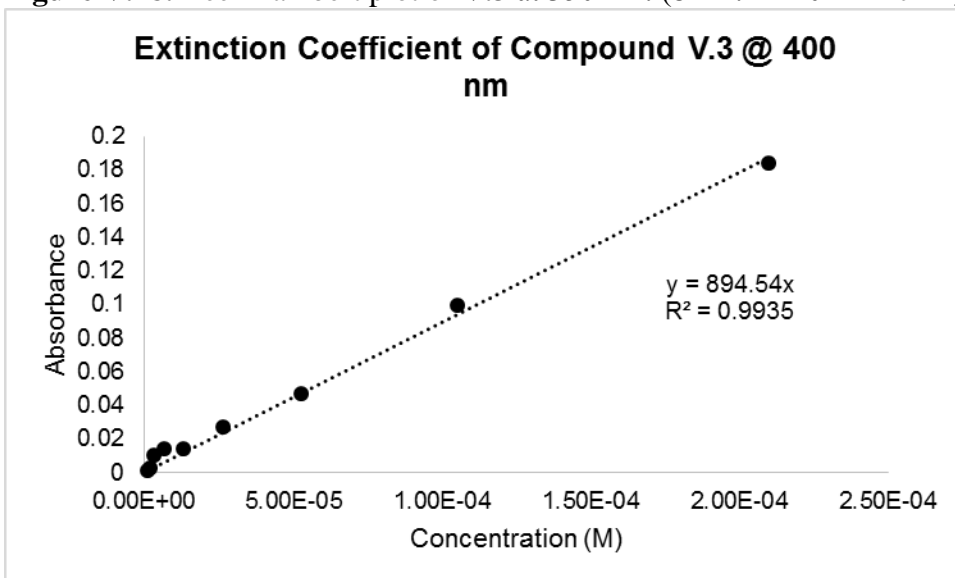


Figure V.19. Beer-Lambert plot of V.3 at 400 nm. ($\epsilon = 0.089 \times 10^4 \text{ M}^{-1} \text{ cm}^{-1}$)

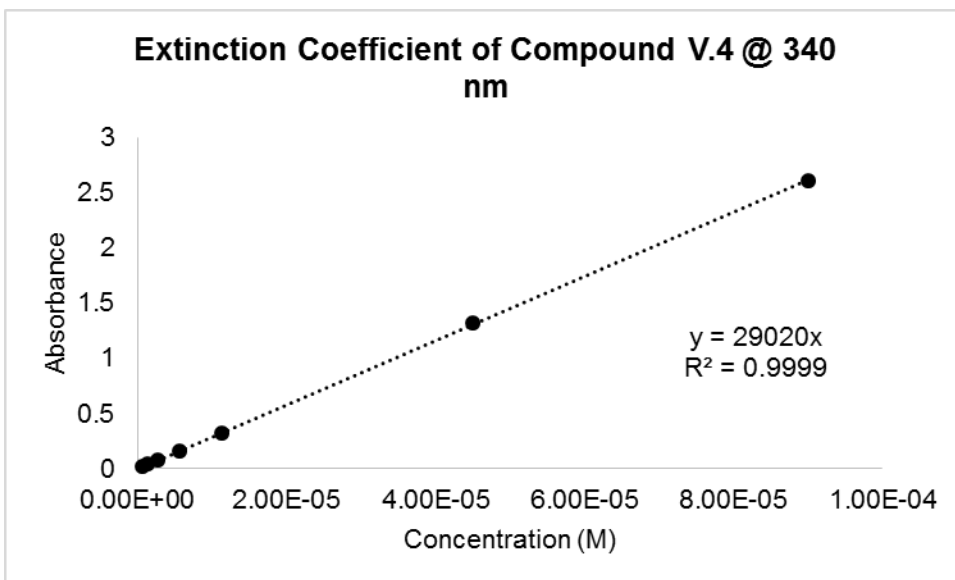


Figure V.20. Beer-Lambert plot of V.4 at 340 nm. ($\epsilon = 2.9 \times 10^4 \text{ M}^{-1} \text{ cm}^{-1}$)

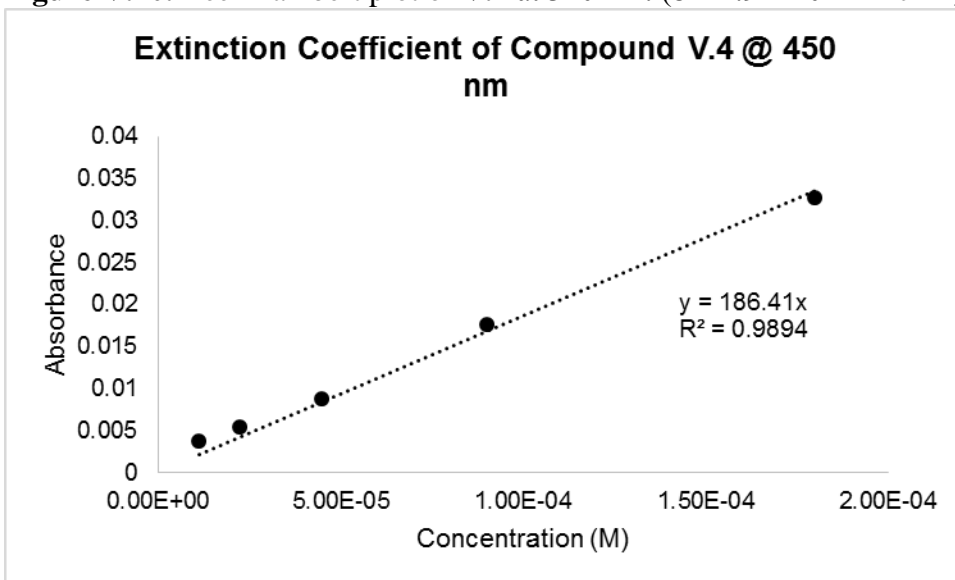


Figure V.21. Beer-Lambert plot of V.4 at 450 nm. ($\epsilon = 0.019 \times 10^4 \text{ M}^{-1} \text{ cm}^{-1}$)

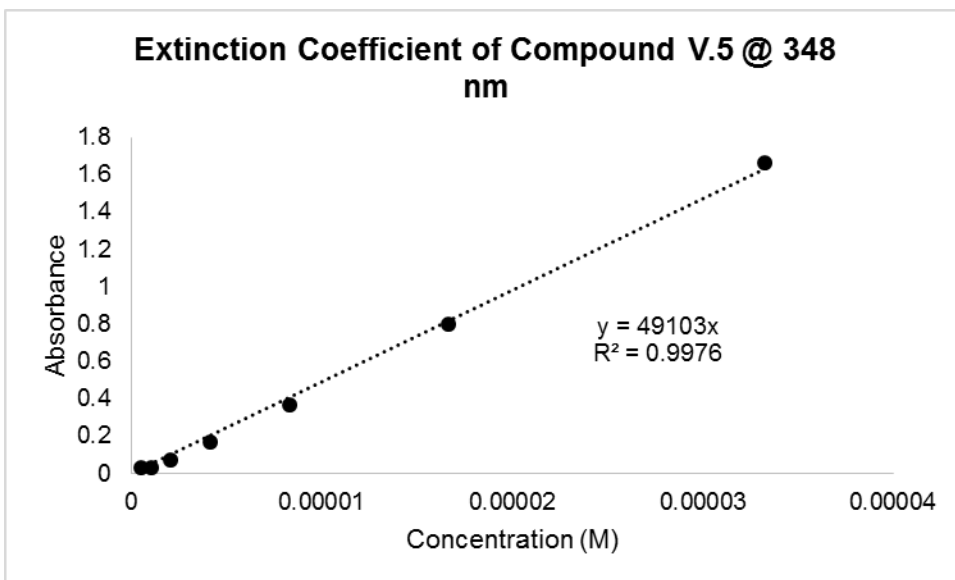


Figure V.22. Beer-Lambert plot of V.5 at 348 nm. ($\epsilon = 4.9 \times 10^4 \text{ M}^{-1} \text{ cm}^{-1}$)

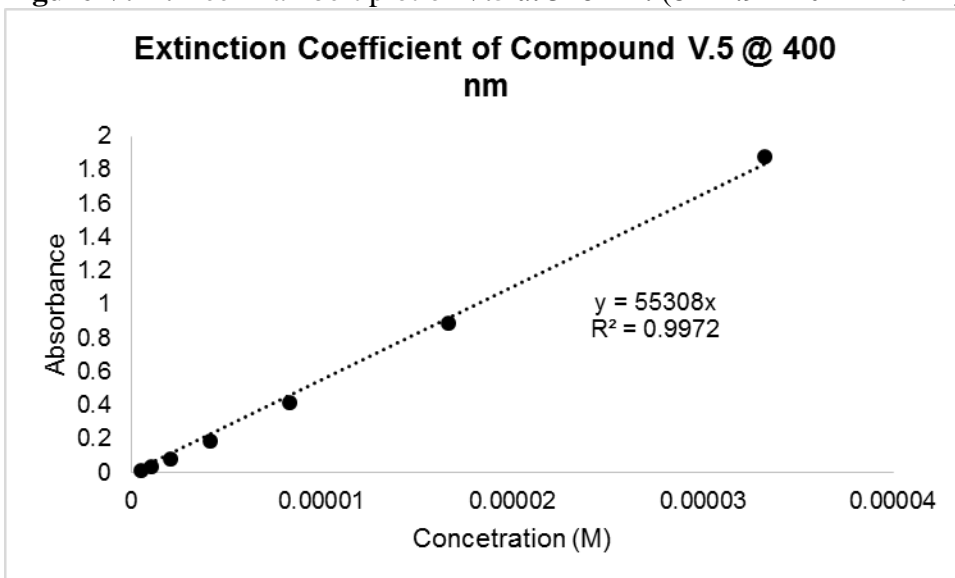


Figure V.23. Beer-Lambert plot of V.5 at 400 nm. ($\epsilon = 5.5 \times 10^4 \text{ M}^{-1} \text{ cm}^{-1}$)

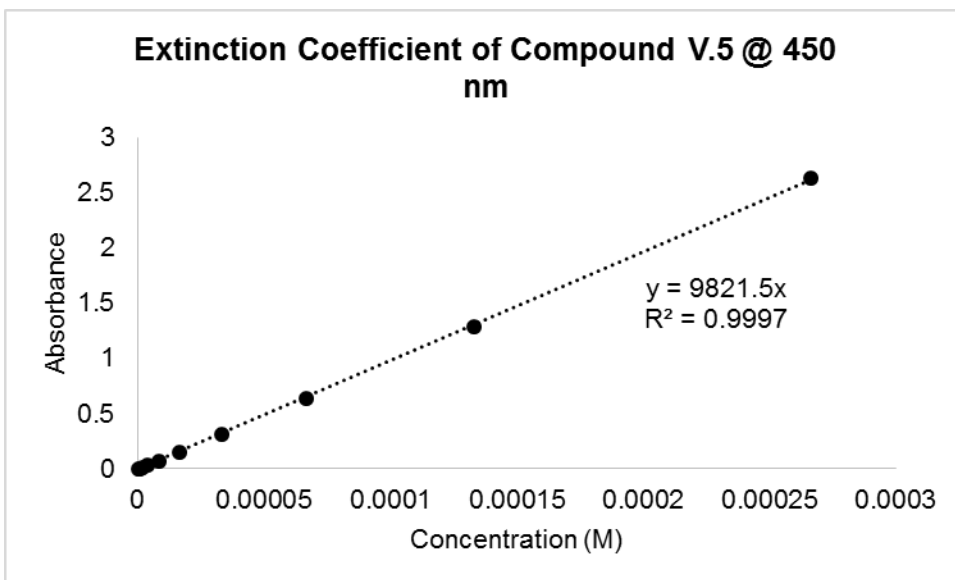


Figure V.24. Beer-Lambert plot of V.5 at 450 nm. ($\epsilon = 0.98 \times 10^4 \text{ M}^{-1} \text{ cm}^{-1}$)

V.6.7. Computational Details.

All calculations were carried out with Gaussian 09 package at B3LYP/6-31g* level of theory.⁶ Geometries were first optimized in the gas phase. Once optimized a single point calculation was carried out using the CPCM solvation model with acetonitrile as the solvent continuum to account for charged species.⁷ All excited state calculations (TD-DFT) were performed on fully optimized structures. The fully optimized structures were confirmed to be true minima by vibrational analysis. Structures were minimized with no symmetry restrictions.

Calculated Optical Transitions using TD-DFT B3LYP/6-31g*

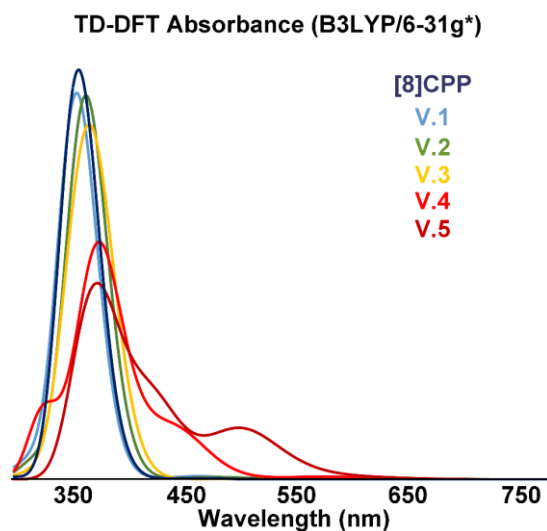


Figure V.25. TD-DFT (B3LYP/6-31g*) Plot for Compounds V.1- V.5 and [8]CPP.

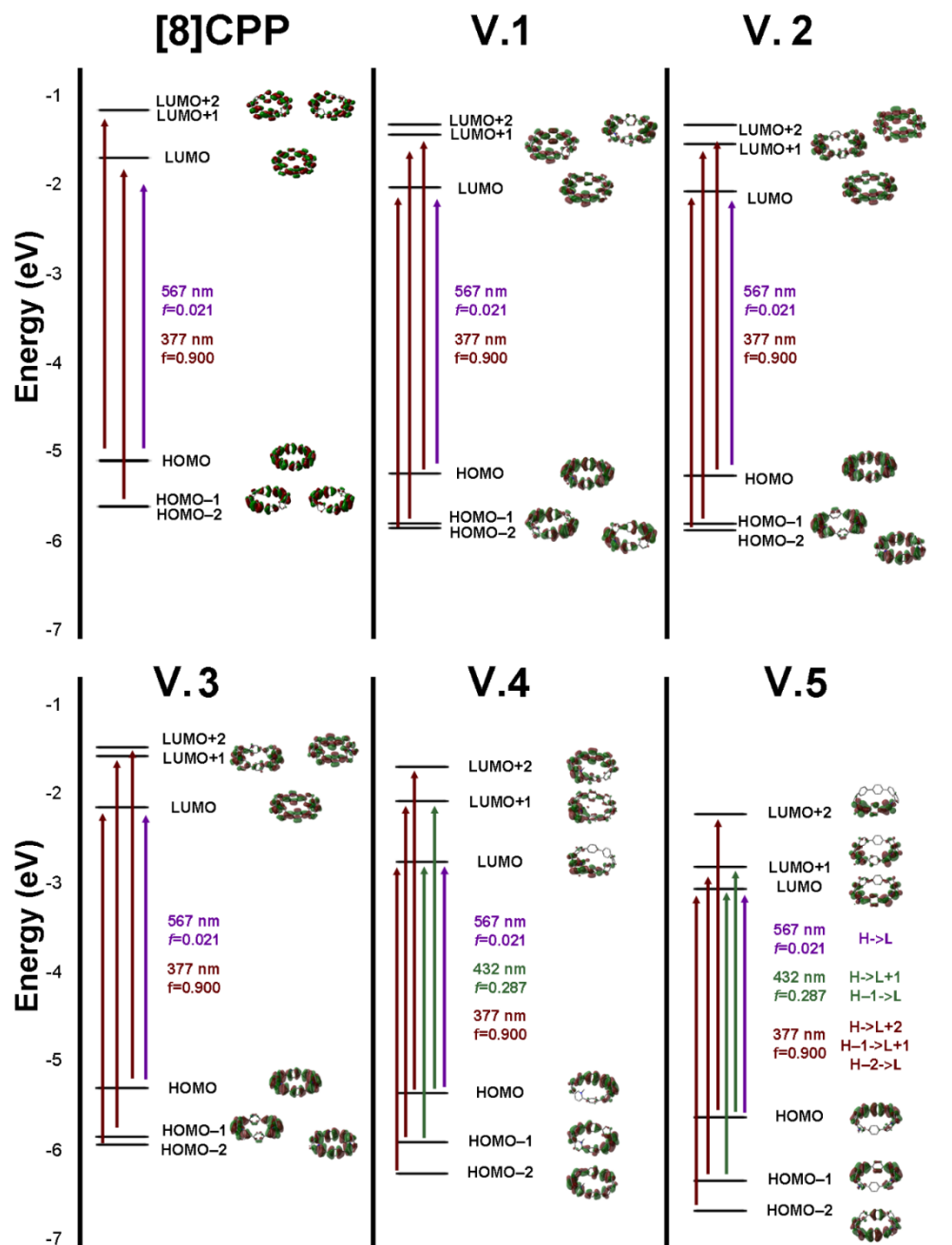


Figure V.26. TD-DFT (B3LYP/6-31g*) Major Transitions and Orbital Densities for Compounds V.1- V.5 and [8]CPP.

Energy (cm ⁻¹)	Wavelength (nm)	Osc. Strength	Major contributions
21813	458	0.0252	HOMO->LUMO (97%)
27563	363	0.2349	H-1->LUMO (76%), HOMO->L+1 (22%)
27841	359	0.4107	H-2->LUMO (37%), H-1->LUMO (14%), HOMO->L+1 (44%)

28068	356	1.4312	H-2->LUMO (60%), HOMO->L+1 (32%)
28800	347	1.092	HOMO->L+2 (96%)
31438	318	0.0443	HOMO->L+3 (81%)
31728	315	0.0577	H-2->L+1 (14%), H-2->L+2 (17%), H-1->L+1 (59%)
32008	312	0.0296	H-2->L+1 (44%), H-1->L+1 (17%), H-1->L+2 (26%)
33290	300	0.0036	H-5->LUMO (12%), HOMO->L+4 (58%)
33354	300	0.0187	H-3->LUMO (36%), H-1->L+2 (13%)
33876	295	0.0021	H-2->L+1 (33%), H-1->L+2 (48%)
33996	294	0.0146	H-2->L+2 (65%), H-1->L+1 (17%)

Table V.2. Major Electronic Transitions for Aza[8]CPP **V.1** Determined by TD-DFT Method Using B3LYP/6-31g*.

Energy (cm-1)	Wavelength (nm)	Osc. Strength	Major contributions
21813	458	0.0252	HOMO->LUMO (97%)
27563	363	0.2349	H-1->LUMO (76%), HOMO->L+1 (22%)
27841	359	0.4107	H-2->LUMO (37%), H-1->LUMO (14%), HOMO->L+1 (44%)
28068	356	1.4312	H-2->LUMO (60%), HOMO->L+1 (32%)
28800	347	1.092	HOMO->L+2 (96%)
31438	318	0.0443	HOMO->L+3 (81%)
31728	315	0.0577	H-2->L+1 (14%), H-2->L+2 (17%), H-1->L+1 (59%)
32008	312	0.0296	H-2->L+1 (44%), H-1->L+1 (17%), H-1->L+2 (26%)
33290	300	0.0036	H-5->LUMO (12%), HOMO->L+4 (58%)
33354	300	0.0187	H-3->LUMO (36%), H-1->L+2 (13%)
33876	295	0.0021	H-2->L+1 (33%), H-1->L+2 (48%)
33996	294	0.0146	H-2->L+2 (65%), H-1->L+1 (17%)

Table V.3. Major Electronic Transitions for 1,15-diaza[8]CPP **V.2** Determined by TD-DFT Method Using B3LYP/6-31g*.

Energy (cm-1)	Wavelength (nm)	Osc. Strength	Major contributions
20895	479	0.0056	HOMO->LUMO (97%)
26474	378	0.3135	H-1->LUMO (10%), HOMO->L+1 (88%)
26966	371	1.2147	H-1->LUMO (87%)
27332	366	0.6758	H-2->LUMO (95%)
28522	351	1.0314	HOMO->L+2 (97%)
30548	327	0.0113	H-1->L+1 (84%)
30865	324	0.018	H-2->L+1 (77%), H-1->L+2 (19%)
31323	319	0.0111	HOMO->L+3 (78%)
31671	316	0.0148	HOMO->L+4 (77%)
32907	304	0.0029	HOMO->L+5 (61%)
32973	303	0.011	H-5->LUMO (10%), H-3->LUMO (30%), HOMO->L+5 (13%)
33348	300	0.007	H-2->L+1 (14%), H-1->L+2 (63%)

Table V.4. Major Electronic Transitions for 1,15,31-triaza[8]CPP **V.3** Determined by TD-DFT Method Using B3LYP/6-31g*.

Energy (cm-1)	Wavelength (nm)	Osc. Strength	Major contributions
17642	567	0.0211	HOMO->LUMO (97%)
22549	443	0.2872	H-1->LUMO (96%)
23135	432	0.0754	HOMO->L+1 (91%)
24872	402	0.2284	H-2->LUMO (86%)
26530	377	0.9003	HOMO->L+2 (81%)
26958	371	0.6285	HOMO->L+3 (92%)
27713	361	0.3411	H-1->L+1 (96%)
30261	330	0.1507	H-2->L+1 (90%)
30575	327	0.0542	H-3->LUMO (81%)
30753	325	0.0062	H-4->LUMO (76%)
30829	324	0.3272	H-1->L+2 (80%)
31115	321	0.0277	H-1->L+3 (80%)

Table V.5. Major Electronic Transitions for *N*-methylaza[8]CPP Triflate **V.4** Determined by TD-DFT Method Using B3LYP/6-31g*.

Energy (cm-1)	Wavelength (nm)	Osc. Strength	Major contributions
17128.11	583.8356	0.021	HOMO->LUMO (97%)
20140.61	496.5093	0.3892	HOMO->L+1 (100%)
23722.54	421.54	0.5499	H-1->LUMO (96%)
24537.17	407.545	0.027	HOMO->L+2 (86%)
24910.61	401.4354	0.026	H-2->LUMO (24%), H-1->L+1 (49%), HOMO->L+3 (11%)
25917.19	385.8443	0.1648	H-2->LUMO (57%), H-1->L+1 (39%)
26478.56	377.6641	0.7374	HOMO->L+3 (84%)
27597.26	362.3549	0.5307	HOMO->L+4 (91%)
27845.68	359.1222	0.2789	H-2->L+1 (94%)
29147.47	343.083	0.0067	H-3->LUMO (89%)
29804.01	335.5254	0.0012	H-4->LUMO (79%)
30058.07	332.6893	0.0075	H-1->L+2 (95%)

Table V.6. Major Electronic Transitions for *N,N*-dimethylaza[8]CPP Ditriflate **V.5** Determined by TD-DFT Method Using B3LYP/6-31g*.

TD-DFT Absorbance (B3LYP/6-31g*)

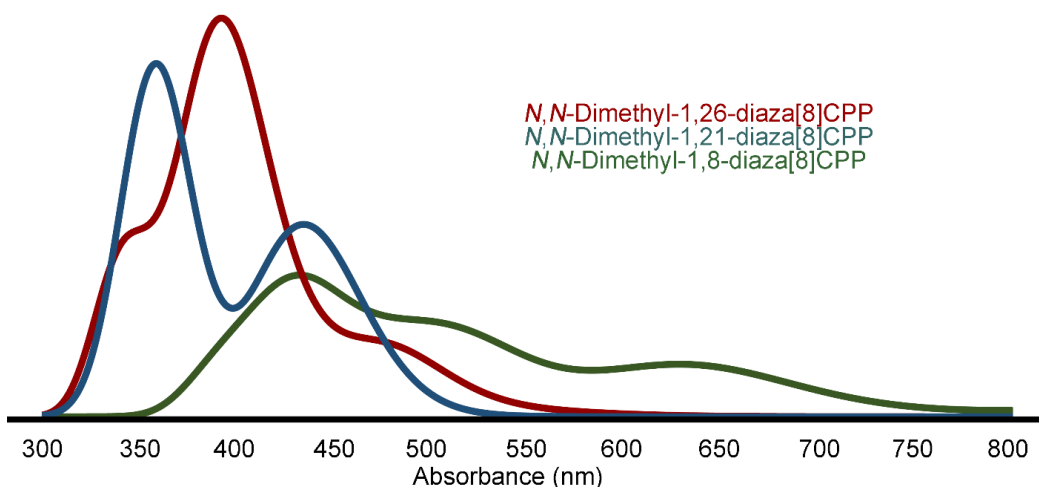


Figure V.27. TD-DFT (B3LYP/6-31g*) Plots for Theoretical Structures *N,N*-Dimethyl-1,26-diaza[8]CPP, *N,N*-Dimethyl-1,21-diaza[8]CPP, and *N,N*-Dimethyl-1,8-diaza[8]CPP.

Energy (cm ⁻¹)	Wavelength (nm)	Osc. Strength	Major contribs
20050.28	498.7463	0.0006	HOMO->LUMO (96%)
22248.15	449.4756	0.3873	HOMO->L+1 (98%)
23544.29	424.7314	0.4828	H-1->LUMO (97%)
24300.04	411.522	0.001	H-1->L+1 (95%)
26658.42	375.116	0.0032	HOMO->L+2 (92%)
27455.3	364.2284	0.3974	H-2->LUMO (89%)
27720.66	360.7418	0.7907	HOMO->L+3 (91%)
28378.81	352.3755	0.0047	H-2->L+1 (87%)
29091.81	343.7393	0.3808	H-1->L+2 (95%)
29895.15	334.5025	0.0001	H-1->L+3 (87%)
30956.58	323.0331	0.0001	H-3->LUMO (86%)
31111.44	321.4252	0.0129	H-4->LUMO (85%)

Table V.7. Major Electronic Transitions for *N,N*-Dimethyl-1,26-diaza[8]CPP Determined by TD-DFT Method Using B3LYP/6-31g*.

Energy (cm ⁻¹)	Wavelength (nm)	Osc. Strength	Major contribs
18031.46	554.5864	0.0182	HOMO->LUMO (96%)
20902	478.4231	0.2643	HOMO->L+1 (98%)
23527.36	425.0371	0.1906	H-1->LUMO (74%), HOMO->L+2 (19%)
24769.46	403.723	0.587	H-1->LUMO (21%), HOMO->L+2 (72%)
25784.92	387.8236	0.5172	H-2->LUMO (79%)
25867.19	386.5902	0.146	H-1->L+1 (30%), HOMO->L+3 (64%)
26030.92	384.1586	0.389	H-2->LUMO (16%), H-1->L+1 (57%), HOMO->L+3 (25%)

27589.19	362.4608	0.0975	H-2->L+1 (86%)
29068.42	344.0159	0.5039	HOMO->L+4 (90%)
29570.91	338.1702	0.0016	H-3->LUMO (91%)
29945.96	333.9349	0.1504	H-1->L+2 (94%)
30617.02	326.6157	0.0021	H-4->LUMO (70%), H-3->L+1 (14%)

Table V.8. Major Electronic Transitions for *N,N*-Dimethyl-1,21-diaza[8]CPP

Determined by TD-DFT Method Using B3LYP/6-31g*.

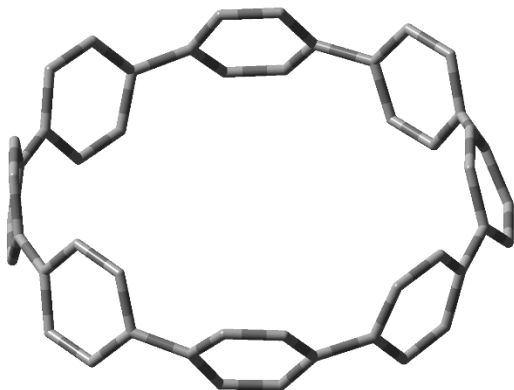
Energy (cm-1)	Wavelength (nm)	Osc. Strength	Major contribs
10786.93	927.0475	0.0437	HOMO->LUMO (99%)
15746.47	635.0629	0.2011	H-1->LUMO (99%)
19117.09	523.0923	0.2372	H-2->LUMO (91%)
20606.8	485.2767	0.0869	HOMO->L+1 (98%)
20860.87	479.3664	0.114	HOMO->L+2 (88%)
23061.16	433.6295	0.4661	HOMO->L+3 (98%)
23502.35	425.4893	0.002	H-3->LUMO (95%)
23957.25	417.4101	0.0031	H-6->LUMO (11%), H-4->LUMO (87%)
24416.18	409.5644	0.0037	H-5->LUMO (91%)
24540.39	407.4914	0.0351	H-1->L+1 (95%)
24807.37	403.1061	0.0026	H-6->LUMO (80%), H-4->LUMO (12%)
25446.16	392.9866	0.189	H-7->LUMO (45%), H-1->L+2 (49%)

Table V.9. Major Electronic Transitions for *N,N*-Dimethyl-1,8-diaza[8]CPP Determined

by TD-DFT Method Using B3LYP/6-31g*.

Minimized Geometries

Dipole moments are shown pictorially and numerically



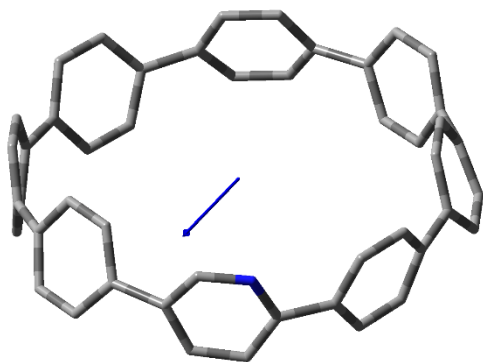
[8]CPP

Calculated Dipole: 0.0085 D

C	-5.24779	1.26112	-0.58206
C	-4.72856	2.5419	-0.75326
C	-4.42158	3.36301	0.3514
C	-4.89724	2.92482	1.60214
C	-5.42765	1.65228	1.77292
C	-5.50345	0.74429	0.70221
H	-5.38101	0.62585	-1.45418
H	-4.48099	2.86906	-1.75906
H	-4.7186	3.52101	2.49031
H	-5.63686	1.30775	2.78132
C	-3.41314	4.49746	-0.09638
C	-2.69183	4.4503	1.11261
C	-2.86142	5.3042	-1.11094
C	-1.38914	4.92951	1.19652
H	-3.10504	3.93465	1.97404
C	-1.57149	5.81381	-1.01439
H	-3.39374	5.43877	-2.04725
C	-0.7477	5.51544	0.08822
H	-0.82689	4.72681	2.10284

H	-1.16903	6.36108	-1.86158
C	-5.52744	-0.72669	-0.09491
C	-5.02433	-1.65834	0.83285
C	-5.70961	-1.18475	-1.41157
C	-4.52412	-2.89009	0.41825
H	-4.94927	-1.38569	1.88258
C	-5.19827	-2.40814	-1.82592
H	-6.11489	-0.51069	-2.1604
C	-4.48476	-3.24449	-0.94614
H	-4.08127	-3.5453	1.16292
H	-5.23096	-2.63653	-2.88563
C	5.68517	1.57218	-0.92697
C	5.14918	2.85702	-0.94803
C	4.43162	3.36486	0.15263
C	4.4871	2.61854	1.34317
C	5.02058	1.33457	1.36334
C	5.52606	0.7357	0.19511
H	6.16064	1.18521	-1.82456
H	5.21757	3.44176	-1.86181
H	3.96452	2.9779	2.22471
H	4.89534	0.73631	2.26071
C	5.52539	-0.74798	0.09942
C	5.65755	-1.58477	1.22476
C	5.04469	-1.34572	-1.07978
C	5.11828	-2.86838	1.23386
H	6.1138	-1.19883	2.13271
C	4.50792	-2.62846	-1.07151
H	4.94084	-0.74721	-1.97972
C	4.42423	-3.3746	0.1175
H	5.16498	-3.45323	2.14894
H	4.00426	-2.98664	-1.96446

C	3.36401	-4.40945	0.23364
C	2.88995	-5.15874	-0.8602
C	2.56793	-4.41557	1.39264
C	1.60219	-5.68999	-0.86721
H	3.50665	-5.26317	-1.74935
C	1.28095	-4.93711	1.38136
H	2.89629	-3.86703	2.27017
C	0.71984	-5.48764	0.21358
H	1.25579	-6.1997	-1.76204
H	0.65971	-4.77305	2.25518
C	-3.38892	-4.4211	-0.2003
C	-2.27984	-4.44627	-1.06833
C	-1.07209	-5.01698	-0.68194
C	-0.91578	-5.6264	0.57793
C	-2.10002	-5.84653	1.30767
C	-3.29827	-5.24615	0.93794
H	-2.31762	-3.91844	-2.01631
H	-0.20864	-4.87048	-1.32352
H	-2.06947	-6.40538	2.23824
H	-4.13978	-5.3262	1.61883
C	0.73511	5.48629	-0.02597
C	1.32082	4.93435	-1.18095
C	2.60652	4.40987	-1.16353
C	3.37661	4.4021	0.01289
C	2.87999	5.15253	1.09589
C	1.5936	5.68671	1.0742
H	0.71877	4.77165	-2.06835
H	2.9531	3.86047	-2.0335
H	3.47694	5.25561	1.99857
H	1.2285	6.19726	1.96109



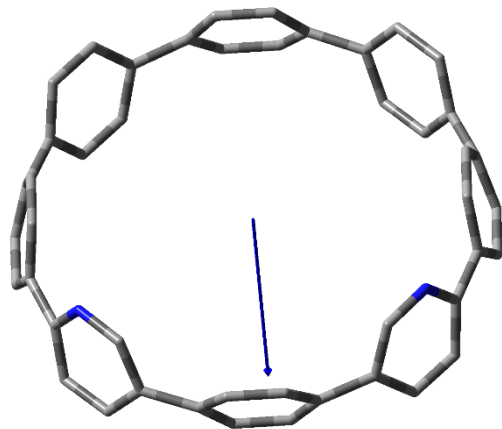
Aza[8]CPP V.1

Dipole: 2.9265 D

C	5.52888	2.15328	1.06614
H	5.6616	2.76786	1.95132
C	4.91116	2.70047	-0.07999
C	4.00676	3.88246	-0.01544
C	3.26745	4.10505	1.16538
H	3.55752	3.60164	2.08117
C	2.05889	4.79839	1.1408
H	1.44927	4.81269	2.0379
C	1.53022	5.30134	-0.06618
C	0.05691	5.48691	-0.17715
C	-0.75786	5.81577	0.92801
H	-0.31432	6.2804	1.80354
C	-2.10968	5.46802	0.95662
H	-2.68606	5.67405	1.85331
C	-2.708	4.7713	-0.11653
C	3.91301	-3.95993	0.25618
C	4.04774	-3.15308	1.40673
H	3.4603	-3.3685	2.29129
C	4.7767	-1.96722	1.3808
H	4.72541	-1.30763	2.2403
C	5.40617	-1.52114	0.20023
C	5.63045	-0.05896	0.03047

C	5.24122	0.54538	-1.1831
H	5.0599	-0.07498	-2.0543
C	4.88875	1.89267	-1.23642
H	4.44428	2.27612	-2.1484
C	3.59345	4.58753	-1.16703
H	4.18486	4.52779	-2.07564
C	2.38145	5.27994	-1.19248
H	2.05751	5.7421	-2.12007
C	4.74333	-3.6325	-0.83989
H	4.76277	-4.27296	-1.71574
C	5.46738	-2.43895	-0.87034
H	6.02205	-2.1823	-1.76798
C	-0.59788	5.00038	-1.32778
H	-0.01577	4.75004	-2.20804
C	-1.94575	4.65006	-1.29768
H	-2.36598	4.13876	-2.1564
C	5.87861	0.803	1.12096
H	6.27285	0.39705	2.04778
C	-5.38672	-1.85806	-1.10595
H	-5.44122	-2.25688	-2.11411
C	-4.92091	-2.65389	-0.03304
C	-3.97834	-3.78053	-0.24113
C	-3.15327	-3.76073	-1.38593
H	-3.37714	-3.07874	-2.19827
C	-1.50595	-5.22041	-0.32181
C	-0.04799	-5.49111	-0.18557
C	0.81948	-5.43669	-1.298
H	0.42116	-5.54894	-2.30094
C	2.16568	-5.10923	-1.14813
H	2.75402	-4.93676	-2.04244
C	2.72293	-4.84879	0.12347

C	-3.90705	3.90495	0.05479
C	-5.3552	2.20838	-0.94677
H	-5.79651	1.76323	-1.83022
C	-5.40473	1.48899	0.26634
C	-5.65617	0.02701	0.25262
C	-5.55225	-0.7875	1.39881
H	-5.66158	-0.37107	2.39306
C	-5.14756	-2.11343	1.24979
H	-4.89918	-2.69121	2.13391
C	-3.63577	-4.70366	0.77133
H	-4.28328	-4.82536	1.63452
C	-2.42975	-5.40721	0.73079
H	-2.17554	-6.05534	1.56365
C	-4.14519	3.30011	1.30755
H	-3.63318	3.67107	2.18866
C	-4.88029	2.12102	1.41228
H	-4.92463	1.62984	2.37796
C	0.56447	-5.47849	1.08629
H	-0.04394	-5.57645	1.97914
C	1.91881	-5.18194	1.23565
H	2.32155	-5.10502	2.23978
C	-1.95284	-4.46166	-1.42485
H	-1.29242	-4.29625	-2.26769
H	-4.55457	3.88269	-2.01309
C	-4.63157	3.39539	-1.04624
N	-5.7064	-0.56331	-0.97307



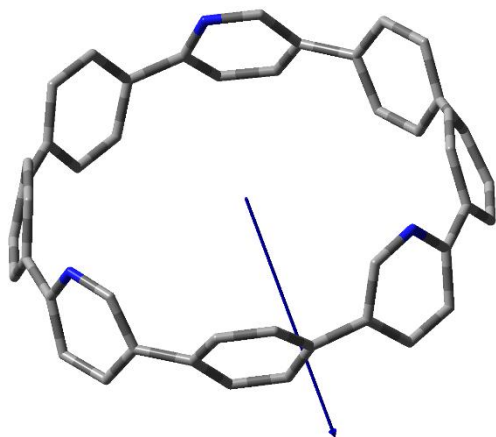
1,15-Diaza[8]CPP V.2

Dipole: 4.6799 D

C	-0.6875	5.82207	1.115
H	-1.21399	6.09464	2.02609
C	-1.41573	5.37544	-0.00493
C	-2.78114	4.79804	0.10262
C	-3.11413	4.08497	1.26822
H	-2.49701	4.19085	2.15521
C	-4.09044	3.09609	1.25433
H	-4.19864	2.46667	2.13202
C	-4.78517	2.77131	0.07493
C	-5.35489	1.40571	-0.06315
C	-5.75175	0.63605	1.04766
H	-5.97627	1.12546	1.99147
C	-5.74714	-0.75503	0.99747
H	-5.95104	-1.30324	1.91277
C	-5.36078	-1.43712	-0.17166
C	4.7935	2.7573	0.07481
C	4.0997	3.08404	1.25421
H	4.20608	2.45428	2.13188
C	3.12624	4.07573	1.26812
H	2.50944	4.18338	2.15511
C	2.79532	4.78978	0.10255

C	1.43161	5.37119	-0.00496
C	0.70284	5.15932	-1.18909
H	1.22064	4.83042	-2.08509
C	-0.68761	5.16141	-1.18908
H	-1.20639	4.83403	-2.08507
C	-3.63384	4.63203	-1.00603
H	-3.47695	5.22936	-1.90054
C	-4.61383	3.64279	-1.01897
H	-5.19878	3.4954	-1.92294
C	4.62465	3.62929	-1.01908
H	5.20914	3.4802	-1.92308
C	3.6475	4.62133	-1.00612
H	3.49232	5.21913	-1.90062
C	-5.19711	0.72027	-1.28313
H	-4.9216	1.27214	-2.17668
C	-5.20151	-0.66699	-1.33798
H	-4.93854	-1.17186	-2.26012
C	0.70473	5.81998	1.11499
H	1.23204	6.091	2.02606
C	0.68773	-5.78844	-0.95345
H	1.21243	-6.11729	-1.84639
C	1.41635	-5.28594	0.14237
C	2.79889	-4.76397	0.02076
C	3.20291	-4.14692	-1.18119
H	2.66632	-4.35027	-2.10621
C	4.7896	-2.82724	-0.14126
C	5.35639	-1.45282	-0.1717
C	5.19903	-0.68228	-1.338
H	4.93425	-1.18641	-2.26003
C	5.19887	0.70499	-1.28323
H	4.92473	1.25766	-2.17672

C	5.35912	1.39001	-0.06335
C	-4.79802	-2.81318	-0.14143
C	-3.21493	-4.13712	-1.18137
H	-2.67867	-4.34174	-2.10631
C	-2.81296	-4.75567	0.0205
C	-1.43199	-5.28172	0.14222
C	-0.70209	-4.98608	1.30795
H	-1.22027	-4.60664	2.18367
C	0.68721	-4.98813	1.30802
H	1.20641	-4.61021	2.18379
C	3.65254	-4.5436	1.11479
H	3.48245	-5.06342	2.05432
C	4.66432	-3.59183	1.03357
H	5.27553	-3.38453	1.90597
C	-4.67524	-3.57847	1.03321
H	-5.28609	-3.36968	1.9055
C	-3.66619	-4.53315	1.11441
H	-3.49781	-5.05374	2.05383
C	5.74522	-0.77185	0.99725
H	5.94789	-1.32063	1.91248
C	5.75404	0.61923	1.04738
H	5.98037	1.10801	1.99108
C	-0.70474	-5.78636	-0.95353
H	-1.23033	-6.11365	-1.84651
N	-4.15236	-3.20132	-1.26099
N	4.14307	-3.21384	-1.26085



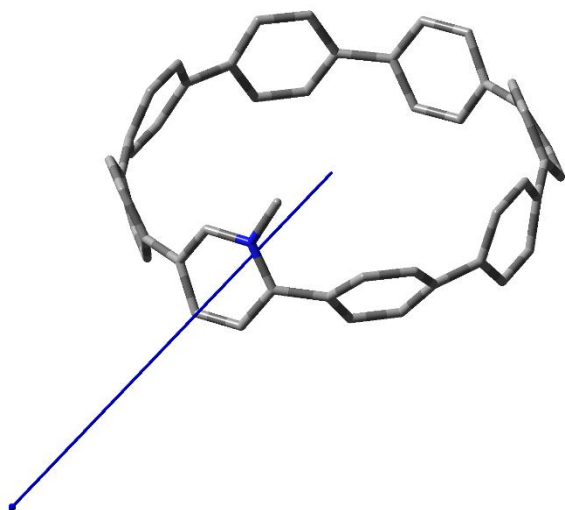
1,15,31-Triaza[8]CPP V.3

Dipole: 6.8770 D

C	1.83155	-5.48384	0.92901
H	2.41205	-5.62526	1.83609
C	2.43041	-4.94301	-0.2243
C	3.69001	-4.15393	-0.17423
C	4.4118	-3.91767	1.01045
H	4.30486	-4.56779	1.87272
C	5.17206	-2.75697	1.11684
H	5.64436	-2.51279	2.06508
C	5.24923	-1.86082	0.03783
C	5.50996	-0.40859	0.18603
C	5.05763	0.23573	1.35189
H	4.76584	-0.35735	2.21357
C	4.7925	1.59941	1.36402
H	4.30227	2.0244	2.23477
C	4.96765	2.38668	0.21144
C	-4.19895	-3.56962	0.13533
C	-3.4126	-3.77639	1.28311
H	-3.62628	-3.21547	2.18804
C	-2.25136	-4.5371	1.23493
H	-1.60098	-4.54256	2.10387
C	-1.81447	-5.12815	0.03548

C	-0.36912	-5.43547	-0.12053
C	0.27141	-5.11396	-1.33225
H	-0.32485	-4.90532	-2.21533
C	1.63836	-4.87594	-1.38491
H	2.08575	-4.49589	-2.29582
C	-3.87942	-4.33914	-1.00034
H	-4.50762	-4.28436	-1.88543
C	-2.71435	-5.10058	-1.04818
H	-2.46479	-5.6201	-1.96946
C	5.89086	0.41592	-0.89054
H	6.33024	-0.02599	-1.78081
C	5.62691	1.78303	-0.87749
H	5.86819	2.37245	-1.75786
C	0.46258	-5.73101	0.97694
H	0.02384	-6.07276	1.91049
C	-1.62315	4.82382	-1.35243
H	-2.0774	4.40604	-2.24489
C	-2.36907	4.90435	-0.16054
C	-3.61889	4.10924	-0.03415
C	-4.34732	3.67225	-1.16048
H	-4.21717	4.17373	-2.11516
C	-5.27622	1.80167	0.08647
C	-5.61075	0.35565	0.06255
C	-5.08841	-1.57547	-1.0869
H	-4.79128	-2.00417	-2.04217
C	-5.06158	-2.3641	0.08253
C	4.18396	3.63932	0.08454
C	1.88444	5.1908	-0.12897
C	0.4241	5.46002	-0.20349
C	-0.35762	5.75509	0.92934
H	0.10954	6.10967	1.84375

C	-1.72467	5.49169	0.94642
H	-2.27766	5.6661	1.86519
C	-3.92623	3.4956	1.19419
H	-3.40653	3.80321	2.09599
C	-4.74117	2.36999	1.2548
H	-4.83134	1.84737	2.20252
C	3.75403	4.40902	1.17861
H	4.26293	4.33091	2.13606
C	2.61624	5.20312	1.07297
H	2.25326	5.73613	1.94576
C	-5.9135	-0.39601	1.21217
H	-6.28968	0.08594	2.10957
C	-5.6161	-1.75516	1.22146
H	-5.74897	-2.32648	2.13672
C	-0.26324	5.09818	-1.37603
H	0.31178	4.90064	-2.27294
C	-5.14194	2.53355	-1.10757
H	-5.58254	2.13997	-2.01729
N	-5.33663	-0.2702	-1.10045
N	3.96985	-3.4341	-1.28063
N	2.43683	4.66086	-1.24033
C	4.72459	-2.34772	-1.17743
H	4.84101	-1.7697	-2.09245
C	3.53969	3.93108	-1.13561
H	3.88178	3.46629	-2.05852



***N*-methylaza[8]CPP Triflate V.4**

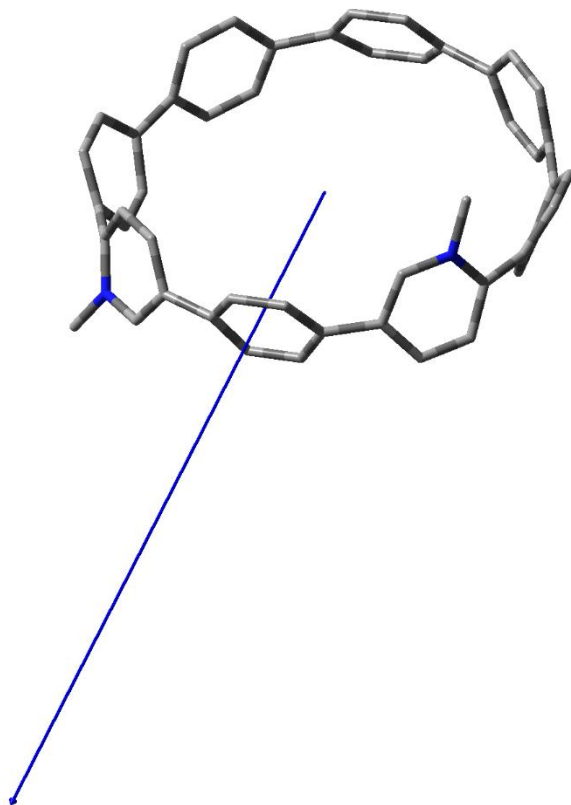
Dipole: 20.8018 D

C	3.94474	-4.60472	-0.85084
H	3.85266	-5.2555	-1.7157
C	3.03932	-4.72389	0.22397
C	1.68951	-5.32334	0.06904
C	1.1072	-5.42779	-1.21209
H	1.73231	-5.36841	-2.09671
C	-0.26958	-5.4413	-1.38041
H	-0.66932	-5.4368	-2.39033
C	-1.13819	-5.34622	-0.27428
C	-2.48119	-4.74136	-0.40009
C	-2.72612	-3.8493	-1.46416
H	-2.03125	-3.79543	-2.29402
C	-3.73048	-2.90016	-1.39511
H	-3.77628	-2.14546	-2.17312
C	-4.56104	-2.79017	-0.25584
C	5.4637	1.54744	-0.15828
C	5.24553	0.74245	-1.29243
H	4.89516	1.1874	-2.21705
C	5.29225	-0.64382	-1.21806
H	4.9741	-1.22103	-2.08106

C	5.55153	-1.29886	-0.00141
C	5.01368	-2.67097	0.17982
C	4.27964	-2.94931	1.34657
H	4.35328	-2.27916	2.19752
C	3.31315	-3.94681	1.36581
H	2.66987	-4.01434	2.23673
C	0.82324	-5.51454	1.165
H	1.22396	-5.56121	2.17256
C	-0.55712	-5.50754	0.9994
H	-1.18335	-5.50514	1.88693
C	5.96289	0.89146	0.98635
H	6.25526	1.46615	1.86003
C	5.99651	-0.49775	1.06725
H	6.30402	-0.96374	1.99981
C	-3.46395	-4.7877	0.615
H	-3.40412	-5.54568	1.39003
C	-4.47104	-3.83155	0.69538
H	-5.17738	-3.89214	1.51641
C	4.90759	-3.60048	-0.8736
H	5.53245	-3.48861	-1.75548
C	-3.64626	4.54906	0.99255
H	-3.50115	5.1098	1.91089
C	-2.78891	4.77431	-0.10791
C	-1.43664	5.35813	0.04498
C	-0.74158	5.11269	1.24366
H	-1.27963	4.76282	2.11939
C	1.41516	5.39043	0.13753
C	2.80826	4.87956	0.05999
C	3.50482	4.4514	1.2071
H	3.20686	4.80165	2.1906
C	4.50039	3.4853	1.12726

H	4.90505	3.093	2.05447
C	4.87416	2.91299	-0.10504
C	-5.20145	-1.46937	-0.10284
C	-5.09649	0.62947	1.02701
H	-4.8553	1.11169	1.96463
C	-5.29362	1.37023	-0.13293
C	-4.78419	2.75475	-0.19253
C	-4.10582	3.15139	-1.36086
H	-4.22504	2.58501	-2.28004
C	-3.13466	4.14371	-1.31891
H	-2.53325	4.31792	-2.20496
C	-0.67807	5.84195	-1.0395
H	-1.17509	6.14433	-1.9576
C	0.7116	5.87142	-0.98809
H	1.25526	6.20006	-1.86846
C	-5.68698	-0.761	-1.2208
H	-5.94847	-1.3315	-2.1045
C	-5.73627	0.62095	-1.24812
H	-6.0557	1.12856	-2.15302
C	3.35806	4.49459	-1.17823
H	2.91224	4.84329	-2.10441
C	4.37608	3.55133	-1.25799
H	4.70865	3.23876	-2.24262
C	-4.61128	3.55117	0.9581
H	-5.20159	3.35914	1.85121
N	-5.06312	-0.72864	1.05296
C	0.64538	5.12743	1.28734
H	1.12796	4.78993	2.1975
C	-4.73219	-1.36035	2.3497
H	-5.5715	-1.96851	2.68969
H	-3.84444	-1.98341	2.23989

H -4.54201 -0.57502 3.07938



***N,N*-Dimethyl-1,15-diaza[8]CPP Ditriflate V.5**

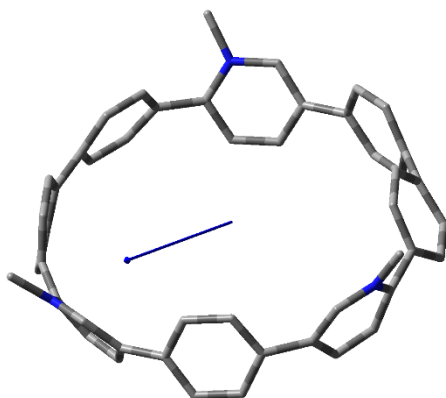
Dipole: 24.5243 D

C	1.71094	5.80444	-0.81505
H	2.25355	6.14189	-1.69331
C	2.38051	5.08568	0.19705
C	3.6499	4.35151	-0.02986
C	3.99491	3.92573	-1.32975
H	3.52341	4.38481	-2.19252
C	4.80873	2.82037	-1.53095
H	4.98049	2.48278	-2.54846
C	5.31389	2.08157	-0.44
C	5.60582	0.63915	-0.55534
C	5.02949	-0.09881	-1.61148

H	4.60658	0.41665	-2.46539
C	4.81544	-1.46028	-1.50715
H	4.23035	-1.94192	-2.28276
C	5.17092	-2.17617	-0.33573
C	-4.24241	3.68538	-0.00078
C	-3.62435	4.24578	-1.13979
H	-3.99512	4.01857	-2.1343
C	-2.47265	5.01084	-1.02726
H	-1.96157	5.31183	-1.93587
C	-1.88314	5.26416	0.22899
C	-0.43017	5.54572	0.32783
C	0.27941	5.03169	1.42944
H	-0.25646	4.67223	2.30107
C	1.64682	4.80803	1.36579
H	2.11707	4.28364	2.19046
C	4.38372	3.7871	1.0335
H	4.25287	4.16233	2.04346
C	5.18489	2.66976	0.83588
H	5.61783	2.18686	1.70653
C	-3.79871	4.15991	1.25253
H	-4.28137	3.82972	2.16658
C	-2.65743	4.94226	1.36286
H	-2.31535	5.22627	2.35285
C	6.21192	-0.12172	0.47385
H	6.81544	0.3723	1.22851
C	5.98984	-1.48669	0.59364
H	6.45492	-2.01215	1.41951
C	0.33905	6.02869	-0.75131
H	-0.14493	6.53442	-1.58173
C	-1.54376	-5.25337	1.21267
H	-2.06546	-5.44885	2.14519

C	-2.23313	-4.69748	0.11791
C	-3.5076	-3.95361	0.27745
C	-3.75379	-3.20609	1.45683
H	-3.1653	-3.39544	2.34857
C	-5.26845	-1.74701	0.24767
C	-5.62046	-0.34652	0.02534
C	-5.953	0.51184	1.10135
H	-6.38205	0.10071	2.01127
C	-5.6896	1.8698	1.0355
H	-5.92823	2.48562	1.89603
C	-5.03059	2.44024	-0.08357
C	4.39679	-3.40666	-0.13113
C	2.61075	-4.40099	1.10207
H	2.1331	-4.44368	2.07199
C	2.0137	-4.9394	-0.02573
C	0.55219	-5.20235	-0.0248
C	-0.17523	-4.83965	-1.17167
H	0.34128	-4.6211	-2.10087
C	-1.54047	-4.58907	-1.1001
H	-2.03559	-4.18021	-1.97564
C	-4.38863	-3.72481	-0.76769
H	-4.40766	-4.34032	-1.6601
C	3.98243	-4.20101	-1.22684
H	4.56619	-4.15173	-2.13838
C	2.82123	-4.94523	-1.18855
H	2.50661	-5.4939	-2.07121
C	-5.2032	0.26569	-1.17989
H	-4.95074	-0.33512	-2.0469
C	-4.92348	1.61936	-1.22891
H	-4.48024	2.01107	-2.13644
C	-0.17596	-5.50327	1.14203

H	0.33106	-5.89142	2.02118
N	3.77409	-3.69374	1.06918
C	-4.61678	-2.13212	1.43697
H	-4.67417	-1.46754	2.2907
C	4.25473	-3.13846	2.35407
H	5.25092	-3.52545	2.57147
H	4.28138	-2.04937	2.30074
H	3.57437	-3.45291	3.14388
C	-6.23282	-2.60274	-1.89126
H	-6.96597	-1.82679	-1.68162
H	-5.71426	-2.38019	-2.82662
H	-6.73796	-3.56754	-1.97326
N	-5.26953	-2.68099	-0.76411



***N,N,N*-Trimethyl-1,15,31-triaza[8]CPP**

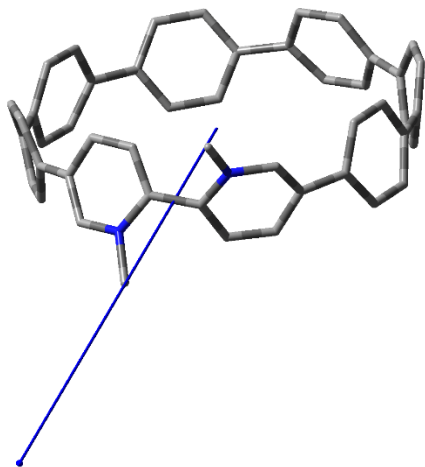
Dipole: 6.4829 D

C	4.01873	-3.09359	-1.6274
H	3.43252	-3.27269	-2.52147
C	3.87978	-3.94223	-0.50479
C	2.69185	-4.81689	-0.36005
C	1.87926	-5.12731	-1.46721
H	2.27039	-5.06057	-2.47765
C	0.53333	-5.43226	-1.29858
H	-0.08178	-5.54691	-2.18496

C	-0.0543	-5.45578	-0.01839
C	-1.51517	-5.225	0.13373
C	-2.44765	-5.45902	-0.90115
H	-2.19172	-6.11329	-1.72847
C	-3.6734	-4.80299	-0.92652
H	-4.33486	-4.95127	-1.77567
C	-4.03316	-3.90942	0.10506
C	4.76516	2.55971	0.22089
C	5.51166	2.13005	-0.8986
H	5.7333	2.81611	-1.70917
C	5.90844	0.80377	-1.03695
H	6.41142	0.49537	-1.94917
C	5.60222	-0.14532	-0.04108
C	5.41699	-1.57757	-0.35722
C	4.78909	-3.70086	0.52563
H	4.92753	-4.38529	1.35461
C	2.15967	-5.07289	0.91942
H	2.76102	-4.91674	1.81003
C	0.82026	-5.40244	1.08526
H	0.44104	-5.53889	2.0928
C	4.65555	1.65173	1.29248
H	4.14292	1.93134	2.20461
C	5.06136	0.33107	1.16917
H	4.82891	-0.35297	1.9786
C	-1.96894	-4.49251	1.24775
H	-1.30715	-4.31256	2.08701
C	-3.19658	-3.84806	1.2386
H	-3.43255	-3.18671	2.06554
C	4.76987	-1.93638	-1.54835
H	4.73463	-1.21355	-2.35491
C	-3.99143	3.15137	0.94302

H	-3.44204	3.45216	1.83025
C	-3.82852	3.85399	-0.26325
C	-2.6404	4.733	-0.41317
C	-2.11513	5.52218	0.60325
H	-2.70538	5.84596	1.45358
C	0.07585	5.50314	-0.34706
C	1.51603	5.31399	-0.09195
C	1.95451	4.87539	1.17574
H	1.33571	5.00348	2.0564
C	3.12329	4.13888	1.30992
H	3.38432	3.78394	2.30005
C	3.88728	3.7626	0.18666
C	-4.94129	-2.77223	-0.12989
C	-5.87459	-0.80443	0.84308
H	-6.33244	-0.39246	1.73561
C	-5.54885	-0.02347	-0.26056
C	-5.3004	1.43949	-0.18607
C	-5.31885	2.25625	-1.33353
H	-5.85543	1.94066	-2.22357
C	-4.5916	3.442	-1.37272
H	-4.57567	4.01938	-2.2928
C	-1.82219	4.59488	-1.55683
H	-2.20124	4.07817	-2.43244
C	-0.49278	4.9625	-1.51353
H	0.16182	4.69609	-2.33368
C	-4.89513	-2.08834	-1.35558
H	-4.46327	-2.59298	-2.21185
C	-5.19358	-0.74109	-1.42601
H	-5.02408	-0.21173	-2.35782
C	2.41563	5.16201	-1.16983
H	2.18081	5.58187	-2.14338

C	3.56991	4.403	-1.03122
H	4.17632	4.23721	-1.91458
C	-4.71351	1.96267	0.97973
H	-4.69909	1.37954	1.89556
N	-5.60472	-2.13974	0.89246
N	-0.8112	5.92615	0.61332
N	5.53599	-2.5638	0.58779
C	6.50367	-2.44481	1.71314
H	7.11346	-1.55562	1.57021
H	5.97216	-2.38698	2.66528
H	7.14525	-3.32831	1.70203
C	-6.07648	-2.88698	2.09098
H	-5.9046	-3.95053	1.94155
H	-7.14761	-2.70532	2.20117
H	-5.55038	-2.54417	2.98438
C	-0.4076	6.87479	1.68782
H	-1.11535	7.70609	1.68556
H	0.58975	7.25455	1.47742
H	-0.42652	6.3798	2.6612



N,N-Dimethyl-1,8-diaza[8]CPP

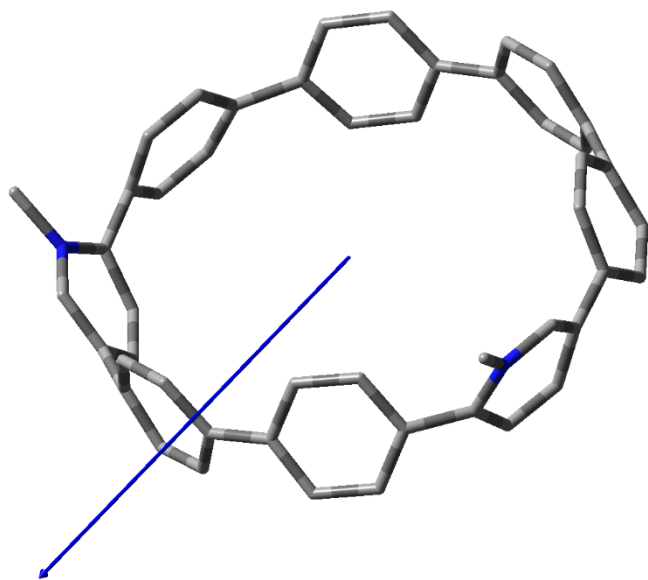
Dipole: 24.9785 D

C	0.12608	0.26867	-0.00586
C	1.35835	0.27645	-0.67305
C	2.03848	1.49503	-0.8086
C	1.33516	2.70374	-0.6987
C	0.09913	2.69585	-0.03379
C	-0.36899	1.48191	0.49097
H	-0.40214	-0.64801	0.15216
H	1.78746	-0.6331	-1.03961
H	1.7462	3.61366	-1.07993
H	-0.45439	3.6009	0.10216
C	3.56985	1.48969	-0.9773
C	4.28685	2.69365	-1.00425
C	4.255	0.26793	-1.01498
C	5.64092	2.67263	-0.62951
H	3.80755	3.61107	-1.26955
C	5.60616	0.2445	-0.64335
H	3.74993	-0.63345	-1.28822
C	6.21067	1.44595	-0.24936
H	6.21356	3.57725	-0.60124
H	6.1526	-0.67648	-0.62648

C	7.43904	1.41464	0.67986
C	7.95613	0.18734	1.11628
C	7.98228	2.61262	1.15968
C	8.66374	0.15727	2.32544
H	7.78293	-0.71012	0.56121
C	8.68601	2.58281	2.3712
H	7.8328	3.53284	0.63612
C	8.80299	1.35617	3.03591
H	9.05221	-0.76094	2.71236
H	9.08986	3.47938	2.79401
C	-1.34673	1.47723	1.68053
C	-1.7545	2.67761	2.26121
C	-1.75706	0.26479	2.24912
C	-2.14739	2.63199	3.59803
H	-1.73342	3.59737	1.71772
H	-1.73351	-0.64057	1.68056
C	-2.11436	1.38812	4.24342
H	-2.43002	3.52264	4.12287
C	-1.84156	0.08695	6.41897
C	-1.16228	0.04656	7.63628
C	-0.62639	1.24733	8.10167
C	-1.13917	2.46033	7.62848
C	-1.94195	1.32702	5.7713
H	-2.24	-0.80149	5.97916
H	-1.02578	-0.87169	8.16966
H	-0.97697	3.36904	8.17018
C	0.58637	1.23574	9.04711
C	1.19117	2.44011	9.43211
C	1.14098	0.01372	9.44699
C	2.53997	2.41054	9.80829
H	0.65119	3.36404	9.40518

C	2.49179	-0.01471	9.81633
H	0.55551	-0.88287	9.43707
C	3.21587	1.18371	9.77812
H	3.05324	3.31206	10.07891
H	2.96533	-0.9343	10.08747
C	4.74527	1.17395	9.6072
C	5.44312	-0.0349	9.46962
C	5.42705	2.39221	9.50217
C	6.68635	-0.01539	8.81679
H	5.02415	-0.95301	9.82258
C	6.66443	2.41289	8.84898
H	4.99523	3.29395	9.88134
C	7.165	1.21158	8.33037
H	7.23763	-0.91982	8.66487
H	7.19802	3.33254	8.72083
C	8.16355	1.24845	7.1587
C	8.56475	2.48273	6.62311
C	8.59708	0.05258	6.56839
C	8.99081	2.51913	5.28972
H	8.51229	3.38047	7.20472
C	9.01914	0.09013	5.23377
H	8.57356	-0.87057	7.10861
C	8.97657	1.32045	4.56318
H	9.28153	3.44111	4.82983
H	9.32803	-0.80214	4.72898
C	-2.32084	3.72958	5.91193
H	-3.18476	3.52598	5.31532
H	-2.58699	4.38459	6.71485
H	-1.56975	4.19439	5.30778
C	-2.53566	-1.01128	4.17582
H	-2.97613	-1.65651	3.44381

H	-1.67259	-1.4831	4.59687
H	-3.24562	-0.81092	4.95029
N	-1.80013	2.47021	6.45894
N	-2.13879	0.25063	3.53543



***N,N*-Dimethyl-1,21-diaza[8]CPP**

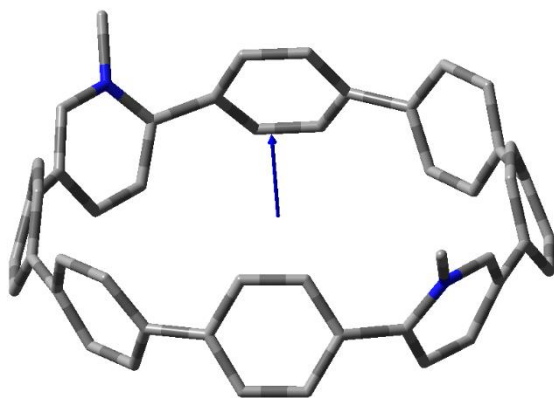
Dipole: 11.4715 D

C	-1.80455	1.70888	-0.45512
C	-0.57678	1.77839	0.21695
C	0.11643	2.99633	0.21007
C	-0.57142	4.19093	-0.04244
C	-1.79913	4.12139	-0.71461
C	-2.2755	2.86085	-1.09939
H	-2.35011	0.78976	-0.50513
H	-0.16291	0.91357	0.69204
H	-0.15355	5.13514	0.23822
H	-2.34058	5.01127	-0.95927
C	1.64706	3.01115	0.3792
C	2.34515	1.80664	0.53956
C	3.69652	4.17466	-0.10694
C	3.69115	1.76208	0.152

H	1.85409	0.93299	0.91437
C	4.26945	2.92431	-0.37592
H	4.26121	5.07527	-0.22913
H	4.25185	0.8536	0.22401
C	-3.23779	2.73429	-2.29505
C	-3.63608	3.87979	-2.99731
C	-3.64158	1.46732	-2.73738
C	-4.02626	3.73645	-4.33566
H	-3.60874	4.8445	-2.53525
C	-4.03176	1.32399	-4.07571
H	-3.61836	0.62308	-2.0804
C	-3.99795	2.45506	-4.90241
H	-4.30378	4.58916	-4.91942
H	-4.31343	0.36776	-4.46453
C	5.47208	2.81875	-1.33206
C	5.98685	1.56064	-1.67277
C	5.99238	3.97311	-1.93265
C	6.66291	1.4276	-2.89306
H	5.83657	0.71472	-1.03502
C	6.66846	3.84007	-3.15298
H	5.84624	4.93614	-1.4898
C	6.7892	2.55957	-3.7095
H	7.04092	0.47772	-3.20886
H	7.05063	4.69915	-3.6637
C	-0.73521	0.67555	-10.02679
C	0.61081	0.631	-10.41443
C	1.31427	1.83906	-10.51294
C	0.61616	3.04357	-10.6733
C	-0.72985	3.08813	-10.28574
C	-1.30816	1.9259	-9.7578
H	-1.29991	-0.22506	-9.90461

H	1.09786	-0.30442	-10.59521
H	1.1072	3.91722	-11.04813
H	-1.29056	3.9966	-10.35777
C	2.84492	1.85388	-10.34379
C	3.53814	3.07182	-10.35067
C	3.53278	0.65929	-10.09128
H	3.12429	3.93665	-10.82576
C	4.7605	0.72883	-9.41908
H	3.11494	-0.28492	-10.37195
C	5.23686	1.98937	-9.0343
H	5.30194	-0.16104	-9.17442
C	6.19914	2.11593	-7.8386
C	6.59742	0.97044	-7.13633
C	6.60293	3.38291	-7.39626
C	6.98757	1.11377	-5.79797
H	6.57009	0.00573	-7.59839
C	6.99309	3.52623	-6.05793
H	6.57971	4.22715	-8.05323
C	6.95927	2.39516	-5.23123
H	7.26508	0.26106	-5.21421
H	7.27474	4.48246	-5.66909
C	-2.5108	2.03146	-8.80163
C	-3.02558	3.28957	-8.46091
C	-3.0311	0.8771	-8.20102
C	-3.70163	3.42261	-7.24061
H	-2.87533	4.13549	-9.09866
C	-3.70717	1.01015	-6.98068
H	-2.88498	-0.08593	-8.64387
C	-3.82791	2.29065	-6.42415
H	-4.07964	4.37249	-6.9248
H	-4.08934	0.15107	-6.46995

N	4.76591	3.14134	-9.67858
N	2.3505	4.21922	0.28069
C	5.51541	4.40405	-9.60986
H	5.27061	4.91518	-8.70228
H	6.56505	4.19737	-9.63083
H	5.25614	5.01869	-10.44645
C	1.68137	5.50432	0.52903
H	1.17882	5.82251	-0.36041
H	0.96917	5.38879	1.31918
H	2.40906	6.23708	0.80908



***N,N*-Dimethyl-1,26-diaza[8]CPP**

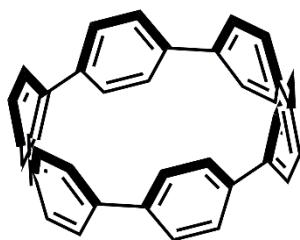
Dipole: 1.9950 D

C	-2.89847	-0.32846	-6.2934
C	-2.51334	-0.25031	-4.94752
C	-2.11318	0.99421	-4.44197
C	-2.51104	2.17187	-5.08918
C	-2.89697	2.09372	-6.43454
C	-2.86335	0.84201	-7.06379
H	-3.17725	-1.26477	-6.72983
H	-2.49112	-1.12564	-4.33228
H	-2.48669	3.11276	-4.58007
H	-3.17524	2.97335	-6.97667
C	-1.15538	1.06435	-3.23739

C	-0.68079	2.3056	-2.79206
C	-0.68659	-0.11613	-2.64513
C	0.54417	2.34405	-2.11176
H	-1.22157	3.20575	-2.99746
C	0.53843	-0.07774	-1.9648
H	-1.23166	-1.03188	-2.7402
C	1.23176	1.13913	-1.91194
H	0.96026	3.2743	-1.78572
H	0.95028	-0.96361	-1.52838
C	2.76218	1.14662	-1.73539
C	3.46154	-0.06343	-1.62816
C	4.80936	-0.08864	-2.01248
H	2.97041	-0.95402	-1.29554
C	4.8126	2.33295	-2.15841
C	5.38822	1.09748	-2.48323
H	5.3709	-0.99887	-1.98098
H	5.37689	3.23884	-2.23622
C	6.595	1.03931	-3.43818
C	7.1159	2.2224	-3.97926
C	7.11319	-0.19991	-3.83776
C	7.79748	2.15059	-5.20174
H	6.96624	3.16223	-3.4901
C	7.7949	-0.27191	-5.06045
H	6.96138	-1.07637	-3.24265
C	7.92303	0.89927	-5.82028
H	8.18033	3.03451	-5.66778
H	8.176	-1.20456	-5.42056
C	0.42424	-0.68056	-12.25335
C	1.77176	-0.70595	-12.63745
C	2.47471	0.50572	-12.67644
C	0.42756	1.74103	-12.39916

C	-0.1514	0.5549	-11.92857
H	-0.14011	-1.58643	-12.17564
H	2.26001	-1.6315	-12.8601
H	-0.134	2.65128	-12.43067
C	-1.35814	0.61308	-10.97351
C	-1.87623	1.85231	-10.57386
C	-1.87901	-0.57004	-10.43245
C	-2.55795	1.92427	-9.3512
H	-1.72448	2.72878	-11.16896
C	-2.56057	-0.49824	-9.20998
H	-1.72943	-1.50984	-10.92166
C	-2.68614	0.75306	-8.59142
H	-2.93904	2.85691	-8.99104
H	-2.94346	-1.38216	-8.74395
C	4.00516	0.51319	-12.49986
C	4.69849	1.73007	-12.44694
C	4.69276	-0.69173	-12.30005
C	5.9235	1.76844	-11.76662
H	4.28664	2.61593	-12.88335
C	5.91773	-0.65328	-11.61977
H	4.2767	-1.62197	-12.62616
C	6.39244	0.58795	-11.17447
H	6.46861	2.68419	-11.67159
H	6.45857	-1.55344	-11.41447
C	7.35017	0.65809	-9.96977
C	7.74813	-0.51957	-9.32258
C	7.75035	1.90262	-9.46423
C	8.13403	-0.4414	-7.9772
H	7.72384	-1.46044	-9.83169
C	8.13545	1.98077	-8.11833
H	7.72813	2.77795	-10.07946

C	8.10036	0.8103	-7.3479
H	8.41234	-1.32102	-7.43506
H	8.41421	2.9171	-7.68188
N	1.77535	1.7158	-12.78353
N	3.46506	2.35832	-1.77436
C	2.45005	2.93927	-13.24047
H	2.9502	3.40043	-12.41458
H	3.16497	2.69105	-13.9969
H	1.72611	3.61688	-13.64252
C	2.79413	3.63003	-1.46856
H	2.29568	3.98992	-2.3443
H	2.07823	3.47697	-0.6882
H	3.52013	4.34887	-1.15059

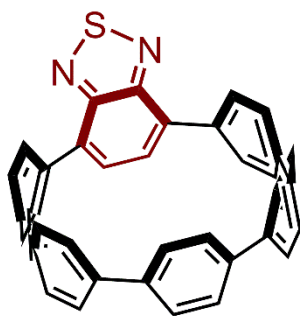


[6]CPP

C	2.58501	3.67073	1.03622
C	1.33524	4.28618	1.03614
C	0.46814	4.17027	-0.07039
C	1.04529	3.69396	-1.26264
C	2.29245	3.07967	-1.26249
C	3.02174	2.91268	-0.07025
H	3.17278	3.68195	1.95068
H	0.98571	4.759	1.95053
H	0.44053	3.62206	-2.16131
H	2.60413	2.55603	-2.16087
C	-1.01193	4.07254	0.07015
C	-1.88673	4.07354	-1.03636

C	-1.52156	3.52496	1.26249
C	-3.0449	3.2994	-1.03633
H	-1.60223	4.588	-1.95081
C	-2.67745	2.75246	1.26255
H	-0.91251	3.53303	2.16106
C	-3.37835	2.49072	0.07029
H	-3.62902	3.23326	-1.95082
H	-2.9177	2.19267	2.16106
C	-1.04528	-3.6941	1.26255
C	-2.29244	-3.07981	1.26247
C	-3.02173	-2.91269	0.07024
C	-2.58501	-3.67062	-1.03631
C	-1.33523	-4.28606	-1.0363
C	-0.46813	-4.17027	0.07024
H	-0.44052	-3.62229	2.16122
H	-2.60412	-2.55627	2.1609
H	-3.17278	-3.68176	-1.95077
H	-0.98571	-4.75877	-1.95075
C	1.01193	-4.07253	-0.07029
C	1.52157	-3.52484	-1.26258
C	1.88672	-4.07363	1.03623
C	2.67745	-2.75234	-1.26257
H	0.91253	-3.53282	-2.16115
C	3.04489	-3.29949	1.03627
H	1.60221	-4.58817	1.95063
C	3.37835	-2.49071	-0.07027
H	2.91771	-2.19247	-2.16102
H	3.62899	-3.23342	1.95078
C	4.03415	-1.1602	0.0702
C	3.81515	-0.44508	1.26258
C	4.47241	-0.40307	-1.03633

C	3.72369	0.94221	1.26261
H	3.51786	-0.9766	2.16116
C	4.38065	0.98699	-1.03635
H	4.77585	-0.90655	-1.95081
C	3.84681	1.68002	0.07023
H	3.35942	1.43003	2.16137
H	4.61538	1.52596	-1.95082
C	-4.03416	1.1602	-0.07005
C	-4.47223	0.40307	1.03656
C	-4.38045	-0.98699	1.03657
C	-3.84681	-1.68003	-0.0701
C	-3.72388	-0.94222	-1.2625
C	-3.81535	0.44507	-1.26246
H	-4.77551	0.90655	1.95109
H	-4.61503	-1.52596	1.95108
H	-3.35976	-1.43004	-2.16132
H	-3.51822	0.97659	-2.16109

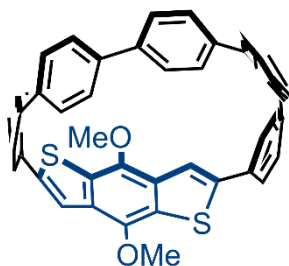


1,4-BT[6]CPP

C	-3.29365	-1.81557	0.01828
C	-2.96459	-2.34063	1.2751
C	-2.80266	-2.4239	-1.14405
C	-1.73638	-3.00842	1.37969
H	-3.59617	-2.1966	2.12668
C	-1.57749	-3.09383	-1.03972
H	-3.31434	-2.33983	-2.08004

C	-0.95775	-3.09059	0.21672
H	-1.3892	-3.39424	2.31537
H	-1.11396	-3.54446	-1.89233
C	-3.36081	3.73053	-0.28665
C	-2.88371	4.22142	-1.50883
C	-3.04611	4.39646	0.90537
C	-1.67523	4.92829	-1.47958
H	-3.39236	4.02423	-2.42934
C	-1.83435	5.10078	0.9352
H	-3.67511	4.33057	1.76839
C	-1.05668	5.07548	-0.23109
H	-1.22213	5.29551	-2.37665
H	-1.49741	5.59361	1.82318
C	3.92882	1.7017	-0.95086
C	3.94593	0.30251	-0.87405
C	3.59196	-0.27578	0.35247
C	3.80062	0.4328	1.54402
C	3.78365	1.83316	1.46716
C	3.55944	2.4019	0.2055
H	4.14319	2.21055	-1.86732
H	4.17403	-0.29822	-1.72961
H	3.92075	-0.07121	2.48019
H	3.89041	2.43935	2.34237
C	2.85374	-1.62828	0.37738
C	2.393	-2.15664	1.59174
C	2.53611	-2.26971	-0.82748
C	1.20226	-2.89645	1.55549
H	2.90095	-1.96482	2.51374
C	1.34539	-3.00715	-0.86363
H	3.15065	-2.16268	-1.69682
C	0.57855	-3.03852	0.30844

H	0.76559	-3.29306	2.44824
H	1.01394	-3.48504	-1.76178
C	2.78877	3.73074	0.08337
C	2.31354	4.37678	1.23344
C	2.45771	4.22945	-1.18385
C	1.10539	5.07927	1.11823
H	2.82455	4.29869	2.17025
C	1.24987	4.93016	-1.2988
H	3.07597	4.04301	-2.03703
C	0.48045	5.07023	-0.13622
H	0.65785	5.55973	1.96309
H	0.90878	5.2999	-2.24323
C	-4.10846	2.38612	-0.24226
C	-4.53749	1.76803	1.08811
C	-4.2851	1.66048	-1.38634
C	-4.52124	0.25304	1.17541
C	-4.26582	0.09913	-1.29961
H	-4.38695	2.15003	-2.33237
C	-4.07438	-0.49317	-0.08241
H	-4.35327	-0.4937	-2.18601
N	-4.86586	2.34089	2.19478
N	-4.83925	-0.22334	2.34314
S	-5.13658	1.01904	3.2355



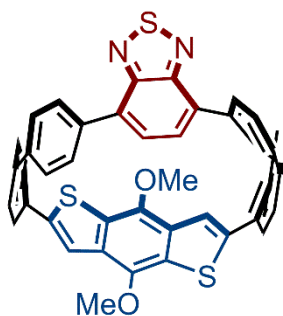
2,6-BDT[6]CPP

C	-5.36504	-0.17325	-1.49856
C	-5.07181	-1.17614	-0.56431

C	-5.22322	-0.9578	0.81535
C	-5.47641	0.31417	1.344
C	-5.35627	1.35899	0.42259
C	-5.398	1.12411	-0.96279
S	-4.95801	-2.45848	1.70131
S	-5.40222	2.6609	-1.83199
C	-4.0415	-3.0089	0.29011
C	-4.51819	-2.4491	-0.85897
C	-4.68946	3.37425	-0.37433
C	-5.09246	2.71301	0.74683
O	-5.76867	0.52947	2.7272
O	-5.55391	-0.43986	-2.89245
C	-4.54762	0.7175	3.44963
H	-4.03154	1.57067	3.06121
H	-4.76502	0.87392	4.48609
H	-3.93222	-0.15117	3.34227
C	-4.29503	-0.39559	-3.57018
H	-3.64236	-1.13719	-3.159
H	-4.44433	-0.59007	-4.61187
H	-3.85663	0.57276	-3.44753
C	-2.76751	-3.8706	0.32406
C	-2.19571	-4.23226	1.55094
C	-2.12092	-4.19808	-0.8745
C	-0.80332	-4.40683	1.58932
H	-2.78967	-4.32774	2.4356
C	-0.73558	-4.38663	-0.83569
H	-2.66067	-4.26044	-1.79682
C	-0.09175	-4.22013	0.39502
H	-0.29978	-4.63362	2.50526
H	-0.18248	-4.60706	-1.72504
C	-3.622	4.48161	-0.32733

C	-3.05235	4.9719	-1.51034
C	-3.14047	4.91853	0.91336
C	-1.72259	5.42127	-1.44683
H	-3.5914	4.96227	-2.43418
C	-1.82301	5.38212	0.97676
H	-3.7469	4.86065	1.7929
C	-1.07201	5.36427	-0.2032
H	-1.211	5.7569	-2.325
H	-1.39202	5.69755	1.90362
C	3.87189	1.66707	-0.9979
C	4.01121	0.27432	-0.91901
C	3.78121	-0.34252	0.31855
C	3.91359	0.39667	1.50017
C	3.77045	1.78946	1.42251
C	3.50526	2.35523	0.1662
H	4.00198	2.18172	-1.9275
H	4.2474	-0.3038	-1.78698
H	4.07863	-0.08905	2.43858
H	3.82266	2.3964	2.30188
C	3.27326	-1.79707	0.37555
C	2.96483	-2.38998	1.60869
C	3.02145	-2.49253	-0.81366
C	1.97849	-3.38733	1.62885
H	3.43692	-2.06377	2.51133
C	2.03202	-3.48224	-0.79388
H	3.53794	-2.24798	-1.7177
C	1.36228	-3.71563	0.41423
H	1.67859	-3.84887	2.54668
H	1.76758	-4.0137	-1.68391
C	2.71151	3.67351	0.06586
C	2.23854	4.29048	1.23175

C	2.37264	4.20229	-1.18914
C	1.06948	5.057	1.13795
H	2.7303	4.14753	2.17139
C	1.20543	4.97611	-1.28303
H	2.96342	3.98911	-2.055
C	0.45248	5.16233	-0.116
H	0.64047	5.51374	2.00455
H	0.88078	5.3749	-2.22164
H	-5.1362	3.13174	1.73143
H	-4.42735	-2.87112	-1.83644



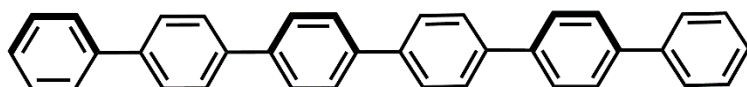
2,6-BDT-1,4-BT[6]CPP

C	3.89375	-0.19491	1.42277
C	3.82313	-1.29564	0.54354
C	3.85308	-1.08011	-0.86344
C	3.89446	0.19452	-1.42214
C	3.82358	1.29526	-0.54294
C	3.85284	1.07973	0.86404
S	3.4701	-2.56813	-1.73152
S	3.46959	2.56777	1.73196
C	2.98604	-3.36746	-0.21094
C	3.36732	-2.61714	0.8718
C	2.98633	3.36718	0.21115
C	3.36807	2.61682	-0.87141

O	3.85908	0.39036	-2.78482
O	3.85766	-0.39071	2.78543
C	2.55123	0.37966	-3.37647
H	1.91629	1.16371	-2.94664
H	2.70271	0.57367	-4.44046
H	2.06107	-0.59108	-3.24744
C	2.54949	-0.37993	3.3764
H	1.9147	-1.16387	2.94615
H	2.70039	-0.57405	4.44044
H	2.05952	0.59088	3.24718
C	1.88875	-4.35119	-0.20075
C	1.05216	-4.48269	-1.32602
C	1.39113	-4.87345	1.0143
C	-0.29533	-4.79528	-1.18082
H	1.40449	-4.16863	-2.30327
C	0.04484	-5.18751	1.15452
H	2.03572	-4.9192	1.88776
C	-0.86322	-5.00121	0.08911
H	-0.93906	-4.69967	-2.04978
H	-0.32366	-5.47895	2.13453
C	1.88919	4.35106	0.20055
C	1.05259	4.4832	1.32575
C	1.39166	4.87284	-1.01474
C	-0.29486	4.79592	1.18037
H	1.40484	4.16958	2.30316
C	0.04542	5.18703	-1.15515
H	2.03627	4.91809	-1.88821
C	-0.86268	5.00133	-0.08967
H	-0.93862	4.70083	2.04936
H	-0.32302	5.47806	-2.1353
C	-5.22788	0.85204	1.08733

C	-5.24596	-0.52548	1.27807
C	-5.08872	-1.41477	0.19659
C	-5.22835	-0.85149	-1.08724
C	-5.24628	0.52603	-1.27798
C	-5.08858	1.41528	-0.19656
H	-5.18685	-1.48828	-1.96557
H	-5.26311	0.90389	-2.29592
C	-4.44473	-2.74657	0.36428
C	-4.29948	-3.66914	-0.69296
C	-3.64247	-2.97622	1.49814
C	-3.24314	-4.57684	-0.7221
H	-4.96297	-3.61942	-1.55197
C	-2.59159	-3.88349	1.47178
H	-3.72696	-2.32683	2.3627
C	-2.28125	-4.61109	0.3079
H	-3.11507	-5.20062	-1.60303
H	-1.90482	-3.89544	2.31214
C	-4.44441	2.74698	-0.36434
C	-3.64209	2.97626	-1.49823
C	-4.29908	3.66971	0.69274
C	-2.59112	3.88342	-1.47205
H	-3.72664	2.32663	-2.36259
C	-3.24262	4.5773	0.72169
H	-4.96259	3.62022	1.55175
C	-2.28075	4.61126	-0.30832
H	-1.90431	3.89511	-2.31239
H	-3.11446	5.20124	1.60251
H	3.13709	2.89895	-1.89086
H	3.13576	-2.89924	1.89113
N	-5.17111	1.71427	2.27654
N	-5.26837	-1.03692	2.65605

S -5.32477 1.09397 3.69537

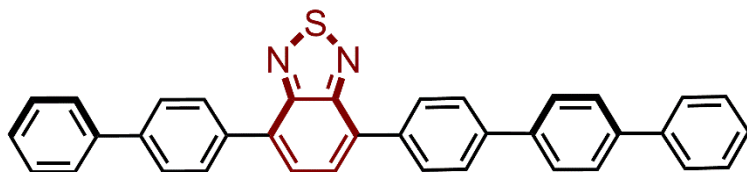


p-Sexiphenyl

C	-3.87745	1.64065	0.77739
C	-2.48229	1.6406	0.77769
C	-1.78457	2.61781	0.06814
C	-2.48203	3.59498	-0.64312
C	-3.87686	3.59468	-0.64376
C	-4.57465	2.61769	0.06686
H	-4.42736	0.87038	1.33724
H	-1.93293	0.87064	1.33859
H	-1.93168	4.36534	-1.20255
H	-4.42683	4.36467	-1.20423
C	-0.24457	2.61836	0.06912
C	0.45262	3.82632	0.06902
C	0.45344	1.41006	0.06972
C	1.84778	3.82672	0.07071
H	-0.09716	4.77867	0.06891
C	1.84826	1.41054	0.07094
H	-0.09649	0.45776	0.06975
C	2.54551	2.61895	0.07183
H	2.39727	4.7792	0.07108
H	2.39866	0.45842	0.07141
C	-6.11465	2.61781	0.06617
C	-6.81218	3.82556	0.065
C	-6.8123	1.4093	0.06712
C	-8.20734	3.82556	0.06358
H	-6.26267	4.77807	0.06388
C	-8.20713	1.40938	0.06618
H	-6.26211	0.45716	0.06811

C	-8.90472	2.61759	0.06401
H	-8.7571	4.77788	0.0622
H	-8.75725	0.4571	0.06693
C	4.08551	2.61913	0.07345
C	4.78251	1.64263	0.78468
C	4.78371	3.59674	-0.6365
C	6.17767	1.64241	0.78544
H	4.23258	0.87189	1.34394
C	6.17853	3.59674	-0.63531
H	4.23393	4.36661	-1.19716
C	6.87559	2.61928	0.07538
H	6.727	0.87216	1.34588
H	6.72908	4.36708	-1.19473
C	8.41559	2.61939	0.07627
C	9.11313	3.82714	0.0766
C	9.11325	1.41088	0.07635
C	10.50829	3.82714	0.07821
H	8.56362	4.77965	0.07691
C	10.50807	1.41096	0.07748
H	8.56305	0.45874	0.07603
C	11.20567	2.61916	0.0788
H	11.05805	4.77946	0.07892
H	11.05819	0.45868	0.07753
H	12.30527	2.61898	0.07989
C	-10.44472	2.61733	0.06269
C	-11.1428	1.64054	0.77247
C	-11.14184	3.59436	-0.64912
C	-12.53796	1.64087	0.77186
H	-10.59371	0.8707	1.33379
C	-12.53667	3.59434	-0.65007
H	-10.59122	4.36439	-1.20873

C	-13.2348	2.61777	0.06079
H	-13.08814	0.87093	1.3319
H	-13.08636	4.36421	-1.21096
H	-14.33441	2.61806	0.06006

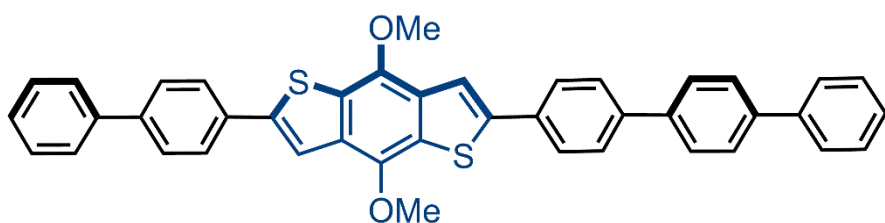


BT-*p*-sexiphenyl

C	-3.04673	-4.5979	0.29701
C	-2.53808	-5.3634	1.35498
C	-3.72367	-5.22369	-0.75847
C	-2.70661	-6.75465	1.35753
H	-2.02108	-4.88562	2.16081
C	-3.8921	-6.61491	-0.75595
H	-4.11194	-4.63925	-1.5663
C	-3.38369	-7.38039	0.30208
H	-2.31833	-7.33912	2.16532
H	-4.40891	-7.0927	-1.56187
C	-1.32481	2.17459	0.51598
C	-1.03971	3.08051	-0.51456
C	-1.06323	2.52349	1.84781
C	-0.49417	4.33577	-0.21317
H	-1.23863	2.81384	-1.53153
C	-0.51778	3.77873	2.14922
H	-1.28006	1.8315	2.63461
C	-0.23374	4.68512	1.1188
H	-0.27658	5.02744	-1.00004
H	-0.31826	4.04514	3.16614
C	2.33078	10.86456	1.35395
C	2.87326	12.12107	1.65548
C	3.13281	12.47089	2.98747

C	2.84986	11.56425	4.01792
C	2.30741	10.30776	3.71641
C	2.04775	9.95794	2.38444
H	2.1327	10.59745	0.33696
H	3.08925	12.81333	0.86871
H	3.04798	11.83138	5.03492
H	2.0915	9.61546	4.50318
C	-3.90631	-11.69163	0.30915
C	-3.95911	-10.97748	1.51379
C	-3.68499	-11.01454	-0.89768
C	-3.79054	-9.58624	1.51158
H	-4.12814	-11.49446	2.43525
C	-3.51647	-9.62333	-0.89989
H	-3.64469	-11.55979	-1.81744
C	-3.56913	-8.90918	0.30473
H	-3.83086	-9.04098	2.43134
H	-3.34755	-9.10636	-1.82136
C	1.4513	8.57725	2.05334
C	0.51285	7.99449	2.91565
C	1.84682	7.90363	0.88983
C	-0.0306	6.73844	2.61418
H	0.21121	8.50861	3.80423
C	1.30344	6.64748	0.58836
H	2.56364	8.34843	0.23163
C	0.36439	6.06504	1.45037
H	-0.74717	6.29356	3.27258
H	1.60549	6.13317	-0.29998
C	-2.86189	-3.06904	0.29421
C	-2.63854	-2.39553	-0.90651
C	-2.91748	-2.35747	1.49329
C	-2.47189	-1.01036	-0.90904

H	-2.59504	-2.95596	-1.85164
C	-2.75039	-0.97269	1.49074
C	-2.52796	-0.29902	0.28945
H	-2.29625	-0.4795	-1.85587
N	-3.15283	-3.06763	2.75867
N	-2.80888	-0.22272	2.75368
S	-1.49621	-1.43638	5.50446
H	3.54704	13.43022	3.21769
H	-4.03499	-12.75386	0.31082

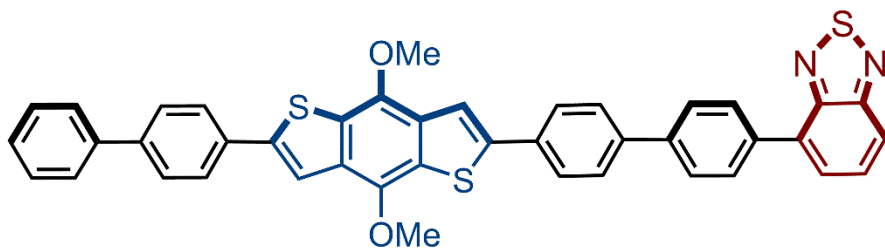


2,6-BDT-*p*-sexiphenyl

C	-2.6729	-1.3573	-1.3
C	-2.97984	-2.34304	-0.35256
C	-2.98435	-2.04579	1.01648
C	-2.57984	-0.80034	1.51521
C	-2.22411	0.17036	0.56916
C	-2.32507	-0.09411	-0.80295
S	-3.54957	-3.43385	1.9404
S	-1.95445	1.35448	-1.73247
C	-3.5123	-4.4497	0.48796
C	-3.29172	-3.69889	-0.6374
C	-1.42424	2.19398	-0.26375
C	-1.7269	1.46863	0.85928
O	-2.5324	-0.53346	2.91927
O	-2.7127	-1.62707	-2.70377
C	-1.23957	-0.87524	3.4259
H	-0.49499	-0.2911	2.92663
H	-1.20406	-0.67582	4.47655

H	-1.05227	-1.91454	3.25362
C	-1.43054	-2.08879	-3.13709
H	-1.17665	-2.98403	-2.60888
H	-1.46047	-2.29071	-4.18744
H	-0.69516	-1.33717	-2.93918
C	-3.69715	-5.97858	0.49076
C	-3.18849	-6.74408	1.54873
C	-4.37409	-6.60437	-0.56471
C	-3.35702	-8.13533	1.55129
H	-2.6715	-6.2663	2.35456
C	-4.54251	-7.99559	-0.56219
H	-4.76236	-6.01993	-1.37254
C	-4.03411	-8.76107	0.49584
H	-2.96875	-8.7198	2.35907
H	-5.05933	-8.47339	-1.36812
C	-0.71032	3.55856	-0.25139
C	-1.06118	4.54155	-1.1866
C	0.29007	3.81743	0.69527
C	-0.41252	5.78381	-1.17438
H	-1.8244	4.34364	-1.90995
C	0.93866	5.05968	0.70756
H	0.55861	3.06663	1.40877
C	0.58702	6.04309	-0.22691
H	-0.6805	6.53432	-1.88841
H	1.70233	5.25734	1.43051
C	2.95088	12.24476	-1.10387
C	3.59717	13.48819	-1.08965
C	4.59602	13.74793	-0.14162
C	4.94856	12.76428	0.79222
C	4.3023	11.52086	0.77799
C	3.30337	11.26112	-0.16996

H	2.18832	12.04643	-1.82776
H	3.32797	14.23925	-1.80263
H	5.71115	12.96262	1.51609
H	4.57157	10.76978	1.49092
C	-4.55673	-13.07231	0.5029
C	-4.60953	-12.35816	1.70755
C	-4.33541	-12.39522	-0.70393
C	-4.44096	-10.96692	1.70533
H	-4.77856	-12.87514	2.629
C	-4.16689	-11.00401	-0.70614
H	-4.29511	-12.94047	-1.62369
C	-4.21955	-10.28987	0.49848
H	-4.48128	-10.42166	2.62509
H	-3.99796	-10.48704	-1.6276
C	2.59305	9.89478	-0.18518
C	2.32383	9.23174	1.01971
C	2.21582	9.31449	-1.40375
C	1.67679	7.98874	1.00614
H	2.61225	9.6746	1.95007
C	1.56883	8.07139	-1.41736
H	2.42172	9.82058	-2.32374
C	1.29896	7.40867	-0.21234
H	1.4712	7.48256	1.92614
H	1.28088	7.62833	-2.34778
H	-1.58958	1.83809	1.85403
H	-3.33647	-4.09712	-1.62951
H	5.08951	14.69728	-0.13079
H	-4.68541	-14.13454	0.50458



2,6-BDT-1,4-BT-*p*-sexiphenyl

C	-1.99966	-1.43916	0.12796
C	-3.12517	-0.59866	0.05457
C	-2.9421	0.81245	-0.01148
C	-1.68265	1.40296	-0.01432
C	-0.55658	0.56098	0.02816
C	-0.73966	-0.84986	0.09842
S	-4.48317	1.64819	-0.11137
S	0.80294	-1.68849	0.12728
C	-5.36475	0.10692	-0.04418
C	-4.51217	-0.95981	0.03379
C	1.68427	-0.14829	0.037
C	0.83077	0.91974	-0.0097
O	-1.54092	2.77037	-0.10439
O	-2.14337	-2.80833	0.17658
C	-1.46518	3.43936	1.15988
H	-0.59535	3.09929	1.73607
H	-1.36251	4.50348	0.93638
H	-2.37512	3.27563	1.75009
C	-2.21571	-3.34726	1.50219
H	-3.0826	-2.94865	2.0441
H	-2.32191	-4.42807	1.38642
H	-1.30308	-3.12832	2.06982
C	-6.82974	0.08894	-0.09308
C	-7.59843	1.19592	0.30831
C	-7.51759	-1.05288	-0.54597

C	-8.98775	1.16028	0.26516
H	-7.10326	2.08637	0.68601
C	-8.90576	-1.08742	-0.58037
H	-6.95487	-1.90976	-0.90414
C	-9.67591	0.0181	-0.17683
H	-9.54988	2.02259	0.61208
H	-9.4036	-1.97343	-0.96413
C	3.14957	-0.13263	0.0129
C	3.89743	-1.24297	-0.41814
C	3.85975	1.01147	0.4238
C	5.28699	-1.20781	-0.44343
H	3.38435	-2.13498	-0.76703
C	5.2477	1.04569	0.39012
H	3.31536	1.87192	0.80124
C	5.99711	-0.06316	-0.04317
H	5.83065	-2.07246	-0.81311
H	5.76353	1.93431	0.74273
C	12.55157	-1.01781	-0.61477
C	13.94479	-0.98282	-0.64173
C	14.62846	0.15607	-0.21199
C	13.90515	1.25914	0.24535
C	12.51198	1.22304	0.27317
C	11.80911	0.08422	-0.15659
H	12.02974	-1.89895	-0.97776
H	14.49709	-1.84429	-1.00808
C	-13.97649	-0.09402	-0.30567
C	-13.29347	1.08154	-0.62301
C	-13.25307	-1.23266	0.05391
C	-11.9007	1.11791	-0.58158
H	-13.84584	1.97155	-0.91303
C	-11.86035	-1.19558	0.09599

H	-13.77435	-2.15102	0.31124
C	-11.15814	-0.01992	-0.22117
H	-11.37943	2.03005	-0.85842
H	-11.30926	-2.07978	0.40408
C	10.32585	0.04651	-0.12754
C	9.56146	1.18544	-0.43246
C	9.63281	-1.12956	0.2057
C	8.17115	1.15036	-0.40499
H	10.06347	2.10176	-0.7302
C	8.24251	-1.16539	0.23265
H	10.19198	-2.01895	0.48246
C	7.478	-0.02605	-0.07191
H	7.61273	2.03992	-0.68282
H	7.74127	-2.08205	0.53068
H	1.16527	1.94452	-0.11897
H	-4.8485	-1.98837	0.0868
H	15.71453	0.18371	-0.23336
H	-15.06223	-0.12256	-0.33849
N	11.76597	2.37829	0.79257
N	14.61069	2.46133	0.71209
S	13.02015	4.32578	-0.03079

CONCLUDING REMARKS

This work represents advancements in the synthesis of carbon nanohoops and their application in organic electronics. We have successfully developed scalable, size-selective syntheses of [5]-[12]cycloparaphenylene and fully characterized their optical, electronic, and solid-state properties. In addition we have developed a method to incorporate nitrogen into the nanohoop scaffold. The addition of nitrogen allowed further functionalization which allowed modulation of the optical, electronic, and solid-state properties.

REFERENCES CITED

Chapter I

- (1) Hoffmann, R.; Hopf, H. *Angew. Chem. Int. Ed.* **2008**, *47*, 4474.
- (2) Kekulé, A. *Liebigs Ann.* **1866**, *137*, 129.
- (3) Kammermeier, S.; Jones, P. G.; Herges, R. *Angew. Chem. Int. Ed.* **1996**, *35*, 2669.
- (4) Nakamura, E.; Tahara, K.; Matsuo, Y.; Sawamura, M. *J. Am. Chem. Soc.* **2003**, *125*, 2834.
- (5) Scott, L.; Boorum, M.; McMahon, B. *Science* **2002**, *295*, 1500.
- (6) Jasti, R.; Bertozzi, C. *Chem. Phys. Lett.* **2010**, *494*, 1.
- (7) Fort, E.; Donovan, P.; Scott, L. *J. Am. Chem. Soc.* **2009**, *131*, 16006.
- (8) Omachi, H.; Nakayama, T.; Takahashi, E.; Segawa, Y.; Itami, K. *Nat. Chem.* **2013**, *5*, 5726.
- (9) Parekh, V.; Guha, P. *J. Indian. Chem. Soc.* **1934**, *11*, 95.
- (10) Friederich, R.; Nieger, M.; Vögtle, F. *Chem. Ber.* **1993**, *126*, 1723.
- (11) Jasti, R.; Bhattacharjee, J.; Neaton, J.; Bertozzi, C. *J. Am. Chem. Soc.* **2008**, *130*, 17646.
- (12) Takaba, H.; Omachi, H.; Yamamoto, Y.; Bouffard, J.; Itami, K. *Angew. Chem. Int. Ed.* **2009**, *48*, 6112.
- (13) Yamago, S.; Watanabe, Y.; Iwamoto, T. *Angew. Chem. Int. Ed.* **2010**, *49*, 757.
- (14) Sisto, T.; Golder, M.; Hirst, E.; Jasti, R.; *J. Am. Chem. Soc.* **2011**, *133*, 15800.
- (15) Xia, J.; Jasti, R. *Angew. Chem. Int. Ed.* **2012**, *51*, 2474.
- (16) Xia, J.; Bacon, J.; Jasti, R. *Chem. Sci.* **2012**, *3*, 3018.
- (17) Darzi, E.; Sisto, T.; Jasti, R. *J. Org. Chem.* **2012**, *77*, 6624.
- (18) Evans, P.; Darzi, E.; Jasti, R. *Nat. Chem.* **2014**, *6*, 404.
- (19) Iwamoto, T.; Watanabe, Y.; Sakamoto, Y.; Suzuki, T.; Yamago, S. *J. Am. Chem. Soc.* **2011**, *133*, 8354.
- (20) Kayahara, E.; Sakamoto, Y.; Suzuki, T.; Yamago, S. *Org. Lett.* **2012**, *14*, 3284.
- (21) Kayahara, E.; Iwamoto, T.; Suzuki, T.; Yamago, S. *Chem. Lett.* **2013**, *42*, 621.
- (22) Kayahara, E.; Patel, V.; Yamago, S. *J. Am. Chem. Soc.* **2014**, *136*, 2284.
- (23) Segawa, Y.; Miyamoto, S.; Omachi, H.; Matsuura, S.; Šenel, P.; Sasamori, T.; Tokitoh, N.; Itami, K. *Angew. Chem. Int. Ed.* **2011**, *50*, 3244.
- (24) Segawa, Y.; Senel, P.; Matsuura, S.; Omachi, H.; Itami, K. *Chem. Lett.* **2011**, *40*, 423.
- (25) Ishii, Y.; Nakanishi, Y.; Omachi, H.; Matsuura, S.; Matsui, K.; Shinohara, H.; Segawa, Y.; Itami, K. *Chem. Sci.* **2012**, *3*, 2340.
- (26) Sibbel, F.; Matsui, K.; Segawa, Y.; Studer, A.; Itami, K. *Chem. Commun.* **2014**, *50*, 954.
- (27) Omachi, H.; Segawa, Y.; Itami, K. *Org. Lett.* **2011**, *13*, 2480.
- (28) Hitosugi, S.; Nakanishi, W.; Yamasaki, T.; Isobe, H. *Nat. Commun.* **2011**, *2*, 492.
- (29) Tran-Van, A.; Huxol, E.; Basler, J.; Neuburger, M.; Adjizian, J.; Ewels, C.; Wegner, H. *Org. Lett.* **2014**, *16*, 1594.
- (30) Huang, C.; Huang, Y.; Akhmedov, N.; Popp, B.; Petersen, J.; Wang, K. *Org. Lett.* **2014**, *16*, 2672.
- (31) Fujitsuka, M.; Cho, D.; Iwamoto, T.; Yamago, S.; Majima, T. *Phys. Chem. Chem. Phys.* **2012**, *14*, 14585.

- (32) Fujitsuka, M.; Lu, C.; Iwamoto, T.; Kayahara, E.; Yamago, S.; Majima, T. *J. Phys. Chem. A* **2014**, *118*, 4527.
- (33) Adamska, L.; Nayyar, I.; Chen, H.; Swan, A.; Oldani, N.; Fernandez-Alberti, S.; Golder, M.; Jasti, R.; Doorn, S.; Tretiak, S. *Nano Lett.* **2014**, *14*, 6539.
- (34) Reddy, V.; Camacho, C.; Xia, J.; Jasti, R.; Irle, S. *J. Chem. Theory Comput.* **2014**, *10*, 4025.
- (35) Segawa, Y.; Fukazawa, A.; Matsuura, S.; Omachi, S.; Yamaguchi, S.; Irle, S.; Itami, K. *Org. Biomol. Chem.* **2012**, *10*, 5979.
- (36) Nishihara, T.; Segawa, Y.; Itami, K.; Kanemitsu, Y. *J. Chem. Phys. Lett.* **2012**, *3*, 3125.
- (37) Camacho, C.; Niehaus, T.; Itami, K.; Irle, S. *Chem. Sci.* **2013**, *4*, 187.
- (38) Nishihara, T.; Segawa, Y.; Itami, K.; Kanemitsu, Y. *Chem. Sci.* **2014**, *5*, 2293.
- (39) Li, P.; Sisto, T.; Darzi, E.; Jasti, R. *Org. Lett.* **2014**, *16*, 182.
- (40) Banerjee, M.; Shukla, R.; Rathore, R. *J. Am. Chem. Soc.* **2009**, *131*, 1780.
- (41) Wong, B. *J. Phys. Chem. C* **2009**, *113*, 21921.
- (42) Srinivasan, M.; Sankararaman, S.; Hopf, H.; Varghese, B. *Eur. J. Org. Chem.* **2003**, *4*, 660.
- (43) Segawa, Y.; Omachi, H.; Itami, K. *Org. Lett.* **2010**, *12*, 2262.
- (44) Fan, X.; Ju, X.; Xia, Q.; Xiao, H. *J. Hazard. Mater.* **2008**, *151*, 255.
- (45) Chen, H.; Golder, M.; Wang, F.; Jasti, F.; Swan, A. *Carbon* **2014**, *67*, 203.
- (46) Jagadeesh, M.; Makur, A.; Chandrasekhar, J. *J. Mol. Modeling* **2000**, *6*, 226.
- (47) Burns, N.; Krylova, I.; Hannoush, R.; Baran, P. *J. Am. Chem. Soc.* **2009**, *131*, 9172.
- (48) Hope, H.; Bernstein, J.; Trueblood, K. *Acta Crystallog. Sec. B* **1972**, *28*, 1733.
- (49) Tsuji, T.; Ohkita, M.; Konno, T.; Nishida, S. *J. Am. Chem. Soc.* **1997**, *119*, 8425.
- (50) Friebolin, H. *Basic One- and Two Dimensional NMR Spectroscopy*, 3 edn., WILEY-VCH New York, **1998**.
- (51) Alvarez, M.; Burrezo, P.; Kertesz, M.; Iwamoto, T.; Yamago, S.; Xia, J.; Jasti, R.; Navarrete, J.; Taravillo, M.; Baonza, V.; Casado, J. *Angew. Chem. Int. Ed.* **2014**, *53*, 7033.
- (52) Fujitsuka, M.; Iwamoto, T.; Kayahara, E.; Yamago, S.; Majima, T. *ChemPhysChem*, **2013**, *14*, 1570.
- (53) Fujitsuka, M.; Tojo, S.; Iwamoto, T.; Kayahara, E.; Yamago, S.; Majima, T. *J. Phys. Chem. Lett.* **2014**, *5*, 2302.
- (54) Hines, D.; Darzi, E.; Jasti, R.; Kamat, P. *J. Phys. Chem. A* **2014**, *118*, 1595.
- (55) Sundholm, D.; Taubert, S.; Pichierri, F. *Phys. Chem. Chem. Phys.* **2010**, *12*, 2751.
- (56) Kasha, M. *Discuss. Faraday Soc.* **1950**, *9*, 14.
- (57) Condon, E. *Phys. Rev.* **1928**, *32*, 858.

Chapter II

- (1) Jasti, R.; Bertozzi, C. *Chem. Phys. Lett.* **2010**, *494*, 1.
- (2) Fort, E.; Donovan, P.; Scott, L. *J. Am. Chem. Soc.* **2009**, *131*, 16006.
- (3) Fort, E.; Scott, L. *Angew. Chem., Int. Ed.* **2010**, *49*, 6626.
- (4) Fort, E.; Scott, L. *J. Mater. Chem.* **2011**, *21*, 1373.
- (5) Bunz, U.; Menning, S.; Martín, N. *Angew. Chem., Int. Ed.* **2012**, *124*, 7202.

- (6) Jasti, R.; Bhattacharjee, J.; Neaton, J.; Bertozzi, C. *J. Am. Chem. Soc.* **2008**, *130*, 17646.
- (7) Iwamoto, T.; Watanabe, Y.; Sakamoto, Y.; Suzuki, T.; Yamago, S. *J. Am. Chem. Soc.* **2011**, *133*, 8354.
- (8) Sisto, T.; Golder, M.; Hirst, E.; Jasti, R. *J. Am. Chem. Soc.* **2011**, *133*, 15800.
- (9) Miyaura, N.; Suzuki, A. *Chem. Rev.* **1995**, *95*, 2457.
- (10) Sundholm, D.; Taubert, S.; Pichierri, F. *Phys. Chem. Chem. Phys.* **2010**, *12*, 2751.
- (11) Wong, B. *J. Phys. Chem.* **2009**, *113*, 21921.
- (12) Segawa, Y.; Fukazawa, A.; Matsuura, S.; Omachi, H.; Yamaguchi, S.; Irle, S.; Itami, K. *Org. Biomol. Chem.* **2012**, *10*, 5979.
- (13) Iwamoto, T.; Watanabe, Y.; Sadahiro, T.; Haino, T.; Yamago, S. *Angew. Chem.* **2011**, *123*, 8492.
- (14) Takaba, H.; Omachi, H.; Yamamoto, Y.; Bouffard, J.; Itami, K. *Angew. Chem. Int. Ed.* **2009**, *48*, 6112.
- (15) Yamago, S.; Watanabe, Y.; Iwamoto, T. *Angew. Chem. Int. Ed.* **2010**, *49*, 757.
- (16) Omachi, H.; Matsuura, S.; Segawa, Y.; Itami, K. *Angew. Chem. Int. Ed.* **2010**, *49*, 10202.
- (17) Segawa, Y.; Miyamoto, S.; Omachi, H.; Matsuura, S.; Senel, P.; Sasamori, T.; Tokitoh, N.; Itami, K. *Angew. Chem. Int. Ed.* **2011**, *50*, 3244.
- (18) Segawa, Y.; Senel, P.; Matsuura, S.; Omachi, H.; Itami, K. *Chem. Lett.* **2011**, *40*, 423.
- (19) Ishii, Y.; Nakanishi, Y.; Omachi, H.; Matsuura, S.; Matsui, K.; Shinohara, H.; Segawa, Y.; Itami, K. *Chem. Sci.* **2012**, *3*, 2340.
- (20) Xia, J.; Jasti, R. *Angew. Chem. Int. Ed.* **2012**, *51*, 2474.
- (21) Matsui, K.; Segawa, Y.; Itami, K. *Org. Lett.* **2012**, *14*, 1888.
- (22) Omachi, H.; Segawa, Y.; Itami, K. *Org. Lett.* **2011**, *13*, 2480.
- (23) Hitosugi, S.; Nakanishi, W.; Yamasaki, T.; Isobe, H. *Nat. Commun.* **2011**, *2*, 492.
- (24) Compound 5 was prepared in a similar fashion as previously reported 3 and 4. The experimental procedures and details are reported in the supporting information.
- (25) A similar strategy has been suggested earlier for the synthesis of cyclophynes. See: Srinivasan, M.; Sankararaman, S.; Hopf, H.; Varghese, B. *Eur. J. Org. Chem.* **2003**, *4*, 660.
- (26) Barder, T.; Walker, S.; Martinelli, J.; Buchwald, S. *J. Am. Chem. Soc.* **2005**, *127*, 4685.
- (27) Frisch, M.; et al. Gaussian03, revisionC.02, Gaussian, Inc., Wallingford, CT, 2004. For full reference, see the Supporting Information.
- (28) Sisto, T.; Jasti, R. *Synlett* **2012**, *23*, 483.
- (29) Williams, A.; Winfield, S.; Miller, J. *Analyst* **1983**, *108*, 1067.
- (30) The discrepancy between our measured quantum yield for [9]CPP as compared to that reported by Itami is likely due to the differing techniques used.
- (31) Pangborn, A.; Giardello, M.; Grubbs, R.; Rosen, R.; Timmers, F. *Organometallics* **1996**, *15*, 1518.

Chapter III

- (1) Eaton, P.; Cole, T. *J. Am. Chem. Soc.* **1964**, *86*, 3157.

- (2) Lawton, R.; Barth, W. *J. Am. Chem. Soc.* **1971**, *93*, 1730.
- (3) Dauben, W.; Cargill, R. *Tetrahedron* **1961**, *15*, 197.
- (4) Kane, V.; Wolf, A.; Jones, M. *J. Am. Chem. Soc.* **1996**, *96*, 2643.
- (5) Scott, L.; Boorum, M.; McMahon, B. *Science* **2002**, *295*, 1500.
- (6) Hopf, H. *Classics in Hydrocarbon Chemistry*. (Wiley-VCH, Weinheim; **2000**).
- (7) Scott, L. *Angew. Chem. Int. Ed.* **2003**, *42*, 4133.
- (8) Parekh, V.; Guha, P. *J. Indian Chem. Soc.* **1934**, *11*, 95.
- (9) Xia, J.; Jasti, R. *Angew. Chem. Int. Ed.* **2012**, *51*, 2474.
- (10) Golder, M.; Wong, B.; Jasti, R. *Chem. Sci.* **2013**, *4*, 4285.
- (11) Zabula, A.; Filatov, A.; Xia, J.; Jasti, R.; Petrukhina, M. *Angew. Chem. Int. Ed.* **2013**, *52*, 5033.
- (12) Iwamoto, T.; Watanabe, Y.; Sadahiro, T.; Haino, T.; Yamago, S. *Angew. Chem. Int. Ed.* **2011**, *50*, 8342.
- (13) Xia, J.; Bacon, J.; Jasti, R. *Chem. Sci.* **2012**, *3*, 3018.
- (14) Hirst, E.; Jasti, R. *J. Org. Chem.* **2012**, *77*, 10473.
- (15) Omachi, H.; Nakayama, T.; Takahashi, E.; Segawa, Y.; Itami, K. *Nat. Chem.* **2013**, *5*, 572.
- (16) Darzi, E.; Sisto, T.; Jasti, R. *J. Org. Chem.* **2012**, *77*, 6624.
- (17) Iwamoto, T.; Watanabe, Y.; Sakamoto, Y.; Suzuki, T.; Yamago, S. *J. Am. Chem. Soc.* **2011**, *133*, 8354.
- (18) Ishii, Y.; Nakanishi, Y.; Omachi, H.; Matsuura, S.; Matsui, K.; Shinohara, H.; Segawa, Y.; Itami, K. *Chem. Sci.* **2012**, *3*, 2340.
- (19) Jasti, R.; Bhattacharjee, J.; Neaton, J.; Bertozzi, C.; *J. Am. Chem. Soc.* **2008**, *130*, 17646.
- (20) Sisto, T.; Golder, M.; Hirst, E.; Jasti, R. *J. Am. Chem. Soc.* **2011**, *133*, 15800.
- (21) Kayahara, E.; Iwamoto, T.; Suzuki, T.; Yamago, S. *Chem. Lett.* **2013**, *42*, 621.
- (22) Kayahara, E.; Sakamoto, Y.; Suzuki, T.; Yamago, S. *Org. Lett.* **2012**, *14*, 3284.
- (23) Iwamoto, T.; Watanabe, Y.; Sakamoto, Y.; Suzuki, T.; Yamago, S. *J. Am. Chem. Soc.* **2011**, *133*, 8354.
- (24) Yamago, S.; Watanabe, Y.; Iwamoto, T. *Angew. Chem. Int. Ed.* **2010**, *49*, 757.
- (25) Sibbel, F.; Matsui, K.; Segawa, Y.; Studer, A.; Itami, K. *Chem. Commun.* **2014**, *50*, 954.
- (26) Ishii, Y.; Nakanishi, Y.; Omachi, H.; Matsuura, S.; Matsui, K.; Shinohara, H.; Segawa, Y.; Itami, K. *Chem. Sci.* **2012**, *3*, 2340.
- (27) Segawa, Y.; Senel, P.; Matsuura, S.; Omachi, H.; Itami, K. *Chem. Lett.* **2011**, *40*, 423.
- (28) Segawa, Y.; Miyamoto, S.; Omachi, H.; Matsuura, S.; Šenel, P.; Sasamori, T.; Tokitoh, N.; Itami, K. *Angew. Chem. Int. Ed.* **2011**, *50*, 3244.
- (29) Omachi, H.; Matsuura, S.; Segawa, Y.; Itami, K. *Angew. Chem. Int. Ed.* **2010**, *49*, 10202.
- (30) Hitosugi, S.; Nakanishi, W.; Yamasaki, T.; Isobe, H. *Nat. Commun.* **2011**, *2*, 492.
- (31) Yagi, A.; Venkataramana, G.; Segawa, Y.; Itami, K. *Chem. Commun.* **2014**, *50*, 957.
- (32) Matsui, K.; Segawa, Y.; Itami, K. *Org. Lett.* **2012**, *14*, 1888.
- (33) Sisto, T.; Tian, X.; Jasti, R. *J. Org. Chem.* **2012**, *77*, 5857.
- (34) Wong, B. *J. Phys. Chem. C* **2009**, *113*, 21921.

- (35) Frisch, M.; Trucks, G.; Schlegel, H.; Scuseria, G.; Robb, M.; Cheeseman, J.; Scalmani, G.; Barone, V.; Mennucci, B.; Petersson, G.; Nakatsuji, H.; Caricato, M.; Li, X.; Hratchian, H.; Izmaylov, A.; Bloino, J.; Zheng, G.; Sonnenberg, J.; Hada, M.; Ehara, M.; Toyota, K.; Fukuda, R.; Hasegawa, J.; Ishida, M.; Nakajima, T.; Honda, Y.; Kitao, O.; Nakai, H.; Vreven, T.; Montgomery, J.; Peralta, J.; Ogliaro, F.; Bearpark, M.; Heyd, J.; Brothers, E.; Kudin, K.; Staroverov, V.; Kobayashi, R.; Normand, J.; Raghavachari, K.; Rendell, A.; Burant, J.; Iyengar, S.; Tomasi, J.; Cossi, M.; Rega, N.; Millam, J.; Klene, M.; Knox, J.; Cross, J.; Bakken, V.; Adamo, C.; Jaramillo, J.; Gomperts, R.; Stratmann, R.; Yazyev, O.; Austin, A.; Cammi, R.; Pomelli, C.; Ochterski, J.; Martin, R.; Morokuma, K.; Zakrzewski, V.; Voth, G.; Salvador, P.; Dannenberg, J.; Dapprich, S.; Daniels, A.; Farkas; Foresman, J.; Ortiz, J.; Cioslowski, J.; Fox, D. Wallingford CT, **2009**.
- (36) All DFT calculations performed with Gaussian09 at the B3LYP/6-31g* level of theory. All strain energies calculated using homodesmotic reactions. See the supplementary material for details.
- (37) Anslyn, E.; Dougherty, D. *Modern Physical Organic Chemistry*. (University Science Books, Mill Valley, CA; **2008**).
- (38) Punna, S.; Díaz, D.; Finn, M. *Synlett* **2004**, *13*, 2351.
- (39) Moreno-Mañas, M.; Pérez, M.; Pleixats, R. *J. Org. Chem.* **1996**, *61*, 2346.
- (40) Based on solubility and MALDI-MS data the decomposed mixture appears qualitatively to contain oligophenylenes.
- (41) Tobe, Y.; Jimbo, M.; Saiki, S.; Kakiuchi, K.; Naemura, K. *J. Org. Chem.* **1993**, *58*, 5883.
- (42) Tobe, Y.; Ueda, K.; Kaneda, T.; Kakiuchi, K.; Odaira, Y.; Kai, Y.; Kasai, N. *J. Am. Chem. Soc.* **1987**, *109*, 1136.
- (43) Jagadeesh, M.; Makur, A.; Chandrasekhar, J. *J Mol. Model.* **2000**, *6*, 226.
- (44) Allinger, N.; Walter, T.; Newton, M. *J. Am. Chem. Soc.* **1974**, *96*, 4588.
- (45) Tobe, Y.; Ueda, K.; Kakiuchi, K.; Odaira, Y.; Kai, Y.; Kasai, N. *Tetrahedron* **1986**, *42*, 1851.
- (46) Baran, P.; Burns, N.; *J. Am. Chem. Soc.* **2006**, *128*, 3908.
- (47) Takiguchi, H.; Ohmori, K.; Suzuki, K. *Angew. Chem. Int. Ed.* **2013**, *52*, 10472.
- (48) Fujitsuka, M.; Cho, D.; Iwamoto, T.; Yamago, S.; Majima, T. *Phys. Chem. Chem. Phys.* **2012**, *14*, 14585.
- (49) Kawasumi, K.; Zhang, Q.; Segawa, Y.; Scott, L.; Itami, K. *Nat. Chem.* **2013**, *5*, 739.

Chapter IV

- (1) Nguyen, S.; Johnson, L.; Grubbs, R.; Ziller, J. *J. Am. Chem. Soc.* **1992**, *114*, 3974.
- (2) Bielawski, C.; Grubbs, R. *Prog. Polym. Sci.* **2007**, *32*, 1.
- (3) Schrock, R. *Acc. Chem. Res.* **1990**, *23*, 158.
- (4) Schrock, R.; Hoveyda, A. *Angew. Chem. Int. Ed.* **2003**, *42*, 4592.
- (5) Gulder, T.; Baran, P. *Nat. Prod. Rep.* **2012**, *29*, 899.
- (6) Villar, E.; Beglov, D.; Chennamadhavuni, S.; Porco Jr, J.; Kozakov, D.; Vajda, S.; Whitty, A. *Nat. Chem. Biol.* **2014**, *10*, 723.
- (7) Xia, J.; Bacon, J.; Jasti, R. *Chem. Sci.* **2012**, *3*, 3018.

- (8) Iwamoto, T.; Watanabe, Y.; Sadahiro, T.; Haino, T.; Yamago, S. *Angew. Chem. Int. Ed.* **2011**, *50*, 8342.
- (9) Iwamoto, T.; Watanabe, Y.; Takaya, H.; Haino, T.; Yasuda, N.; Yamago, S. *Chem. Eur. J.* **2013**, *19*, 14061.
- (10) Iwamoto, T.; Slanina, Z.; Mizorogi, N.; Guo, J.; Akasaka, T.; Nagase, S.; Takaya, H.; Yasuda, N.; Kato, T.; Yamago, S. *Chem. Eur. J.* **2014**, *20*, 14403.
- (11) Isobe, H.; Hitosugi, S.; Yamasaki, T.; Iizuka, R. *Chem. Sci.* **2013**, *4*, 1293.
- (12) Hitosugi, S.; Iizuka, R.; Yamasaki, T.; Zhang, R.; Murata, Y.; Isobe, H. *Org. Lett.* **2013**, *15*, 3199.
- (13) Sato, S.; Yamasaki, T.; Isobe, H. *Proc. Natl. Acad. Sci.* **2014**, *111*, 8374.
- (14) Matsuno, T.; Sato, S.; Iizuka, R.; Isobe, H. *Chem. Sci.* **2015**, *6*, 909.
- (15) Baran, P.; Burns, N. *J. Am. Chem. Soc.* **2006**, *128*, 3908.
- (16) Burns, N.; Krylova, I.; Hannoush, R.; Baran, P. *J. Am. Chem. Soc.* **2009**, *131*, 9172.
- (17) Lloyd-Williams, P.; Giralt, E. *Chem. Soc. Rev.* **2001**, *30*, 145.
- (18) Evans, D.; Wood, M.; Trotter, B.; Richardson, T.; Barrow, J.; Katz, J. *Angew. Chem. Int. Ed.* **1998**, *37*, 2700.
- (19) Nicolaou, K.; Li, H.; Boddy, C.; Ramanjulu, J.; Yue, T.; Natarajan, S.; Chu, X.; Bräse, S.; Rübsam, F. *Chem. Eur. J.* **1999**, *5*, 2584.
- (20) Boger, D.; Miyazaki, S.; Kim, S.; Wu, J.; Castle, S.; Loiseleur, O.; Jin, Q. *J. Am. Chem. Soc.* **1999**, *121*, 10004.
- (21) Cram, D.; Cram, J. *Acc. Chem. Res.* **1971**, *4*, 204.
- (22) Golder, M.; Jasti, R. *Acc. Chem. Res.* **2015**, *48*, 557.
- (23) Darzi, E.; Jasti, R. *Chem. Soc. Rev.* **2015**, *44*, 6401.
- (24) Negishi, E. *Handbook of Organopalladium Chemistry for Organic Synthesis*; John Wiley & Sons: New York, **2002**; Vol. 1.
- (25) Evans, P.; Darzi, E.; Jasti, R. *Nat. Chem.* **2014**, *6*, 404.
- (26) Dhital, R.; Sakurai, H. *Asian J. Org. Chem.* **2014**, *3*, 668.
- (27) Iafe, R.; Kuo, J.; Hochstatter, D.; Saga, T.; Turner, J.; Merlic, C. *Org. Lett.* **2013**, *15*, 582.
- (28) Iafe, R.; Chan, D.; Kuo, J.; Boon, B.; Faizi, D.; Saga, T.; Turner, J.; Merlic, C. *Org. Lett.* **2012**, *14*, 4282.
- (29) Ogura, T.; Usuki, T. *Tetrahedron* **2013**, *69*, 2807.
- (30) Miyaura, N.; Yanagi, T.; Suzuki, A. *Synth. Commun.* **1981**, *11*, 513.
- (31) Butters, M.; Harvey, J.; Jover, J.; Lennox, A.; Lloyd-Jones, G.; Murray, P. *Angew. Chem. Int. Ed.* **2010**, *49*, 5156.
- (32) Moreno-Mañas, M.; Pérez, M.; Pleixats, R. *J. Org. Chem.* **1996**, *61*, 2346.
- (33) Lakmini, H.; Ciofini, I.; Jutand, A.; Amatore, C.; Adamo, C. *J. Phys. Chem. A* **2008**, *112*, 12896.
- (34) Adamo, C.; Amatore, C.; Ciofini, I.; Jutand, A.; Lakmini, H. *J. Am. Chem. Soc.* **2006**, *128*, 6829.
- (35) Liu, Q.; Li, G.; He, J.; Liu, J.; Li, P.; Lei, A. *Angew. Chem. Int. Ed.* **2010**, *49*, 3371.
- (36) Yoshida, H.; Yamaryo, Y.; Ohshita, J.; Kunai, A. *Tetrahedron Lett.* **2003**, *44*, 1541.
- (37) Punna, S.; Díaz, D.; Finn, M. *Synlett* **2004**, *13*, 2351.

- (38) Braga, A.; Ujaque, G.; Maseras, F. *Organometallics* **2006**, *25*, 3647.
- (39) Carrow, B.; Hartwig, J. *J. Am. Chem. Soc.* **2011**, *133*, 2116.
- (40) Lennox, A. J.; Lloyd-Jones, G. *Angew. Chem. Int. Ed.* **2013**, *52*, 7362.
- (41) Thomas, A.; Denmark, S. *Science* **2016**, *352*, 329.
- (42) McLaughlin, P.; Verkade, J. *Organometallics* **1998**, *17*, 5937.
- (43) Mason, M.; Verkade, J. *Organometallics* **1992**, *11*, 2212.
- (44) Lanci, M.; Brinkley, D.; Stone, K.; Smirnov, V.; Roth, J. *Angew. Chem. Int. Ed.* **2005**, *44*, 7273.
- (45) Yamamoto, Y. *Synlett* **2007**, *2007*, 1913.
- (46) Miyaura, N.; Suzuki, A. *Main Group Met. Chem.* **1987**, *10*, 295.
- (47) Lennox, A.; Lloyd-Jones, G. *Chem. Soc. Rev.* **2014**, *43*, 412.
- (48) Xia, J.; Jasti, R. *Angew. Chem. Int. Ed.* **2012**, *51*, 2474.
- (49) Li, P.; Sisto, T.; Darzi, E.; Jasti, R. *Org. Lett.* **2014**, *16*, 182.
- (50) Takagi, J.; Takahashi, K.; Ishiyama, T.; Miyaura, N. *J. Am. Chem. Soc.* **2002**, *124*, 8001.
- (51) Billingsley, K.; Barder, T.; Buchwald, S. *Angew. Chem. Int. Ed.* **2007**, *46*, 5359.
- (52) Ainley, A.; Challenger, F. *J. Chem. Soc.* **1930**, 2171.
- (53) Patel, V.; Kayahara, E.; Yamago, S. *Chem. Eur. J.* **2015**, *21*, 5742.
- (54) Kayahara, E.; Patel, V.; Yamago, S. *J. Am. Chem. Soc.* **2014**, *136*, 2284.
- (55) Darzi, E.; Sisto, T.; Jasti, R. *J. Org. Chem.* **2012**, *77*, 6624.
- (56) Sisto, T.; Golder, M.; Hirst, E.; Jasti, R. *J. Am. Chem. Soc.* **2011**, *133*, 15800.
- (57) Sibbel, F.; Matsui, K.; Segawa, Y.; Studer, A.; Itami, K. *Chem. Commun.* **2014**, *50*, 954.
- (58) Agard, N.; Prescher, J.; Bertozzi, C. *J. Am. Chem. Soc.* **2004**, *126*, 15046.
- (59) Laughlin, S.; Baskin, J.; Amacher, S.; Bertozzi, C. *Science* **2008**, *320*, 664.
- (60) Iha, R.; Wooley, K.; Nyström, A.; Burke, D.; Kade, M.; Hawker, C. *Chem. Rev.* **2009**, *109*, 5620.
- (61) Srinivasan, M.; Sankararaman, S.; Hopf, H.; Varghese, B. *Eur. J. Org. Chem.* **2003**, *2003*, 660.
- (62) Kayahara, E.; Patel, V.; Xia, J.; Jasti, R.; Yamago, S. *Synlett* **2015**, *26*, 1615.
- (63) Jasti, R.; Bhattacharjee, J.; Neaton, J.; Bertozzi, C. *J. Am. Chem. Soc.* **2008**, *130*, 17646.
- (64) Garrido, L.; Zubía, E.; Ortega, M.; Salvá, J. *J. Org. Chem.* **2003**, *68*, 293.

Chapter V

- (1) Lewis, N.; Nocera, D. *Proc. Nat. Acad. Sci. U.S.A.* **2006**, *103*, 15729.
- (2) Anthony, J. *Chem. Rev.* **2006**, *106*, 5028.
- (3) (a) McQuade, D.; Pullen, A.; Swager, T. *Chem. Rev.* **2000**, *100*, 2537; (b) Izuhara, D.; Swager, T. *J. Mater. Chem.* **2011**, *21*, 3579; (c) Izuhara, D.; Swager, T. *J. Am. Chem. Soc.* **2009**, *131*, 17724.
- (4) Brédas, J.; Calbert, J.; da Silva Filho, D.; Cornil, J. *Proc. Nat. Acad. Sci. U.S.A.* **2002**, *99*, 5804.
- (5) (a) Golder, M.; Jasti, R. *Acc. Chem. Res.* **2015**, *48*, 557; (b) Darzi, E.; Jasti, R. *Chem. Soc. Rev.* **2015**, *44*, 6401.
- (6) Brédas, J.; Heeger, A. *Chem. Phys. Lett.* **1994**, *217*, 507.

- (7) Iwamoto, T.; Watanabe, Y.; Sakamoto, Y.; Suzuki, T.; Yamago, S. *J. Am. Chem. Soc.* **2011**, *133*, 8354.
- (8) Segawa, Y.; Omachi, H.; Itami, K. *Org. Lett.* **2010**, *12*, 2262.
- (9) Alvarez, M.; Burrezo, P.; Kertesz, M.; Iwamoto, T.; Yamago, S.; Xia, J.; Jasti, R.; Navarrete, J.; Taravillo, M.; Baonza, V.; Casado, J. *Angew. Chem. Int. Ed.* **2014**, *53*, 7033.
- (10) Unsubstituted linear [n]oligoparaphenylenes become completely insoluble when n>6.
- (11) (a) Takase, M.; Narita, T.; Fujita, W.; Asano, M.; Nishinaga, T.; Benten, H.; Yoza, K.; Müllen, K. *J. Am. Chem. Soc.* **2013**, *135*, 8031; (b) Berger, R.; Giannakopoulos, A.; Ravat, P.; Wagner, M.; Beljonne, D.; Feng, X.; Müllen, K. *Angew. Chem. Int. Ed.* **2014**, *53*, 10520; (c) Ito, S.; Tokimaru, Y.; Nozaki, K. *Angew. Chem. Int. Ed.* **2015**, *54*, 7256.
- (12) (a) Keshavarz-K, M.; Gonzalez, R.; Hicks, R.; Srdanov, G.; Srdanov, V.; Collins, T.; Hummelen, J.; Bellavia-Lund, C.; Pavlovich, J.; Wudl, F.; Holczner, K. *Nature* **1996**, *383*, 147; (b) Chen, P.; Chew, L.; Kostka, A.; Muhler, M.; Xia, W. *Catal. Sci. Tech.* **2013**, *3*, 1964; (c) Stephan, O.; Ajayan, P.; Colliex, C.; Redlich, P.; Lambert, J.; Bernier, P.; Lefin, P. *Science* **1994**, *266*, 1683.
- (13) (a) Matsui, K.; Segawa, Y.; Itami, K. *Org. Lett.* **2012**, *14*, 1888; (b) Ito, H.; Mitamura, Y.; Segawa, Y.; Itami, K. *Angew. Chem. Int. Ed.* **2015**, *54*, 159; (c) Huang, C.; Huang, Y.; Akhmedov, N.; Popp, B.; Petersen, J.; Wang, K. *Org. Lett.* **2014**, *16*, 2672; (d) Tran-Van, A.; Huxol, E.; Basler, J.; Neuburger, M.; Adjizian, J.; Ewels, C.; Wegner, H. *Org. Lett.* **2014**, *16*, 1594; (e) Tran-Van, A.; Wegner, H. *Beilstein J. Nanotechnol.* **2014**, *5*, 1320; (f) Bachrach, S.; Stück, D. *J. Org. Chem.* **2010**, *75*, 6595.
- (14) During the preparation of this manuscript, two related concepts were reported. The first was reported by Nuckolls et al. Ball, M.; Fowler, B.; Li, P.; Joyce, L.; Li, F.; Liu, T.; Paley, D.; Zhong, Y.; Li, H.; Xiao, S.; Ng, F.; Steigerwald, M.; Nuckolls, C. *J. Am. Chem. Soc.* **2015**, *137*, 9982. The second was reported by Itami et al. Kuwabara, T.; Orii, J.; Segawa, Y.; Itami, K. *Angew. Chem.* **2015**, *127*, 9782.
- (15) Frisch, M.; Schlegel, H.; Scuseria, G.; Robb, M.; Cheeseman, J.; Scalmani, G.; Barone, V.; Mennucci, B.; Petersson, G.; Nakatsuji, H.; Caricato, M.; Li, X.; Hratchian, H.; Izmaylov, A.; Bloino, J.; Zheng, G.; Sonnenberg, J.; Hada, M.; Ehara, M.; Toyota, K.; Fukuda, R.; Hasegawa, J.; Ishida, M.; Nakajima, T.; Honda, Y.; Kitao, O.; Nakai, H.; Vreven, T.; Montgomery, J.; Peralta, J.; Ogliaro, F.; Bearpark, M.; Heyd, J.; Brothers, E.; Kudin, K.; Staroverov, V.; Kobayashi, R.; Normand, J.; Raghavachari, K.; Rendell, A.; Burant, J.; Iyengar, S.; Tomasi, J.; Cossi, M.; Rega, N.; Millam, N.; Klene, M.; Knox, J.; Cross, J.; Bakken, V.; Adamo, C.; Jaramillo, J.; Gomperts, R.; Stratmann, R.; Yazyev, O.; Austin, A.; Cammi, R.; Pomelli, C.; Ochterski, J.; Martin, R.; Morokuma, K.; Zakrzewski, V.; Voth, G.; Salvador, P.; Dannenberg, J.; Dapprich, S.; Daniels, A.; Farkas, Ö.; Foresman, J.; Ortiz, J.; Cioslowski, J.; Fox, D. *Gaussian 09, Revision D.01*, Gaussian 09, Wallingford CT **2009**.
- (16) Méndez-Hernández, D.; Gillmore, J.; Montano, L.; Gust, D.; Moore, T.; Moore, A.; Mujica, V. *J. Phys. Org. Chem.* **2015**, *28*, 320.

- (17) (a) Evans, P., Darzi, E., Jasti, R. *Nat. Chem.* **2014**, *6*, 404; (b) Xia, J.; Bacon, J.; Jasti, R., *Chem. Sci.* **2012**, *3*, 3018; (c) Darzi, E.; Sisto, T.; Jasti, R. *J. Org. Chem.* **2012**, *77*, 6624; (d) Sisto, T.; Golder, M.; Hirst, E.; Jasti, R. *J. Am. Chem. Soc.* **2011**, *133*, 15800; (e) Jasti, R.; Bhattacharjee, J.; Neaton, J.; Bertozzi, C. *J. Am. Chem. Soc.* **2008**, *130*, 17646.
- (18) (a) Cai, D.; Hughes, D.; Verhoeven, T. *Tetrahedron Lett.* **1996**, *37*, 2537; (b) Wang, X.; Rabbat, P.; O'Shea, P.; Tillyer, R.; Grabowski, E.; Reider, P. *Tetrahedron Lett.* **2000**, *41*, 4335.
- (19) Xia, J.; Jasti, R. *Angew. Chem. Int. Ed.* **2012**, *51*, 2474.
- (20) Yamago, S.; Watanabe, Y.; Iwamoto, T. *Angew. Chem. Int. Ed.* **2010**, *49*, 757.
- (21) (a) Adamska, L.; Nayyar, I.; Chen, H.; Swan, A. K.; Oldani, N.; Fernandez-Alberti, S.; Golder, M.; Jasti, R.; Doorn, S.; Tretiak, S. *Nano Lett.* **2014**, *14*, 6539; (b) Kasha, M. *Farad. Discuss.* **1950**, *9*, 14.
- (22) Duan, C.; Huang, F.; Cao, Y. *J. Mater. Chem.* **2012**, *22*, 10416.
- (23) Iwamoto, T.; Kayahara, E.; Yasuda, N.; Suzuki, T.; Yamago, S. *Angew. Chem. Int. Ed.* **2014**, *53*, 6430.
- (24) Lin, Y.; Li, Y.; Zhan, X. *Chem. Soc. Rev.* **2012**, *41*, 4245.
- (25) (a) Kubota, N.; Segawa, Y.; Itami, K. *J. Am. Chem. Soc.* **2015**, *137*, 1356; (b) Patel, V.; Kayahara, E.; Yamago, S. *Chem. Eur. J.* **2015**, *21*, 5742.